

Earth and Environmental Sciences Library

Ayad M. Fadhil Al-Quraishi
Yaseen T. Mustafa
Abdelazim M. Negm *Editors*

Environmental Degradation in Asia

Land Degradation, Environmental
Contamination, and Human Activities

 Springer

Earth and Environmental Sciences Library

Series Editor

Abdelazim M. Negm, Faculty of Engineering, Zagazig University, Zagazig, Egypt

Earth and Environmental Sciences Library (EESL) is a multidisciplinary book series focusing on innovative approaches and solid reviews to strengthen the role of the Earth and Environmental Sciences communities, while also providing sound guidance for stakeholders, decision-makers, policymakers, international organizations, and NGOs.

Topics of interest include oceanography, the marine environment, atmospheric sciences, hydrology and soil sciences, geophysics and geology, agriculture, environmental pollution, remote sensing, climate change, water resources, and natural resources management. In pursuit of these topics, the Earth Sciences and Environmental Sciences communities are invited to share their knowledge and expertise in the form of edited books, monographs, and conference proceedings.


Ayad M. Fadhil Al-Quraishi · Yaseen T. Mustafa ·
Abdelazim M. Negm
Editors


Environmental Degradation in Asia

Land Degradation, Environmental
Contamination, and Human Activities

 Springer

Editors

Ayad M. Fadhil Al-Quraishi 
Petroleum and Mining Engineering
Department
Tishk International University
Erbil, Iraq

Yaseen T. Mustafa 
University of Zakho
Zakho, Duhok, Iraq

Abdelazim M. Negm
Zagazig University
Zagazig, Egypt

ISSN 2730-6674

ISSN 2730-6682 (electronic)

Earth and Environmental Sciences Library

ISBN 978-3-031-12111-1

ISBN 978-3-031-12112-8 (eBook)

<https://doi.org/10.1007/978-3-031-12112-8>

© The Editor(s) (if applicable) and The Author(s), under exclusive license to Springer Nature Switzerland AG 2022

This work is subject to copyright. All rights are solely and exclusively licensed by the Publisher, whether the whole or part of the material is concerned, specifically the rights of translation, reprinting, reuse of illustrations, recitation, broadcasting, reproduction on microfilms or in any other physical way, and transmission or information storage and retrieval, electronic adaptation, computer software, or by similar or dissimilar methodology now known or hereafter developed.

The use of general descriptive names, registered names, trademarks, service marks, etc. in this publication does not imply, even in the absence of a specific statement, that such names are exempt from the relevant protective laws and regulations and therefore free for general use.

The publisher, the authors, and the editors are safe to assume that the advice and information in this book are believed to be true and accurate at the date of publication. Neither the publisher nor the authors or the editors give a warranty, expressed or implied, with respect to the material contained herein or for any errors or omissions that may have been made. The publisher remains neutral with regard to jurisdictional claims in published maps and institutional affiliations.

This Springer imprint is published by the registered company Springer Nature Switzerland AG
The registered company address is: Gewerbestrasse 11, 6330 Cham, Switzerland

Preface

This volume came into the mind of the editors to help Asian countries in taking the necessary steps to protect the environment against human-induced degradation. As a result, the book titled “Environmental Degradation in Asia: Land Degradation, Environmental Contamination, and Human Activities” will assist Asian countries in meeting the SDGs connected to the environment. The volume consists of four parts and 29 chapters written by more than 70 authors from different Asian countries. The four parts cover (i) Land Degradation in eight chapters, (ii) Part II: Soil Degradation and Environmental Contamination in eight, (iii) Part III: Climate Change and Human Activities in nine chapters, and (iv) Part IV: Drought, Vegetation Degradation in four chapters.

Chapter 1 is titled “[Land Use Land Cover Mapping in Support of Land Degradation Mapping Using Tree-Based Classifiers](#)”. The authors developed land cover mapping of the study area of Shiraz using Landsat-8 and Sentinel-2A satellite images based on several supervised machine learning classifiers, including a complex tree, a medium tree, a simple tree, and a fine gaussian SVM, developed in the MATLAB programming language. The OA and KI statistical indices are used to evaluate the obtained classification results. Additionally, the results are compared with the previously mentioned supervised methods of tree-based algorithms against the fine Gaussian SVM method for Landsat-8 and Sentinel-2A satellite image classification.

Chapter 2 is titled “[Detection of Anthropogenic and Environmental Degradation in Mongolia Using Multi-Sources Remotely Sensed Time Series Data and Machine Learning Techniques](#)”. The chapter presents the detected environmental change and land degradation of Mongolia for the period 1990-2019 using multi-sources RS time-series data. The impacts of several factors are investigated including (1) climate factor impact on land degradation and environmental change, (2) impact of land cover change on land degradation and environmental change, (3) impact of vegetation index on land degradation and environmental change, and (4) impact of drought on land degradation and environmental change.

Chapter 3 is titled “[Assessment of Land Degradation Vulnerability Using GIS-Based Multicriteria Decision Analysis in Zakho District, Kurdistan Region of Iraq](#)”. The authors evaluate land degradation vulnerability and identify vulnerable zones in the Zakho district in the Kurdistan Region of Iraq using GIS, RS, and a multicriteria decision analysis approach. They analyze the susceptibility of land degradation in the study area using a variety of physical and socio-economic criteria.

Chapter 4 is titled “[Evaluation of Geo-hazard Induced by Zarand Earthquake in Central Iran Using Thermal Remote Sensing Data and GIS](#)”. In this chapter, the geo-hazard evaluation of the Zarand Earthquake in central Iran, which occurred February 10th–28th, 2005, is analyzed, and the land surface temperature (LST) variation for the years 2004, 2005, and 2007 is mapped. Finally, the in-situ air temperature variation for the entire month of February 2005 (1st–28th February) is analyzed and compared with data from the ten years before (1994–2004) and six years (2006–2011) after the earthquake. The authors use the satellite data of the MODIS daytime LST product (MOD11A1) from the thermal band during the period from February 10th to 28th, 2005.

Chapter 5 is titled “[Environmental Control of the Sand Dunes in Iraq](#)”. The authors use three methods to detect the changes in the shape, size, and area of the different studied dunes. The three approaches are (a) field work, (b) Iraqi geological maps, and (c) GIS technique.

Chapter 6 is titled “[Amu Darya Dynamics in Afghanistan Using Remote Sensing Data](#)”. This chapter applies remote sensing data and geo-information techniques to understand the temporal and spatial channel changes and dynamics of the Amu Darya river along Afghanistan’s border. Also, mapping and analyzing the land cover changes of four classes over the study area are being investigated. Moreover, determining land conversion from 1990–2020 between the investigated classes has been conducted. Also, seasonal land degradation is being investigated. The authors used four Landsat images (1990, 2000, 2011, and 2020) from the same period (May–July) to avoid seasonal changes. The seasonal changes are investigated in 2020, in all four seasons. Their analysis has been made on the Google Earth Engine platform.

Chapter 7 is titled “[A New Method for Land Degradation Assessment in the Arid Zone of Republic of Kazakhstan](#)”. The authors use the following major processes altogether to characterize the land degradation phenomenon: decreasing productivity, i.e., changes in vegetation; soil degradation (erosion); desertification (increasing of bare land area); and salinization of the soil. These processes are well recognizable using satellite data in the form of direct observation, band ratio computations, or other more or less sophisticated approaches.

Chapter 8 is titled “[Land Degradation Issues in Uzbekistan](#)”. The chapter focuses on showing that existing soil degradation problems are under the effects of climate change and suggests different ways of solving them.

Chapter 9 is titled “[Soil Erosion Catastrophe in Iraq-Preview, Causes, and Study Cases](#)”. In this chapter, the authors review most of the available research articles and reports that are interested in and involved in estimating and managing soil erosion in Iraq.

Chapter 10 is titled “[Assessment of Aircraft Noise Pollution on Students’ Performance](#)”. Here, the authors explore the effects of aircraft noise on students’ learning performance and teachers’ teaching performance at selected schools near Abu Dhabi International Airport.

Chapter 11 is titled “[Role of Effective Factors on Soil Erosion and Land Degradation: A Review](#)”. The authors conducted a comprehensive review and discussed the main factors affecting land degradation, with a major focus on soil erosion. Land degradation sources fall into two main categories: natural and anthropogenic sources affecting land degradation. The main anthropogenic sources, including the role of agriculture, soil salinity, building and urbanity, culture, people’s outcomes, environmental pollution, and war, are presented and discussed.

Chapter 12 is titled “[Cadmium Fractionation Technique as a Chemical Degradation Indicator for Some Soils Near Diyala River in Iraqi Center](#)”. The authors, in this chapter, investigate pollution with cadmium as a chemical degradation indicator for some soils irrigated by the Diyala River (southern part) in the Iraqi center.

Chapter 13 is titled “[Land Degradation Due to MSW Dumping and Sanitary Landfilling: Iraq as a Case Study](#)”. The chapter focuses on finding out the rate of land degradation due to open dumping and landfilling of solid waste in the short and long term. The social and environmental impacts and the measures to stop this tragedy and land rehabilitation in the long term are presented.

Chapter 14 is titled “[RUSLE Model in the Northwest Part of the Zagros Mountain Belt](#)”. Investigation of this topic is essential to suggest mitigations and extend the life of the Mosul Dam. The Mosul Dam, which impounds the Tigris River, suffers from different problems, one of which is siltation. This kind of investigation helps in understanding the nature and type of land erosion processes. Also, many sectors of society in a concerned region will benefit from this investigation. The authors estimate the mean annual loss of soil in the Al-Khabur River Basin (KhRB) on the northwest side of the western Zagros Range (Kurdistan Region/Iraq).

Chapter 15 is titled “[Changes in the Water Quality of Large Rivers in the Asian Part of Russia from the Standpoint of Achieving Sustainable Development Goals](#)”. The authors studied the interim tendencies in water quality in the large rivers of the Asian part of Russia applying Indicator SDG 6.3.2 methodology. The primary objective was to choose the so-called target values characterizing good water quality. In Level 1 evaluation, they used national water quality standards, those recommended by UNEP, and individual target values for each region under discussion.

Chapter 16 is titled “[A Sustainable Way for Fish Health Management by Replacement of Chemical and Drugs by Earthworm](#)”. The authors investigated the need for a sustainable method for fish health management. They also found that earthworms play a key role in this approach.

Chapter 17 is titled “[Integration of Field Investigation and Geoinformatics for Urban Environmental Quality Appraisal of Bankura Town, West Bengal, India](#)”. This chapter endeavor thus attempts to look into all the parameters required for a sustainable Bankura town and assess the environmental quality to address policy initiatives.

Chapter 18 is titled “[Urban Heat Island Under the Background of Urbanization: A Case Study in Nan Jing City, China](#)”. The authors attempt to look into all the parameters required for a sustainable Bankura town and assess the environmental quality to address policy initiatives.

Chapter 19 is titled “[Optimization of Ecological Environment Sensor Network Sites with Multiple Monitoring Targets](#)”. In this chapter, the authors elaborated on a sampling optimization methodology for multi-objective factors. In addition to considering spatial coverage, they also consider the need for information redundancy and economic efficiency. They planned a two-stage site design and layout plan. The goal of the first phase is to show the spatial relationship between precipitation, land surface temperature, soil moisture, and environmental covariates and to obtain their spatial trends. The goal of the second phase is to reflect the relationship between precipitation, surface temperature, soil moisture, and other constraints.

Chapter 20 is titled “[The Influence of Large Scales of Reservoir Construction in the Upper Yangtze River Basin on Regional Precipitation](#)”. The study work provides a first reference for understanding the relationship between regional reservoir planning and precipitation changes. Therefore, this chapter focuses on revealing the total and local impact of the existing reservoirs on precipitation change in the UYRB using multi-source precipitation data for the first time. To accomplish this, the suitability of satellite precipitation products on each sub-basin and time scales of day, month, and year was assessed in order to use them to find and analyze temporal and spatial changes in precipitation and extreme precipitation in the UYRB.

Chapter 21 is titled “[Impact of Climate Changes and Landuse/Land Cover Changes on Water Resources in Malaysia](#)”. This chapter presents a comprehensive review on climate and anthropogenic activities to incorporate the major findings of the previous studies to help policymakers identify specific basins that need to be improved and prioritized. The review highlights the most recent trends and potential impacts of land use change, climate change, and combined land use and climate change impacts on water quantity and quality in various parts of Malaysia and identifies the major sources of water resource degradation. The authors suggest mitigation and adaptation strategies for managing water resources, i.e. sources in Malaysia based on the conducted review.

Chapter 22 is titled “[Impact of Land Use—Land Cover and Socio-economic Changes on Groundwater Availability: A Case Study of Barrackpore-II Block, West Bengal, India](#)”. This chapter is intended to find out the extent of groundwater scarcity, identify the change in LULC and hotspots of water, and access the water insufficiency and awareness of rooftop RWH (RRWH) by rural households.

Chapter 23 is titled “[Unplanned Urban Sprawl Impact on Cultivable Soil Degradation](#)”. It aims to determine the extent of cultivatable soil degradation caused by changing the type of soil use from agricultural to urban (slums). The Normalized Difference Building Index (NDBI) and the Built-up Index (UI) are used to assess the decline of cultivatable soils as soil use changes.

Chapter 24 is titled “[Variability Analysis of Local Climate Change and Its Association with Urbanization in the Beijing-Tianjin-Hebei Region, China](#)”. In this chapter, the authors selected four contiguous cities in China’s Beijing-Tianjin-Hebei region

as the study area. The meteorological, socio-economic, and LUCC data are synthetically used to explore the correlation and variability between urbanization and local climate change. The authors constructed urbanization indicators based on population size, population density, GDP, built-up area, and socio-economic data. Several data analysis methods, including Pearson's moment correlation, Spearman's rank correlation, and EOF were selected to achieve the goals.

Chapter 25 is titled "[Spatial-Environmental Assessment of the Transport System in the Northern Emirates, UAE: Toward Policies and Practices](#)". The chapter examines the relationship between economic growth, environmental degradation, and infrastructure development in the UAE. The authors bring into focus the development of the transport system in the northern emirates, an emerging economic region in the UAE, and the effects this has had on environmental degradation. The authors assess and devise a variety of proposed policies and practices that curb the inevitable environmental degradation associated with the development of the transport system.

Chapter 26 is titled "[Influence of Cryogenic Processes and Phenomena on Minimum Runoff in Russia](#)". The main purpose of this chapter is to assess the cumulative impact on the groundwater recharge of Russian rivers, including those located in the Asian part of the country, of many cryogenic phenomena and processes occurring in riverbeds, catchments, swamps, wetlands, soils, and fissured and loose rocks. The chapter presents the authors' reflections on the evolution of stable and unstable structures in «water flow-ice-channel sediments» system (in annual and multiyear cycles) as air temperature decreases. Also, according to the authors, it lists the main problems arising in the assessment of minimum runoff and groundwater recharge of rivers under climate change.

Chapter 27 is titled "[Forest Successional Change and Its Effect on Plant Species Diversity: A Case Study for Euxine Forests, NE Turkey](#)". The chapter focuses on four main objectives. They are (1) to determine the variation of plant species diversity in the stages of forest succession; (2) to evaluate how the succession stages in tree, shrub, and herbaceous layers affect plant species replacement; (3) to determine the distribution of abundance according to the seral stages of succession; and (4) to explore the distribution of endemic and rare taxa in the succession stages.

Chapter 28 is titled "[Desertification in China: Role of Natural Succession in the Sustainable Revegetation of Drylands](#)". This chapter reviews relevant studies that identify the factors leading to successful and long-term sustainable revegetation of degraded semi-arid and arid drylands. The authors compare ecological methods of revegetation, focusing on the process of natural succession and its implementation in China's drylands during the last 15 years. Furthermore, the authors discuss the actual value of large-scale restoration with sustainable vegetation for the agronomy and reversal of desertification trends and as a potential tool to directly mitigate climate warming and aridity on a local, regional, and maybe even country level.

Chapter 29 is titled "[Estimation of Satellite-Based Regional-Scale Evapotranspiration for Agriculture Water Management Using Penman-Monteith Method](#)". In this chapter, the authors estimate the monthly reference evapotranspiration (ET₀) based on the FAO Penman-Monteith method using the Landsat-7 ETM+ and Landsat-8 OLI seasonal data of 2014, 2015, and 2016 over the Dwarakeswar-Gandheswari

river basin. The model input parameters are emissivity, land surface temperature (LST), net radiation, soil heat flux (G), air temperature, actual and saturation vapor pressure, and wind speed. Correlation analyses have been performed of ET and field-based soil moisture data in the proposed command area. Additionally, results are validated by using MODIS LST for estimated LST and MODIS ET for estimated ET. Moreover, the assessment of regional-scale-based evapotranspiration is a challenge to the agricultural and hydrological frame. This analysis demonstrates the potential applicability of this methodology.

Special thanks are due to all the authors who contributed to this volume. Without their efforts and patience, it would not have been possible to produce this unique volume on Environmental Degradation in Asia. Also, thanks should be extended to include the Springer team, particularly the publishing editor: Alexis Vizcaino, who largely supported the authors and editors during the production of this volume.

Erbil, Kurdistan Region, Iraq
Zakho, Kurdistan Region, Iraq
Zagazig, Egypt
April 2022

Ayad M. Fadhil Al-Quraishi
Yaseen T. Mustafa
Abdelazim M. Negm

Contents

Land Degradation

Land Use Land Cover Mapping in Support of Land Degradation Mapping Using Tree-Based Classifiers	3
Ali Jamali and İsmail Rakıp Karas	
Detection of Anthropogenic and Environmental Degradation in Mongolia Using Multi-Sources Remotely Sensed Time Series Data and Machine Learning Techniques	17
Otgonbayar Munkhdulam, Atzberger Clement, Damdinsuren Amarsaikhan, Satoshi Yokoyama, Sumiya Erdenesukh, and Dalantai Sainbayar	
Assessment of Land Degradation Vulnerability Using GIS-Based Multicriteria Decision Analysis in Zakho District, Kurdistan Region of Iraq	49
Hazhir Karimi, Yaseen T. Mustafa, Hooshyar Hossini, and Ayad M. Fadhil Al-Quraishi	
Evaluation of Geo-hazard Induced by Zarand Earthquake in Central Iran Using Thermal Remote Sensing Data and GIS	69
Hamid Allahvirdiasl, Himan Shahabi, Ayub Mohammadi, Ataollah Shirzadi, Wei Chen, Mehdi Ahmadi, and Masood Khodadadi	
Environmental Control of the Sand Dunes in Iraq	89
Hasan K. Jasim, Ahmed J. Al-Shakeri, and Thamer A. Al-Shimmary	
Amu Darya Dynamics in Afghanistan Using Remote Sensing Data	117
Mohammad Asef Mobariz and Gordana Kaplan	
A New Method for Land Degradation Assessment in the Arid Zone of Republic of Kazakhstan	135
Dmitry Malakhov, Madina Batyrbayeva, and Irina Vitkovskaya	

Land Degradation Issues in Uzbekistan	163
Mukhiddin Juliev, Lazizakhon Gafurova, Olimaxon Ergasheva, Makhsud Ashirov, Kamila Khoshjanova, and Mirvasid Mirusmanov	
Soil Degradation and Environmental Contamination	
Soil Erosion Catastrophe in Iraq-Preview, Causes and Study Cases	179
Nabil Ibrahim Eltaif and Mamoun A. Gharaibeh	
Assessment of Aircraft Noise Pollution on Students' Performance	209
Khaula Abdulla Alkaabi, M. M. Yagoub, and Keith G. Debbage	
Role of Effective Factors on Soil Erosion and Land Degradation: A Review	221
Hooshyar Hossini, Hazhir Karimi, Yaseen T. Mustafa, and Ayad M. Fadhil Al-Quraishi	
Cadmium Fractionation Technique as a Chemical Degradation Indicator for Some Soils Near Diyala River in Iraqi Center	237
Hazim Aziz Al-Robai and Salman Khalaf Essa	
Land Degradation Due to MSW Dumping and Sanitary Landfilling: Iraq as a Case Study	257
Salah Farhan A. Sharif	
RUSLE Model in the Northwest Part of the Zagros Mountain Belt	287
Arsalan Ahmed Othman, Ahmed K. Obaid, Varoujan K. Sissakian, Ahmed F. Al- Maamar, and Ahmed T. Shihab	
Changes in the Water Quality of Large Rivers in the Asian Part of Russia from the Standpoint of Achieving Sustainable Development Goals	307
Alesya O. Danilenko, Lyudmila S. Kosmenko, Olga S. Reshetnyak, Maria Yu. Kondakova, and Mikhail M. Trofimchuk	
A Sustainable Way for Fish Health Management by Replacement of Chemical and Drugs by Earthworm	329
Rahul Kumar, Renu Yadav, Rajender Kumar Gupta, and Pooja	
Climate Change and Human Activities in Nine Chapters	
Integration of Field Investigation and Geoinformatics for Urban Environmental Quality Appraisal of Bankura Town, West Bengal, India	355
Abira Dutta Roy, Jaya Gorai, Rinku Dey, Sujata Pal, and Sunipa Mandal	
Urban Heat Island Under the Background of Urbanization: A Case Study in Nan Jing City, China	391
Zhanya Xu, Xiao Liu, Xiangang Luo, Shuang Zhu, Ning Zhang, and Qi Guo	

Optimization of Ecological Environment Sensor Network Sites with Multiple Monitoring Targets 411
 Xiangang Luo, Kai Luo, Yangchun Li, Fukun Zhu, Libo Zhou, and Bei Xu

The Influence of Large Scales of Reservoir Construction in the Upper Yangtze River Basin on Regional Precipitation 439
 Shuang Zhu, Jianan Wei, Jiang Li, Yuying Wang, and Siwen Cao

Impact of Climate Changes and Landuse/Land Cover Changes on Water Resources in Malaysia 465
 Hadi Hamaaziz Muhammed, Nuraddeen Mukhtar Nasidi, and Aimrun Wayayok

Impact of Land Use—Land Cover and Socio-economic Changes on Groundwater Availability: A Case Study of Barrackpore-II Block, West Bengal, India 485
 Satabdi Biswas, Satiprasad Sahoo, and Anupam Debsarkar

Unplanned Urban Sprawl Impact on Cultivable Soil Degradation 505
 Suhad M. Al-Hedny and Qassim A. Talib Alshujairy

Variability Analysis of Local Climate Change and Its Association with Urbanization in the Beijing-Tianjin-Hebei Region, China 521
 Shaobo Zhong, Min Xu, Chunxiang Cao, and Wei Zhu

Spatial-Environmental Assessment of the Transport System in the Northern Emirates, UAE: Toward Policies and Practices 541
 Robert M. Bridi, Naeema Al Hosani, and Ahmed Al Murshidi

Drought, Vegetation Degradation

Influence of Cryogenic Processes and Phenomena on Minimum Runoff in Russia 567
 M. L. Markov, M. V. Georgievsky, and M. A. Mamaeva

Forest Successional Change and Its Effect on Plant Species Diversity: A Case Study for Euxine Forests, NE Turkey 587
 Alper Uzun and Salih Terzioğlu

Desertification in China: Role of Natural Succession in the Sustainable Revegetation of Drylands 615
 Lorenz Huebner and Ayad M. Fadhil Al-Quraishi

Estimation of Satellite-Based Regional-Scale Evapotranspiration for Agriculture Water Management Using Penman–Monteith Method 633
 Satiprasad Sahoo, Tanushree Basu Roy, Anirban Dhar, and Anupam Debsarkar

Land Degradation

Land Use Land Cover Mapping in Support of Land Degradation Mapping Using Tree-Based Classifiers



Ali Jamali and İsmail Rakıp Karas

Abstract Currently, land degradation is among one of the most challenging environmental issues globally. Land degradation has been affected considerably by the land cover change at the national and global scales. On the other hand, recent ecological changes, including droughts and flash floods associated with climate change, directly link with the land cover change. It has been reported that the most affected people worldwide are in developing countries where their economy is directly connected with agriculture. In this study, to map the land cover of Shiraz city, a fine gaussian Support Vector Machine (SVM) algorithm is compared against three tree-based algorithms of complex, medium, and simple tree. Landsat-8 and Sentinel-2A imageries of the study area are classified with the beforementioned supervised classifiers. Based on the results, the fine gaussian SVM classifier had an overall accuracy (OA) of 99.29% and a kappa index (KI) of 98.26%, outperforming the other tree-based classifiers. In addition, with the values of 99.54 and 98.88% for the OA and KI, the fine gaussian SVM had better results for classifying the Sentinel-2A imagery of the study region.

Keywords Land cover · Land use · Land degradation · Machine learning · Decision tree · SVM

1 Introduction

Currently, land degradation has become a topic of research as it is regarded as a global issue. Deforestation, climate change issues such as droughts and flash floods, and on

A. Jamali (✉)

Civil Engineering Department, Faculty of Engineering, University of Karabük, 78050 Karabük, Turkey

e-mail: alijamali@karabuk.edu.tr

İ. R. Karas

Department of Computer Engineering, Faculty of Engineering, University of Karabük, 78050 Karabük, Turkey

e-mail: ismail.karas@karabuk.edu.tr

© The Author(s), under exclusive license to Springer Nature Switzerland AG 2022

A. M. F. Al-Quraishi et al. (eds.), *Environmental Degradation in Asia*,

Earth and Environmental Sciences Library,

https://doi.org/10.1007/978-3-031-12112-8_1

the other hand, a rapid increase in population growth are the main factors associated with land degradation on the global scale [1]. In addition, land cover land-use change is among the main factors that considerably affect land degradation globally [2]. Land degradation is defined by the decline in biological productivity of the forest, wetland, rangeland, semi-arid and dry land. Land use land cover change (LULC) has been mapped with the use of various supervised and unsupervised machine learning algorithms [3–7].

In the literature, advanced algorithms such as Random Forest (RF), Decision Trees and Support Vector Machine (SVM) have shown their superiority over the conventional classification methods, including Maximum Likelihood (ML), due to their capability in dealing with high-dimensional and complex data [8, 9]. It is worth highlighting that the most critical capability of SVM is that it can generalize complex objects. On the other hand, the SVM algorithm had good results in research with a limited number of training data [10]. It was reported that the SVM classifier had outperformed other tree-based algorithms such as RF, specifically in LULC mapping [11–14].

It is worth noting that the SVM method does the classification by utilization of an optimally separating hyperplane [15]. For instance, for the classification of tree species, Nguyen et al. [16] developed a weighted SVM algorithm, improving the kappa index (KI) and overall accuracy (OA) of the conventional SVM by 2%. The proposed method improved the mean class accuracy by 10% compared to the traditional method of SVM. Gapper et al. [17] used the SVM classifier for the change detection of coral reef in pacific islands, obtaining accuracies of 87.9%, 85.7%, 69.2%, and 81.2% for the classification of Palmyra Atoll, Kingman Reef, Baker Island Atoll, and Howland Island, respectively. Based on their results, it was found that the SVM method is a more accurate classifier over Ridge, LASSO, and logistic regression methods. On the other hand, decision trees are regarded as the most used and popular methods for the classification of remote sensing imageries due to their structure's simplicity and high capabilities of image classification [9, 18–20].

In this research, for accurate land cover mapping of the study area of Shiraz using the Landsat-8 and Sentinel-2A satellite images, several supervised machine learning classifiers, including a complex tree, medium tree, simple tree, and a fine gaussian SVM, are developed in MATLAB programming language. Besides, the OA and KI statistical indices are used to evaluate the obtained classification results. This chapter compares the results of the previously mentioned supervised methods of tree-based algorithms against the fine gaussian SVM method for the Landsat-8 and Sentinel-2A satellite image classification.

2 The Study Area

The study area is Shiraz city, located on the south side of Iran (see Fig. 1). In the last decades, the land cover of the city has experienced dramatic changes. It is worth

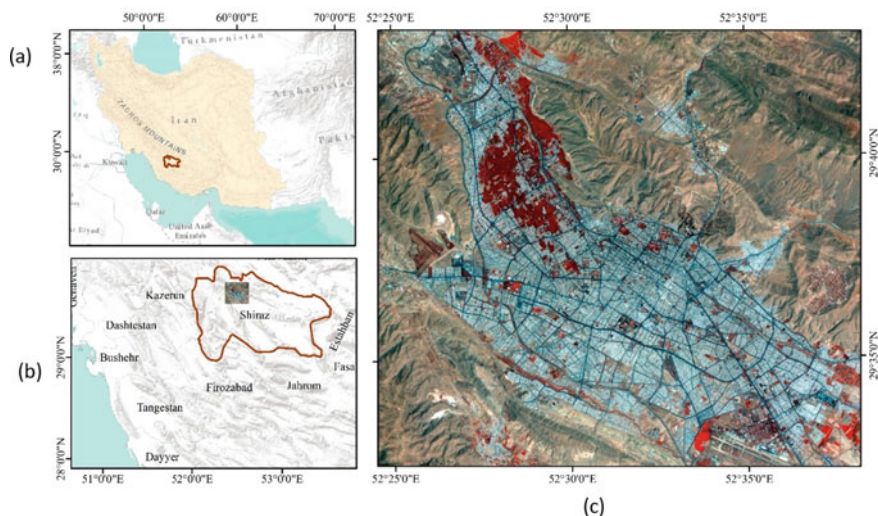


Fig. 1 a Map of Iran; b city of Shiraz; c Landsat-8 image of the study area

highlighting that urbanization is the predominant factor of the land-use change over the last fifty years in Shiraz.

3 Methodology

The workflow of this research is shown in Fig. 2. First, ENVI software is utilized for the Landsat-8 image atmospheric and radiometric correction. In addition, the SNAP software is used for the atmospheric correction of the Sentinel-2A imagery. Then, to classify the Landsat-8 and Sentinel-2A images, several machine learning classifiers, including a complex tree, medium tree, simple tree, and a fine Gaussian SVM, are developed. Finally, the classification results are evaluated based on the OA and KI statistical indices.

It should be noted that reflectance values were extracted from digital numbers for the Landsat-8 satellite image. Besides, radiometric calibration and atmospheric correction were applied using the ENVI 5.3 software. Dark Object Subtraction (DOS) [21] was used in this research as it is not dependent on the field measurements. In other words, the DOS technique does not require ground control points measured in the study area of interest.

Additionally, for the atmospheric correction of the Sentinel-2A imagery, Sen2Cor in SNAP software was used [22]. It is worth mentioning that the SNAP was used due to its simplicity and efficiency in dealing with Sentinel satellite imagery. The Normalized Difference Vegetation Index (NDVI) [10] was used to improve the classification results of the Landsat-8 image (Eq. 1).

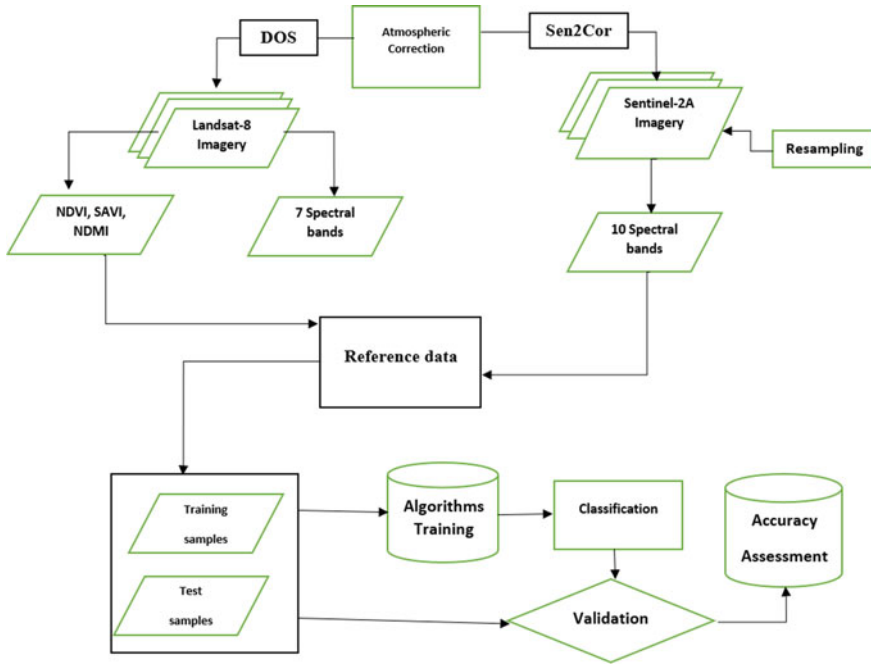


Fig. 2 The workflow of this research

$$NDVI = \frac{(NIR - RED)}{(NIR + RED)} \quad (1)$$

Moreover, the Landsat-based Normalized Difference Moisture Index (NDMI) was employed (Eq. 2).

$$NDMI = \frac{(NIR - SWIR)}{(NIR + SWIR)} \quad (2)$$

On the other hand, for the classification of the Sentinel-2A imagery, ten spectral bands of Coastal aerosol, blue, green, red, three vegetation red edges, near infra-red, narrow near infra-red, and water vapor bands were used. It should be noted that the Sentinel-2A imagery was resampled using the nearest neighbor algorithm in SNAP software to a 10 m pixel resolution. The number of training and test data used in this research are shown in Table 1.

Table 1 The number of training and test data for each LULC classes

Class	Class ID	Landsat-8 (test/training)	Sentinel-2A (test/training)
Build-up	1	821/1924	7514/17,398
Soil	2	3010/6998	27,102/63,329
Vegetation	3	245/588	2226/5238

4 Land Cover Land Use Maps

The Landsat-8 and Sentinel-2A imageries of the research region are presented in Figs. 3 and 4.

The LULC maps based on the fine gaussian SVM, the complex tree, the medium tree, and the simple tree is shown in Fig. 4 (i.e., based on the Landsat-8 imagery).

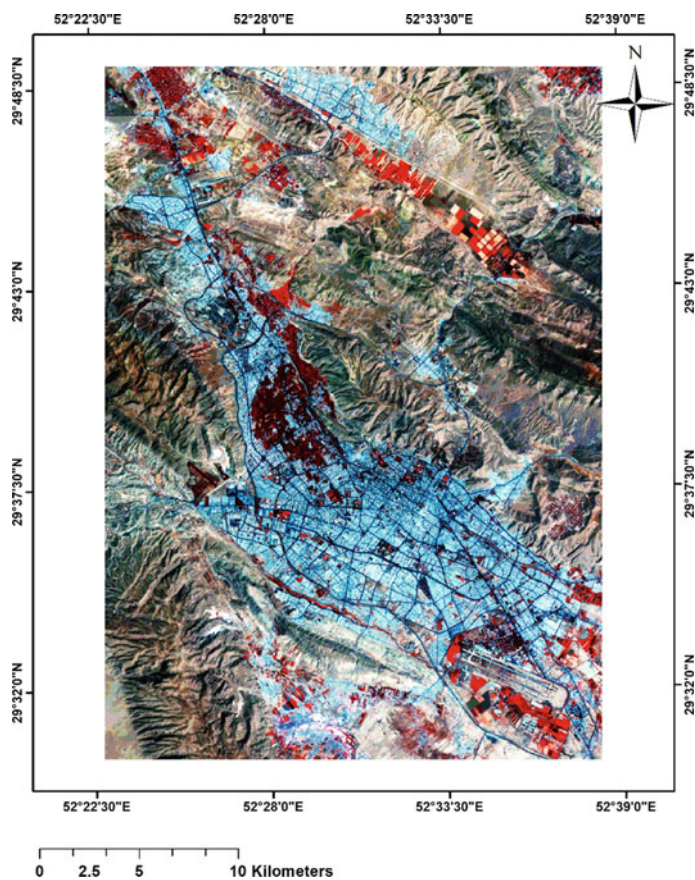


Fig. 3 The Landsat-8 image of the research location

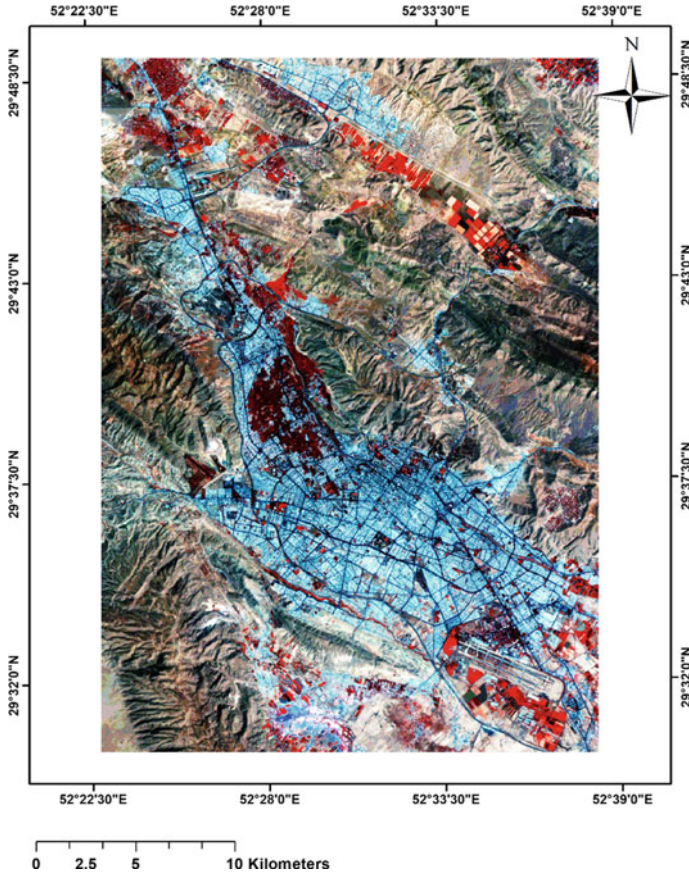


Fig. 4 The Sentinel-2A imagery of the study area

The number of nodes for the simple, medium, and complex trees is equal to 7, 33, and 141, respectively. From Fig. 5, it is evident that the simple tree method had a high level of misclassification for the build-up regions. In contrast, other tree-based classifiers of the medium and complex tree visually produced better classification results. It should be noted that better classification results of the medium and complex trees than the simple tree are due to their higher number of trees and complexity.

Figure 6 shows the LULC maps of the study area based on the Sentinel-2A imagery using the fine gaussian SVM, the complex tree, the medium tree, and the simple tree classifiers. The number of nodes for the simple, medium, and complex trees is equal to 9, 37, and 175, respectively. Based on the results and as evident from Fig. 6, the simple tree method had a high level of build-up misclassification for the classification of the Sentinel-2A image as well. The lower number of trees in the simple tree classifier than the other two more complex tree-based classifiers should be the main reason for its higher misclassification for the build-up areas.

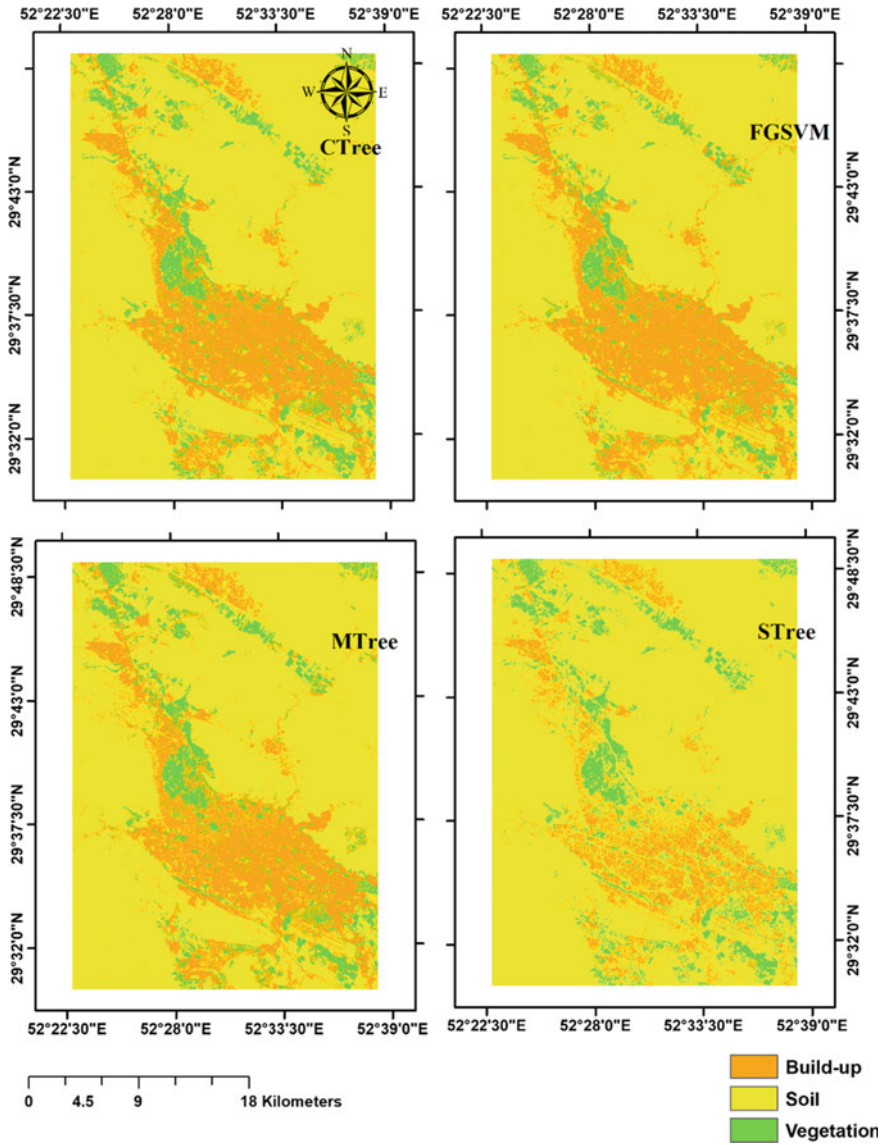


Fig. 5 The land use/cover map of the research area from Landsat-8 imagery

5 Evaluation of the Results

In this chapter, the OA and KI statistical indices were used to evaluate the results of the tree-based algorithms of the simple, medium, and complex trees against the fine gaussian SVM method (Eqs. 3 and 4).

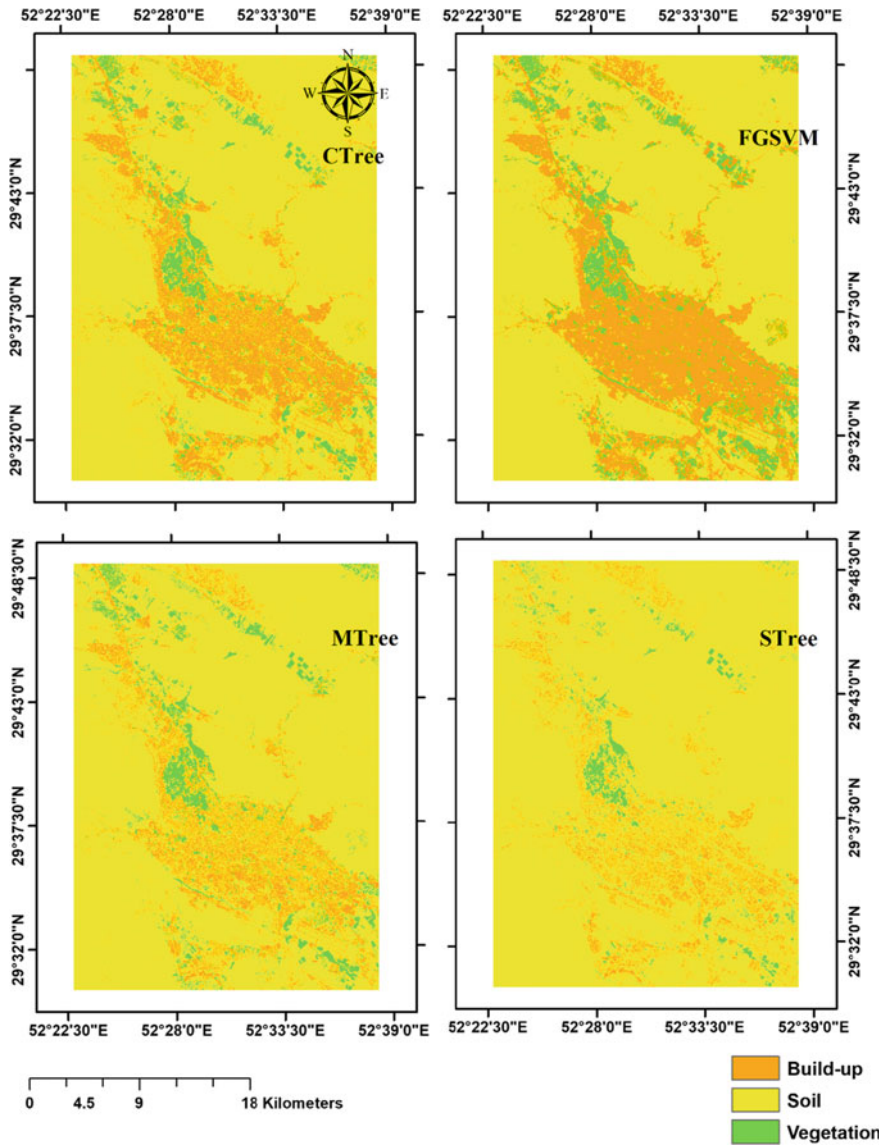


Fig. 6 Land cover/use of the research location using the Sentinel2-A image

$$OA = \frac{\text{number of correct classified pixels}}{\text{total number of pixels}} \tag{3}$$

$$KI = \frac{p_0 - p_e}{1 - p_e}, p_0 = \frac{\sum x_{ii}}{N}, p_e = \frac{\sum x_{i+}x_{+i}}{N^2} \tag{4}$$

where x_{i+} is the marginal total of row I, the total number of observations is shown by N, and x_{ij} is observation in row i and column i.

For the Landsat-8 satellite imagery, the fine gaussian SVM with 99.29 and 98.26% values for the OA and KI outperformed the other tree-based algorithms. On the other hand, the Complex decision tree had better performance than the medium and the simple tree classifiers with 98.33% and 95.92% for the OA and KI, respectively (see Fig. 7). It can be explained by its higher number of trees and complexity than the other tree-based classifiers of the simple and medium trees.

Moreover, with 99.54 and 98.88% for the statistical metrics of OA and KI, the fine gaussian SVM had better results for the classification of the Sentinel-2A imagery. Besides that, the complex tree had better performance than the medium and simple tree methods, with the values of 95.25% and 88.35% for the OA and KI, respectively (see Fig. 8).

The matrix of confusions of the classifiers for the Landsat-8 and Sentinel-2A imageries are shown in Tables 2 and 3.

The highest level of misclassification was for the simple tree algorithm, where it had difficulty in recognition of build-up regions from soil areas. The reason should be similar spectral reflectance in the optical imageries of Landsat-8 and Sentinel-2A for the build-up and soil regions. However, better classification results were obtained by increasing the number of trees and the complexity of the tree-based algorithms.

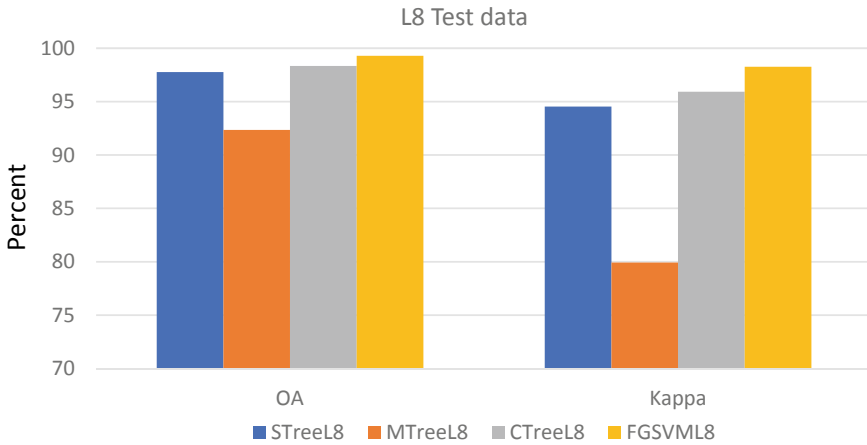


Fig. 7 The classification results in terms of OA and KI for the Landsat-8 image (values are in percent)

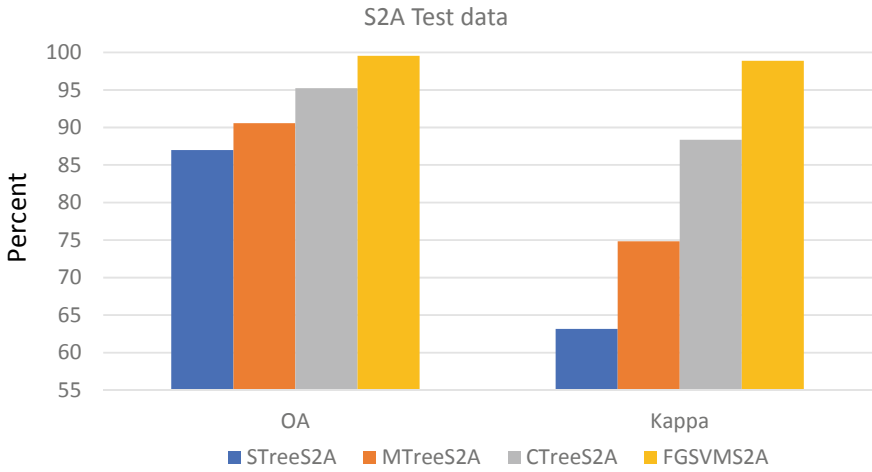


Fig. 8 The results of classification algorithms for the OA and KI for the Sentinel-2A imagery (values are in percent)

Table 2 The confusions matrix of the classifiers for the Landsat-8 imagery (for the test data)

CTreeL8	Build-up	Soil	Vegetation
Build-up	782	38	1
Soil	29	2981	0
Vegetation	0	0	245
MTreeL8	Build-up	Soil	Vegetation
Build-up	767	54	0
Soil	37	2973	0
Vegetation	0	0	245
STreeL8	Build-up	Soil	Vegetation
Build-up	554	267	0
Soil	45	2965	0
Vegetation	0	0	245
FGSVML8	Build-up	Soil	Vegetation
Build-up	805	16	0
Soil	12	2998	0
Vegetation	0	1	245

6 Discussions

Figure 9 presents the area percentage covered by the three LULC classes of build-up, soil, and vegetation regions for the study area of Shiraz city.

Table 3 The confusions matrix of the classifiers for the Sentinel-2A imagery (for the test data)

CTreeS2A	Build-up	Soil	Vegetation
Build-up	6388	1121	5
Soil	547	26,555	0
Vegetation	23	40	2163
MTreeS2A	Build-up	Soil	Vegetation
Build-up	4471	3017	26
Soil	344	26,757	1
Vegetation	31	48	2147
STreeS2A	Build-up	Soil	Vegetation
Build-up	3335	4179	0
Soil	353	26,749	0
Vegetation	1	263	1962
FGSVMS2A	Build-up	Soil	Vegetation
Build-up	7392	115	7
Soil	31	27,071	0
Vegetation	13	4	2209

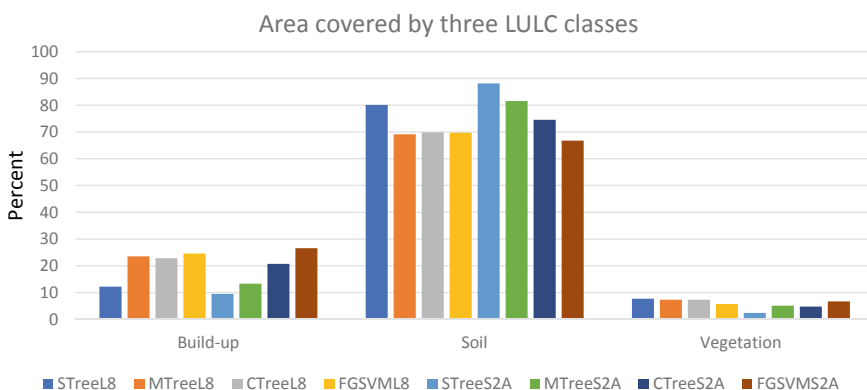


Fig. 9 Area covered by the three LULC classes (in percent) (L8 presents Landsat-8 imagery and S2A presents Sentinel-2 imagery) (values are in percent)

Based on the results of the SVM algorithm for the Landsat-8 imagery, vegetation, build-up, and soil regions covers 5.71%, 24.58%, and 69.71% of the study area, respectively. In addition, based on the results of the SVM algorithm obtained from the Sentinel-2A image, vegetation, build-up, and soil areas cover 6.69%, 26.57%, and 66.74% of the study region, respectively. The SVM algorithm had produced approximately similar results for the two satellite imageries, respectively, considering the different spatial resolutions of 30 and 10 m for the Landsat-8 and Sentinel-2A imageries, respectively (see Fig. 9).

In terms of the statistical indices of OA and KI, the fine gaussian SVM was superior over the other tree-based machine learning algorithms for the image classification of Landsat-8 and Sentinel-2 imagery. It is worth highlighting that we used a limited number of training data to train our machine learning classifiers. As such, the limited number of training data can be attributed as the main reason for the superiority of the SVM classifier over the other tree-based classification techniques. In other words, one of the most significant advantages of the SVM classifier over other supervised methods is its capability to be trained with a low number of training data. Such capability is essential in remote sensing projects in which creating training data is costly and time-consuming.

7 Conclusions

Land degradation is significantly affected by the recent climate change. At the same time, urbanization is increasing rapidly due to phenomena directly or indirectly linked to climate change, including desertification. Moreover, LULC change is regarded among parameters related to land degradation. It is worth highlighting that as poor people's livelihood and food security depend on natural resources, they are the most affected people globally. Consequently, in this research, several supervised machine learning techniques were utilized for the precise land cover mapping of the study area of Shiraz city. The fine gaussian SVM classifier outperformed the other tree-based methods to classify the Landsat-8 and Sentinel-2A imageries based on the results. The fine gaussian SVM algorithm had the OA and KI values of 99.29% and 98.26%, respectively, for the classification of the Landsat-8 image. Besides, values of 99.54% and 98.88% were obtained by the fine gaussian SVM to classify the Sentinel-2A image for the indices of the OA and KI, respectively.

8 Recommendations

As land degradation is directly or indirectly linked to food security, the environment, and the quality of life in areas that are dependent on natural resources, it will remain one of the most challenging issues worldwide in the twenty-first century. Urbanization, climate changes such as droughts, and human interventions have negatively affected the rate of land degradation globally. As such, the development of advanced algorithms for monitoring the natural resources and areas affected by land degradation is an essential task for the local government. The provincial government and stakeholders can use the results of this research to use suitable remote sensing imagery, algorithms, and tools for the preservation of natural resources (i.e., gardens) in the study area of Shiraz.

Acknowledgements We would like to thank the editors and reviewers for the time and effort given to our paper.

References

1. Gashaw T, Behaylu A, Tilahun A, Fentahun T (2014) Population growth nexus land degradation in Ethiopia. *Population* 4
2. Nkonya E, Anderson W, Kato E, Koo J, Mirzabaev A, von Braun J, Meyer S (2016) Global cost of land degradation. In: *Economics of land degradation and improvement—a global assessment for sustainable development*. Springer, Cham, pp 117–165
3. Jamali A (2021) Land use land cover modeling using optimized machine learning classifiers: a case study of Shiraz, Iran. *Model Earth Syst Environ* 7:1539–1550. <https://doi.org/10.1007/s40808-020-00859-x>
4. Jamali A, Mahdianpari M, Brisco B, Granger J, Mohammadimanesh F, Salehi B (2021) Wetland mapping using multi-spectral satellite imagery and deep convolutional neural networks: a case study in Newfoundland and Labrador, Canada. *Can J Remote Sens* 47:243–260. <https://doi.org/10.1080/07038992.2021.1901562>
5. Jamali A, Mahdianpari M, Brisco B, Granger J, Mohammadimanesh F, Salehi B (2021) Comparing solo versus ensemble convolutional neural networks for wetland classification using multi-spectral satellite imagery. *Remote Sens* 13:2046. <https://doi.org/10.3390/rs13112046>
6. Hosseiny B, Mahdianpari M, Brisco B, Mohammadimanesh F, Salehi B (2022) WetNet: a spatial-temporal ensemble deep learning model for wetland classification using Sentinel-1 and Sentinel-2. *IEEE Trans Geosci Remote Sens* 60:1–14. <https://doi.org/10.1109/TGRS.2021.3113856>
7. Ghorbanian A, Kakooei M, Amani M, Mahdavi S, Mohammadzadeh A, Hasanlou M (2020) Improved land cover map of Iran using Sentinel imagery within Google Earth Engine and a novel automatic workflow for land cover classification using migrated training samples. *ISPRS J Photogramm Remote Sens* 167:276–288. <https://doi.org/10.1016/j.isprsjprs.2020.07.013>
8. Berhane TM, Lane CR, Wu Q, Autrey BC, Anenkhonov OA, Chepinoga VV, Liu H (2018) Decision-tree, rule-based, and random forest classification of high-resolution multispectral imagery for wetland mapping and inventory. *Remote Sens* 10
9. Ghatkar JG, Singh RK, Shanmugam P (2019) Classification of algal bloom species from remote sensing data using an extreme gradient boosted decision tree model. *Int J Remote Sens* 40:9412–9438
10. Jamali A (2019) A fit-for algorithm for environmental monitoring based on maximum likelihood, support vector machine and random forest. *ISPRS Ann Photogramm Remote Sens Spat Inf Sci* 25–32
11. Foody GM, Mathur A (2004) Toward intelligent training of supervised image classifications: directing training data acquisition for SVM classification. *Remote Sens Environ* 93:107–117
12. Otukei JR, Blaschke T (2010) Land cover change assessment using decision trees, support vector machines and maximum likelihood classification algorithms. *Int J Appl Earth Obs Geoinf* 12:S27–S31
13. Mountrakis G, Im J, Ogole C (2011) Support vector machines in remote sensing: a review. *ISPRS J Photogramm Remote Sens* 66(3):247–259
14. Shao Z, Cai J (2018) Remote sensing image fusion with deep convolutional neural network. *IEEE J Sel Top Appl Earth Obs Remote Sens* 11:1656–1669
15. Jozdani SE, Johnson BA, Chen D (2019) Comparing deep neural networks, ensemble classifiers, and support vector machine algorithms for object-based urban land use/land cover classification. *Remote Sens* 11

16. Nguyen HM, Demir B, Dalponte M (2019) Weighted support vector machines for tree species classification using lidar data. Presented at the IGARSS 2019–2019 IEEE international geoscience and remote sensing symposium
17. Gapper JJ, El-Askary H, Linstead E, Piechota T (2019) Coral Reef change detection in remote Pacific islands using support vector machine classifiers. *Remote Sens* 11
18. Kilpatrick KA, Podestá G, Williams E, Walsh S, Minnett PJ (2019) Alternating decision trees for cloud masking in MODIS and VIIRS NASA sea surface temperature products. *J Atmos Oceanic Tech* 36:387–407
19. Moayedi H, Jamali A, Gibril MBA, Kok Foong L, Bahiraei M (2020) Evaluation of tree-base data mining algorithms in land used/land cover mapping in a semi-arid environment through Landsat 8 OLI image; Shiraz, Iran. *Geomat Nat Hazards Risk* 11:724–741
20. Jamali A, Mahdianpari M, Brisco B, Granger J, Mohammadimanesh F, Salehi B (2021) Deep forest classifier for wetland mapping using the combination of Sentinel-1 and Sentinel-2 data. *GISci Remote Sens* 1–18. <https://doi.org/10.1080/15481603.2021.1965399>
21. Chavez PS (1988) An improved dark-object subtraction technique for atmospheric scattering correction of multispectral data. *Remote Sens Environ* 24:459–479. [https://doi.org/10.1016/0034-4257\(88\)90019-3](https://doi.org/10.1016/0034-4257(88)90019-3)
22. Louis J, Debaecker V, Pflug B, Main-Knorn M, Bieniarz J, Mueller-Wilm U, Cadau E, Gascon F (2016) Sentinel-2 Sen2Cor: L2A processor for users. Presented at the Proceedings living planet symposium 2016

Detection of Anthropogenic and Environmental Degradation in Mongolia Using Multi-Sources Remotely Sensed Time Series Data and Machine Learning Techniques



Otgonbayar Munkhdulam, Atzberger Clement, Damdinsuren Amarsaikhan, Satoshi Yokoyama, Sumiya Erdenesukh, and Dalantai Sainbayar

Abstract The main objective of this study is to investigate land degradation and environmental change in Mongolia using time series of multi-sources remotely sensed data and advanced approaches. As the data analysis techniques, the Random Forest (RF) classifier, Ordinary Least Square (OLS), and Partial Least Square (PLS) regressions, Break for Additive Season and Trend (BFAST) algorithm, Sen's slope and Restrend method were applied. For detecting land degradation and environmental change, we have investigated several factor impacts: (1) climate factor impact on land degradation and environmental change, (2) impact of land cover change on land degradation and environmental change, (3) impact of vegetation index on land degradation and environmental change, (4) impact of drought on land degradation and environmental change. The meteorological time series analysis showed that

O. Munkhdulam (✉) · D. Amarsaikhan · D. Sainbayar
Institute of Geography and Geocology, Mongolian Academy of Sciences (MAS), 15170 Ulaanbaatar, Mongolia
e-mail: munkhdulam@mas.ac.mn; otgonbayar.munkhdulam.a0@s.mail.nagoya-u.ac.jp

D. Amarsaikhan
e-mail: amarsaikhan@mas.ac.mn

D. Sainbayar
e-mail: sainbayard@mas.ac.mn

A. Clement
Institute of Geomatics, University of Natural Resources and Life Sciences (BOKU), Peter-Jordan-Straße 82, 1190 Vienna, Austria
e-mail: clement.atzberger@boku.ac.at

O. Munkhdulam · S. Yokoyama
Department of Geography, Graduate School of Environmental Studies, Nagoya University, Nagoya 464-8601, Japan
e-mail: s-yokoyama@nagoya-u.jp

S. Erdenesukh
School of Arts and Sciences, National University of Mongolia (NUM), 14201, 46A Ulaanbaatar, Mongolia
e-mail: erdenesukh@num.edu.mn

between 1990 and 2019, air temperature over Mongolia has increased by 1.8 °C, while annual total precipitation over Mongolia had decreased from 714 to 640 mm. The land cover analysis indicated that between 1990 and 2019, forest, steppe, dry steppe, and cropland were decreased. In contrast, the meadow steppe, wetland, sand land, broken area, urban land, and water were increased. The trend analysis result indicated that positive trends were observed in Mongolia's central, northern, and northeastern parts. In contrast, the negative trends were detected in all areas of the west, southern region, forested areas in the north and east, around the Ulaanbaatar city, and in the grassland area of eastern Mongolia. The drought detection analysis showed that the years 1993, 1994, 1997, 2000–2002, 2004–2007, 2009, and 2017 could very well detect the droughts during the growing season for the period 1990–2019. The trend analysis result showed that negative and positive trends of time series NDVI were strongly related to land cover change.

Keywords Land degradation · Time series data analysis · Random Forest classifier · Least square regression · Sen's slope value · BFAST algorithm

1 Introduction

Land degradation and environmental change are global issues recognized by the United Nations Conventions on Combat Desertification (UNCCD), climate change, and biodiversity [1–3]. The literature contains numerous definitions, giving the idea of the complexity of the phenomenon [4–8]. The UNCCD, and the Millennium Ecosystem Assessment (MEA) programs used more inclusive definitions:

- Environmental degradation is a process through which the natural system is compromised, decreasing biodiversity, and the health of the environment [9]. Environmental degradation is also an umbrella concept including a variety of issues [10] through which loss of natural resources (water, air, and soil), reduction of the ecosystem productivity, the extinction of wildlife, and increase of pollution are envisaged [11]. Environmental degradation a reduction of the environment's capacity to support ecological objectives and social-economic needs [12].
- Land degradation is a long-term by reducing biological and economic productivity, and loss of heterogeneity in the landscape [13]. Land degradation leads to long-term collapse to balance the demand for and supply of ecosystem goods and services [14] caused by disturbances from which the system cannot recover [15], and its effects on food security, livelihoods, and production. Land degradation is associated with carrying capacity, resilience, and sensitivity of land and the susceptibility of people living on and from this land [16].

Moreover, the UNCCD adopted land degradation neutrality (LDN) in 2015. LDN in which no land is lost or least degradation was adopted as a common target under the Sustainable Development Goals [17].

Early land degradation assessment was commonly focused on expert judgment [18]. In the past two decades, international agencies (UNEP, and GEF) and scholars have joined efforts to develop standardized methods, and tools for map and monitor land degradation and achieve specific advance [19]. Most methods to assess land degradation have been defined by the “Land Degradation Assessment in Drylands (LADA-FAO)” approach [20, 21]. Accurate evaluation of land degradation is vitally important in drylands [22]. In practice, synergistic uses that integrate field and long-term observational studies are more important. However, facing challenges of estimation of environmental change and land degradation have been identified as uncertain and specious, but results were at different success levels because it depends on small scale field study and expert opinion [23]. Therefore, the lack of long-term and small-scale field monitoring programs and problems involving projects to detect land degradation have been noted [22, 24, 25]. More advances with the broad application of geospatial and artificial intelligence technology to research the cause, effect, and trend of land degradation have been observed in recent years. The studies have shown that long term vegetation and climate observation data for assessing land degradation can be from remote sensing (RS) data. Because satellite data provide highly informative outputs of remote measurements at different resolutions [26]. Furthermore, this multi-source information can be used to detect and monitor environmental changes and land degradation for researchers and decision-makers dealing with environmental management.

Over the past two decades, two kinds of approaches have been commonly applied to assess environmental change and land degradation or change of land productivity [23, 27]. The first approach is based on assessment change in vegetation phenology acquired from remotely sensed time-series imagery [28–31]. Vegetation indices (VIs) have been applied to determine and explain a range of phenology metrics that determine annual vegetation life period occurrence [32]. Several approaches have been introduced for quantifying vegetation dynamics using time series of VI products such as TIMESAT [33], TSPT/PPET [34], Breaks for the additive season and trend (BFAST) [35], NDVIts [36], TimeStats [37], PenoSat [38], the software for the processing and interpretation of RS image time series (SPIRITS) [39], and DATimeS [40]. From those approaches, BFAST and TIMESAT are commonly applied to evaluate vegetation phenology [41]. The second approach for degradation examination is based on detection changes in the interrelation between a VI and climate variables which is an estimate of vegetation greenness and a proxy evaluation of land degradation [32, 42]. In this part, one of the widely used methods is the Residual trend (RESTREND) analysis [42]. RESTREND is widely applied to assess ecosystem productivity changes not caused by inter-annual climatic variability [42, 43].

In 1990, Mongolia transitioned from a socialist economy to a democratic society. Since the transition to a market economy, Mongolia has experienced lots of social, economic, and environmental changes. For example, between 1990 and 2019, the total population of the country has gradually increased (from 2.1 to 3.2 million or 53.1%), while there was observed a tremendous increase in the amount of livestock (from 25.8 to 70.9 million or by a factor 2.74) [44]. This rapid increase of population and livestock have different negative environmental impacts in Mongolia such as

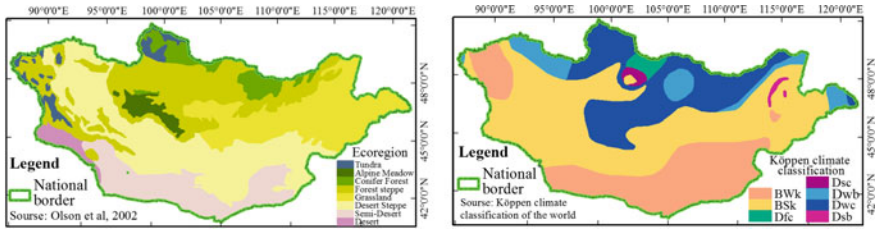


Fig. 1 Study area: (left) Terrestrial Ecoregions of the World Wide Fund (Olson et al. 2001), (right) Köppen climate classification of Mongolia extracted from world map of the Köppen climate classification

pasture deterioration, overgrazing, deforestation, and land degradation caused by mining activities. This chapter aimed to detect the environmental change and land degradation of Mongolia for the period 1990–2019 using multi-sources RS time-series data. Here, we have investigated several factor impacts: (1) climate factor impact on land degradation and environmental change, (2) impact of land cover change on land degradation and environmental change, (3) impact of vegetation index on land degradation and environmental change, (4) impact of drought on land degradation and environmental change.

2 Study Area

We selected the entirety of Mongolia (1.56×10^6 km²) as the study area, of which about 45.3% can be featured as desert steppe, semi-desert, and desert ecoregion (Fig. 1a). The climate conditions are extremely conditional and dry. Annual average air temperature, and annual total precipitation fluctuations -8 °C to 6 °C, and 50 – 500 mm, respectively. By Köppen’s climate classification, Mongolia is divided into 7 climatic regions (Fig. 1b). The largest widespread climates are cold desert climate (BWk), cold semi-arid (BSk), and monsoon-influenced subarctic (Dwc). By contrast, subarctic (Dfc), Mediterranean-influenced (Dsc), monsoon-influenced warm-summer humid continental (Dwb), and Mediterranean-influenced warm-summer humid continental (Dsb) are less prevalent as shown in Fig. 1b.

3 Data and Methods

For the analysis, we used five different datasets. Three of the five datasets have been derived from Landsat, Moderate Resolution Imaging Spectroradiometer (MODIS), and Global Inventory Modeling and Mapping Studies (GIMMS). The two remaining datasets are the metrological and training data. Details about datasets are shown in Table 1. Within the framework of the current study, all remotely sensed data have

Table 1 Data sources and characteristics

Sensor/source	Product name/band	Path/row	Acquisition date	Temporal resolution	Spatial resolution
Landsat 4, 5	B2–B7	123–124/27–28, 125/27–29, 126/25–29, 127/25–30, 128–130/26–31, 131–133/25–31, 134–136/25–30, 137/24–30, 138/24–29, 139–140/25–29, 141/25–28, 142/25–27, 143/25–26	1990 ± 1 from May to Sep	16-day	30 m
Landsat 8			2019–1 from May to Sep	16-day	
MODIS Aqua and Terra	NDVI (MCD13Q1)	h23v03, h23v04, h24v03, h24v04, h25v03, h25v04, h26v04	2002–2019	16-day	250 m
GIMMS	NDVI3g	Extracted from global data	1981–2013	15-day	8 km
Climate Research Unit-Time series (CRU-TS)	Temperature, precipitation	Extracted from global data	1961–2019	Monthly	1 km
FROM-GLC	Validation sample point	Extracted from global data	–		

been reprojected to a Universal Transverse Mercator (UTM)/World Geodetic System (WGS) 84 coordinates systems applying the nearest neighbor resampling approach.

3.1 Remotely Sensed Data

Landsat imagery

For the land cover classification, a total of 216 scenes of Landsat Thematic Mapper (TM) and Operational Land Imager (OLI) imageries take into account the period from May to September of 1990 and 2019 at a spatial resolution of 30 m. For analysis, six spectral bands, and downloaded from the United States Geological Survey (USGS) Earth Explorer have been applied (Table 1). Radiometric and atmospheric corrections were conducted applying Semi-automatic Classification Plugin (SCP) based on the Quantum Geographic Information System (QGIS).

MODIS data

This study used MODIS Aqua, and Terra satellites NDVI (MOD13Q1 and MYD13Q1) products for the period 2002–2019 acquired from the Land Processes Distributed Active Archive Center (LP DAAC) (Table 1). This NDVI data had a spatial resolution of ~250 m in sinusoidal projection. We applied mosaicking, resampling, reprojecting modules, and performed an image cropping applying the “MODIS” R package [45].

GIMMS data

The third-generation (3 g) of GIMMS NDVI is the more recent new version of the GIMMS data. The original GIMMS datasets were generated from the AVHRR (Advanced Very High-Resolution Radiometer) sensor data taking into account different deleterious effects [46]. NDVI3g is a bi-monthly composite derived from AVHRR sensor data of National Oceanic and Atmospheric Administration (NOAA) 7–18 satellites, and it covers for 1981–2013 period at a spatial resolution of 1/12°. For the processing of the GIMMS NDVI3g, we used the “GIMMS” R package [47].

3.2 Meteorological Data

Time series of meteorological data (monthly average air temperature and monthly total precipitation) were collected from the Climate Research Unit Time Series (CRU-TS) for 1961–2019 at a resolution of 0.5°. These datasets are downscaled from CRU-TS v4.03 by the CRU, University of East Anglia, and applying WorldClim 2.1 [48, 49]. The grid is an interpolation station-based meteorological data in real-time. Therefore, more precision might be expected at the levels of the weather stations [50].

3.3 Training Samples

For training samples, we focused on synthesis strategy including the majority-class. The validation sample points have been extracted from the Finer Resolution Observation and Monitoring of Global Land Cover (FROM-GLC) validation sample data. FROM-GLC is a global LC map produced using Landsat imagery at a resolution of 30 m in 2010, 2015, and 2017 [51, 52]. For the LC classification was focused on the FROM-GLC version 2 classification system. This classification system defined 11 main classes easily created to the FAOLC classification system and International Geo-Biosphere Program (IGBP) classification system. The additional sampling points were obtained from Google high-resolution images.

3.4 Methods

Random Forest (RF) classifier, Ordinary Least Square (OLS), and Partial Least Square (PLS) regressions, Break for Additive Season and Trend (BFAST) algorithm, Sen’s slope and Restrend method have been applied as the data analysis techniques. Over the years, different classification methods have been used to map LC derived from RS data (from unsupervised algorithms to machine learning algorithms) [53]. Many authors judged that machine learning algorithms such as an artificial neural network (ANN) [54], decision tree [55, 56], support vector machine (SVM) [57], and ensembles of classifiers [58] were more accurate and efficient compared to the conventional parametric algorithms [59, 60]. ANN and SVM need to adjust a large number of parameters [61, 62]. In contrast, the classification method (bagging, boosting, and RF) is high classification accuracy and can determine variable importance. In order to generate, LC map used an RF classifier, a non-linear statistical ensemble method. There were 500 trees with out-of-bag (OOB) error. The variables per splits were set to zero.

We used trend analysis methods to assess land degradation including the linear regression model and Sen’s Slope. Firstly, the study applied the ordinary least square (OLS) regression model. The method estimates the relationship between the response and predictor variables in Eq. 1.

$$y = \alpha + \beta x + \epsilon \tag{1}$$

where x —the predictor or explanatory variable and y —response variable which represents time and NDVI value, respectively. α —intercept of the regression line, which represents the average value of y when x is 0, β —the slope of the regression line, ϵ —the error term. Accurate trend measures are strongly impacted by the variability and noise process [63]. The number of years is required to determine the trend’s importance. Two widely used non-parametric methods to detect trend significance include Sen’s Slope and Mann–Kendall (MK) test [64, 65]. We applied Sen’s Slope (2) test to detect trend significance.

$$Slope = Median \left[\frac{x_j - x_i}{j - i} \right] \tag{2}$$

where x_i and x_j are the values at times i and j , respectively ($1 \leq i < j \leq n$, n indicates the data length) [66]. For data analysis, Rstudio was applied [67]. The linear trend is easy to compute however, contrasting trends could balance out so it is significant to confirm that hypothesis for determining the linear trend is met for each analysis. There is needs to use nonlinear NDVI time series models including a trend, seasonal and stochastic components, external variables, seasonal components, and white noise [68]. For detecting, abrupt change and annual dynamics of land cover

from NDVI time-series data, we applied the BFAST algorithm. The BFAST algorithm integrates a decomposition model that decomposes the time series into trend, seasonality, and residuals components with an iterative algorithm to detect breakpoints using structural change methods [35]. The decomposition model is used to iteratively fit a piecewise linear trend and a seasonal model (see Eq. 3) [69].

$$Y_t = T_t + S_t + e_t (t = 1, \dots, n) \quad (3)$$

where Y_t —NDVI at the time t , T_t —the trend components, S_t —the seasonal components, e_t —the noise component (or represents the remaining variation). Trend and seasonal models are fitted to the section of time series according to the changes that detected breakpoints [70]. The ordinary least squares (OLS) residual focused on the transferring of the sum test was applied to the test including one or more breakpoints [71]. But the BFAST requires a maximum number of breakpoints [70].

Over the past period, many different approaches have been used for monitoring drought mainly focused on RS indices [72, 73] for instance, Palmer Drought Index (PDSI) [74], Standardized Precipitation Index (SPI) [75, 76], Standardized Precipitation Evapotranspiration Index (SPEI) [77], Enhanced Combined Drought Index (ECDI) [78], Multivariate Standardized Drought Index (MSDI) [79], and Vegetation Condition Index (VCI) [73, 80, 81]. Of these, VCI and SPI are commonly applied in research of drought monitoring [82]. In this research, we estimated NDVI anomaly using the following Eqs. (4–6). NDVI anomaly is a commonly used approach based on NDVI for drought monitoring [72, 83].

$$NDVI_{mean_i} = (NDVI_1 + NDVI_2 + \dots, NDVI_n)/n \quad (4)$$

where $NDVI_{mean_i}$ —mean value of NDVI, $NDVI_1, NDVI_n$ —the first, and the last day composite of the NDVI, which represents the growing season of i year. The sum NDVI value is computed using Eq. (5).

$$\overline{NDVI} = \sum_{i=1}^n \frac{NDVI_{mean_i}}{n} \quad (5)$$

where, $NDVI$ —means of the NDVI, n —the number of years. In order to compute the seasonally of the NDVI anomaly used Eq. (6) [84].

$$NDVI_{anomaly_i} = \frac{NDVI_{mean_i} - \overline{NDVI}}{\overline{NDVI}} \times 100 \quad (6)$$

where $NDVI_{anomaly_i}$ —NDVI anomaly represents the growing season (from May to September) i year. In order to estimate the climate factors' influences in land degradation, we used the residual trend analysis method (RESTREND). RESTREND investigates the trend of residual differences between observed and predicted NDVI [85]. This approach is widely used to assess and monitor land degradation by analyzing time series NDVI data. Linear regression models might be applied to fit the seasonal vegetation variation well into a line in the NDVI time-series analysis (Eq. 7). The slope of the line can be used to detect the direction of vegetation variation and the strength of variation from the steepness of the trend line [32].

$$NDVI_i = a \times t + NDVI_0 \quad (7)$$

where $NDVI_0$ —the constant, a —the trend, t —the time. Firstly, Evans and Geerken [42] used the linear regression on time series NDVI data and precipitation to determine the NDVI signals calculable to climatic conditions. The difference between observed and predicted NDVI was highlighted as residuals. The residuals were measured pixel by pixel to identify climate signals [42]. Climate signal is recognized and eliminated from the trend in vegetation action, the remaining vegetation variation might be associated with the human-induced activity [32]. Because there is a high correlation between vegetation and climate factors [85–88].

4 Results

4.1 Meteorological Data Time Series Analysis

Estimation of annual mean air temperature and annual total precipitation from CRU-TS data related to entire Mongolia has been made by a zonal and local statistics approach. The 1961–1989 period is used as the base year for the calculation of temperature and precipitation anomalies. The result of the study showed that between 1990 and 2019, air temperature over Mongolian territory has increased by 1.8 °C compared to the annual mean air temperature of the period 1961–1990 (Fig. 2). The trend of 1961–2019s illustrated that the annual mean air temperature has been gradually increased demonstrating significant fluctuation (Fig. 3 (left)). Over the past 58 years, the annual mean temperature was at its highest in 2007, reaching 2.3 °C, and the lowest in 1984, and decreased by –1.5 °C (Fig. 3 (left)). Air temperature anomaly results showed that the years of 1964, 1968, 1969, 1970, 1974, 1981, 1984, 1985, and 2012 were cold and temperature anomalies exceeded –0.5 °C (Fig. 3 (right)). However, the years of 1979, 1980, 1995, 1997–1999, 2002, 2004, 2006–2008, 2013–2015, and 2017–2019 were warm and temperature anomalies exceeded 1.0 °C (Fig. 3 (right)).

Between 1990 and 2019, the annual total precipitation over Mongolia had decreased from 714 to 640 mm (Fig. 4). However, annual total precipitation has

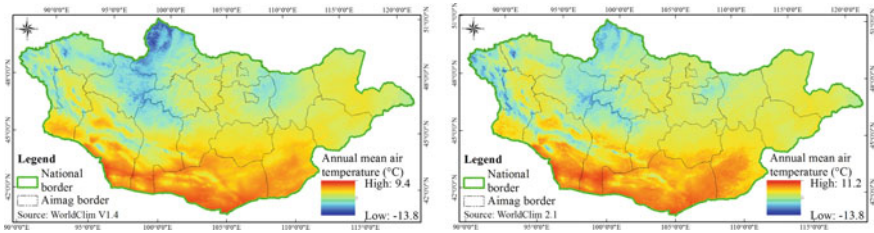


Fig. 2 Annual mean air temperature, °C: (left) for period 1961–1989, (right) for period 1990–2019

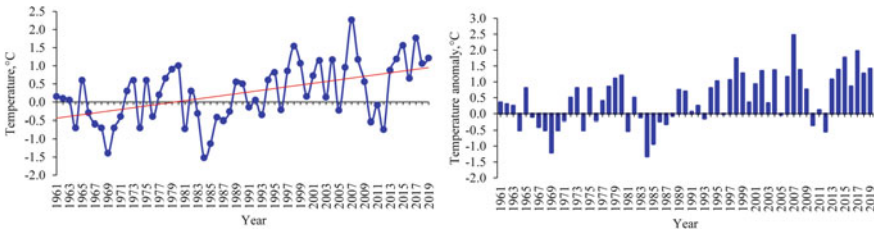


Fig. 3 (Left) Yearly mean air temperature from 1981 to 2019, (right) Yearly average air temperature anomaly

greatly fluctuated since 1961 (Fig. 5 (left)). From the long-term trend (i.e. 1961–2019), it is seen that annual total precipitation has been gradually increasing (Fig. 5 (left)). Over the past 58 years, annual total precipitation was at its highest in 1990, reaching 284.2 mm, and lowest in 1980, and dropped to 159.2 mm (Fig. 5 (left)).

The annual total precipitation anomaly results showed that the years of 1964, 1984, 1990, 1993, 1994, 1998, 2003, 2013, 2016, and 2018 were wet, and precipitation anomalies fluctuated from 42.2 mm to 75.5 mm. In contrast, the years of 1965, 1968, 1972, 1978, 1980, 2002, 2004, and 2017 were driest and precipitation anomalies ranged from -23.2 mm to -49.5 mm (Fig. 5 (right)).

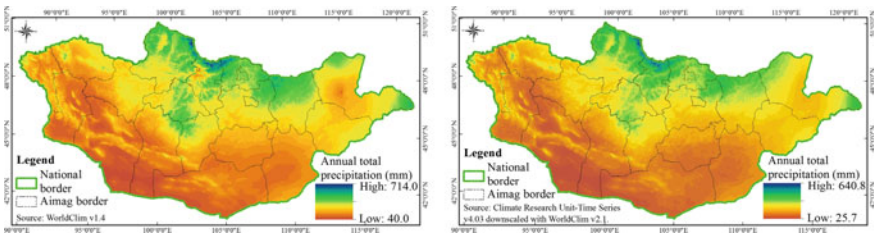


Fig. 4 Annual total precipitation, mm: (left) for period 1961–1989, (right) for period 1990–2019

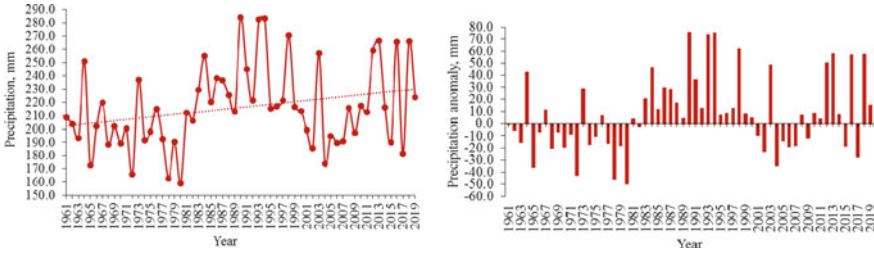


Fig. 5 (Left) Yearly total precipitation from 1961 to 2019, (right) Yearly precipitation anomaly

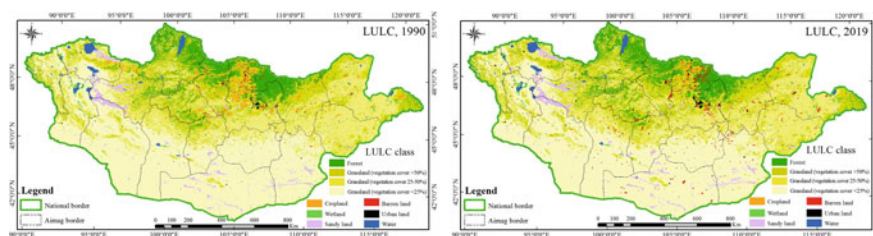
4.2 Land Cover Classification Derived from Landsat Data

Land is a valuable resource for food, energy, and many other vital goods that are demanded to meet human and animal needs [89]. LC information is also vitally important in land management, nature conservation, food security, and many others. In addition, the LC change affects surface characteristics, climate change, ecosystem services [90, 91], energy balance, and biogeochemical cycles [92]. In the present study, for the LC classification, 216 scenes of Landsat TM, OLI imageries from May to September in 1990 and 2019 with a spatial resolution of 30 m have been used. For the actual analysis, six spectral bands were used. We focused on 11 LC classes defined by the FROM-GLC version 2 classification system. However, we revised some classes based on the main characteristics of the Mongolian landscape, and vegetation coverage. Also, we considered the suggestions made in the previous studies [50, 93–95]. For instance, vegetation coverage, grassland was divided into two types such as meadow steppe and steppe. Barren land was also divided into sand and broken areas by mining activity. The final LC classification scheme used in this study is shown in Table 2, and Fig. 6. The validation sample points have been obtained from the FROM-GLC (<http://data.ess.tsinghua.edu.cn/>), and Google high-resolution images. After the radiometric and atmospheric corrections, we used a random forest (RF) classifier for the LC mapping [96]. There were 500 trees with out-of-bag (OOB) error. The variables per splits were set to 0.

The result indicated that between 1990 and 2019, forest, steppe, dry steppe, and cropland were decreased by 4135×10^3 pixels, 4747×10^3 pixels, $19,659 \times 10^3$ pixels, 9925×10^3 pixels, respectively (Table 3). In contrast, meadow steppe, wetland, sand land, broken area, urban land, water were increased by $32,916 \times 10^3$ pixels, 29×10^3 pixels, 3320×10^3 pixels, 1570×10^3 pixels, 561×10^3 pixels, and 120×10^3 pixels, respectively (Table 3).

Table 2 The land cover type

Level 1		Level 2		Level 3		Description
LC type	Code	LC type	Code	LC type	Code	
Forest	1	–	–	–	–	All type of forest
Cropland	2	–	–	–	–	All type of fallow and sown area
Grassland	3	Meadow steppe	31	Steppe	32	There are includes two type of steppe: meadow steppe (vegetation coverage (VC) > 50%), steppe (VC 25–50%)
Shrub land	4	Dry steppe	41	–	–	Where land is sparsely vegetated and largely barren (VC < 25%)
Wetland	5	–	–	–	–	All types of wetland
Water	6	–	–	–	–	Fresh and salt water lake, ephemeral lake, and pond
Urban land	7	–	–	–	–	Town and rural settlement area
Barren land	8	Sand	81	Mining	82	Sand or sand dunes; broken area by mining activity

**Fig. 6** LULC maps in 1990 and 2019 derived from Landsat TM, OLI imagery applying an RF classifier with 303 training samples

4.3 Change Detection Analysis

4.3.1 Analysis of MODIS and GIMMS NDVI Time Series for Detection of Land Degradation

Over the years, satellite (e.g. Landsat at 30 m, MODIS at 250 m, and AVHRR at 1 km resolution) data-based NDVIs have been widely used for land degradation assessment [32]. One of the most popular practices of NDVI applications in the assessment and monitoring of land degradation could be the analysis of time-series remotely sensed

Table 3 Assessment of classification accuracy using confusion matrix (overall accuracy was 82.3%, 1 pixel represent 10³)

LULC class	Forest	Grassland (VC > 50%)	Grassland (VC 25–50%)	Shrub land (VC < 25%)	Cropland	Wetland	Sand land	Broken area	Urban land	Water	Total pixel	User accuracy, %
Forest	147,578	6526	1289	211	85	62	43	229	21	0	156,044	94.6
Grassland (VC > 50%)	1958	378,601	2371	937	781	0	321	327	148	0	385,445	98.2
Grassland (VC 25–50%)	1781	15,353	367,809	5122	536	1	324	519	102	27	391,575	93.9
Shrub land (VC < 25%)	39	10,187	12,215	718,881	78	1	2692	519	76	125	744,814	95.6
Cropland	550	7647	3143	4	2718	11	5	0	61	0	14,140	19.2
Wetland	0	24	0	0	16	4178	5	0	0	2	4225	98.9
Sand land	0	0	0	0	0	0	34,535	0	104	0	34,639	99.7
Broken area	2	23	0	0	0	0	0	262	0	0	286	91.5
Urban land	0	0	0	0	0	0	0	0	1457	0	1457	100.0
Water	0	0	0	0	0	0	34	0	0	17,375	17,410	99.8
Total pixel	151,909	418,361	386,828	725,155	4215	4254	37,959	1856	1968	17,530	1,750,035	–
Producer accuracy, %	97.1	90.5	95.1	99.1	64.5	98.2	91.0	14.1	74.0	99.1	–	82.3

NDVI. The positive trend of NDVI represents the areas of vegetation recovery, and the negative trend is represents human induced degradation of vegetation cover. For detecting anthropogenic and environmental degradation, Mongolia used the Trend and BFAST analysis methods derived from MODIS and GIMMS NDVI time series for the period 1990–2019. The trend analysis summarized patterns over the period in the data to show the trend of change and could be applied to examine ambiguities in different period points and relations with other factors [97].

The slope of the line can be applied to figure out the direction of vegetation variation, and the strength of variation from the steepness of the trend line [32]. Therefore, we have estimated the linear regression slope values for trends using GIMMS and MODIS NDVI products from 1990 to 2019 (Fig. 7). Estimated trend significance values derived from GIMMS and MODIS NDVI from 1990 to 2019 are shown in Fig. 8. The trend analysis result showed that the positive trends are observed in the central, north, and northeastern Mongolia increased from the north to the northeast (Fig. 7). On the other hand, negative trends are observed in southern Mongolia and in all areas of the west, some forested areas in the north and northeast, as well as grassland areas in the east and around Ulaanbaatar (Fig. 7). Especially in the northwest and south parts of Mongolia, the land is also sparsely vegetated. In order to illustrate the significance of the trend, we used Sen’s slope method. Figure 8 shows, high-density vegetated areas were not significant, for instance, in the northern and northeastern parts of Mongolia. However, contrasting trends could balance out, so it is significant to ensure that hypothesis for the determining the linear trend is met for each analysis [32]. BFAST algorithm is more powerful to determine changes of trend [70].

This algorithm integrates a decomposition model of time series components (i.e., trend components, seasonality components, and residual components) with an iteration of the algorithm to determine breakpoints applying methods of the structural change [35]. In other words, the algorithm iteratively calculates the number change

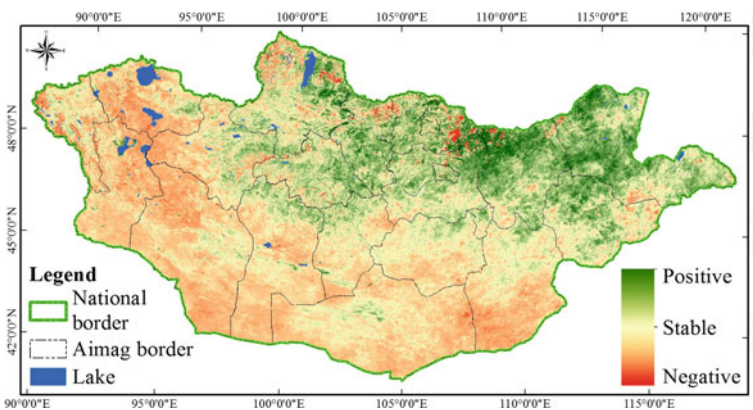


Fig. 7 The trend of slope value of linear regression estimated from GIMMS and MODIS NDVI for the period 1990–2019

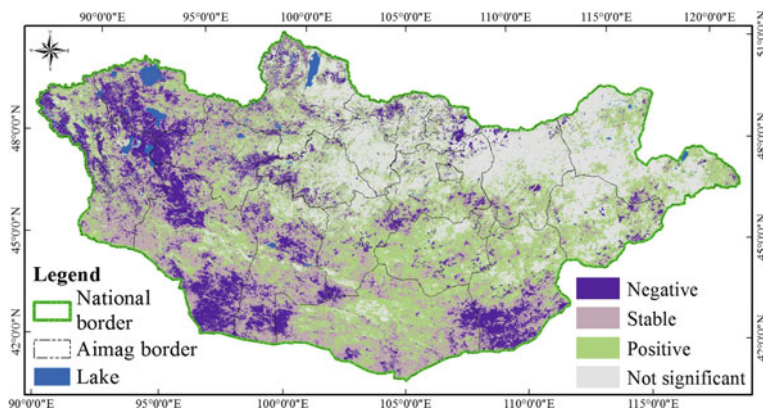


Fig. 8 The trend of slope value of significant linear regression estimated from GIMMS and MODIS NDVI for the period 1990–2019

and time, and features of change by their amplitude and direction [50]. For detection of the trend, seasonal, and remainder components, both gradual and abrupt changes of time series monthly NDVI (MODIS of 2002–2019 and GIMMS of 1981–2013), we used the BFAST algorithm.

As could be seen from the BFAST analysis (see Fig. 9a–f), the areas of positive and negative NDVI trends are strongly related to land cover change. Validation of smaller, more localized NDVI trends can be done with the fine-resolution satellite imagery. By the use of the NDVI time series analysis and BFAST algorithm, we detected negative trends in the areas with forest fire, deforestation, mining activities, and urban expansion.

4.3.2 Analysis of MODIS and GIMMS NDVI Time Series for Drought Detection

Drought is a complicated process having an impact on human life [82, 98, 99]. The United Nations Office for Outer Space Affairs (UNOOSA) depicted four types of droughts, including meteorological, hydrological, agricultural, and socio-economic [100]. In Mongolia, several researchers [72, 101–104] have used various RS-based drought indices for detecting and monitoring the drought at different success levels. The previous studies have shown that NDVI could be widely used to detect and investigate meteorological, hydrological, and agricultural droughts globally. For detecting drought, we computed the NDVI anomaly from MODIS and GIMMS NDVI time series data for the period 2002–2019 (Fig. 10) and 1982–2013 (Fig. 11), respectively. The results of the study showed that the years of 1985, 1993, 1994, 1997, 2000–2002, 2004–2007, 2009, and 2017 could very well detect the droughts during the growing season for the period 1982–2019 (Fig. 12).

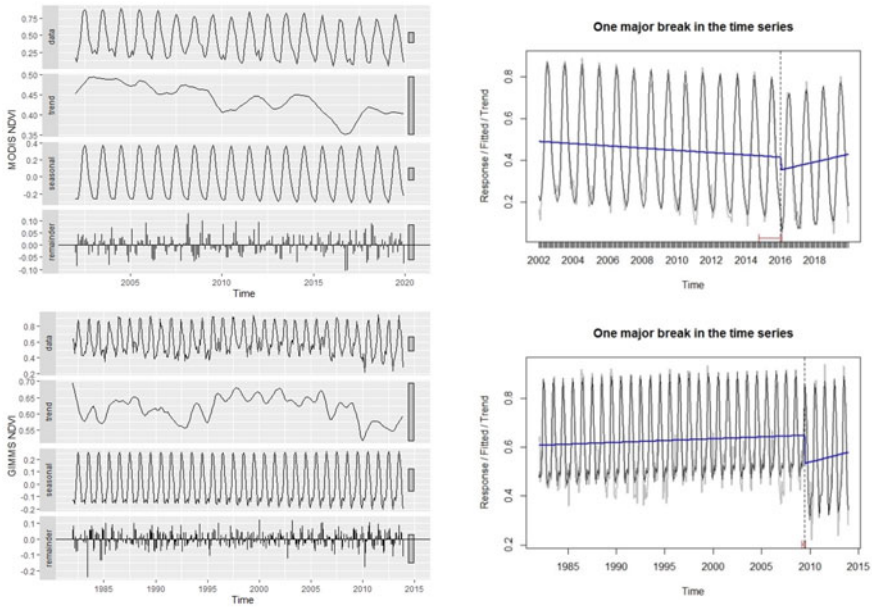


Fig. 9 a Forest to barren land by mining activity (Latitude: 49.640, Longitude: 107.721). Here, fitted components of trend, seasonal, and the remainder (evaluated noise) for the time series monthly NDVI of MODIS (left above) and GIMMS (left below). The abrupt change was observed in the trend component of the NDVI time series (right above and below). The grey, black, red, and blue lines were represented a primary NDVI curve, fitted NDVI curve, direction and magnitude of abrupt change, and trend for before and after the change, respectively. **b** Forest to grassland by fire (Latitude: 49.124, Longitude: 112.061). Explanations are found in (a). **c** Grassland (vegetation coverage > 50%) to forest (Latitude: 50.167, Longitude: 106.498). Explanations are found in (a). **d** Grassland (vegetation coverage > 50%) to cropland (Latitude: 49.415, Longitude: 105.628). Explanations are found in (a). **e** Grassland (vegetation coverage 25–50%) to barren land (Latitude: 48.423, Longitude: 104.529). Explanations are found in (a). **f** Grassland (vegetation coverage < 25%) to urbanland (Latitude: 43.040, Longitude: 106.84). Explanations are found in (a)

4.3.3 Land Degradation Induced by Human Factors

If the important climate influence can be eliminated from long-term trends of NDVI, human-induced land degradation might be discriminate against [86]. As it is known, the RESTREND method is widely used to eliminate factors from the vegetation trend [43]. The method is focused on the assumption that considers the relationship between vegetation production and climate factors [105]. Anthropogenic land degradation is separated from climate driven one [106]. In order to detect climate factors impact, examined the RESTREND includes regressing NDVI from precipitation (P), temperature (Ta), and potential evapotranspiration (PET) for the period 1982–2019, and then calculated the residuals or difference between observed and predicted NDVIs. Firstly, seven statistical models have been created to study the relationship between the response and 3 predictor variables (Table 4).

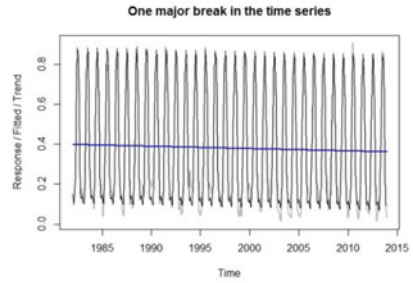
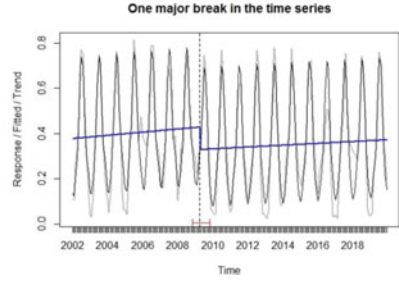
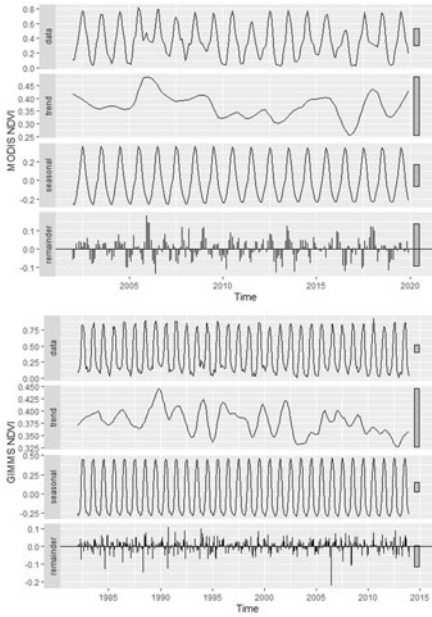


Fig. 9 (continued)

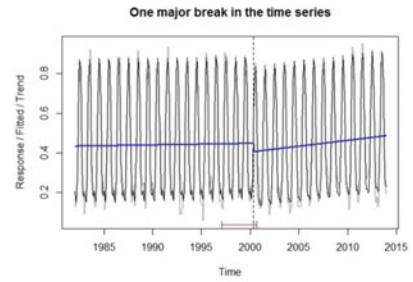
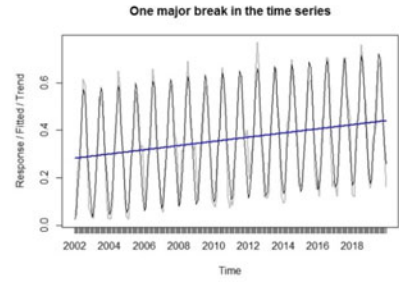
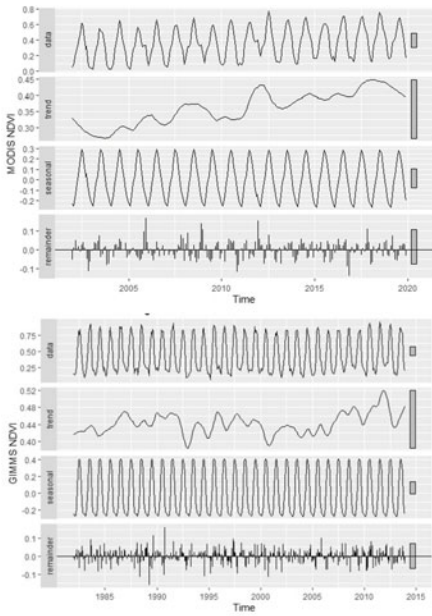


Fig. 9 (continued)

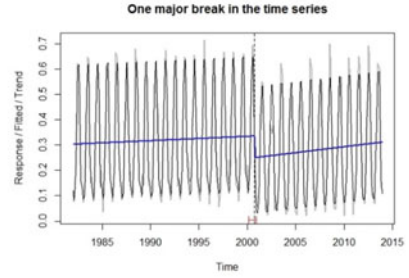
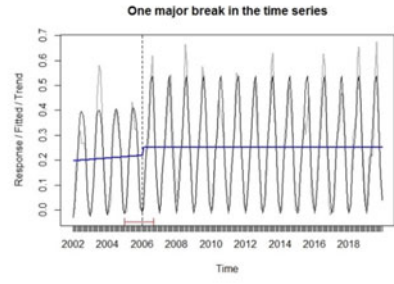
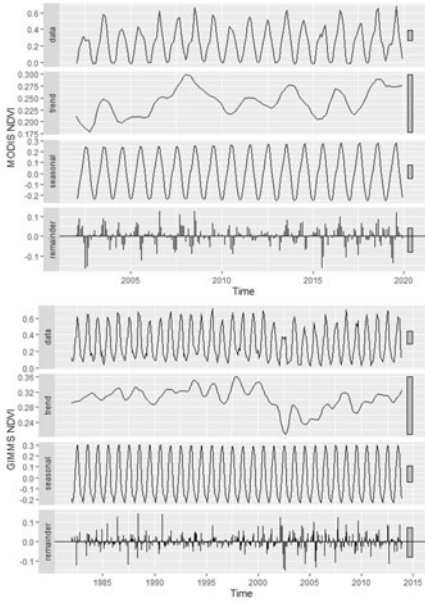


Fig. 9 (continued)

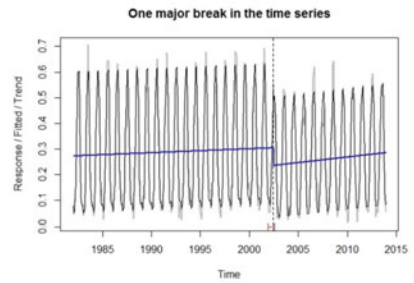
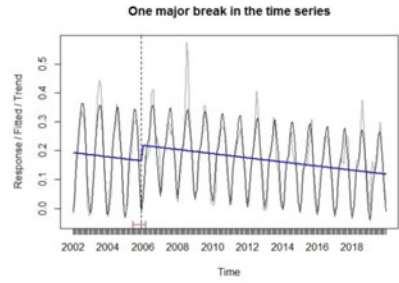
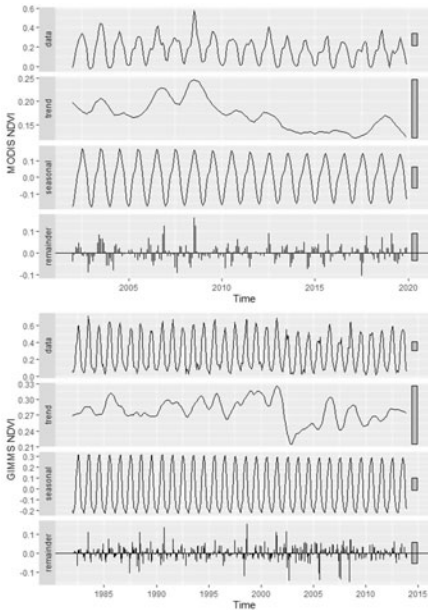


Fig. 9 (continued)

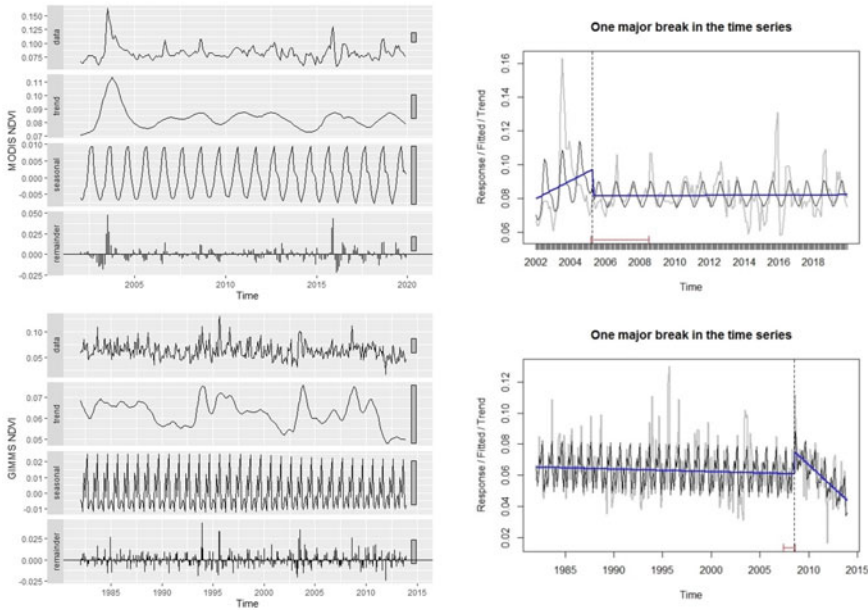


Fig. 9 (continued)

RF and Partial Least Square (PLS) models were used to predict NDVIs using temperature, precipitation, and potential evapotranspiration. The RF is a non-linear machine learning approach while the PLS is a classical linear regression model [107]. For the analysis, response and predictor variables were extracted from the full image ($n = 74,988$ pixels). The study results showed that vegetation production or NDVI is positively correlated with three climate variables (Table 5). The results of the previous studies [106] and our result indicated that NDVI is strongly correlated with precipitation compared to the temperature. Moreover, a number of researchers stated that precipitation is a major climate factor of vegetation production especially in semi-arid and arid regions [108, 109]. Therefore, we used precipitation to estimate predictor NDVI (Fig. 13).

This study used various statistical approaches and multi-sources RS products and imageries. From the data analysis, we generated two kinds of land degradation maps. The first map shows a strongly degraded area, evaluated from the MODIS and GIMMS NDVI time series for the period 1990–2019, using trend, BFAST, and RESTREND methods (Fig. 14). The second map illustrates a human-induced degraded area, generated from the Landsat OLI imagery, Google Earth map, and vector data. The vector data was obtained from the environmental geo-database of Mongolia (Fig. 15).

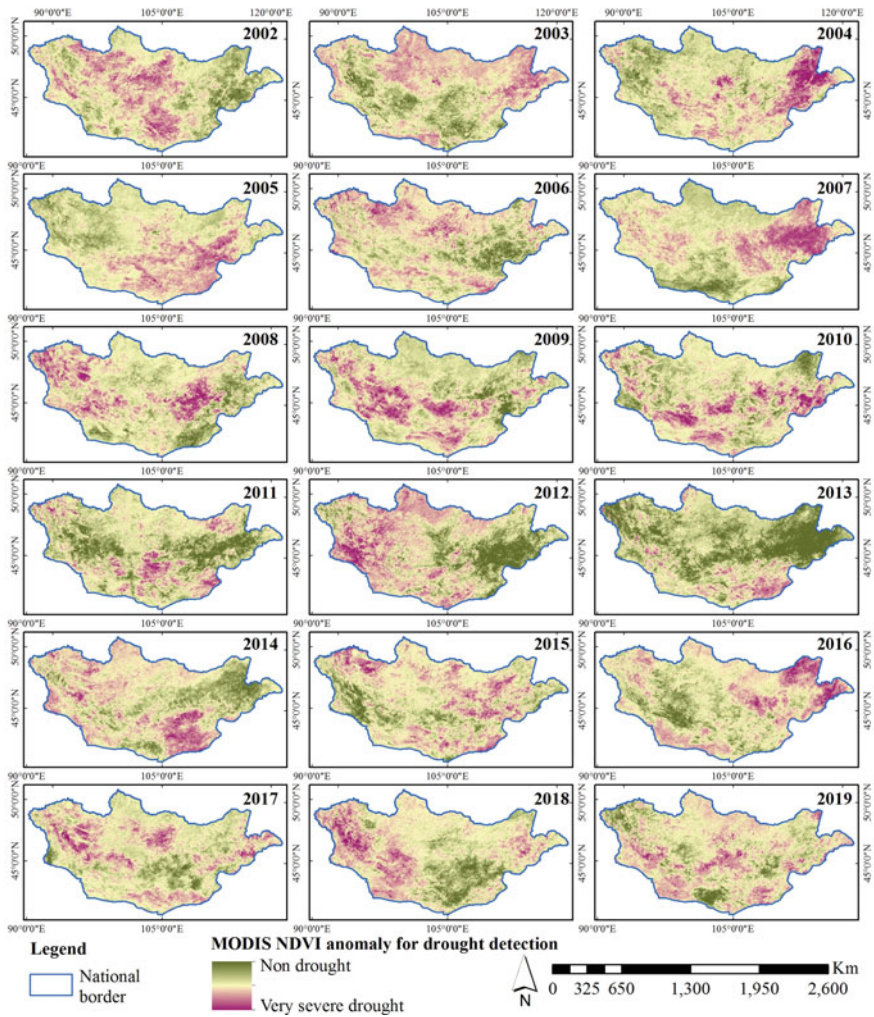


Fig. 10 Spatial distribution map of drought based on MODIS NDVI anomaly during the growing season (May–September) for period 2002–2019

5 Discussions

Since the 1990s, the assessment of Mongolia’s land degradation and desertification process has been done four times [110]. The first assessment of the state of land degradation and desertification have done between 1992 and 1996. At that time, researchers have used the Turkmen Institute of Desert study methodology, and the result showed that 44.7% of the total territory affected desertification. The second, third, and fourth

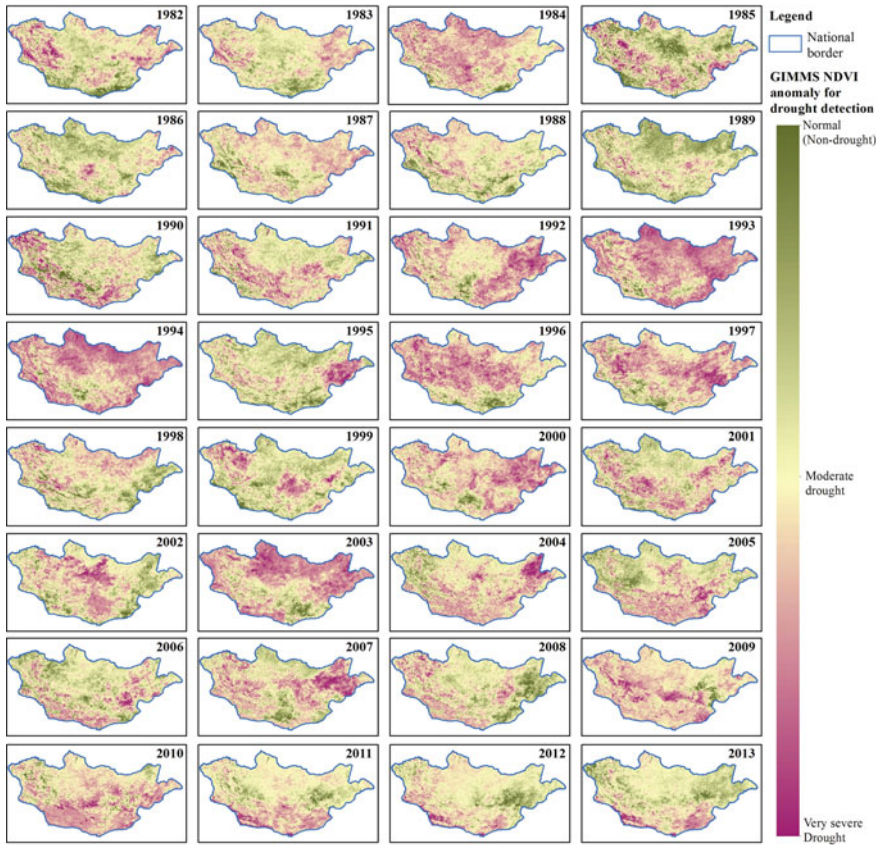


Fig. 11 Spatial distribution map of drought based on GIMMS NDVI anomaly during the growing season (May–September) for period 1982–2013

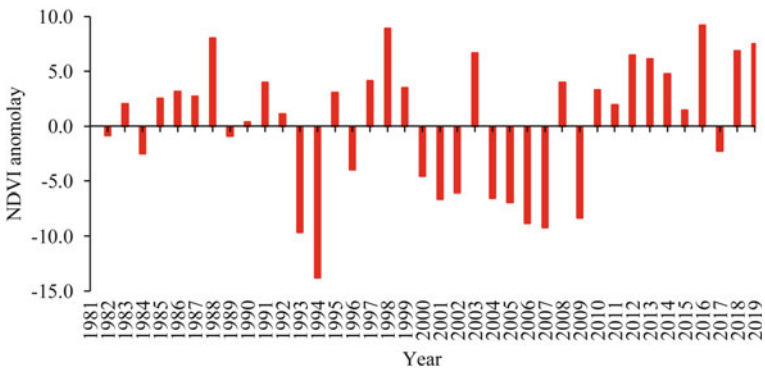


Fig. 12 The combined result of MODIS and GIMMS NDVI anomaly during the growing season (May–September) for period 1982–2019

Table 4 The seven models were created to study the relations between the independent variable and 3 dependent variables. N_{var} indicates the number of predictor variables in each group

	Acronym	Variables	N_{var}
Group 1	G1	Temperature (temp)	1
Group 2	G2	Precipitation (prec)	1
Group 3	G3	Potential evapotranspiration (PET)	1
Group 4	G4	Temperature and precipitation	2
Group 5	G5	Temperature and potential evapotranspiration	2
Group 6	G6	Precipitation and potential evapotranspiration	2
Group 7	G7	Temperature, precipitation, and evapotranspiration	3

Table 5 Modeling results obtained using RF and PLS regression

	n	RF model		PLS model		Formula (by PLS)
		R^2	RMSE	R^2	RMSE	
Group 1	74,988	0.435	0.105	0.201	0.136	$0.164 + 0.005*temp$
Group 2	74,988	0.970	0.015	0.667	0.088	$0.068 + 0.006*prec$
Group 3	74,988	0.413	0.109	0.121	0.142	$0.103 + 0.027*PET$
Group 4	74,988	0.451	0.097	0.243	0.132	$0.060 - 0.001*temp + 0.007*prec$
Group 5	74,988	0.905	0.019	0.677	0.086	$0.269 + 0.011*temp - 0.046*PET$
Group 6	74,988	0.962	0.012	0.695	0.084	$0.094 + 0.007*prec - 0.016*PET$
Group 7	74,988	0.959	0.013	0.710	0.082	$0.156 + 0.004*temp + 0.007*prec - 0.041*PET$

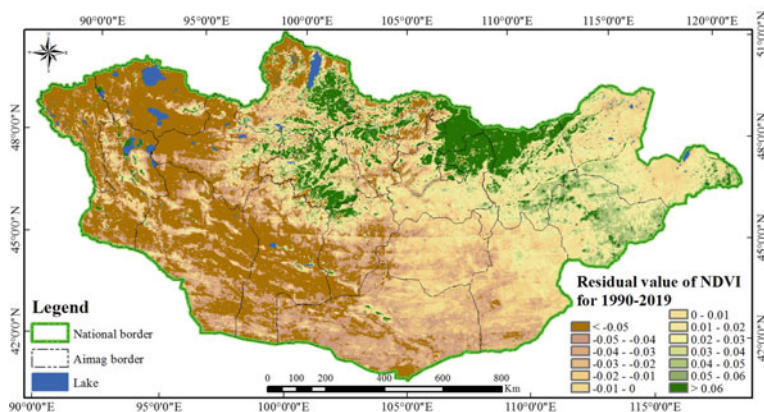


Fig. 13 Residual value or difference between measured and estimated NDVI for 1990–2019 using RF regression model with group 2

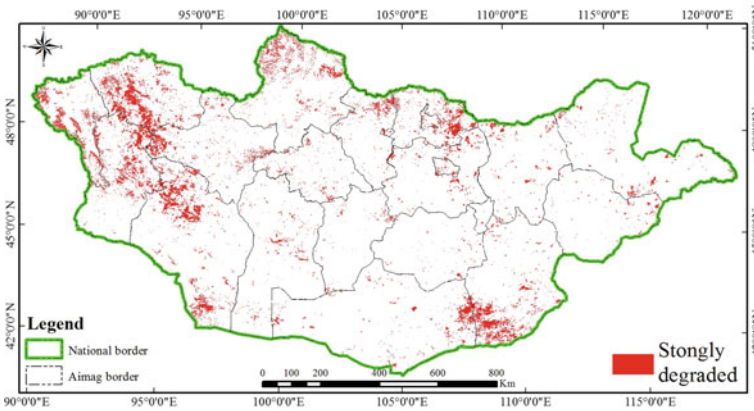


Fig. 14 Estimated strongly degraded area from MODIS and GIMMS NDVI time series for period 1990–2019 using trend, BFAST, and RESTREND analysis methods

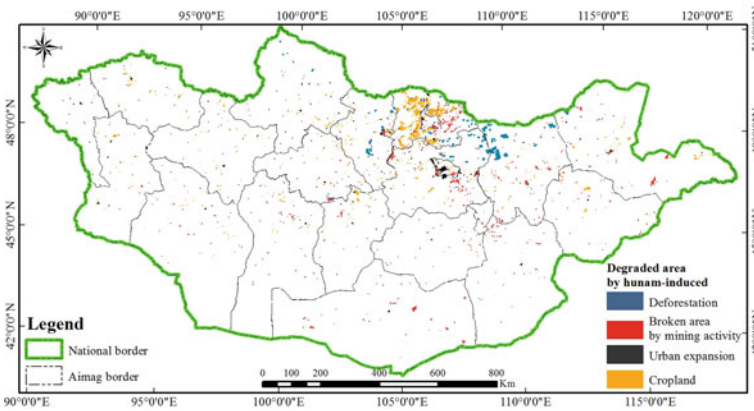


Fig. 15 Generated strongly degraded area by human activity from Landsat OLI imagery, Google earth map, and environmental geo-database of Mongolia

nation-wide assessment was done in 2000, 2006, and 2010 when using FAO methodology, MEDALLUS approach, and LADA methodology. These studies concluded that drylands are strongly susceptible to degradation. Moreover, several studies have been implemented over the past period relevant to environmental change and land degradation in Mongolia. For instance, Mandakh et al. [110] developed criteria for assessing Mongolia’s land degradation and desertification process. These researchers selected 5 criteria such as aridity (Mezentsev’s humidity coefficient), wind erosion (RUSLE model), water erosion (WEQ model), vegetation (Mann–Kendall trend analysis of MODIS NDVI time series), and livestock density. Their study results showed that 77.8% of the total territory of Mongolia affected degradation which of 6.7%

severely, and 9.9% extremely degraded. They concluded that the main factors of land degradation and desertification are drought/aridity, wind erosion, increased livestock density, and raised centralization. Hilker et al. [111] determined Mongolian land degradation by NDVI. Decline in NDVI to explain with air temperature, precipitation, and livestock density. The study showed that the Mongolian steppe has strongly degraded, and attributed to an increase in livestock. Eckert et al. [50] to assess land degradation in Mongolia used the NDVI time series. The result showed that the linear slope value for the trend NDVI time series is suitable for detecting Mongolia's land degradation process. However, these researchers mentioned their next study will focus on the BFAST algorithm. Our study used 3 different methods, including RF classification, linear regression, and BFAST algorithm. This study result showed that the BFAST algorithm was more effective compared to trend analysis.

6 Conclusions

Our research focused on detecting land degradation and environmental change using time series of environmental variables and machine learning techniques. For detecting land degradation and environmental change, we have investigated several factor impacts: (1) climate factor impact on land degradation and environmental change, (2) impact of land cover change on land degradation and environmental change, (3) impact of vegetation index on land degradation and environmental change, (4) impact of drought on land degradation and environmental change. As the data analysis techniques, the Random Forest (RF) classifier, Ordinary Least Square (OLS), and Partial Least Square (PLS) regressions, Break for Additive Season and Trend (BFAST) algorithm, Sen's slope and Restrend method were applied.

- The meteorological time series analysis showed that between 1990 and 2019, air temperature over Mongolian territory has increased by 1.8 °C, while annual total precipitation over Mongolia had decreased from 714 to 640 mm. The production of soil organic matter has impacted growing temperature and declining precipitation over Mongolia. Loss of soil organic matter is impacted extremely land bio-potential as a result of increasing erosion of wind and water.
- The land cover analysis indicated that between 1990 and 2019, forest, steppe, dry steppe, and cropland were decreased. In contrast, the meadow steppe, wetland, sand land, broken area, urban land, and water were increased. The land cover change affects different types of emissions as a greenhouse gas. Changed land is also directly affected the potential of carbon sequestration.
- To detect vegetation impact on land degradation and environmental change, we used multi-temporal MODIS 16-day composite and GIMMS 15-day composite NDVI time series for 2002–2019 and 1982–2013. The time series data were analyzed for the trends using the linear regression, Sen's slope, BFAST algorithm, and RESTREND analysis methods. The results indicated that positive trends were observed in Mongolia's central, northern, and northeastern parts. In contrast, the

negative trends were detected in all areas of the west, southern region, forested areas in the north and east, around the Ulaanbaatar city, and in the grassland area of eastern Mongolia. As could be seen from the analysis, the observed trends were not significant in the high density vegetated areas (e.g. north and northeast of the country). Moreover, the study revealed that negative and positive trends of the NDVI were strongly related to the land cover changes. Validation of NDVI trends could be done with the assistance of fine-resolution satellite imageries. As seen, the negative trends or changes occurred due to such influencing factors as forest fire, forest pests, deforestation, overgrazing, mining activities, and urban expansion. Generally, the trend analysis result showed that negative and positive trends of time series NDVI were strongly related to land cover change.

- The drought detection analysis showed that the years 1993, 1994, 1997, 2000–2002, 2004–2007, 2009, and 2017 could very well detect the droughts during the growing season for the period 1990–2019. Drought is a short-term process however, the frequency of drought has extremely influenced by land degradation.

7 Recommendations

In order to obtain more reliable information on the process of land degradation in Mongolia linking remote sensing data, field-measured data and advanced statistical methods. Environmental change and land degradation coverage all the natural processes and affect each ecosystem service, therefore, we recommended following an ecosystem-focused approach.

Acknowledgements The authors would like to thank many organizations that provided data for this study especially, Institute of Geography and Geoecology, Mongolian Academy of Sciences (IGG MAS), National University of Mongolia (NUM), and the Information and Research Institute of Meteorology, Hydrology, and Environment (IRIMHE). The authors also appreciate the provider's time series of satellite and meteorological data to allow us to download and use these datasets. We thank the editors for their valuable comments and suggestions on the chapter who is Dr. Ayad M. Fadhil Al-Quraishi, Dr. Abdelazim M Negrn and Dr. Yaseen T. Mustafa.

References

1. United Nations Conventions on Combat Desertification [UNCCD] secretariat (2013) Mid-term evaluation of the 10-year strategic plan and framework to enhance the implementation of the Convention (2008–2018), Report by the inter sessional working group, conference of the parties, eleventh session, Windhoek, Namibia
2. United Nations Environmental Program [UNEP] (1992) The status of desertification and implementation of the United Nations plan of action to combat desertification, Nairobi
3. United Nations Conference on Environment and Development [UNCED] (1992) Managing fragile ecosystems, combating desertification and drought, chapter 12 of agenda, 21. Rio de Janeiro, Brazil

4. Eswaran H, Lal R, Reich PF (2001) Land degradation: an overview, responses to land degradation. In: Bridges EM, Hannam ID, Oldeman LR, Pening de Vries FWT, Scherr SJ, Sompatpanit S (eds) Proceeding 2nd the international conference on land degradation and desertification, Khon Kaen, Thailand. Oxford Press, New Delhi, India
5. Middleton N, Thomas D (1997) World atlas of desertification, edn 2. Arnold, Hodder Headline, PLC
6. Lal R, Stewart BA (1994) Research priorities for soil processes and water quality in 21st century. In: Lal R, Stewart BA (eds) Soil processes and water quality
7. Oldeman LR (1992) Global extent of soil degradation. In Bi-Annual Report 1991–1992/ISRIC 19 p
8. Dregne HE (1992) Degradation and restoration of arid lands
9. McMahan M (2020) Accessed on 10 Oct 2020. Available online: <https://www.wisegeek.com/what-is-environmental-degradation.htm>
10. Mahendra Kumar T (2015) Morphological characterization, quality, yield and DNA fingerprinting of bio-field energy treated alphonso mango (*Mangifera indica* L.). J Food Nutr Sci 3(6):245. <https://doi.org/10.11648/j.jfns.20150306.18>
11. Johnson DL, Ambrose SH, Bassett TJ, Bowen ML, Crumme DE, Isaacson JS, Johnson DN, Lamb P, Saul M, Winter-Nelson AE (1997) Meanings of environmental terms. J Environ Qual 26:581. <https://doi.org/10.2134/jeq1997.00472425002600030002x>
12. International Strategy for Disaster Reduction [ISDR] (2010) Disaster risk reduction: an instrument for achieving the millennium development goals: Advocacy kit for parliamentarians
13. United Nations Conventions on Combat Desertification [UNCCD] (2004) In final report on the workshop on forest and forest ecosystems: promoting synergy in the three Rio conventions, 5 p
14. Millennium Ecosystem Assessment [MEA] (2005) Ecosystems and human well-being: synthesis. Island Press, Washington, DC, USA. <http://www.bioquest.org/wp-content/blogs.dir/files/2009/06/ecosystems-and-health.pdf>
15. United Nations Environmental Program [UNEP]-Fi M, Asset Management Working Group (2007) Demystifying responsible investment performance. A review of key academic and border research on ESG factors
16. Zorn M, Komac B (2013) Land degradation. Encyclopedia of natural hazards. In: Bobrowsky PT (ed) Encyclopedia of earth sciences series. Springer, Dordrecht
17. United Nations Convention to Combat Desertification [UNCCD] (2015) Impulse report-climate change and desertification: anticipating, assessing and adapting to future change in drylands. United Nations Convention to Combat Desertification, Rome, Italy
18. Stocking M, Murnaghan N (2001) Handbook for the field assessment of land degradation. Earthscan
19. Metternicht G, Zinck JA, Blanco PD, Del Valle HF (2010) Remote sensing of land degradation: experiences from Latin America and the Caribbean. J Environ Qual 39(1):42. <https://doi.org/10.2134/jeq2009.0127>
20. Liniger H, Schwilch G, Mekdaschi R, Providoli I, Bunning S, Biancalani R, Van Lynden G (2013) Tools for better SLM knowledge management and informed decision-making in addressing land degradation at different scales: the WOCAT–LADA–DESIRE methodology
21. Koochafkan P, Lantieri D, Nachtergaele F (2003) Land Degradation Assessment in Drylands (LADA): guidelines for a methodological approach. Land and water development division, FAO, Rome
22. Burrell AL, Evans JP, Liu Y (2018) The impact of dataset selection on land degradation assessment. ISPRS J Photogrammetry Remote Sens 146:22. <https://doi.org/10.1016/j.isprsjprs.2018.08.017>
23. Higginbottom TP, Symeonaki E (2014) Assessing land degradation and desertification using vegetation index data: current frameworks and future directions. Remote Sens 6(10):9552. <https://doi.org/10.3390/rs6109552>
24. Healy MA, Forrest K, Bastin G (2016) The role of a knowledge broker in improving knowledge and understanding of climate change in the Australian rangelands. Rangeland J 37(6):541. <https://www.publish.csiro.au/RJ/RJ15060>

25. Ludwig JA, Tongway DJ, Bastin GN, James CD (2004) Monitoring ecological indicators of rangeland functional integrity and their relation to biodiversity at local to regional scales. *Austral Ecol* 29(1):108. <https://doi.org/10.1111/j.1442-9993.2004.01349.x>
26. Otgonbayar M, Atzberger C, Mattiuzzi M, Erdenedalai A (2019) Estimation of climatologies of average monthly air temperature over Mongolia using MODIS land surface temperature (LST) time series and machine learning techniques. *Remote Sens* 11(21):2588. <https://doi.org/10.3390/rs11212588>
27. Rishmawi K, Prince SD (2016) Environmental and anthropogenic degradation of vegetation in the Sahel from 1982 to 2006. *Remote Sens* 8(11):948. <https://doi.org/10.3390/rs8110948>
28. Atkinson PM, Jeganathan C, Dash J, Atzberger C (2012) Inter-comparison of four models for smoothing satellite sensor time-series data to estimate vegetation phenology. *Remote Sens Environ* 123:400. <https://doi.org/10.1016/j.rse.2012.04.001>
29. Atzberger C (2014) Special issue on geodata processing at the institute of surveying, remote sensing and land information at BOKU in Vienna. PFG Photogrammetry, Fernerkundung, Geoinformation, 309 p. <https://doi.org/10.1127/1432-8364/2014/0225>
30. Eerens H, Haesen D, Rembold F, Urbano F, Tote C, Bydekerke L (2014) Image time series processing for agriculture monitoring. *Environ Model Softw* 53:154. <https://doi.org/10.1016/j.envsoft.2013.10.021>
31. Atzberger C, Eilers PH (2011) A time series for monitoring vegetation activity and phenology at 10-daily time steps covering large parts of South America. *Int J Digital Earth* 4(5):365. <https://doi.org/10.1080/17538947.2010.505664>
32. Yengoh GT, Dent D, Olsson L, Tengberg AE, Tucker CJ (2015) Use of the Normalized Difference Vegetation Index (NDVI) to assess land degradation at multiple scales: current status, future trends, and practical considerations
33. Jonsson P, Eklundh L (2002) Seasonality extraction by function fitting to time-series of satellite sensor data. *IEEE Trans Geosci Remote Sens* 40(8):1824. <https://doi.org/10.1109/TGRS.2002.802519>
34. McKellip RD, Ross KW, Spruce JP, Smoot JC, Ryan RE, Gasser GE, Vaughan RD (2010) Phenological parameters estimation tool
35. Verbesselt J, Hyndman R, Newnham G, Culvenor D (2010) Detecting trend and seasonal changes in satellite image time series. *Remote Sens Environ* 114(1):106. <https://doi.org/10.1016/j.rse.2009.08.014>
36. Brown ME, De Beurs K, Vrieling A (2010) The response of African land surface phenology to large scale climate oscillations. *Remote Sens Environ* 114(10):2286. <https://doi.org/10.1016/j.rse.2010.05.005>
37. Udelhoven T (2010) TimeStats: a software tool for the retrieval of temporal patterns from global satellite archives. *IEEE J Select Top Appl Earth Obs Remote Sens* 4(2):310. <https://doi.org/10.1109/JSTARS.2010.2051942>, <https://ieeexplore.ieee.org/document/5512552>
38. Rodrigues A, Marcal AR, Cunha M (2011) PhenoSat A tool for vegetation temporal analysis from satellite image data. In: 2011 6th international workshop on the analysis of multi-temporal remote sensing images (multi-temp). *IEEE*, 45 p. <https://doi.org/10.1109/Multi-Temp.2011.6005044>, <https://ieeexplore.ieee.org/abstract/document/6005044>
39. Rembold F, Meroni M, Urbano F, Royer A, Atzberger C, Lemoine G, Haesen D (2015) Remote sensing time series analysis for crop monitoring with the SPIRITS software: new functionalities and use examples. *Front Environ Sci* 3(46). <https://doi.org/10.3389/fenvs.2015.00046>
40. Belda S, Pipia L, Morcillo-Pallarés P, Rivera-Caicedo JP, Amin E, De Grave C, Verrelst J (2020) DATimeS: a machine learning time series GUI toolbox for gap-filling and vegetation phenology trends detection. *Environ Model Softw* 104666 p. <https://doi.org/10.1016/j.envsoft.2020.104666>
41. Bai ZG, Dent DL, Olsson L, Schaepman ME (2008) Proxy global assessment of land degradation. *Soil Use Manag* 24(3):223. <https://doi.org/10.1111/j.1475-2743.2008.00169.x>
42. Evans J, Geerken R (2004) Discrimination between climate and human-induced dryland degradation. *J Arid Environ* 57(4):535. [https://doi.org/10.1016/S0140-1963\(03\)00121-6](https://doi.org/10.1016/S0140-1963(03)00121-6)

43. Wessels KJ, Prince SD, Malherbe J, Small J, Frost PE, VanZyl D (2007) Can human-induced land degradation be distinguished from the effects of rainfall variability? A case study in South Africa. *J Arid Environ* 68(2):271. <https://doi.org/10.1016/j.jaridenv.2006.05.015>
44. National statistics office of Mongolia [NSOM] (2019) Number of population and livestock, Mongolian statistical information service. Accessed 29 Sept 2020. <http://www.1212.mn>
45. Mattiuzzi M, Verbesselt J, Hengel T, Klisch A, Stevens F, Mosher S, Evans B, Lobo A, Hufkens K, Detsch F (2019) MODIS: MODIS acquisition and processing package. R package version 1.1.5. Accessed on 29 Sept 2019. Available online: <https://cran.r-project.org/web/packages/MODIS/MODIS.pdf>
46. Tucker CJ, Pinzon JE, Brown ME, Slayback DA, Pak EW, Mahoney R, El Saleous N (2005) An extended AVHRR 8-km NDVI dataset compatible with MODIS and SPOT vegetation NDVI data. *Int J Remote Sens* 26(20):4485. <https://doi.org/10.1080/01431160500168686>
47. Detsch F (2016) Package ‘GIMMS’. Accessed on 25 Nov 2020, Available online: <https://cran.r-project.org/web/packages/gimms/gimms.pdf>
48. Harris I, Osborn TJ, Jones P, Lister D (2020) Version 4 of the CRU TS monthly high-resolution gridded multivariate climate dataset. *Sci Data* 7(1):1. <https://doi.org/10.6084/m9.figshare.11980500>
49. Fick SE, Hijmans RJ (2017) WorldClim 2: new 1-km spatial resolution climate surfaces for global land areas. *Int J Climatol* 37(12):4302. <https://doi.org/10.1002/joc.5086>
50. Eckert S, Hüsler F, Liniger H, Hodel E (2015) Trend analysis of MODIS NDVI time series for detecting land degradation and regeneration in Mongolia. *J Arid Environ* 113:16. <https://doi.org/10.1016/j.jaridenv.2014.09.001>
51. Gong P, Wang J, Yu L, Zhao Y, Zhao Y, Liang L, Li C (2013) Finer resolution observation and monitoring of global land cover: first mapping results with Landsat TM and ETM+ data. *Int J Remote Sens* 34(7):2607. <https://doi.org/10.1080/01431161.2012.748992>
52. Liu H, Gong P, Wang J, Clinton N, Bai Y, Liang S (2020) Annual dynamics of global land cover and its long-term changes from 1982 to 2015. *Earth Syst Sci Data* 12(2):1217. <https://doi.org/10.5194/essd-12-1217-2020>
53. Amarsaikhan D (2020) Advanced classification of optical and SAR images for urban land cover mapping. In: Invited paper published in international archives of the photogrammetry, RS and spatial information sciences, XXIV ISPRS congress, Nice, France, 1417 p. <https://doi.org/10.5194/isprs-archives-XLIII-B3-2020-1417-2020>
54. Mas JF, Flores JJ (2008) The application of artificial neural networks to the analysis of remotely sensed data. *Int J Remote Sens* 29(3):617. <https://doi.org/10.1080/01431160701352154>
55. Breiman L, Friedman J, Stone CJ, Olshen RA (1984) Classification and regression trees. CRC Press
56. Damdinsuren A, Douglas T (2004) Data fusion and multisource data classification. *Int J Remote Sens* 17(25):3529. <https://doi.org/10.1080/0143116031000115111>
57. Mountrakis G, Im J, Ogole C (2011) Support vector machines in remote sensing: a review. *ISPRS J Photogramm Remote Sens* 66(3):247. <https://doi.org/10.1016/j.isprsjprs.2010.11.001>
58. Breiman L (1996) Bagging predictors. *Mach Learn* 24(2):123. <https://doi.org/10.1007/BF00058655.pdf>
59. Rogan JM, Grayson DJ (2003) Towards a theory of curriculum implementation with particular reference to science education in developing countries. *Int J Sci Educ* 25(10):1171. <https://doi.org/10.1080/09500690210145819>
60. Atzberger C, Klisch A, Mattiuzzi M, Vuolo F (2014) Phenological metrics derived over the European continent from NDVI3g data and MODIS time series. *Remote Sens* 6(1):257. <https://doi.org/10.3390/rs6010257>
61. Rodriguez-Galiano VF, Ghimire B, Rogan J, Chica-Olmo M, Rigol-Sanchez JP (2012) An assessment of the effectiveness of a random forest classifier for land-cover classification. *ISPRS J Photogrammetry Remote Sens* 67:93. <https://doi.org/10.1016/j.isprsjprs.2011.11.002>

62. Nyamjargal E, Amarsaikhan D, Munkh-Erdene A, Battsengel V, Bolorchuluun C (2020) Object-based classification of mixed forest types in Mongolia. *Geocarto Int* 35(14):1615. <https://doi.org/10.5564/pmas.v60i4.1504>
63. Weatherhead EC, Reinsel GC, Tiao GC, Meng XL, Choi D, Cheang WK, Miller AJ (1998). Factors affecting the detection of trends: Statistical considerations and applications to environmental data. *J Geophys Res Atmosp* 103(D14):17149–17161. <https://doi.org/10.1029/98JD00995>
64. Kendall MG (1938) A new measure of rank correlation. *Biometrika* 30(1/2):81p. <https://doi.org/10.2307/2332226>
65. Sen PK (1968) Estimates of the regression coefficient based on Kendall's tau. *J Am Stat Assoc* 63(324):1379
66. Meng X, Gao X, Li S, Lei J (2020) Spatial and temporal characteristics of vegetation NDVI changes and the driving forces in Mongolia during 1982–2015. *Remote Sens* 12(4):603. <https://doi.org/10.3390/rs12040603>
67. R Core Team: a language and environment for statistical computing. Available online: <https://www.r-project.org/>. Accessed on 31 Oct 2021
68. Erian WF (2005) Arab network of the remote sensing centers for desertification monitoring and assessment. Remote sensing and geo-information processing in the assessment and monitoring of land degradation and desertification, Trier, Germany, 452–459
69. Haywood J, Randall J (2008) Trending seasonal data with multiple structural breaks. *NZ visitor arrivals and the minimal effects of 9*
70. Xu Z, Shen X, Cao L, Coops NC, Goodbody TR, Zhong T, Wu X (2020) Tree species classification using UAS-based digital aerial photogrammetry point clouds and multispectral imageries in subtropical natural forests. *Int J Appl Earth Obs Geoinform* 92:102173. <https://doi.org/10.1016/j.jag.2020.102173>
71. Zeileis A (2005) A unified approach to structural change tests based on ML scores, F statistics, and OLS residuals. *Economet Rev* 24(4):445. <https://doi.org/10.1080/07474930500406053>
72. Nanzad L, Zhang J, Tuvdendorj B, Nabil M, Zhang S, Bai Y (2019) NDVI anomaly for drought monitoring and its correlation with climate factors over Mongolia from 2000 to 2016. *J Arid Environ* 164:69. <https://doi.org/10.1016/j.jaridenv.2019.01.019>
73. Klisch A, Atzberger C (2016) Operational drought monitoring in Kenya using MODIS NDVI time series. *Remote Sens* 8(4):267. <https://doi.org/10.3390/rs8040267>
74. Palmer WC (1965) Meteorological drought, vol 30. US Department of Commerce, Weather Bureau
75. McKee TB (1995) Drought monitoring with multiple time scales. In: Proceedings of 9th conference on applied climatology, Boston
76. McKee TB, Doesken NJ, Kleist (1993) The relationship of drought frequency and duration to time scales. *Proc 8th Conf Appl Climatol* 17(22):179. <https://climate.colostate.edu/pdfs/relationshippofdroughtfrequency.pdf>
77. Vicente-Serrano SM, Beguería S, López-Moreno JI (2010) A multiscalar drought index sensitive to global warming: the standardized precipitation evapotranspiration index. *J Clim* 23(7):1696. <https://doi.org/10.1175/2009JCLI2909.1>
78. Enekel M, Steiner C, Mistelbauer T, Dorigo W, Wagner W, See L, Rogenhofer E (2016) A combined satellite-derived drought indicator to support humanitarian aid organizations. *Remote Sens* 8(4):340. <https://doi.org/10.3390/rs8040340>
79. Hao Z, AghaKouchak A (2013) Multivariate standardized drought index: a parametric multi-index model. *Adv Water Resour* 57:12. <https://doi.org/10.1016/j.advwatres.2013.03.009>
80. Kogan FN (1990) Remote sensing of weather impacts on vegetation in non-homogeneous areas. *Int J Remote Sens* 11(8):1405. <https://doi.org/10.1080/01431169008955102>
81. Liu WT, Kogan FN (1996) Monitoring regional drought using the vegetation condition index. *Int J Remote Sens* 17(14):2761. <https://doi.org/10.1080/01431169608949106>
82. Adede C, Oboko R, Wagacha PW, Atzberger C (2019) Model ensembles of artificial neural networks and support vector regression for improved accuracy in the prediction of vegetation conditions and droughts in four Northern Kenya counties. *ISPRS Int J Geo Inf* 8(12):562. <https://doi.org/10.3390/ijgi8120562>

83. Anyamba A, Tucker CJ (2012) Historical perspective of AVHRR NDVI and vegetation drought monitoring. *Remote Sens Drought: Innovative Monit Approaches* 23(20). <https://digitalcommons.unl.edu/cgi/viewcontent.cgi?article=1217&context=napasub>
84. Anyamba A, Tucker CJ, Eastman JR (2001) NDVI anomaly patterns over Africa during the 1997/98 ENSO warm event. *Int J Remote Sens* 22(10):1847
85. Ibrahim YZ, Balzter H, Kaduk J, Tucker CJ (2015) Land degradation assessment using residual trend analysis of GIMMS NDVI3g, soil moisture and rainfall in Sub-Saharan West Africa from 1982 to 2012. *Remote Sens* 7(5):5471. <https://doi.org/10.3390/rs70505471>
86. Wessels KJ, Van Den Bergh F, Scholes RJ (2012) Limits to detectability of land degradation by trend analysis of vegetation index data. *Remote Sens Environ* 125:10. <https://doi.org/10.1016/j.rse.2012.06.022>
87. Huber S, Fensholt R, Rasmussen K (2011) Water availability as the driver of vegetation dynamics in the African Sahel from 1982 to 2007. *Glob Planet Change* 76(3–4):186. <https://doi.org/10.1016/j.gloplacha.2011.01.006>
88. Giannini A, Saravanan R, Chang P (2003) Oceanic forcing of Sahel rainfall on inter-annual to inter-decadal time scales. *Science* 302(5647):1027. <https://doi.org/10.1126/science.1089357>
89. Wallace KJ (2007) Classification of ecosystem services: problems and solutions. *Biol Cons* 139(3–4):235. <https://doi.org/10.1016/j.biocon.2007.07.015>
90. Reyers B, O'Farrell PJ, Cowlin RM, Egoh BN, Le Maitre DC, Vlok JH (2009) Ecosystem services, land-cover change, and stakeholders: finding a sustainable foothold for a semiarid biodiversity hotspot. *Ecol Soc* 14(1). <https://www.jstor.org/stable/26268036>
91. Gibbard S, Caldeira K, Bala G, Phillips TJ, Wickett M (2005) Climate effects of global land cover change. *Geophys Res Lett* 32(23). <https://doi.org/10.1029/2005GL024550>
92. DeFries RS, Field CB, Fung I, Collatz GJ, Bounoua L (1999) Combining satellite data and biogeochemical models to estimate global effects of human-induced land cover change on carbon emissions and primary productivity. *Global Biogeochem Cycles* 13(3):803. <https://doi.org/10.1029/1999GB900037>
93. Wang J, Wei H, Yao J, Shao Y, Liang X, Chonokhuu S, Davaasuren D (2020). Analysis of spatiotemporal patterns and driving forces for land degradation and restoration in Mongolia from 1990 to 2015. In: EGU general assembly conference abstracts, May 2020, 2363 p. <https://ui.adsabs.harvard.edu/abs/2020EGUGA..22.2363W/abstract>
94. Lamchin M, Lee JY, Lee WK, Lee EJ, Kim M, Lim CH, Kim SR (2016) Assessment of land cover change and desertification using remote sensing technology in a local region of Mongolia. *Adv Space Res* 57(1):64. <https://doi.org/10.1016/j.asr.2015.10.006>
95. Dugarsuren N, Lin C, Tsogt K (2011) Land cover change detection in Mongolia in last decade using MODIS imagery. In: *Proceeding of ACRS2011*. Taipei, Taiwan, 688 p. <https://dl.wqxts1xzle7.cloudfront.net/>
96. Pal M (2005) Random forest classifier for remote sensing classification. *Int J Remote Sens* 26(1):217. <https://doi.org/10.1080/01431160412331269698>
97. Chao YS, Wu CJ, Wu HC, Chen WC (2018) Trend analysis for national surveys: application to all variables from the Canadian health measures survey cycle 1 to 4. *PLoS one*, 13(8):e0200127. <https://doi.org/10.1371/journal.pone.0200127>
98. Ali Z, Hussain I, Faisal M, Nazir HM, Hussain T, Shad MY, Hussain Gani S (2017) Forecasting drought using multilayer perceptron artificial neural network model. *Adv Meteorol*. <https://doi.org/10.1155/2017/5681308>
99. Morid S, Smakhtin V, Bagherzadeh K (2007) Drought forecasting using artificial neural networks and time series of drought indices. *Int J Climatol J Roy Meteorol Soc* 27(15):2103. <https://doi.org/10.1002/joc.1498>
100. United Nations Office for Outer Space Affairs [UNOOSA]. Accessed 29 Sept 2020
101. Chang S, Wu B, Yan N, Davdai B, Nasanbat E (2017) Suitability assessment of satellite-derived drought indices for Mongolian grassland. *Remote Sens* 9(7):650. <https://doi.org/10.3390/rs9070650>
102. Dorjsuren M, Liou YA, Cheng CH (2016) Time series MODIS and in situ data analysis for Mongolia drought. *Remote Sens* 8(6):509. <https://doi.org/10.3390/rs8060509>

103. Erdenetuya M, Bulgan D, Erdenetsetseg B (2011) Drought monitoring and assessment using multi-satellite data in Mongolia. In: Processing 32nd asian conference remote sensing. <http://toc.proceedings.com/14023webtoc.pdf>
104. Bayarjargal Y, Karnieli A, Bayasgalan M, Khudulmur S, Gandush C, Tucker CJ (2006) A comparative study of NOAA-AVHRR derived drought indices using change vector analysis. *Remote Sens Environ* 105(1):9. <https://doi.org/10.1016/j.rse.2006.06.003>
105. Wang XM, Zhang CX, Hasi E, Dong ZB (2010) Has the Three Norths Forest Shelterbelt Program solved the desertification and dust storm problems in arid and semiarid China? *J Arid Environ* 74(1):13. <https://doi.org/10.1016/j.jaridenv.2009.08.001>
106. Huang S, Kong J (2016) Assessing land degradation dynamics and distinguishing human-induced changes from climate factors in the Three-North Shelter forest region of China. *ISPRS Int J Geo Inf* 5(9):158. <https://doi.org/10.3390/ijgi5090158>
107. Otgonbayar M, Atzberger C, Chambers J, Damdinsuren A (2019) Mapping pasture biomass in Mongolia using partial least squares, random forest regression and Landsat 8 imagery. *Int J Remote Sens* 40(8):3204. <https://doi.org/10.1080/01431161.2018.1541110>
108. Rosenzweig ML (1968) Net primary productivity of terrestrial communities: prediction from climatological data. *Am Nat* 102(923):67. <https://doi.org/10.1086/282523>
109. Lehouérou HN, Bingham RL, Skerbek W (1988) Relationship between the variability of primary production and the variability of annual precipitation in world arid lands. *J Arid Environ* 15(1):1. [https://doi.org/10.1016/S0140-1963\(18\)31001-2](https://doi.org/10.1016/S0140-1963(18)31001-2)
110. Nyamtseren M (2014) The land degradation and desertification process in Mongolia. Mongolia second assessment report on climate change, Chapter: Climate change impact, Publisher: The Ministry of Environment and Green Development, 1
111. Hilker T, Natsagdorj E, Waring RH, Lyapustin A, Wang Y (2014) Satellite observed widespread decline in Mongolian grasslands largely due to overgrazing. *Glob Change Biol* 20(2):418–428. <https://doi.org/10.1111/gcb.12365>

Assessment of Land Degradation Vulnerability Using GIS-Based Multicriteria Decision Analysis in Zakho District, Kurdistan Region of Iraq



Hazhir Karimi, Yaseen T. Mustafa, Hooshyar Hossini,
and Ayad M. Fadhil Al-Quraishi 

Abstract The combination of GIS and multicriteria decision analysis approach was applied for assessment of land degradation vulnerability in Zakho District in Kurdistan Region of Iraq. First, a literature review was conducted to select effective parameters related to land degradation vulnerability. Three main groups of parameters, including physical, chemical, and socio-economic, were defined as effective criteria. The selected parameters were land use/land cover, slope, soil erosion rate, soil salinity, soil sodicity, soil organic carbon, soil acidity, and population density. The data were acquired from several sources, and the maps of the parameters were created in ArcGIS 10.3 version. The maps were standardized and adjusted in similar units and then aggregated using a weighted overlay method to show the spatial pattern of land degradation risk in the study area. The result indicated that only 7% be susceptible in the study area, while 50 and 43% were categorized as low and moderate levels, respectively. The land degradation risk is mainly due to natural factors such as slope and soil erosion. The result of this research could be useful for national organizations and agencies for sustainable land use planning and land management.

H. Karimi (✉)

Department of Biological Sciences, University of Alabama, Tuscaloosa, AL 35401, USA
e-mail: hkarimi@crimson.ua.edu; hazhir.karimi25@gmail.com

Y. T. Mustafa

Department of Environmental Science, Faculty of Science, University of Zakho, Zakho, Kurdistan Region, Iraq
e-mail: yaseen.mustafa@uoz.edu.krd

Computer Science Department, College of Sciences, Nawroz University, Duhok, Kurdistan Region, Iraq

H. Hossini

Department of Environmental Health Engineering, Faculty of Health, Kermanshah University of Medical Sciences, Kermanshah, Iran

A. M. F. Al-Quraishi

Petroleum and Mining Engineering Department, Faculty of Engineering, Tishk International University, Erbil 44001, Kurdistan Region, Iraq
e-mail: ayad.alquraishi@tiu.edu.iq; ayad.alquraishi@gmail.com

© The Author(s), under exclusive license to Springer Nature Switzerland AG 2022

49

A. M. F. Al-Quraishi et al. (eds.), *Environmental Degradation in Asia*,
Earth and Environmental Sciences Library,
https://doi.org/10.1007/978-3-031-12112-8_3

Keywords Land degradation · Soil erosion · GIS · Multicriteria decision analysis · Zakho

1 Introduction

Land degradation is a worldwide environmental issue, happening in a short to long trend with an alarming rate that might worsen without proper emergent measures [1]. Land degradation influences human beings through food insecurity, decreased land fertility, climate change, and the threat to ecosystem services [2]. It also poses significant threats to the biodiversity and ecological health of grasslands, shrubs, and savannas [3]. Globally, nearly one-quarter of the total land area has been degraded, affecting about 3.2 billion inhabitants, especially in rural societies and poor countries [2]. As a result, land degradation seriously affects the ecosystem, economy, society, and human health [4].

Both natural hazards and anthropogenic factors contribute to land degradation. Natural hazards or phenomena are the conditions of the physical environment that cause a high degradation occurrence [1, 5]. Erosion and land degradation occur quickly in arid areas when exposed to seasonal or temporary storms [3]. Also, areas with steep slopes are subject to severe erosion, mainly when cultivated in the slope direction. Lack of vegetation can provide a good condition for land degradation since vegetation act as a physical barrier to erosion forces [6].

Furthermore, anthropogenic activities and land-use changes cause substantial soil erosion and land degradation [7]. Traditional agriculture, especially in low crop yields, cause consuming nutrients and soil organic matter that might increase land degradation [4]. Excessive pesticides represented soil degradation because microbial communities are responsible for soil fertility and nutrient element cycles [8]. Overgrazing directly decreases the quantity and quality of the vegetation cover, leading to an increase in soil erosion [9, 10]. Additionally, there is a strong relationship between land degradation and socio-economic and cultural situation [11, 12]. Direct dependence on the livelihood of rural communities on natural resources has caused degradation [9]. Some studies also highlighted that wars and armed conflicts directly turn in lands through physical damage and its significant effect on land uses and land degradation [13].

The evaluation of land degradation state depend on various characteristics such as soil features, climate condition, land use types, physiography, and socioeconomic properties [14]. The remote sensing (RS) and geographic information systems (GIS) are very helpful techniques to understand the state of land degradation and monitor its trends [15]. RS and GIS techniques have widely been used for different environmental studies such as land use/cover change detection [16–20] and land degradation and drought monitoring [e.g., 14, 21–26]. However, in the analysis of land degradation various effective parameters should be considered. Multicriteria decision analysis (MCDA) is a common approach used to facilitate the consideration of multiple criteria by decision-makers to make the best possible decision [27]. MCDA

has effectively been integrated with GIS and applied in various environmental studies [14, 28–35] but a few studies used GIS-MCDA to evaluate land degradation risks.

This study aims to evaluate land degradation vulnerability and identify vulnerable zones in the Zakho district in the Kurdistan Region of Iraq using GIS, RS, and multicriteria decision analysis approach. Various physical and socio-economic criteria were used to assess vulnerability of land degradation in the study area. The case study, methods, results, discussion, and conclusion are explained in detail in the following sections.

2 Material and Methods

2.1 Case Study

The case study is Zakho district located in Duhok province in the Kurdistan Region of Iraq. Zakho is located in the north of Iraq and is suited approximately between latitudes $36^{\circ} 18' 12.64''$ – $37^{\circ} 20' 33.55''$ N, and longitudes $42^{\circ} 20' 25.36''$ – $44^{\circ} 17' 40.50''$ E. Its elevation ranges between 430 and 2500 m above the sea level. This district covers an area of 1452 km². Turkey surrounds it from the north, Syria from the west, Semel and Duhok districts from the south, and Amedi district from the east (Fig. 1). The climate of this region is hot and dry summers and mild winters [36]. The annual averages rainfall has been recorded at 600 mm and the winter months have the highest precipitation. The annual temperature varies from 3 to 42 °C.

Land degradation vulnerability in the study area was assessed using the multicriteria decision analysis (MCDA) approach combined with GIS and remote sensing techniques. The MCDA involves various steps: aim definition, criteria determination, map standardization, criteria weighting, map aggregation, and final decision-making. According to previous studies, various factors were defined [1, 11, 14, 22, 37–39], availability of the data, expert opinions, and features of the study area. The selected factors were categorized into three main groups: physical indicators, chemical indicators, and socioeconomic indicators (Fig. 2). The environmental indicators include land use, slope, and soil erosion. The chemical indicators used in this study were organic matter, acidity, salinity, and soil sodicity. The socio-economic indicators represent the cause of land degradation due to human pressures and activities. Such causes as population, income level, lifestyle, culture, and infrastructure can potentially contribute to degradation risk. Due to the absence of spatial data, we used only population density as an influential and essential factor for the socio-economic criteria.

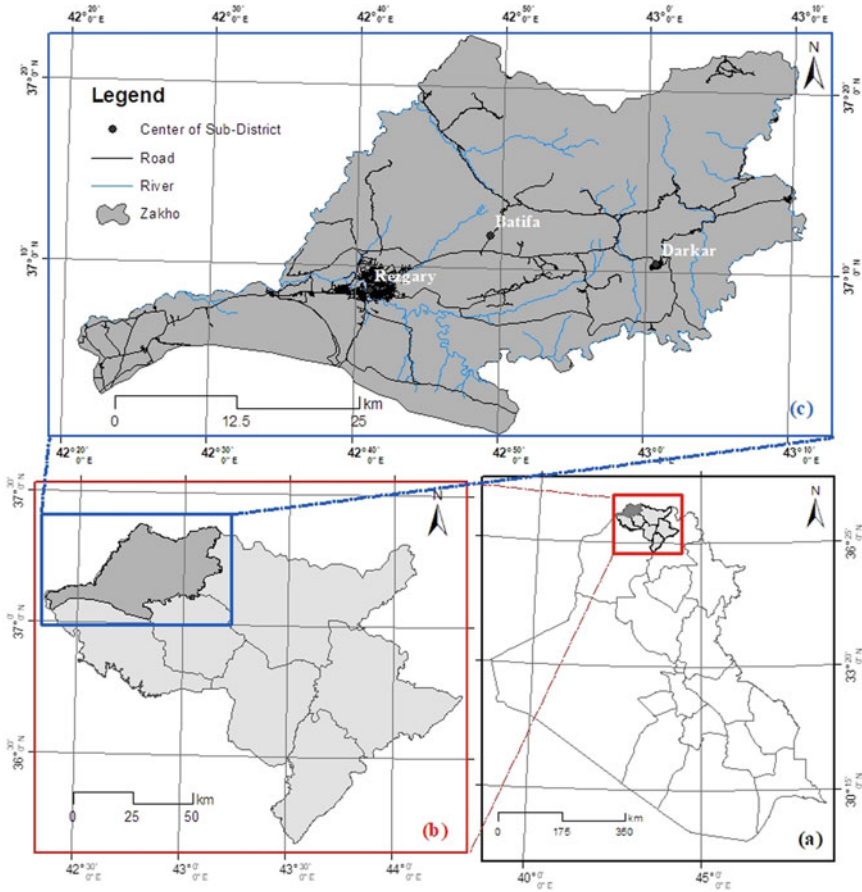


Fig. 1 a Map of Iraq, b Map of Duhok Province, c Map of the study area (Zakho)

2.2 Data Collection and Preparation

The data used were collected from various sources such as satellite imagery, field study, Directorate of Regional Statistics of Duhok, Ministry of Planning, National Meteorology Agency of Kurdistan Region, and College of Agriculture of the University of Duhok. The data were acquired and the spatial layers were created in the ArcGIS 10.3. All maps were classified into 5 levels from level 1 to level 5 means class 1 indicates low vulnerability, and class 5 represents a very high vulnerability for land degradation. The following sections describe data collection, data preparation, and classification.

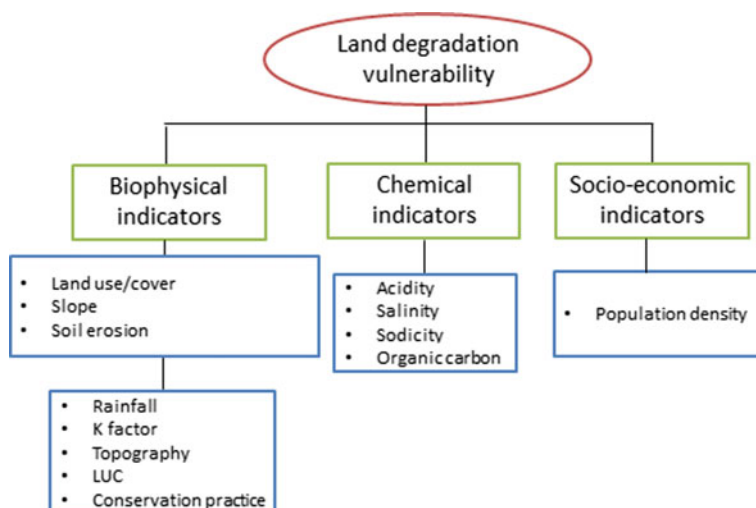


Fig. 2 Hierarchical structure of land degradation vulnerability in our study

2.2.1 Physical Indicators

- *Land Use/Land Cover (LULC)*

Sentinel-2 level 1-C data acquired on 14 August 2019 was used to prepare the LULC map. It was scaled to the top of the atmosphere (TOA) level, including orthorectification and spatial registration on a global reference system [40]. The image was resampled to 10 m spatial resolution using the nearest neighbor method. Finally, the study area is obtained through subsetting. The next step was to classify the image as we used K-Means Cluster Analysis as an unsupervised land classification. K-Means Cluster Analysis was performed by a false-color composite map and applied to all bands where the image is classified into six types of LULC. They are Built-up areas, Forest, Agriculture, Water, Soil, and Rock. Then, accuracy of the image was assessed and classified image as a raster was converted to a vector to prepare LULC map.

- *Soil erosion*

Revised Universal Soil Loss Equation (RUSLE) model was used to estimate soil erosion loss. RUSLE is one of the commonly-used methods of soil erosion estimation that calculates the rate of soil loss based on the rainfall, topography and slope, vegetation cover, soil parameters, and conservation practice. The formula of RUSLE is given as following.

$$A = R \times K \times L \times S \times C \times P \quad (1)$$

A: annual soil erosion
R: rainfall erosivity
K: soil erodibility
LS: slope length and stepness
C: land use/cover
P: management practices

- *Rainfall erosivity factor (R)*

Rainfall has a direct relationship with soil erosion. Monthly rainfall data for 12 years (2002–2014) were analyzed and the spatial map of average annual precipitation (*P*) in the study area was estimated using interpolation methods. Modified Fournier Index (MFI) based on Eq. 2 [41] was used to calculate *R* factor.

$$MFI = 1/N \sum_{j=1}^n \frac{P_{ij}^2}{P_j} \quad (2)$$

P_{ij} is mean monthly rainfall (mm); P_j is mean annual rainfall (mm); *N* is numbers of years

$$R = \frac{0.07397MFI^{1.847}}{17.02} \quad \text{if } MFI < 55 \quad (3)$$

$$R = \frac{95.77 - 6.081MFI + 0.477MFI^2}{17.02} \quad \text{if } MFI \geq 55 \quad (4)$$

- *Soil erodibility factor (K)*

K factor describes the influence of soil properties on soil loss [42]. The statistical data of these parameters are from the College of Agricultural at the University of Duhok. They included 5 sampling points within the study area. The values of the parameters were put into ArcGIS, and the point sources were converted to a polygon. The *K* was estimated based on the Eq. 4 [42].

$$K = \left\{ 0.2 + 0.3 \exp \left[-0.0256SAN \frac{1-SIL}{100} \right] \right\} + \frac{SIL}{CLA+SIL} 0.3 \\ * \left(1.0 - \frac{0.25C}{C + \exp(3.72 - 2.95C)} \right) \left(1.0 - \frac{0.75NI}{5NI + \exp(-5.51 + 22.95NI)} \right) \quad (5)$$

Fraction of sand (SAN), silt (SIL), clay (CLA), soil organic carbon content (C).

- *Land cover and land use factor (C)*

The *C* factor represents the effect of land-use types on soil erosion. It was prepared based on the LULC map of the study area.

- *Topographic factor (LS)*

Length (L) and slope steepness (S) factors describe the topographic factors. The overland flow velocity can be increased if the slope increases, leading to a higher soil erosion rate. The L and S factors were extracted from the DEM layer. The surface analysis was used in GIS to calculate slope percent and degree layers from DEM. The DEM was obtained from ASTER data (ASTER-GDEM 2013). ASTER Global Digital Elevation Model (GDEM). Retrieved August 15, 2018, from Global Data Explorer [43]. The Shuttle Radar Topography Mission. Retrieved May 10, 2013, from <http://gdex.cr.usgs.gov/gdex/>.

The LS factor was estimated based on the equation presented by Renard et al. [41].

$$L = \left(\frac{\lambda}{22.13} \right) \times m \tag{6}$$

λ ; the slope length and m ; an adjustable slope length exponent.

$$m = \frac{\beta}{1 + \beta} \beta = \frac{\sin\left(\frac{\theta}{0.0896}\right)}{3.0(\sin\theta)^{0.8} + 0.56} \tag{7}$$

- *Conservation practices factor (P)*

In the study area, no significant conservation practices to minimize soil erosion are implemented; thus, a value of 1 was assigned for this factor.

- *Estimation of soil erosion*

All maps were prepared in raster grid layers and transformed into similar reference systems (Zone 38 UTM) and resolution (30 m grid) in the ArcGIS10.6. To estimate the rate of soil erosion in the study area, the maps were integrated. The highest susceptibility areas are given the highest rate, and the minimum rate is given to the lowest susceptible feature.

2.2.2 Chemical Indicators

Undesirable changes in soil chemicals behavior that decrease soil quality represent chemical degradation [44]. The most important indicators of chemical degradation vulnerability are losses of organic matter, acidity, sodicity, and salinity; thus, these parameters were analyzed for the chemical land degradation index. These parameters' information was obtained from the College of Agriculture at the University of Duhok, Iraq.

- *Organic matter*

Table 1 Organic matter classes and risks to land degradation [3]

Organic matter	Density	Risk class
0–1	Very low density	Very high
1–3	Low density	High
3–10	Moderate density	Moderate
>10	High density	Low

Organic matter includes the soil's living and dead organic materials and has an important impact on the soil function. Continuous cultivation areas may lead to the loss of organic matter, resulting in a decrease in soil fertility [44]. Soil organic matter can be estimated from organic carbon. It can be calculated using the following equation (Combs and Nathan 1998).

$$\text{Percentage of organic matter} = \text{Percentage of total organic carbon} \times 1.72 \quad (8)$$

The values of organic matter were added into ArcGIS and the point sources were converted to polygon sources using interpolation methods. The map was classified into four classes according to FOA. Table 1 shows the defined classes that are 0–1, 1–3, 3–10, and greater than 10, representing very low, low, moderate, and high soil organic matter, respectively.

- *Soil salinity*

Soil salinity describes soils based on their soluble salt content. Salinity may occur in different climatic conditions. In arid areas, salinity is mainly a result of water shortage and a high evapotranspiration rate [1]. However, in humid areas, the increase in groundwater table due to excessive discharge from uncontrolled irrigation activities or poor drainage conditions may lead to salinity. The rate of salinity can be determined by electrical conductivity (*EC*) measurements. The values of *EC* were put into ArcGIS and the point data were converted to polygon surface using geostatistical methods. The map was reclassified based on the value ranges given in Table 2 to prepare the rate of soil salinity for land degradation in the study area.

Table 2 Soil salinity classes and risks to land degradation [3]

Electrical conductivity (dS/m)	Soil salinity class	Risk class
0–2	Non-saline	Very low
2–4	Slightly saline	Low
4–8	Moderately saline	Moderate
8–16	Strongly saline	High
>16	Very strongly saline	Very high

Table 3 Soil acidity classes and risk to land degradation [3]

Soil pH	Description	Risk class
<5.5	Acid soils	High
5.5–6.7	Slightly acid soils	Low
6.7–7.3	Neutral soils	Very low
7.3–7.8	Slightly alkaline soils	Medium
>7.8	Very alkaline soils	High

Table 4 Exchangeable sodium percentage (ESP) and sodicity hazard [3]

ESP	Percentage	Risk class
Low	<15	None to slight
Moderate	15–30	Light to moderate
High	30–50	Moderate to high
Very high	>50	High to very high

- *Soil acidity*

Soil acidity is another important indicator of chemical soil degradation. The human-made or natural factors may cause soil acidity, resulting in deficiency or unavailability of essential nutrients and may cause a reduction in crop productivity and increases dependency on chemical fertilizers [44, 45]. Based on the pH the acidity of soil can be measured. The state of acidity in our study was calculated from the pH values, and the values were put into ArcGIS, and the point data were converted to polygon surface using interpolation methods. The acidity map has been classified based on the class ranges of FAO used to classify soil acidity (Table 3).

- *Soil sodicity*

Sodicity represents the amount of sodium in the soil. In the current study, the exchangeable sodium percentage (ESP) value were put into ArcGIS, and the point data were converted to polygon surface using interpolation methods. The sodicity map has been classified into four levels, as Table 4.

2.2.3 Socio-economic Indicator

- *Population Density*

Population density intensifies the pressure of humans on land resources and thus is a main factor in land degradation vulnerability. The study area's population information was obtained from the Directorate of Regional Statistics of Duhok. The population density was calculated by population number divided into the area. The spatial distribution of the population density was prepared and reclassified to a scale of 1 to 5,

Table 5 AHP scales [27]

Intensity of importance	Description
1	Equal importance
2	Equal to average importance
3	Average importance
4	Average to strong importance
5	Strong importance
6	Strong to very strong importance
7	Very strong importance
8	Very strong or super-strong importance
9	Super strong importance

Source Saaty [46]

indicating very low to very high density. In the areas of high rate population density, the pressure on the land resources is high; therefore, land vulnerability degradation is considered as high.

2.3 Weighting Criteria

Since the importance of the criteria in a specific aim differs from others, it is necessary to make a comparison between factors and determine the weight of each factor. Weight represents the importance or significance of the criteria for other criteria. Ranking, rating, and analytical hierarchy process (AHP) are the three most widely used weighting methods [27]. In this study, we used AHP to determine the relative importance or weight of the criteria. AHP has been developed by Saaty [46] and is a pairwise comparison comparing two criteria at one time based on the scale (Table 5). In AHP, a scale of values ranging from 1 to 9 is defined, in which 9 represents the most important and 1 represents the least important.

2.4 Aggregating Criteria

In the final step, all prepared maps were aggregated. First, physical indicators maps (LULC, slope, and soil erosion) were aggregated and physical land degradation vulnerability maps were obtained. Then, chemical parameters maps, including organic matter, salinity, acidity, and sodicity, were aggregated and the chemical land degradation vulnerability was created. Finally, three maps of physical land degradation, chemical land degradation, and population density were combined using the

Table 6 Pairwise comparison matrix for biophysical land degradation indicators

Criteria	Sub-criteria	Weights
Biophysical indicators 0.70	Soil erosion	0.55
	Slope	0.25
	LULC	0.20
Chemical indicators 0.30	Organic matter	0.45
	Salinity	0.20
	Acidity	0.20
	Sodicity	0.15

weighted overlay method. Each map was multiplied by its weight in the overlay process.

3 Results and Discussion

3.1 Physical Land Degradation Vulnerability

The weights of the three physical indicators, including LULC, soil erosion, and slope, were derived through the weighting process and the obtained weights are presented in Table 6. Soil erosion is considered the most important factor in physical degradation vulnerability. The maps of soil erosion, slope, and LULC were prepared and shown in Fig. 3. These maps were then combined by considering their weights for the result of physical degradation vulnerability. The spatial distribution of physical land degradation vulnerability is shown in Fig. 4. The result shows that 60% of the study area has low risk, and a small portion of the study area has a high level of risk.

3.2 Chemical Degradation Vulnerability

The weights of the chemical degradation indicators are shown in Table 6. As can be seen, organic matter, salinity, acidity, and sodicity were assigned as the most to least important factors, respectively. These maps of chemical indicators (Fig. 5) were aggregated to show the chemical degradation vulnerability in the study area. The spatial distribution of chemical land degradation is shown in Fig. 6.

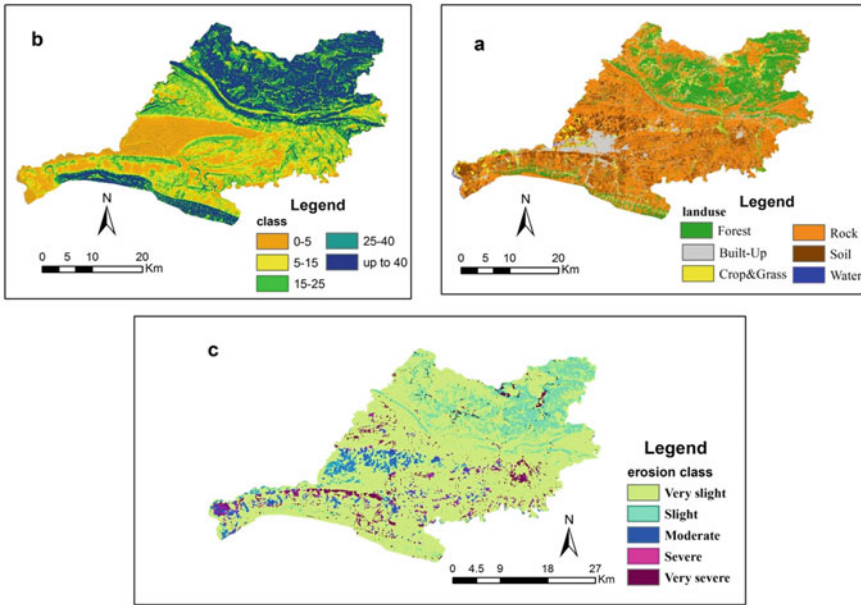


Fig. 3 a LULC cover, b slope, and c soil erosion maps of Zakho district

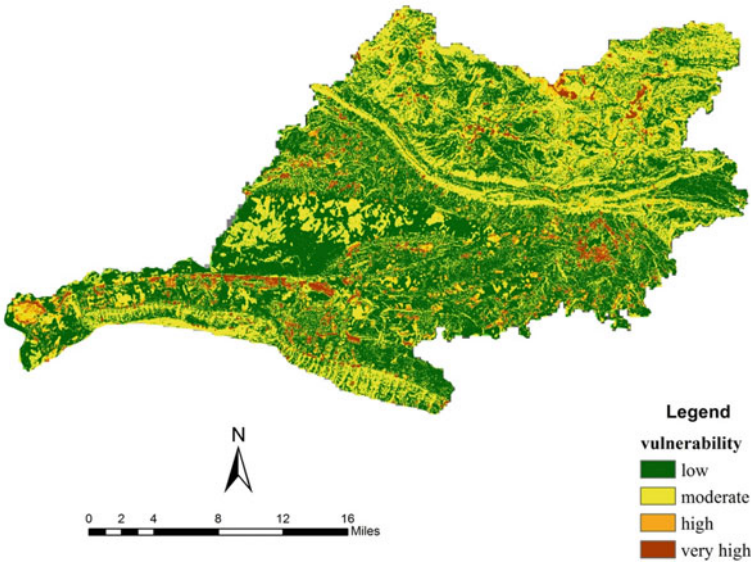


Fig. 4 Physical land degradation vulnerability in Zakho district

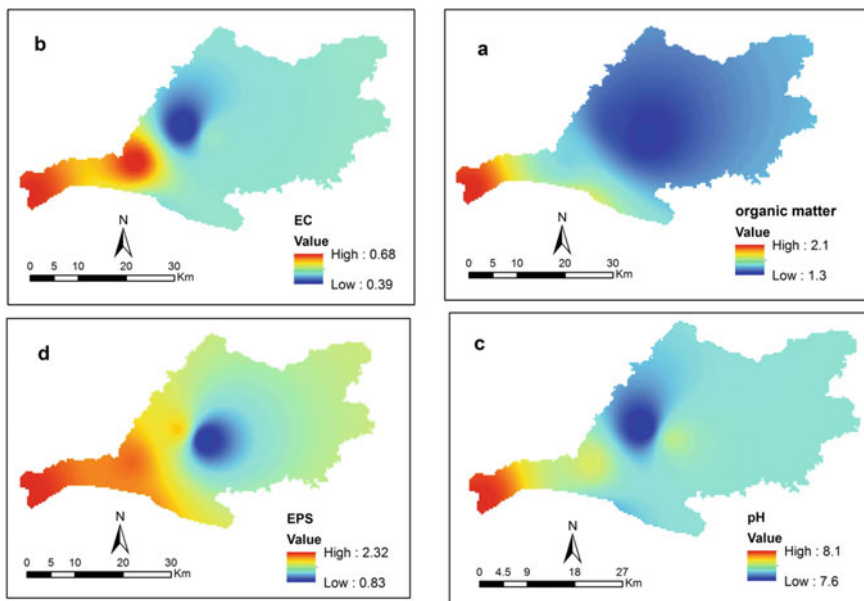


Fig. 5 a Spatial distribution of organic matter, b salinity, c acidity, and d sodicity in Zakho district

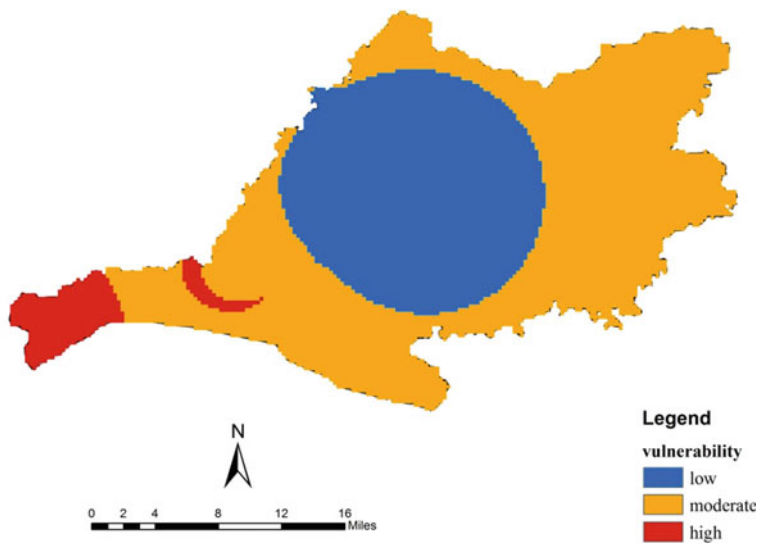


Fig. 6 Chemical land degradation vulnerability in Zakho district

3.3 Land Degradation Vulnerability

By considering the weight of the biophysical vulnerability, chemical vulnerability, and reclassified population density indicators (Fig. 7), these three maps were integrated to show the spatial distribution of land degradation vulnerability in the study area. Based on the weighting, physical degradation vulnerability is the most important index with a weight of 0.5. The chemical degradation index and reclassified population density were assigned the second and third priorities with 0.30 and 0.20, respectively. The final map that represents the land degradation vulnerability is shown in Fig. 8. The final map was classified into three levels of risk; low, moderate, and high vulnerability. According to the result, approximately 50% of the study area is low vulnerable to land degradation, while the vulnerability of the 7% is high. Also, 43% of the district falls in the moderate land degradation vulnerability class.

The figure shows that the moderate and high risk is mostly found in the north-eastern, western, and southwestern parts of the study area. The higher weight was assigned to physical indicators, including LULC, slope, and soil erosion. Therefore, these indices play an essential role in land degradation assessment. The low risks of soil erosion, dense forest, and dense vegetation cover decrease the risk of degradation in the Zakho district. Also, it is found that the central parts have the lowest portion of the degradation. These areas have the promising condition of erosion and degradation and the chemical features have an acceptable condition along with a very high population density, resulting in a low risk of land degradation in these areas.

The vulnerability to land degradation and indicators, including natural and human-made, were considered. To exact understand land degradation vulnerability, it is

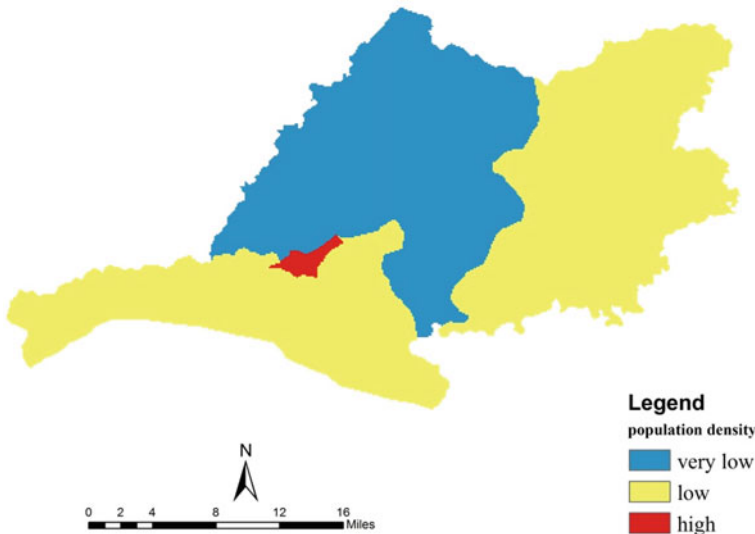


Fig. 7 Population density (person per area) in Zakho district

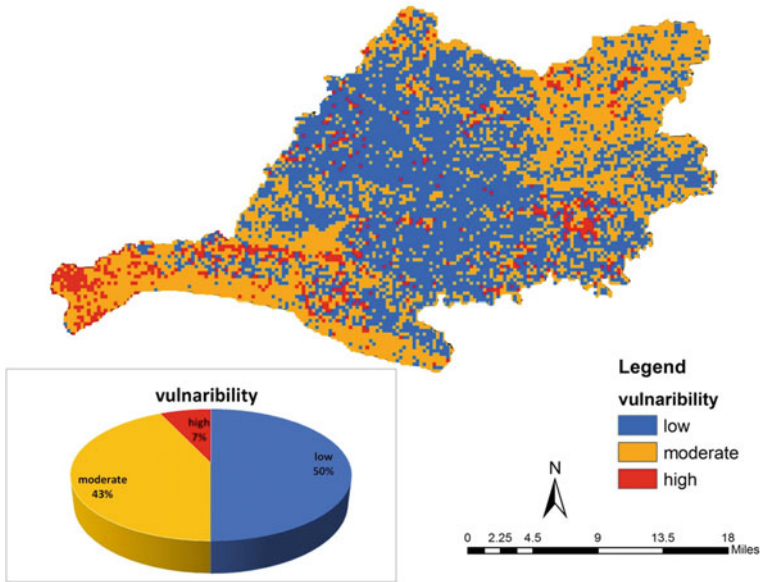


Fig. 8 Map of land degradation vulnerability in Zakho district

essential to deal with various natural and human-made indices. However, based on weighting, some factors can be given higher importance. Similar studies that have assessed the land degradation vulnerability considered integrated factors. Imbrenda et al. [26] assessed land degradation vulnerability based on integrated criteria. They considered the socio-economic parameters demonstrating the effect of farming with analyses of the vegetation trends. In a study by AbdelRahman et al. [14], land degradation state was evaluated in Chamrajanagar district in India. The land degradation then was categorized in five classes from very low to very high ranges. Also, in the study area hotspot regions were identified and it was shown that in surface and sub-surface horizons the soil was mostly exposed to degradation. In a study by Vu et al. [6], environmental and socio-economic factors affecting land degradation in Vietnam were identified. They assessed land degradation extent based on geology, slope, soil type, and percent of the total population. The results illustrated that population growth and farming, especially in rural areas, had strong effects on land degradation intensity.

4 Conclusions

Integrating multi-criteria evaluation and GIS has a great potential to assess land degradation vulnerability and identify the hotspot areas. In this study, we applied the multi-criteria evaluation approach in combination with GIS for Zakho district, Kurdistan Region-Iraq. The overall results showed that the Zakho district has a low

land degradation risk. The acceptable results clearly illustrated the GIS capability for vulnerability assessment and suitability analysis. Also, it was concluded that MCE is an efficient approach in suitability assessment; however, proper field validation provides more accurate results and predictions.

In this chapter, the analysis was performed based on a comprehensive set of criteria. We used three groups of criteria and related sub-criteria. The availability of data are important in the selection of effective parameters. Despite this fact, some key factors might be ignored that could yield different decision alternatives. We strongly recommend that future studies consider further parameters, especially socio-economic parameters such as agriculture production income, education, and the rate of development.

5 Recommendations

The rate of land degradation in Zakho district was assessed at low risk; however, it is recommended that the national organizations and decision-makers will support further studies to study the more exact status of land degradation across the province to minimize the possible hazards and soil erosion. Also, in recent years some parts of the forests in the Duhok province and Zakho district have been degraded due to political conflicts; therefore, it is better to overcome threats by avoiding further degradation and new reclamation of forest lands.

Acknowledgements We thank Department of Agriculture of the University of Duhok for providing the required data and information.

References

1. Oldeman L (1992) The global extent of soil degradation. In: ISRIC bi-annual report 1991–1992, 19–36. International Soil Reference and Information Centre, Wageningen
2. Global Environment Facility-GEF (2019) Land degradation report. https://www.thegef.org/sites/default/files/publications/gef_land_degradation_bifold_2019.pdf
3. FAO (2011) Land degradation assessment in drylands: manual for local level assessment of land degradation and sustainable land management. Part 2: Field methodology and tools. food and agriculture organization of the United Nations, Rome, Italy
4. Pirsahab M, Nouri M, Karimi H, Mustafa Y, Hossini H, Naderi Z (2020) Occurrence of residual organophosphorus pesticides in soil of some Asian countries, Australia and Nigeria. In: IOP conference series: materials, science and engineering, vol 737, p 012175
5. Neamat S, Karimi H (2020) A systematic review of GIS-based landslide hazard mapping on determinant factors from international databases. In: 2020 international conference on advanced science and engineering (ICOASE), 2020, pp 180–183. <https://doi.org/10.1109/ICOASE51841.2020.9436611>
6. Vu QM, Le QB, Frossard E, Vlek PLG (2014) Socio-economic and biophysical determinants of land degradation in Vietnam: an integrated causal analysis at the national level. Land Use Policy 36:605–617. <https://doi.org/10.1016/j.landusepol.2013.10.012>

7. Senjobi B, Ogunkunle A (2011) Effect of different land use types and their implications on land degradation and productivity in Ogun State, Nigeria. *Int J Agric Biotechnol Sustain Dev* 3(1):7–18
8. Joko T, Anggoro S, Sunoko HR, Rachmawati S (2017) Pesticides usage in the soil quality degradation potential in Wanasari subdistrict, Brebes, Indonesia. *Appl Environ Soil Sci*. <https://doi.org/10.1155/2017/5896191>
9. Hostert P, Röder A, Hill J, Udelhoven T, Tsiourlis G (2003) Retrospective studies of grazing-induced land degradation: a case study in central Crete, Greece. *Int J Remote Sens* 24(20):4019–4034. <https://doi.org/10.1080/0143116031000103844>
10. Fadhil AM (2013) Sand dunes monitoring using remote sensing and GIS techniques for some sites in Iraq. In: P SOC PHOTO-OPT INS 8762, PIAGENG 2013: intelligent information, control, and communication technology for agricultural engineering, vol 876206, Sanya, China. <https://doi.org/10.1117/12.2019735>
11. Al-Quraishi AMF, Hu GD, Chen JG (2004) Land degradation detection, mapping, and monitoring in the northwestern part of Hebei Province, China, using RS and GIS Technologies. In: 2004, Map Asia 2004, the international conference on geospatial sciences, Beijing, China
12. Stocking MA, Murnaghan N (2013) A handbook for the field assessment of land degradation. Routledge
13. Mitri G, Nader M, Van der Molen I, Lovett J (2014) Evaluating exposure to land degradation in association with repetitive armed conflicts in North Lebanon using multi-temporal satellite data. *Environ Monit Assess* 186:7655–7672. <https://doi.org/10.1007/s10661-014-3957-5>
14. AbdelRahman MAE, Natarajan A, Hegde R, Prakash SS (2019) Assessment of land degradation using the comprehensive geostatistical approach and remote sensing data in GIS-model builder. *Egypt J Remote Sens Space Sci* 22(3):323–334. <https://doi.org/10.1016/j.ejrs.2018.03.002>
15. Dubovyk O (2017) The role of remote sensing in land degradation assessments: opportunities and challenges. *Eur J Remote Sens* 50(1):601–613. <https://doi.org/10.1080/22797254.2017.1378926>
16. Karimi H, Jafarnezhad J, Khaledi J, Ahmadi P (2018) Monitoring and prediction of land use/land cover changes using CA-Markov model: a case study of Ravansar County in Iran. *Arab J Geosci* 11(592). <https://doi.org/10.1007/s12517-018-3940-5>
17. KouroshNiya A, Huang J, Karimi H, Keshkar H, Naimi B (2019) Use of intensity analysis to characterize land use/cover change in the biggest island of Persian Gulf, Qeshm Island, Iran. *Sustainability* 11:4396
18. KouroshNiya A, Huang J, Kazemzadeh-Zow A, Karimi H, Karimi B (2020) Comparison of three hybrid models to simulate land use changes: a case study in Qeshm Island, Iran. *Environ Monit Assess* 192:302. <https://doi.org/10.1007/s10661-020-08274-6>
19. Karimi H, Jafarnezhad J, Kakhani A (2020) Landsat time-series for land use change detection using support vector machine: case study of Javanrud District, Iran. In: 2020 international conference on computer science and software engineering (CSASE). Duhok, Iraq, pp 128–131. <https://doi.org/10.1109/CSASE48920.2020.9142087>
20. Mustafa YT (2020) Multi-temporal satellite data for land use/cover (LULC) change detection in Zakho, Kurdistan Region-Iraq. In: Al-Quraishi A, Negm A (eds) *Environmental remote sensing and GIS in Iraq*. Springer Water, Cham. https://doi.org/10.1007/978-3-030-21344-2_7
21. Fadhil AM (2011) Drought mapping using geoinformation technology for some sites in the Iraqi Kurdistan Region. *Int J Digit Earth* 4(3):239–257. <https://doi.org/10.1080/17538947.2010.489971>
22. Prakash S, Sharma MC, Kumar R, Dhinwa PS, Sastry KLN, Rajawat AS (2016) Mapping and assessing land degradation vulnerability in Kangra district using physical and socio-economic indicators. *Spat Inf Res* 24:733–744. <https://doi.org/10.1007/s41324-016-0071-5>
23. Al-Quraishi AMF, Gaznayee HA, Crespi M (2021) Drought trend analysis in a semi-arid area of Iraq based on normalized difference vegetation index, normalized difference water index and standardized precipitation index. *J Arid Land* 13:413–430. <https://doi.org/10.1007/s40333-021-0062-9>

24. Reith J, Ghazaryan G, Muthoni F, Dubovyk O (2021) Assessment of land degradation in semi-arid Tanzania—using multiscale remote sensing datasets to support sustainable development goal 15.3. *Remote Sens* 13(9):1754. <https://doi.org/10.3390/rs13091754>
25. Mzuri RT, Mustafa YT, Omar AA (2021) Land degradation assessment using AHP and GIS-based modelling in Duhok District, Kurdistan Region, Iraq. *Geocarto Int.* <https://doi.org/10.1080/10106049.2021.1987534>
26. Imbrenda V, D’Emilio M, Lanfredi M, Simoniello T, Ragosta M, Macchiato M (2013) Integrated indicators for the estimation of vulnerability to land degradation, soil processes and current trends in quality assessment. Maria C. Hernandez Soriano, *IntechOpen*. <https://doi.org/10.5772/52870>. <https://www.intechopen.com/books/soil-processes-and-current-trends-in-quality>
27. Malczewski J, Rinner C (2015) *Multicriteria decision analysis in geographic information science*. Springer, New York
28. Karimi H, Soffianian A, Mirghaffari N, Soltani S (2016) Determining air pollution potential using geographic information systems and multi-criteria evaluation: a case study in Isfahan Province in Iran. *Environ Process* 3:229–246. <https://doi.org/10.1007/s40710-016-0136-4>
29. Siefi S, Karimi H, Soffianian A, Pourmanafi S (2017) GIS-based multi criteria evaluation for thermal power plant site selection in Kahnuj county, SE Iran. *Civil Eng Infrastruct J* 50(1):179–189. <https://doi.org/10.7508/cej.2017.01.011>
30. Chehrazar F, Nahavandchi M, Balist J, Amiri M (2018) Capability Evaluation of tourism with fuzzy logic in mountain areas in GIS environment (case study: Hamedan City). *J Environ Sci Stud* 3(1):659–672
31. Karimi H, Amiri S, Huang J, Karimi A (2019) Integrating GIS and multi-criteria decision analysis for landfill site selection, case study: Javanrood County in Iran. *Int J Environ Sci Technol* 16:7305–7318. <https://doi.org/10.1007/s13762-018-2151-7>
32. Karimi K, Soffianian A, Seifi S, Pourmanafi S, Ramin H (2020) Evaluating optimal sites for combined-cycle power plants using GIS: comparison of two aggregation methods in Iran. *Int J Sustain Energy* 39(2):101–112. <https://doi.org/10.1080/14786451.2019.1659271>
33. Adil Z, Jabbar S, Sulaiman RH, Mustafa YT, Karimi H (2021) Land suitability analysis for identifying industrial zones in Duhok District, Kurdistan Region of Iraq. *JoCEF* 2(02):51–56
34. Balist J, Nahavandchi M, Bidar GS (2021) Landfill site selection using fuzzy logic & AHP & WLC (case study: Razan city—Iran). *JoCEF* 2(01):01–07. <https://doi.org/10.38094/jocef20129>
35. Karimi H, Hossini H, Amin AA (2022) Municipal landfill site selection and environmental impacts assessment using spatial multicriteria decision analysis: a case study. *Comput Earth Environ Sci* 235–244. <https://doi.org/10.1016/B978-0-323-89861-4.00030-0>
36. Muhammed AH, Karimi H, Ghareeb BK, Neamat N, Mirzaei K (2020) Assessment of the quality of the environment in Duhok Province, Kurdistan Region of Iraq. *JoCEF* 1(1):20–24
37. Wodaje ST (2016) Land degradation vulnerability assessment using GIS and remote sensing in Beshilo River Basin, Ethiopia. MSc Thesis, NTNU, The Netherlands
38. Haregeweyn N, Tsunekawa A, Poesen J, Tsubo M, Meshesha DT, Fenta AA, Nyssen J, Adgo E (2017) Comprehensive assessment of soil erosion risk for better land use planning in river basins: a case study of the Upper Blue Nile River. *Sci Total Environ* 574:95–108
39. Imane H, Tahri M, Mohamed M, Mustapha H (2019) Efficiency of fuzzy analytic hierarchy process to detect soil erosion vulnerability. *Geoderma* 354:113853. <https://doi.org/10.1016/j.geoderma.2019.07.011>
40. Sentinel-2 Team (2015) *Sentinel-2 user hand book*, European Space Agency
41. Renard KG, Foster GR, Weesies GA, McCool DK, Yoder DC (1997) *Predicting soil erosion by water: a guide to conservation planning with the revised universal soil loss equation (RUSLE)*. U.S. Department of Agriculture-Agriculture Handbook No. 7

42. Sun W, Shao Q, Liu J, Zhai J (2014) Assessing the effects of land use and topography on soil erosion on the Loess Plateau in China. *CATENA* 121:151–163
43. USGS (2005)
44. Saeedi R, Safaei E, Lee Y, Lužnik J (2019) Oxidation of sulfides including DBT using a new vanadyl complex of a non-innocent o-aminophenol benzoxazole based ligand. *Appl Organomet Chem*
45. Osman KT (2013) *Soil degradation, conservation and remediation*. Springer, New York
46. Saaty TL (2008) Decision making with the analytic hierarchy process. *Int J Serv Sci* 1(1):83–98

Evaluation of Geo-hazard Induced by Zarand Earthquake in Central Iran Using Thermal Remote Sensing Data and GIS



Hamid Allahvir diasl, Himan Shahabi, Ayub Mohammadi, Ataollah Shirzadi, Wei Chen, Mehdi Ahmadi, and Masood Khodadadi

Abstract Land degradation is one of the environmental hazards that can occur in most countries during the last century. Geo-hazards induced by earthquakes have caused environmental degradation. Inevitably, stresses occurring prior to an earthquake in tectonically active places are able to boost the near-ground temperature of a region. Thermal remote sensing can usually detect these transformations, which can provide substantial clues about future earthquakes. The aim of this study is to analyze land surface temperature (LST) variations due to the Zarand Earthquake,

H. Allahvir diasl

Faculty of Built Environment and Surveying, Universiti Teknologi Malaysia (UTM), 81310 Johor Bahru, Malaysia

e-mail: p_hamid84@yahoo.com

H. Shahabi (✉)

Department of Geomorphology, Faculty of Natural Resources, University of Kurdistan, Sanandaj, Iran

e-mail: h.shahabi@uok.ac.ir

A. Mohammadi

Department of Remote Sensing and GIS, University of Tabriz, 51666-16471 Tabriz, Iran

e-mail: mohammadi.ayub@tabrizu.ac.ir

A. Shirzadi

Department of Rangeland and Watershed Management, Faculty of Natural Resources, University of Kurdistan, Sanandaj, Iran

e-mail: a.shirzadi@uok.ac.ir

W. Chen

College of Geology & Environment, Xi'an University of Science and Technology, Xi'an 710054, China

e-mail: chenwei0930@xust.edu.cn

M. Ahmadi

Department of Geomorphology, Faculty of Planning and Environmental Sciences, University of Tabriz, 51666-16471 Tabriz, Iran

M. Khodadadi

School of Business and Creative Industries, University of the West of Scotland, Paisley PA1 2BE, UK

e-mail: masood.khodadadi@uws.ac.uk

© The Author(s), under exclusive license to Springer Nature Switzerland AG 2022

A. M. F. Al-Quraishi et al. (eds.), *Environmental Degradation in Asia*,

Earth and Environmental Sciences Library,

https://doi.org/10.1007/978-3-031-12112-8_4

which occurred in south–central Iran during 10–28 February 2005, by using the MODIS LST product. In addition, ten and six years of air temperature anomaly average data from before and after the Zarand earthquake, respectively, were used in this study. The results showed that the LST on 16th February was 28 °C, while on 21st February was 37 °C. Therefore, there was an LST difference of about 9 °C between both dates, so that there was a temporary abnormal rise in temperature before the earthquake occurred. On the other hand, the time series analysis of LST maps from 10 to 28th February 2005 showed that anomalies started six days before the main shock. Also, based on the correlation of MODIS LST and in-situ air temperature, interestingly, either the LST or air temperature started to rise on 16 February, or both soared on 21st February 2005.

Keywords Earthquake · Land surface temperature · Thermal remote sensing · Environmental degradation · Central Iran

1 Introduction

Earthquakes as one of environmental degradation is a major problem worldwide, especially in developing countries [1, 2]. With the increase in economic development, much more serious economic and social damage can be caused by unexpected earthquakes than ever before [3, 4]. Therefore, monitoring and studying of natural catastrophes, such as flood [5, 6], wildfire [7, 8], sinkhole [9], droughtiness [10], landslide [11], gully erosion [12], land cover [13], land/ground subsidence [14], groundwater [15], and earthquake [16] presents a severe scientific challenge [17]. Clearly, one of the most effective ways of minimizing the earthquakes' effects is predicting the event before it occurs, so that necessary measures can be taken to evacuate and warn those in danger [18]. Furthermore, understanding temperature anomalies in the land associated with earthquakes can help predict the earthquake and reduce the extreme earthquake impacts. The anomaly can be observed within two weeks up to few hours before the earthquake [19].

Ouzounov and Freund [20] proposed a mechanism to explain the temperature rise preceding an earthquake is the presence of positive hole-type charge carriers in rocks. LST as an important factor in investigating the temperature of areas close to the epicenter can provide new attitudes to study this catastrophic phenomenon [21]. This temperature difference is quite obvious in temperatures obtained from satellite images estimated from the Earth's emission information and from instruments placed 1.5 m above the ground, collecting air temperature data [22]. The observed thermal anomalies are related to the strong interaction between the lithosphere and atmosphere [23].

Satellite thermal infrared (TIR) imaging data show not only long-lived thermal fields associated with large fault systems and linear structures in the Earth's crust [24], but also short-lived anomalies prior to major earthquakes [25]. The short-lived anomalies in the land typically appear 7–14 days before an earthquake.

Recently, several techniques, including co-registration and geo-referencing of all relevant imagery from GOES and AVHRR have been developed to analyze satellite TIR imagery to identify anomalies [26]. Furthermore, other applied techniques are single image comparison of pre- versus post-earthquake TIR imageries, multispectral infrared component analysis of the MODIS Terra and Aqua data by using LST [20], and an analysis of pixel temperature variance from long-term scene threshold temperatures to identify “hot” areas [26].

Some researchers have also observed anomalies from two weeks to a few hours before the event at distances of 200–1000 km from the epicenter (China, Japan, Russia, Turkey, Chile, Mexico, and Greece) [27–30]. In addition, there are several satellite-based methods that show potential precursors to earthquakes [22]. It is worth mentioning that remote sensing has proved to be a useful tool for observing LST variations. Therefore, understanding the near real-time and large spatial scale LST variations from remote sensing images is of great importance because this domain has not been thoroughly explored, and it may provide valuable information for seismic studies in tectonically-active areas.

A change in the thermal regime of an epicenter region is one of the most striking changes and can be detected by space-borne sensors such as AVHRR and MODIS [31, 32]. Several studies have shown that numerous geophysical parameters are strongly related to earthquakes. If changes can be recognized before the earthquake, these parameters may be possible precursors of an earthquake occurrence. In particular, one of these parameters is LST, which can change before the earthquake. If LST anomalies before an earthquake could be observed, the prediction of earthquakes may be possible. Therefore, this research may make a valuable contribution to reducing the damage to the environment and manmade infrastructure and loss of life. This study will also be important to scientists who work on seismic research or research related to seismic activity.

In-situ air temperature data were used to show the increasing air temperature variation associated with the earthquake. Moreover, LST variation maps were produced from satellite data to show the temperature anomaly associated with the earthquake. Additionally, LST maps for the years 2004 and 2007 were produced to compare with 2005 (10th–28th February). Furthermore, this study covered the variation of LST that happened prior to the earthquake. The study area is the Zarand district earthquake in Kerman Province. The earthquake occurred on 22nd February 2005, with a magnitude of 6.4. However, the particular dates were 10th to 28th February 2005. The earthquake prediction is a challenging task to reduce the earthquake impact and hence reduce the damage by taking necessary precautions.

In this study, geo-hazard evaluation of Zarand Earthquake in central Iran, which occurred during 10th–28th February 2005, is analyzed and the land surface temperature (LST) variation for the years 2004, 2005, and 2007 are mapped. Finally, the in-situ air temperature variation for the entire month of February 2005 (1st–28th February) is analyzed and compared with data from the ten years before (1994–2004) and six years (2006–2011) after the earthquake. In this study, the satellite data utilized were the MODIS daytime LST product (MOD11A1) from the thermal band for 10th to 28th February 2005.

2 Study Area

The study area is located in Zarand district, Kerman Province, central Iran. On 22 February 2005 at 05:55 local time (02:25 GMT), an earthquake with a magnitude of 6.4 on the Richter scale struck the area. The epicenter was identified at 30.726 N, 56.817 E at a depth of 42 km at 55 km north-west of Kerman. The earthquake lasted for 12 s, caused extensive damage to the rural areas in Ravar district and Kerman district, and was much more disastrous for the Zarand district. More than 50 villages suffered between 30 and 100% damage as a consequence of this earthquake. Almost 612 were killed and 15,000 were injured. The population adversely affected is around 32,000 (Fig. 1). A great proportion of the population in several villages was severely affected due to poor building conditions.

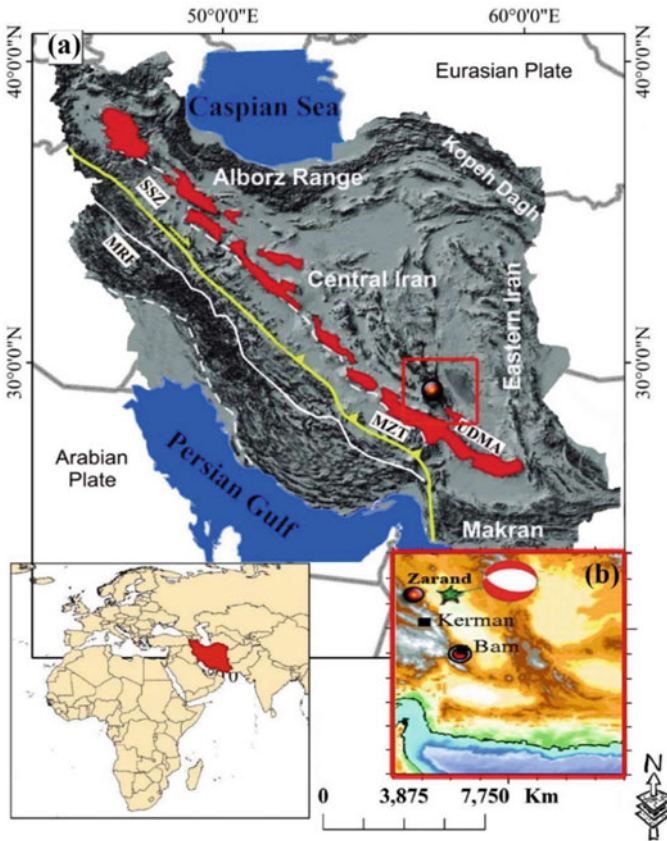


Fig. 1 The geographical position of the study area in Iran; **a** structural units and tectonic features of the Arabia-Eurasia collision zone in Iran: SSZ (Sanandaj-Sirjan Zone), MRF (Main Recent Fault), MZT (Main Zagros Thrust), UDMA (Urumieh-Dokhtar Magmatic Arc); **b** geographical location of Zarand earthquake

The study area is based on the geological structure, is located between two tectonic units—the Urumieh-Dokhtar Magmatic Arc (UDMA) and Main Zagros thrust (MZT) [33]. The UDMA is situated between the Sanandaj-Sirjan Zone (SSZ) and central Iran, running parallel to the Zagros Mountains and the SSZ (Fig. 1a) [34].

3 Materials and Method

3.1 Satellite Data Acquisition

MODIS was launched by NASA with on-board polar orbiting. This study used MODIS Terra because moderate-resolution remote sensing provides a way to quantify land surface characteristics such as snow cover extent, land cover type and extent, leaf area index, surface temperature, and fire occurrence. The MODIS Terra satellite launched on December 18th, 1999. It has 705 km orbit and descending node in which the local time is 10:30 A.M. It has sun-synchronous, near-polar orbiting. The swath angle for this satellite is 2330 km (cross track) by 10° of latitude (along track) [35]. In addition, it has 36 bands with spatial resolutions of 250 m for bands 1–2, 500 m for bands 3–7, and 1000 m for bands 8–36 [36].

The data used for this research was MODIS Terra Land level 3 Daily Tiled LST Products (MOD11A1 Level 3 Daily Land Surface Temperature/Emissivity-1 km). The spatial resolutions for applied Aqua MODIS data for the current study are 1 and 5 km. The source of the data was through this website (<http://ladsweb.nascom.nasa.gov/>).

3.2 Satellite Data Analysis

Needless to say, high-resolution LST is usually derived from thermal infrared satellite observations using a multi-channel technique. In general, surface-emitted TIR radiance depends on its temperature and emissivity, varying with the wavelength. In the current study, 19 images have been used to analyze the temperature variation in 2005. The images which have been downloaded are as follows: 12 images before the earthquake were downloaded within the period of 10th–21st February 2005. In addition, one image was downloaded during the earthquake on 22nd February 2005, and six more images after the earthquake were downloaded for the period of February 23th–28th 2005.

The same data before, during, and after the earthquake for 2005 were used for the years 2004 and 2007. Hence, in the current study, the data for one year before the earthquake (2004) and two years after the earthquake (2007) were considered as well. The MODIS satellite data for both 2004 and 2007 were downloaded from the same source as for 2005. So, 19 images were considered for 2004 and 2007

from February 10th to 28th. The same data was also downloaded for the 10th to 28th for 2007 and compared to 2005 to indicate that the temperature anomaly was due to the earthquake. The air temperature was also used to show the increase in air temperature during the earthquake. Therefore, the air temperature for February 2005 was downloaded for the whole month. Air temperature for 2004 and 2007 were also used to compare with 2005. So, to measure the air temperature, the average of ten years before since 1994–2004, and six years after the earthquake since 2006–2011, compared with 2005 as background.

3.3 Detection of LST Variation

Detection of thermal anomalies has been described by Wan and Dozier [37]. In this technique, they used a split window and some statistical techniques to calculate thermal anomalies. Fortunately, MODIS has a product of LST, which can be used for research in order to indicate LST variation. Therefore, this study uses MODIS satellite LST data to indicate LST variation during the earthquake. As explained in the previous section, after downloading the images, the data were processed: first, pre-processing, the MODIS LST data have already been pre-processed. Secondly, the LST product data should be converted to LST in Kelvin and then Celsius. So, the first step is to convert LST data to Kelvin. In order to do this conversion, the LST data should be multiplied by a scale factor of 0.02. Hence, the conversion of LST data to Kelvin has been used (Eq. 1):

$$LST (K) = RD * 0.02 \quad (1)$$

where, $LST (K)$ is the land surface temperature in Kelvin, RD is the raw data of MODIS LST, and 0.02 is the scale factor.

Remote sensing software like ENVI was used to convert the first equation. The LST data in Kelvin was achieved through this conversion. Therefore, for this purpose, LST Kelvin was subtracted from 273. Then, all values have been changed to Celsius. Therefore, the conversion equation is given as Eq. (2):

$$LST (°C) = LST (K) - 273 \quad (2)$$

where, $LST (°C)$ is LST data in Celsius.

In order to indicate the growth of the thermal anomaly, the LST data in Celsius were transferred to ArcGIS software to show LST variation during the earthquake. Therefore, the data were transferred to ArcGIS 10.2. Then, the data was divided into nine classes using the symbology function. Finally, the data was exported and saved as a final LST map, so the variation of LST can be easily observed. The flow chart of this research is shown in Fig. 2.

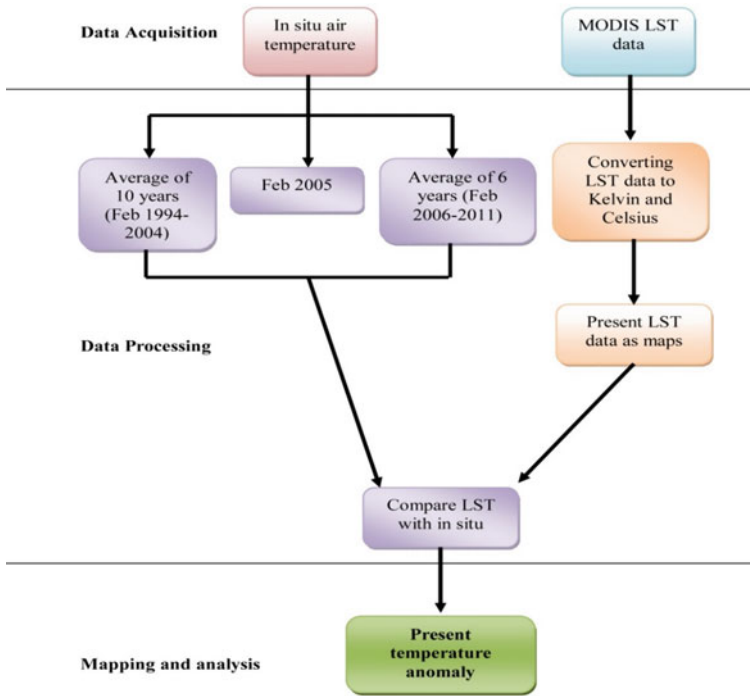


Fig. 2 Flow chart of research methodology adopted in this study

4 Results and Discussion

4.1 LST Variation Prior to Earthquake for 2005

The results of the MODIS daytime series LST maps from 10 to 28th February 2005 are provided in Fig. 3. The LST maps show a thermal anomaly that appeared before the devastating Zaran earthquake, which occurred on 22nd February 2005. The LST maps show that the LST on 16th February was 28 °C, while on 21st February it was 37 °C. Therefore, there was an LST difference of about 9 °C between both dates (Fig. 3). At some places, the LST was about 6–10 °C higher than the usual temperature in that period. In the daytime maps, it can be seen that before 15th February 2005, the LST in the region was indeed at the normal level. The development of a thermal anomaly around the earthquake epicenter started from 16th February 2005 and peaked on 21st February 2005, a day before the earthquake. After experiencing a thermal anomaly of about 5–9 °C, the LST in the region recovered to normal conditions on 25th February 2005 (Fig. 3).

The investigation of pre- and post-earthquake thermal anomalies by analyzing LST images has shown valuable information about changes in the TIR regime of the affected area. The analysis of the time series of the LST maps from 10 to 28th

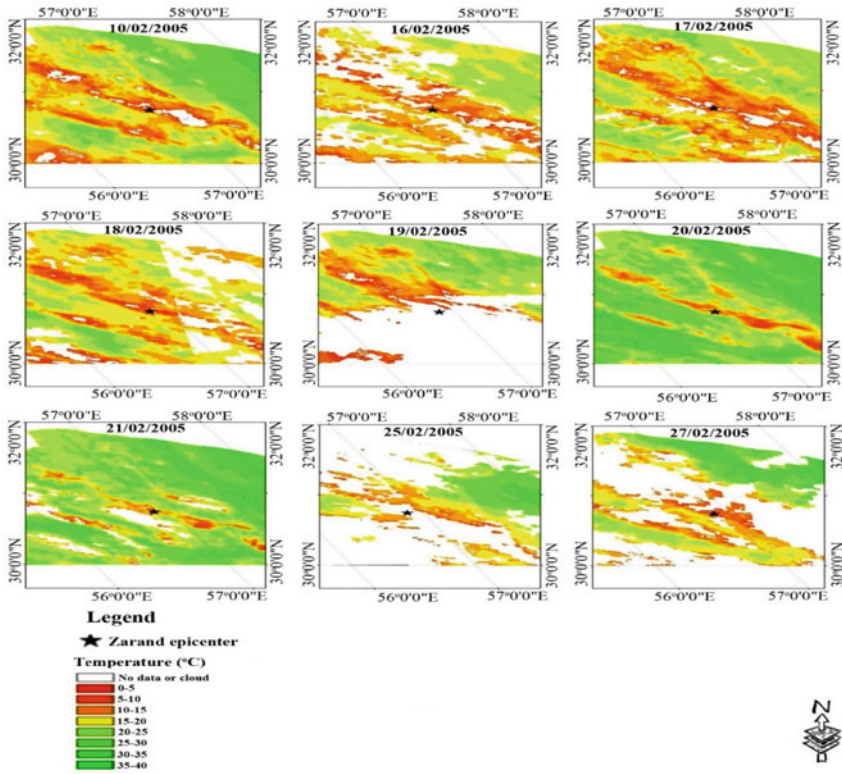


Fig. 3 MODIS day time series LST maps since 10th–28th February 2005; white region indicates no data or cloud

February 2005 showed that anomalies started six days before the main shock. This anomalous LST region increases spatially and in intensity (Fig. 3). The results of this study are in line with previously published works including Choudhury et al. [38], Kancharla et al. [27], and Saraf et al. [22].

Panda et al. [31] analyzed the daytime MODIS LST product to the investigation of obtained LST and occurred Kashmir earthquake. The anomaly started to develop to the south-west of the epicenter and spread out to a large area with LST of 37–44 °C. The earthquake occurred on 8th October 2005. On 7th October 2005, just one day before the earthquake, the epicentral region experienced its highest temperature, which was around 4–8 °C different. In this study, during the Zarand earthquake the peak temperature was seen before the earthquake, and the thermal anomaly started six days before the earthquake.

As a matter of fact, one of the causes of LST anomalies is tectonic stresses. It is known that an increase in rock pressure leads to an increase in temperature.

4.2 Correlation Between MODIS LST and In-Situ Air Temperature

The LST retrieved from the MODIS thermal infrared sensor was compared with in-situ air temperatures observed on the same dates. The MODIS LST and maximum air temperature data are listed in Table 1.

Table 1 shows the correlation between the MODIS LST and in-situ air temperatures from the 10th to 28th February 2005. To better understand the variations of LST and air temperature, they are graphically presented as mentioned in Fig. 4. As shown in Fig. 4, the MODIS-retrieved LST agreed well with the ground observation of air temperature. Interestingly, both LST and air temperature started to increase from 16th February and both also peaked on 21st February 2005.

As can be seen in Fig. 4, the air temperature for day 15th–17th February was around 8 °C, which started to rise gradually. A surface air temperature of 17 °C was recorded on 20th February 2005. Also, the region experienced its maximum rise in air temperature on 21st February 2005, which was 4–8 °C higher than the temperature of the previous days (19th–21st February), while the MODIS LST increased about 1–7 °C compared to that during the period of 19th–21st February.

Table 1 MODIS LST and in-situ air temperature data

Dates of February 2005	In-situ air temperature	MODIS LST
10	11.0	34.1
11	7.0	24.0
12	8.0	28.2
13	7.0	21.5
14	11.0	29.8
15	8.0	30.8
16	8.0	28.2
17	8.0	29.5
18	9.0	29.6
19	13.0	30.8
20	17.0	37.0
21	21.0	37.0
22	13.0	28.1
23	10.0	28.4
24	14.0	34.6
25	16.0	32.8
26	6.0	39.0
27	13.0	25.3
28	15.0	41.4

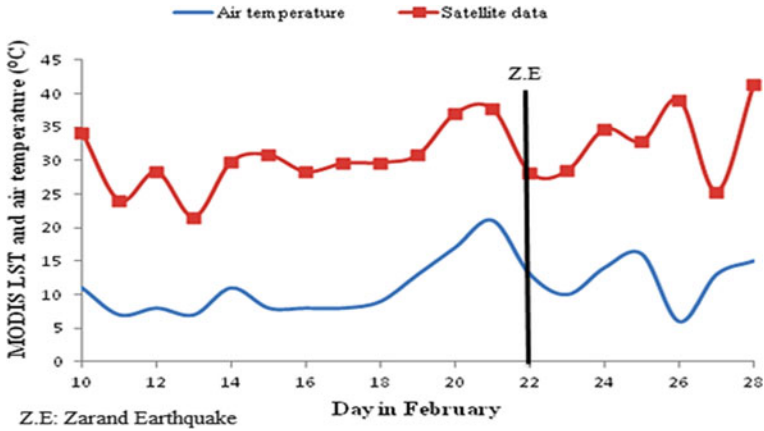


Fig. 4 Variation of MODIS LST and in-situ air temperature before and after the Zarand earthquake within the period from 10 to 28th February 2005. The black bar indicates the date of the Zarand earthquake

The MODIS LST on the 19th was 30.8 °C, while on 21st February, the temperature rose to 37 °C (Fig. 4). As is clear in Table 2 and Fig. 4, the MODIS LST reached a maximum on 21st February with the temperature of 37 °C, but on 22nd February a lower temperature was recorded. 28 °C was recorded for the MODIS LST and 13 °C for air temperature for 22nd February 2005. After the 21st, both the MODIS LST and air temperature continued to decrease until 23rd February, and then both air temperature and the MODIS LST showed small increases on the 25th, which was 16 °C for air temperature and 32 °C for the MODIS LST.

4.3 Comparisons of 2005 LST with 2004 and 2007 LSTs

In order to ensure whether the increase in MODIS LST from 16th February 2005 was associated with the Zarand earthquake, the same analysis was also conducted for the years 2004 and 2007 within the same period (10th to 28th February). Furthermore, compared to the year 2005, there was no unusual MODIS LST increase which started from 16th February in both years 2004 and 2007 (Fig. 5).

Overall, the MODIS LST was in its normal condition in both 2004 and 2007. The MODIS LST for the years 2004, 2005, and 2007 are shown in Table 2. As can be seen in Table 2, for 2005 the peak temperature was recorded on 21st February at 41.6 °C. This is the maximum value for this year in the period of 19 days from 10 to 28th February. In order to compare 21st February 2005 with the previous year, i.e. 2004, the LST recorded was 34.6 °C, which is 7 °C lower than 2005. On the 21st February 2007, the LST was 37.3 °C, which is 4 °C lower than on 21st February 2005. In addition, in 2005 within the period of 16th–22nd February, the MODIS LST

Table 2 MODIS LST for the years 2004, 2005, and 2007

Day	Year 2004	Year 2005	Year 2007
10	36.5	34.1	35.0
11	38.5	24.0	36.4
12	37.6	28.2	35.6
13	40.5	21.5	34.8
14	42.3	29.8	36.4
15	44.0	30.8	33.3
16	37.8	28.2	40.0
17	33.7	29.5	38.6
18	40.3	29.6	37.4
19	41.6	30.8	36.8
20	39.5	37.0	36.6
21	34.6	41.6	37.3
22	40.0	28.1	32.2
23	37.0	28.4	36.3
24	35.8	34.6	35.2
25	40.8	32.8	43.7
26	41.0	39.0	35.9
27	42.7	25.3	30.7
28	40.4	41.4	36.4

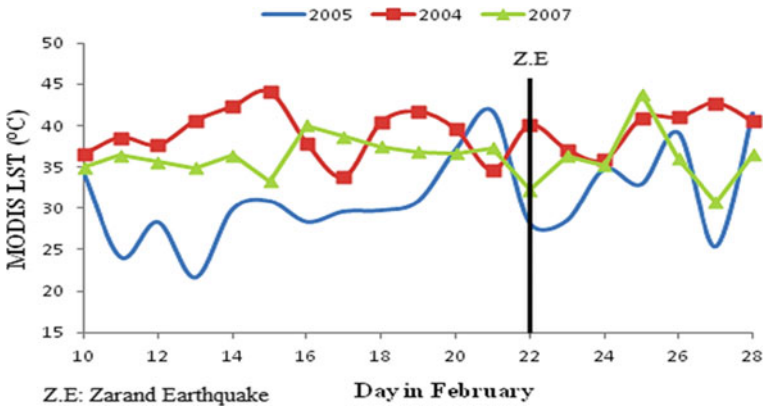


Fig. 5 MODIS LST variation for the years 2004, 2005, and 2007. The black bar indicates the date of the Zarand earthquake

increased gradually from 28 to 41 °C, while in the previous year the same increase cannot be seen. For 2004, within the 16th–22nd February period, the LST values were 33–40 °C (Table 2).

In order to better understand the MODIS LST for the years 2004, 2005, and 2007, they are presented in Fig. 5. Furthermore, the time series LST maps for the years 2004 and 2007 are provided for the period of 10th–28th February in order to compare with 2005. In 2005, the thermal anomaly started to increase from 6th–21st February, while no such thermal anomaly was observed in the years 2004 and 2007 (Fig. 6).

Research has been done by Saraf and Choudhury [21] into an earthquake in Bhuj, Gujarat, India. The earthquake occurred on 26th January 2001. In this research, thermal channels were used to calculate LST over the study area. The LST maps over the region have been provided to indicate the thermal anomaly. The data from the year 2003 from the same region and same dates were also used to study the LST situation and compare between LST in 2001, when the earthquake occurred, and 2003, two years after the earthquake. It was seen that in 2003 there was a completely normal thermal scenario in and around the epicenter. This research shows that the increasing thermal anomaly in 2001 was due to the earthquake and there was no such thermal anomaly in 2003.

4.4 Air Temperature Anomaly

The in-situ air temperature data for the whole month of February were analyzed to understand the correlation between earthquake events and the air temperature variation. The air temperature data from the Zarand meteorological stations are available from the daily climate and weather data statistics website. The maximum temperature values were plotted against the dates within the period 1st–28th February. The maximum air temperature variation for February 2005 was compared with the normal air temperature (generated from ten years of data from 1994 to 2004, and six years from 2006 to 2011—Fig. 7).

The air temperature in Zarand showed a rise of around 4 °C on 19th February 2005 and 5.5 °C on 20th February 2005 with respect to the mean normal air temperature (Fig. 7). On 22nd February 2005, the air temperature deviated as high as 7.5 °C from the normal air temperature, and on 26th February 2005, it was almost the same as that of normal conditions. Although the magnitude of the in-situ air temperature is lower than MODIS LST, the observed in-situ air temperature variation supported the LST variation observed by MODIS, showing that the thermal anomaly seemed to occur a few days before the earthquake and dissipated after the earthquake, which agreed well with previous results [31].

The difference between the in-situ air temperature magnitudes and MODIS LST is normal as the instrument used to measure in-situ air temperature is usually placed at 1.5 m above the ground [22]. Furthermore, the LST obtained from MODIS is the surface skin temperature estimated from the Earth's emission [21]. The in-situ air temperature data from the daily climate weather data statistics website for the year

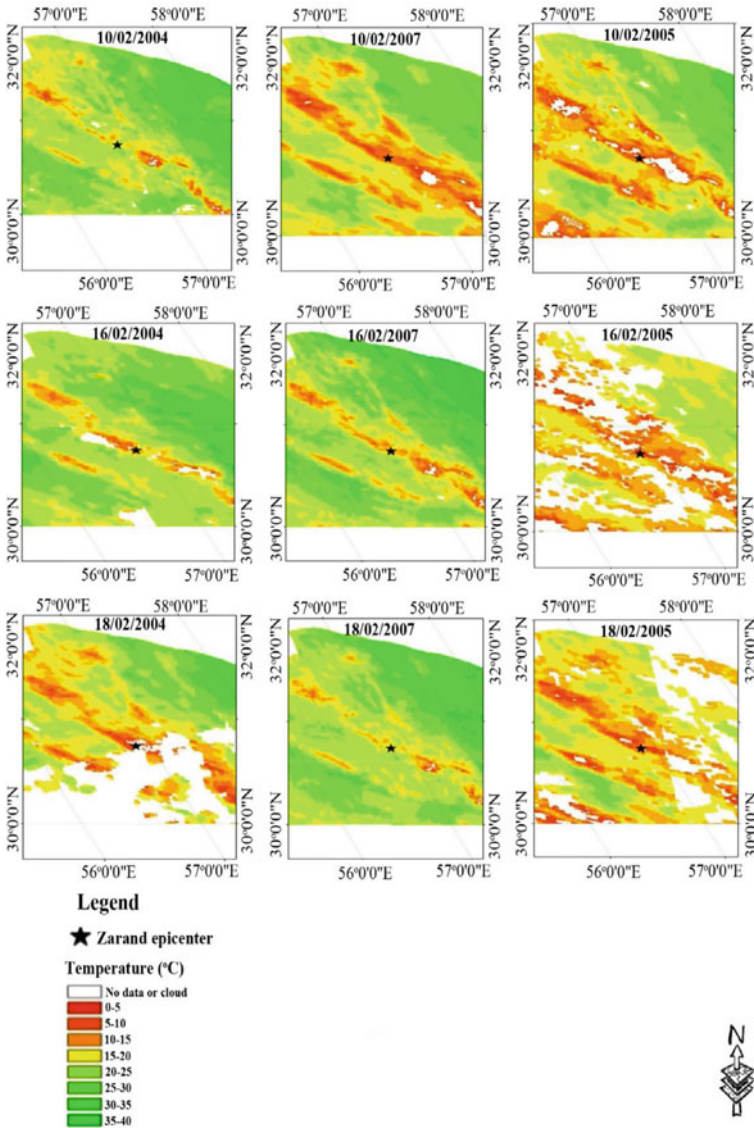


Fig. 6 a Time series of LST maps for years 2004 and 2007 to be compared with 2005 (9 days). b Time series of LST maps for 2004 and 2007 to be compared 2005 (another 9 days)

2005 and the average of 10 years before the earthquake (1994–2004) and six years after the earthquake (2006–2011) are listed in Table 3.

Furthermore, before the earthquake on 21st February 2005, there was an increase in air temperature of 4–6 °C, which did not occur in 2004 and 2007. From 1st February to 10th February in 2004, 2005, and 2007, the in-situ air temperature showed similar

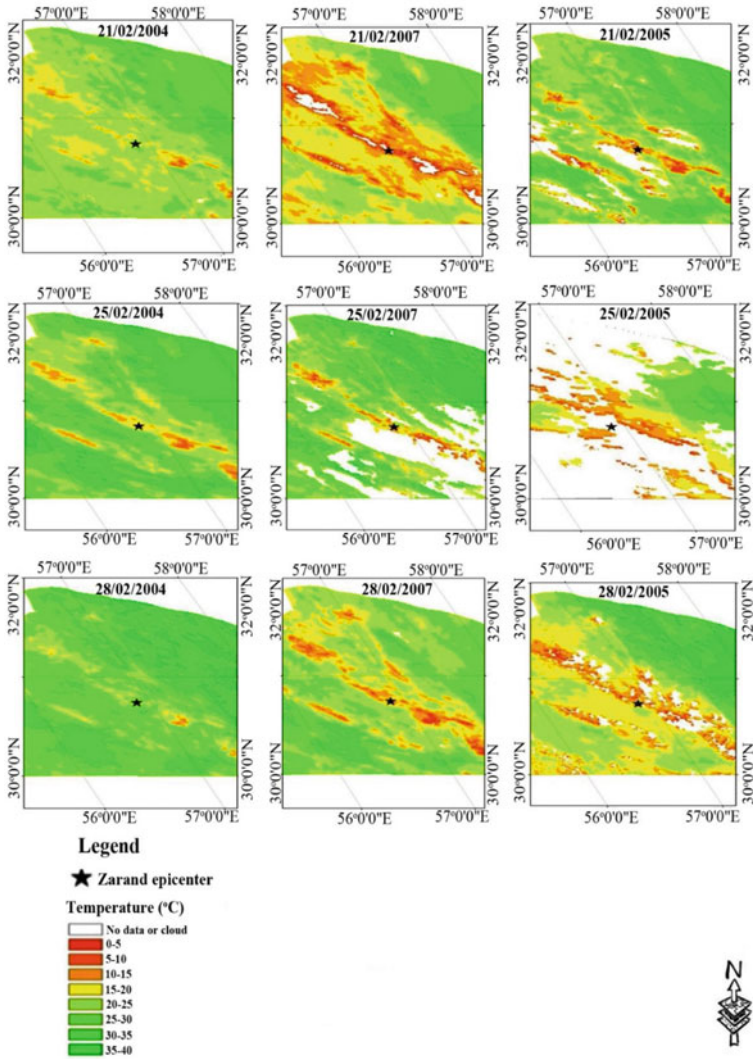


Fig. 6 (continued)

patterns. From 16th February the air temperatures started to rise from 8 to 21 °C on 21st February. After 21st February, the temperature decreased and on 24th February, the temperature relaxed to the normal condition (Fig. 8).

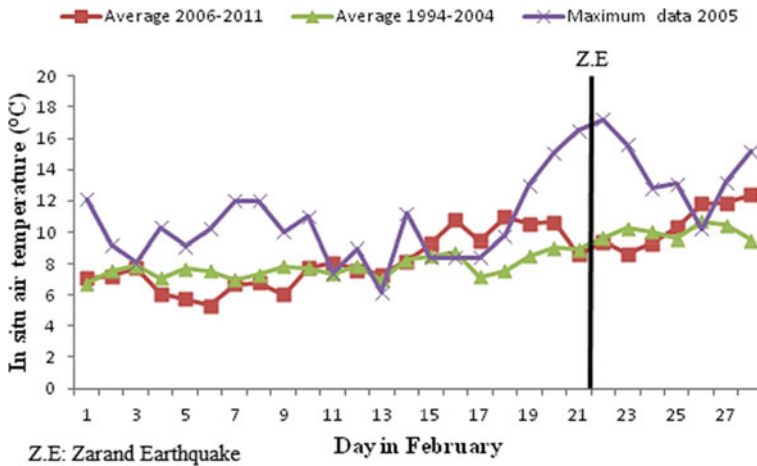


Fig. 7 Temporal variation of in-situ air temperature collected at Zarand meteorological station for the year 2005 (maximum temperature), and mean of average values for the years 2006 to 2011 and the years 1994 to 2004. The black bar indicates the date of the Zarand earthquake

5 Conclusions

The Zarand earthquake in Kerman Province in central Iran triggered numerous geo-hazards, including landslides, rock avalanches, and debris flows. These geo-hazards caused heavy losses by destroying roads, burying villages, blocking rivers and damaging vegetation. It is noted that MODIS Terra thermal data sets have been confirmed to be valuable in successfully detecting earthquake thermal anomalies. The analysis of MODIS daytime LST and in-situ air temperature data for the whole month of February 2005 reveals a distinct, robust, and rapid rise in LST before the Zarand earthquake. The affected region may take days to weeks to attain normal temperature conditions after the main event.

As successfully demonstrated in the present study to analyze LST variation for 2005, the Zarand earthquake was associated with pre-earthquake thermal anomalies. The anomalies appeared six days before the earthquake. The increase in temperature ranges between 5 and 10 °C. The MODIS LST data for 2004 and 2007 data were also analyzed from 10th to 28th and compared to those of 2005, since there is no temperature variation in 2004 and 2007. The LST maps indicated normal conditions in 2004 and 2007, with no thermal anomaly, such as that seen in 2005. The analysis relates to the observational study for the detection of pre-earthquake anomalies, and it provides an understanding of the pattern of growth for TIR anomalies and may assist in the development of a reliable potential earthquake thermal precursor. Besides, regarding the air temperature, a pattern of growth has been observed in 2005. In-situ air temperature, like LST, has indicated growth before and during the earthquake.

Table 3 Maximum of in-situ air temperature data for 2005 and mean of air temperature for the years 1994–2004 and 2006–2011, collected from Zarand meteorological stations

Date	Mean values 2006–2011	Mean values 1994–2004	Maximum values 2005
1	7.1	6.7	12.1
2	7.2	7.5	9.2
3	7.7	7.9	8.1
4	6.1	7.0	10.3
5	5.7	7.6	9.1
6	5.3	7.5	10.2
7	6.7	6.9	12.0
8	6.7	7.3	12.0
9	6.0	7.8	10.0
10	7.7	7.7	11.0
11	8.1	7.3	7.4
12	7.6	7.9	9.0
13	7.3	6.9	6.2
14	8.1	8.2	11.2
15	9.2	8.5	8.4
16	10.8	8.7	8.4
17	9.4	7.1	8.4
18	10.9	7.5	9.8
19	10.5	8.5	13.0
20	10.6	9.0	15.1
21	8.5	8.9	16.5
22	9.3	9.6	17.2
23	8.6	10.2	15.6
24	9.3	10.0	12.8
25	10.2	9.5	13.1
26	11.8	10.6	10.2
27	11.8	10.4	13.2
28	12.3	9.4	15.2

6 Recommendations

It is noted that the remote sensing missions in the future have an important role in calculating LST before each earthquake in the world. The new satellites with equipment sensors in better spatial, spectral, and radiometric resolutions can detect more anomalies before occurring of an earthquake.

For example, in optical remote sensing, Landsat 9 will be equipped with the Thermal Infrared Sensor 2 (TIRS-2) to provide the LST and act as an upgraded version of the Landsat 8 TIRS instrument by solving the known stray light and

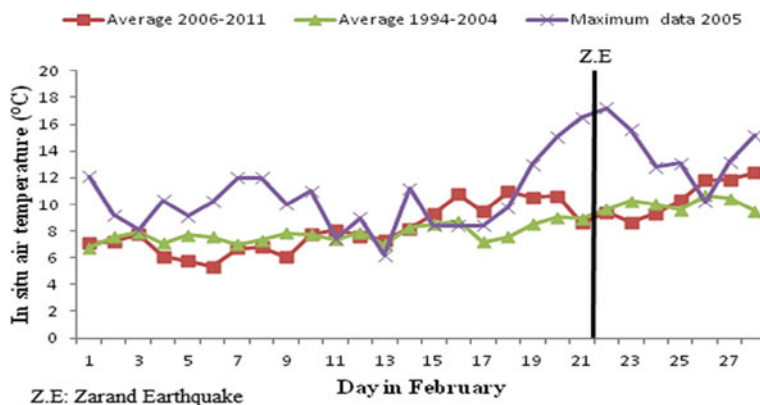


Fig. 8 Temporal variation of maximum in-situ air temperature collected at Zarand meteorological station for 2004, 2005, and 2007. The black bar indicates the date of the Zarand earthquake

reliability issues with the TIRS. Furthermore, in radar remote sensing, Sentinels 4, 5, and Sentinel-5P with orbits of geostationary and sun-synchronous can detect and measure the omitted surface temperature with more precision. Finally, although the prediction of earthquakes in the present time is impossible but more research on the earthquakes in different geographical locations by the advanced equipment in remote sensing data can predict an earthquake precisely and on time.

References

1. Symeonakis E, Karathanasis N, Koukoulas S, Panagopoulos G (2016) Monitoring sensitivity to land degradation and desertification with the environmentally sensitive area index: the case of Lesbos island. *Land Degrad Dev* 27:1562–1573
2. Taheri K, Shahabi H, Chapi K, Shirzadi A, Gutiérrez F, Khosravi K (2019) Sinkhole susceptibility mapping: a comparison between Bayes-based machine learning algorithms. *Land Degrad Dev* 30:730–745
3. Alizadeh M, Alizadeh E, Asadollahpour Kotenaee S, Shahabi H, Beiranvand Pour A, Panahi M, Bin Ahmad B, Saro L (2018) Social vulnerability assessment using artificial neural network (ANN) model for earthquake hazard in Tabriz city, Iran. *Sustainability* 10:3376
4. Lee S, Panahi M, Pourghasemi HR, Shahabi H, Alizadeh M, Shirzadi A, Khosravi K, Melesse AM, Yekrangnia M, Rezaie F (2019) Sevucas: a novel gis-based machine learning software for seismic vulnerability assessment. *Appl Sci* 9:3495
5. Wang Y, Hong H, Chen W, Li S, Panahi M, Khosravi K, Shirzadi A, Shahabi H, Panahi S, Costache R (2019) Flood susceptibility mapping in Dingnan County (China) using adaptive neuro-fuzzy inference system with biogeography based optimization and imperialistic competitive algorithm. *J Environ Manage* 247:712–729
6. Shahabi H, Shirzadi A, Ronoud S, Asadi S, Pham BT, Mansouripour F, Geertsema M, Clague JJ, Bui DT (2021) Flash flood susceptibility mapping using a novel deep learning model based on deep belief network, back propagation and genetic algorithm. *Geosci Front* 12:101100

7. Jaafari A, Zenner EK, Panahi M, Shahabi H (2019) Hybrid artificial intelligence models based on a neuro-fuzzy system and metaheuristic optimization algorithms for spatial prediction of wildfire probability. *Agric For Meteorol* 266:198–207
8. Oliveira S, Gonçalves A, Zêzere JL (2021) Reassessing wildfire susceptibility and hazard for mainland Portugal. *Sci Total Environ* 762:143121
9. Nefeslioglu HA, Tavus B, Er M, Ertugrul G, Ozdemir A, Kaya A, Kocaman S (2021) Integration of an InSAR and ANN for sinkhole susceptibility mapping: a case study from Kirikkale-Delice (Turkey). *ISPRS Int J Geo Inf* 10:119
10. Mokarram M, Pourghasemi HR, Hu M, Zhang H (2021) Determining and forecasting drought susceptibility in southwestern Iran using multi-criteria decision-making (MCDM) coupled with CA-Markov model. *Sci Total Environ* 781:146703
11. Van Dao D, Jaafari A, Bayat M, Mafi-Gholami D, Qi C, Moayedi H, Van Phong T, Ly H-B, Le T-T, Trinh PT (2020) A spatially explicit deep learning neural network model for the prediction of landslide susceptibility. *CATENA* 188:104451
12. Arabameri A, Cerda A, Pradhan B, Tiefenbacher JP, Lombardo L, Bui DT (2020) A methodological comparison of head-cut based gully erosion susceptibility models: combined use of statistical and artificial intelligence. *Geomorphology* 359:107136
13. Bhattacharya RK, Das Chatterjee N, Das K (2021) Land use and land cover change and its resultant erosion susceptible level: an appraisal using RUSLE and logistic regression in a tropical plateau basin of West Bengal, India. *Environ Dev Sustain* 23:1411–1446
14. Ebrahimi H, Feizizadeh B, Salmani S, Azadi H (2020) A comparative study of land subsidence susceptibility mapping of Tasuj plane, Iran, using boosted regression tree, random forest and classification and regression tree methods. *Environ Earth Sci* 79:1–12
15. Mosavi A, Hosseini FS, Choubin B, Abdolshahnejad M, Gharechae H, Lahijanzadeh A, Dineva AA (2020) Susceptibility prediction of groundwater hardness using ensemble machine learning models. *Water* 12:2770
16. Maqsoom A, Aslam B, Awais M, Hassan U, Alaloul WS, Musarat MA, Qureshi MI (2021) Efficiency of multiple hybrid techniques for the earthquake physical susceptibility mapping: the case of Abbottabad District, Pakistan. *Environ Earth Sci* 80:1–20
17. Lu X, Meng Q, Gu X, Zhang X, Xie T, Geng F (2016) Thermal infrared anomalies associated with multi-year earthquakes in the Tibet region based on China's FY-2E satellite data. *Adv Space Res* 58:989–1001
18. Li, J, Liu C, Zheng Y, Xiong X (2017) Rupture process of the M_s 7.0 Lushan earthquake determined by joint inversion of local static GPS records, strong motion data, and teleseismograms. *J Earth Sci* 28:404–410
19. Tramutoli V, Cuomo V, Filizzola C, Pergola N, Pietrapertosa C (2005) Assessing the potential of thermal infrared satellite surveys for monitoring seismically active areas: the case of Kocaeli (Izmit) earthquake, August 17, 1999. *Remote Sens Environ* 96:409–426
20. Ouzounov D, Freund F (2004) Mid-infrared emission prior to strong earthquakes analyzed by remote sensing data. *Adv Space Res* 33:268–273
21. Saraf A, Choudhury S (2005) Cover: satellite detects surface thermal anomalies associated with the Algerian earthquakes of May 2003. *Int J Remote Sens* 26:2705–2713
22. Saraf AK, Rawat V, Das J, Zia M, Sharma K (2012) Satellite detection of thermal precursors of Yamnotri, Ravar and Dalbandin earthquakes. *Nat Hazards* 61:861–872
23. Tronin A, Biagi P, Molchanov O, Khatkevich Y, Gordeev E (2004) Temperature variations related to earthquakes from simultaneous observation at the ground stations and by satellites in Kamchatka area. *Phys Chem Earth Parts A/B/C* 29:501–506
24. Carreno E, Capote R, Yague A, Tordesillas J, Lopez M, Ardizzone J, Suarez A, Lzquierdo A, Tsige M, Martinez J (2001) Observations of thermal anomaly associated to seismic activity from remote sensing. General Assembly of European Seismology Commission, Portugal, p 269
25. Tronin AA, Hayakawa M, Molchanov OA (2002) Thermal IR satellite data application for earthquake research in Japan and China. *J Geodyn* 33:519–534

26. Ouzounov D, Liu D, Chunli K, Cervone G, Kafatos M, Taylor P (2007) Outgoing long wave radiation variability from IR satellite data prior to major earthquakes. *Tectonophysics* 431:211–220
27. Kancherla VK, Mandla VR, Arrowsmith C (2018) Study of thermal IR phenomena associated with 27 February 2010 Chile Mw 8.8 earthquake using MODIS data. *Geocarto Int* 33:293–309
28. Liu C, Zheng Y, Xiong X (2015) Focal mechanism and rupture process of the 2012 Mw 7.0 Santa Isabel, Mexico earthquake inverted by teleseismic data. *J Earth Sci* 26:384–390
29. Lü Q-Q, Ding J-H, Cui C-Y (2000) Probable satellite thermal infrared anomaly before the Zhangbei M_s= 6.2 earthquake on January 10, 1998. *Acta Seismologica Sinica* 13:203–209
30. Qin X, Tan C, Chen Q, Wu M, Feng C (2014) Crustal stress state and seismic hazard along southwest segment of the Longmenshan thrust belt after Wenchuan Earthquake. *J Earth Sci* 25:676–688
31. Panda S, Choudhury S, Saraf A, Das J (2007) MODIS land surface temperature data detects thermal anomaly preceding 8 October 2005 Kashmir earthquake. *Int J Remote Sens* 28:4587–4596
32. Pulinet S, Ouzounov D, Karelin A, Boyarchuk K, Pokhmelnikh L (2006) The physical nature of thermal anomalies observed before strong earthquakes. *Phys Chem Earth Parts A/B/C* 31:143–153
33. Ahmadian J, Murata M, Nadimi A, Ozawa H, Kozai T (2014) Active tectonics of Iran deduced from earthquakes, active faulting, and GPS evidence. *Bull Cent Collab Comm Naruto Univ Edu* 28:11–22
34. Talebian M, Jackson J (2002) Offset on the main recent fault of NW Iran and implications for the late Cenozoic tectonics of the Arabia-Eurasia collision zone. *Geophys J Int* 150:422–439
35. Xiong X, Wolfe R, Barnes W, Guenther B, Vermote E, Saleous N, Salomonson V (2010) Terra and Aqua MODIS design, radiometry, and geometry in support of land remote sensing. In: *Land remote sensing and global environmental change*. Springer, pp 133–164
36. Roodposhti MS, Safarrad T, Shahabi H (2017) Drought sensitivity mapping using two one-class support vector machine algorithms. *Atmos Res* 193:73–82
37. Wan Z, Dozier J (1996) A generalized split-window algorithm for retrieving land-surface temperature from space. *IEEE Trans Geosci Remote Sens* 34:892–905
38. Choudhury S, Dasgupta S, Saraf AK, Panda S (2006) Remote sensing observations of pre-earthquake thermal anomalies in Iran. *Int J Remote Sens* 27:4381–4396

Environmental Control of the Sand Dunes in Iraq



Hasan K. Jasim, Ahmed J. Al-Shakeri, and Thamer A. Al-Shimmary

Abstract Mesopotamia (Iraq) is considered as one of the fertile lands extending back thousands of years. Despite the presence of the two rivers (Tigris and Euphrates), vast desertification and degradation effects were encountered during the past forty years. Four large sand dune fields extending along five governorates (Missan, Al-Mithana, Thi-Qar, Al-Qadisiyah, and Al-Najaf) were studied in the field, and by GIS technique. The creeping sand dunes affected roads, railways, farmlands, archaeological sites, and artificial and natural irrigation channels. Monitoring these sand dune fields shows a pronounced expansion causing more severe and harsh consequences. One possible remedy for limiting the disastrous consequences is establishing vegetation belts along the main wind direction that will restrain the sand dunes accumulation and migration.

Keywords Sand dunes · Aeolian hazards · Migration of sand dunes · Desertification

1 Introduction

Dust/sand storms are considered to be one of the most important environmental hazards in Iraq and the region [1]. Wind erosion affects 39% of arid areas susceptible to human degradation [2]. The real problem of sand dunes is their creep that affects the development of projects; such as highways, railways, irrigation and drainage canals, agricultural lands, and other projects. Dunes are causing a decrease in the efficiency and increase in the maintenance costs for these projects [3]. Migrating dunes, especially large dunes, can be a real menace as they march across roads and even through forests and over Farmland, roads, and buildings were buried under shifting, windblown soil during the dust bowl era. The cost to clear and maintain roads along sandy beaches and through deserts can be high because dunes can move several meters or more in a year [4].

H. K. Jasim (✉) · A. J. Al-Shakeri · T. A. Al-Shimmary
Department of Geology, College of Science, University of Baghdad, Baghdad, Iraq
e-mail: hasan.jasim@sc.uobaghdad.edu.iq; hassan1500000@yahoo.com

© The Author(s), under exclusive license to Springer Nature Switzerland AG 2022
A. M. F. Al-Quraishi et al. (eds.), *Environmental Degradation in Asia*,
Earth and Environmental Sciences Library,
https://doi.org/10.1007/978-3-031-12112-8_5

2 Aeolian Hazards

Arid environments are characterized by sparse or no vegetation. Thus free, mobile sand dunes are common in these areas. Dune soils have proved popular for agriculture in some regions, as they are less prone to salinization than other areas. However, these resources can be easily overexploited so that vegetation is lost. Once the vegetation is removed, moisture loss is increased and restabilization is unlikely. The drifting sand becomes a problem for road transport and can bury settlements [5].

Land degradation and desertification are menaces in many parts of the world with serious implications for sustainable use of the natural environment. According to [6, 7], it is mainly the semiarid regions of the most susceptible world. At the same time, these regions, both rich and poor, are experiencing some of the highest population growth rates worldwide [8]. The term ‘desertification’ has been the subject of much controversy in the literature [9], but is used here in accordance with the concept adopted by [10]. This concept includes the following key features: (a) reduction in vegetation productivity (particularly due to the loss of perennial shrub cover), (b) decrease in species diversity and (c) increase in aeolian processes such as the erosion, transportation and deposition of sand.

3 Migration of Sand Dunes

Sand dunes may be fixed, active, or partially active, mainly due to wind power and vegetation cover. Thus, ongoing climatic changes may turn some currently fixed dunes into active ones and vice versa [11–13]. Sand movement by wind is a complex process involving several styles of grain movement that occur more or less simultaneously [14] in [15]. Geomorphologists usually quantify dune mobility in terms of mobility indexes [16]. These are usually based on parameters such as wind power, precipitation rate, and potential evapotranspiration. According to conventional beliefs, dunes in the same geographical area can be active, fixed or partially active dependent on changing climatological conditions that determine mobility indexes [17]. However, it was recently shown that active and fixed dunes coexist under similar climatic conditions [11, 18–20]. The general movement of dunes in Iraq is in a south-east direction as a result of prevailing northwest winds [21].

4 Hazards of Sand Dunes in Iraq

Most Iraqi lands are affected by wind erosion and the formation and movement of sand dunes, particularly in the middle and south of Iraq [22]. The total area covered by sand dunes is approximately 2 million hectares. Furthermore, millions of hectares are threatened by sand dunes [23].

The state of desertification in Iraq has worsened after 1990. Areas of lands affected by salinity, waterlogging and deterioration of the vegetation cover increased. In addition, areas covered by moving sand dunes increased owing to wind erosion. Besides these factors, the population increase, migration and urban creep are all becoming an added adverse factors leading to desertification [24]. There are enormous changes in different climatic factors in the Middle East due to global climate change; since the last decade. Global climate change and the GAP project in Turkey are both contributing to the water shortages in Iraq. The area experienced enormous changes in annual average temperature and rainfall. As a result, the number of annual dust storms witnessed serious alarms in Iraq. As a result, there are growing concerns that most of the agricultural land in Iraq will be converted to desert areas [25–27].

5 Methodology

Three methods were followed to detect the changes in the shape, size and area of the different studied dune fields these are:

1. Field Work.
2. Geological Maps of Iraq.
3. GIS Technique.

5.1 Field Work

Through **ten** field trips covering the sand dunes in Missan, Thi-Qar, and Al-Muthana Governorates during the time from 2014 to 2016, several aeolian hazards were observed to affect many civilian and human activity establishments these include the following:

5.1.1 Archeological and Holy Sites Burial

Two localities of hazard were noticed; the first site lies within Missan dune fields (Syaid Subair dune field), representing a hill area about 15 m high and a 3000 m² area. This hill represents an archeological site listed in the Ministry of Tourism and Antiquities under Qara-Taba Archeological Hill's name (see Fig. 1).

In this area, many shattered archeological pieces were found scattered all around the place (see Fig. 2).

This site lies along the main wind direction thus, it was affected by the accumulation of sand dunes all around the hill (see Fig. 1). Ministry of Agriculture tried to solve this problem by stabilizing the dunes by covering the dunes with soil layers. However, this was not successful, in fact. It worsens the conditions like the soil

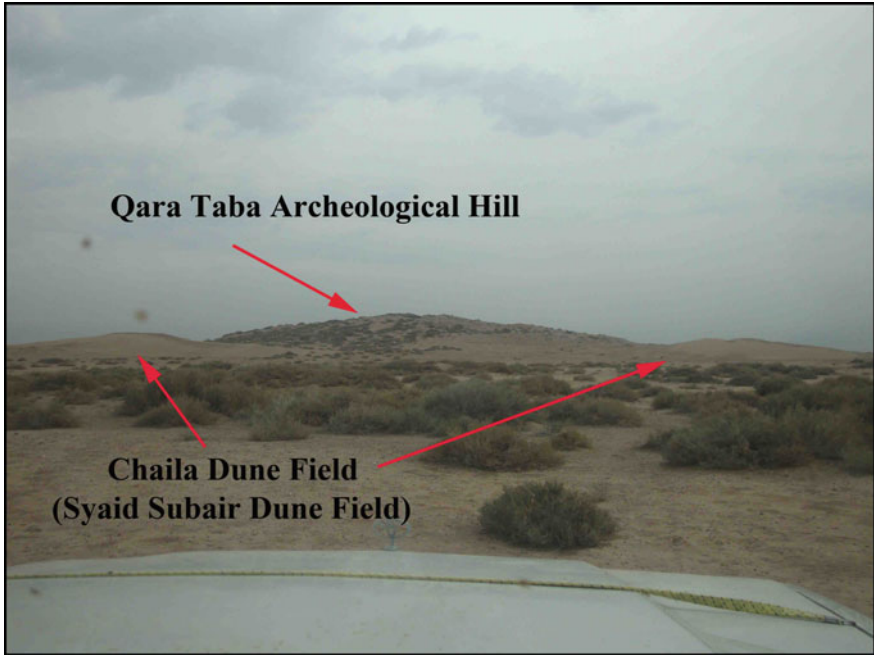


Fig. 1 Qara Taba Archeological Site in Sayid Subair dune field. Missan Governorate



Fig. 2 Archeological pieces in Qara-Taba Hill area. Missan Governorate

cover were eroded and the sand has exposed again. Additionally, the dune shape was extensively distorted, which caused the area to be converted into badland (see Fig. 3).

As a consequence, more supply of dune sand was deposited around the hill (see Fig. 4).

A more convenient method to protect this site may be suggested which is establishing a belt of vegetation surrounding the area of the archeological hill. The second site lies in the Thi-Qar Governorate (Albu Tarfa Dune Field). This site represents

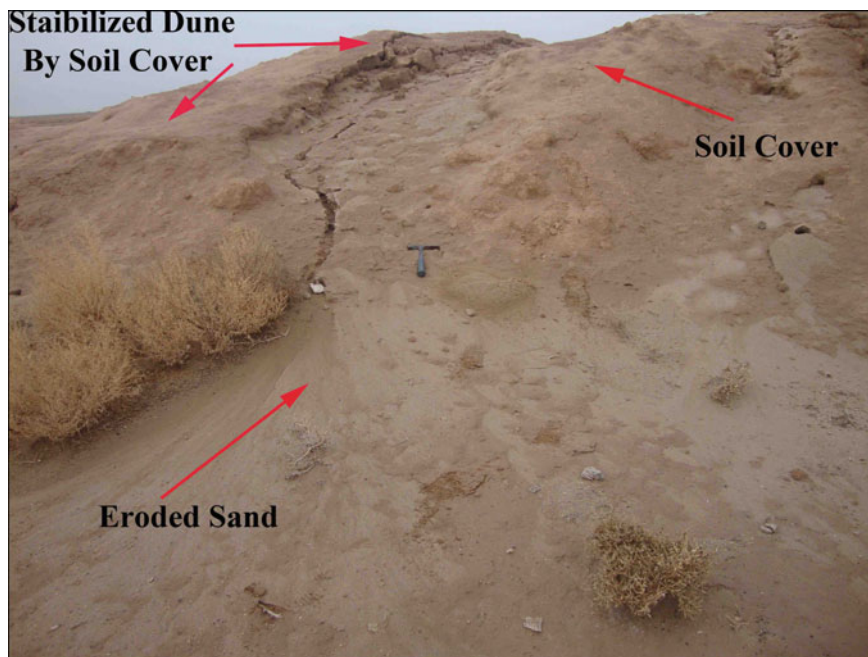


Fig. 3 Stabilized dune by soil cover around Qara Taba Archeological Site eroded. Chailat dune fields, Missan Governorate

a holy site, in which the sand dunes of Albu-Tarfa Dune Field are creeping on the building of the holy site (see Fig. 5). Vegetation of the surrounding area may protect this place from a further accumulation of sand dunes.

5.1.2 Road and Railway Obstruction

Creeping of sand dunes on roads forming obstacles to the transportation network was observed in most of the studied areas in Missan, Thi-Qar, and Al-Muthana Governorates (Figs. 6, 7, 8, 9 and 10).

These hazardous effects lead to environmental and economic losses to many governorates as many important local and main roads are interrupted or closed. As a suggestion to solve this problem, one must determine the mainstream direction of the wind regime in which the sand dunes are transported. The information gathered from these directions may be exploited to prevention the arrival of the sand dunes to preserve the established roads and highways. Upon future roads and highways constructions, dune forming winds may be avoided depending on the selection of least affected areas. Sand dunes cover the mainline of the Baghdad-Basra railway, which passes through Al-Muthana Governorate in many scattered locations (see Fig. 11). This problem is may cause many problems and accidents, and it needs adequate solutions.



Fig. 4 New sand dune deposited in the QaraTaba archeological hill, Missan Governorate, southern Iraq

5.1.3 Soil Destruction and Agricultural Benefits

Many agricultural areas within Missan, Thi-Qar, and Al-Muthana dune fields are observed to be affected by sand dunes migration resulting in decreased agricultural areas and an increase in dunes area (Figs. 12, 13, 14, 15 and 16).

A practical solution in such areas is by mixing a certain amount of sand dunes with the soil, and such a solution was found very successful in eliminating the dune sands on the one hand and fertilizing the soil on the other hand (see Fig. 17).

5.1.4 Creeping on Oil Installations and Buildings

Many buildings and oil installations in Thi-Qar and Missan Governorates are affected by the sand dunes migration causing many economic and environmental hazards. The fences surrounding these installations are observed to cause the accumulation of sand dunes, as these fences act as traps. Thus, the situation worsened as the creeping sand moved over these fences and overridden these installations (Figs. 18, 19 and 20).

A solution that may be suggested in such a case is to cover the surrounding area with vegetation belts that stabilize the active sand dunes. The main wind direction

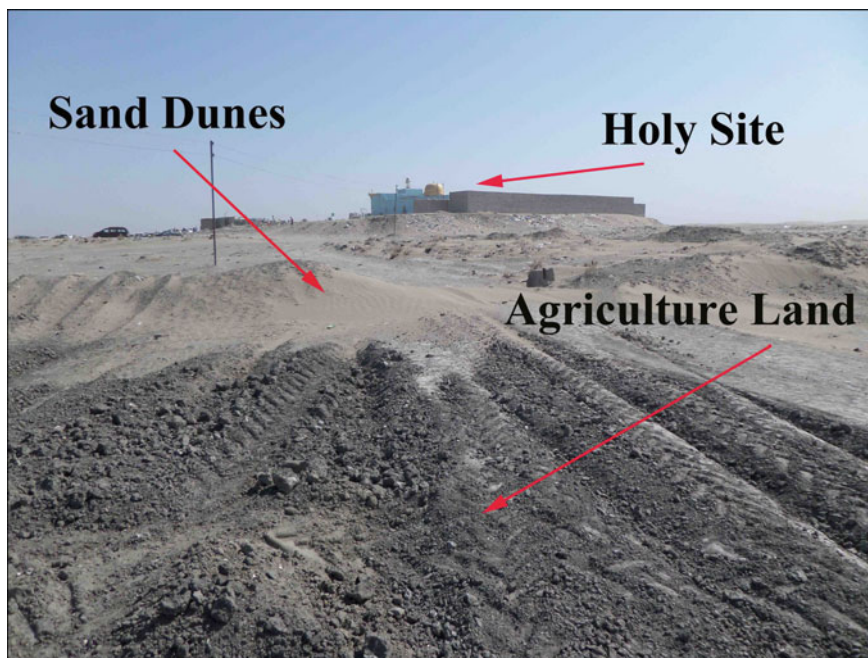


Fig. 5 Holy site in Thi-Qar Governorate showing creeping by sand dunes

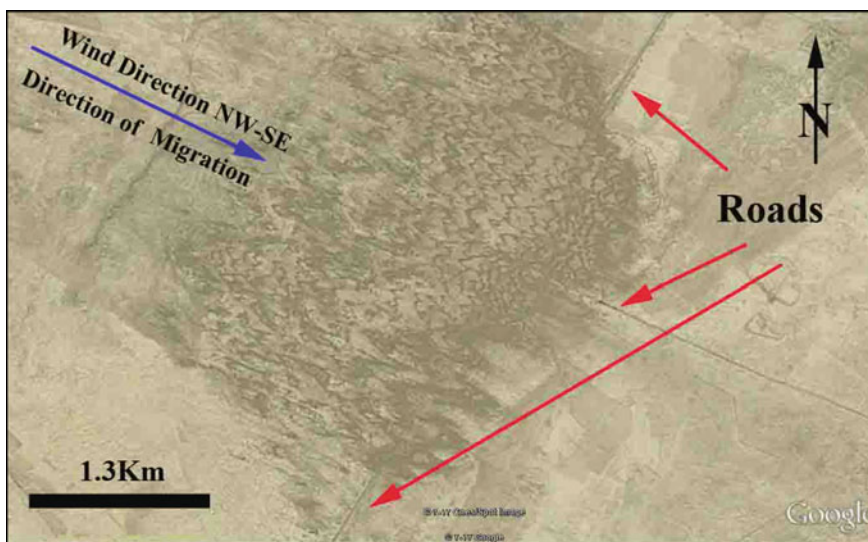


Fig. 6 Google Earth image shows the migration of dunes on the net of roads in Missan Governorate dune fields



Fig. 7 Main road closed by migration of sand dunes in Missan Governorate, Middle Chailat dune field

causing the sand dunes may be considered when planning future installations in establishing these projects.

5.1.5 Burial of Seasonal and Artificial Channels

One of the outstanding geomorphological features is the seasonal rivers found due to the higher slope of the Himreen Anticline in the east of Missan dune fields and the artificial channels for groundwater pumping. During sand movement and migration periods (in Spring and Summer), these channels are filled with dune sands (Figs. 21, 22 and 23). However, in winter and during rainy seasons and water supplies, the sand dunes will be collapsed and be obliterated.

5.2 Geological Maps of Iraq

Geological maps of Iraq for the years 1986, 2000, and 2012 constructed by [28–30], were used to compare the changes in the spatial model of the different sand dune fields. These comparisons include the following Fields:



Fig. 8 Road closed by migration of sand dunes in Missan Governorate, Middle Chailat dune field

5.2.1 Missan Dune Fields

Comparison between the geological map of Missan dune fields for the years 1986, 2000, 2012 shows that there is a evident change in the area of Missan dune fields, in which an increase in the trend of the main belt towards the north west of Missan Governorate (to Shihabi and Badra in Wasit Governorate) (see Fig. 24).

Al-Shakeri and Jasim [31] state that the new creep area is considered an early stage of dune formation in the form of Nabkha dunes in Badra area. These dunes represent a direct indication of the expansion of the eastern belt of sand dunes of Iraq (see Fig. 25).

Al-Muthana Dune Fields

Comparison between the geological maps of Al-Muthana dune fields for the years 1986, 2000, and 2012. Figure 26 shows that 1986 an absence of Samawa-Najaf dune field was absent, while in 2000, this field formed between Al-Muthana and Al-Najaf Governorates. In 2012 the field expanded towards the south west of Samawa. Nowadays, the belt expanded to the south east of Samawa towards Nasiriyah and Basra and may continue to the Kuwait Borders.

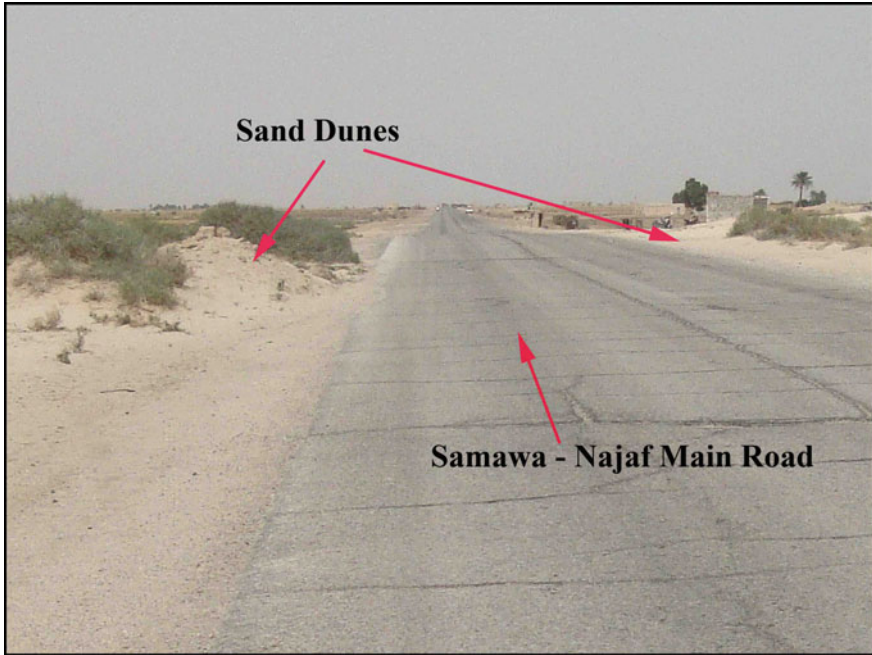


Fig. 9 Main road of Samawa-Najaf showing the sand dune creeping

5.2.2 Thi-Qar Dune Fields

Comparison between the geological maps of these fields for the years 1986, 2000, and 2012, show the central belt of sand dunes (Nasiriyah Dune Field) has endured several stages of accumulations, and migrations leading to the expansion of the fields towards south east, north west, and laterally (see Fig. 27).

In 1986, this field occupied areas reaching closer to Nasiriyah city in the south and away from Hor Al-Dalmaj in North West of Nasiriyah. Al-Ezerajawi [32] noticed the presence of sand dunes surrounding the Hor Al-Dalmaj in Wasit Governorate. In 2000, and 2012 the affected areas are stretched laterally, thus covering areas such as the old arid marshes of Albu-Tarfa at the north of Nasiriyah City (see Fig. 28), [33]. Nowadays, the expansion of Nasiriya dune field reaches the out outskirts of Nasiriyah city.

5.3 Remote Sensing and GIS Techniques

Remote sensing can be defined as “the art, science, and technology of obtaining reliable information about physical objects and the environment through which the processes of recording, measuring, and interpreting imagery patterns derived from



Fig. 10 Sand dunes deposited on the side of the road in Thi-Qar Governorate



Fig. 11 Creeping of sand dunes on railway in Al-Muthana Governorate

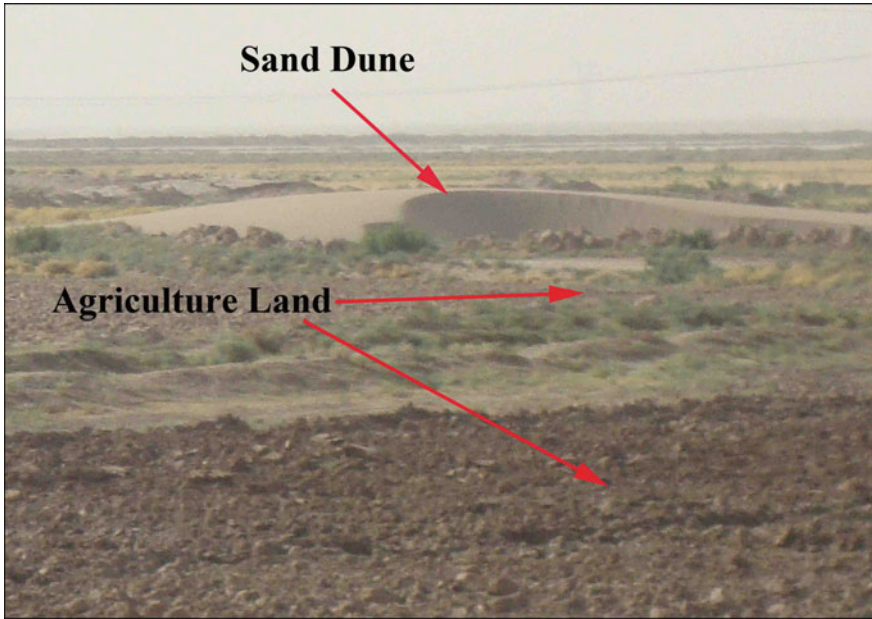


Fig. 12 Sand dune deposited on farmland in Chailat area, Missan Governorate

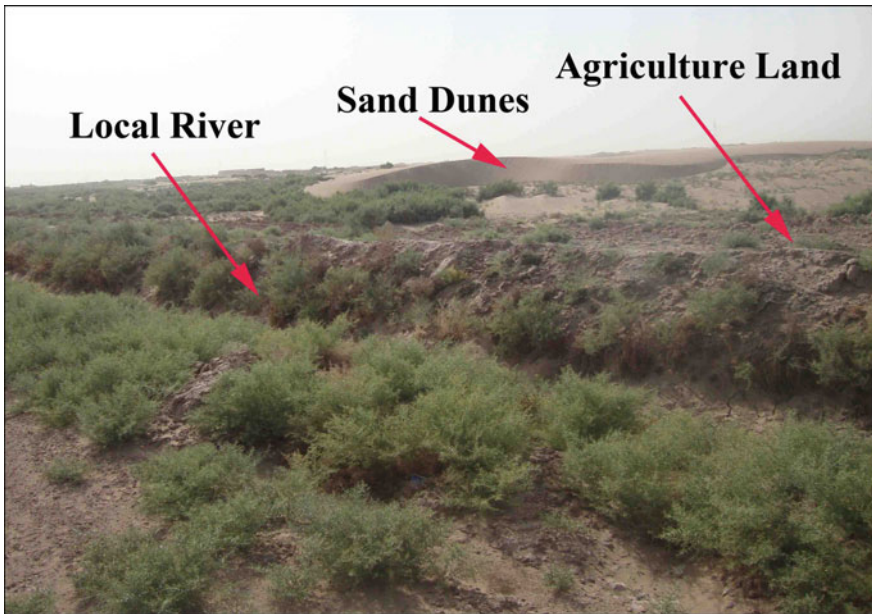


Fig. 13 Sand dune deposited on farmland in Chailat area, Missan Governorate

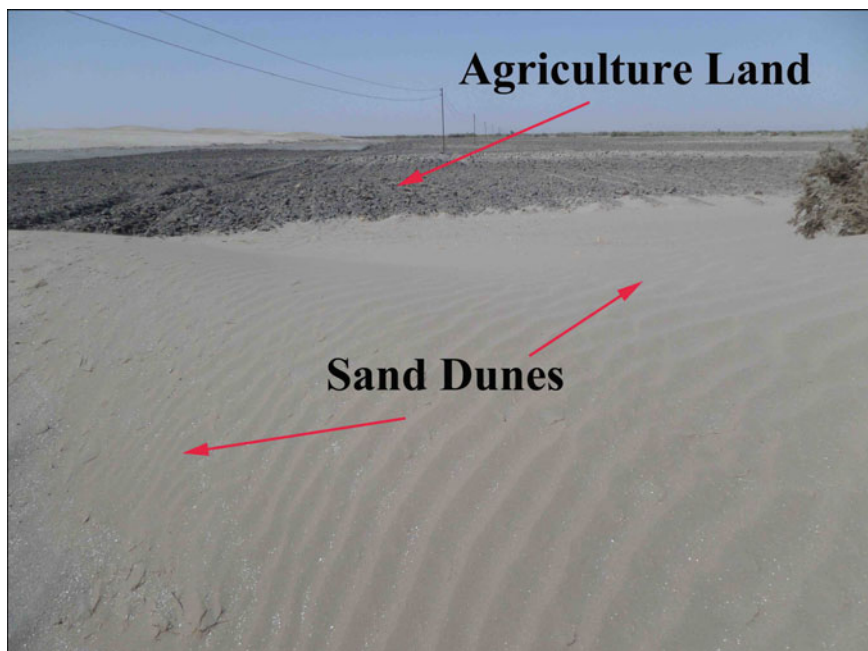


Fig. 14 Sand dune deposited on farm and in Albu-Tatfa dune field, Thi-Qar Governorate

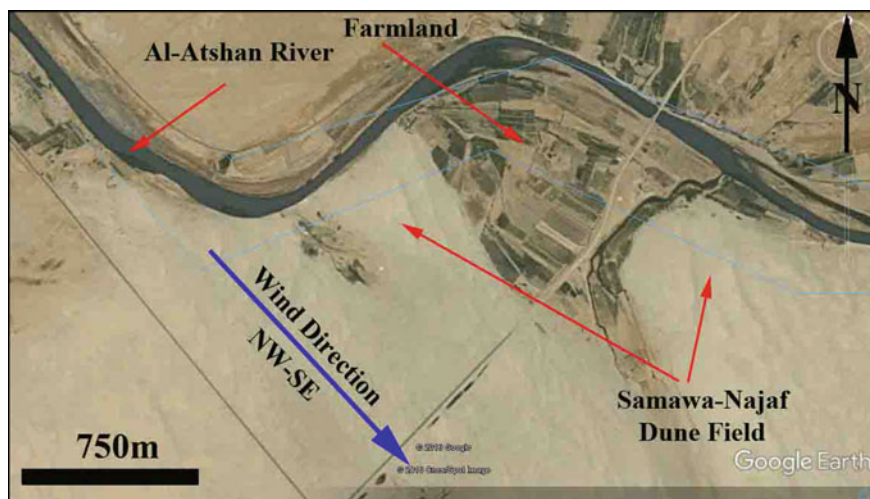


Fig. 15 Google Earth image shows the migration of dunes on the farmland in the Al-Muthana Governorate

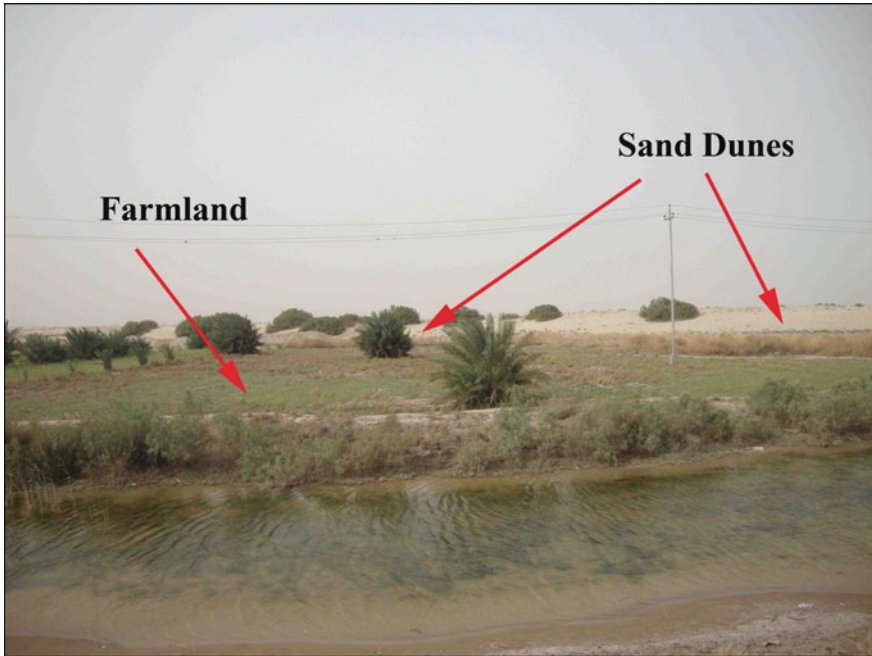


Fig. 16 Creeping of sand dunes on the farmland in Al-Muthana Governorate

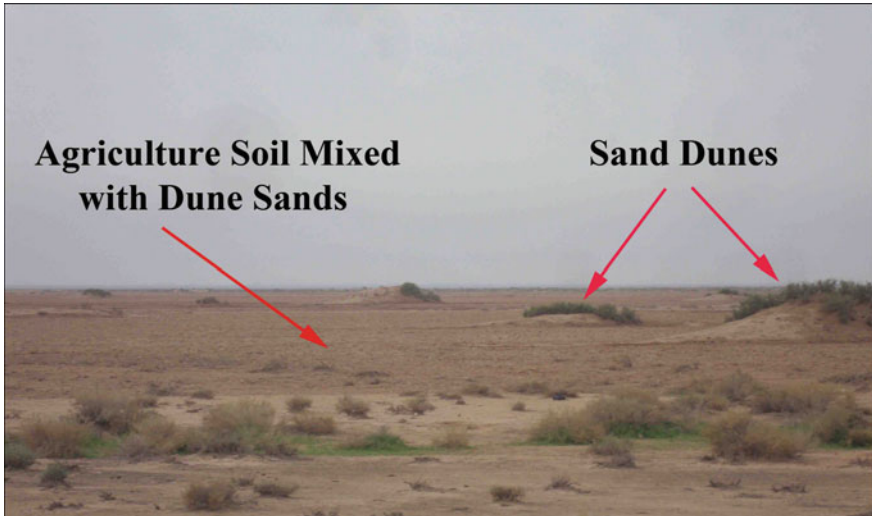


Fig. 17 Agricultural soil mixed with dune sand in Middle Chailat dune field. Missan Governorate



Fig. 18 Sand dunes creeping over fences of oil insulation in Thi-Qar Governorate



Fig. 19 Sand dunes inside the oil insulation camp in Thi-Qar Governorate

non-contact sensor systems” [34]. Remote sensing techniques could be used effectively to monitor sand dune movements by comparing the multi-temporal satellite images [35]. The importance of remote sensing in monitoring and mapping degradation and desertification in arid and semi-arid regions is widely recognized and well



Fig. 20 Dune sand creeping on the soil bar for stabilizing sand dunes migration (the bar traps the dune sands) in Middle Chailat dune field. Missan Governorate

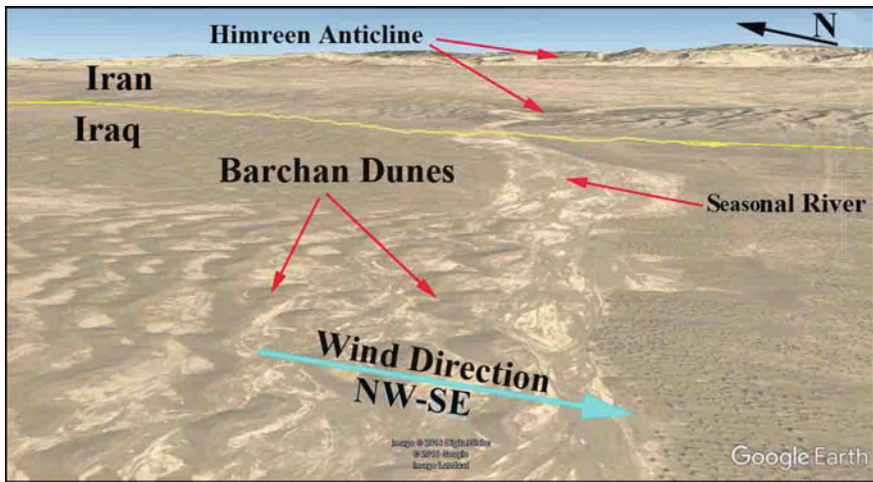


Fig. 21 Inclined Google Earth view shows the sand dune occupying temporary the channels in Missan dune field

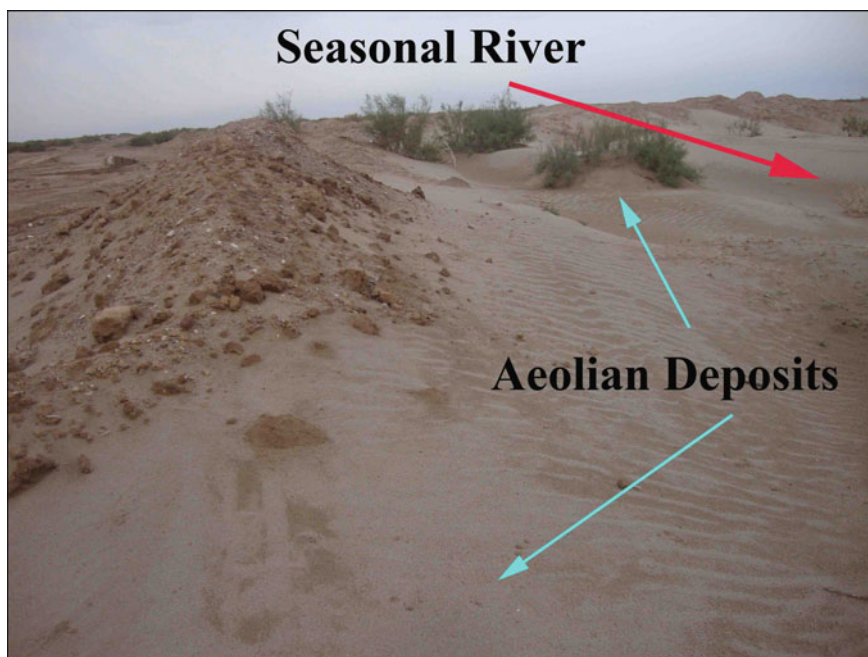


Fig. 22 Aeolian deposits were occupying the seasonal river in Missan dune field

developed in various fields. It is well known that remote sensing has initially been used primarily for resource mapping and inventory. Many experiments, however, proved that remote sensing systems and, in particular, earth observation satellites provide significant contributions to desertification assessment and monitoring. The developments in satellite technologies and remotely sensed image acquisition and analysis offer adequate opportunities for monitoring land cover change in such areas. The integration of remote sensing and Geographic Information Systems (GIS) has been widely applied and been recognized as a powerful and effective tool in detecting land use and land cover change [36–39]. Satellite images (Landsat 5 and Landsat 8) covering the period from 1992 to 2016 were used to monitor the various changes within the studied area; such an approach requires more information to reach a conclusive result. This work tackled the following areas:

5.3.1 Samawa-Najaf Dune Field

This field shows changes during the period from 2006 to 2014. A notable expansion in area is observed (see Fig. 29). The cause of such expansion seems to be related to the desertification conditions that affected this area causing the vegetation cover to decrease. A possible solution is to maintain the water resources necessary to increase the vegetation cover and stabilize the soil and thus the dunes.



Fig. 23 Artificial channel for pumping ground water occupied by dune sands in Missan Governorate

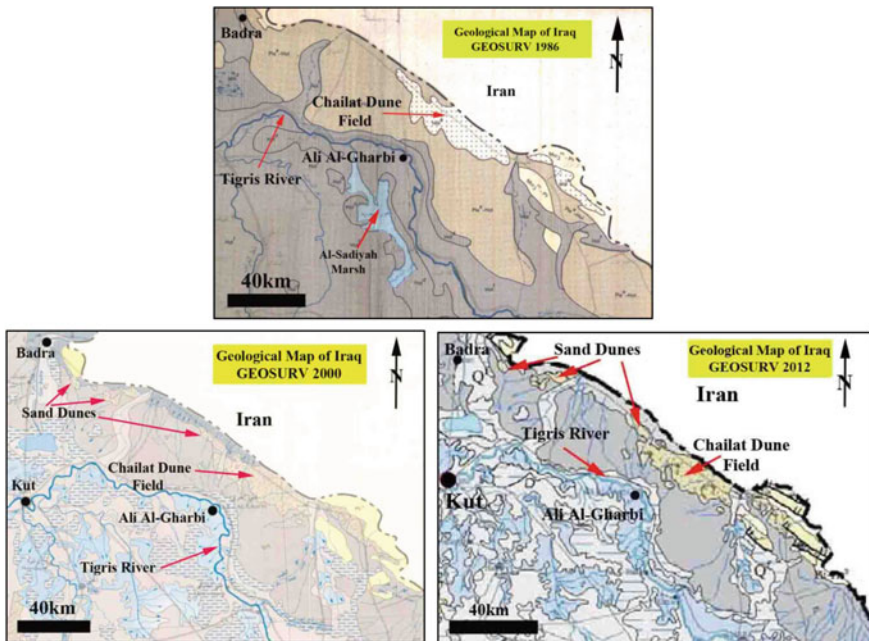


Fig. 24 Geological maps of east Missan and Wasit Governorates after [28–30]



Fig. 25 Nabkha dunes in Badra area, Wasit Governorate (after [31])

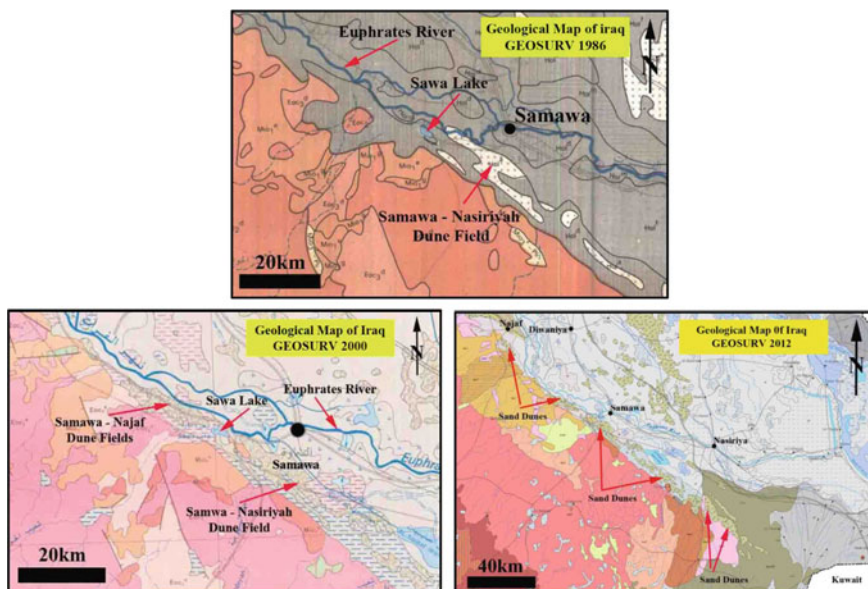


Fig. 26 Geological maps of Al-Muthana Governorate after [28–30]

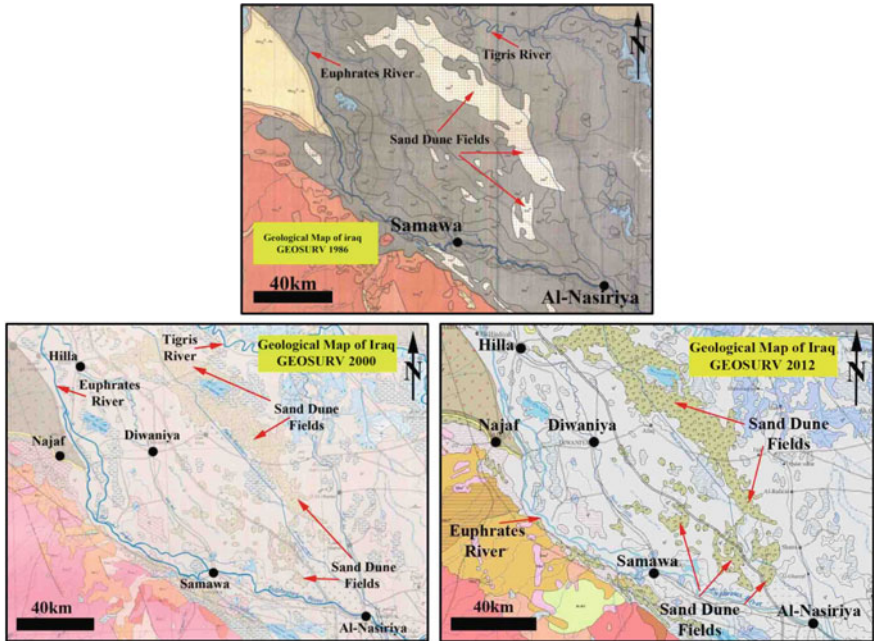


Fig. 27 Geological maps of Thi-Qar Governorate after [28-30]

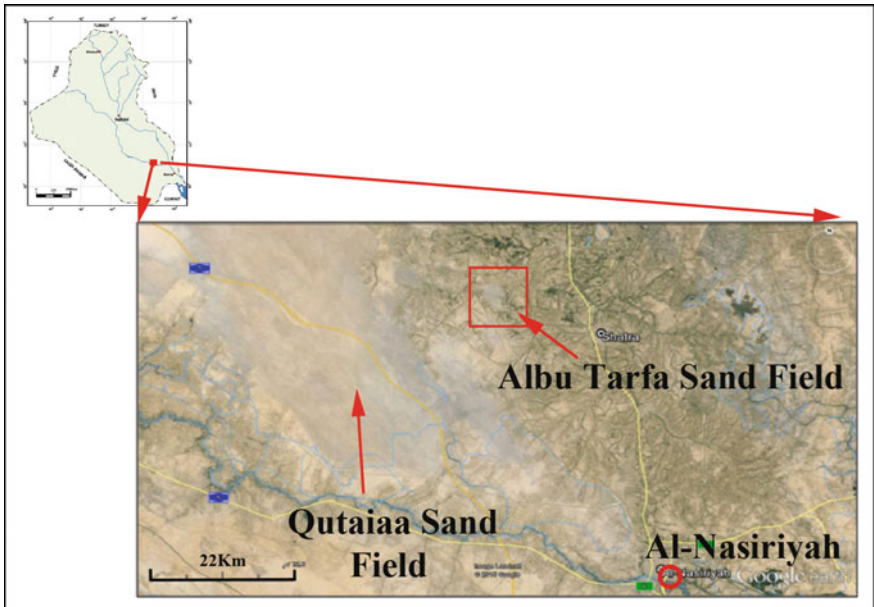


Fig. 28 Google Earth image of Albu-Tarfa Dry Marsh occupied by sand dune field

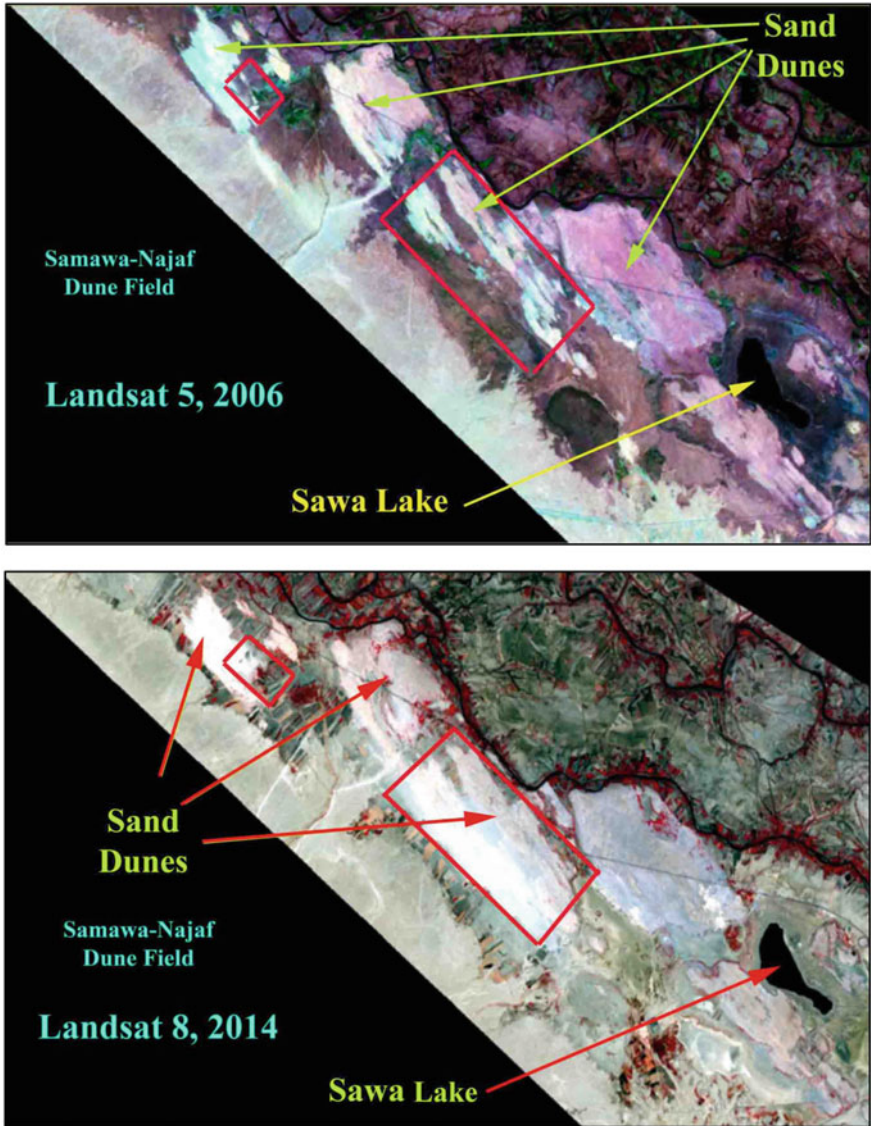


Fig. 29 Satellite images of Samawa-Najaf dune field (Landsat, 5 and Landsat, 8)

5.3.2 Samawa-Nasiriyah Dune Field

This field shows an expansion in the area from 2006 to 2014, as shown in Fig. 30. In which the area during 2006 was well vegetated and have a low occurrence of sand dunes, while in 2014, the vegetated area has vanished and been replaced by significant

accumulations of sand dunes. These changes are a good proof of the desertification stage in the area.

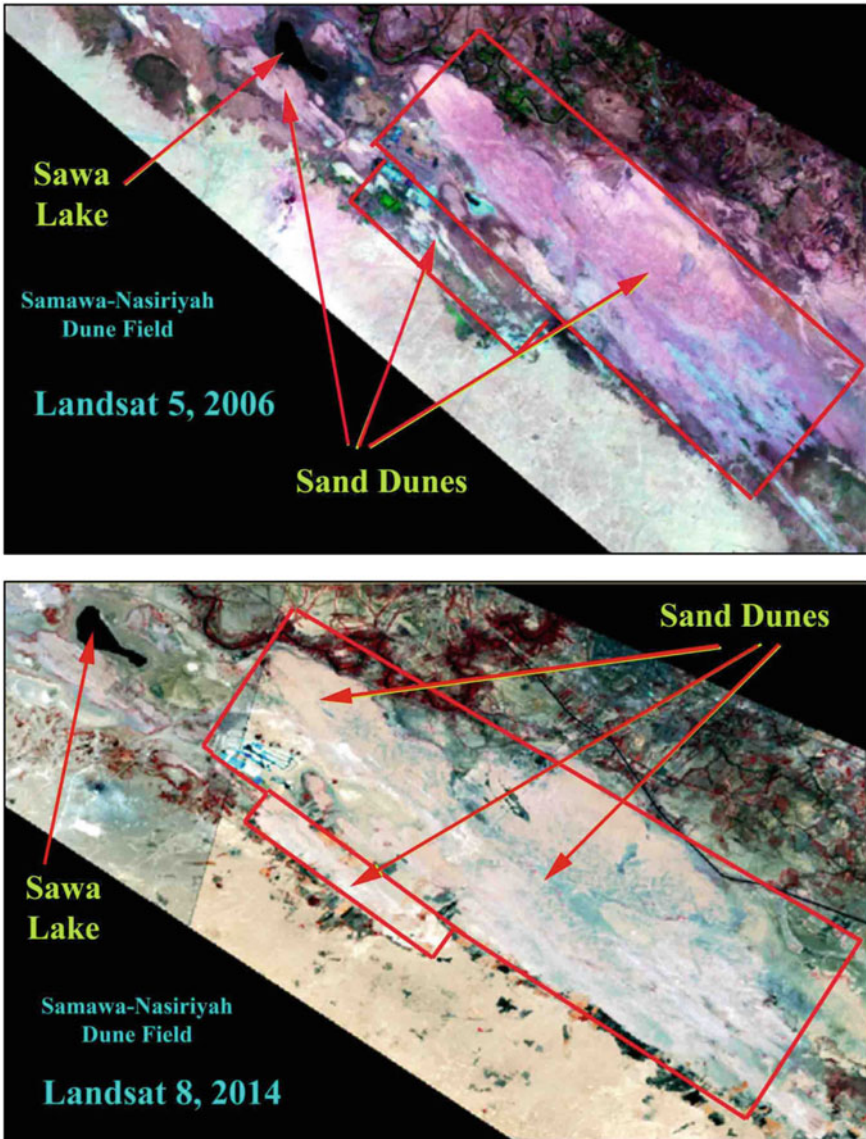


Fig. 30 Satellite images of Samawa-Nasiriyah dune field (after [40] and [41])

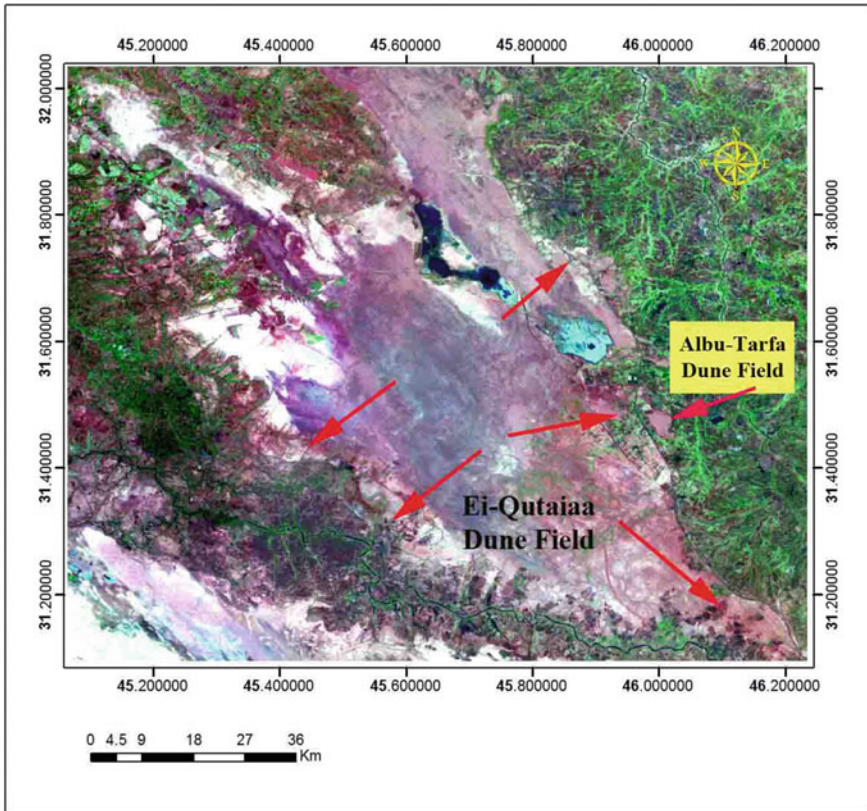


Fig. 31 Satellite image of Nasiriyah dune field (after [40])

5.3.3 Thi-Qar Governorate Dune Fields

This large field shows lateral and longitudinal expansions in which the former is situated in the eastern side of the field (east of El-Qtaiaa dune field) to Albu-Tarfa dune field, while the latter shows an extension towards Nasiriyah city (to the south east), which is shown in Fig. 31.

5.3.4 Missan Governorate Dune Fields

During the period between 1992 to 2016, this is shown in Fig. 32. Missan dune fields show an expansion laterally and longitudinally. In 1992, the area had good drainage in which many local and seasonal rivers were occupying the area, as a result, the area was well vegetated. The water resources to the area began to deteriorate and cause the area to enter the desertification stage, which is well shown in 2016. The sand dunes area increased at the expense of the high water supplied area.

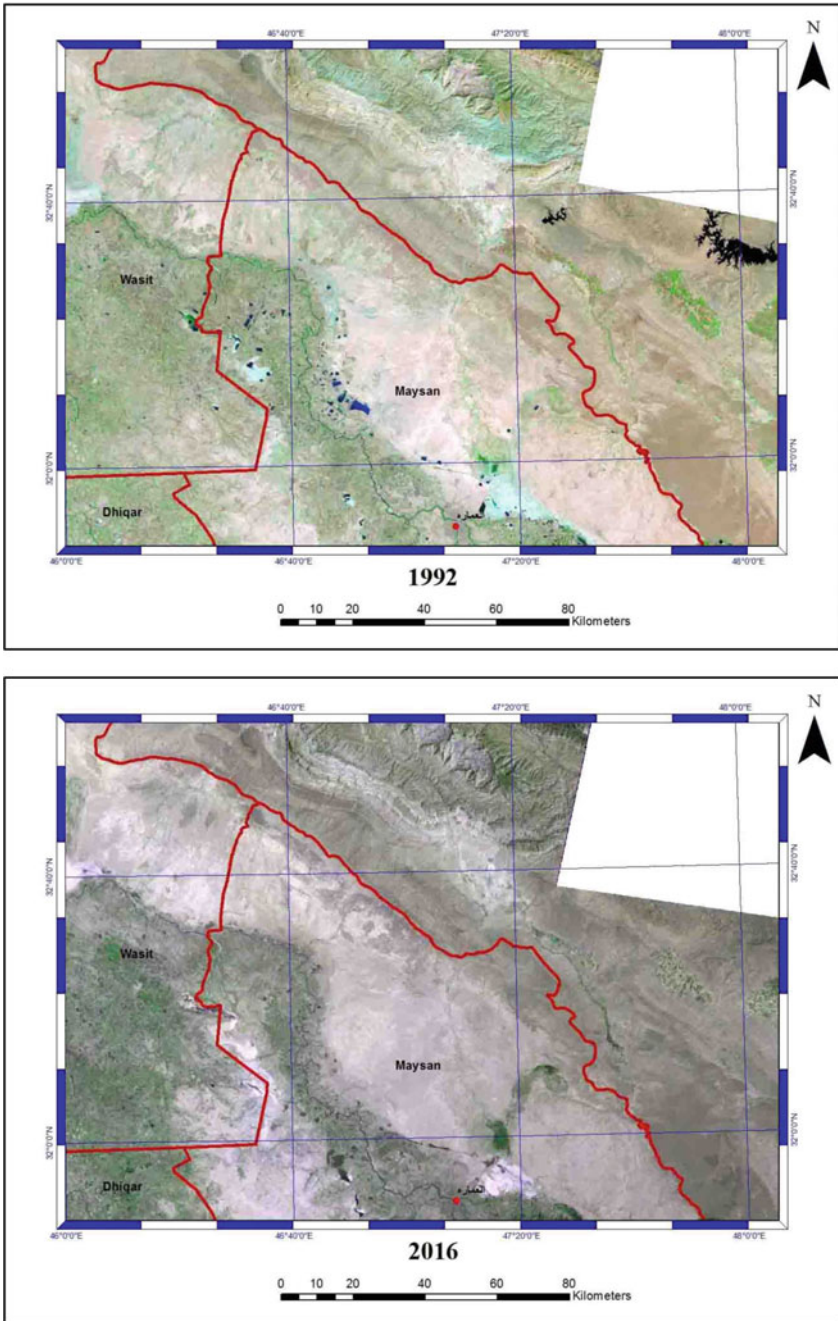


Fig. 32 Satellite images of Missan dune fields from period 1992 to 2016 (after [41])

6 Conclusions

There is a great deal of matching between the field-work, a geological map of Iraq, and GIS data concerning the distribution of dunes fields in the different studied belts, in which the well-vegetated area and good water supplied areas show a decline in which the area of sand dunes attained a high pace of accumulation which is mainly caused by desertification conditions in the area of study. Summing up the solution to the aeolian hazards in the studied area following suggested methods for limiting the sand dunes accumulation migration on the different observed sites and areas. An alternative solution might suggest dealing with this problem in which the dunes may be considered an economic deposit depending on their mineralogical composition and texture.

7 Recommendations

The sand dune fields must be monitored periodically by carrying out seasonal field work, and dune fields, especially creeping and active fields, by means of satellite images, and periodically to control the hazards resulting from the encroachment of sand dunes. Before constructing the various types of civil structures, a study should be made of wind directions and the extent to which sand dunes are close to these facilities. The agricultural lands must be protected from the creeping of sand dunes on them by making belts of suitable trees that prevent the creeping of sand dunes on the agricultural lands.

References

1. UNEP. WMO. UNCCD (2016) Global assessment of sand and dust storms. United Nations Environment Program, Nairobi, 139 pp
2. UNEP (1992) World Atlas of desertification. Edward Arnold, Seven Oaks, 69 pp
3. Albusoda BS, Salem LA (2012) Stabilization of dune sand using Cement Kiln Dust (CKD). *J Earth Sci Geotech Eng* 2(1):131–143
4. Montgomery CW (2006) Environmental geology, 7th edn. McGraw and Hill Companies Inc., Boston, 346 pp
5. Perry C, Taylor K (2007) Environmental sedimentology. Blackwell Publishing Ltd., 441 pp
6. Kassas M (1995) Desertification: a general review. *J Arid Environ* 30:115–128
7. Agnew C, Warren A (1996) A framework for tackling drought and land degradation. *J Arid Environ* 33:309–320
8. Warren A, Sud YC, Rozanov B (1996) The future of deserts. *J Arid Environ* 32:75–89
9. Verstraete MM (1986) Defining desertification: a review. *Clim Change* 9:5–18
10. Dregne HE (1986) Desertification of arid lands. In: El-Baz F, Hassam MHA (eds) *Physics of desertification*. Martinus Nijhoff Publishers, Dordrecht, pp 4–34, 473 pp
11. Muhs DR, Maat PB (1993) The potential response of Aeolian sands to greenhouse warming and precipitation reduction on the Great Plains of the U.S.A. *J Arid Environ* 25:351–361

12. Thomas DS, Knight GM, Wiggs GFS (2005) Remobilization of Southern African desert dune systems by twenty-first century global warming. *Nature* 435:1218–1221
13. Alexander W (2007) Locally-developed climate model verified: climate prediction. *Water Wheel* 6(1):27–29
14. Bagnold RA (1941) *The physics of blown sand and Desert Dunes* Methuen and Co. Ltd. London, 256 pp
15. Walker AS (2007) Introduction to Aeolian land forms, *Goddard Earth Sciences. Data and Information Services Center Chap. 8: 1–14*
16. Lancaster N (1997) Response of Aeolian geomorphic systems to minor climate change: examples from the Southern Californian Deserts. *Geomorphology* 19:333–347
17. Knight MD, Thomas SG, Wiggs GFS (2004) Challenges of calculating dune field mobility over the 21st century. *Geomorphology* 59:197–213
18. Tosar H (2005) Sand dunes mobility and stability in relation to climate. *Phys A* 357(1):50–56
19. Yizhaq H, Ashkenazy Y, Tosar H (2007) Why do active and stabilized dunes coexist under the same climatic conditions. *Phys Rev Lett* 98:188001
20. Arens SM, Slings Q, Geelen L, Van der Hagen H (2007) Implications of environmental change for dune mobility in the Netherlands, Paper Presented at International conference on management and restoration of coastal dunes, Minist. De Medio Ambiente, Santander, Spain, 3–5 Oct
21. Dougrameji JS (1979) Some physical properties of sandy soil sand dunes in Iraq. *FAO Soil Bulletin No 25, Rome, Italy*
22. Fadhil AM (2002) Sand dunes fixation in Baiji District of Iraq. *J China Univ Geosci* 13(7):67–72
23. Dougrameji JS, Kaul RN (1999) Aeolian sediment movements in the Lower alluvial plan, Iraq. *Desertification Control Bull* 35:45–49
24. UNCSCO (2015) *Newsletter III(1)*
25. Al-Ansari NA (2013) Management of water resources in Iraq: perspectives and prognoses. *Engineering* 5:667–684
26. Chulov M (2009) Water shortage threatens two million people in southern Iraq. *The Guardian*. <http://www.theguardian.com/world/2009/aug/26/water-shortage-threat-iraq>
27. Al-Ansari NA, Knutsson S, Ali A (2012) Restoring the Garden of Eden, Iraq. *J Earth Sci Geotech Eng* 2:53–88
28. Jassim SZ, Hagopian D, Al-Hashimi H (1986) Geological map of Iraq, 1:1 000 000 scale series. Geological Map Publication of GEOSURV, Iraq, Baghdad
29. Sissakian V (2000) Geological map of Iraq, 1:1 000 000 scale series. Geological Map Publication of GEOSURV, Baghdad
30. Sissakian V, Fouad SF (2012) Geological map of Iraq, 1:1 000 000 scale series. Geological Map Publication of GEOSURV, Baghdad
31. Al-Shakeri AJ, Jasim HK (2016) Juvenile Aeolian Deposits at Badra Area—Eastern Iraq. *J Environ Earth Sci* 6(1). ISSN: 2225-0522
32. Al-Ezerajawi WM (2012) Environmental study of Dalmaj Marsh Area—Wasit Governorate-Iraq. Unpublished, MSc, thesis University of Baghdad, 123 pp
33. Jasim HK, Al-Shammery Th (2016) Environmental degradation in Albu Tarfa Area Thi-Qar Governorate Southern Iraq. *J Environ Earth Sci* 6(8). ISSN 2224-3216 (Paper). ISSN 2225-0948 (Online)
34. Colwell RN (1997) *Manual of remote sensing, 2nd edn.* American Society of Photogrammetry, Falls Church, Virginia
35. Hereher M (2000) A study on sand dunes fields in North Sinai and the environmental risk assessment of Aeolian processes. MSc thesis, Faculty of Science (Dumyat), Mansoura University, Egypt. <http://landsat.usgs.gov/banddesignationsLandsatsatellites>
36. Elhers M, Edwards G, Bedar Y (1990) Integration of remote sensing with geographic information systems: a necessary evolution. *Photogramm Eng Remote Sens* 55(11):1619–1627
37. Trietz PM, Howarth PJ, Gong P (1992) Application of satellite and GIS technologies for land cover and land use mapping at the rural urban fringe: a case study. *Photogram Eng Remote Sens* 58(4):127–150

38. Fadhil AM (2009) Land degradation detection using geo-information technology for some sites in Iraq. *J Al-Nahrain Univ* 12(3):94–108. <https://doi.org/10.22401/JNUS.12.3.13>
39. Fadhil AM (2013) Sand dunes monitoring using remote sensing and GIS techniques for some sites in Iraq. In: Proceedings volume 8762, PIAGENG 2013: intelligent information, control, and communication technology for agricultural engineering, p 876206. <https://doi.org/10.1117/12.2019735>
40. USGS (2015) Landsat8 Operational Land Imager (OLI) and Thermal Infrared Sensor (TIRS)
41. USGS (2006) Landsat5 Operational Land Imager (OLI) and Thermal Infrared Sensor (TIRS)

Amu Darya Dynamics in Afghanistan Using Remote Sensing Data



Mohammad Asef Mobariz and Gordana Kaplan

Abstract Land degradation due to river dynamics is a significant problem worldwide. As people have settled near rivers, river dynamics cause severe material damage. This situation is getting more complicated when the same water bodies are the international border between two or more countries, making it a geopolitical problem. This natural disaster's mapping and monitoring are possible with remote sensing data and geoinformation technologies. The land cover changes and river dynamics of international borders and their surroundings were investigated using remote sensing satellite imagery in Google Earth Engine's cloud-based platform. The most significant contribution of this chapter is that it points out a significant problem many local people are facing, mainly in developing countries. However, it should also be stated that this is also a global problem. The Amu Darya river case study is just an example of what many local people mainly depend on agriculture. Here we use remote sensing data to investigate the channel changes and dynamics of the Amu Darya river along Afghanistan's border. The main goal is to map and analyze the land cover changes of four classes over the study area and determine land degradation from 1990 to 2020. Also, seasonal land degradation has been investigated. The results showed that monitoring river dynamics could be done with satellite remote sensing data, and it can be used to timely monitor water bodies dynamics. National and international administrations can use such data to resolve geopolitical problems due to due to unresolved water-sharing policies.

Keywords Remote sensing · GIS · River dynamics · Land degradation · Geopolitics

M. A. Mobariz

Institute of Earth and Space Sciences, Eskisehir Technical University, Eskisehir 25555, Turkey
e-mail: m.asefmobariz@gmail.com

G. Kaplan (✉)

Institute of Graduate School, Eskisehir Technical University, Eskisehir 25555, Turkey
e-mail: gkaplan@eskisehir.edu.tr

1 Introduction

The inability of the ecosystem to heal itself unaided after a significant loss is called land degradation. Land degradation as one type of environmental degradation can happen in different types, namely physical, chemical, and biological. Water erosion, or soil erosion, is the primary type of physical land degradation. Physical land degradation is a significant problem for the local people and the environment all around the world. People's dependence on water is clear as more than 80% of the world's population live on previously flooded land, whereas 90% are settled along a river [1]. Thus, water erosion is a significant problem in undeveloped countries, especially for the local people who mainly depend on agriculture. Water erosion is one of the natural degradation hazards. This type of land degradation is; high-intensity rains, steep slopes, and soils with a low resistance to water erosion. More than 20% of the international borders are represented by rivers [2]. The number of international borders as the river is the highest in South America and lowest in Asia. The division of states, cities, and countries with water bodies often causes political controversies. Also, river dynamics cause a considerable hazard to those in the surrounding area [3]. River dynamics are natural occurrences mainly caused by anthropogenic activities such as dam constructions, irrigation infrastructure construction, land-use changes, and climatic factors [4]. Understanding, monitoring, and mapping the rivers are essential to prevent and lower the hazards caused by the river channel dynamics. If the river is transboundary and has natural hazards, it can also cause geopolitical problems [5, 6]. Shared waters have been a reason for conflict in many parts of the world [7].

The Amu Darya river is prone to conflicts and to land degradation. The Amu Darya river, shared by Tajikistan, Afghanistan, Uzbekistan, and Turkmenistan, also represents Afghanistan, Tajikistan, and Uzbekistan. Flowing from the highest mountains in the region, Amu Darya continues its journey in the flat areas of Central Asia and Afghanistan. The river dynamics make it challenging for the local people to claim their rights [5]. Researchers [8] have been searching for solutions for managing shared water resources in the Aral Sea Basin. The lack of effective management of the water caused severe consequences for the natural environment, the human population, and the economies of the sharing countries [9]. The Aral Sea Basin is extending over parts of five Central Asian Republics. The spring of the Amu Darya river is in the mountains of Afghanistan and Tajikistan. Through Uzbekistan and Turkmenistan, the river flows into the Aral Sea [10]. As agreements for shared water resources did not succeed, the economic and environmental state's vulnerability can increase, and a political conflict can emerge [9]. Bekchanov et al. clearly stated the importance of action in the Aral Sea Basin to stop the crisis that affects millions of people, with increased mortality rates, disease and health disorders [11].

Geospatial data and tools have become valuable tools for mapping and monitoring land use and river dynamic changes worldwide. However, remote sensing has not been widely used for waterways as political borders. Using Landsat data, Popelka and Smith [2], recently a new geospatial database of the world's river borders for

large rivers has been made. In their study, Langat et al. [4] combined satellite imagery from Landsat with aerial imagery to monitor the river dynamics over Tana, Kenya. Thus, they were able to analyze the temporal and spatial channel changes of the river from 1975 to 2017. Similarly, Billah [12] used Landsat imagery to map and monitor the erosion and accretion in the Padma river, Bangladesh, from 1975 to 2015. Remote sensing data and geoinformation techniques have been successfully used for river channel dynamics [1, 4, 13–17]. With geoinformation systems, remote sensing data can provide excellent river channel dynamics, processing, visualization, and analysis tools. Remote sensing data can be used for land use/land cover maps, and with spatial analysis, the land cover changes can be determined. Also, not many studies can be found in the literature investigating transboundary waters. This leaves space in the literature to monitor transboundary rivers and river dynamics using remote sensing and geo-information systems. River morphology changes in varying environmental conditions due to the shifts of the river bank and the river's water flow through natural and anthropogenic inputs.

Some of the river morphology processes are channel dynamics, discharge, runoff events, sediment supply, and vegetation cover. Also, channel shifting and its response to changing environmental conditions are highly reliant on local factors (for example, channel type, hydrologic, and vegetation conditions) affected by anthropogenic activities. The processes attributed to channel shifting and assessing river morphological change has long been of interest to geologists, geomorphologists, and engineers. Geo-information systems and remote sensing technologies have proven helpful for mapping and monitoring river resources [4, 12, 14, 15]. To better understand the importance of remote sensing data and technologies for river channel dynamics, first, we need to define the term river channel dynamics. Before we investigate the dynamics of Amu Darya, a detailed literature review of remote sensing use will be given.

1.1 River Channel Dynamics

River dynamics are a significant cause of land degradation. Riverbank changes and are connected to both natural and anthropogenic activities. The anthropogenic activities have become more recent than the natural causes, such as excessive or insufficient precipitation [4].

The importance of water is clear as it is essential for life on Earth. Waterways create distinctive stream designs such as braided and meandering depending on the discharge regime, sediment load, hydrodynamic forces, and floodplain properties [18]. Stream morphology changes in changing natural conditions over spatial and temporal scales due to the erosion and accretion of the waterway bank and the river's water stream through common and anthropogenic inputs. Control waterway morphology forms incorporate channel flow, release, runoff occasions, dregs supply, and vegetation cover. In expansion, channel moving and its reaction to changing

natural conditions depend on nearby components influenced by anthropogenic unsettling influences. Thus, understanding the processes attributed to channel shifting and assessing river morphological change has long been of interest to geologists, geomorphologists, and engineers [19]. In the last few years, significant progress has been noticed in understanding channel morphology and elucidating the channel's shifting in the platform of a river basin. Subsequently, studies of channel morphology are fundamental to assess the common and human impacts on morphometric parameters and channel flow amid this time. However, forecasts of channel's reactions are a complicated assignment. Successful variations react to the changes within the waterway bowl. In recent studies, most channel morphology studies have focused on the deterministic model; however, the river system is energetic and stochastic. Freshwater resources such as lakes and rivers are the most politicized natural resources. There are over 250 rivers worldwide transboundary borders. Worldwide basins cover more than 45% of Earth's surface. With a dynamically water-stressed world, shared water resources can along these lines be utilized as political inferences. In expansion, more than 40% of the world's populace depends on universal streams, and approximately 25% of these individuals live in creating nations. The battles and clashes for shared water assets increment political pressures between neighboring nations. Later research appeared that more than 300 arrangements bargain with shared water assets between nations [6].

In any case, since waterways are dynamic natural features, the moving of streams due to common erosion and sedimentation forms can make political issues between nations in terms of boundary definitions. In expansion, as normal assets are shared, stream boundaries are powerless to debate concerning viewpoints of water administration. Over the final 60 years, the Hirmand Waterway has changed its morphology. This is likely due to the changes that have happened within the hinterland. Several studies appeared that the land use inside a catchment incorporates a critical affect on the fluvial forms. Changes within the upstream regions of a catchment influence the hydrological, geomorphological, sedimentological, and biological working of a waterway.

1.2 Remote Sensing and River Dynamics

With geo-information systems, remote sensing techniques and data provide vital information on the erosional dynamics and intensity over time and space, that are useful for soil erosion assessment, control, and prediction. Research shows that soil erosion, crucial component of land degradation, comprising water and wind erosion, chemical degradation, excessive salts, and physical and biological degradation, is a severe global environmental problem [20]. Rapid population growth, deforestation, unsuitable land cultivation, uncontrolled, and overgrazing have accelerated soil erosion in the world's principally in developing countries [21].

The most convenient way to identify changes in water areas is by mapping and observing how they have changed over time. Due to erosion and deposition,

coastal zone management shifts in coastline position are a significant concern as very dynamic coastlines can cause considerable hazards to human use and development. Therefore, coastline mapping and measurement of coastline position changes are moreover fundamental for secure navigation, asset administration, natural assurance, and maintainable coastal improvement and arranging. Also, many coastal habitats are designated as particular conservation areas under the European Union's (EU) Habitats Directive. Thus, it is evident that rapid, replicable techniques are required to update coastline maps and monitor movement rates [22].

Earth Observation gives a well-suited innovation system for environmental mapping and observing, and it can give information required for spatial examination. The ability of Earth Observation technologies to provide accessible and continuous data is a significant advantage over the conventional methods. The detection of water bodies changes using satellite data has gained high importance in the last few decades. With satellite imagery is possible to define water areas and other land covers. Earth Observation provides a practical set of tools for analyzing and extracting spatial information to support reliable and consistent decision-making. The integration with GIS, provides an excellent framework for data capture, storage, synthesis measurements and analysis, all of which are essential in coastline changes investigations.

Integrating remote sensing data and technologies with geo-information systems has become an effective tool for mapping and spatial-temporal monitoring of land-use change. It provides a detailed understanding of the different functioning of ecosystems. Therefore, remote sensing data and techniques are the main tools in Earth observation sciences. Several studies have been carried out worldwide to study land-use and land cover changes through processing satellite images. The primary data source of this kind of study is the Landsat images. The Landsat program provides satellite images with a temporal resolution of 16 days that have provided free up-to-date images across the globe since 1972 [23, 24]. Image processing is the process of improving the quality of an image for analysis and manipulation.

Remote sensing technology is opening up modern conceivable outcomes for waterway science and management. With the use of multispectral data, water bodies can be mapped and monitored. With remote sensing data availability at broader scales and suitable accuracy, the possibilities to survey and characterize the hydro morphological features of river systems extensively at multiple scales, from catchment to reaches, is unprecedented. However, the information accessibility challenges existing information investigation abilities and requires modern statistical modeling systems to gotten to be reasonable for waterway characterizations and management [24].

Land degradation caused by stream bank erosion and its effects on channel evolution are essential geomorphic research problems relevant to many scientific and engineering fields. Remote sensing can provide large area data at regular intervals with a quick turnaround time integrated with GIS techniques. Remote sensing data has been used to study and monitor river erosion and its bank line shifting [25].

River morphological dynamics are natural autogenic occurrences for fluvial rivers resulting from discharge flow processes, debris and sediment transport, channel migration, and floodplain erosion and accretion. Riverbank erosion and accretion

and channel course changes are more related to climate change, discharge quantity and sediment type, and hydrologic regimen variations. However, basin-wide Anthropogenic advancement activities such as hydroelectric dam development, water system framework development along the riverbank, and land-use changes are accelerators of the river's characteristic geomorphologic dynamic behavior. These human alterations have gotten to be more powerful than the characteristic strengths of floods and dry spells. They undermine the autogenic waterway channel dynamics coming about in major channel degradation, disturbance of sediment supply and water pathways, as well as waterway provisioning administrations. [15].

Expert and experienced human interpreters extract thematic information from satellite images through visual interpretation. Visual interpretation takes into account tonal differences, texture, size, shape, context etc. Though visual analysis is extensively used for interpreting remote sensing data, it cannot provide quantitative information. With big volume of data, the information extraction through visual analysis is shallow. The visual analysis also makes it challenging to use all spectral bands effectively. Thus, computer processing of remotely sensed data is essential to take full advantage of the capabilities of this data to identify and quantify features. Land cover classes are ordinarily mapped from advanced remotely sensed information through the method of directed digital image classification [26].

The task of digital classification is to assign a value or label to each pixel of the remote sensing image. Suppose this labeling is done for all the pixels in the scene. In that case, we get a thematic map as in the case of visual interpretation. The objects are discriminated based on reflectance/emittance variation of their Electromagnetic radiation and other characteristic properties. There is no unique value of the reflectance/emittance associated with each class. Spectral response patterns from various surface classes will generally have a mean value and a spread/variability around the mean. Several factors like atmospheric scattering, topography, class mixture, illumination and view angles etc. cause this spread or variability within a class [27].

Combining satellite image processing techniques, surveys, and field data to study land cover change and its relation to water availability, demand, and consumption has effectively assessed water balances. Many studies with a similar research topic in the literature and remote sensing have shown a strong performance in the study of land use/cover changes, the development and generation of land cover change scenarios for hydrological modeling [28]. Monitoring river channel dynamics is also helpful in preventing and mitigating flood and drought disasters, particularly in developing countries. Remote sensing data have become a valuable tool for change detection in rivers and their floodplain dynamics. Different RS and GIS methods are utilized to supply knowledge into the river channel vulnerability and an understanding of the transient and spatial channel changes and elements of this waterway reach [4]. River morphological dynamics are natural autogenic occurrences for fluvial rivers resulting from discharge flow processes, debris and sediment transport, channel migration, and floodplain erosion and accretion. Riverbank disintegration and growth and channel course changes are more related to climate alter, release amount and sort of silt, and varieties of hydrologic regime [4].

This chapter applies remote sensing data and geo-information techniques are applied to understand the temporal and spatial channel changes and dynamics of the Amu Darya river along Afghanistan's border. The objective is to map and analyze the land cover changes of four classes over the study area and to determine land conversion from 1990 to 2020 between the investigated classes. Also, seasonal land degradation has been investigated. To achieve the goals in this study, we use four Landsat images (1990, 2000, 2011, 2020) from the same period (May–July) to avoid seasonal changes. The seasonal changes were investigated in 2020, in all four seasons. The analyses have been made in the Google Earth Engine platform. This kind of application is needed for decision-making when conventional monitoring of river dynamics. Both local and international administrations can use the information to resolve problems due to unresolved water-sharing policies. Also, the results can be significant to help make geopolitical decisions beneficial for the water-sharing parties.

2 Study Area

Afghanistan is an extremely poor country, and it is highly dependable on agriculture. For the past few decades, the war that has been going on put economic considerations secondary to political and military problems [5]. Afghanistan is an arid country where mountains occupy two-thirds of the land with little or no vegetation. Still, 90% of the population depends on agriculture. Most of the agricultural land is located in the northern part of Afghanistan, in the basin of the Amu Darya river, and it is the largest river in Central Asia, with a total length of about 1,400 km. The river is formed as a result of the confluence of two rivers, Pyandzh and Vakhsh. Before diverting their flow, together with Syr Darya, Amu Darya was the main source of the formerly fourth-largest lake globally, the Aral Sea [29]. The total catchment area is estimated as 465,000 km², the area of the effective drainage basin is 300,000 km² [30]. The river is formed in the Tigrovaya Balka Nature Resource on the border between Afghanistan and Tajikistan and flows into the Aral Sea. The river's upper course is part of Afghanistan's border with Tajikistan, Uzbekistan, and Turkmenistan. The river then continues across the desert of eastern Turkmenistan and its lower course forms part of the boundary between Uzbekistan and Turkmenistan.

The Amu Darya river is approximately 1,415 km long, but if measured from the sources of its headstream, the Panj River, in the Pamirs, its length is 2,540 km. In the past, Amu Darya was one of the main rivers discharging into the Aral Sea before river diversion. Precipitation and temperature in the basin vary mainly according to topography. The main source of precipitation are mid-latitude westerlies, and it mainly falls as snow during the winter. That way, at the highest places with extremely low temperatures, the glaciers are fed with precipitation that may exceed 1,015 mm. As the elevation decrease, the mean monthly temperatures increase and precipitation decreases. In the river's lower reaches, mean annual precipitation is less than 100 mm, with mean July temperatures above 25 °C and mean January temperatures ranging

between 0 and 10 °C. The climate is more often than not dry mainland in Afghanistan, with cold and generally stormy winters (and a stormy top in spring) and hot and sunny summers. In any case, considerable contrasts are depending on region and height.

The border between Afghanistan, Tajikistan, and Uzbekistan starts at the beginning of the Amu Darya river, on the joint point of the rivers Pyandzh and Vakhsh. It continues until the Afghanistan border with Turkmenistan (Fig. 1). The surrounding of the river from both sides is occupied with croplands. The surrounding small towns are vulnerable as the area is flooded almost every year, usually from March till May, when floods happen due to the heavy rains in the mountainous regions, filling the river basin, causing hazards and challenging the local people (Fig. 2) [5].



Fig. 1 Amu Darya basin, and location of the study area, the border between Afghanistan and Tajikistan [10]



Fig. 2 Land degradation caused by water erosion in Amu Derya (Photographs taken by Ali Reza Danis, May 2021)

3 Google Earth Engine Classification

To classify the study area into four classes: Water, Bare Land, Cropland, and Wetland, image collections from Landsat—5 (1990, 2000, and 2010), Landsat—8 (2020), in the cloud computing platform, Google Earth Engine was utilized. The image collections were filtered by date, and images from June and July were used in further processing. The obtained images were reduced to a single image to get cloud-free imagery, calculating their median values. Six Landsat bands (Blue, Green, Red, Near Infrared, ShortWave Infrared-1, ShortWave Infrared-2) were used for the classification. In addition to the mentioned bands, two spectral indices calculated from Landsat data were added to the investigation; Normalized Difference Vegetation Index (NDVI), Normalized Difference Water Index (NDWI), Modified Normalized Difference Water Index (MNDWI). Details and equations of the indices are given in Table 1. Frequently used water indices in the literature using remote sensing data are commonly used for water detection [31]. High index values usually correspond

Table 1 Spectral indices used in the GEE classification

	Index	Used bands	Equation
1	NDVI	Red, NIR	$\text{NIR} - \text{Red} / \text{NIR} + \text{Red}$
2	NDWI	Green, NIR	$\text{Green} - \text{NIR} / \text{Green} + \text{NIR}$
3	MNDWI	Green, SWIR	$\text{Green} - \text{SWIR} / \text{Green} + \text{SWIR}$

to water and low values to land. The indices can be calculated from any satellite collecting data in the conserving wavelength. Thus, for calculating MNDWI from Sentinel-2, the green (Band 3 at 559.8 nm) and the short-wave infrared (SWIR) bands (Band 11 at 1613.7 nm) are used [32]. The NDWI is calculated using the green (Band 4 at 664.6 nm) and NIR bands (Band 8 at 832.8 nm) from Sentinel-2 sensor. Different to the water indices, the NDVI high values corresponds to vegetation and low values to land. The NDVI is calculated using Sentinel-2's green (Band 8 at 832.8 nm) and Red bands (Band 4 at 664.6 nm).

For the four classifications, the same samples have been used. Thus, the samples were carefully selected from the unchanged land covers over the years. The sample training was done over the Landsat data, with validation over high-resolution imagery from Google Earth. The classification was performed using a LIBSVM classifier. Fifty percent of the samples were used in the classification. Overall accuracy and kappa statistics were calculated for every year for the accuracy assessment. The same methodology has been used for the seasonal analysis. Details about the used methodology are given in the flowchart in Fig. 3.

Recently, Support Vector Machine (SVM) is a very popular supervised classification and regression algorithm. SVM grew up on the concept of perpendicular distance or margin between decision planes (defined as decision boundary) and data points. In the present study, the most used Mapping and Monitoring Amu Darya River Dynamics of SVM were employed to classify the river mapping. A detailed flowchart of the methodology is given in Fig. 3. After the study area has been selected, it has been added as a Geometry in the GEE platform.

Furthermore, the four classes, Water, Cropland, Bare land, and wetland, have been distinguished in the study area. Using Landsat for the yearly and Sentinel-2 for the seasonal analyses, 30 sample points for each class have been selected. Then, image collections have been selected and processed. According to the study area, the image collections have been clipped according to the study area, date, cloud cover, and the same bands have been used for Landsat—5 and Landsat—8 for the yearly analysis. The same procedure has been done for the Sentinel-2 seasonal analyses.

After stacking the multispectral bands and the calculated indices, the model has been trained using the samplings for each class. The classification accuracy assessment has been done using 50% of the collected samples. Thus, 50% of the samples were used for classification, while 50% were used for testing the developed model. Afterward, the results have been exported and analyzed in a GIS software where spatial analyses for land conversion have been made.

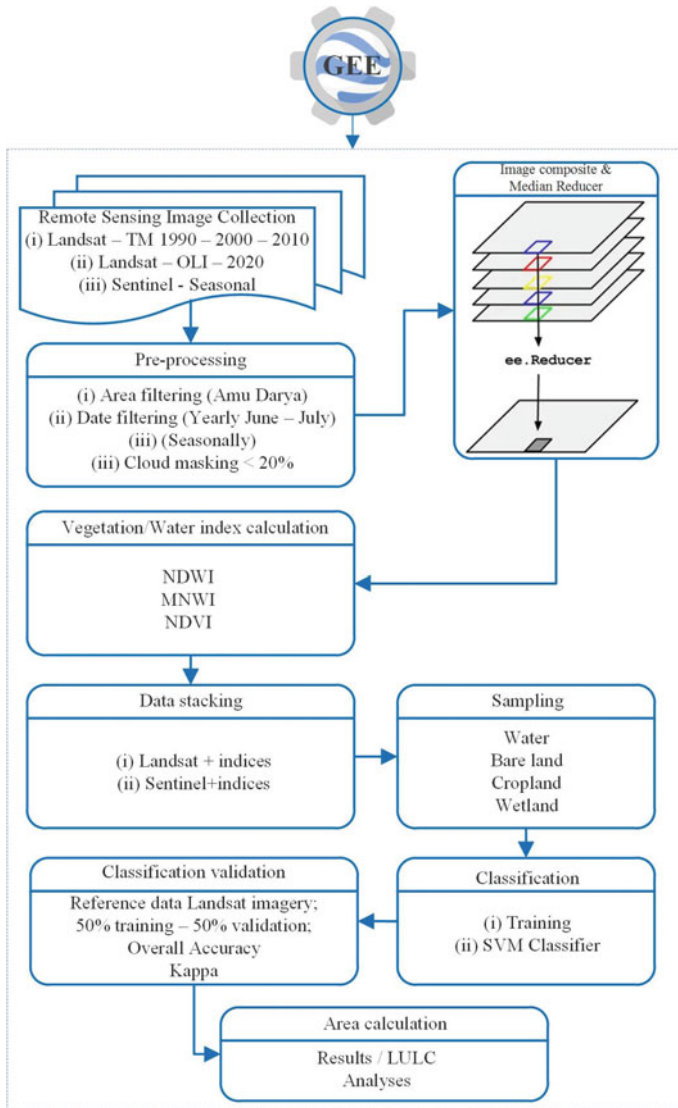


Fig. 3 Flowchart of the GEE classification

4 Results

Interpreting results from satellite imagery classification is the most important part of remote sensing analysis. For land degradation caused by river dynamics, the water body changes are needed to assess the erosion and acceleration of the river over a specific period. Also, the accuracy of the results is crucial for accurate interpretation

Table 2 Accuracy assessment results

	Year	Validation overall accuracy (%)	kappa
1	1990	90	0.86
2	2000	96	0.95
3	2010	87	0.83
4	2020	98	0.97

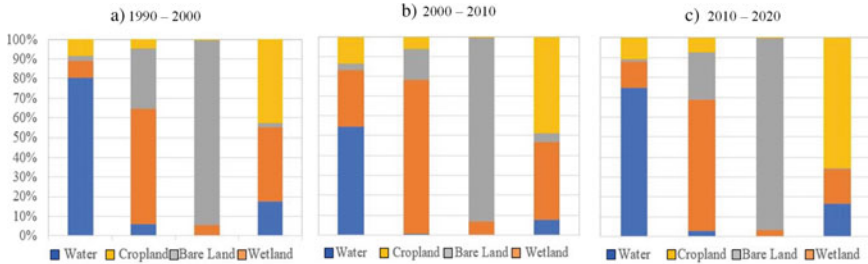


Fig. 4 Land conversion results; **a** 1990–2000; **b** 2000–2010; **c** 2010–2020

of the results. Thus, 50% of the training samples were then used for the accuracy assessment analyses, and the results are presented in Table. For remote sensing images with middle spatial resolution as Landsat and Sentinel, a minimum accuracy of 75% needs to be obtained. The accuracy of the classifications made in GEE over the Amu Darya river was between 87 and 98% (Table 2).

The results of the classifications are shown in Fig. 4. While there are no significant changes in the Bare Land class, a shift of the river bed can be noticed in several points of the study area. Land conversion during the three investigated periods (1990–2000; 2000–2010; 2010–2020) has been made for more detailed investigation. The conversions between the classes are shown in Fig. 4.

In all three periods, the class Bare Land did not receive any additional area from the other classes, but small Bare Land areas were converted to, generally, cropland. Wetland and water’s classes changed the most, with more than 40% conversion of the Water class to Wetland and Cropland. From 1990 to 2000 and 2010 to 2020, this conversion was 20% and 25%, respectively. As expected, the results showed that the river bed mainly shifts towards the Wetland and Cropland, or areas with soft soil. For a more detailed investigation, we recommend considering the geological characteristics of the river bed and its surroundings.

The land degradation can be clearly seen in Fig. 5, where the erosion and acceleration between 1990 and 2020 have been shown. Results show evident land degradation over the Amy Derya river bank. According to the statistical analyses, the water area in 2000 was approximately 30.000 ha smaller than the area in 1990. The water area then gains around 19.000 ha in 2010 compared to 2000, and then it got lowered in 2020 to 11.000 ha. The results showed that the river dynamics mainly occupy the wetlands and croplands area, thus causing damage in farmers’ land and some small

villages around the river bed. It should also be mentioned that the river dynamics are constantly changing the natural border between the sharing countries, which causes even more significant problems for local farmers to claim their rights [5].

For the seasonal analyses, Sentinel-2 satellite data has been used. The same methodology as with the yearly analyses has been applied. The accuracy results were significantly higher in comparison with the results from the Landsat imagery. This is expected as Sentinel-2 has a higher spatial, spectral, and temporal resolution than Landsat. The results are given in Table 4.

Figure 6 shows the river in the four seasons in 2020. The results of the classifications are shown in Fig. 7. While there are no significant changes in the Bare Land class, a shift of the river bed can be noticed in several points of the study area.

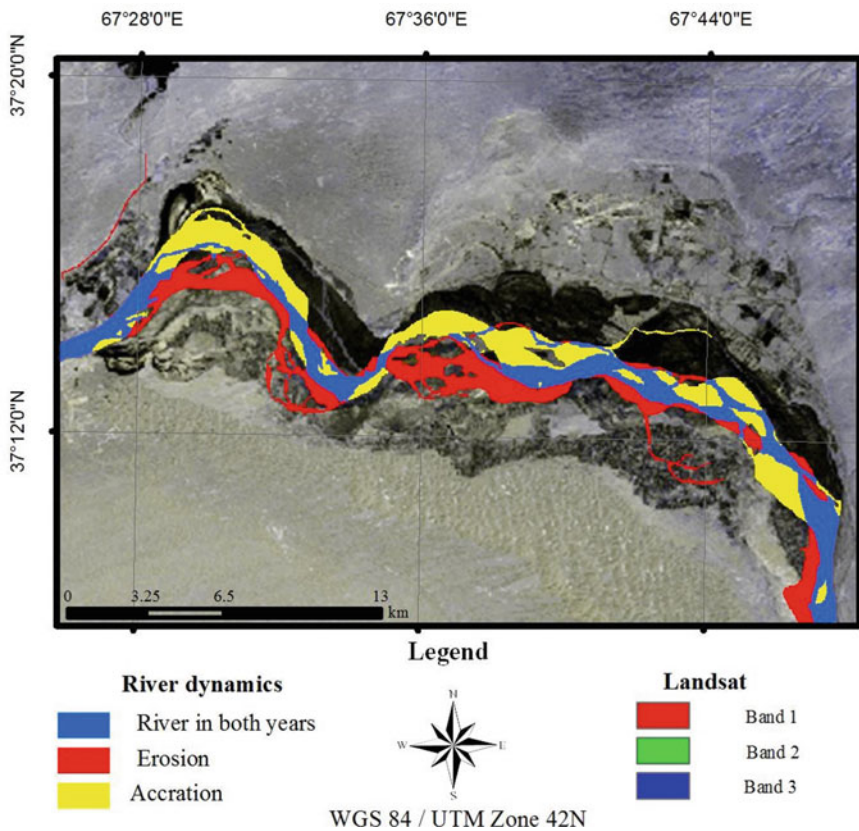


Fig. 5 Amu Darya river dynamics 1990–2020, erosion and accretion

Table 4 Accuracy assessment for the seasonal analyses using Sentinel-2

	Season	Validation overall accuracy (%)	Kappa
1	Winter	94	0.93
2	Fall	96	0.95
3	Summer	93	0.91
4	Spring	96	0.95

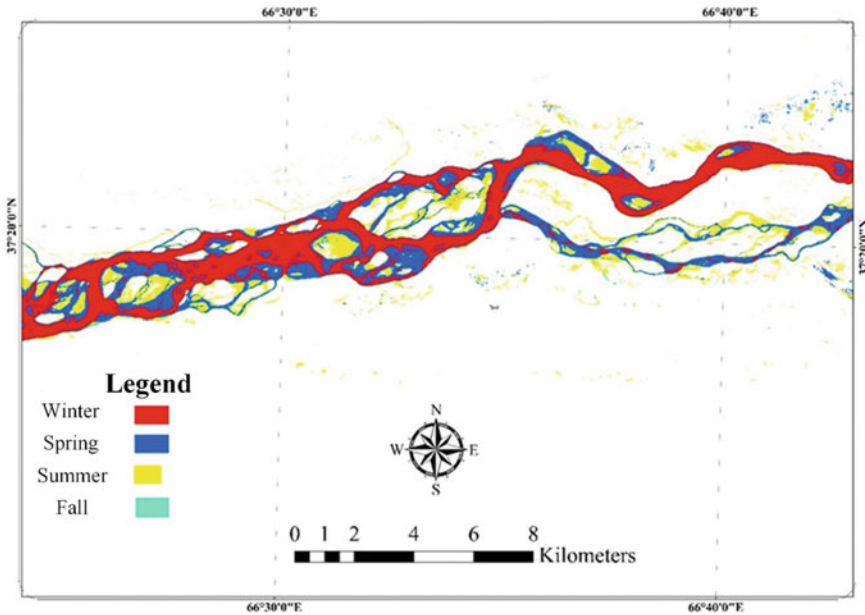


Fig. 6 Classification result from four seasons for the river

5 Discussion

Land degradation is a major problem all over the world. Land degradation caused by river channel dynamics can be a significant problem for the local people, especially farmers in developing countries who depend on agriculture. With the use of remote sensing data and geo-information techniques, this study once again showed the role of satellite remote sensing data in river channel dynamics. Once again mentioned, a number of water bodies worldwide are also an international border between two or more countries. This can be extremely difficult as some of the local farmers lose their land in some cases. As shown in this study, with the shifting of the river body, Afghanistan’s agricultural land gets flooded, while the other side “gains” land. This is a serious problem, as the locals are living in an extremely poor country and cannot fight for their rights. However, this is a major problem that needs to be addressed geo-politically. Remote sensing and geo-information systems can be of aid to the

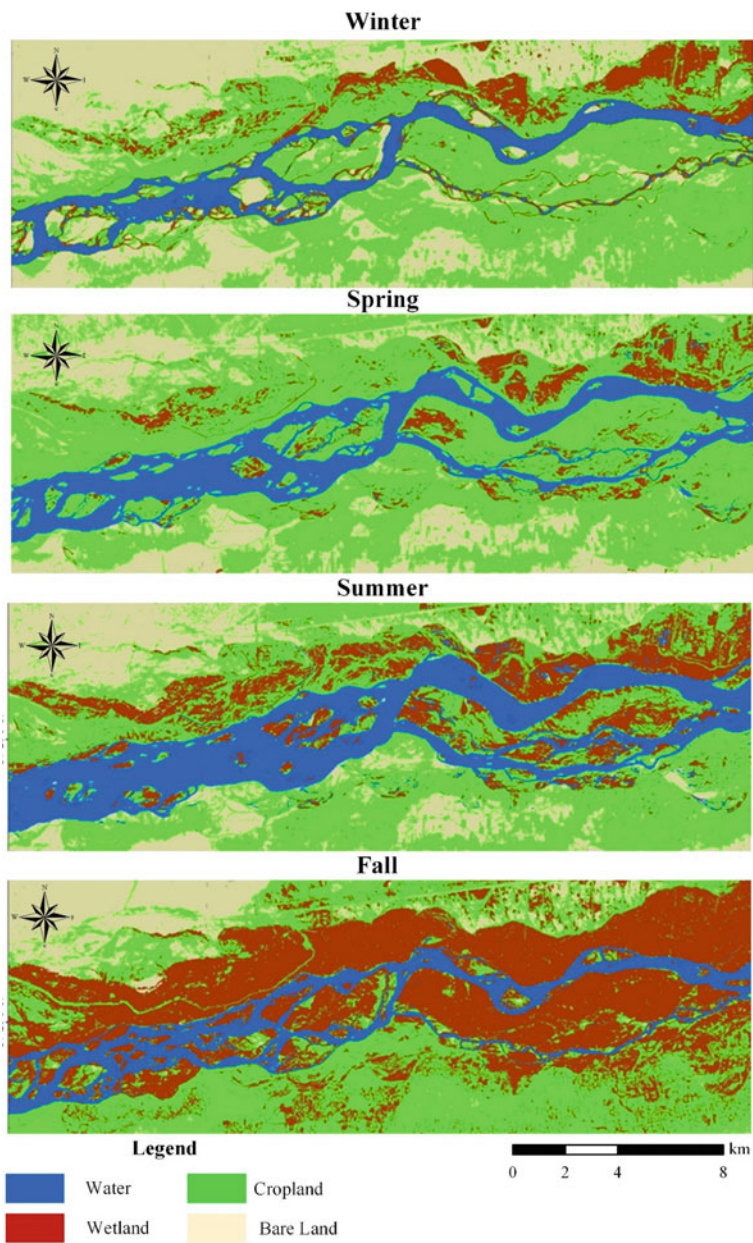


Fig. 7 Seasonal river dynamics of Amy Darya

resolution of this problem, as with satellite imagery, large areas can be timely monitored. In order to help decision-makers and solve geopolitical problems between the countries, continuous monitoring of the water areas and their surroundings is crucial. Most of the studies in the literature investigate river dynamics [4, 12] or land cover changes [33]. The main contribution of this study is the evaluation of both land cover changes and river dynamics of Amu Darya river. For that purpose, a classification has been made over the study area with four classes (Bare land, Cropland, Water, Wetland) in the cloud-based platform Google Earth Engine. Furthermore, the land conversion has been calculated between 1990 and 2020.

According to the results, large areas of wetland (possibly highly watered cropland) and cropland are being flooded by the river's new course, meaning that the river causes damages to local peoples' lands. More than 50% of the wetland areas transitioned to cropland (approximately 30%), and water and bare land (10%) in the investigated period. Part of the river is the border between Afghanistan and Tajikistan, and with every change of the riverbed, the international border between these two countries changes. The results are curtailed in decision making, and both local and international administrations can benefit from them. Also, the results can be helpful in risk management, irrigation plans, monitoring systems, etc.

As the pressures of increasing destruction by the waters of the Amu Darya on the people and the inhabitants around the sea were greater and a large number of people suffered irreparable damage due to these devastating events, and people were forced to leave their homes. It is also noteworthy that climate change is affecting the low-water areas. Neighboring countries have increasingly managed and controlled the infrastructure and management of transboundary waters in Afghanistan, and unfortunately, have suffered the most from Afghanistan. Similarly, over the past few years, the Government of Afghanistan has raised its awareness of the importance of addressing cross-border issues with low-water neighbors to ensure the most efficient use of the region's precious water resources. This chapter is a step towards strengthening Afghanistan's transboundary water dialogue by reviewing the situation and proposing possible solutions to promote cooperation and water management in the Amu Darya Basin.

6 Conclusions

The part of Amu Darya basin in Afghanistan and Tajikistan is prone to major river dynamics. This causes land degradation as an erosion, causing significant problems in the area. As the river is also the international border between these two countries, this can also be referred to as a global, geopolitical problem. Using remote sensing data and technologies and geospatial technologies can be beneficial for such an important matter. With the ability to collect daily, weekly, or monthly data, remote sensing is the ideal tool for mapping and monitoring river dynamics. Due to seasonal changes, the Amu Darya river is constantly changing its riverbed, making it hard for the local people settled around the river who mostly depend on agriculture. The results showed

that the river/international border between Afghanistan and Tajikistan has shifted to the south, which resulted in the loss of land and houses, and most importantly, the lives of the local Afghanistan people.

7 Recommendations

Conventional methods for mapping and monitoring riverbed shifting can be challenging and expensive. Therefore, modern technologies and techniques should be considered to overcome threats and possible damage to the surroundings. As the Amu Darya river is constantly changing, such methods can be impractical as well. As the main source for Earth Observation, remote sensing should be used for monitoring such changes.

Acknowledgements The content in the book chapter is part of Mohammad Asef Mobariz's master thesis under the mentorship of Dr. Gordana Kaplan. Parts of the study have been presented at IDRC2020 and 5th International Electronic Conference on Water Sciences.

References

1. Tomsett C, Leyland J (2019) Remote sensing of river corridors: a review of current trends and future directions. *River Res Appl* 35:779–803
2. Popelka SJ, Smith LC (2020) Rivers as political borders: a new subnational geospatial dataset. *Water Policy*
3. Hirabayashi Y, Mahendran R, Koirala S, Konoshima L, Yamazaki D, Watanabe S, Kim H, Kanae S (2013) Global flood risk under climate change. *Nat Clim Chang* 3:816–821
4. Langat PK, Kumar L, Koech R (2019) Monitoring river channel dynamics using remote sensing and gis techniques. *Geomorphology* 325:92–102
5. Glantz MH (2005) Water, climate, and development issues in the amu darya basin. *Mitig Adapt Strat Glob Change* 10:23–50
6. Yousefi S, Keesstra S, Pourghasemi HR, Surian N, Mirzaee S (2017) Interplay between river dynamics and international borders: the hirmand river between iran and afghanistan. *Sci Total Environ* 586:492–501
7. Ovezova A (2015) Managing water conflict and cooperation in central asia
8. Haleemzai HA, Sediqi A (2018) Impacts of water development plans on regional water cooperation—a case study of amu river basin. *J Water Resour Prot* 10:1012–1030
9. Vinogradov S, Langford VP (2001) Managing transboundary water resources in the aral sea basin: in search of a solution. *Int J Glob Environ Issues* 1:345–362
10. Mobariz MA, Kaplan G (2021) Moving borders: Mapping and monitoring amu darya river dynamics using remote sensing data and techniques. *Geodetski list* 75:29–44
11. Bekchanov M, Ringler C, Bhaduri A (2018) A water rights trading approach to increasing inflows to the aral sea. *Land Degrad Dev* 29:952–961
12. Billah MM (2018) Mapping and monitoring erosion-accretion in an alluvial river using satellite imagery—the river bank changes of the padma river in Bangladesh. *Quaestiones Geographicae* 37:87–95

13. Tadese M, Kumar L, Koech R, Kogo BK (2020) Mapping of land-use/land-cover changes and its dynamics in awash river basin using remote sensing and gis. *Remote Sens Appl Soc Environ* 19:100352
14. Cai X, Feng L, Hou X, Chen X (2016) Remote sensing of the water storage dynamics of large lakes and reservoirs in the yangtze river basin from 2000 to 2014. *Sci Rep* 6:36405
15. Langat PK, Kumar L, Koech R, Ghosh MK (2019) Monitoring of land use/land-cover dynamics using remote sensing: a case of tana river basin, kenya. *Geocarto Int* 1–19
16. Legleiter CJ, Manley PV, Erwin SO, Bulliner EA (2020) An experimental evaluation of the feasibility of inferring concentrations of a visible tracer dye from remotely sensed data in turbid rivers. *Remote Sens* 12:57
17. Sichangi AW, Wang L, Yang K, Chen D, Wang Z, Li X, Zhou J, Liu W, Kuria D (2016) Estimating continental river basin discharges using multiple remote sensing data sets. *Remote Sens Environ* 179:36–53
18. Hemmelder S, Marra W, Markies H, De Jong SM (2018) Monitoring river morphology & bank erosion using uav imagery—a case study of the river buëch, hautes-alpes, france. *Int J Appl Earth Obs Geoinf* 73:428–437
19. Akhter S, Eibek KU, Islam S, Islam ARMT, Chu R, Shuanghe S (2019) Predicting spatiotemporal changes of channel morphology in the reach of teesta river, Bangladesh using gis and arima modeling. *Quatern Int* 513:80–94
20. Sepuru TK, Dube T (2018) An appraisal on the progress of remote sensing applications in soil erosion mapping and monitoring. *Remote Sens Appl Soc Environ* 9:1–9
21. Gelagay HS, Minale AS (2016) Soil loss estimation using gis and remote sensing techniques: a case of koga watershed, northwestern ethiopia. *Int Soil Water Conserv Res* 4:126–136
22. Petropoulos GP, Kalivas DP, Griffiths HM, Dimou PP (2015) Remote sensing and gis analysis for mapping spatio-temporal changes of erosion and deposition of two mediterranean river deltas: the case of the axios and aliakmonas rivers, greece. *Int J Appl Earth Obs Geoinf* 35:217–228
23. Sajjad A, Lu J, Chen X, Chisenga C, Saleem N, Hassan H (2020) Operational monitoring and damage assessment of riverine flood-2014 in the lower chenab plain, punjab, pakistan, using remote sensing and gis techniques. *Remote Sens* 12:714
24. Bizzi S, Demarchi L, Grabowski RC, Weissteiner C, Van de Bund W (2016) The use of remote sensing to characterise hydromorphological properties of european rivers. *Aquat Sci* 78:57–70
25. Zanditon M, Hellman S (1981) The complicated business of setting up residential alternatives. *Psychiatr Serv* 32:335–339
26. Wu Q (2017) Gis and remote sensing applications in wetland mapping and monitoring
27. Bhosale MA, Veer V Land use/land cover and change detection analysis of upper Krishna river sub basin using gis and remote sensing
28. El Hafyani M, Essahlaoui A, Rompaey AV, Mohajane M, El Hmaid A, El Ouali A, Moudden F, Serrhini N-E (2020) Assessing regional scale water balances through remote sensing techniques: a case study of boufakrane river watershed, meknes region, morocco. *Water* 12:320
29. Kostianoy AG, Lebedev SA, Solovyov DM (2013) Satellite monitoring of the caspian sea, kara-bogaz-gol bay, sarykamysh and alty n asyr lakes, and amu darya river. In: *The turkmen lake alty n asyr and water resources in Turkmenistan*. Springer, pp 197–231
30. Asarin AE, Kravtsova VI, Mikhailov VN (2010) Amudarya and syrdarya rivers and their deltas. In: *The aral sea environment*. Springer, pp 101–121
31. Kordelas GA, Manakos I, Aragonés D, Díaz-Delgado R, Bustamante J (2018) Fast and automatic data-driven thresholding for inundation mapping with sentinel-2 data. *Remote Sens* 10:910
32. Brombacher J, Reiche J, Dijkma R, Teuling AJ (2020) Near-daily discharge estimation in high latitudes from sentinel-1 and 2: a case study for the icelandic þjórsá river. *Remote Sens Environ* 241:111684
33. Cai L, Shi W, Miao Z, Hao M (2018) Accuracy assessment measures for object extraction from remote sensing images. *Remote Sens* 10:303

A New Method for Land Degradation Assessment in the Arid Zone of Republic of Kazakhstan



Dmitry Malakhov , Madina Batyrbayeva, and Irina Vitkovskaya 

Abstract The problem of land degradation, being extremely actual over the planet and especially in arid zones, requires imminent scientific attention to outline territories affected with degradation, and develop effective measures to withstand the problem. The use of remotely sensed data proves as a cost-effective and informative tool for land surface monitoring. Moreover, remote sensing is sometimes the only way to comprehensively imagine the current processes over huge territories. The main question of remote sensing data application is the accuracy of methods used to obtain certain land characteristics. The joint analysis of ground and satellite data is indispensable at all the remote sensed algorithm development stages. In the current chapter the new index of land degradation assessment is described. The index has been under development for several years and has strong ground-truth support with data gathered in the arid zone of Kazakhstan. The new index considers the condition of plant cover, the moistening regime, and bare soil's spectral parameters. Initially developed for Landsat-8 data in south-eastern Kazakhstan, the index was applied for the entire arid zone of Kazakhstan. There is no doubt, the new index could be of use at various applications related to the problem of environmental degradation all over the arid belt of Eurasia, where the problem of aridization becomes most actual for Asian countries.

Keywords Land degradation · Arid zone · Spectral index · Landsat-8 · TERRA/MODIS

M. Batyrbayeva · I. Vitkovskaya
Joint Stock Company “National Center of Space Research and Technology”, Almaty 050010,
Kazakhstan

D. Malakhov (✉)
GIS and Remote Sensing Department, Institute of Zoology SC MES RK, Almaty, Kazakhstan
e-mail: d_malakhov_73@mail.ru; dmitry.malakhov@zool.kz

1 Introduction

The deterioration of environmental conditions induced by human activity is a threateningly fast and dangerous phenomenon that is very close to becoming uncontrollable globally. Asian countries having most of their territories laying within the arid or sub-humid belts are especially vulnerable to land degradation and desertification. Methods and technologies of fast, cost-effective and reliable assessment of degradation severity upon vast and often hardly accessible areas are very important for Asian countries allowing identify the degradation foci and provide reasonable and well-timed response. Land degradation is a complex phenomenon, comprising many factors and induced by different reasons. Different schools define land degradation according to their interests [1]. Even a very brief review of the land degradation concepts [2, 3] comprises a set of very different definitions of the degradation process.

General concepts define land degradation as a process that implies reducing the potential productivity of the land [4]. More attenuated concepts define land degradation as a result of collective degradation of different components, including water, soils and biotic resources [5]. The UNCCD defines land degradation as the “reduction or loss in arid, semi-arid and dry sub-humid areas, of the biological or economic productivity and complexity of rainfed cropland, irrigated cropland, or range, pasture, forest and woodlands resulting from land uses or from a process or combination of processes, including processes arising from human activities and habitation patterns” [6]. Degradation of land can be caused by various factors, including climatic variations and human activities. Human-induced land degradation mainly occurs due to overexploitation of land resources for cropping and livestock farming, including irrigation practices, overgrazing of rangelands, and fuelwood exploitation.

Land degradation is a common phenomenon. It includes soil degradation as a component. Soil degradation is a process of decreasing soil capacity to support human life [7]. The loss of vegetation enhances soil erosion and reduces the productive value of the land [8]. In turn, soil degradation reduces biodiversity and natural vegetation [9]. Lal and Stewart [10] grouped soil degradation into three categories: (1) physical degradation, (2) biological degradation, and (3) chemical degradation. Besides vegetation degradation, soil degradation comprises such aspects as: water erosion, wind erosion, salinization, soil fertility loss, soil compaction, and crusting [11].

Key soil parameters affecting vegetation development are nutrients, moisture content, soil acidity (pH), mineralization, humus content, and soil microorganisms' biomass. Change or alteration in the composition of those parameters may indicate the process of soil degradation [12]. Manifestations of land degradation may appear as desertification, soil erosion, salinity increase, etc., often related to each other. Desertification is land degradation in arid, semi-arid, and dry sub-humid areas resulting from various factors, including climatic variations and human activities” [6]. Soil erosion is the displacement of materials like soil, mud, and rock by gravity, wind, water, or ice. The most common agents of soil erosion are water and wind [13].

The alteration of the chemical composition of soil [14] and soil salinity in particular may evident the degradation. Salinity is salt in the wrong place, affecting water quality, water uptake and nutrients by plants, and breaking up roads and buildings. It occurs naturally in drylands and areas prone to tidewater flooding but is often exacerbated by poor soil and water management [15]. Soil erosion is another important aspect of land degradation [16] resulting in the loss of soil nutrients and overall soil destruction. As a particular case of land degradation, pasture degradation may be indicated by altering natural plant species with ruderal and unpalatable species. The method of quantitative estimation of overall pasture grass cover and the ratio of unpalatable species was proposed by Zha et al. [17]. Following this approach, general grass cover and the ratio of ruderals species are counted in percent, allowing quantitative estimation of the pasture.

In general, the variety of degradation definitions may be splitted into “Socioeconomically” and “ecologically” accented ones. There is consensus that land degradation is widespread, it has severe financial and social consequences and may sometimes be irrecoverable on a human timescale at manageable cost [18].

Natural pastures represent an important component of the biosphere resources that outline the biological diversity of the flora and fauna and the quality of human beings’ environment. Under normal conditions, pasture ecosystems possess some important characteristics: the annual renovation of the vegetation with stable biomass value and maintaining soil fertility. The stability of pasture ecosystems is related, among other factors, to the intensity of the grazing. Degradation of natural pastures results in altering the natural plant species and communities, which has a form of depletion of palatable species and decreasing plant coverage density. Ruderal and unpalatable species, existing in normal conditions as a marginal component of plant community, may become abundant and widespread under ecosystem transformation and may serve as indicators of degradation. In the arid regions, where the natural plant coverage is sparse and patched, overgrazing appears to be the most aggressive factor that leads to deflation of the fertile upper horizon of soils and hardening of inner clay loam layers containing salts. Disturbed areas, represented with degraded plant communities, contained mostly ruderal species, often appear along cattle paths, human settlements, wells, and artesian and may spread to huge areas, if cattle owners neglect or, in some reasons, cannot follow the rational regulations of cattle breeding. Arid pastures are fragile as the renovation capacity is very limited in a hot and dry climate, so any disturbance has a prolonged effect on steppe pastures.

Kazakhstan traditionally is an area of intense cattle-breeding. As a result, the area of natural pastures, is as much as 187 million ha, with an additional 5 million ha of hayfields. At the same time, the rough estimation of the area of degraded pastures returns as much as 25–27 million ha [19].

Alterations of pasture are well detectable with satellite imagery. Vegetation and soil appear to be most suitable for the study by remotely sensed data of all the ecosystem components. Changes in these elements possess pronounced spatial and temporal character and may be detected using the information provided by various satellite sensors at different levels of spatial resolution and periodization. There are two possible opportunities for degradation assessment with remotely sensed data:

the estimation of the current situation using few or single scenes, and the long-term observations over the area.

The estimation of a current degradation state may often be very rough, as the manifestations of light degradation are often similar to changes in plant and soil properties caused by seasonal fluctuation of temperature and precipitation. The long-term monitoring of the degradation process is more reliable and thought time-consuming. It provides the possibility to determine land condition trends and track the land cover dynamics together with the analysis of the relations between land cover and climatic changes. Remotely sensed indicator should be easy to use, sensitive to minor land cover changes, and consider several environmental parameters rather than the single one. One of the basic problems of remote sensing data application is the strict necessity to obtain the correlation between ground data and satellite information.

The accuracy of data and calculations is the main question to be answered prior to developing a monitoring system on different scales: from regional to global. Here we present a new index to estimate the degradation in arid areas of Kazakhstan, developed and verified with the Landsat-8 data and ground information obtained during field seasons of 2013 in the Balkhash Lake region (South-East Kazakhstan). The proposed index considers vegetation condition, moisture, and bare soil properties. The observation and validation of the index was taken during the 2013–2019 period at the study area with Landsat-8 data. The index's performance was further tested for the entire arid zone of Kazakhstan and applied to TERRA\MODIS imagery.

Thus, the following major processes all together characterize the land degradation phenomenon: decreasing of productivity, i.e. changes in vegetation; soil degradation (erosion); desertification (increasing of bare land area); salinization of the soil. All the processes listed are well recognizable using satellite data in the form of direct observation, band ratio computations, or other, more or less sophisticated approaches.

2 Study Area

The study area (Fig. 1), located in the South-East Balkhash Lake region, is arid and dry: solar radiation is 130–140 kilocalorie/cm² per year, the annual mean temperature is about 5 °C, mean January temperature varies between (–14) and (–15) °C; mean temperature of July is 24 °C. Annual precipitation does not exceed 150–200 mm [20]. The duration of the vegetation growth is 200–210 days. Soils are characterized by low humus content, relatively high carbonate and gypsum content, and frequent and high salinization caused by a relatively high level of groundwater.

Pogrebensky [21] described the following main geomorphological elements to form the landscape in the study area: river bed; river banks, cellular inter-channel depressions, and flat plains sloping from the channels; hilly and hilly-ridged sands. Sands represent the remnants of a sandy desert that formed as a result of ancient alluvium.

The main elements of the relief in the abrasion-accumulating plain are represented by flat saucer-shaped depressions and numerous delta channels crossing the plain.



Fig. 1 Study area. Red rectangle indicates the location of study area within the territory of Kazakhstan

In addition, phytogenic hillocks form distinct agglomerations. The total slope of the surface, directed to the Balkhash Lake is about 0.0002° [22].

Lepsy and Aksu Rivers are two main water streams of the area. Lepsy River runs in the northern part of the study area, and Aksu River crosses the central part of the study area. Both streams flow into Balkhash Lake. Few human settlements are located within the study area. Landscapes consist mainly of hilly plains; salty marshes are common and associated with microrelief depressions. Vegetation consists mainly of hyper xerophilous and xerophilous plants of different lifeforms, with the dominance of semi-shrubs, shrubs and trees [23, 24]. The study area belongs to the Central-Asian type of deserts [25], possessing more or less even seasonal distribution of annual precipitation. The presence and prevalence of grey sagebrush (*Artemisia terra albae*) characterize the regional desert as a northern type of sandy desert.

2.1 *Physiography of the Arid Zone of Kazakhstan*

Semidesert zone occupies as much as 75 million hectares. It is characterized by an arid, continental climate with annual precipitation of about 175–250 mm and sparse grass cover. However, much of the semi-arid zone is unsuitable for plowing and represents mainly pastures (up to 90% of the entire area) and hayfields. Soils are characterized by moderate humus content and significant areas affected with severe manifestations of salt, associated with relief depressions [19]. Following the classification of Köppen-Geiger [26, 27], semidesert falls mainly into BSk (Arid/Steppe/Cold) zone. Pastures of the semidesert zone are located to the North of 48°N parallel and have mixed vegetation, containing both steppe (fescue, feather grass) and desert (mainly sagebrush) species [28].

Desert zone is the largest climatic zone of Kazakhstan. Desert zone occupies up to 86–87 million ha. The climate is extremely arid and continental. Annual precipitation does not exceed 200 mm with the prevalence of spring precipitation. Soils of the desert zone are weakly developed with a humus content of about 1% [19]. In terms of Köppen-Geiger [26, 27] classification desert area resembles BWk (Arid/Desert/Cold), BSk and Dsa (Cold/Dry Summer/ Hot summer) climatic zones.

Pastures of the desert type are common to the South from 48°N parallel [28]. Desert pastures are traditionally divided into several distinct groups: pastures of sandy desert, pastures of the clayish desert, pastures of gravel desert, and pastures of salty deserts. These types of salty and clayish deserts pastures demonstrate lesser value due to low productivity and relatively high concentration of unpalatable grasses [29]. Most common soils are grey-brown and sandy desert soils [20]. Following Zabler's classification [30], predominant soil units within the arid zones of Kazakhstan are luvisols, haplic, calcic and takyric yermosols, i.e. soils with low humus content, enriched with calcium carbonate, with high clay and sand content. The vast desert pastures make this type the only useable for many people. At the same time, desert pastures are the most vulnerable type to degradation processes due to the weak development of the fertile horizon in soils and the properties of vegetation cover.

3 **Material and Methods**

3.1 *Field Data*

Fieldwork was attended twice (late May and early September) in 2013. Seventy-seven field protocols (Fig. 2) were documented for each observation point with a detailed description of the landscape, soil, vegetation cover, and degradation degree.

A degradation degree was studied following [31]. Predominating type (or several) of the anthropogenic pressure was described, and degraded locations were compared to intact areas. The selection of intact areas has been done among as much as similar areas to degraded ones in regard of soil and vegetation. Special attention has been

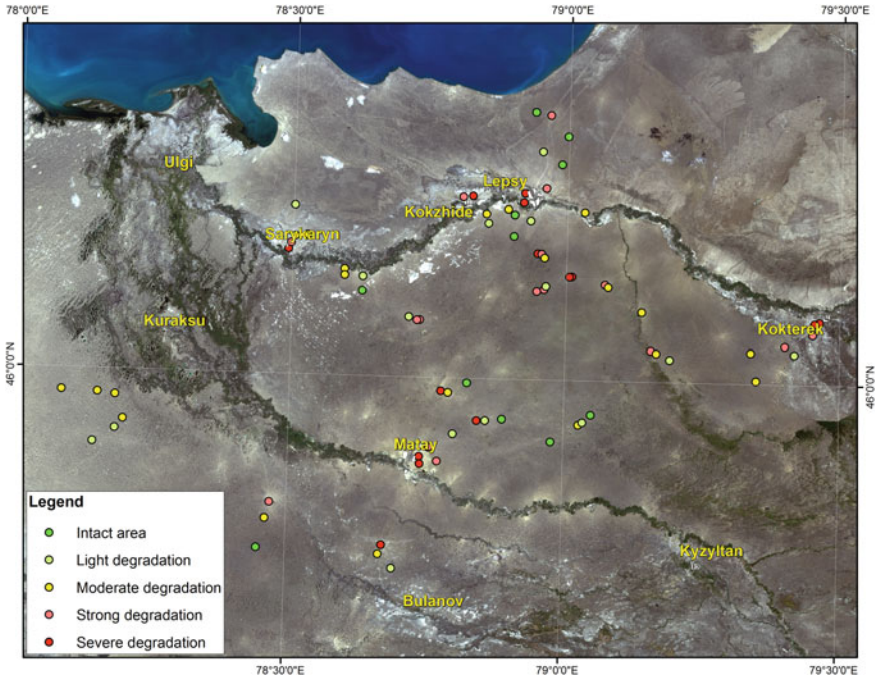


Fig. 2 Observation points during field seasons of 2013. Classification of degradation is based upon the field measurements and descriptions

paid to ruderal species, indicating the process of natural pasture transformation. The list of plant species used as indicators of degradation in the arid areas of Kazakhstan is given in Table 1.

Major indicators of the degradation in desert ecosystems are the following: disturbance of the structure and composition of plant communities, decreasing of the biomass (production), decreasing of the perennial plants ratio in the community, appearance *en masse* of ruderal and unpalatable species [32].

For each ground point, the following data were registered:

- Composition of plant community
- Abundance and distribution of species
- Phenology
- Grass cover
- Biomass (counted for square meter and recalculated for hectare)
- Ratio of indicator species in a community
- Relief description
- Soil composition
- Moistening regime
- The presence and the character of anthropogenic pressure (i.e. grazing, infrastructure, etc.); affected square and the period of pressure (when possible)

Table 1 Plant species indicating the pasture transformation in the desert zone of Kazakhstan

Species	Sandy loam desert	Sandy desert
<i>Anisantha tectorum</i>	+	+
<i>Alhagi pseudalhagi</i>	+	+
<i>Anabasis aphylla</i>	+	–
<i>Atriplex spp.</i>	+	+
<i>Artemisia scoparia</i>	+	+
<i>Allysum teukestanicum</i>	+	+
<i>Bassia spp.</i>	+	–
<i>Ceratocarpus arenarius</i>	+	+
<i>Ceratocarpus urticulosus</i>	+	+
<i>Climacoptera brachiata</i>	+	–
<i>Chenopodium album</i>	+	–
<i>Chondrilla ambigua</i>	–	+
<i>Corispermum spp.</i>	–	+
<i>Heliotropium argusoides</i>	–	+
<i>Heliotropium ellipticum</i>	–	+
<i>Horaninovia ulicina</i>	–	+
<i>Euphorbia seguierana</i>	–	+
<i>Lepidium perfoiatum</i>	+	+
<i>Lepidium ruderales</i>	+	–
<i>Peganum harmala</i>	+	+
<i>Polygonum spp.</i>	+	–
<i>Salsola nitraria</i>	–	+
<i>Tribulus terrestris</i>	–	+

– The degree of degradation.

The degradation degree was estimated based upon the complex criteria [32] and summarized in Table 2.

The numerical value of degradation in Table 2 represents the summarized effect of soil degradation and the vegetation conditions described in each field location. A summarized description of degradation levels was formalized and attributed to numerical values from 1 (no degradation) to 5 (severe degradation) and these values were used for statistical processing satellite data.

3.2 Remote Sensing Data

The study area is covered with Landsat LC08_L1TP_149028 scenes. We used a series of late summer-early autumn images for the period of 2013–2019 to test and

Table 2 Degree of degradation in the study area

Degree	Description	Numerical value
Intact area	Very light soil erosion, degradation has no clear attributes, mineral salts are recognizable in depression were precipitation accumulates. Vegetation cover looks undisturbed	1
Light degradation	Light soil erosion. Fine soil fractions may vanish, and coarse fractions (gravel) may appear at the surface. Light changes of the habitus in some plant species appear, sensitive or rare species may disappear, shrubs may become damaged	2
Moderate degradation	Moderate soil erosion, the lower loamy horizon may become exposed, streaming erosion becomes observable. Features of grazing are observable, ruderal and unpalatable species appear in distinct accumulations, bare soils appear as irregular and relatively small patches around wells and human settlements. Dominant plant species composition still persists. While the role of xerophytic species in communities increases, morphological changes in plants become observable	3
Strong degradation	Strong soil erosion, gravel is often at the surface, upper soil horizon is patched and thin, soil may alter its natural color, ravines appear. Overgrazing, alteration of natural plant communities with ruderal species, wide areas of barren land. The composition of dominant plant species alters, ruderal and unpalatable species prevail, while the overall species abundance in the communities becomes reduced	4
Severe degradation	Extremely strong soil erosion, upper horizon is removed completely. Soil color altered, ravines are active. Vegetation is completely altered, the plant cover is extremely fragmented, consists mainly of ruderal species	5

verify indices sensitivity. For the purposes of this study, the variety of spectral indices was tested and statistically analyzed. As a result of the series of experiments, new spectral index was elaborated. The expression of the index is:

$$\text{Complex Degradation Index (CDI)} = (LDI_{TCW} - LDI_{NDVI}) / (LDI_{TCW} + LDI_{NDVI}) * RED \quad (1)$$

where LDI_{TCW} and LDI_{NDVI} are degradation indices, proposed by Fadhil [33], RED is a value of the red band of Landsat-8.

Firstly mentioned in 2014 [34], this expression combines vegetation, soil wetness and the red band of the spectrum sensitive to barren lands. The index range and intervals study revealed that the range of index values from 0.27 to 0.6 resembles different

stages of land degradation. Values lower than 0.27 apparently indicate intact areas and water bodies, and values exceeding 0.6 resemble the areas with high salinization.

To depict salty areas still unpublished salinity index was applied. The index is under development by the National Center of Space Research and Technology for the purposes of several projects related to irrigated area monitoring. The expression of this index is:

$$(b5 - (b6 - b7)) / (b5 + (b6 - b7)) * \sqrt{b6}, \quad (2)$$

where $b5$, $b6$, and $b7$ are respective bands of Landsat-8 (NIR and SWIR wavelengths).

The salinity index in its current version is aimed to elaborate the quantitative approach, and this work is still in progress. In the meantime, this index demonstrated high spatial accuracy in terms of qualitative analysis, i.e. in the range of index values 0.37–1.0 it returns pixels associated with superficial salt manifestation.

Normalized Difference Water Index [35] was used to outline water objects. NDWI is a simple normalized ratio of Green and NIR bands:

$$(Green - NIR) / (Green + NIR), \quad (3)$$

positive values of the index resemble water surfaces at a satellite image.

Vegetation Condition Index [36, 37] was used to estimate multitemporal moistening conditions of the study area. The equation to compute VCI is as following:

$$VCI = \frac{NDVI_i - NDVI_{min}}{NDVI_{max} - NDVI_{min}} * 100\%, \quad (4)$$

where $NDVI_i$, $NDVI_{min}$ and $NDVI_{max}$ are the smoothed weekly NDVI, its multiyear absolute maximum, and minimum of each pixel, respectively.

The index's main purpose is to analyze weather influence on the vegetation condition during the observing period as a measure of moistening. Raster sets, comprising the VCI distribution within the study area and adjacent territories, were used to illustrate the moistening regime of certain years. Archived data on decadal VCI are available at <https://land.copernicus.eu/global/> (Copernicus Global Land Service). We used data aggregated for the last ten days of each summer months.

Satellite data was processed with L3Harris Geospatial ENVI 5.2, mapping and spatial analysis of data with ESRI ArcGIS 10.4 and statistical workflow were performed with STATSOFT STATISTICA 12.0. Processing of satellite data includes radiometric calibration and atmosphere correction with standard ENVI tools and default settings.

After validating the new index with field data within Almaty Region for the period 2013–2019, it was used in different scales for Almaty and Kyzylorda Regions based on Landsat-8 data as for the entire territory of Kazakhstan with TERRA/MODIS

imagery. Landsat scenes used for Almaty Region and Kyzylorda Region are listed in Table 3.

The general flowchart of data processing is presented in Fig. 3.

4 Results

The scale of degradation presented in Table 2 was used to verify the classification of satellite data with the index herein proposed (CDI). The scale accepted is quite subjective as the class designation depends completely upon specialists' expertise working in the field. However, the integral nature of the scale assumes the joint work of several experts (specialists in soil science, geobotany, and geography). It leaves very few possibilities to misinterpret the degradation degree. CDI demonstrated good correlation with numerical values of degradation ($r = 0.5285$) (Table 4).

Statistical correlation was calculated for 7 years (2013–2019), assuming that landscape changes in the area with the low human population are minor within a short period and depend mainly upon the climate fluctuations rather than upon human activity. The distribution of the CDI remains close to normal during the observable period of 7 years (Fig. 4), so the CDI range is thought to encompass the degradation phenomenon in most of its manifestations, existing within the study area.

The resulted map of degradation degree for the study area, as shown in Fig. 4, demonstrates the accurate spatial distribution of degraded land and degradation severity within the study area and good resemblance to field protocols. However, a disputable spot appears south-west of Kuraksu Village (six field points of bright green and yellow color south-west of Kuraksu Village in Fig. 5). Field protocols reveal weak or moderate degradation in this region, whereas CDI returns rather moderate to strong degradation.

The experimentally established informative range of CDI values is 0.27–0.6; this range comprises all the degradation classes and manifestations except areas of heavy salinization. It was shown that low values of the CDI could describe seasonal fluctuations in the land surface and vegetation cover dependent on the weather envelope of the current season. The disputable spot of Kuraksu Village is referred to as the sandy dune desert (Fig. 6); this kind of desert depends on the weather and, in particular, on the moistening regime.

During the dry year, the entire plant coverage is less developed than that of the wet year, whereas bare soils are spread much wider in the dry season. The reflectance of chlorophyll measured with satellite sensors in a dry year is less, and the reflectance of bare soil is greater during the dry year if compared to the same parameters, measured in the same area for wet years. This would mean a more pronounced manifestation of degradation at the image, taken within the dry year in terms of satellite data. The comparison of CDI distribution for dry and wet years (Fig. 7) shows the significant shift of "intact" and "light degradation" areas. In contrast, strong and severe degradation foci, associated with settlements, wells and permanent barren areas remained pretty constant.

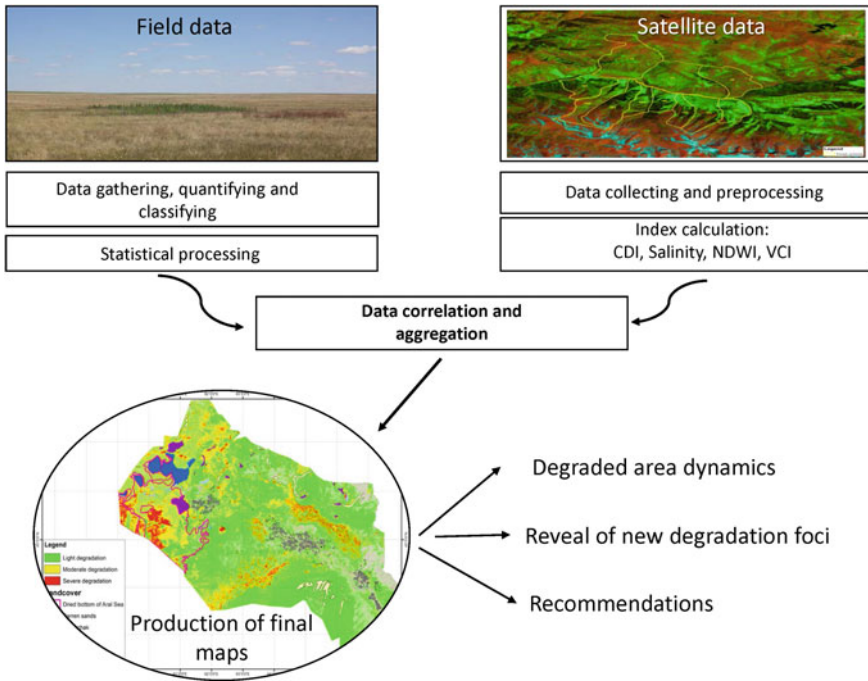


Fig. 3 Simplified flowchart of data retrieval and processing

The entire range of CDI (0.27–0.6) was divided into three equal intervals. The interval 0.27–0.38, comprising the lower third of index values, is supposed to describe seasonal fluctuations and, in general, resembles the light degree of land degradation. The middle interval of 0.38–0.49 encompasses moderate degradation, and the top third of values from 0.49 to 0.6 describes the location of permanent foci of severe degradation. From 2013 through 2019, areas of each CDI’s interval were calculated. The analysis of each class dynamics over the years showed the stability of “moderate” and “strong” degradation foci position, while the area of “light degradation” may vary in wide diapason (Fig. 8, Table 5).

The abrupt increase of lightly degraded area in the year of 2014 is explained with meteorological data. Available data from the meteorological station “Aul-4”, located to the west of the study area in the Delta of Ile River, comprises 2000–2014. The sum of summer precipitation in the region normally varies between 15 and 58 mm. The summer of 2014 was the driest during the period of observation, with the total amount of summer precipitation as about 1 mm (3% of normal summer precipitation).

Another indicator of moistening condition throughout a certain season is Vegetation Condition Index (VCI) developed by Kogan [36] and applied as a drought predictor. Figure 9 represents the distribution of VCI values in Almaty Region for dry, wet and moderately wet years.

Table 4 Correlations of ground degradation classes and CDI values

Var. X and Var. Y	Marked correlations are significant at $p < 0.05000$ (Casewise deletion of missing data)										
	Mean	Std. Dv	$r(X, Y)$	t	p	N	Constant dep: Y	Slope dep: Y	Constant dep: X	Slope dep: X	
Ground degradation	3.06	1.3									
CDI	0.26	0.059	0.528548	14.4	0.05	539	0.189945	0.023966	-0.005365	11.65641	

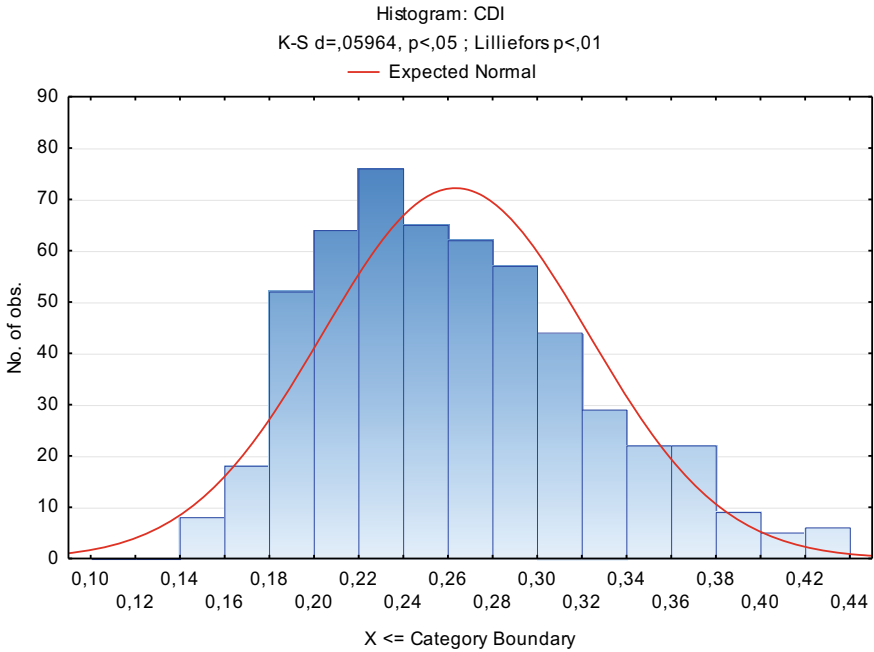


Fig. 4 The normality of CDI values over 7-years period

The distribution of VCI's values over summer months within dry, moderately wet and wet years shows the very poor condition of plain vegetation in dry years. Depleting the vegetation in huge areas returns the rising CDI values, calculated with synchronous satellite data. Suppose the index is calculated for a single satellite image. In that case, that may become hard to explain its range without the information on weather conditions. Nevertheless, it is noticeable that the study area has a fragmented distribution of VCI values even in most favorable year, indicating unevenness of natural plant cover. VCI demonstrated high vegetation cover variability from another vantage point, which follows the weather changes quite rapid even the one-year summer (see Fig. 9, July and August of 2016). So, it is possible to confirm the relation of low CDI range to the vegetation condition and moistening regime (as possible initial stages of degradation process), rather than to deep vegetation and soil structure changes. Analysis of CDI ranges distribution within dry and wet conditions confirms that the lower range of 0.27–0.38, here considered as “light degradation degree” describes seasonal fluctuations of the moistening and vegetation. The range of 0.38–0.6 depicts stable foci of land degradation, where soil is affected with erosion and salinization. As follows from meteorological data analysis and from VCI data (Fig. 9, 2014 year), the moisture scarcity resulted in early wilting of vegetation within a huge area that, in turn, makes the “weak degradation” range of CDI spatially expanded. The use of a single satellite image may lead to misinterpretation of actual degradation statements in terms of “light degradation” overestimation.

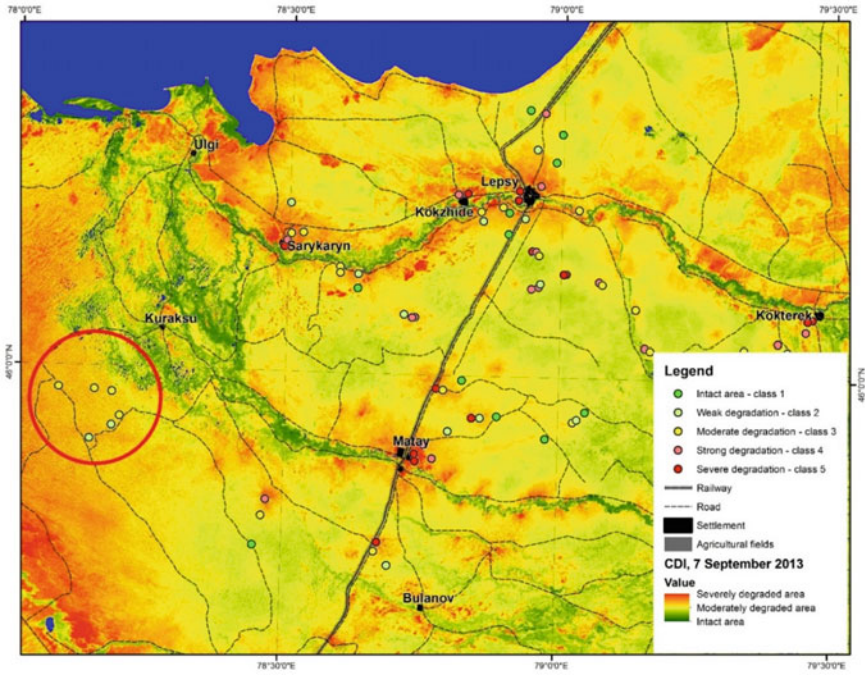


Fig. 5 CDI for the study area, September 2013. CDI scale varies from green (no degradation) to red (severe degradation). Red circle indicates a disputable area



Fig. 6 Typical landscape of the south-west vicinity of Kuraksu Village (Photo by D. Malakhov)

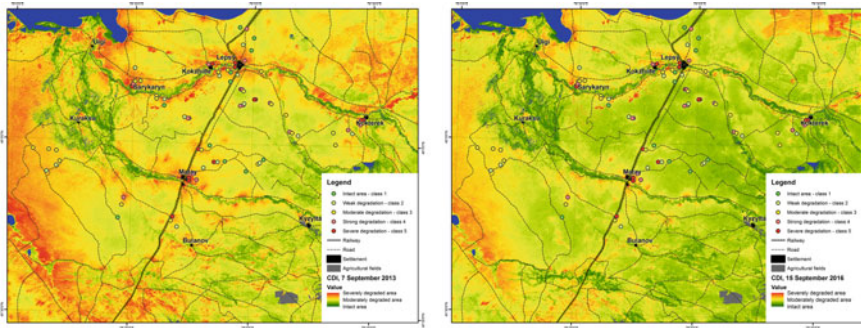


Fig. 7 Distribution of CDI values in dry (left, 2013) and wet (right, 2015) years. Dry conditions of 2013 year resulted in wider distribution of “light and moderate degradation” ranges of CDI. Wet year (2015) demonstrates the significant shrinking of light and moderate degradation areas, whilst the severe degradation foci persisted

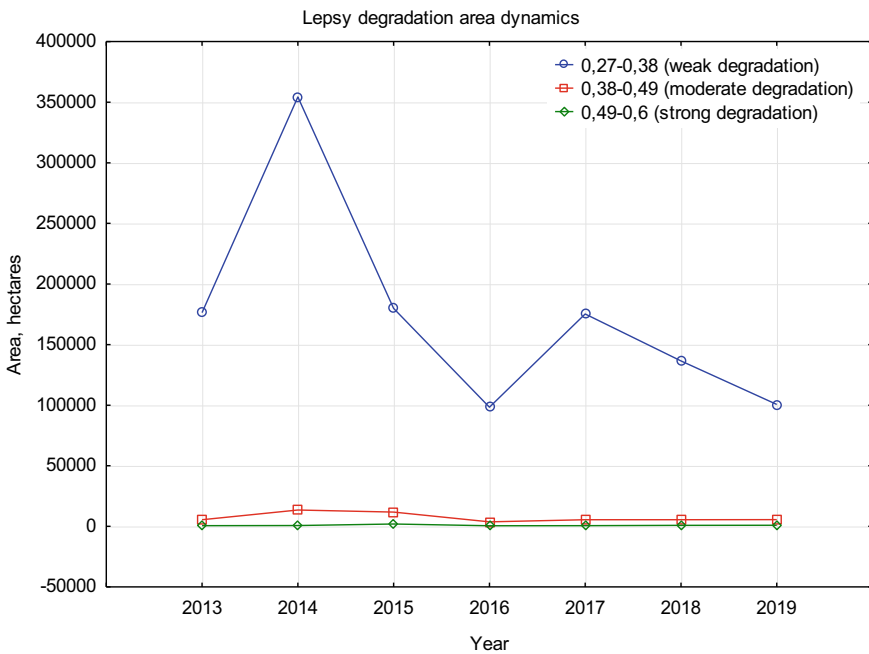


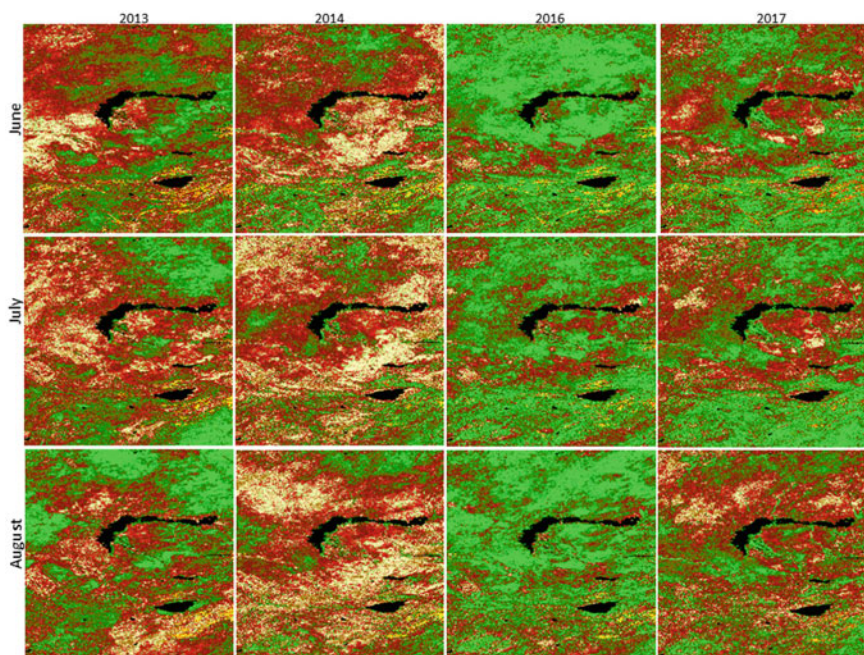
Fig. 8 Changes of CDI ranges’ area over the period of 2013–2019

Results of the CDI study and validation were applied on regional and national scales. Integral maps of land degradation were developed for Almaty and Kyzylorda Regions (Figs. 10 and 11) basing on Landsat-8 data.

Kyzylorda Region, located east of the Aral Sea, is most degraded territory in Kazakhstan. The territory of the Region naturally fits the sandy desert belt, and the

Table 5 Areas of CDI ranges within the study area for the period of 2013–2019

CDI interval	Area, hectares						
	2013	2014	2015	2016	2017	2018	2019
0.27–0.38 (weak degradation)	176,348	354,273	179,843	98,268	175,274	136,464	100,595
0.38–0.49 (moderate degradation)	5510	13,483	11,778	3743	5448	5469	5548
0.49–0.6 (strong degradation)	604	682	1964	534	585	827	901

**Fig. 9** Monthly dynamics of VCI in dry (2013, 2014), wet (2016) and moderately wet (2017) summer. Green pixels resemble good vegetation condition; deep red pixels indicate very bad vegetation condition

shrinking of the Aral Sea causes the further burdening of the ecological situation for this region. On the other hand, Kyzylorda Region is one of most populated in Kazakhstan. The presence of water sources (the main source of water is Syr-Darya River) allows arable farming and traditional cattle-breeding. Both, the geographical position of the Region within desert belt and the huge badlands at the former bottom of Aral Sea, affected with intense wind erosion and producing massive clouds of salty dust, make the region possessing tremendous foci of natural degradation. In

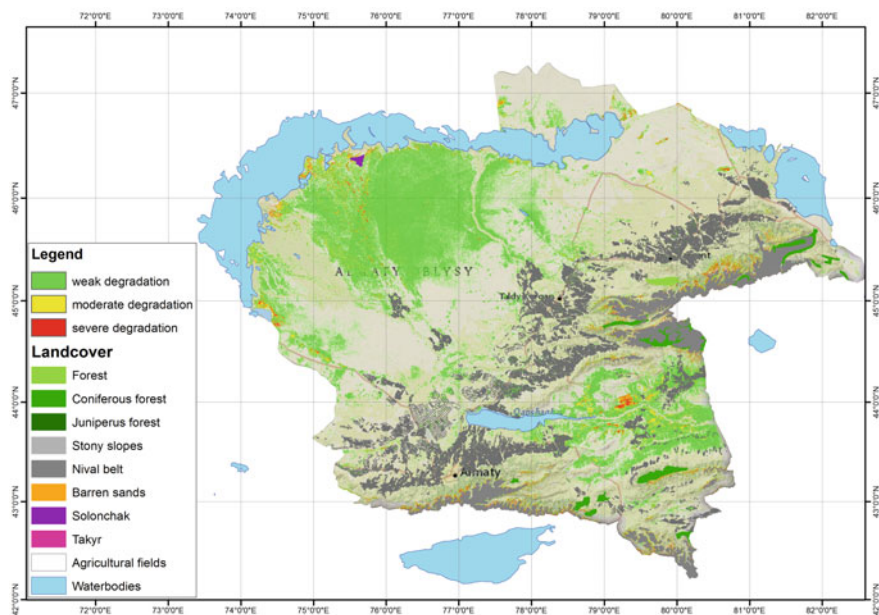


Fig. 10 Map of land degradation in Almaty Region by satellite data of 2019

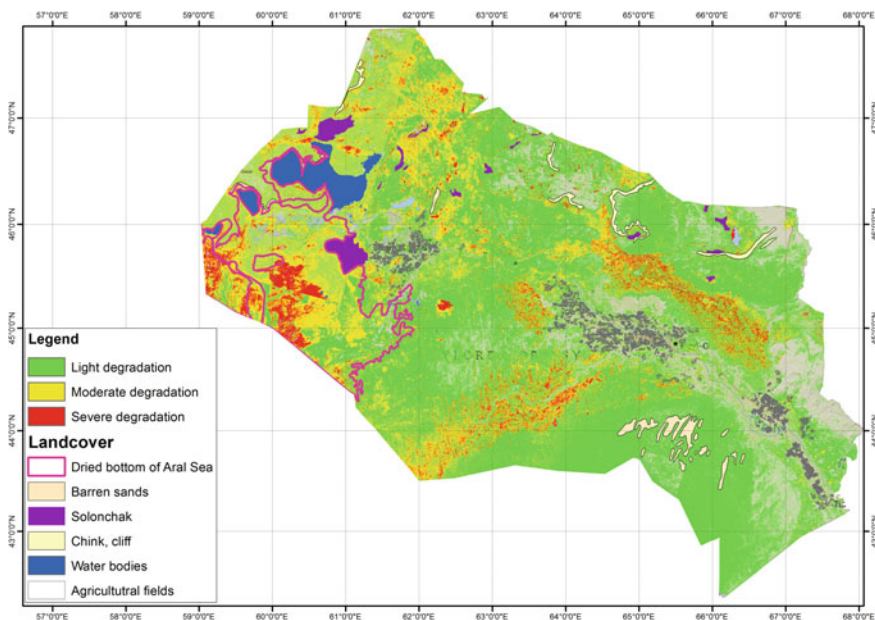


Fig. 11 Map of land degradation in Kyzylorda Region by satellite data of 2019

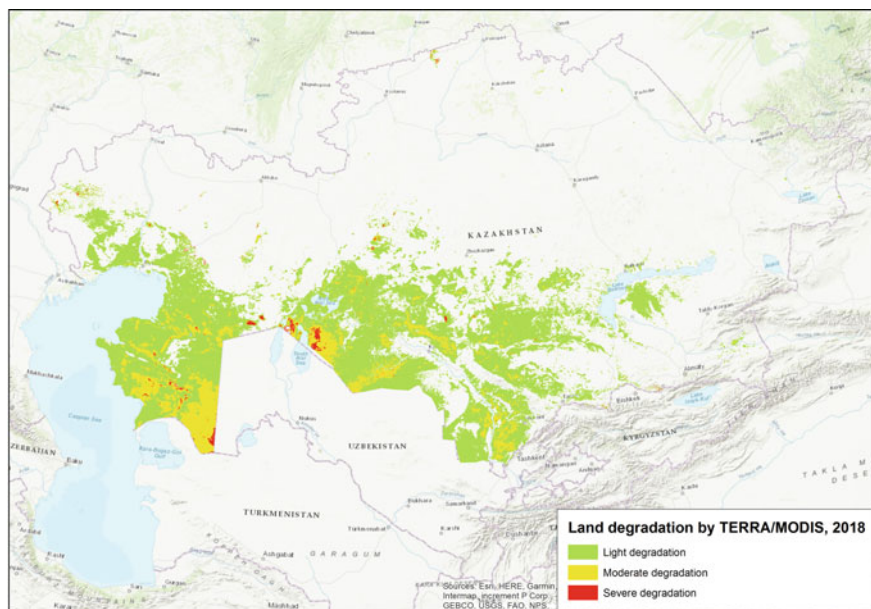


Fig. 12 Map of degraded areas by TERRA/MODIS data, September 2018

this situation, rapid and objective monitoring of degraded areas is highly demanded and useful from ecological and socio-economical positions.

CDI was contributed for the national scale as well with TERRA/MODIS data as a source of satellite information. MOD021KM data, encompassing 36 spectral bands with a spatial resolution of 1 km, were used to develop the map of degraded lands of Kazakhstan. Figure 12 represents the map of degraded areas for the autumn of 2018 (joint project of National Center of Space Research and Technology and KGS Space Technologies).

The comparison of degraded areas and territories, affected with salinization, calculated with the salinity index given in **Material and Methods** reveals a close spatial association of salty and degraded areas (Figs. 12 and 13).

The actual distribution of degraded lands revealed with different sensors may vary depending upon the climatic conditions of the data acquisition period and upon the spatial resolution of imagery. In fact, persistent hotspots of degraded lands do not usually occupy big areas. Instead, small patches of severely degraded territories may be represented as a single or few pixels at CDI's raster derived from TERRA/MODIS imagery, or even absent if the area of the hotspot falls beneath the spatial resolution of satellite data. Figure 14 demonstrates the difference of degradation distribution derived from autumn scenes of Landsat-8 and TERRA/MODIS within the same area.

Applied to MODIS imagery, CDI demonstrates some alteration of degraded areas if considered to CDI derived from Landsat-8. Most of "light" and "moderate" ranges of Landsat are attributed to "light" degradation by MODIS, whereas some of "light

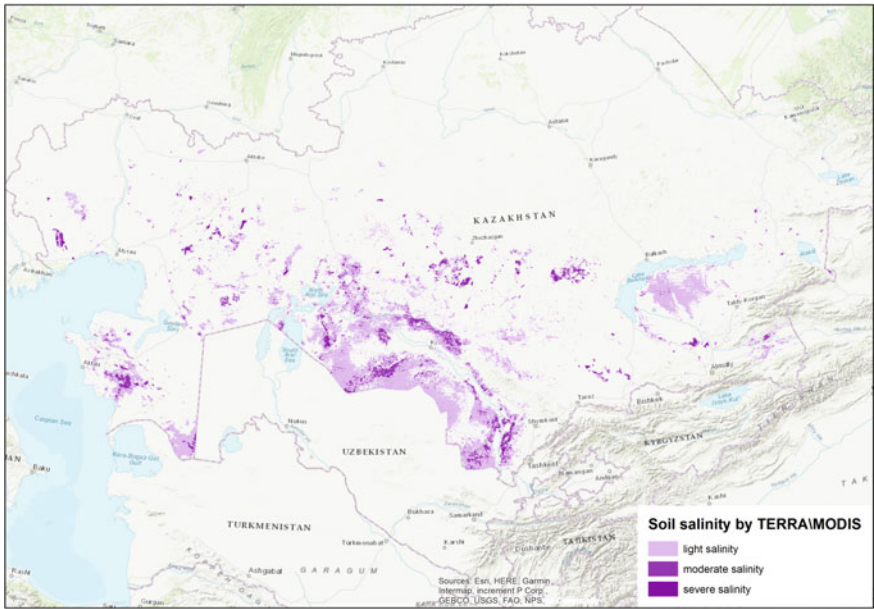


Fig. 13 Map of superficial salinization by TERRA/MODIS data, September 2018

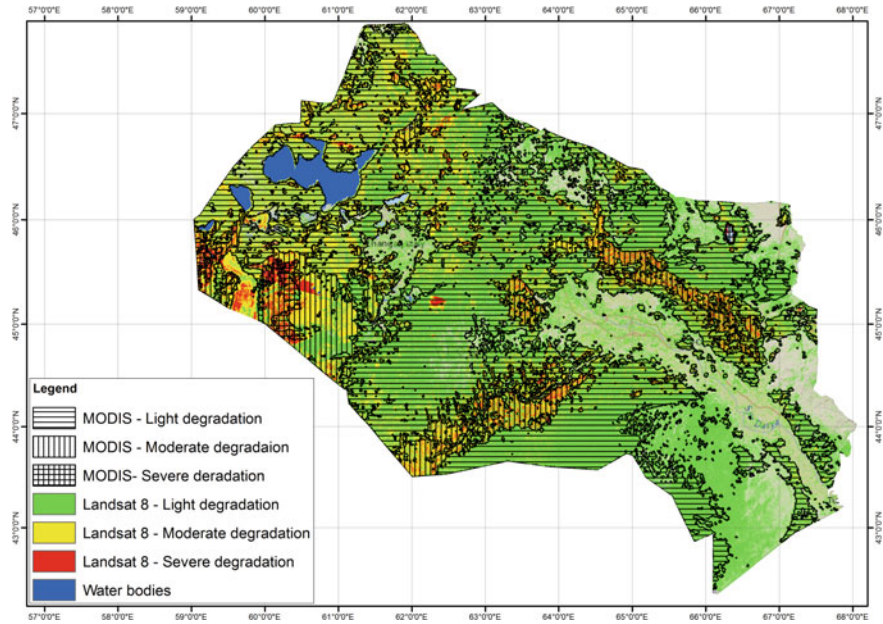


Fig. 14 Different visualization of degraded areas derived from low and moderate resolution satellite data

degradation” areas of Landsat do not fit into degraded areas by MODIS at all. It looks like MODIS-derived CDI has lesser sensitivity to seasonal fluctuations of plant cover. However, it is obvious that those areas, discriminated by MODIS as degraded territories in wide sense, resemble “moderate” and “severe” degradation by Landsat. Apparently, the index calculated with TERRA/MODIS provides adequate recognition of degraded land in the diapason of meaningful values (0.27–0.6). However, the particular ranges within the diapason remain a subject of further study.

5 Discussion

If consider satellite imagery, the increasing of the surface albedo is one of the key features that may indicate soil and vegetation cover degradation. Soil albedo depends on such factors as the moisture content and the richness of organic matter. Wet soils with high humus content have lesser albedo than dry soils with pure humus content. The depletion of vegetation and the fragmentation of continuous plant cover within degraded areas also increase in surface albedo. Soil and vegetation of degraded landscapes may become heavily fragmented due to different erosion activity and, thus, become very spectrally heterogeneous. High spatial and spectral heterogeneity of arid landscapes may indicate an active degradation process in the area. On the other hand, high spectral unevenness of the area makes the use of a single parameter, as vegetation cover, soil moisture, humus content or soil albedo, doubtful when estimating the degradation by means of satellite data. Obviously, the accurate estimation of the degradation degree should consider as many parameters as possible to retrieve with satellite data. However, the results of global studies are disputed because they are different from traditional expert assessments, and are hard to validate in the field. At the same time, local assessments are only snapshots of small areas, generally too detailed for global application [1].

The most common methods to assess land degradation are following [38]: expert opinions, land users’ opinions, field monitoring, observations, and measurement, modeling, estimation of productivity changes, and remote sensing. Methods of the assessment of the degraded areas with remotely sensed data could be divided, in general, into two major groups:

- (a) Direct use of satellite data in the form of spectral indices or image classification [39–43];
- (b) Combined approaches, when satellite data use in any form is combined with ancillary data and/or involved in modeling procedures [44–49].

Remotely sensed approaches appear to be optimal for the global or national levels, as satellites provide up-to-date and regular information on land surface dynamics and vegetation cover dynamics. The data, acquired from satellite sensors may be calibrated with ground data and provide valuable information on the land dynamics over the range of spatial and temporal scales.

Spectral indices used to assess land degradation, provide different results in terms of accuracy and sensitivity. It is hard to outline the “ideal” spectral index for degradation monitoring. Multiple factors and drivers regulate the degradation process itself, and the relation between those factors is far from clear understanding. “Ideal” index should consider many factors and, moreover, to provide the interaction of considered factors within a single algorithm, making the algorithm non-discrete and useable in large-scaled applications. Fadhil [33] proposed a novel index representing a promising direction of degradation indices development combining significant factors: the vegetation and the soil wetness in a single complex approach. However, being tested in their original format at heavily transformed region of oil production [50], this approach demonstrated rather moderate effectiveness. The index proposed (CDI) attempts to further improve the combination of vegetation condition, soil wetness and soil albedo within a single algorithm as another step to “ideal degradation index”.

CDI appears to be a quite effective and informative approach to degradation assessment and may be applied for both highly detailed regional observations and observations at the national scale. This index is sensitive to seasonal fluctuations of soil moistening and vegetation cover in the lower range of values. At the same time, the upper ranges of the index values indicate the area where persistent foci of degradation are developed. The proposed three ranges of CDI values roughly divide the degraded area into three classes: light, moderate and severe degradation. However, these ranges are the subject of further study, both for different landscapes and soil content and for different types of satellite sensors. In its current form, the index accurately describes spatial dynamics of degraded areas with use of satellite imagery of moderate spatial resolution and provides adequate, albeit sometimes disputable, spatial distribution of degraded lands. Subjects of further study are: the applicability of the index in arid steppe zone; the ranging of the CDI informative interval into distinct classes for certain landscapes and climatic conditions; further validation of the index with TERRA/MODIS data. All the activities listed should be based upon adequate and reliable ground data.

6 Conclusions

The multiform interaction of soil and vegetation is the basis of any ecosystem. This interaction provides the transformation of sun and chemical energy into organic components, thus forming a food chain base. Hence the disturbance of one or both of these components caused by any driver will negatively affect the entire ecosystem. The stability of natural ecosystems used as a food resource of livestock is extremely important in arid areas, where there are no other agricultural opportunities and the cattle-breeding is a major if not the only way to maintain human well-being. As land degradation is an extremely complex phenomenon the approach of this phenomenon assessment with remotely sensed should not consider just a single parameter, like vegetation or soil condition. It appears reasonable to assess multiple indicators of

degradation to provide fast and accurate information on the current state of land degradation within a certain area.

Complex Degradation Index (CDI) is a promising attempt to combine the plant cover condition, soil moistening and the reflectance of bare soils in the form of a single algorithm of satellite data processing. The theoretical basis of this index is the assumption of the land degradation process as a complex phenomenon with multiform interaction of possible drivers and major components of ecosystem: soil and vegetation. Empirically derived from the joint analysis of satellite (Landsat-8) and ground data, the informative diapason of CDI values thought to comprehensively describe most of the degradation manifestations in the arid zone of Kazakhstan. Being extended to TERRA/MODIS imagery, the algorithm demonstrated optimistic results for the wide-scale monitoring purposes. However, an additional study of MODIS-based CDI is needed. The difference between Landsat and MODIS CDI's concerns mainly the area of "light degradation" interpretation and loss of details with MODIS data. The shift of CDI ranges in MODIS data with the prevalence of "light degradation" over the area may result from the spatial resolution of MODIS. The sensitivity and accuracy of CDI, calculated with MODIS data, need additional studies to clarify the certain ranges of the index.

7 Recommendations

The estimation of land degradation is an expensive and complicated procedure in waste arid areas of Kazakhstan if attempted by traditional ground survey methods. The algorithm proposed provides cost-effective and reliable results of degraded areas assessment with remotely sensed data. This algorithm could serve as a basis to develop the complex monitoring system of land degradation processes in Kazakhstan as well as in other countries with predominating arid conditions.

Acknowledgements N. N. Karabkina (NCSRT, Kazakhstan) collected and processed meteorological data; A. F. Islamgulova ("Turan" University, Kazakhstan), A. Aysarova (NCSRT, Kazakhstan), R. Iskakov (NCSRT, Kazakhstan), N. E. Bekmuhamedov (NCSRT, Kazakhstan), provided valuable assistance during field expeditions; N. I. Berdygulov (NCSRT, Kazakhstan) helped with satellite data collecting and preprocessing. The work on the CDI development has been initiated in the framework of the project "Development and improvement of methods and technologies for thematic decryption of remote sensing data of the earth and calibration of remote sensing equipment using sub-satellite observations at test sites" associated to the Republic Program "Applied research in the field of space activities" in 2013.

References

1. DeJong R, DeBruin S, Schaepman M, Dent D (2011) Quantitative mapping of global land degradation using Earth observations. *Int J Remote Sens* 32(21):6823–6853
2. Ibrahim YZ (2017) Vegetation and land cover change in the context of land degradation in sub-saharan West Africa. University of Leicester, 179 pp
3. Torrion JA (2002) Land degradation detection, mapping and monitoring in the Lake Naivasha Basin, Kenya. International Institute for Geo-Information Science and Earth observation Enschede, the Netherlands, 93 pp
4. Hill J, Sommer S, Mehl W, Megier J (1995) Use of Earth observation satellite data for land degradation mapping and monitoring in Mediterranean ecosystems: towards a satellite-observatory. *Environ Monitor Assess* 37(1–3):143–158
5. Hennemann R (2001) Elective on land degradation, assessment, monitoring and modelling. Soil Science Division, ITC, Enschede, The Netherlands
6. UNCCD (1994) Elaboration of an international convention to combat desertification in countries experiencing serious drought and/or desertification, particularly in Africa. UN, Bonn
7. GLASOD (1988) Guidelines for general assessment of the status of human induced soil degradation: Global Assessment of Soil Degradation GLASOD, ISRIC, Wageningen, The Netherlands, p 25
8. Hill J, Megier J, Mehl W (1995) Land degradation, soil erosion and desertification monitoring in Mediterranean ecosystems. *Remote Sens Rev* 12(1–2):107–130
9. DeJong SM (1994) Applications of reflective remote sensing for land degradation studies in a mediterranean environment. Utrecht University, Utrecht, The Netherlands, 250 pp
10. Lal R, Stewart BA (1985) Soil degradation: a global threat. In: Lal and Stewart (eds) *Soil degradation*, vol 2. *Advances in soil science*. Springer, New York, pp 13–17
11. Dregne H (1998) Land degradation: assessment and monitoring. *Int Taskforce Land Degradation* 32
12. Elhag MM (2006) Causes and impact of desertification in the Butana Area of Sudan. Bloemfontein, 190 pp
13. Foth HD (1991) *Fundamentals of soil science*. Wiley, 382 pp
14. Ahmad N, Pandey P (2018) Assessment and monitoring of land degradation using geospatial technology in Bathinda district, Punjab, India. *Solid Earth* 9:75–90
15. Metternicht G, Zinck A (2008) Remote sensing of soil salinization: impact on land management. CRC Press, Boca Raton, 377 pp. <https://doi.org/10.1201/9781420065039>
16. Vågen G, Winowiecki LA (2019) Predicting the spatial distribution and severity of soil erosion in the global tropics using satellite remote sensing. *Remote Sens* 11:1800. <https://doi.org/10.3390/rs11151800>
17. Zha Y, Gao J, Ni S, Liu Y, Jiang J, Wei Y (2003) A spectral reflectance-based approach to quantification of grassland cover from Landsat TM imagery. *Remote Sens Environ* 87:371–375
18. Okin GS, Murray B, Schlesinger WH (2001) Degradation of sandy arid shrubland environments: observations, process modelling and management implications. *J Arid Environ* 47:123–144
19. Bekmuhamedov EL, Rysimbetov TK, Assanov AA, Bekmuhamedova NZ (2010) Pasture resources of Kazakhstan. Shymkent, 332 pp
20. Botanical geography of Kazakhstan and Middle Asia (Desert region) (2003) (Rachkovskaya EI, Volkova EA, Khrantsov VN (eds)), Saint Petersburg, 424 pp
21. Pogrebenskiy MA (1963) The valley of Ile River, its nature and resources. Alma-Ata, pp 252–260
22. Plissak RP (1981) Change in the vegetation of the Ili River Delta under flow overregulation. Alma-Ata, 216 pp
23. Rachkovskaya EI (1993) Vegetation of the Gobi Deserts of Mongolia. Saint Petersburg, 132 pp
24. Rachkovskaya EI (1995) On the desert type of vegetation. *Bot J* 80(9):53–58

25. Prozorovsky AV (1935) On the zonal types of deserts in Soviet Middle Asia. *Izvestya Gosudarstvennogo Geographicheskogo Obschestva* 3:318–331
26. Kottek M, Grieser J, Beck C, Rudolf B, Rubel F (2006) World Map of the Köppen-Geiger climate classification updated. *Meteorol Z* 15(3):259–263
27. Peel MC, Finlayson BL, McMahon TA (2007) Updated world map of the Köppen-Geiger climate classification. *Hydrol Earth Syst Sci* 11:1633–1644
28. Kurochkina LY, Osmanova LT, Karibayeva RN (1986) Fodder plants of deserts of Kazakhstan. Alma-Ata, 206 pp
29. Dimeyeva LA, Stogova LL (2001) Natural pastures of Kazakhstan. *Almaty*, pp 143–144
30. Zobler L (1986) A world soil file for global climate modeling. NASA Tech. Memo. 87802, 33 p
31. Bizhanova G, Kurochkina LY (1989) Anthropogenically induced changes of Moinkum Desert pastures and pasture cartography. Alma-Ata, 164 pp
32. Akiyanova FZ, Kurochkina LY (2006) The desertification as a process of land degradation. *Almaty* 3:197–254
33. Fadhil AM (2009) Land degradation detection using geo-information technology for some sites in Iraq. *J Al-Nahrain Univ* 12(3):94–108. <https://doi.org/10.22401/JNUS.12.3.13>
34. Malakhov DV, Islamgulova AF (2014) The quantitative interpretation of pasture image parameters: an experience with low and moderate spatial resolution remotely sensed data application. *Optika Atmosfery i Okeana* 27(7):587–592
35. McFeeters SK (1996) The use of normalized difference water index (NDWI) in the delineation of open water features. *Int J Remote Sens* 17:1425–1432
36. Kogan FN (1990) Remote sensing of weather impacts on vegetation in non-homogeneous areas. *Int J Remote Sens* 11:1405–1419
37. Kogan FN (1996) Global drought watch from space. *Bull Amer Meteorol Soc* 78(4):621–636
38. Kapalanga TS (2008) A review of land degradation assessment methods. Land Restoration Training Programme, Keldnaholt, 112 Reykjavík, Iceland, pp 17–68
39. Ajourlo M (2005) Evaluation and mapping of rangelands degradation using remotely sensed data. *Sociedade & Natureza, Uberlândia, Special Issue* 727–735
40. Hoshino B, Kaneko M, Matsunaka T, Ishii S, Shimada Y, Ono C (2009) A comparative study of pasture degradation of Inner Mongolian fenced and unfenced land based on remotely sensed data. *J Rakuno Gakuen Univ* 34(1):15–22
41. Al-Bakri J, Saoub H, Nickling W, Suleiman A, Salahat M, Khresat S, Kandakji T (2012) Remote sensing indices for monitoring land degradation in a semi-arid to arid basin in Jordan. In: Civco DL, Ehlers M, Habib S, Maltese A, Messinger D, Michel U, Nikolakopoulos KG, Schulz K (eds) *Earth resources and environmental remote sensing/GIS applications III. Proceedings of SPIE* 8538 853810. <https://doi.org/10.1117/12.974333>
42. Liu Y, Zha Y, Gao J, Ni S (2004) Assessment of grassland degradation near Lake Qinghai, West China, using Landsat TM and in situ reflectance spectra data. *Int J Remote Sens* 25(20):4177–4189. <https://doi.org/10.1080/01431160410001680419>
43. Karnielia A, Bayarjargala Y, Bayasgalan M, Mandakh B, Dugarjav Ch, Khudulmur J, Bazha SN, Gunin PD (2013) Do vegetation indices provide a reliable indication of vegetation degradation? A case study in the Mongolian pastures. *Int J Remote Sens* 34(17):6243–6262. <https://doi.org/10.1080/01431161.2013.793865>
44. Lu D, Batistella M, Mausel P, Moran E (2007) Mapping and monitoring land degradation risks in the Western Brazilian Amazon using multitemporal Landsat TM/ETM+ images. *Land Degrad Develop* 18:41–54
45. Bai ZG, Dent DL, Olsson L, Schaepman ME (2008) Proxy global assessment of land degradation. *Soil Use Manag* 24:223–234. <https://doi.org/10.1111/j.1475-2743.2008.00169.x>
46. Fadhil AM (2011) Drought mapping using Geoinformation technology for some sites in the Iraqi Kurdistan region. *Int J Digital Earth* 4(3):239–257. <https://doi.org/10.1080/17538947.2010.489971>
47. Tagore GS, Bairagi GD, Sharma NK, Sharma R, Bhelawe S, Verma PK (2012) Mapping of degraded lands using remote sensing and GIS techniques. *J Agric Phys* 12(1):29–36

48. Pandey PC, Rani M, Srivastava PK, Sharma LK, Nathawat MS (2013) Land degradation severity assessment with sand encroachment in an ecologically fragile arid environment: a geospatial perspective. *QScience Connect* 43. <https://doi.org/10.5339/connect.2013.43>
49. Homère A, Mfondoum N, Etouana J, Nongsi BK, Moto FA, Deussieu FGN (2016) Assessment of land degradation status and its impact in arid and semi-arid areas by correlating spectral and principal component analysis neo-bands. *Int J Adv Remote Sens GIS* 5(2):1539–1560
50. Mjachina KV, Malakhov DV (2013) An experience of moderate spatial resolution remote sensing data application for the discrimination of oil industry objects within technogenic modified landscapes (Orenburg region as example). *Izvestiya Samarskogo nauchnogo centra RAS* 15(7):2260–2265

Land Degradation Issues in Uzbekistan



Mukhiddin Juliev, Lazizakhon Gafurova, Olimaxon Ergasheva, Makhsud Ashirov, Kamila Khoshjanova, and Mirvasid Mirusmanov

Abstract Land degradation in the previous century has become one of the main challenges to the global environment, especially this phenomenon became very common for the dry climate zones. Uzbekistan also faces the land degradation consequences and the application of the up-to-date technologies can help to save a soil. The current chapter describes the land degradation problems, which face Uzbekistan and different ways of finding solutions. Soil erosion and soil salinity are main issues for the land degradation in Uzbekistan. In addition, climate change phenomena effects have been discussed. Climate change regionally will increase by the number of extreme weather events, periods with droughts and high summer temperatures, fluctuations in the regime of water resources formation, and land degradation. Furthermore, the current status of the Aral Sea shows that the region became a zone of applying environmental innovation and technologies. In the last part, we listed the main priorities of soil science development in Uzbekistan. This chapter can be applied as a methodological recommendation for stakeholders in agriculture and water resources management fields in dealing with the consequences of land degradation.

Keywords Land degradation · Soil erosion · Soil salinity · Aral Sea · Climate change · Uzbekistan

M. Juliev (✉)

Tashkent Institute of Irrigation and Mechanization of Agricultural Engineers, Tashkent, Uzbekistan

e-mail: mukhiddinjuliev@gmail.com; mukhiddinjuliev@tiiame.uz

Turin Polytechnic University in Tashkent, Tashkent, Uzbekistan

L. Gafurova · O. Ergasheva · M. Ashirov · K. Khoshjanova

National University of Uzbekistan, Tashkent, Uzbekistan

M. Mirusmanov

Tashkent State Technical University, Tashkent, Uzbekistan

1 Introduction

Uzbekistan is one of the large states of the Central Asian region, with more than 33 million people, extensive experience in irrigated agriculture, and developing industry. According to the scheme of provincial division, Uzbekistan is included in the Central Asian soil-climatic province, characterized by a climate of continental (dry) subtropics and specific soils that are different from soils of the more northern regions of Eurasia [1].

The country's territory has an extremely diverse landscape: plateaus and plains, lowlands and depressions, elevations of foothills, spurs of mountains and mountain ranges. The plains consist of the Ustyurt plateau and the Aral lowland in the northwest, almost the whole Kyzyl Kum desert and the steppes adjoining it (Mirzachul, Karshi), wedging between the mountain ranges far to the east. The steppes smoothly pass into the foothills, and serve as a link connecting the desert plains of the west and the mountainous part of the east. In addition, tectonic processes led to the formation of vast intermountain depressions called valleys (Ferghana, Zerafshan, Kitab-Shakhrisabz, Sherabad-Surkhandarya, etc.) [2].

Facts from the last century declaring that the land degradation has become one of the main challenges to the global environment, catastrophically worsening the productive potential of the earth and violating the integrity and sustainability of natural ecosystems, especially in the arid countries of the world [3, 4].

Key problems of land degradation in Uzbekistan, causing serious concern in terms of providing vital environmental services, are secondary salinization of irrigated lands; waterlogging, flooding and waterlogging of lands under the influence of irrigated agriculture; soil depletion—loss of humus and nutrients, compaction; water and irrigation soil erosion in mountain and foothill areas; deflation and pasture digression in the desert regions of livestock transhumance; deforestation and loss of species diversity; soil pollution by agrochemicals, industrial chemical pollutants; Desertification of lands adjacent to the areas close to the dried site of the Aral Sea [4]. Different studies have been conducted solving issues mentioned before [5, 6]. The current chapter shows existing soil degradation problems under the climate change effect and different ways of solving them.

2 Climatic Condition of the Country

The climate of Uzbekistan is continental, dry, characterized by significant seasonal and daily temperature fluctuations, long dry and hot summers, wet autumn and unstable winter weather. According to the aridity index, the territory of Uzbekistan, except the piedmont and mountainous parts, is characterized as arid. Therefore, it is subject to desertification processes. The arid climate, which determines the features of the modern bioclimatic conditions of the region, has caused the preservation of relict salt reserves in eluvial and eluvial-accumulative landscapes, as well as modern

salt accumulation in hydromorphic conditions. In addition, small slopes of the surface of the plains and the lack of natural outflow of groundwater with the development of irrigation have influenced the migration of soluble salts [2].

Unfavorable weather conditions, such as frost, heavy rains, hail, dry winds and strong winds, with a 15 m/s or more speed, are found throughout the country. The mean wind speed in the plains ranges from 3–4 m/s, wind amplification up to 6–10 m/s, contributing to the occurrence of dust storms, is usual for desert regions. Dust stormy days vary from 10 to 30 on the flat territory, in the Karshi steppe and lower areas of the Amu Darya it can reach 50, and in the Aral Sea region (Muynak)—64. The duration of strong winds at a speed of 15 m/s or more, at which the grazing of sheep stops is 11 days a year. Various types of local winds arise in the foothills (“Bekabad”, “Kokand”). The influence of relief is also manifested in formation of a hairdryer—a warm dry wind blowing from mountains. For the southern part of the country is characterized by the southwest dry wind “Garmsil” and “Afghan”, carrying dust with sand [1].

Thus, the geographic, climatic, geomorphological and hydrogeological features of the territory have made the arid ecosystems of the country highly prone to land degradation and desertification, threatening the economy, agriculture.

3 Land Degradation in Uzbekistan

Land degradation negatively affects the integrity of an ecosystem, either through a decrease in its long-term environmental productivity or through a decrease in natural biological abundance and ability to withstand external influences [6]. In such a way, degradation is a consequence of the complex integration of biological, physical, social, political, cultural and economic factors, that is, it develops under the joint influence of nature and mankind [6].

The listed below aspects of land degradation are predetermined by nature itself, but are strengthened by irrational nature management and economic measures [4]. There are several natural factors of land degradation in Uzbekistan (Fig. 1). They are climatic features causing such phenomena as drought, dry winds, atmospheric transport of sand; steep slopes contributes to water erosion, the formation of and landslides mudflows [7]. At the same time, steady terrain, depressions and depressions create conditions for salinization and waterlogging of land [8]. Orography also contributes to the formation of specific winds (hair dryers, pine forest), which play a role in the development of wind erosion. The features of the parent rock switch to soil properties (mechanical composition, plastering, salinity) and determine the soil's predisposition to wind erosion, subsidence and karst phenomena, and form buffering soil—resistance to various toxic substances. Extreme natural phenomena not caused by human activities, such as forest and steppe fires, floods, etc., supplement the natural impact on the soil cover [9].

Anthropogenic influences on land resources in Uzbekistan:



Fig. 1 Ayaz-Kala fortress and degraded lands (Right bank of Amu-Darya river)

1. Intensive agriculture leading to the depletion of organic matter and nutrients, soil pollution with agricultural pesticides, compaction and destruction of soil structure.
2. Irrigation with inadequate drainage, improper management of collector-drainage runoff causes salinization and waterlogging;
3. Irrational pasture use (lack of pasture rotation and rotation, violation of the regulatory load, etc.), leading to overgrazing, the formation of a bare surface, destruction of the soil structure and, as a result, the development of deflation under the action of wind and high temperatures;
4. Unsustainable forestry (excessive deforestation and deforestation), causing erosion of slopes in the mountains, soil deflation and the onset of sand on fertile lands on the plain [10, 11].

Soil degradation is also associated with a violation of land reclamation measures associated with cotton monoculture. High amounts of fertilizers and pesticides, the extreme inadequate utilization of organic fertilizers and the cultivation of perennial grasses and side crops causing land degradation [6]. Inadequate agricultural practices caused soil dehumidification, soil destruction [4].

One of the global tasks of protecting soils is protecting soils from erosion [12, 13]. Currently, out of the total area of the Republic, 44,410.3 thousand hectares are 26,734 thousand hectares of agricultural land and only 1551 thousand hectares or only 5.8% of them are not subject to erosion [6]. More than 4700 thousand hectares are subject to water erosion. Water erosion processes mainly occur in the mountain slopes, foothills [6].

Soil erosion control is one of the most important tasks. About 56% of lands are subject to wind erosion. About 20% of soils are affected by water erosion; these processes are most widely observed in Kashkadarya, Surkhandarya, and Tashkent regions they reach 50–80%. As a result of irrigation erosion alone, soil loss amount equals to 100–500 t/ha, and loss of humus annually can be 500–800 kg/ha, nitrogen 100–120 kg/ha phosphorus, 75–100 kg/ha or more [14].

A major environmental problem in Uzbekistan is soil salinity. Over the past 3–5 decades, the territory of saline lands was enlarged [6, 14]. As a consequence of climate change, an increase in the intensity of groundwater discharge in the aeration zone is expected, which will lead to the development of secondary salinization. In several areas, salinization is accompanied by the formation of difficultly reclaimed gypsum soils. The total area of gypsum lands is 291.5 thousand ha, and they are most widespread in the Republic of Karakalpakstan, Syrdarya, Jizzakh and Kashkadarya regions, in the Fergana Valley [4, 15, 16]. Thus, to adapt land use to climate change, it is important to prevent secondary salinization and take effective measures that can stop soil degradation.

In that way, there is a need to take urgent measures to increase the effectiveness of land use and soil protection, to carry out land reclamation of disturbed pasture lands. Main reason is to protect soils from erosion and salinization, desertification of pollution, dehumidification of re-compaction and other negative phenomena affecting conservation and increasing soil fertility (Fig. 2).



Fig. 2 Degraded lands of Khojakol basin (Right bank of Amu-Darya river)

4 Effects of Climate Change Phenomena

It is known that the problem of climate change and its effect on the environment is one of the main problems of the XXI century that humanity faces. An important place here is the conservation of soil cover and biological diversity under the active influence of anthropogenic factor [17, 18]. In Uzbekistan, regional climate change will increase the number of extreme weather events, periods with droughts and hot summers, changes in the regime of water resources formation, and land degradation [19]. Climate forecasts indicate that the region will be subject to increase in average annual temperature of 1.9–2.4 °C by 2050, with a difference in regions, with the most significant warming occurring in winter and spring. The average annual rainfall will increase by 15–18% with the greatest increase in the summer season. Deterioration and more risky conditions of agricultural production, due to an increase in temperature there is an increase in evapotranspiration of agricultural crops. Compensation of the predicted increase in rainfall and leading to more arid conditions of agricultural production, increasing its relevance on already scarce water resources, a gradual increase in the predicted water shortage in Aral Sea Basin. It is predicted that as water demand and volume decrease are guaranteed water withdrawal from the Amu Darya and Syr Darya rivers. The water deficit will exceed 500%, increasing from 2 km³ in 2005 to 11–13 km³ in 2050. Finally, an increase in the length of the growing season, especially in the northern regions, which makes it possible to plant new crops [20].

Climate change—is a problem not only of the future, but also of the present. Therefore, the strategy of modern agriculture should consider the appearance of this stress factor [18]. The rational use and conservation of soils in Uzbekistan occupy a special place in the general problem of the protection and rational use of natural resources in the face of climate change. Soil resources are limited in area and quality. The current state of soil resources is alarming. Because over the past 30–50 years, the content of humus and elements in soils decreased. They were subjected to salinization, water and wind erosion, and contamination by heavy metals and agrochemicals [19]. It is known, about 76% of the republic's territory is located in a system of latitudinal soil-climatic zones in the desert zone. It is difficult to use gray-brown, takyrs soils and takyrs, desert sandy, salt marshes and hydromorphic soils of the desert zone are widespread. Here the risk of aridity will increase, the risk of periods is very strong heat, drought and lack of water, resulting in a decrease in crop production. As noted, 23.4% of the soil in the high-altitude zone is light, typical and dark gray soils, carbonate, typical and leached mountain brown, mountain brown, brown forest, light—Borax meadow-steppe, as well as hydromorphic soils of high-altitude zones [20]. As an outcome of climate change—in this zone, the risk of frosts for fruit crops is increased, the risk of aridity increases, and an increase in speed and a change in the snowmelt period are expected, leading to pink or mudflow phenomena.

5 Short Overview on the Aral Sea

A bright example of the menacing scale of environmental and socio-economic disasters caused by improper utilization of natural resources is the tragedy of the Aral Sea [21]. Aral Sea until 1960 was one of the largest enclosed waterbodies in the world with an area of 68.9 sq. km and a volume of water of 1083 km³, the greatest depth of 68 m. Due to the flow of the Syr Darya and Amu Darya rivers, the Aral Sea annually received an average of 50–55 km³ water [22]. The sea was as a climate control factor and reduced extreme weather fluctuations in the whole region, which favorably influenced the population's living conditions, agricultural production, and the ecological situation [14].

In the 1930s, large-scale irrigation canals were established in Central Asia, which was especially intensified in 1950–1960. Since the 1960s, the sea has become shallow. From 1960 to 1990, the area of irrigated lands in Central Asia increased to 4.5 million 907.5 million hectares. The region's water demand increased from 60 to 120 cubic km/year, of which 90% accounted for irrigation. As a result, starting in 1961, sea levels have been falling at an increasing rate [22, 23]. In less than half a century, the total river flow into the Aral Sea has decreased by almost 4.5 times, the water level has decreased by 29 m. The volume of water in the sea has decreased by more than 15 times. The water mineralization has increased to 125–300 g/l. Salinity of the Aral sea was more than 10 times of the salinity of the oceans [14, 22, 23]. On the dried-up part of the sea. The Aralkum Desert has an extensive area of salt fields with an area of more than 5.5 million ha. More than 90 days a year, dust and salt storms rage on it, spreading 100 million tons of dust annually over a distance of 300 km or more [23].

The degradation of land resources has occurred, the area of saline lands has increased, and their reclamation status has worsened [23]. In general, the biological productivity of the Aral Sea region decreased by 10 times. Representatives of endemic species, include the Turanian tiger, Asian cheetah, Ustyurt sheep, striped hyena, etc. (Fig. 3). The situation with the Saigak population is difficult—they were on the verge of extinction. The Red Book was supplemented by 11 species of fish, 12 species of milk feeding, 26 species of birds and 11 species of plants [21]. The number of days with temperatures above 40 °C doubled in the Aral Sea region. Also, recently there has been an increased frequency of days with extremely cold temperatures in wintertime below –30 °C. A further increase in temperature by 1.5–3% will increase water loss by 10–20% due to evaporation from the water surface and by 10–20% due to an increase in transpiration by plants. Nowadays, the Aral Sea disaster has grown beyond the region's borders into a global problem and requires a consideration of international organizations, politicians, scientists and experts from around the world [24].

On May 27, 2018, we were also witnesses when strong winds with dust storms covered the western part of Uzbekistan in Karakalpakstan, Khorezm, Navoi and Bukhara observed (Fig. 4). Dust-salt and clouds spread over long distances, salt settled on roads, houses and vegetation, covering them with a white coating [23]. A



Fig. 3 View of Aral Sea from MODIS satellite data

strong wind lifted a large amount of dust into the air from a desiccated surface of the earth. In addition, the prevailing northern direction of the wind was caused by the transfer of salts from the highly saline lands of the bottom of the dried Aral Sea [23].



Fig. 4 Typical view of the dried bottom of Aral Sea

For solving environmental problems, the Government of the Republic of Uzbekistan adopted a number of strategic documents. They are: 1. National Environmental Health Action Plan 2. National Strategy and Action Plan for the Conservation of Biological Diversity 3. National Action Program to Combat Drought and Desertification [4, 14]. Furthermore, in order to implement them, the National Program of Environmental Protection, the State Program for the Reclamation of Irrigated Lands, etc., are developed and implemented.

Uzbekistan, experiencing the dire consequences of an environmental disaster in 2013–2017, has implemented more than 500 projects to mitigate its effects. In particular, he planted about 350 thousand hectares on the dried area of the Aral Sea with saxaul (haloxylon) and other salt-tolerant plants. The state program on improving life conditions in the Aral Sea region for 2017–2021 with a budget of 8.422 trillion sums (81.08 billion) was approved [23].

Uzbekistan put forward the initiative of creating a multi-partner fund for human security for the Aral Sea region, which received United Nations support. Only in 3 months, more than 1 million hectares of land was prepared and more than 400 thousand seeds were planted on the dried area of the Aral Sea [23]. Plantations will retain salts from the bottom of the dried Aral Sea, saxaul plantations will completely fix the sediment, and they get into the atmosphere not long ago.

One bush of a plant is able to fix around itself from 10 to 100 tons of salt deposits. The reclamation state of more than 2.2 million ha of irrigated land, the area of land with a critical level of groundwater has decreased by almost 10%. The Aral Sea region has been states as a zone application of environmental innovation and technologies.

6 Main Priorities of the Soil Science Development in Uzbekistan

List of the main priorities of the soil science development in Uzbekistan:

- Conducting research activities on the processes of transfer of substances in the soil cover;
- To develop efficient actions against to salinization, erosion, dehumidification, overconsolidation, etc.;
- Development of theoretical foundations and technologies of environmentally sound integrated land reclamation of insufficiently moistened, saline, eroded, gypsum, and other soils;
- Development of adaptive-landscape, environmentally friendly farming systems; Further development and widespread adoption of agroecotechnology, biotechnology, information technology in the field of development of rational use and soil protection;
- Carrying out work to improve the classification of soils;
- Application of precision agriculture technologies;
- Linkage between higher education, research institutes and industry;

- Adaptation of the best practices in soil science and the development of international capacity building.

7 Innovative Technologies for the Prevention of Soil Degradation

- *Improving the fertility of degraded soils.* With this technology, the standard forms of vegetable soy, chickpea and asparagus beans are used as the main culture or as a secondary and intermediate crop. As a result, the agrochemical, agrophysical and water properties of degraded soils improve, their biological activity increases.
- *The utilization of metagenesis waste in the production of biogas to increase soil fertility.* The technology is based on the use of biogas production waste as a highly effective organic fertilizer on farmers' fields. This type of fertilizer can increase soil fertility, provide plants with readily available nutrients and reduce the rate of mineral fertilizers.
- *Improving the fertile parameters of soils by enriching them with organic substance.* The complex of agrotechnical measures, including crop diversification, increased rates of organic fertilizers and crop rotation, the use of plant residues as organic fertilizers, compost from plant residues is applied instead, cooked in advance in special pits. Compost is introduced into the soil under autumn plowing at a rate of 15–20 t/ha.
- *Increasing the fertility of degraded soils of semi-desert pastures.* A set of agroecobiotechnologies: usage of microbiological fertilizers, nanoadapters, pelleting, electrical treatment of plants with high feed value. This technology has increased seed germination and plant survivability, improved soil properties, and increased land productivity.
- *Improving the fertile parameters of rainfed lands and the productivity of winter wheat.* This technology is based on the use of hydrogels, biological products, organic composts and new types of fertilizers, as well as foliar feeding of grain crops. The technology improves grain quality, increases productivity, and optimally uses soil moisture.
- *Improving fertile parameters and preventing secondary salinization on slightly saline irrigated lands.* A set of measures, including autumn soil washing, increased rates of organic fertilizers, diversification of crops, including legumes, and plant residues as a source of humus, prevent the development of secondary salinization and increase soil fertility. For three years, soil flushing is not required, which saves irrigation water. In addition, the accumulation of organic matter leads to the formation of highly fertile structural soils, creating favorable conditions for the formation of a high yield.
- *Agrobiotechnology in the improvement of desert soils polluted with oil and oil products.* The technology is based on bioremediation of contaminated soils, the use of biological products and phytomeliorants, making it possible to rehabilitate soils quickly (5–7 years) and then proceed to restore their fertility.

- *Organic and mineral fertilizers based on secondary resources and their use for reclamation of low-fertile soils.* New organic and mineral fertilizers obtained on the basis of secondary resources (glauconites, bentonites of low-grade phosphorites and phosphomuca) by means of vermicomposting with manure, as well as biohumus with the addition of minerals, are used to optimize the properties of low-fertility soil.
- *Improving the fertile parameters of soils by growing winter-leguminous crops.* The technology allows the rational use of land resources, enriches the soil with nitrogen and other nutrients, biologically active substances, increases the microbiological and enzymatic activity of soils, improves the permeability and water resistance of aggregates, increases soil fertility.
- *Vermicompost preparation technology from solid household waste.* Composting organic waste using earthworms and in the process of microbiological decomposition of organic matter obtain an economical, ecological organic fertilizer containing the basic nutrients and microelements needed by plants. Bioorganic fertilizer can be used for all crops. They enrich the soil with organic matter, macro and micro nutrients, increase the biological activity of the soil, improve the water-physical properties of degraded soils.
- *Nano-irrigation and drainage techniques for increasing soil fertility and crop productivity.* Improving the resistance of plants to extreme conditions based on small-volume adaptogen preparations. Phytomelioration of degraded soils by applying nano-irrigation and drainage techniques that increase bioenergy and ecological resistance of crops to extreme conditions (salinization, soil alkalinity, pesticides, adverse agrometeorological conditions, etc.). Adaptogens increase germination energy and seed germination, increase vegetative mass, productive bushiness and biological productivity of agricultural plants.
- *Productivity management of saline and gypsum-bearing soils.* The technology includes a set of agrotechnical and measures aimed at restoring the productivity of irrigated lands. The technology includes deep loosening of the soil, improved field planning, good work of the collector-drainage network, flushing the root zone from salts, flushing irrigation regime during the growing season, balanced plant nutrition, crop rotation: cotton (April–October)—winter wheat (October–June)—legumes-mash (July–October)—grass on siderat (October–March), soil enrichment with plant residues after harvesting; care for crops (timely interrow cultivation, biological methods of plant protection, the use of bioorganic fertilizers and adaptogens).
- *Growing of *Indigofera tinctoria* to restore saline degraded lands.* *Indigofera* culture (*Indigofera tinctoria*) promotes the restoration of degraded saline lands and synthesizes a natural dye that is in high demand in the world market. Studies in the framework of the ZEF/UNESCO project Bonn, Germany/Urgench State University, Uzbekistan have shown that the legume *Indigofera tinctoria* can be quite successfully cultivated in saline degraded lands.
- *Development of an agro-reclamation soil passport.* The agro-reclamation passport of a farmer's field, which includes complete information about soil-reclamation and climatic conditions of the field, topography, nutrients, salinization, etc., is an

indicative tool for decision-making on effective agricultural production, includes: area, climate, topography, crops, productivity, characteristics of the basic properties of soils; cartograms of the availability of soil with humus and nutrients, salinity and mechanical composition.

8 Conclusions

From the abovementioned, the main priorities for the development of soil science in the agricultural sphere with climate change are as follows:

1. The study of changes in the processes of arid soil formation in the conditions of adaptation of agriculture to climate change;
2. Development of theoretical basis and efficient actions against to salinization, erosion, dehumidification, plastering, soil pollution with heavy metals and agrochemicals;
3. Study and optimization of the biological activity of soils, its pedofauna in various soil and climatic conditions;
4. Development of biological methods to increase soil fertility;
5. Further development and widespread adoption of agroecotechnologies, biotechnologies, GIS technologies in the field of sustainable use and protection of soil resources;
6. Study of the relation between effectiveness of fertilizers and environmental factors;
7. Studying the nutrition of a specific variety of each crop, developing a new system for applying mineral fertilizers as applied to the new adaptation system of agriculture;
8. Development of adaptive landscape, environmentally friendly farming systems;
9. Development of measures for the conservation and rational use of forest resources (mountainous, desert, tugai), forest reclamation measures to protect soils from erosion, salinization, and the negative effects of climate change;
10. Conducting research in order to use the drained bottom of the Aral Sea and adjacent territories;
11. International cooperation and an agreed solution to this global problem and monitoring studies on the impact of climate change on the agricultural sector.

9 Recommendations

Land degradation is a crucial issue for the countries of Central Asia and especially for Uzbekistan. Listed main priorities and innovative methods should be taken into account by the governmental stakeholders. More international joint projects should be conducted in the field of soil quality and fertility.

References

1. Belolipov IV, Zaurov DE, Eisenman SW (2013) The geography, climate and vegetation of Uzbekistan. In: Eisenman SW, Zaurov DE, Struwe L (eds) *Medicinal plants of Central Asia: Uzbekistan and Kyrgyzstan*. Springer, New York, NY, pp 5–7
2. Juliev M, Pulatov A, Hubl J (2017) Natural hazards in mountain regions of Uzbekistan: a review of mass movement processes in Tashkent province. *Int J Sci Eng Res* 8:1102–1108. <https://doi.org/10.14299/ijser.2017.02.013>
3. Lal R, Mohtar RH, Assi AT, Ray R, Baybil H, Jahn M (2017) Soil as a basic nexus tool: soils at the center of the food–energy–water nexus. *Curr Sustain Energy Rep* 4:117–129. <https://doi.org/10.1007/s40518-017-0082-4>
4. Nurbekov A, Akramkhanov A, Kassam A, Sydyk D, Ziyadaullaev Z, Lamers JPA, International Center for Agricultural Research in the Dry Areas (ICARDA) Central Asia and the Caucasus Regional Office, Tashkent, Uzbekistan (2016) *Conservation agriculture for combating land degradation in Central Asia: a synthesis*. *AIMS Agric Food* 1:144–156. <https://doi.org/10.3934/agrfood.2016.2.144>
5. Aw-Hassan A, Korol V, Nishanov N, Djanibekov U, Dubovyk O, Mirzabaev A (2016) Economics of land degradation and improvement in Uzbekistan. In: Nkonya E, Mirzabaev A, von Braun J (eds) *Economics of land degradation and improvement—a global assessment for sustainable development*. Springer International Publishing, Cham, pp 651–682
6. Strikeleva E, Abdullaev I, Reznikova T (2018) Influence of land and water rights on land degradation in Central Asia. *Water* 10:1242. <https://doi.org/10.3390/w10091242>
7. Juliev M, Mergili M, Mondal I, Nurtaev B, Pulatov A, Hübl J (2019) Comparative analysis of statistical methods for landslide susceptibility mapping in the Bostanlik district, Uzbekistan. *Sci Total Environ* 653:801–814. <https://doi.org/10.1016/j.scitotenv.2018.10.431>
8. Vogel H-J, Bartke S, Daedlow K, Helming K, Kögel-Knabner I, Lang B, Rabot E, Russell D, Stöfel B, Weller U, Wiesmeier M, Wollschläger U (2018) A systemic approach for modeling soil functions. *Soil* 4:83–92. <https://doi.org/10.5194/soil-4-83-2018>
9. Pi H, Sharratt B, Lei J (2019) Wind erosion and dust emissions in central Asia: spatiotemporal simulations in a typical dust year. *Earth Surf Process Landf* 44:521–534. <https://doi.org/10.1002/esp.4514>
10. Akramkhanov A, Ul Hassan M, Hornidge A-K (2018) Redrawing soil salinity innovation-focused stakeholder interaction for sustainable land management in Khorezm province, Uzbekistan. *Water* 10:208. <https://doi.org/10.3390/w10020208>
11. Ivushkin K, Bartholomeus H, Bregt AK, Pulatov A (2017) Satellite thermography for soil salinity assessment of cropped areas in Uzbekistan. *Land Degrad Dev* 28:870–877. <https://doi.org/10.1002/ldr.2670>
12. Nicu I (2018) Is Overgrazing really influencing soil erosion? *Water* 10:1077. <https://doi.org/10.3390/w10081077>
13. Olson KR, Al-Kaisi M, Lal R, Cihacek L (2016) Impact of soil erosion on soil organic carbon stocks. *J Soil Water Conserv* 71:61A–67A. <https://doi.org/10.2489/jswc.71.3.61A>
14. Kurochkina LY (2015) Monitoring and mapping of degradation of vegetation formations in the ecosystems of arid Aral Sea region. *Arid Ecosyst* 5:201–215. <https://doi.org/10.1134/S207909611504006X>
15. Aralova D, Kariyeva J, Khujanazarov T, Toderich K (2018) Drought variability and land degradation in Central Asia: assessment using remote sensing data and drought indices. In: Egamberdieva D, Öztürk M (eds) *Vegetation of Central Asia and environs*. Springer International Publishing, Cham, pp 15–47
16. Okuda Y, Onishi J, Shirokova YI, Kitagawa I, Kitamura Y, Fujimaki H (2020) Water and salt balance in agricultural lands under leaching with shallow subsurface drainage used in combination with cut-drains. *Water* 12:3207. <https://doi.org/10.3390/w12113207>
17. Hamidov A, Khamidov M, Ishchanov J (2020) Impact of climate change on groundwater management in the northwestern part of Uzbekistan. *Agronomy* 10:1173. <https://doi.org/10.3390/agronomy10081173>

18. Mukhamedjanov S, Mukhomedjanov A, Sagdullaev R, Khasanova N (2021) Adaptation to climate change in irrigated agriculture in Uzbekistan. *Irrig Drain* 70:169–176. <https://doi.org/10.1002/ird.2529>
19. Mustaeva N, Kartayeva S (2019) Status of climate change adaptation in central Asian region. In: Alam M, Lee J, Sawhney P (eds) *Status of climate change adaptation in Asia and the Pacific*. Springer International Publishing, Cham, pp 41–67
20. Mannig B (2018) OBSOLETE: impacts of climate change in Central Asia. In: Reference module in earth systems and environmental sciences. Elsevier
21. Matsui K, Akhupov Y, Kussainova M, Funakawa S (2017) Management of wood resources: a dilemma between conservation and livelihoods in a rural district in the Aral region. *Energy Sustain Dev* 41:121–127. <https://doi.org/10.1016/j.esd.2017.08.010>
22. Krapivin VF, Mkrtchyan FA, Rochon GL (2019) Hydrological model for sustainable development in the Aral Sea region. *Hydrology* 6:91. <https://doi.org/10.3390/hydrology6040091>
23. Xenarios S, Schmidt-Vogt D, Qadir M, Janusz-Pawletta B, Abdullaev I (2019) *The Aral Sea basin: water for sustainable development in Central Asia*, 1st edn. Routledge
24. Wheeler W (2018) Mitigating disaster: the Aral Sea and (post-)soviet property. *Glob Environ* 11:346–376. <https://doi.org/10.3197/ge.2018.110207>

Soil Degradation and Environmental Contamination

Soil Erosion Catastrophe in Iraq-Preview, Causes and Study Cases



Nabil Ibrahim Eltaif and Mamoun A. Gharaibeh

Abstract Soil erosion is a major global soil degradation threat to land, freshwater and food security. Quantification of soil loss is important for soil and water conservation practitioners and policy makers. In Iraq, about 11 million hectares are affected by water and wind erosion, while the remaining areas experience different degrees of erosion. This chapter reviews available research reports estimating and managing soil erosion in Iraq. It is evident that water erosion in Iraq is caused by both natural processes and human induced activities, while wind erosion is mainly caused by natural process. Land desertification in Iraq is paired with salinization leading to additional soil erosion caused by destructive wind. Both water and wind erosion had reached critical levels in the past three decades as a result of land neglecting and lack of conservation measures. The northern parts of Iraq are suffering from water erosion due to high rainfall intensities and excessive plowing of cultivated soil, whereas wind erosion is affecting most of the southern and western parts. Average erosivity factors were 15,835, 6695, and 2584 MJ mm ha⁻¹ h⁻¹ for the northern, western, and central and southern parts, respectively. Moreover, estimated wind erosion was 65–70.2 Mg ha⁻¹ year⁻¹ for the western and southern parts. More applied work is needed to estimate and solve erosion problems in different parts of Iraq.

Keywords Water erosion · Wind erosion · Degradation · Soil loss · Conservation · Iraq

N. I. Eltaif (✉) · M. A. Gharaibeh
Faculty of Agriculture, Department of Natural Resource and the Environment, Jordan University
of Science and Technology, P.O. Box 3030, Irbid 22110, Jordan
e-mail: nieltiaf@just.edu.jo

M. A. Gharaibeh
e-mail: mamoun@just.edu.jo

1 Introduction

Arid or semi-arid conditions spread over the utmost soils of Iraq, having low water content under natural conditions. The primary soil problem in Iraq is the maintenance of soil productivity under such prevailing conditions. The whole area of Iraq comprises 438 317 km²; agricultural land is spread over 94 500 km², and forest land cover 8 230 km². The Tigris and Euphrates rivers were known as the Fertile Crescent because of the abundance of ancient irrigation and flood protection projects developed and provided by Sumerian rulers.

Soil erosion in Iraq has been prevalent problem ever since the land was first cultivated. Studies have shown that the downfall of early Iraqi civilizations was because of land degradation, especially soil erosion [1]. Water and wind erosion are rather serious problems as about 5 million hectares suffer from severe water erosion. About 8 million hectares are affected by wind erosion, whereas the remains of Iraqi land experience different degrees of water or wind erosion [2–4]. Invasions into Iraq in 1991 and 2003 brought inevitable problems to the country, which caused a human tragedy that was worse than ever before. The economic, agricultural, and industrial infrastructures were lost. Furthermore, educational, health and cultural infrastructures were also destroyed. The lack of protection and control of agricultural land by the occupation authorities resulted in desertification and soil erosion.

This chapter reviews the most important published articles dealing with soil erosion problems in Iraq and tracks all accessible worldwide research on soil erosion. In the last decade, Iraqi researchers published their articles in national and international journals intending to draw the attention of organizations, the government, and other scientific institutes to the catastrophe of soil erosion in Iraq. However, most of the research work about Iraq is not designed to solve the soil erosion problem but rather to evaluate and estimate erosion in the different regions of Iraq. Researchers have used different models available in the existing literature to evaluate soil loss events initiated by water and wind erosion.

2 Preview of Soil Erosion in Iraq

Two important facts have been identified by [5]. These facts are described as follows: First, not all the erosion that results from the human mismanagement of natural resources is accelerated soil erosion; much of the wind erosion for the most of Iraq is natural erosion that is not easy to mitigate using soil conservation practices. Second, the country's detected soil erosion results from actions of water or wind over several thousands of years, and not all of it are recent.

Water erosion is evident in the north of Iraq, on cultivated highlands and foothills, and even in the rolling and level lands. The increase in the plowing of hill slopes in the north of Iraq promotes soil erosion and caused land destruction. This soil erosion occurs because of the deterioration of life after 1991 and a decreasing standard of

living that has forced farmers to engage in the unsuitable cultivating of their lands. Mostly, the only means of conservation in the region is by establishing a permanent grass-cover or forest.

Desertification is one of the consequences of the invasion of the USA and the coalition forces of Iraq in 1991 and 2003. During the military operations, the topsoil in Iraq was destroyed because of the great number of bombs explosion and the moving Lorries in different regions of the country that enhancing the emission of dust and the formation of sand storms. Desertification is the destructive process or damaging of the land's topsoil, which can eventually lead to the creation of desert-like conditions and, in turn, reduce plant and animal production, thus affecting the maintenance of human existence [6, 7]. Such circumstances are recognized by the studies of [8, 9].

As soil conservation measures are put into effect, soil erosion does not become a grim problem as occasionally visualized; therefore, soil losses by erosion could be mitigated in Iraq. However, Protecting or even restoring the productive potential of the land requires improvements in both soil and vegetation management.

3 The Climate of Iraq

Iraq is a country consisting of 19 provinces, and one of them is the self-governing region (Iraqi Kurdistan), including mainly Dohuk, Arbil, and As-Sulaymaniyah (Fig. 1).

The climate in Iraq is described; desert and hot in summer and relatively cold in winter [10, 11]. It is semi-desert in the north with a relatively cold winter, while in the northern mountains, the climate is cold and rainy (or snowy) in winter. The zone 1 on the map is the mountainous area that receives substantial rainfall (≈ 800 mm). Zone 2 on the map is a northern area that receives moderate rainfall (≈ 400 mm). The most parts affected by wind erosion in Iraq are zone 3 (middle-south area) and zone 4 (west) on the map (Fig. 1). The climate in zone 3 and 4 is desert or semi-desert, the blowing wind is usually occurring in the middle and southern parts (zone 3). Zone 4 on the map is desert, quite cold with frequent frosts in winter and hot in summer, and slightly less hot than in the plains because of altitude (Table 1).

In Iraq's summer, dust storms coming from the north "Shimali" hit most of the country for days and were initiated by the northwest wind. Shimali blows almost continually through June and July (Fig. 2). However, Shimali wind may continue blowing in August and September and can stay for many days in a row [12]. According to the Iraqi Environmental Ministry, one hundred twenty-two dust storms recorded in Iraq and 283 dusty days per year. It is mentioned that Iraq could be affected by even 300 dusty days per year [12, 13].



Fig. 1 Iraq map showing the four areas of the country (1—mountainous, 2—northern, 3—middle-south, and 4—northwest) (<https://www.climatestotravel.com/climate/iraq>)

4 Soil Erosion Concepts

4.1 Water Erosion

Natural resources conservation service (NRCS-USDA) defines water erosion as the loss of soil materials as a result of detachment and removal by water. Water erosion may take place naturally (geological) or by human activity (accelerated). The rate of erosion generally varies from very slow to very rapid, depending on the soil, the topography, and weather conditions.

Table 1 Mean annual rainfall (mm), temperature (°C), dust storms (days), and dryness index for of different areas in Iraq (Iraqi Metrological Organization) Climatic atlas of Iraq 1951–1990

Governorate	Mean annual rainfall (mm)	Mean annual temperature (°C)	Mean annual dust storms (days)	Dryness index
Baghdad	150–200	23	12	20–25
Mosul	300–600	18–20	1–4	5–10
Basra	75–150	24	8–24	15–20
Erbil	400–>800	<16–19	1–4	<5
Suliamaniyah	500–>800	<16–18	1–2	<5
Dohuk	600–>800	18	1	<5
Kirkuk	200–400	20–22	2–4	5–10
Salah Al-Deen	100–300	22–23	4–12	10–20
Diyala	150–450	23	4–12	15–20
Anbar	<75–150	18–22	4–8	20–35
Wasit	150–200	23	2–6	20–25
Misan	150–200	23	2–8	15–25
Babil	100–150	23	10–12	25–30
Karbala	75–100	22–24	8–12	30–35
Najaf	75–100	22–24	8–12	30–36
DhiQar	100–150	24	6–12	20–30
Qadisiyah	100–150	23–24	6–24	25–30
Al-Muthan'na	<75–100	24	12–24	25–35

**Fig. 2** Dunes formation as a result of wind blowing in arid regions [14]

4.2 Types of Water Erosion

4.2.1 Splash Erosion

When raindrops hit the soil surface, the soil disperses and splash by impacting raindrops, transferring particles from their locations [15, 16]. Both [17, 18] designate the splash erosion developments as raindrop impact, a splash of soil particles, and craters' formation, which is a function of raindrop characteristics.

4.2.2 Sheet Erosion

A thin layer of soil is removed by raindrop effect in sheet erosion, and a shallow surface flow is formed. As a result, most of the smallest soil particles that hold nutrients and organic matter are lost. Soil loss by sheet erosion occurs continuously, unseen, and causing a great quantity of soil loss. Particle detachment, rainfall intensity, and field slope affect sheet erosion. Nearly 70% of total water erosion is a result of both splash and sheet erosion. These two erosion types happen concurrently; even so, splash erosion governs the initial process.

4.2.3 Rill Erosion

In rill erosion, shallow channels (less than 30 cm deep) are formed by concentrated water of runoff on these channels. Rill erosion is often described as the transitional step between sheet and gully erosion [19, 20].

4.2.4 Gully Erosion

Gullies form channels typically more than 30 cm deep that are difficult to remove by ordinary cultivation. Gullies' occurrence needs that water flows concentrate on the soil surface and cut the soil. Two types of gullies are designated: Ephemeral and permanent gullies. The first type is shallow channels that are easy to be removed by ordinary tillage. The second type is relatively too large a channel; therefore, they need special control and management measures [20–23].

4.2.5 Tunnel Erosion

In tunnel erosion, surface water seeps into the subsoil and causes the soil's inner eroding, especially when the soil is dispersive. Enlargement of these cavities (tunnels) may cause the failure of soil surface, creating gullies in the fields [24–26].



Fig. 3 Soil erosion (Rill and interrill) by water in North of Iraq [29]

4.2.6 Streambank Erosion

Streambank erosion is the downfall of soil along the riversides due to the water flow power. This erosion is a naturally occurring process, but human activities may increase the rate of erosion. Streambank erosion is the dominant source of sediment in many river systems. As a result, some conservation measures are commonly taken to protect the banks from further erosion [27, 28].

Water erosion means the removal of surface soil via the action of water runoff. In Iraq; different types of water erosion are recognized, namely splash, sheet, rill, gully, tunnel, and streambank erosion [29]. Interrill erosion involves both splash and sheet erosion (Fig. 3).

Moreover, [22] prepared a map of gully erosion in the northwest of Iraq with the aid of a computer program (Surfer 32). The map showed the existence of moderate to substantial gully erosion.

4.3 Quantifying Water Erosion

4.3.1 Field Methods

Direct erosion measurements are the most accurate method of quantifying soil erosion; such measurements are laborious and expensive [30]. They comprise collecting the depositions in a volumetric barrel and weight sediments (Fig. 4).

Prediction of soil loss using models such as Universal Soil Loss Equation (USLE) and Revised USLE (RUSLE) is done with the aid of runoff plots, which are used extensively for conducting erosion research works [31]. Moreover, standardized plots



Fig. 4 Collecting sediments from runoff plots. Hailun field experimental station, Heilongjiang, China after [30]

could be used to rank relative soil erosion among treatments [32]. The runoff plot method was also used for measuring soil loss by water erosion [33–36].

Runoff plots were used to demonstrate to the farmers the occurrences of water erosion in their fields and show the role of vegetative cover in reducing erosion [23, 37, 38]. Another possible use is to create or to validate a model or equation to predict runoff or soil loss [39, 40].

4.3.2 Erosion and Runoff Plots Used in Iraq

The cheapest and most straightforward method to study soil erosion is to install the plots and then wait for natural rainfall, but unpredicted rain can make this frustrating. Natural runoff plots were used to collect sediment yield at three different experimental sites in northern Iraq [41]. Such plots were used to study the effect of tillage treatments on soil erosion under natural rainfall in the Aski-Kalak site, and Erbil, in, Iraq [42]. Runoff and sediment yield data were collected from runoff plots and evaluated by taking volumetric and weight measurements. In twenty rainfall events occurring from 1988 to 1992, runoff and sediments were recorded from $20 \times 4 \text{ m}^2$ plots. The runoff materials in the collecting tanks were thoroughly mixed, quantified and sediment concentration was determined using the method of [43, 44]. Rainfall simulators have been designed to apply uniform rainfall rates to measure runoff over land surfaces because of the natural rainfall variability. Different rainfall simulators (Fig. 5) are designed with different shapes, types, and sizes. Most of them usually use nozzles to apply water at chosen rates and durations. By changing the nozzle size, the rate and duration of rainfall can be handled. Soil erosion by water has been widely used to study rainfall simulators [15, 45–49].



Fig. 5 Rainfall simulator, Experimental Farm Wijnandsrade, South-Limburg, The Netherlands after [50]

Little attempts have been made in Iraq to exploit simulators for studying water erosion. Using a simulator in Iraq is to speed up results and control of the amount and type of rainfall.

4.3.3 Water Erosion Prediction (Empirical Models)

The Universal Soil Loss Equation (USLE) is the simplest mathematical model proposed by [51, 52]. Every model has unique characteristics and application in a different field. The USLE has been used worldwide since the 1960s to predict soil erosion [39]. It is an empirical model serving to estimate average annual soil loss in the long term from agricultural watersheds.

Researchers used different techniques to achieve rapid and efficient info about soil erosion. For example, the input data sets can be generated by using the model of remote sensing for soil erosion distribution through the merging of GIS, remote sensing, and RUSLE.

The RUSLE model uses the same formula as the USLE but with improvements in evaluating some factors. RUSLE model predicts soil degradation and sediment concentrations better by using some parameters with some new key features. The USLE remains the easiest method available for soil erosion studies on large watersheds [39, 53]. The USLE has been used extensively worldwide [39, 53–55]. Modified USLE (MUSLE) and Revised USLE (RUSLE 1 and 2) result from the continual upgrading of the USLE [55]. Additionally, in Iraq, researchers have used USLE and RUSLE directly or indirectly to evaluate water erosion [41, 56–60].

However, the USLE/RUSLE is considered better than other advanced models because of its simplicity, usability, and no need for extensive data for soil loss prediction. Instead, simple equations and charts (e.g. nomographs) are usually used to evaluate the factors of USLE/RUSLE.

The form of USLE/RUSLE is written as follows:

$$A = R \times K \times LS \times C \times P \quad (1)$$

Here, A is the soil loss expressed in Mg ha^{-1} , R is erosivity factor (rain and runoff), K is soil erodibility factor, LS is length and degree of land slope factor, C is the vegetation management, and P is soil conservation factor. Tables and nomographs (charts) are usually used to solve the basic versions of USLE.

4.4 Solving Water Erosion Equation (USLE)

4.4.1 Rainfall and Runoff Erosivity Index (EI)

The EI is computed as the total storm energy (E) product and the maximum 30-min intensity (I_{30}) of the rain.

$$EI = E \times I_{30} \quad (2)$$

The total of computed EI values from single storms that happened during the year is related closely to the amount of soil loss from a field [52]. The USLE computed EI is applicable for a rainfall intensity of ≤ 63.5 . In the tropical zone with heavy rains, the EI values used in USLE to evaluate erosivity usually yield overestimating values. Therefore, adjustments to EI have been suggested by [61] for tropical regions.

Assessment of the term 30-min intensity is done by calculating the intensity for a maximum amount of rainfall in any 30 min during the rainstorm from the rain gauge charts. An erosivity map (iso-erodent map) was developed in the USA after analyzing about four thousand sites for different rainfall-return periods. An example to calculate erosivity from rainfall data is shown in Table 2.

4.4.2 Soil Erodibility Factor (K)

Soil erodibility is affected by several physical and chemical soil properties. The K values were attained by direct soil erosion measurements under simulated rainfall [14]. By using the following equation, K value can be determined [52, 63]:

$$K = \frac{2.1 * 10^{-4}(12 - a)M^{1.14} + 3.25(b - 2) + 2.5(c - 3)}{100} \quad (3)$$

Table 2 Calculation of erosivity factor in USLE, modified after [62]

(1) Time from the start of the storm	(2) Rainfall (mm)	(3) Intensity (mm h ⁻¹)	(4) Kinetic energy (MJ ha ⁻¹ mm ⁻¹)	(5) Total kinetic energy (MJ ha ⁻¹) (Col 1 × Col 4)
0–14	1.52	6.08	0.0877	0.1333
15–29	14.22	56.88	0.2755	3.918
30–44	26.16	104.64	0.2858	7.4761
45–59	31.5	126	0.2879	9.0674
60–74	8.38	33.52	0.2599	2.1776
75–89	0.25	1	0	0

Wischmeier index (EI_{30})

Maximum 30-min rainfall = 26.16 + 31.50 mm = 57.66 mm

Maximum 30-min intensity = 57.66 × 2 = 115.32 mm h⁻¹

Total kinetic energy (total of column 5) = 22.7724 MJ ha⁻¹

EI_{30} = 22.7724 × 115.32 = 262.12 MJ mm ha⁻¹ h⁻¹

$$M = (\% \text{ very fine sand} + \% \text{ silt})(100 - \% \text{ clay}) \tag{4}$$

where M is particle-size parameter, a is the percentage (%) of soil organic matter content (SOM), b is soil structure code (1 = very fine granular; 2 = fine granular; 3 = medium or coarse granular; 4 = blocky, platy, or massive), and c profile permeability (saturated hydraulic conductivity) class [1 = rapid (150 mm h⁻¹); 2 = moderate to rapid (50–150 mm h⁻¹); 3 = moderate (12–50 mm h⁻¹); 4 = slow to moderate (5–15 mm h⁻¹); 5 = slow (1–5 mm h⁻¹); 6 = very slow (<1 mm h⁻¹)]. SOM content is computed as the product of organic C (%) and 1.72.

A chart (nomograph) can be used to estimate the K value shown in Fig. 6.

4.4.3 Topographic Factor (LS)

Slope length and its degree are both represented quantitatively in USLE as LS factor. LS is the ratio of soil loss from a field slope at particular conditions to that from a 72.6-ft (22.1-m) length of uniform 9% slope for a field of the same conditions. Slope length and its degree value for the LS factor can be determined from direct measurements or using topographic maps and Digital Elevation Models (DEM). In the Agriculture Handbook number 537 (23), both a table and a slope-effect chart are available, demonstrating values of LS for specific combinations of slope length and degree [14, 65].

The chart and the table were derived by the equation;

$$LS = \left(\frac{L}{22.1} \right)^m + (65.41\sin^2\theta + 4.56\sin\theta + 0.065) \tag{5}$$

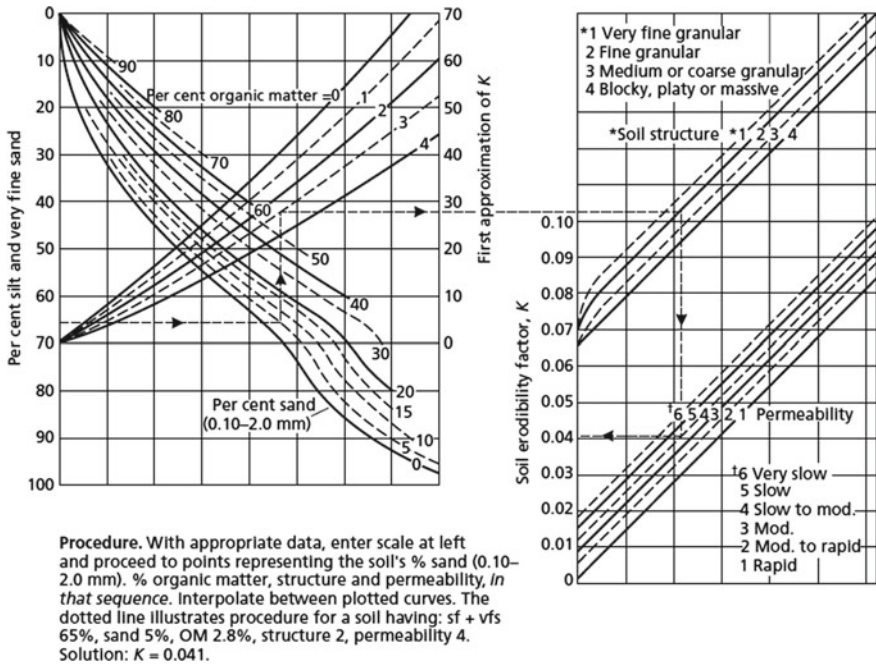


Fig. 6 Chart for calculating soil erodibility K in metric units [64] To change K to American units divide K value by 0.13

$$m = 0.6[1 - \exp(-35.835 \times S)] \tag{6}$$

$$\theta = \tan^{-1}\left(\frac{S}{100}\right) \tag{7}$$

where S is field slope (%) and θ is field slope steepness in degrees.

4.4.4 Cover-Management Factor (C)

The C-factor in USLE characterizes the impact of vegetation on soil loss during different stages period of the crop. It can be calculated via dividing soil loss from a field under a definite crop stage period by soil loss under a bare unplanted field with conventional tillage [66].

4.4.5 Support Practice Factor (P)

The P-factor in USLE denotes the field practices that are usually used for controlling soil erosion. It can be computed via dividing soil loss from a field with supporting practices by soil loss from a field under conventional tillage with no field practices. P-factor values range from zero to one [67].

4.5 Study Cases of Soil Erosion by Water in Iraq

A key indicator of soil erosion is erosivity that is important in predicting erosion. The potential erosion risk in Iraq can be evaluated by rainfall erosivity data, despite the dry climate dominating Iraq most of the year. Erosion is mainly resulting from irregular and heavy rainfall intensities. However, erosivity in seven regions in Iraq, namely Baghdad, Baji, Khanakeen, Kirkuk, Mosul, Zakho, and As-Sulaymaniah, was determined using Eltaif and Abbas' easy procedure [68]. Results showed that the values of the annual erosivity fluctuated between 145 and 1359 MJ mm ha⁻¹ h⁻¹ year⁻¹.

The highest annual erosivity was recorded in northeast regions of Iraq (As-Sulaymaniyah), while the regions heading south recorded the lowest annual erosivity values. The total monthly and annual rainfall data from 1993 to 2010 for eighteen monitoring stations in Iraq was used to estimate rainfall erosivity [56] by using sophisticated statistics (Fig. 7). They concluded that water erosion is greatly related to rainfall, and with the low rainfall, other factors are not activating to cause erosion.

A key source for water erosion prediction in Iraq is the spatial differences in erosivity values. Therefore, it is worthwhile to compare erosivity values in Iraq with those in nearby countries. A regional rain erosivity map project could be used as a framework. The simplicity of the USLE is most likely the main reason it is still widely used in case of data insufficiency.

The universal soil loss equation (USLE) is an effective tool (when combined with GIS) for the determination of soil loss [59, 69–71]. Soil loss was evaluated from the Alibag catchment in Iraqi Kurdistan (north of Iraq) with the integrated GIS and USLE [29]. Different layers of the USLE were prepared and processed in the ArcGIS. Values soil loss reached 16.6 Mg ha⁻¹y⁻¹ with a mean value of nearly 6 Mg ha⁻¹y⁻¹. In Iraq, erosion was estimated and erosion forms were determined based on different info (e.g. location visits, remote sensing, and soil assessment reports [60]). This information was then assembled into a soil degradation map for the region.

It was concluded that out of the total 12-million-hectare area in the northern part of Iraq, about 33% is subject to serious water erosion [60]. Additionally, about 23% and 22% of the total land area in Iraq have slight and severe water erosion, respectively. However, severe water erosion occurred mostly in the mountainous northeastern region (zone1 in Fig. 1). The rest of the total area is affected by minor to moderate water erosion.

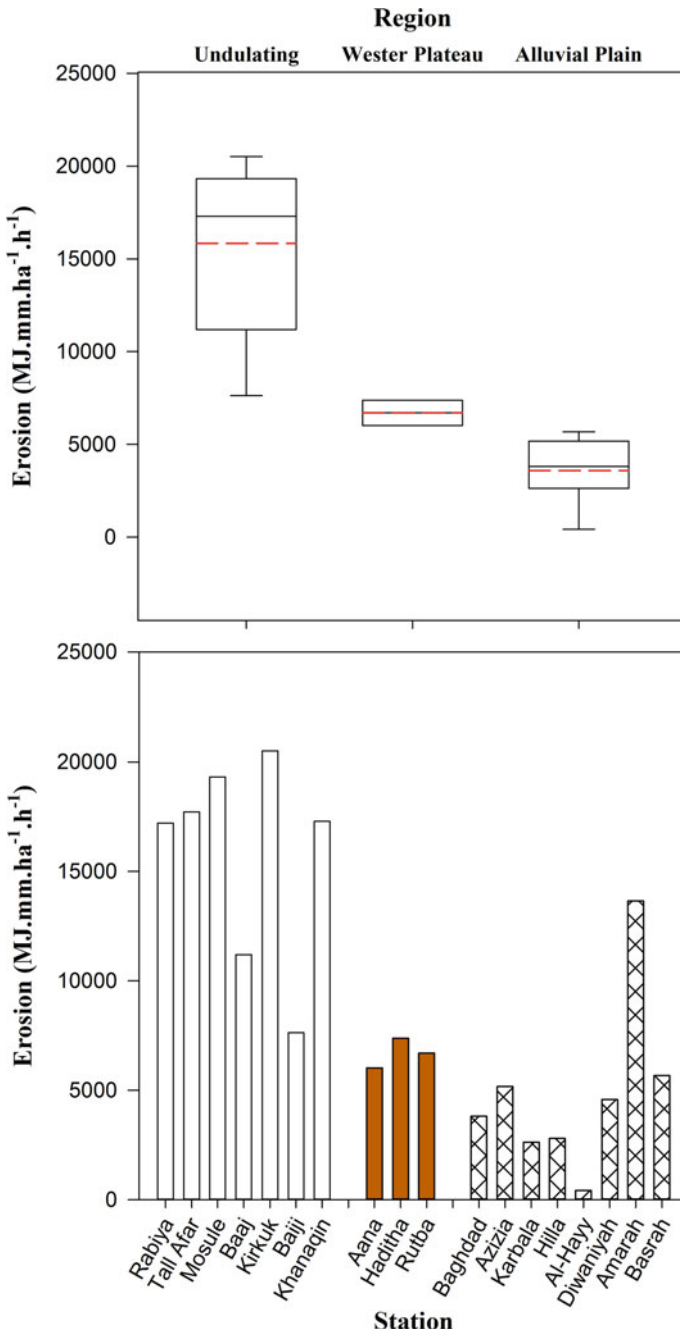


Fig. 7 Annual distribution of water erosion (MJ mm ha⁻¹ h⁻¹) of the soil for the 18 study stations (undulating, western plateau, and alluvial plain) in Iraq. Redrawn form [56]

The integration of remote sensing, GIS, and empirical RUSLE model were used to evaluate annual water erosion in Kirkuk, north of Iraq [58]. The RUSLE five factors for determining soil loss were derived from field survey, archival data, digital elevation model, and LANDSAT 8 multi-bands imagery. Using a raster calculator (ArcGIS 10.2 software), the annual soil loss was computed by multiplying the five RUSLE factors.

Estimation of the R factor was conducted by analyzing the annual and monthly rainfall attained from the meteorological stations near the study area. The R values ranged between 108 and 716 with an average of $368 \text{ MJ mm ha}^{-1} \text{ h}^{-1} \text{ yr}^{-1}$. The K values ranged between 0.04 and 0.38 with an average of $0.14 \text{ t ha}^{-1} \text{ h}^{-1} \text{ MJ mm}^{-1}$. The length and degree factor (LS) can be estimated by the Digital Elevation Model (DEM). The values of LS ranged from 0 to 10.76, with an average value of 0.02. The mean values of C by using remote sensing data and Normalized Difference Vegetation Index (NDVI) were ranged from 0.38 to 0.76 with a mean value of 0.55. The P factor is taken 1.0 in the study area because there was no management practice. The spatial distribution of soil loss averaged $2 \text{ t ha}^{-1} \text{ yr}^{-1}$ and fluctuated from 0 and $245 \text{ t ha}^{-1} \text{ yr}^{-1}$.

Erosion potential model (EPM) is combined with geographic information systems (GIS) for predicting erosion and sedimentation in the Garmiyān basin at Kurdistan Region, Iraq [57]. The basin with an area of about $1,620 \text{ km}^2$ and has a mixture of vegetation, slope, soil texture, and land use. Three main gullies were recognized in the study area when the spatial distribution of gully erosion was programmed. The slight to moderate gully covers 10%, the high gully covers 89%, and severe fluvial gully erosion covers about 1%. The values of the erosion coefficient as shown by EPM indicated that the intensity of erosion could be classified as moderate to high.

5 Wind Erosion

Wind erosion is the main reason causing land degradation in most dry conditions [72]. These conditions, such as the region's exposure to the severe wind blowing and dust storms, are common in Iraq (Fig. 8). The impact of war and external sanctions (1991, 2003) combined to threaten Iraq with a high risk of desertification. However, no significant research works were done on the wind erosion control and its developments in Iraq.

Desertification in Iraq is paired with salinization. It is worth pointing out that the salinization phenomenon in the irrigated land of southern Iraq is covering a large area and is not that easy to control. The most affected areas by wind erosion are sedimentary (alluvial) plains, extending from the eastern areas of the Euphrates River to the southern areas of Baghdad (part of zone 3, in Fig. 1). However, the most known area susceptible to wind erosion is sedimentary plains' central and upper lands [6].

In his description of wind erosion in the south of Iraq, [5] stated that the saline areas (solonchak soils) with a friable surface layer, the irrigated silty levees are more

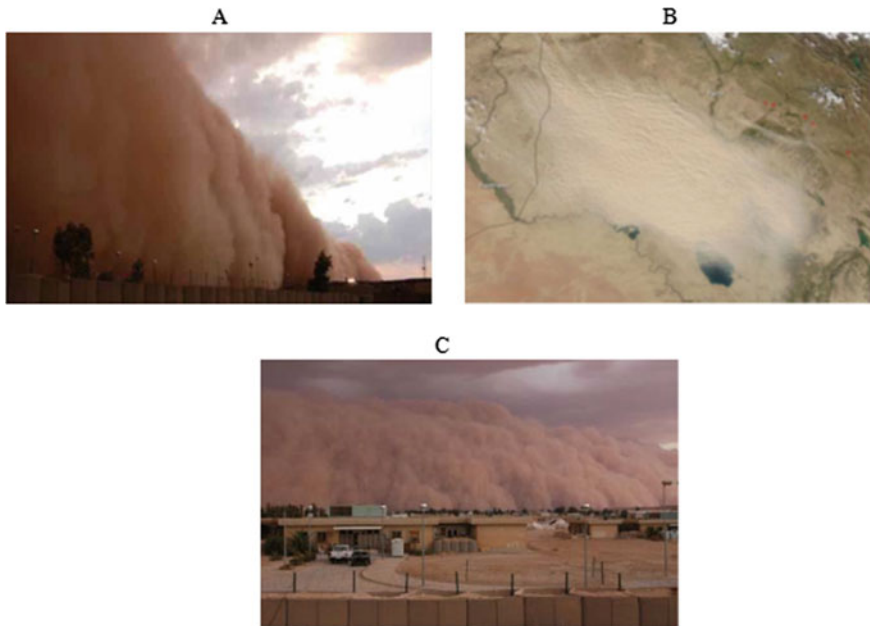


Fig. 8 **a** General view of a dust storm in the west desert of Iraq. **b** Airborne dust storm in the north-west desert of Iraq visualized by the Moderate Resolution Imaging Spectroradiometer (MODIS). **c** Dust storm, Western Desert, west of Falluja, Iraq. After [12]

subject to destructive wind. The flocculated fine particles in these levees resemble the sand particles forming the dunes or sheets (pseudo sand) [73, 74].

The prevailing arid and semi-arid conditions, such as in Iraq environments, with low rainfall amounts, imposed significant limitations on crop production [75]. Iraq is generally characterized by aridic soil moisture regime and typically saline soils with low organic matter. Wind erosion can be enhanced and stimulated in conditions such as weak soil structure, wide fields, low vegetative cover, and high wind speed [76].

The pseudo-dunes in that area cover about one million hectares of land in dry, unprotected conditions and are strongly affected by wind erosion and this accordingly restricts crop production [13, 77]. Attempts to improve soil and water management practices for Iraqi conditions were done and verified successfully, but one of the most challenging problems fronting such attainment is the social problems [78].

World Meteorological Organization (WMO) defines dust storms as mobilization of the huge amount of wind-blown particles through turbulent atmospheric flows that reduce horizontal visibility to less than 1000 m [79].

The nomination of the dust events is derived from four types of dust as shown in Fig. 9. The land degradation by wind erosion in Iraq is attributed to exceptional prevailed climatic conditions, misuse of land, and poor management practices. Strip

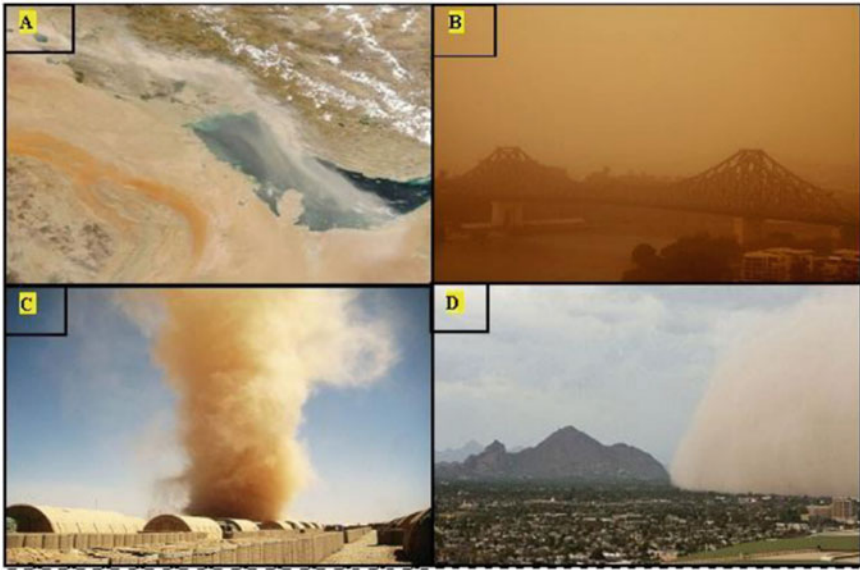


Fig. 9 Types of dust storms: blowing dust (a), dust haze (b), dust devil (c), and Haboob (d) [80]

cropping and adapting the modern irrigation management practices are seldom used in Iraq.

5.1 Prediction of Soil Loss by Wind Erosion

The wind erosion equation (WEQ) was proposed to predict soil loss by wind action [81]. A simple computer solution was presented by [82] to solve the WEQ. The general functional form of WEQ is $E = f(IKCLV)$; Where (I) is soil erodibility factor, (K) is a roughness factor, (C) is a climatic factor, (L) is the distance of wind transport across a field and (V) is the vegetative cover equivalent. The WEQ model is derived experimentally and adopting that erosion by wind is linearly related to the variations in climatic conditions, properties of soil, and surface conditions. The model does not take into account, for example, the possibility of spatial erosion variability or the interactions and combinations between some wind erosion factors [78, 83, 84].

The main advantages of the WEQ application are as follows: First is to guess the amount of soil loss by the wind from cultivated fields. The second is to identify the conservation practices to reduce soil loss by the wind to an acceptable amount. The equation can then be set to govern the conditions required to diminish soil loss to the tolerable limits by applying some conservation practices such as increasing the residue on the soil surface and shortening field length [85, 86]. A stepwise procedure

was used to solve WEG [87]. The stepwise procedure involves first determining soil erodibility, I (E_1); and then determining E_2 and E_3 as follows: $E_1 = I$; $E_2 = IK$; $E_3 = IKC$. Determining E_4 and E_5 depending on E_2 and E_3 as follows: $E_4 = (WF^{0.348} + E_3^{0.348} - E_2^{0.348})^{2.87}$; $E_5 = \psi I \cdot E_4^{\psi^2}$. Where WF is the field length. However, a different procedure was adopted by [14] to solve WEQ and it is as follows.

5.1.1 Erodibility Factor (I)

Erodibility factor (I) in WEQ signifies the potential annual soil loss from an uncultivated, flat, and indefinite length field. A conventional flat or rotary sieve is usually used to determine the part of dry soil fraction in a soil sample [86].

One kilogram of the dry soil (0–15 cm) weighs and screens with a 0.84 mm diameter opening sieve to allow for peds <0.84 mm diameter to pass through. The following regression equation was developed to estimate I ;

$$I = 525 \times 2.718^{-0.04F} \quad (8)$$

where I and F are soil erodibility (Mg ha^{-1}), and dry soil fraction >0.84 mm (%), respectively.

5.1.2 Soil Ridge Roughness Factor (K)

A simple technique to measure soil surface roughness was presented by [88–90] by using a roller chain. The principle of the technique is simple. A chain of known length (L_1) is positioned on the land surface, and as the horizontal distance (L_2) between the ends of the chain decreases, the roughness increases [91]. The following equation was used to evaluate the soil surface roughness (C_r):

$$C_r = [1 - (L_2/L_1)] \times 100 \quad (9)$$

The ridge alignment in the field was designed by knowing the prevailing wind direction.

5.1.3 Climatic Factor (C)

The climatic factor (C) in WEQ was first presented by [92]. The Food and Agriculture Organization [93] improved the factor to suit the conditions of dryness. The monthly C factor involves the mean monthly weather parameters that are effective in evaluating wind erosion as follows:

$$C = \frac{1}{100} \sum_{i=1}^{i=12} U^3 \left(\frac{ETP_i - P_i}{ETP_i} \right) d \quad (10)$$

where U , ETP_i , P_i , and d : are the wind velocity at 2 m height (m s^{-1}), potential evaporation (mm), precipitation (mm), and the number of days in the month of consideration; respectively.

5.1.4 Field Length Factor (L)

The field length (L) is in the dominant wind direction, according to [81]. In some cases, the wind comes from different directions; therefore, the wind direction becomes difficult to be determined [94].

5.1.5 Vegetative Cover Factor (V)

This factor is evaluated by relating some elements of vegetative material to its equivalent small grain residue equivalent. The following equation was used by [95] to express the vegetative cover factor (V) as the small grain equivalent (SG)_e.

$$(SG)_e = aR_w^b \quad (11)$$

where a , and b are crop constants (Use Table from [14]). R_w is the amount of residue expressed in terms of small grain equivalent (kg ha^{-1}).

The annual soil loss was computed using the term (IKCL) [96, 97]. If the product of nominated factors in this term $>5.5 \times 10^6$; use the following equation:

$$E = 2.178 \left(\frac{-V}{4500} \right) \times \left(I \times K \times \frac{C}{100} \right) \quad (12)$$

But if the product $\leq 5.5 \times 10^6$; use the following equation:

$$E = 0.0015 \times 2.178 \left(\frac{-V}{4500} \right) \times \left(I^{1.87} \times K^2 \times \left(\frac{C}{100} \right)^{1.3} \times L^{0.3} \right) \quad (13)$$

It is worth pointing out that a guide is prepared by the Department of Water, Land and Biodiversity Conservation (DWLBC) to identify the minimum and desired soil cover required to reduce wind erosion and provide soil protection under most conditions [98]. It is established that grasses amount $>2 \text{ Mg ha}^{-1}$ is enough to entirely avoid wind erosion hazard in the field [95]. The DWLBC [98] suggested the following amounts of surface cover required to protect soil from wind erosion (Table 3).

Table 3 Amount of surface cover required for soil protection from wind erosion [98]

Soil type	Minimum cover		Desirable cover	
	%	Mg t ha ⁻¹	%	Mg t ha ⁻¹
Loam	15	0.5	35	1
Sandy loam	20	0.6	50	1.5
Sands	50	1.5	70	2.5

A broad modification of the wind erosion equation (WEQ) was made since the 1960s. The WEQ model has been exposed to many refinements which led to a very sophisticated model. This stimulates the emergence of new equations such as the well-planned model Revised Wind Erosion Equation (RWEQ) by [83]. The model links field information with computer models to estimate spatial soil erosion, therefore, it is better defined the processes of wind erosion. However, REWEQ predicts wind erosion depending on factors related to weather, soil surface, and crop factors [99, 100]. Wind erosion prediction system (WEPS) is another model set to improve the prediction technology. WEPS is a more complex model than WEG and REWEQ and requires additional input parameters [101–106].

5.2 Study Cases of Wind Erosion in Iraq

Wind erosion in Iraq seems to be concentrated in zone 3 (middle-south area) and zone 4 (northwest area) (see Fig. 1). The potential wind erosion reported by [107] reached 65 Mg ha⁻¹ year⁻¹ in zone 3 and zone 4 with comparable soil surface and climate conditions. However, a simple mathematical model was used by [108] to predict soil loss by wind erosion annually in different locations. Six fallow barley fields were randomly chosen from semi-arid sedimentary plain south of Baghdad, Iraq (zone 3 in Fig. 1). An average potential erosion of 70.2 Mg ha⁻¹ y⁻¹ was attained (Table 4).

The WEQ was used to estimate potential erosion for designing the optimal measures to adjust soil losses by wind erosion in Iraq by defining a group of K, L, and V that required declining losses to an acceptable level [108]. For example, if a soil roughness K of 0.5 is associated with particular environments, this would decrease the peak soil loss by wind by 50% for fields where ridges established perpendicularly to the dominant wind direction. According to the prevailed environments, their calculations suggest an amount of 250–500 kg ha⁻¹ plant residues to be applied on the soil surface to diminish soil loss to the tolerable level (2 Mg ha⁻¹). However, when arid conditions are prevailing most of the year, such as in Iraq, tillage operation associated with an inadequate amount of residues covering soil surface induce rough soil surface most of the year. This is considered the main reason for effective wind erosion control (Fig. 10).

The main causes of desertification in Iraq are unsustainable agricultural practices through soil and crop management processes [110]. Desertification also decreased

Table 4 Potential wind erosion (E_3) \times depending on soil roughness (K) and climate (C) (After [108])

Location	$E_1 = I$ (Mg. ha ⁻¹ year ⁻¹)	K	$E_2 = I \times K$ (Mg. ha ⁻¹ year ⁻¹)	C	$E_3 = E_2 \times C$ (Mg. ha ⁻¹ year ⁻¹)	Observation
1	354	1	354	0.45	159.3	Regions of flow
2	169	1	169	0.45	76.1	
3	132	1	132	0.45	59.4	Climatic factor
1	89	1	89	1.43	127.3	Regions of high
2	38	1	38	1.43	54.3	
3	17	1	17	1.43	24.3	Climatic factor
Geometric mean	87.7	1	87.7	0.8	70.2	



Fig. 10 Establishing soil ridges to control wind erosion in a field [109]

the biological productivity of dry areas, which comprise about 92% of the total area in Iraq. It is indicated that Iraq is now witnessing an increase in sand storms compared with those that happened during the last century [12]. The study concluded that the extreme change in the annual rainfall and temperature is the main cause of enhancing the local dust. Moreover, other reasons that escalated the local dust occurrences were attributed to the messy armed activities and roads.

Some researchers used new techniques to define the extent of desertification in Iraq. For example, in his study of dunes monitoring, [111] included six districts in

Iraq suffering from dunes creeping. The dry weather and low amount of rainfall have characterized these districts, especially in the latest years. The study was designed to monitor, evaluate, and map the dune advance in the north-central zone (zone 4 Fig. 1). Remote sensing “RS” and in specific, Earth observation satellites and also Geographical Information Systems “GIS” were used to monitor dunes advance. The study concluded that the dunes accumulation is increased by 2,020.6 km in Baiji site and 29.1 km in Al-Aith site throughout the 21 years (1988–2009).

Management practices designed to mitigate wind erosion may include the use of soil conditioners besides windbreaks. In the two preceding sites, the rates of dunes movement were 1,155.9 and 494.2 m year⁻¹ for the same period. Generally, these results indicated that the dune invasion represents a great risk to the study area. Based on [111] study results, it seems that remote sensing and GIS techniques are suitable for dune advanced monitoring. Minute attempts have been carried out in Iraq to fix dunes advance using soil stabilizers and evaluation of dunes stabilization.

Attempts have been made to stabilize dunes in the Baiji district, Iraq (Zone 4 Fig. 1) using local soil conditioners derived from oil derivatives and plant residuals [112, 113]. The author exploits some parameters related to wind erosion (i.e. mean weight diameter, dry aggregate percentage) to evaluate the effectiveness of these conditioners to stabilize dunes [112]. Results indicated that the natural vegetation cover in the first level of bitumen emulsion treatment (1%) is much better than the second (2.5%) and the third level treatments (5%). Plant residuals treatments generally have positive effects on the natural vegetation cover. Plant residuals increase soil organic matter, and consequently, it improves soil structure, reduces bulk density, increases the soil pores and, ultimately increases soil moisture.

5.3 The Need for a Soil Conservation Foresight in Iraq

Solutions for land degradation in Iraq, particularly soil erosion problems, have been neglected since 1991. Subsequently, no actual attempts have been made to face the consequences of soil erosion and their effects on the different aspects of the Iraqi people’s lives. The successive governments, especially after 2003, ignored the problems associated with soil and plant production deterioration, and they have not suggested any plans or strategies to cope with the soil erosion problems. Also, little attention has been paid by the Iraqi institutions, establishments, and authorities to the same. This deliberate ignorance by the politicians has led to poverty, unemployment, low productivity, and disorder in rural societies.

The land is the most ignored resource that is misused by almost everyone, either knowingly or unknowingly. Nearly all the soil erosion research work in Iraq focuses on monitoring the phenomenon without finding resolutions to the problem. However, some researchers who were concerned about the soil erosion problems published negligible and scattered articles in some scientific journals to indicate the occurrence of soil erosion in Iraq.

Iraq needs an ad hoc project, which involves a group of participants that mainly come from academic and research organizations and the government and include scientists, politicians, and foresight experts. The group must review a set of relevant literature (national and international) and build a scenario to identify the steps required to solve the main soil erosion problems in Iraq.

In summary, the soil erosion rate in Iraq results from interaction with a group of factors, namely climate, soil surface characteristics, topography, land use, and land cover. Wind erosion is widespread over almost all parts of the country, but water erosion dominates mainly in the north and northeastern of the country. This study can be used as a base to further advanced erosion studies and to assess the extent of water and wind erosion over time. Moreover, such a study may be used as a guide to understanding the erosion problems in Iraq.

6 Conclusions

Water and wind erosion are reaching catastrophic levels in Iraq due to lack of control measures and neglecting of land especially in the past three decades. Water erosion is related to natural and human induced activities, whereas much of the wind erosion for the most of Iraq is natural erosion that is not easy to mitigate using soil conservation practices. Water erosion dominates in the northern parts, while wind erosion prevails in the central and southern parts of Iraq. While limited number of studies is available on the estimation of soil erosion in different parts of Iraq, the management part is neglected in most of reports.

7 Recommendations

Field and applied research are needed in the imminent future to accurately estimate erosion levels and to manage increased loss of agricultural and rangelands in Iraq. Moreover, soil erosion management goals have to be established to regulate practices and ultimately to conserve soil quality in the long-term soil management policies and programs. A key source for water erosion prediction in Iraq is the spatio-temporal differences in erosivity values. Therefore, it is worthwhile to compare erosivity values in Iraq with those in nearby countries. A regional rain erosivity map project could be used as a framework objective.

Acknowledgements The authors are thankful for the distinctive comments offered by editors and reviewers that have improved the text and chapter. We are grateful to Dr. Ayad M. Fadhil Al-Quraishi, Professor of Applied Remote Sensing and GIS, Tishk, International University for his continuous motivation and support.

References

1. Lowdermilk WC (1953) Conquest of the land through 7,000 years. *Agric Inf Bull* 99(99):24
2. FAO-ITPS (2015) Status of the world's soil resources. Main report. Food and Agriculture Organization of the United Nations and Intergovernmental Technical Panel on Soils, Rome, Italy
3. Abdullah M, Al-Ansari N, Laue J (2020) Water harvesting in Iraq: status and opportunities. *J Earth Sci Geotech Eng* 10:1792–9660
4. Abdul-Munaim AM, Lightfoot DA, Watson DG (2020) Could conservation tillage farming be the solution for agricultural soils in Iraq? *AMA Agric Mech Asia Africa Lat Am* 51:7–9
5. Buringh P (1960) Soils and soil conditions of Iraq, Ministry of Agriculture. *Agric Res Proj Baghdad* 1
6. Dregne HE (1986) Desertification of arid lands. In: El-Baz F, Hassan MHA (eds) *Physics of desertification*. Springer, Netherlands, Dordrecht, pp 4–34
7. Goudie AS (2019) IPCC climate change and land: desertification. *Encycl Environ Heal*
8. Caldwell TG, McDonald EV, Bacon SN, Stullenbarger G (2008) The performance and sustainability of vehicle dust courses for military testing. *J Terramechanics* 45:213–221. <https://doi.org/10.1016/j.jterra.2008.10.002>
9. Bacon SN, McDonald EV, Dalldorf GK, Lucas W, Nikolich G (2014) Recommendations for the development of a dust-suppressant test operations procedure (TOP) for U.S. Army materiel testing. *GSA Rev Eng Geol* 22:83–100. [https://doi.org/10.1130/2014.4122\(09\)](https://doi.org/10.1130/2014.4122(09))
10. United Nations Economic and Social Commission for Western Asia (ESCWA) (2017) Arab climate change assessment report—executive summary. *Reg Initiat Assess Clim Chang Impacts Water Resour Socio-Economic Vulnerability Arab Reg* 57
11. Zakaria S, Al-Ansari N, Knutsson S (2013) Historical and future climatic change scenarios for temperature and rainfall for Iraq. *J Civ Eng Archit* 7. <https://doi.org/10.17265/1934-7359/2013.12.012>
12. Sissakian VK, Al-Ansari N, Knutsson S (2013) Sand and dust storm events in Iraq. *Nat Sci* 05:1084–1094. <https://doi.org/10.4236/ns.2013.510133>
13. Albarakat R, Lakshmi V (2019) Monitoring dust storms in Iraq using satellite data. *Sensors (Switzerland)* 19. <https://doi.org/10.3390/s19173687>
14. Blanco-Canqui H, Lal R (2010) Principles of soil conservation and management
15. Bellocchi G, Diodato N (2020) Rainfall erosivity in soil erosion processes. *Water (Switzerland)* 12. <https://doi.org/10.3390/w12030722>
16. Fu Y, Li G, Wang D, Zheng T, Yang M (2019) Raindrop energy impact on the distribution characteristics of splash aggregates of cultivated dark loessial cores. *Water (Switzerland)* 11. <https://doi.org/10.3390/w11071514>
17. Ghadiri H (2004) Crater formation in soils by raindrop impact. *Earth Surf Process Landforms* 29:77–89. <https://doi.org/10.1002/esp.1014>
18. Fernández-Raga M, Palencia C, Keesstra S, Jordán A, Fraile R, Angulo-Martínez M, Cerdà A (2017) Splash erosion: a review with unanswered questions. *Earth-Sci Rev* 171:463–477
19. Popa N (2017) Sheet and rill erosion. In: Radoane M, Vespremeanu-Stroe A (eds) *Landform dynamics and evolution in Romania*. Springer Geography. Springer, Cham, pp 347–369
20. Bernatek-Jakiel A, Poesen J (2018) Subsurface erosion by soil piping: significance and research needs. *Earth-Sci Rev* 185:1107–1128
21. Capra A (2013) Ephemeral gully and gully erosion in cultivated land: a review. In: *Drainage basins and catchment management: classification, modelling and environmental assessment*, pp 109–141
22. Al-Allaf M (2009) Study of gully erosion of kand structure Nw of Iraq by using remote sensing data. *Mesopotamia J Agric* 37:170–176. <https://doi.org/10.33899/magrij.2009.27396>
23. Boardman J, Evans R (2020) The measurement, estimation and monitoring of soil erosion by runoff at the field scale: challenges and possibilities with particular reference to Britain. *Prog Phys Geogr* 44:31–49. <https://doi.org/10.1177/0309133319861833>

24. Yang H, Zou X, Wang J, Shi P (2019) An experimental study on the influences of water erosion on wind erosion in arid and semi-arid regions. *J Arid Land* 11:208–216. <https://doi.org/10.1007/s40333-019-0097-3>
25. Lemboye K, Almajed A, Alnuaim A, Arab M, Alshibli K (2021) Improving sand wind erosion resistance using renewable agriculturally derived biopolymers. *Aeolian Res* 49. <https://doi.org/10.1016/j.aeolia.2020.100663>
26. Tanner S, Katra I, Haim A, Zaady E (2016) Short-term soil loss by eolian erosion in response to different rain-fed agricultural practices. *Soil Tillage Res* 155:149–156. <https://doi.org/10.1016/j.still.2015.08.008>
27. Myers DT, Rediske RR, McNair JN (2019) Measuring streambank erosion: a comparison of erosion pins, total station, and terrestrial laser scanner. *Water (Switzerland)* 11. <https://doi.org/10.3390/w11091846>
28. Castro-Bolinaga CF, Fox GA (2018) Streambank erosion: advances in monitoring, modeling and management. *Water (Switzerland)* 10
29. Keya DR (2018) Integration of GIS with USLE in assessing soil loss from Alibag catchment, Iraqi Kurdistan Region. *Polytech J* 8:12–16
30. Zhang S, Zhang X, Huffman T, Liu X, Yang J (2011) Soil loss, crop growth, and economic margins under different management systems on a sloping field in the black soil area of Northeast China. *J Sustain Agric* 35:293–311. <https://doi.org/10.1080/10440046.2011.554307>
31. Tessema YM, Jasińska J, Yadeta LT, Świtoniak M, Puchalka R, Gebregeorgis EG (2020) Soil loss estimation for conservation planning in the welmel watershed of the Genale Dawa Basin, Ethiopia. *Agronomy* 10. <https://doi.org/10.3390/agronomy10060777>
32. Mitchell JK, Mostaghimi S, Freeny DS, McHenry JR (1983) Sediment deposition estimation from cesium-137 measurements. *JAWRA J Am Water Resour Assoc* 19:549–555. <https://doi.org/10.1111/j.1752-1688.1983.tb02769.x>
33. Boix-Fayos C, Martínez-Mena M, Arnau-Rosalén E, Calvo-Cases A, Castillo V, Albaladejo J (2006) Measuring soil erosion by field plots: understanding the sources of variation. *Earth-Sci Rev* 78:267–285. <https://doi.org/10.1016/j.earscirev.2006.05.005>
34. Bagarello V, Ferro V (2017) Measuring soil loss and subsequent nutrient and organic matter loss on farmland. In: *Oxford research encyclopedia of environmental science*
35. Williams BL (2004) Trees, crops and soil fertility. In: Schroth G, Sinclair FL (eds) *Concepts and research methods*. CABI Publishing, Wallingford, UK, pp 437. £65.00. ISBN 0-85199-593-4. *Exp Agric* 40:143–143. <https://doi.org/10.1017/s0014479703321520>
36. Gupta VP (2020) Role of agroforestry in soil conservation and soil health management: a review. *J Pharmacogn Phytochem* 9:555–558
37. Du X, Jian J, Du C, Stewart RD (2021) Conservation management decreases surface runoff and soil erosion. *Int Soil Water Conserv Res*. <https://doi.org/10.1016/j.iswcr.2021.08.001>
38. Zhao J, Wang Z, Dong Y, Yang Z, Govers G (2022) How soil erosion and runoff are related to land use, topography and annual precipitation: Insights from a meta-analysis of erosion plots in China. *Sci Total Environ* 802. <https://doi.org/10.1016/j.scitotenv.2021.149665>
39. Alewell C, Borrelli P, Meusburger K, Panagos P (2019) Using the USLE: chances, challenges and limitations of soil erosion modelling. *Int Soil Water Conserv Res* 7:203–225
40. Borrelli P, Alewell C, Alvarez P, Anache JAA, Baartman J, Ballabio C, Bezak N, Biddoccu M, Cerdà A, Chalise D, Chen S, Chen W, De Girolamo AM, Gessesse GD, Deumlich D, Diodato N, Efthimiou N, Erpul G, Fiener P, Freppaz M, Gentile F, Gericke A, Haregeweyn N, Hu B, Jeanneau A, Kaffas K, Kiani-Harchegani M, Villuendas IL, Li C, Lombardo L, López-Vicente M, Lucas-Borja ME, Märker M, Matthews F, Miao C, Mikoš M, Modugno S, Möller M, Naipal V, Nearing M, Owusu S, Panday D, Patault E, Patriche CV, Poggio L, Portes R, Quijano L, Rahdari MR, Renima M, Ricci GF, Rodrigo-Comino J, Saia S, Samani AN, Schillaci C, Syrris V, Kim HS, Spinola DN, Oliveira PT, Teng H, Thapa R, Vantas K, Vieira D, Yang JE, Yin S, Zema DA, Zhao G, Panagos P (2021) Soil erosion modelling: a global review and statistical analysis. *Sci Total Environ* 780

41. Hussein MH, Awad MM, Abdul-Jabbar AS (1994) Predicting rainfall-runoff erosivity for single storms in northern Iraq. *Hydrol Sci J* 39:535–547. <https://doi.org/10.1080/02626669409492773>
42. Al-Banna AR, Eltayef NI, Karim TH (1986) The effect of tillage treatments on soil and water losses under natural rainfall in Aski-Kalak region (in Iraq). *Zanco (Iraq)* 4:15–21
43. Vanoni VA (2006) *Sedimentation engineering*
44. Boiten W (2021) Measurement of sediment transport. In: *Hydrometry*
45. Mutchler CK, Hermsmeier LF (1965) A review of rainfall simulators. *Trans ASAE* 8:0067–0068. <https://doi.org/10.13031/2013.40428>
46. Yakubu ML, Yusop Z (2017) Adaptability of rainfall simulators as a research tool on urban sealed surfaces—a review. *Hydrol Sci J* 62:996–1012. <https://doi.org/10.1080/02626667.2016.1267355>
47. Marston RA, Gillespie BM, Haire DH (2020) Portable controlled field experiments to resolve human impacts in geomorphology. *Geomorphology* 366. <https://doi.org/10.1016/j.geomorph.2019.106992>
48. Menezes Sanchez Macedo P, Ferreira Pinto M, Alves Sobrinho T, Schultz N, Altamir Rodrigues Coutinho T, Fonseca de Carvalho D (2021) A modified portable rainfall simulator for soil erosion assessment under different rainfall patterns. *J Hydrol* 596. <https://doi.org/10.1016/j.jhydrol.2021.126052>
49. Mhaske SN, Pathak K, Basak A (2019) A comprehensive design of rainfall simulator for the assessment of soil erosion in the laboratory. *CATENA* 172:408–420. <https://doi.org/10.1016/j.catena.2018.08.039>
50. Kwaad FJPM, Van Der Zijp M, Van Dijk PM (1998) Soil conservation and maize cropping systems on sloping loess soils in the Netherlands. *Soil Tillage Res* 46:13–21. [https://doi.org/10.1016/S0167-1987\(98\)80103-7](https://doi.org/10.1016/S0167-1987(98)80103-7)
51. Wischmeier WH, Smith DD (1965) Predicting rainfall-erosion losses from cropland east of the rocky mountains: guide for selection of practices for soil and water conservation. Agricultural Research Service, U.S. Dept of Agriculture in cooperation with Purdue Agricultural Experiment Station, Washington, D.C.
52. Wischmeier WH, Smith DD (1958) Rainfall energy and its relationship to soil loss
53. Lin BS, Thomas K, Chen CK, Ho HC (2016) Evaluation of soil erosion risk for watershed management in Shenmu watershed, central Taiwan using USLE model parameters. *Paddy Water Environ* 14:19–43. <https://doi.org/10.1007/s10333-014-0476-5>
54. Khosrokhani M, Pradhan B (2014) Spatio-temporal assessment of soil erosion at Kuala Lumpur metropolitan city using remote sensing data and GIS. *Geom Nat Hazards Risk* 5:252–270. <https://doi.org/10.1080/19475705.2013.794164>
55. Djoukbal O, Hasbaia M, Benselama O, Mazour M (2019) Comparison of the erosion prediction models from USLE, MUSLE and RUSLE in a Mediterranean watershed, case of Wadi Gazouana (N-W of Algeria). *Model Earth Syst Environ* 5:725–743. <https://doi.org/10.1007/s40808-018-0562-6>
56. Al-Taai OT, Al-Hassani DA, Mehdi AM (2016) Estimating the soil erosion by using rainfall data for selected stations in Iraq. *OALib* 03:1–15. <https://doi.org/10.4236/oalib.1102494>
57. Salahalddin SA, Al-Umary FA, Salar SG, Al-Ansari N, Knutsson S (2016) GIS based soil erosion estimation using EPM method, Garmiyān Area, Kurdistan Region, Iraq. *J Civ Eng Archit* 10. <https://doi.org/10.17265/1934-7359/2016.03.004>
58. Al-Abadi AMA, Ghalib HB, Al-Qurnawi WS (2016) Estimation of soil erosion in northern Kirkuk governorate, IRAQ using rusle, remote sensing and GIS. *Carpathian J Earth Environ Sci* 11:153–166
59. Khassaf SI, Jaber HA, Al-Abadi AMA, Ghalib HB, Al-Qurnawi WS, Hussein MH, Keya DR (2018) Estimation of soil erosion risk of the Euphrates River watershed using RUSLE model, remote sensing and GIS techniques. *Polytech J* 8:8–21
60. Hussein MH (1998) Water erosion assessment and control in Northern Iraq. *Soil Tillage Res* 45:161–173. [https://doi.org/10.1016/S0933-3630\(97\)00007-X](https://doi.org/10.1016/S0933-3630(97)00007-X)

61. Lal R (1976) Soil erosion on Alfisols in Western Nigeria. III. Effects of rainfall characteristics. *Geoderma* 16:389–401. [https://doi.org/10.1016/0016-7061\(76\)90003-3](https://doi.org/10.1016/0016-7061(76)90003-3)
62. Morgan RP (2005) Soil erosion and conservation, 3rd edn
63. Foster GR, Lane LJ, Nowlin JD, Lafflen JM, Young RA (1980) Chapter 3. A model to estimate sediment yield from field-sized areas: development of model. In: Knisel WG (ed) CREAMS: a field-scale model for chemicals, runoff, and erosion from agricultural management systems, p 640
64. Wischmeier WH, Johnson CB, Cross BV (1971) A soil erodibility nomograph for farmland and construction sites. *J Soil Water Conserv* 26:189–193
65. Schmidt S, Tresch S, Meusburger K (2019) Modification of the RUSLE slope length and steepness factor (LS-factor) based on rainfall experiments at steep alpine grasslands. *MethodsX* 6:219–229. <https://doi.org/10.1016/j.mex.2019.01.004>
66. Panagos P, Borrelli P, Meusburger K, Alewell C, Lugato E, Montanarella L (2015) Estimating the soil erosion cover-management factor at the European scale. *Land Use Policy* 48:38–50. <https://doi.org/10.1016/j.landusepol.2015.05.021>
67. Xiong M, Sun R, Chen L (2019) Global analysis of support practices in USLE-based soil erosion modeling. *Prog Phys Geogr* 43:391–409. <https://doi.org/10.1177/0309133319832016>
68. Eltaif NI, Abbas MK (1987) Estimation of erosivity indices for universal soil-loss equation in central and northern Iraq. *J Agric Water Resour Soil Water Resour* 6:1–13
69. Beskow S, Mello CR, Norton LD, Curi N, Viola MR, Avanzi JC (2009) Soil erosion prediction in the Grande River Basin, Brazil using distributed modeling. *CATENA* 79:49–59. <https://doi.org/10.1016/j.catena.2009.05.010>
70. Batista PVG, Silva MLN, Silva BPC, Curi N, Bueno IT, Acérbí Júnior FW, Davies J, Quinton J (2017) Modelling spatially distributed soil losses and sediment yield in the upper Grande River Basin—Brazil. *Catena* 157:139–150. <https://doi.org/10.1016/j.catena.2017.05.025>
71. Fattah Sheikh Suleimany JM (2020) Determination of potential runoff coefficient using geographic information system for a small basin in Balakayety Watershed, Kurdistan Region of Iraq. *Polytech J* 10:38–43. <https://doi.org/10.25156/ptj.v10n2y2020.pp38-43>
72. Duniway MC, Pfennigwerth AA, Fick SE, Nauman TW, Belnap J, Barger NN (2019) Wind erosion and dust from US drylands: a review of causes, consequences, and solutions in a changing world. *Ecosphere* 10. <https://doi.org/10.1002/ecs2.2650>
73. Buringh P, Edelman CH (1955) Some remarks about the soils of the alluvial plain of Iraq, South of Baghdad. *Netherlands J Agric Sci* 3:40–49. <https://doi.org/10.18174/njas.v3i1.17825>
74. Fenta AA, Tsunekawa A, Haregeweyn N, Poesen J, Tsubo M, Borrelli P, Panagos P, Vanmaercke M, Broeckx J, Yasuda H, Kawai T, Kurosaki Y (2020) Land susceptibility to water and wind erosion risks in the East Africa region. *Sci Total Environ* 703. <https://doi.org/10.1016/j.scitotenv.2019.135016>
75. Lal R (2013) Climate change and soil quality in the WANA region. In: Climate change and food security in West Asia and North Africa, pp 55–74
76. Malek C (2018) Desertification an imminent threat, creating unstable grounds for development. In: Arab News
77. Webb NP, Galloza MS, Zobeck TM, Herrick JE (2016) Threshold wind velocity dynamics as a driver of aeolian sediment mass flux. *Aeolian Res* 20:45–58. <https://doi.org/10.1016/j.aeolia.2015.11.006>
78. Dougrameji J (1999) Aeolian sediment movements in Lower Alluvial Plain, Iraq. *Desertif Control Bull* 45–49
79. WMO (2015) Sand and dust storm warning advisory and assessment system (SDS–WAS): science and implementation plan 2015–2020
80. Bolorani AD, Nabavi SO (2015) Dust storms in the West Asia Region
81. Woodruff NP, Siddoway FH (1965) A wind erosion equation. *Soil Sci Soc Am J* 29:602. <https://doi.org/10.2136/sssaj1965.03615995002900050035x>
82. Skidmore EL, Fisher PS, Woodruff NP (1970) Wind erosion equation: computer solution and application. *Soil Sci Soc Am J* 34:931–935. <https://doi.org/10.2136/sssaj1970.03615995003400060032x>

83. Fryrcar DW, Chen W, Lester C (2001) Revised wind erosion equation. *Ann Arid Zone* 40:265–279
84. Zhou Z, Zhang Z, Zou X, Zhang K, Zhang W (2020) Quantifying wind erosion at landscape scale in a temperate grassland: Nonignorable influence of topography. *Geomorphology* 370. <https://doi.org/10.1016/j.geomorph.2020.107401>
85. Rose CW (2017) Research progress on soil erosion processes and a basis for soil conservation practices. In: *Soil erosion research methods*, pp 159–180
86. Skidmore EL (2017) Wind erosion. In: *Soil erosion research methods*, pp 265–294
87. Williams JR, Jones CA, Dyke PT (1984) A modelling approach to determining the relationship between erosion and soil productivity. *Trans Am Soc Agric Eng* 27:129–144
88. Saleh A (1993) Soil roughness measurement: chain method. *J Soil Water Conserv* 48:527–529
89. Saleh A (1994) Measuring and predicting ridge-orientation effect on soil surface roughness. *Soil Sci Soc Am J* 58:1228–1230. <https://doi.org/10.2136/sssaj1994.03615995005800040033x>
90. Saleh A, Fryrear DW (1999) Soil roughness for the revised wind erosion equation (RWEQ). *J Soil Water Conserv* 54:473–476
91. de Oro LA, Colazo JC, Buschiazzo DE (2016) RWEQ—wind erosion predictions for variable soil roughness conditions. *Aeolian Res* 20:139–146. <https://doi.org/10.1016/j.aeolia.2016.01.001>
92. Armbrust DV (1962) Climatic factor for estimating wind erodibility of farm fields. *Water* 17:1–4
93. FAO, UNDP, UNEP (1994) *Land degradation in south Asia: its severity, causes and effects upon the people*
94. Schmidt S, Meusburger K, de Figueiredo T, Alewell C (2017) Modelling hot spots of soil loss by wind erosion (SoLoWind) in Western Saxony, Germany. *L Degrad Dev* 28:1100–1112. <https://doi.org/10.1002/ldr.2652>
95. Lyles L, Allison BE (1981) Equivalent wind-erosion protection from selected crop residues. *Trans Am Soc Agric Eng* 24:405–408. <https://doi.org/10.13031/2013.34265>
96. Schwab GO, Fangmeier DD, Elliot WJ, Frevert RK (1993) *Soil and water conservation engineering*, 4th edn. *Soil water Conserv Eng 4th Ed*
97. Panigrahi B, Goyal MR (2016) *Soil and water engineering: principles and applications of modeling*
98. McCord A, Rix R (2007) *Land management monitoring in the agricultural areas of South Australia. Report No 1. South Australia. Department of Water, Land and Biodiversity Conservation. DWLBC Report 2008/28*
99. Jarrah M, Mayel S, Tatarko J, Funk R, Kuka K (2020) A review of wind erosion models: data requirements, processes, and validity. *Catena* 187
100. Zou X, Li H, Liu W, Wang J, Cheng H, Wu X, Zhang C, Kang L (2020) Application of a new wind driving force model in soil wind erosion area of northern China. *J Arid Land* 12:423–435. <https://doi.org/10.1007/s40333-020-0103-9>
101. Pi H, Sharratt B (2017) Evaluation of the RWEQ and SWEEP in simulating soil and PM10 loss from a portable wind tunnel. *Soil Tillage Res* 170:94–103. <https://doi.org/10.1016/j.still.2017.03.007>
102. Zhang JQ, Zhang CL, Chang CP, Wang R De, Liu G (2017) Comparison of wind erosion based on measurements and SWEEP simulation: a case study in Kangbao County, Hebei Province, China. *Soil Tillage Res* 165. <https://doi.org/10.1016/j.still.2016.08.006>
103. Hagen LJ (2004) Evaluation of the wind erosion prediction system (WEPS) erosion submodel on cropland fields. In: *Environmental modelling and software*, pp 171–176
104. Wagner LE (2013) A history of wind erosion prediction models in the United States Department of Agriculture: the wind erosion prediction system (WEPS). *Aeolian Res* 10:9–24
105. Tatarko J, Wagner L, Fox F (2019) The wind erosion prediction system and its use in conservation planning. In: *Bridging among disciplines by synthesizing soil and plant processes*, pp 71–101

106. Guo Z, Zobeck TM, Stout JE, Zhang K (2012) The effect of wind averaging time on wind erosivity estimation. *Earth Surf Process Landforms* 37:797–802. <https://doi.org/10.1002/esp.3222>
107. Eltaif NI, Abass K, Kozikyan A (1989) Estimation potential wind erosion in the Bajii region. *Iraqi J Agric Sci* 20:5–10
108. Eltaif NI, Gharaibeh MA (2011) Aplicación De Un Modelo Matemático Para Predecir Y Reducción De La Erosión Eólica En Tierras Áridas No Protegidas. *Rev Chapingo Ser Ciencias For y del Ambient XVII*:195–206. <https://doi.org/10.5154/r.rchscfa.2010.08.061>
109. Tatarko J, Trujillo W, Schipanski M (2019) Wind Erosion Processes and Control Quick Facts
110. Aliyas I (2016) Dimensions of desertification on sustainable development in Iraq. *Int J Adv Res* 4:1553–1562
111. Fadhil AM (2013) Sand dunes monitoring using remote sensing and GIS techniques for some sites in Iraq. In: *PIAGENG 2013: intelligent information, control, and communication technology for agricultural engineering*. p 876206
112. Fadhil AM (2002) Sand dunes fixation in Baiji District, Iraq. *J China Univ Geosci* 13:67–72
113. Fadhil AM (2003) Evaluation of sand dunes stabilization in Baiji district, Iraq. *J China Univ Geosci* 14:59–64

Assessment of Aircraft Noise Pollution on Students' Performance



Khaula Abdulla Alkaabi, M. M. Yagoub, and Keith G. Debbage

Abstract One of the most serious issues associated with the aviation sector is aircraft noise, which negatively impacts nearby communities. It can lead to community annoyance, diminished educational attainment, and various health issues such as sleep disturbance, loss of concentration, and cardiovascular illness. Therefore, this study aims to explore the effect of aircraft sound on students' learning and teachers' performance using a binary logit model. A total of 2,023 students in two different schools, near Abu Dhabi International Airport, age between 15 and 18 years, and 214 teachers in the schools participated in a survey. The model findings demonstrate that airplane noise has no effect on the health, cognitive performance, or learning performance of students of both genders. Moreover, the survey results revealed that there is no substantial impact on teaching performance. The results of the noise measurements show that the noise level in all of the classes is less than the limit value (40 dB). The survey is coupled with noise level measurements at the selected schools. Overall, the survey results and noise level measurements indicate that there is no impact of aircraft sound on students' performance. This is maybe partly due to the nature of buildings and the difference between airport flight scheduling and schools workday hours. Future study could develop new noise impact measurements and indicators that correlate with health impacts.

Keywords School students · Aircraft noise pollution · Students' health · Airport

K. A. Alkaabi (✉) · M. M. Yagoub
Department of Geography and Urban Sustainability, College of Humanities and Social Sciences,
United Arab Emirates University, P.O. Box 15551, Al Ain, United Arab Emirates
e-mail: khaula.alkaabi@uaeu.ac.ae

M. M. Yagoub
e-mail: myagoub@uaeu.ac.ae

K. G. Debbage
Department of Geography, Environment and Sustainability & Department of Marketing,
Entrepreneurship, Hospitality and Tourism UNC-Greensboro, Greensboro, NC 27402, USA

1 Introduction

The influence of airport noise pollution on surrounding communities and ecosystem has gotten considerable of attention in the literature [1–5]. For example, the impact of airport noise on the value of residential houses and units in the Gold Coast airport zone were investigated from 2012 to 2016 using the statistical t-test to assess qualitative data on residential values located both inside and outside the flight route [1]. The study analysis showed that the average sales price difference for houses was 26%, which was statistically significant ($P = 0.00527576$); while the difference in unit pricing was 4% ($P = 0.222046$), which was not statistically significant, indicating that noise levels have a moderate effect on property values under the flight path [1].

Recently, the impact of aircraft noise on students' health was investigated experimentally through laboratory studies, while a methodological investigation was started to find the effects on students due to aircraft noise exposure [6]. Student's development could be potentially impaired by exposure to aircraft noise during the critical periods of learning at school [6]. This is because children are vulnerable to aircraft noise or other environmental noises as they may interfere with the cognition and learning development stage. In addition, students have less ability than adults do to tolerate aircraft noise. The noise can have a considerable impact on the level of data that is often encoded in memory, processed, saved, and brought back [7].

Aircraft noise interferes with children's learning in different skills such as reading, speech, acquisition, and memory. Various studies showed that children who lived near aircraft noise zones are negatively impacted when noise levels are at Leq of 65 dB or higher. The impact could be on phonological precursors of reading acquisition [6, 8, 9]. Mechanisms are available to lower the impact of aircraft noise on students, including changing structures and sound insulation [10].

This study aims to assess the effect of aircraft noise on students' learning and performance in schools around the Abu Dhabi International Airport. The airport was selected because of the accessibility and availability of some data. Previous studies showed that a huge urban development during the last two decades around the airport area. This highlights that the importance of studying the impact of aircraft noise pollution on students cognitive and performance. Student performance measures were based on a questionnaire distributed to students and teachers in the schools. This study is the first of its kind that is conducted in the UAE to investigate the effect of aircraft noise on students' learning performance [5, 6, 11, 12].

Several studies examined the impact of aircraft noise on primary school children's reading comprehension, cognition, and long-term memory [13, 14]. Most of the previous investigations were conducted on students of age between 5 and 12 years. This period is considered critical in learning acquisition. Previous results showed that students exposed to aircraft noise face some cognitive impairments with different levels [15, 16]. The most affected task by aircraft noise was found to be related to central processing and language comprehension [15, 17].

Different studies investigated and explored the potential impact of aircraft noise on reading performance, memory, and attention [17–24]. The most important studies

concerning the impact of aircraft noise on students' cognition are carried out by Hygge et al. [17] and Stansfeld et al. [23]. The first study analyzed the effects of aircraft noise on German students in Munich for the age group of eight to twelve years. The test took place in a sound attenuated mobile laboratory. The test was conducted through different phases. The first phase took place prior to relocation of the airport. Exposed students were compared with less exposed students in the same area, and it was found that the exposed students performed low on the most challenging reading test items. Following the shutdown of the old airport, the group difference disappeared in reading test and for long-term memory. Stansfeld et al. [23] studied students (eight to twelve years) living around three airports. These include Amsterdam–Schiphol (The Netherland), London–Heathrow (United Kingdom), and Madrid–Barajas (Spain) airports. Aircraft noise value at the schools was found range between 30 and 77 db LAeq. The analyses showed positive a linear correlation between airplane noise exposure and reading comprehension and recognition memory in schools. The analyses revealed increasing annoyance responses in students as the aircraft noise increases, and no aircraft noise impact on working memory.

A study conducted by de Oliveira Nunes and Sattler [25] in Brazil (Filho Airport) concluded that aircraft noise pollution results in problems in school performance. Students who exposed to aircraft noise experienced low performance in contrast to those who are not exposed to the noise [9, 25–33]. A similar study taken for ten schools around Heathrow Airport concluded the same results on the impact of aircraft noise on reading comprehension [20, 21]. The study concluded that students in the exposed schools experienced greater annoyance and had a poorer reading performance on the difficult items of a national standardized reading test.

Abu Dhabi International Airport is the UAE's second largest airport and one of the world's fastest expanding aviation hubs, serving more than 100 destinations in more than 50 countries. Abu Dhabi International Airport serviced over 23 million passengers in 2015, with 169,989 aircraft movements [34]. Alkaabi and Yaqoup [3] conducted a study that used Landsat classification and change detection techniques to analyze the effects of aircraft noise pollution on local communities and facilities near Abu Dhabi International Airport, and discovered that some schools are located along the flight path with a Ldn value greater than 610 dB. Therefore, it is critical to study the impact of airport aviation activities' impact on students learning in the adjacent schools. Thus, this chapter aims to explore the effect of aircraft noise on students' learning performance and teachers' teaching performance at the selected schools near Abu Dhabi International Airport. The following methodology section provides further information on the research survey and the noise level measurements implemented at the selected neighboring schools.

2 Methods

2.1 Data Collection

To investigate the impact of aircraft noise on students' learning performance, data was collected through self-administered questionnaires and face-to-face interviews with school students and teachers. Both questionnaires (for teachers and students) are designed to be anonymous and require less than fifteen minutes to be filled. The questionnaires include questions related to demographic variables such as gender, age, and income. In addition to, questions related to annoyance and difficulty of hearing from aircraft noise. Three faculty members reviewed the questionnaires, and some questions were modified to ensure the survey's validity. A pilot survey was conducted to check understanding and clarity of the questions. The purpose of the study was explained to participants in advance.

A stratified sampling method was used and the target was students and teachers who teach or study in schools around Abu Dhabi International Airport. The questionnaire was distributed to two schools in Abu Dhabi city. Um Al Emarat School and Al Hosn School are adjacent to the airport (within a 9–10 km radius of the airport runway center) and are therefore highly exposed to aircraft noise (where the dB LAeq is equal to around 60).

A total of 2,023 students in both schools (1025 from Um Al Emarat School and 998 from Al Hosn School) and 214 teachers in both schools (110 from Um Al Emarat School and 104 from Al Hosn School) were interviewed and completed the questionnaires. Students in high school classes (14–18 years old) were selected to participate in the survey. The survey was carried out during January and February, 2015.

Noise level measurements are conducted in the two schools (Al Hosn School and Um Al Emarat School in Al Shamkha district) to evaluate existing aircraft noise inside two classrooms. The selection was based on closeness to the airport, along the flight path, and one for males and females. The measurements process started in 2015 and completed in December, 2017. The procedure for noise measurement follows the ISO 1996-2:2007 methodology to determine environmental noise levels. Sound level meter SVANTEK, SV200, 39,731, and Calibrator CEL-177 were used to take the measurements. The measurements were used to validate the survey results. The specifications of classrooms are shown in Table 1. The measurements were conducted on two alternative days. The instrument was placed middle of the classroom and measurement was taken for 24 h.

Table 1 Details of surveyed classrooms

Sl. No.	Class rooms	Room size	Number of windows and size	Carpet	No. of tables/chairs	Other items for absorbing sound
1	Al Hosn School—Class Room 1	6.26 m × 8.92 m	3 windows, 2 m × 1.5 m Closed windows	No	30	Billboards, charts
2	Al Hosn School—Class Room 2	6.35 m × 8.74 m	3 windows, 2 m × 2 m Closed windows	No	30	Billboards, charts
3	Um Al Emarat School—Class Room 1	6.17 m × 10.8 m	2 windows, 2.5 m × 2 m Closed windows	No	30	Billboards, charts
4	Um Al Emarat School—Class Room 2	5.95 m × 10.87 m	2 windows, 2.5 m × 2 m Closed windows	No	34	Billboards, charts

2.2 Statistical Analysis and Model Development

SPSS software was used to analyze the survey data from schools located near from Abu Dhabi Airport. Statistical significance was tested using Chia-square test to determine if there are any differences between the socio-economic characteristics of the respondents.

A Binary Logit regression model was utilized to analyze aircraft noise's effect on students' cognitive and learning performance. Potential determinants such as gender, age, and income are controlled to predict a categorical variable from a set of predictor variables based on the odds ratio between the variables. One variable was chosen as a base case, and its coefficients were set to zero.

2.3 Demographic and Socioeconomic Characteristics of the Samples

Demographic and socio-economic characteristics show that the students from both schools (Um Al Emarat School and Al Hosn School) are between 15 and 18 years old. The percentage of female students in both schools outweigh the percentage of male students. They have same income profile (Fig. 1). Similar socioeconomic characteristics have been collected and provided to school teachers (Fig. 1). Table 2 shows no significant differences between the students and the teachers of schools located near from the airport in terms of their socioeconomic characteristics.

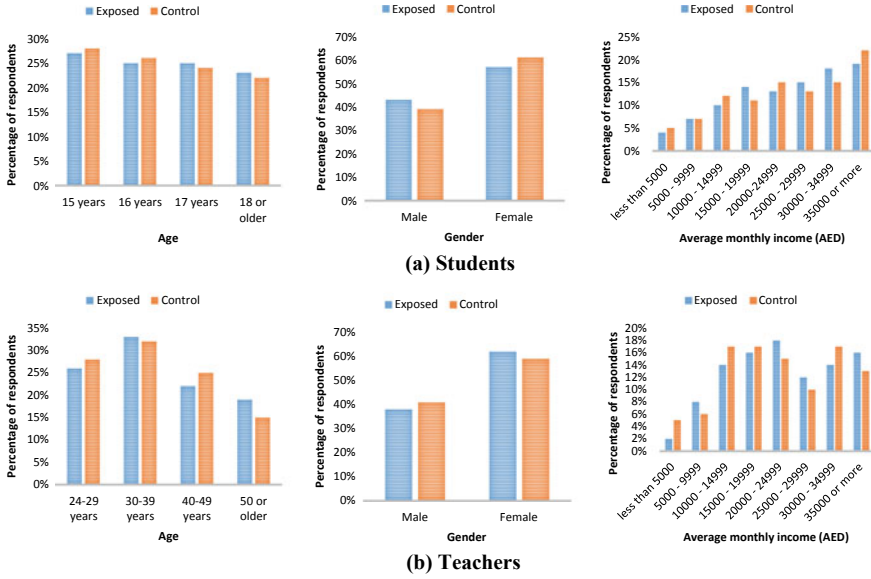


Fig. 1 Comparison between the socioeconomic characteristics between the exposed and control population areas: **a** students, **b** teachers

Table 2 Comparison of socio-economic characteristics between the two samples

Students		
	X ² -value	P-value
Gender	4.835	0.305
Age	23.216	0.599
Income	37.671	0.661
Teachers		
	X ² -value	P-value
Gender	5.919	0.432
Age	20.474	0.200
Income	13.240	0.152

3 Data Analysis and Discussion

Students and teachers in Um Al Emarat School were asked if they are annoyed by aircraft noise and, if yes, to rate the degree of annoyance level from 1 (not annoyed) to 10 (very annoyed) scale. Most of the respondents (79% of students and 82% of teachers) indicated that they are not annoyed by aircraft noise. The mean aircraft noise annoyance results for students are 3.24 and for teachers are 2.63, which clearly indicate that either students or teachers are annoyed.

The questionnaire asked students and teachers if aircraft noise causes disruption of verbal communication, such as “raise voice during asking questions or during teaching”, speech interference in the classroom”, have difficulties hearing the students or teachers and classroom discussion”. The majority of the teachers (87.2%) and students (82.6%) reported that aircraft noise has no major impact on disruption of speech. The teachers and students reported no need to raise their voices during teaching or asking questions to be heard. The results for “shout further support this finding” and “pause” during students asking questions, discussion sessions, or during teaching when aircraft passes by. The percentage of students and teachers who “pause” or “shout”, when an aircraft passes by, is low. Raising voice from both students and teachers, to overcome interference, is not adopted by them. Very few teachers and students attempt to raise their voices against high aircraft noise. The findings indicate that aircraft noise has no impact on students' cognitive development around Abu Dhabi Airport, and the educational environment is not affected by aircraft noise.

A binary logit model was used to assess the presence/absence of chronic aircraft noise on students' health, cognitive and learning performance based on the gender of students. The model results show that aircraft noise is not affecting students from both genders in terms of their health, cognitive performance, and learning performance (Table 3). There is no relationship between exposure to aircraft noise and noise annoyance, health, cognitive, and learning performance between male and female students. Aircraft noise does not annoy students of both genders. In addition, Table 3 clearly shows that students have no difficulties hearing the teachers and classroom discussion or talk loudly during the class to be heard. In addition, there are no impacts of aircraft noise on study disturbance, speech and communication, or on the students' daily activities. The self-reported health survey shows that students from both genders have no health issues such as hearing problems, stress, headache, or hypertension due to aircraft noise.

A binary logit model was also used to analyze the effect of aircraft noise on teacher performance. The results showed that there is no significant effect on teaching performance. Table 4 shows the results of the binary model, which clearly indicate that there is no relationship between aircraft noise and hearing the students or talking loudly. The teachers from both genders are not annoyed by the noise, and the table shows an insignificant difference between them. In addition, the result shows no significant differences between teachers from male and female schools in terms of health issues. No significant differences were found between teachers in different schools in terms of using hearing aids, medicine, headache, and hypertension.

Table 5 shows the noise level measurement results in classrooms. The UAE Federal Law No. (24) of 1999 for the Protection and Development of the Environment regulation and the Cabinet Decree (12) of 2006 do not stipulate classroom noise limits. Therefore, the results were compared to comfort values based on international standards. Several international and national standards define the noise exposure levels in schoolrooms. The noise limit was taken into account as 30–40 dB (A) in school rooms. The survey results show that the noise levels in each classroom are within (30–40 dB (A)). Therefore, the aircraft noise is not affecting the students and teachers of

Table 3 Result of predicting the impact of aircraft noise on students’ cognitive and learning performance based on gender (males as reference) using binomial logit models

	B	S.E	Wald	df	Sig	Exp (B)
Do you experience any aircraft noise pollution during lunch break?	0.162	0.112	2.095	1	0.148	1.176
Does Aircraft noise annoy you on a daily basis	-0.172	0.108	2.528	1	0.112	0.842
Is it more difficult to study in the presence of aircraft noise?	0.153	0.134	1.315	1	0.252	1.166
Do you have difficulties hearing the teacher and classroom discussion?	0.145	0.113	1.636	1	0.201	1.156
Do you feel it was necessary to talk loudly in class in order to be heard?	0.240	0.167	2.071	1	0.150	1.272
Does aircraft noise bother you?	0.271	0.410	0.435	1	0.510	1.311
Your health (excellent to poor)	0.677	0.498	1.849	1	0.174	1.969
Do you use any type of medicine	-0.184	0.243	0.572	1	0.449	0.832
Do you use any hearing aids	-1.415	1.259	1.263	1	0.261	0.243
Study disturbance	0.134	0.090	2.202	1	0.138	1.144
Effect on speech and communication	1.497	0.932	2.579	1	0.108	4.469
Effect on daily activities	-0.114	0.224	0.257	1	0.612	0.893
<i>Health issues due to aircraft noise</i>						
No disturbance (can tolerate)	-0.370	0.393	0.886	1	0.347	0.691
General disturbance (irritation)	0.161	0.108	2.223	1	0.136	1.175
Headache	0.119	0.190	0.393	1	0.531	1.127
Hypertension	0.501	0.326	2.366	1	0.124	1.651
Hearing problems	0.017	0.073	0.055	1	0.815	1.017
Constant	0.722	0.885	0.667	1	0.414	2.059

the schools. This result aligns with the model results obtained from the questionnaire (Tables 3 and 4). The results from the survey and noise measurements at the schools (Table 5) indicated that the UAE government-mandated schools’ construction with specifications to reduce noise. This research study can be viewed as a preliminary academic attempt to assess the influence of aircraft noise on students’ cognition at schools near Abu Dhabi International Airport.

4 Conclusion and Limitations

This study assessed the impact of aircraft sound on students’ health, cognitive, and learning performance in schools near Abu Dhabi International Airport. Both the model and the survey results indicate that aircraft noise has no overall impact on

Table 4 Binomial logit models for predicting the effect of aircraft noise on teachers teaching performance based on gender (males as reference)

	B	S.E	Wald	df	Sig	Exp(B)
Does Aircraft noise annoy you on a daily basis?	-1.424	2.570	0.307	1	0.579	0.241
Is it more difficult to teach in the presence of aircraft noise?	-1.276	0.893	2.039	1	0.153	0.279
Do you have difficulties hearing the student and classroom discussion?	0.283	0.939	0.091	1	0.763	1.327
Do you feel it was necessary to talk loudly in class in order to be heard?	0.852	0.629	1.835	1	0.176	2.344
Do aircraft noise bothers you?	-0.203	0.495	0.168	1	0.682	0.816
Your health (excellent to poor)	1.541	2.022	0.581	1	0.446	4.670
Do you use any type of medicine	0.751	1.812	0.172	1	0.679	2.119
Do you use any hearing aids	-1.167	1.487	0.616	1	0.433	0.311
<i>Problems due to noise pollution</i>						
No disturbance (can tolerate)	0.688	1.446	0.227	1	0.634	1.990
General disturbance (irritation)	2.271	2.059	1.216	1	0.270	9.685
Headache	-0.155	1.462	0.011	1	0.916	0.857
Hypertension	-0.898	1.811	0.246	1	0.620	0.407
Hearing problems	0.593	0.687	0.745	1	0.388	1.809
Constant	-4.041	3.636	1.235	1	0.266	0.018

Table 5 Evaluated noise level values of the aircrafts

School	Classroom	Noise level in daytime (07.00–20.00)	Noise level in night time (20.00–07.00)
Al Hosn School	Class 1	37.3 dB (A)	38.0 dB (A)
	Class 2	38.5 dB (A)	39.2 dB (A)
Um Al Emarat School	Class 1	38.7 dB (A)	39.4 dB (A)
	Class 2	31.5 dB (A)	32.3 dB (A)

students' health and learning performance and this holds true when the students are broken out by gender. The measurement results show that all the classrooms' noise levels are less than the limit value (40 dB (A)). Future research can consider monitoring and studying the effect of long-term exposure to the aircraft sound on students' health and learning performance.

Recommendations

Even though the study found that airport activities have no effect on the performance of the nearby schools' students or teachers, given the airport's ambitious aviation growth plan, it is recommended that communication channels be established between airports and schools' boards to closely monitor and manage potential aviation noise activities. Future research could develop new noise impact metrics and indicators that better correspond with health effects.

Acknowledgements We acknowledge the Research and Sponsored Projects Office at the United Arab Emirates University, which funded this research (Fund No. G00001260/4).

References

1. Bishop R, Laing K (2020) Impact of airport noise on residential property values: Cairns Airport. *J New Bus Ideas Trends* 18(2):22–29
2. Zhao L, Wang T, Guo R, Zhai X, Zhou L, Cui J, Wang J (2021) Differential effect of aircraft noise on the spectral-temporal acoustic characteristics of frog species. *Anim Behav* 182:9–18
3. Alkaabi KAS, Yagoub MM (2019) Variation in land use/land cover and aircraft sound levels around Abu Dhabi International Airport. *Eur J Geogr* 10(1):68–84
4. Athirah B, Shahida N (2019) Occupational noise exposure among airport workers in Malaysia: an ergonomic investigation. *J Phys Conf Ser* 1262. <https://doi.org/10.1088/1742-6596/1262/1/012010/pdf>
5. Alkaabi KA (2017) Studying the effects of aircraft noise around Abu Dhabi International Airport, UAE on the surrounding residential and workplaces. *Civil Eng Urban Plann Int J (CiVEJ)* 4(2):59–78. <https://doi.org/10.5121/civej.2017.4205>
6. Klatte M, Spilski J, Mayerl J, Moehler U (2016) Effects of aircraft noise on reading and quality of life in primary school children in Germany: results from the NORAH study. *Environ Behav* 49(4). <https://doi.org/10.1177/0013916516642580>
7. Stansfeld SA, Haines MM, Brown B (2000) Noise and health in the urban environment. *Rev Environ Health* 15(43):82. <https://doi.org/10.1515/reveh.2000.15.1-2.43>
8. Astolfi A, Pellerey F (2008) Subjective and objective assessment of acoustical and overall environmental quality in secondary school classrooms. *J Acoust Soc Am* 123(1):163–173. <https://doi.org/10.1121/1.2816563>
9. Evans G, Maxwell L (1997) Chronic noise exposure and reading deficits: the mediating effects of language acquisition. *Environ Behav* 29(5):638–656. <https://doi.org/10.1177/0013916597295003>
10. Bridget MS, Dockrell JE (2003) The effects of noise on children at school: a review. *Build Acoust* 10(2):97–106
11. Bergström K, Spilski J, Mayerl J, Moehler U, Lachmann T, Klatte M (2015) Effects of aircraft noise on annoyance and quality of life in German children near Frankfurt/Main airport: results of the NORAH (noise-related annoyance, cognition, and health)-study. In: 23rd international congress on acoustics. <https://doi.org/10.18154/RWTH-CONV-239176>

12. Verneil AL, Lavandier C (2017) Study of the impact of aircraft noise on annoyance and cognitive task performance regarding the distance from the airport. *J Acoust Soc Am* 141:3967. <https://doi.org/10.1121/1.4989034>
13. Boman E, Enmarker I (2004) Factors affecting pupils' noise annoyance in schools: the building and testing of models. *Environ Behav* 36(2):207–228. <https://doi.org/10.1177/0013916503256644>
14. Jones K (2010) Aircraft Noise and Children's Learning. Environmental Research and Consultancy Department, UK CAA, ERCD Report 0908. <https://publicapps.caa.co.uk/docs/33/ERC D200908.pdf>
15. Evans G, Lepore S (1993) Non-auditory effects of noise on children: a critical review. *Children's Environ* 10(1):42–72
16. Hiramatsu K, Tokuyama T, Matsui T, Miyakita T, Osada Y, Yamamoto T (2004) The Okinawa Study: effect of chronic aircraft noise exposure on memory of school children. In: Proceedings of noise public health problem international congress, 8th, Schiadam, The Netherlands, 179–180 pp
17. Hygge S, Evans GW, Bullinger M (2002) A prospective study of some effects of aircraft noise on cognitive performance in schoolchildren. *Psychol Sci* 13(5):469–474. <https://doi.org/10.1111/1467-9280.00483>
18. Clark C, Sorqvist P (2012) A 3 year update on the influence of noise on performance and behavior. *Noise Health* 14(61):292–296. <https://doi.org/10.4103/1463-1741.104896>
19. FICAN (2007) Findings of the FICAN pilot study on the relationship between aircraft noise reduction and changes in standardized test scores. https://fican1.files.wordpress.com/2015/10/findings_test_scores.pdf
20. Haines MM, Stansfeld SA, Job RF, Berglund B, Head J (2001) Chronic aircraft noise exposure, stress responses, mental health and cognitive performance in school children. *Psychol Med* 31:265–277
21. Haines MM, Stansfeld SA, Brentnall S, Head J, Berry B, Jiggins M, Hygge S (2001) The West London Schools Study: the effects of chronic aircraft noise exposure on child health. *Psychol Med* 31(8):1385–1396. <https://doi.org/10.1017/s003329170100469x>
22. Matheson M, Clark C, Martin R, van Kempen E, Haines M, Barrio IL, Hygge S, Stansfeld S (2010) The effects of road traffic and aircraft noise exposure on children's episodic memory: the RANCH Project. *Noise Health* 12(49):244–254. <https://doi.org/10.4103/1463-1741.70503DOI:10.4103/1463-1741.70503>
23. Stansfeld SA, Berglund B, Clark C, Lopez-Barrio I, Fischer P, Öhrström E, Haines MM, Head J, Hygge S, van Kamp I, Berry BF (2005) Aircraft and road traffic noise and children's cognition and health: a cross-national study. *Lancet* 365(9475):1942–1949. [https://doi.org/10.1016/S0140-6736\(05\)66660-3](https://doi.org/10.1016/S0140-6736(05)66660-3)
24. van Kempen E, van Kamp I, Lebreit E, Lammers J, Emmen H, Stansfeld S (2010) Neurobehavioral effects of transportation noise in primary schoolchildren: a cross-sectional study. *Environ Health* 9(1):25. <https://doi.org/10.1186/1476-069X-9-25>
25. de Oliveira Nunes MF, Sattler MA (2006) Aircraft noise perception and annoyance at schools near Salgado Filho International Airport, Brazil. *J Build Acoust* 13(2):159–172. <https://doi.org/10.1260/135101006777630418>
26. Boman E, Enmarker I, Hygge S (2005) Strength of noise effects on memory as a function of noise source and age. *Noise Health* 7(27):11–26. <https://doi.org/10.4103/1463-1741.31636>
27. Evans GW, Hygge S (2007) Noise and performance in children and adults. In: Luxon L, Prasher D (eds) *Noise and its effects*. Whurr Publishers, London
28. Clark C, Stansfeld SA (2007) The effect of transportation noise on health and cognitive development: a review of recent evidence. *Int J Comp Psychol* 20(2–3):145–158
29. Clark C, Martin R, Kempen EV, Alfred T, Head J, Davies HW, Haines MM, Barrio IL, Matheson M, Stansfeld SA (2006) Exposure-effect relations between aircraft and road traffic noise exposure at school and reading comprehension: the RANCH project. *Am J Epidemiol* 163(1):27–37. <https://doi.org/10.1093/aje/kwj001>

30. Eagan ME, Anderson G, Nicholas B, Horonjeff R, Tivnan T (2004) Relation between aircraft noise reduction in schools and standardized test scores. Washington, DC, FICAN
31. Haines MM, Stansfeld SA, Head J, Job RF (2002) Multilevel modelling of aircraft noise on performance tests in schools around Heathrow Airport London. *J Epidemiol Community Health* 56:139–144. <https://doi.org/10.1136/jech.56.2.139>
32. Stansfeld SA, Clark C, Cameron RM, Alfred T, Head J, Haines MM, van Kamp I, van Kempen E, Lopez-Barrio I (2009) Aircraft and road traffic noise exposure and children's mental health. *J Environ Psychol* 29(2):203–207. <https://doi.org/10.1016/j.jenvp.2009.01.002>
33. Schreckenberg D, Meis M, Kahl C, Peschel C, Eikmann T (2010) Aircraft noise and quality of life around Frankfurt Airport. *Int J Environ Res Public Health* 7(9):3382–3405. <https://doi.org/10.3390/ijerph7093382>
34. Statistics Centre Abu Dhabi (2016) Statistical Yearbook of Abu Dhabi. <https://www.scad.ae/Release%20Documents/SYB-2016%20EN%202016AUG14.pdf>

Role of Effective Factors on Soil Erosion and Land Degradation: A Review



Hooshyar Hossini, Hazhir Karimi, Yaseen T. Mustafa,
and Ayad M. Fadhil Al-Quraishi 

Abstract Land degradation is one of the leading environmental problems in the world. It defines as any change in the original condition of the land that may affect soil productivity, including topsoil erosion, the loss of vegetation, and salinity. In this chapter, we discussed the main factors affecting land degradation and soil erosion. At first, land degradation sources fell into two main categories: natural and anthropogenic. Among, anthropogenic sources with greater effects on land degradation were more noted. The main anthropogenic sources which have been discussed are agricultural activities, soil salinity, building and infrastructure, culture, economic situation, environmental pollution, and war.

Keywords Land degradation · Soil erosion · Natural and anthropogenic sources · Agriculture land degradation · Land use change

H. Hossini

Department of Environmental Health Engineering, Faculty of Health, Kermanshah University of Medical Sciences, Kermanshah, Iran
e-mail: hoo.husseini@gmail.com

H. Karimi (✉)

Department of Biological Sciences, University of Alabama, Tuscaloosa, AL 35401, USA
e-mail: hkarimi@crimson.ua.edu

Y. T. Mustafa

Department of Environmental Science, University of Zakho, Duhok, Kurdistan Region, Iraq
e-mail: yaseen.mustafa@uoz.edu.krd

Computer Science Department, College of Sciences, Nawroz University, Duhok, Kurdistan Region, Iraq

A. M. F. Al-Quraishi

Petroleum and Mining Engineering Department, Faculty of Engineering, Tishk International University, Kurdistan Region, Erbil 44001, Iraq
e-mail: ayad.alquraishi@tiu.edu.iq; ayad.alquraishi@gmail.com

1 Introduction to Land Degradation

Globally, rangelands cover about a quarter of Earth's land surface, and land degradation is the major problem [1]. Population growth, development, and urbanization have destroyed lands and urban green spaces. The development of urbanization often coincides with more consumption from natural sources, affecting nature and, consequently, weak sustainable development. Inappropriate planning, poor management system, and lack of specialist resources in urban management have increased the rate of destruction of natural lands [2]. Rangeland degradation is generally affected by interactions between climate, soil type, geology, vegetation type, and humans' and animals' interference. Degradation in ecosystems can occur in a short time with rapid progression from low to severe levels. As result of land degradation, it poses a threat to the ecological health of grasslands, shrubs, and savannas and could reduce the fertility of lands. Ecosystems degradation also has a severe effect on economic and social life. Several important indices could be used for land management. They may include lack of organic matter in the soil, decreases in soil fertility, disruption of soil structure and erosion, maladaptive changes in salinity, acidity, alkalinity, and presence of toxic chemicals [3]. On the other hand, land degradation includes the impact of biophysical factors, especially drought and anthropogenic, leading to the overuse of natural sources. These factors are illustrated in Fig. 1. According to this figure, the proximate and root causes of land degradation can be seen.

2 Environmental Destruction

Destruction of the environment can be classified from different perspectives, and one of them is assorting by reversible (renewable) or irreversible (non-renewable) destruction. Other classifications are including limited or extended destruction, and living or non-living destruction. Some examples that could be of help to better understanding are as follow:

- Limited destruction that is for one or several cases such as: hunting for an animal, cutting down a tree;
- Extended type examples: losing a lot of fish, extensive fires in a forest, or hunting many animals;
- Reversible impacts example: decreasing the land vegetation;
- Irreversible impacts such as ozone depletion, extinction of a genre of the animal;
- Living destruction example: destroying of habitat with its biota;
- Non-living destruction: soil degradation and erosion.

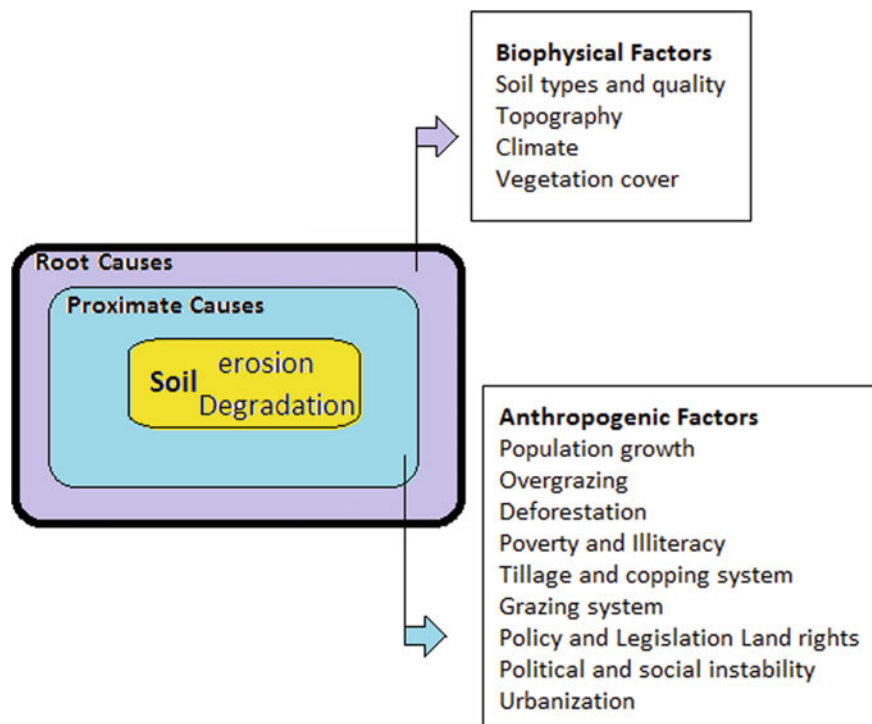


Fig. 1 A schematic of the root and proximate causes of land degradation [4]

3 Soil Erosion

Soil erosion is considered a potential threat to human and animal life that can be happened by soil depletion and reduced fertility. Therefore, it causes a decline in production, human and animal migrations, and the abandonment of farms. Soil erosion also reduces the useful volume of dams and lakes, which affects water storage capacity. The erosion forces are shown in Fig. 2 concerning its evidence in addition to powerful physical forces (wind and water), and other forces that can be caused by soil erosion such as chemical and biological agents. Generally, rocks and soils are eroded by wind, water under three stages: rock or soil erosion, the phase of soil transfer, and soil accumulation. Figure 3 displays the primary mechanism of soil erosion.

- *Stage of soil excavation*

At this stage, the soil aggregates lose their adhesion and disintegrate due to the loss of humus and colloids. Here, the soil is ready to erode, and then the topsoil gradually disappears by water or wind.

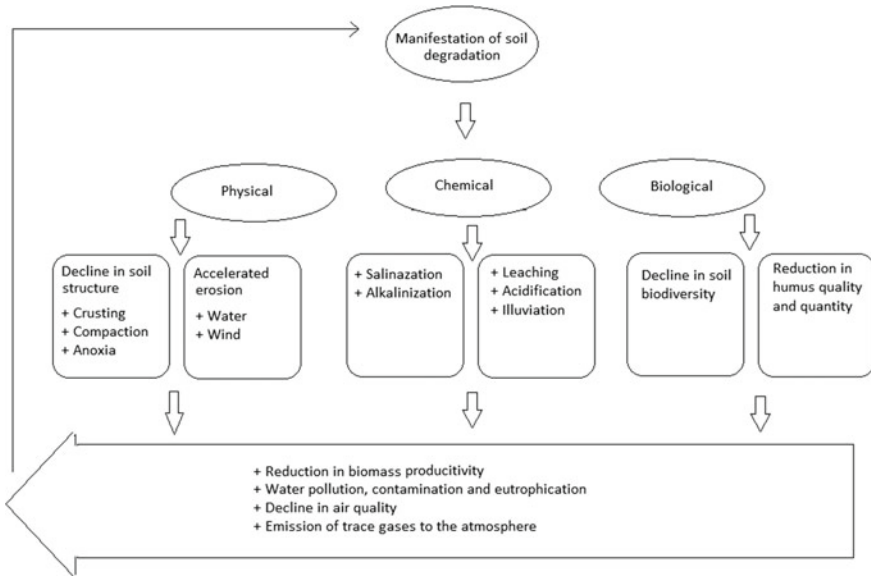


Fig. 2 Soil degradation by physical, chemical, and biological factors [5]

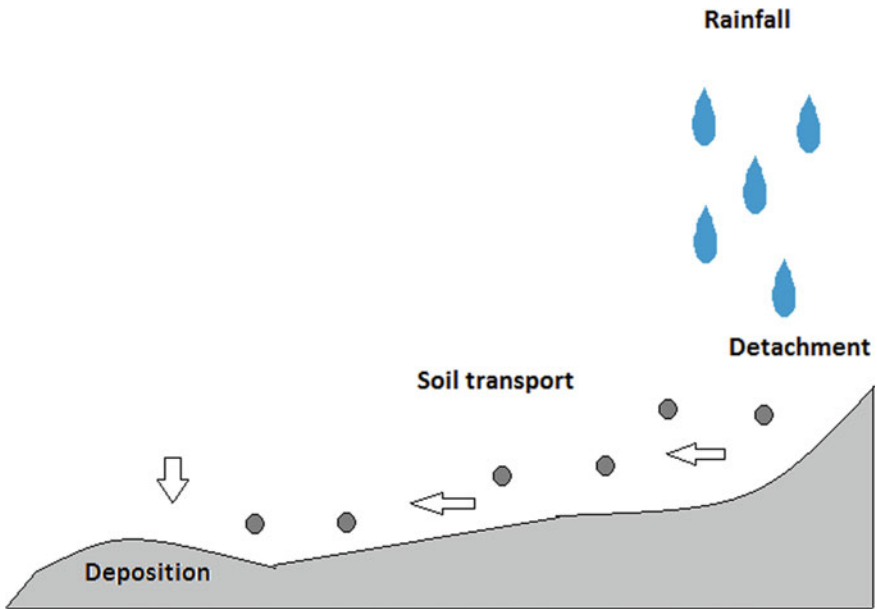


Fig. 3 A schematic pattern of soil degradation [6]

- *Soil transporting*

Because of no adhesion between aggregates, they slip out of place and move to another location.

- *Soil accumulation*

Wherever the wind carried particles hit an obstacle such as a plant, wall, stone, etc., they immediately fall to the ground and accumulate there. They can form large hills and even massive sand or mountain-like masses in extreme conditions. Alluvies gradually stop and precipitate when the water flows decrease (initially larger particles and then smaller particles). In some cases, the accumulation of alluvial material is so high that it forms a significant sedimentary layer.

3.1 The Importance of Erosion

By ignoring the formation of fertile alluvial downstream lands, soil formation is time-consuming and inconsiderable at the erosion point. According to researches, it generally takes about 500–800 years to form a centimeter of soil [6]; erosion is one of the most concerns in environmental circles.

3.2 Types of Erosion

3.2.1 Based on Erosion Factors

There are Naturally two forces, or two factors, which can cause soil displacement or soil erosion: water and wind. The most important natural processes in arid semi-arid and hyper-arid areas are wind erosion. This process occurs in conditions that have sensitive soil where the wind is permanently and at high velocity. Soil particles are transported in various forms of suspended, leaked, and creepy, which is ultimately causing serious environmental damage.

3.2.2 Based on the Influence of Nature and Human Intervention

Natural erosion, also known as normal erosion, is continually occurring in nature by water or wind at a slow rate that leads to soil production. Human activities such as mining, land excavations, road construction, agriculture, and livestock have disturbed the natural balance of erosion, and soil degradation has become significantly faster.

4 Land Degradation Sources

4.1 *Natural: Geography, Topography, and Climate*

The area where is located in arid and semi-arid regions; when exposed to seasonal or temporary storms, erosion occurs quickly. On the other hand, due to a short "time of concentration," high floods occur; topsoil of arid-base area erodes. Also, the arid area always is exposed to wind erosion due to low soil moisture. Areas with steep slopes are also subject to severe erosion, especially when the plowing and cultivation are in the direction of the slope, especially when the slope is more than 10–12%. Lack of vegetation can provide a good condition for erosion because plants and herbs help maintain the structure of soils and act as a physical barrier to erosion forces.

4.2 *Anthropogenic*

4.2.1 *Agricultural*

Improper Cultivation, Irrigation, and Overgrazing

The area with low land and low crop yields, especially in traditional agriculture, put much stress on the soil. Therefore, large parts of nutrients and soil organic matter like humus are consumed. This way causes degradation of aggregated soil and erosion. Reducing the organic material in soil is accompanied by soil adhesion and, finally, land degradation. Traditional irrigation also has adverse effects on soil. Degradation can be increased when traditional irrigation and furrow irrigation being used together. In comparison, drip irrigation is a better alternative to reduce soil erosion and water consumption. In some areas, cultivation is carried out with an improper frequency, for example, twice a year, where the erosion rate will be significantly higher than in other places.

Overuse of Chemical Fertilizers and Pesticides

To respond to the nutritional needs of communities and increase crop yields, nitrogenized and phosphorus fertilizers are common. This way reduces fertility and soil quality over a long time, and consequently, fattens lead to erosion. Also, overuse and uncontrolled pesticides into the soil can contaminate soil, and it possibly kills microorganisms such as bacteria, fungi, and earthworms [7]. Excessive pesticides represented soil degradation because microbial communities are responsible for soil fertility and nutrient element cycles.



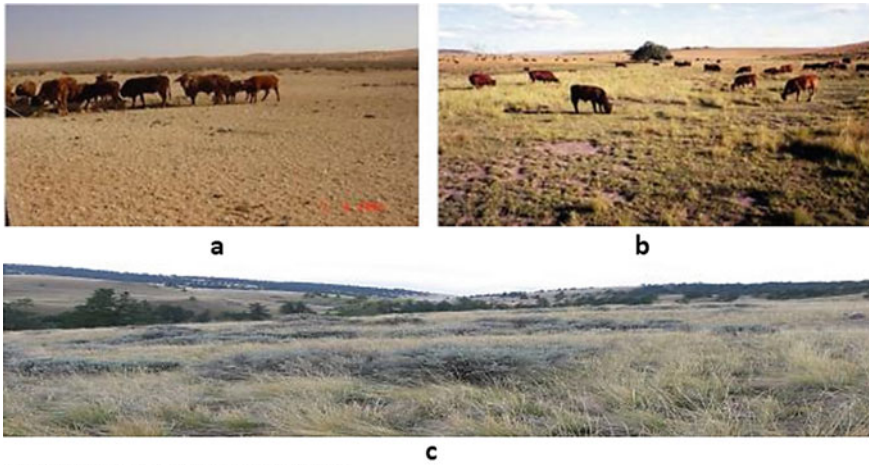
Fig. 4 Aeroponics grow and hydroponic [9]

No Use of New Agricultural Methods

Recently plants grow with a method called "hydroponics," which is a new method and agricultural machinery to protect the soil and land from degradation. In this method, plants can grow in a saturated nitrogen nutrient solution without soil (Fig. 4). Aeroponics grow is another new method that works without soil or aggregate material and supplies the growth in an air–water space where the nutrients are provided to the bare root system [8]. These promising methods can decrease the rate of soil degradation. Higher efficiency, more yielding, and environment-friendly can be provided by modern technology. Modern agricultural machinery allows better tilling, planting, fertilizer application, and pest control conditions. Also, it can be mentioned about the new irrigation system, which can reduce the rate of soil erosion. For example, in the use of sprinklers and micro-irrigation, the risk of erosion is decreased. Genetic manipulation engineering is another specialization that can help agriculture and slowing down erosion and land degradation. For example: try to come up the resistant crops against pests and environmental stresses.

Grazing Pressure

It is understood that livestock is a primary danger to biodiversity [10]. In central Crete, Greece, the study showed that approximately 40% of the central Cretan rangelands have declined in vegetation cover for 20 years between 1977 and 1996 [11]. This study reported that grazing pressure is responsible for decreasing vegetation cover throughout the long term. The effect of livestock on decreasing vegetation cover



a) Totally degraded; b) Partially degraded c) Restored

Fig. 5 a, b Livestock and c land degradation examples [12]

is noticeable. A graphical image of grazing pressure on rangelands is illustrated in Fig. 5. The effect of livestock on decreasing vegetation cover is noticeable.

4.2.2 Soil Salinization

Soil salinity is a wide-spreading concern and a major threat to growth, development, and plant yield production [13]. Salinity stress can affect plants growth because of their sensitivity to high salts concentrations (sodium and potassium ions). Research has shown that 20% of total cultivated lands and 33% of irrigated area are afflicted by high salinity [14]. Also, the salinized areas are increasing at a rate of 10% annually due to some reasons, such as low rainfall, high evaporation from the land surface, weathering of aggregate soil and rocks, irrigation using saline water, and inferior cultural methods. It has also been measured that more than 50% of the cultivable farms would be salinized by 2050 [14].

4.2.3 Building and Urbanity

A significant part of the destruction of vegetation is because of development activities such as road networks, construction of large dams, oil and gas pipelines, and exploitation of mines. A study entitled “Effect of different land-use types and their implications on land degradation and productivity in Ogun State, Nigeria” was carried out to compare land use types, including arable cropping, oil palm, secondary forest, and building sites [15]. It illustrated that land nutrients vary depending on the type of land use. This study determined that soil nutrients loss can be very high in all

types of land uses; thus, a proper choice is necessary to reduce soil nutrient depletion and enhances productivity. Among different land uses, it becomes clear that the soil nutrients depletion followed as Building sites > Arable cropping > Oil palm > Secondary forest. Also, more soil depletion and soil degradation were prominent from building sites and arable cropping rather than others.

4.2.4 Effects of Dam Building

According to the current situation in Iran, about 647 dams have been used, which provide utilization for industrial, agricultural, and domestic purposes. Although these dams have increment roles in development programs and utilizing water resources, their adverse effects on the environment should be noted. As seen in Fig. 6, Isfahan City and the Daran and East Isfahan weather stations are seen. Zayandehrood as the largest source in the center of Iran begins in the Zagros mountains and stretches 400 km eastward before ending in the Gavkhouni international wetland, southeastern Isfahan city. The Zayandehrood-Dam was made up on the Zayandehrood river in 1970 for many utilities, including hydroelectricity, protecting floods, and industrial, agricultural, and domestic needs. Jafari et al. [16] reported an assessment of the effects of the dam on land degradation. This evaluation was conducted through Spatio-temporal dynamics of land use/land cover and land surface temperature to desertify in an arid environment resulting from Zayandehrood-Dam construction. Figure 7, illustrates the photographs of Zayandehrood dam (a), Zayandehrood River (b), abandoned agricultural land (c), and salinized agricultural land (d). To emphasize the negative effects of the dam on land degradation, the finding of Jafari et al. [16] revealed that salty and bare areas significantly increased, while agricultural areas declined considerably from 1987 to 2014. The main reason for agriculture declining was related to the drying up of the Zayandehrood River caused by the dam construction.

4.2.5 Land Subsidence

Subsidence is an important and serious cause of erosion in mountainous areas. Natural subsidence mainly occurs in tectonic zones and heavy rainfall areas. Road construction and cutting the forest trees are considered as the main important subsidence factors [17]. Figure 8 shows the mainland subsidence in Iran. In the recent decade, many areas of Iran have been suffered from land subsidence caused by the large exploitations of groundwater and available aquifers withdrawal [18]. Aliabad plain, plateau of Qom, Iran, which is one of the main important plains at risk of ground subsidence in Iran. Concerning the figure, the effect and level of subsidence are seen obviously.

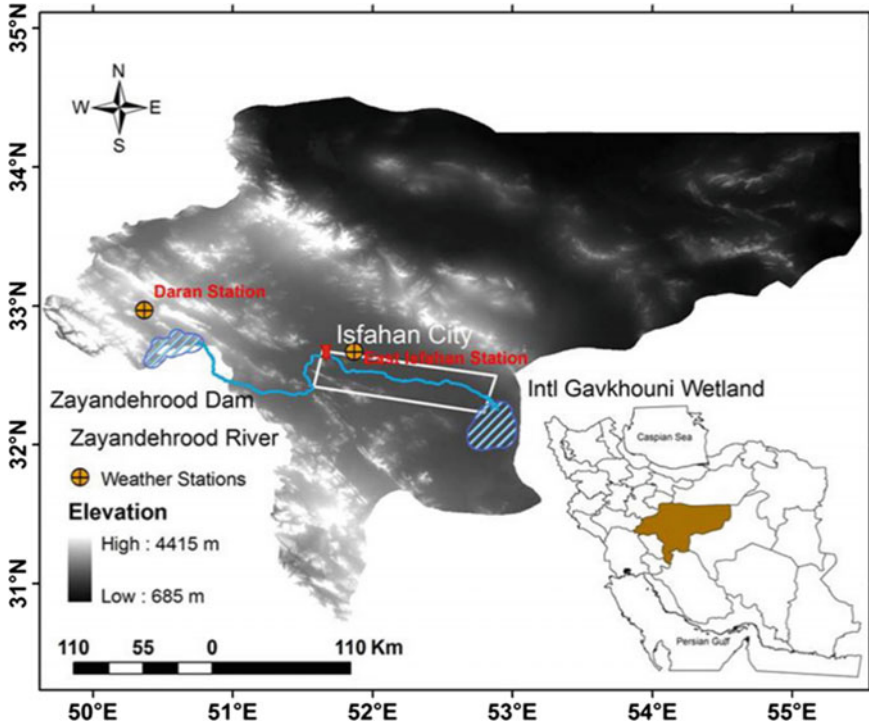


Fig. 6 Location of the study area for assessing the effects of dams on land degradation [16]

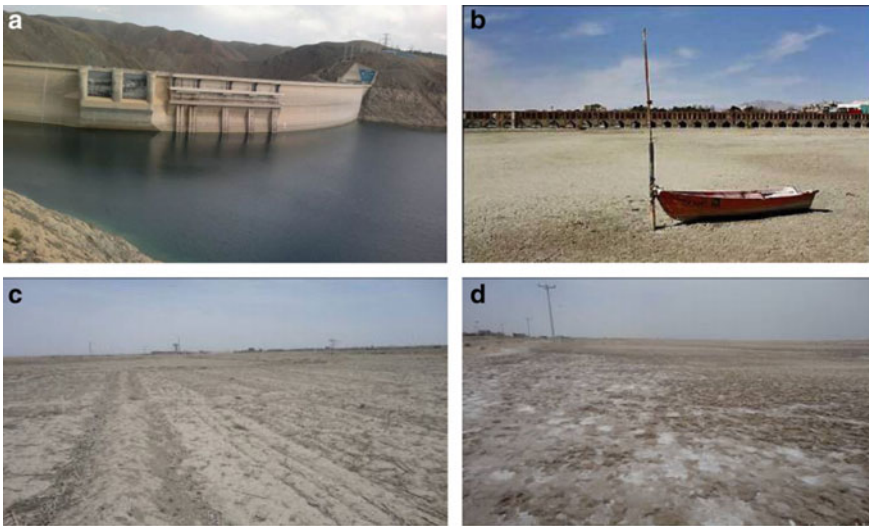


Fig. 7 Zayandehrood Dam and its effect on desertification[16]

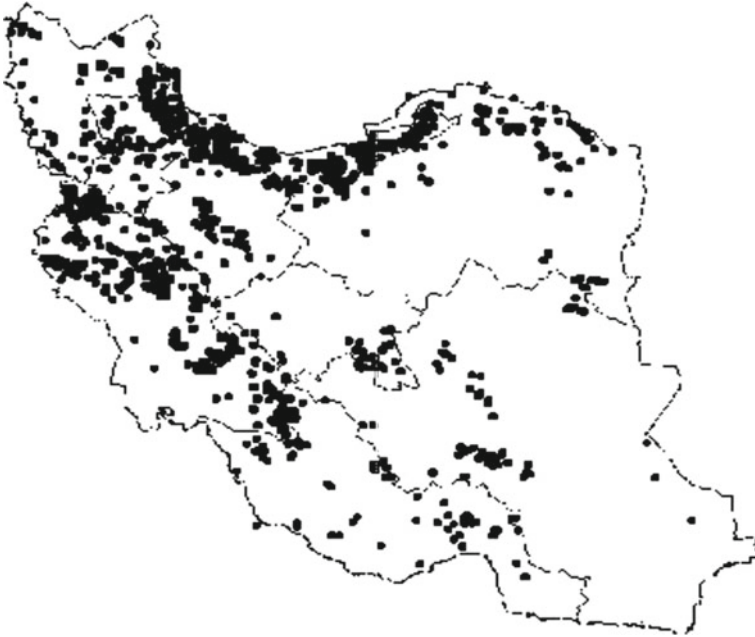


Fig. 8 Map of mainland subsidence in Iran [19]

4.2.6 Economic and Culture

Although land degradation is a physical mechanism, it strongly relates to socio-economic, political, and cultural factors [20]. Traditional practices in livestock and agriculture play an important role in the recent land degradation crisis. Overgrazing, long-time usages, destruction of surface vegetation, dry farming, and cultivation of on-ramp surfaces are the most critical land degradation related to socio-economic and cultural factors. Direct dependence on the livelihood of rural and traditional communities on natural resources has caused degradation. On the other hand, high competition for greater utilization of rangelands due to the limited capacity increased. The higher pressure of livestock, surplus grazing, hurry to entry, delay in departure and livestock, and bushing has increased the rate of land degradation. Fuel supply is one of the most important factors in rangeland destruction by rural and low-income livelihoods, leading to *desertification*.

In countries with high economic inflation, providing forage and other family necessities has directly increased the overuse of rangelands and natural resources. In some countries, due to the increasing population and poverty of the local communities, many people earn a living by utilizing forest resources to feed livestock, build crafts and sell the wood to small woodworking and fuel companies. Also, unnecessary harvesting of medicinal plants and excessive forest land utilization as dry

farming—which is usually low yield—and forest timber fuel the degradation and depletion of natural resources.

- Dry farming

Intensive cultivation has been known as an important source of land degradation and soil erosion. For instance, according to an estimation, about 10 million hectares of the country are under rainfed cultivation in Iran. Unfortunately, most farmers do not follow the correct rainfed principles. They often use sloping lands that are eroded so much. In most cases, paying attention to soil fertility and fertilizer needs is neglected because of poverty or insufficient dry farming knowledge. Iranian studies show that on average, erosion in rainfed lands is twice as much as irrigated lands [19]. In this regard, lots of researches have been reported. For instance, in the study of Zehtabian et al. [21], the effect of dry farming cultivation on land degradation was evaluated [21]. The result of this study indicated that dryland farming with sloping land of more than 8% was nominated as the most unsuitable condition for land degradation.

To protect from land degradation some researches have been conducted. For example, the study of Maghami et al. 2013 [22], revealed to optimum use lands and reduce their destruction, pay attention to some measurements include land using and land production capacity are necessary. This work showed that the lands with this work showed that the lands with a slope of more than 20% or a southern slope direction are not suitable for rain-fed cereal cultivation. But alfalfa species because of lower its effect on soil organic carbon, is permitted for the southern slope. However, this research, recommended the implementation of the optimal cultivation pattern needs to be promoted and informed by the farmers. In another study to prevent land degradation and reduction of soil quality, some measurements should be addressed such as a long-term solution, reduction the tillage operations, and addition of organic matter. Furthermore, in the pasture lands, the grazing must be controlled before pasture preparation.

4.2.7 Environmental Pollution

The widespread increase of fertilizers, pesticides, the extensive release of municipal and hazardous industrial wastewater (that is highly toxic with various types of chemicals), and droughts have caused environmental degradation [23, 24]. More examples of these hazardous sources are heavy metals, waste, and effluents containing petroleum and hydrocarbons, which threaten soil resources [25]. Since most industrial areas are near cities, surrounding lands are of great economic value. Hence, each year thousands of hundreds of square meters of land are turned into dead land, “so-called brownfields” by pollution from waste and effluent. In many cases, contaminated lands lose their fertility. Mining and oil activities are other causes of soil contamination and degradation, which operates in various forms [26]. Generally, mines, where minerals contain heavy metals or other harmful elements to the soil, will adversely affect the surface and depth of the soil after excavation.

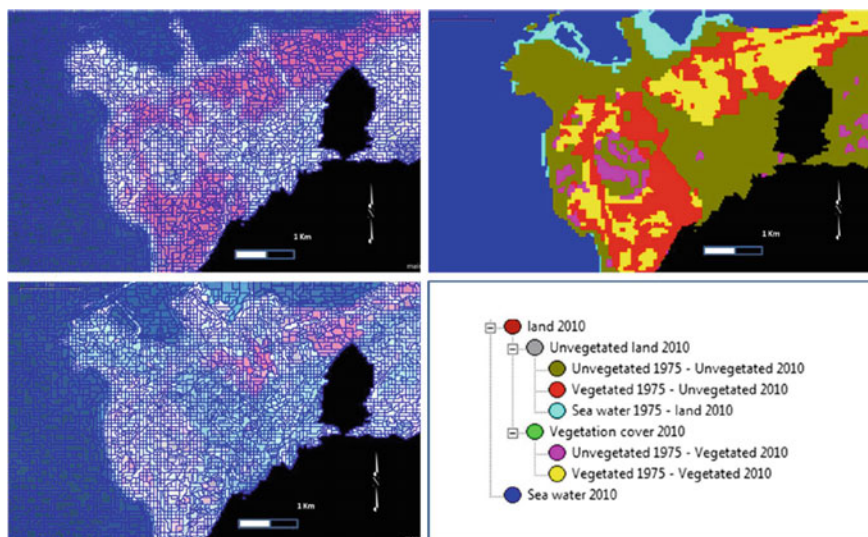


Fig. 9 Land cover change in some parts of Lebanon that reported by [27]

4.2.8 War-Induced Soil Degradation

Wars and armed conflicts make the turn in lands/directly through physical damage or by changing peoples' everyday practices and their use of natural resources [27]. Some Asian countries that were subject to war and civil war, such as Lebanon, Syria, Iraq, and Afghanistan, are more affected by the problems of war. Due to the long-lasting effects of war, the lands of these countries are more susceptible to soil erosion and degradation. Evaluating exposure to land degradation by war and armed conflicts in North Lebanon using multi-temporal satellite data was reported by [27]. This study showed that the war could significantly affect land uses and also land degradation. Figure 9 illustrates the comparison between land cover change within a segmented subset of 1975 (top image) and 2010 (bottom image). War and armed conflicts have significant pressure on lands and soils.

4.2.9 Land-Use Change and Soil Erosion Relationship

Many studies have reported that environmental problems such as soil erosion, water quality, ecosystem services, and biodiversity have been accelerating worldwide due to land use and land cover change (LULCC) [28, 29]. Uddin et al. [30], analyzed the consequence of land-use change on soil erosion risk from 1990 to 2010 in Nepal [30]. The results showed that soil erosion in the period studied increased from 129.30 million tons to 110.53 million tons. In similar research by Weldu Woldemariam and Edo Harka [31], the consequent changes in land use/land cover on soil erosion

were studied between 2000 and 2008 in Ethiopia. The estimated total soil loss showed an increase in that period, from 1.01 million tons to 1.52 million tons. The results also illustrated that extensive soil loss was found in croplands and bare lands.

5 Conclusions and Recommendation

This review has highlighted both natural and anthropogenic factors affecting land degradation and soil erosion. Soil erosion is one of the important phenomena that is occurring globally. Understanding soil erosion causes is an essential step toward developing effective soil conservation practices and actions. In this review, it is clearly revealed anthropogenic causes such as soil salinity, building and urbanity, agriculture, environmental pollution, and war have intensified the state of soil erosion, especially in developing countries.

References

1. Palmer MA, Poff NL (1997) The influence of environmental heterogeneity on patterns and processes in streams. *J N Am Benthol Soc* 16(1):169–173
2. Karimi H, Jafarnejhad J, Kakhani A (2020) Landsat time-series for land use change detection using support vector machine: case study of Javanrud District, Iran. In: 2020 international conference on computer science and software engineering (CSASE)
3. Hubert G (2003) Land degradation assessment in Drylands. Land and water development division. FAO
4. Kiage LM (2013) Perspectives on the assumed causes of land degradation in the rangelands of Sub-Saharan Africa. *Prog Phys Geogr* 37(5):664–684
5. Lal R (2001) Soil degradation by erosion. *Land Degrad Dev* 12(6):519–539
6. Matsumoto S et al. (2016) Application of coal ash to postmine land for prevention of soil erosion in coal mine in Indonesia: utilization of fly ash and bottom ash. *Adv Mater Sci Eng*
7. Joko T et al. (2017) Pesticides usage in the soil quality degradation potential in wanasari subdistrict, Brebes, Indonesia. *Appl Environ Soil Sci*
8. Nir I (1981) Growing plants in aeroponics growth system. In: Symposium on substrates in horticulture other than soils in situ, p 126
9. NASA (2014) Hydroponics gardening. Advanced nutrients raising the bud weight and reputation of top growers. Aeroponics and NASA. <http://www.advancednutrients.com/articles/aeroponics-and-nasa/>
10. Pringle HJ, Landsberg J (2004) Predicting the distribution of livestock grazing pressure in rangelands. *Austral Ecol* 29(1):31–39
11. Hostert P et al (2003) Retrospective studies of grazing-induced land degradation: a case study in central Crete, Greece. *Int J Remote Sens* 24(20):4019–4034
12. Zerga B (2015) Rangeland degradation and restoration: a global perspective. *Point J Agric Biotechnol Res* 1:37–54
13. Riaz M et al (2019) A comprehensive review on rice responses and tolerance to salt stress. *Advances in rice research for abiotic stress tolerance*. Elsevier, pp 133–158
14. Shrivastava P, Kumar R (2015) Soil salinity: a serious environmental issue and plant growth promoting bacteria as one of the tools for its alleviation. *Saudi J Biol Sci* 22(2):123–131

15. Senjobi B, Ogunkunle A (2011) Effect of different land use types and their implications on land degradation and productivity in Ogun State, Nigeria. *J Agric Biotechnol Sustain Develop* 3(1):7–18
16. Jafari R, Hasheminasab S (2017) Assessing the effects of dam building on land degradation in central Iran with Landsat LST and LULC time series. *Environ Monit Assess* 189(2):74
17. Neamat S, Karimi H (2020) A systematic review of GIS-based landslide Hazard mapping on determinant factors from international databases. In: 2020 international conference on advanced science and engineering (ICOASE). IEEE.
18. Rajabi AM (2018) A numerical study on land subsidence due to extensive overexploitation of groundwater in Aliabad plain, Qom-Iran. *Nat Hazards* 93(2):1085–1103
19. Mahdian M (2005) Investigating the situation of land degradation in Iran. In: National conference on erosion and sediment
20. Stocking MA, Murnaghan N (2013) *A handbook for the field assessment of land degradation*. Routledge
21. Zehtabian GR et al. (2005) The approach of desertification mapping using MEDALUS methodology in Iran
22. Moghim FM et al (2013) Evaluation of land use and suitability for rainfed crops in Roin, North Khorasan. *Agroecology* 5(2):143–152
23. Pirsahab M et al (2020) Occurrence of residual organophosphorus pesticides in soil of some Asian countries, Australia and Nigeria. *MS&E* 737(1):012175
24. Pirsahab M et al (2016) Evaluation of heavy metals (chromium, nickel and lead) in topsoil of the residential and industrial area of Kermanshah, Iran. *IIOAB J* 7(2):410–415
25. Pirsahab M et al (2017) A systematic review on organochlorine and organophosphorus pesticides content in water resources. *Toxin Rev* 36(3):210–221
26. Sadeghi A, Galalizadeh S, Zehtabian G, Khosravi H (2021) Assessing the change of groundwater quality compared with land-use change and precipitation rate (Zrebar Lake's Basin). *Appl Water Sci* 11(11):170. <https://doi.org/10.1007/s13201-021-01508-z>
27. Mitri G et al (2014) Evaluating exposure to land degradation in association with repetitive armed conflicts in North Lebanon using multi-temporal satellite data. *Environ Monit Assess* 186(11):7655–7672
28. Karimi A, Moghani N, Mohammadi J, Naderi M (2018) Investigation of some soil physical quality properties in different land uses In Bardeh catchment, Shahrekord (Chaharmahal and Bakhtiari province). *J Water Soil Conserv* 25(5):249–263
29. Borrelli P et al (2017) An assessment of the global impact of 21st century land use change on soil erosion. *Nat Commun* 8(1):1–13
30. Uddin M, Chow C, Su S (2018) Classification methods to detect sleep apnea in adults based on respiratory and oximetry signals: a systematic review. *Physiol Measure* 39(3): 03TR01
31. Weldu Woldemariam G, Edo Harka A (2020) Effect of land use and land cover change on soil erosion in erer sub-basin, Northeast Wabi Shebelle Basin, Ethiopia. *Land* 9(4):111
32. Karimi H, Amiri S, Huang J, Karimi A (2019) Integrating GIS and multi-criteria decision analysis for landfill site selection case study: Javanrood County in Iran. *Int J Environ Sci Technol* 16(11):7305–7318. <https://doi.org/10.1007/s13762-018-2151-7>
33. Sadeghi A, Shirzadi S, Galalizadeh S, Malekmohammadi B, Karimi H (2020) Environmental risk assessment and mapping of oil installations to Chamshir Dam water basin using GIS and HAZOP method. *Int J Risk Assess Manag* 23(3/4):207–10037183. <https://doi.org/10.1504/IJRAM.2020.10037183>
34. Karimi H, Jafarnejhad J, Khaledi J, Ahmadi P (2018) Monitoring and prediction of land use/land cover changes using CA-Markov model: a case study of Ravansar County in Iran. *Ara J Geosci* 11(19):592. <https://doi.org/10.1007/s12517-018-3940-5>
35. Wu W, Zucca C, Muhaimed AS, Al-Shafie WM, Fadhil Al-Quraishi AM, Nangia V, Zhu M, Liu G (2018) Soil salinity prediction and mapping by machine learning regression in Central Mesopotamia Iraq. *Land Degrad Dev* 29(11):4005–4014 <https://doi.org/10.1002/ldr.3148>
36. Fadhil AM (2011) Drought mapping using Geoinformation technology for some sites in the Iraqi Kurdistan region. *Int J Digital Earth* 4(3):239–257. <https://doi.org/10.1080/17538947.2010.489971>

Cadmium Fractionation Technique as a Chemical Degradation Indicator for Some Soils Near Diyala River in Iraqi Center



Hazim Aziz Al-Robai and Salman Khalaf Essa

Abstract Soil degradation can occur due to physical or chemical processes that are promoted by natural phenomena or prompted by humans. This study aimed to investigate the pollution with cadmium as a chemical degradation indicator for some soils irrigated by Diyala River in the Iraqi center. Six Profiles were selected, four of them are located near the Diyala River and two are located near the Tigris River, starting from Baqubah city to AL-Boiatha area in Baghdad city. Cadmium chemical phases (soluble, exchangeable, bound to carbonates, oxides, organic matter, and residue) were determined, using single and sequential extractions procedure (Tessier's method) to demonstrate the bindings of cadmium ions with various soil components, plus determinate the dangerous degree of cadmium element. The results clearly showed the superiority of some soil components in the retention of cadmium, despite their low content in these soils. It was clear with oxides that holding the most significant amount of cadmium (34.89%) followed by organic matter (27.36%), while carbonates had 18.17%. Finally, the residue fraction was retained cadmium around 14.40%. The results also showed that the content of extractable cadmium ions was very low in the soluble phase ($0.001\text{--}0.003\ \mu\text{g mL}^{-1}$), to ensure the rareness of ions in all Profiles. The concentration of exchangeable cadmium was rather low compared with other forms of the element to making 4.99% of the total ion content. The vertical distribution of cadmium was not very clear but generally decreased with a depth. Sometimes it follows the total content of the component that binding with it or shows random distribution with a depth.

Keywords Degradation · Cadmium · Diyala River · Tessier · Distribution

H. A. Al-Robai (✉)

Department of Soil and Water Resources, College of Agriculture, Al-Qasim Green University, Babil, Iraq

e-mail: dr.hazim@environ.uoqasim.edu.iq

S. K. Essa

Department of Soil and Water Resources, College of Agricultural Engineering Sciences, University of Baghdad, Baghdad, Iraq

e-mail: salman.essa.52@gmail.com

1 Introduction

Soil is not just the material on which soil life forms live yet, in addition to assumes critical functions in the material cycles and the exchange of energy in biological systems. Industrialization and urbanization have transformed soil contamination into severe ecological challenges which can not be dismissed [1].

Soil degradation can occur due to physical or chemical processes that are generated by natural phenomena or prompted by humans. Processes such as salinization, depletion of nutrients by draining, or accumulation of pollutants are all factors that can be regarded as agents and indicators of chemical soil degradation [2]. Soils are viewed as the significant sinks for poisonous metals inter into the biological systems by the previously mentioned human exercises and, not at all like, pollutants oxidized by microbial activity to carbon (IV) oxide. Heavy elements create mostly from basic igneous rocks, in which element content is higher than other rocks such as sandstones, granites, and siltstones [3, 4]. Throughout the world, there are 5 million sites of soil contaminated by heavy metals/metalloids with current concentrations above the regulatory levels [5].

Physio-chemical processes such as leaching and oxidation can start the availability of heavy elements accumulated in the soil environment, permitting the elements to reach water bodies and be uptake by plants and finally affect public health through water supply and the food chain [6]. Heavy elements released from numerous natural and human sources into the water environment, like agricultural or residential wastewater, chemical and inorganic fertilizer products, sewage leaching, transport and port operation, atmospheric deposits, and physio-chemical weathering of the Earth's crust [7].

Essential heavy elements are needed for organisms and can be essential in very small concentrations in the body. In living organisms, non-essential heavy elements have no known biological function. Examples of essential heavy elements are Fe, Cu, Mn, and Zn while Pb, Cd, and Hg are poisonous and are considered as biologically unnecessary [8–11]. Heavy elements are among the contaminants of the ecosystems that have been investigated widely. Based on the dose and duration of exposure, almost any heavy element and metalloid may be poisonous to living organisms. Numerous elements are listed in the heavy elements group but some are related to the environmental media. List of the environmentally related most dangerous heavy elements and metalloids involves Cr, Cd, Ni, Cu, Hg, Zn, Pb, and As [12].

There is some argument about suitably what a “heavy metal” is and what elements should be properly classified as such. Some authors established the definition depending on atomic weight, while others point to those elements with a specific gravity of more than 4.0 or more than 5.0. The term ‘heavy metal’ was most recently used as a common term for those metals and semimetals with possible poisonous to the environment [13, 14]. Because of its non-biodegradable nature, heavy metals (elements) are very harmful.

Organic matter of soil, which has a key function in the controlling mobility of elements, consists primarily of humic material-humic and fulvic acids. The heavy

elements in the soil cannot be breakdown as organic pollutants, but can only be moved from one location (polluted location) to another, e.g. landfill, which is a very costly operation, however. Different techniques have therefore been established to decrease the hazards and pollution associated with heavy elements in soils and to mitigate possible effects on plants, animals, and quality of water and consequently on the health of humans. Soil stabilization techniques, which are dependent on the use of appropriate immobilizing compounds, can impede the increase of pollutants in the soil.

The key mechanisms responsible for reducing element mobility, leachability, and bioavailability were the adsorption of pollutants on mineral surfaces, the creation of stable complexes with organic ligands, surface precipitation, and ion exchange [15]. Industrial and sewage wastewater are continuously discarded in open drains whose water is utilized for irrigation [16, 17]. Such wastewaters contain a lot of heavy metals elements such as cadmium (Cd), manganese (Mn), iron (Fe), lead (Pb), zinc (Zn), chromium (Cr), copper (Cu), cobalt (Co), and nickel (Ni), together with organic matter and nutrients. Crops irrigated by wastewaters store and uptake these heavy metals through different parts. These heavy elements cause severe health impacts when consumed through the food chain [16, 18].

Cadmium (Cd) is an unnecessary factor for living organisms with a high poisonous danger that tends to form stable dissolved complexes with inorganic and organic ligands, which inhibits its sorption and precipitation [19]. It is one of the pollutants that influence mainstream researchers, as it is freely absorbed by plant roots and accumulates concentrations in the shoots that could harmfully influence the food chain [20, 21]. Indeed, chronic exposure to Cd causes numerous health effects and illnesses such as lung cancer, complications with prostate, kidney failure, and osteoporosis. Even the intake of essential biologically significant elements may threaten human health.

Generally, when ions are entered into cells, they are influenced by the potential for oxidation and reduction reactions (redox) which can upset the intracellular reaction in living cells [22]. The current research was carried out to investigate pollution with cadmium as a chemical degradation indicator for some soils irrigated by the Diyala River (southern part) in the Iraqi center.

2 Materials and Methods

2.1 Study Area

Six Profiles were selected, four of them are located near the Diyala River and two are located near the Tigris River, starting from Baqubah city to the AL-Boiatha area in Baghdad city.

Profile 1: North of Baqubah city.

Profile 2: Kargholia.

Profile 3: Rustomia.

Profile 4: Sumadia.

Profile 5: AL-Jadiria (before joining point of the Diyala River with Tigris).

Profile 6: AL-Boiatha (after joining point of the Diyala River with Tigris).

2.2 Samples Preparation and Analysis

Soil samples in duplicate were randomly collected from the Profiles. After removing the stones, pebbles, samples were mixed and a part was taken into pre-cleaned plastic bags. Then, the labeled samples were transported to the central laboratories of the college of agricultural engineering sciences, university of Baghdad. Soil samples were dried at laboratory temperature (25 °C) and then powdered by using mortar and pestle to pass through a 2 mm sifter and stored in polyethylene bottles until further physio-chemical analysis.

2.3 Physio-chemical Properties of Soils

Particle-size analysis (soil texture) was made using the hydrometer method [23]. Electrical conductivity (EC) and pH were measured according to Richards [24]. Organic matter (OM) was determined by a wet oxidation method [25]. Carbonates were estimated by the gravimetric method [24]. Total oxides were determined according to Mehra and Jackson [26]. Cation exchange capacity (CEC) was estimated as described by Savant [27].

2.4 Extraction of Cadmium

Tessier's method [28] was used for the extraction of cadmium ions from soils, available phase, and that bound with carbonates, oxides, organic matter, and residue fraction, with a simple modification in the extraction of soluble element ions separately because it's reduced concentrations that are difficult to detect by atomic absorption spectrophotometer.

2.4.1 Single Extraction of Soluble Cadmium

The single extraction method was adopted after Ma and Rao [29]: 10 g soil sample was used with 10 ml of distilled water in a shaker for 2 h and centrifuged. Then, the supernatants were carefully transferred to plastic bottles and analyzed for element concentrations.

2.4.2 Sequential Extraction

The sequential extraction of cadmium ions was carried out as per Tessier's method. 1 g soil was used in the following order:

Fraction 1: Available (soluble and exchangeable): Soils samples were used at 25 °C for 1 h with 8 mL of 1 M NaOAc solution at pH 8.2 with constant shaking.

Fraction 2: Bound to carbonates: The remaining from fraction 1 was used at 25 °C with 8 ml of 1 M NaOAc adjusted to pH 5.0 with HOAc. Constant shaking was kept up and the time required for complete extraction was assessed.

Fraction 3: Bound to oxides. The remaining from fraction 2 was used with 20 ml of 0.04 M hydroxylamine hydrochloride in acetic acid (25% v/v). The latter experiments were performed at 96 ± 3 °C with occasional agitation and the time required to complete the dissolution oxides was evaluated.

Fraction 4: Bound to organic matter (oxidizable): To the remaining from fraction 3 were added 3 ml of 0.02 M HNO₃ and 5 ml of 30% H₂O₂ adjusted to pH₂ with nitric acid, and the mixture was heated to 85 °C for 2 h with constant shaking. A second 3 ml aliquot of 30% H₂O₂ (pH 2 with HNO₃) was then added and the samples were heated again to 85 ± 2 °C for 3 h with intermittent agitation. After cooling, 5 mL of 3.2 M NH₄OAc in 20% (v/v) HNO₃ was added and the samples were diluted to 20 ml and constantly agitated for 30 min.

Fraction 5: Residual: The remaining from fraction 4 was digested according to a wet digestion method [30].

Polypropylene, 50 ml tubes were used to minimize losses of solid material. Centrifugation at 6000 rpm for 20 min was done for separation after each extraction and supernatant was taken by pipette for analysis by Flame Atomic Absorption Spectrophotometer (FAAS). All used glassware for the tests was previously soaked in 14% HNO₃ (v/v) and rinsed with deionized water.

3 Results and Discussion

3.1 *Physio-chemical Properties of Soils*

The measured parameters of collected soil samples from Profiles are listed in Table 1. The pH values varied from 7.0 to 7.5, indicating the natural and slightly alkalinity of the studied soils. Soils content of carbonates, oxides and organic matter are ranged from 245 to 380, 3.4–6.3, and 1.6–22.0 g kg⁻¹ respectively, indicating the calcareous nature and poor oxides and organic content of soils due to the aridity and the carbonate rocks.

Table 1 Properties of soils

Horizon	Dept. cm	pH	EC dS m ⁻¹	Carb.	Oxid.	OM	CEC Cmol _c kg ⁻¹	Texture
				g kg ⁻¹				
<i>Profile 1</i>								
A _p	0–25	7.0	3.88	340	4.6	20.1	10.70	Silty clay
C ₁	25–50	7.0	13.60	330	4.5	16.7	14.17	Silty clay
C ₂	50–75	7.5	2.40	260	4.7	15.0	6.42	Clayey loam
<i>Profile 2</i>								
A _p	0–22	7.2	2.80	300	4.5	19.5	4.49	Clayey loam
C ₁	22–45	7.2	5.61	370	6.0	20.2	9.63	Silty clay loam
C ₂	45–70	7.1	5.67	320	4.4	16.7	9.90	Silty loam
<i>Profile 3</i>								
A _p	0–20	7.5	1.09	370	3.8	16.0	9.90	Clayey loam
C ₁	20–50	7.3	2.28	370	4.6	13.0	7.22	Clayey loam
C ₂	50–80	7.0	2.05	350	3.4	11.0	5.32	Clayey loam
<i>Profile 4</i>								
A _p	0–20	7.4	1.21	350	5.4	22.0	9.90	Silty clay loam
C ₁	20–42	7.4	1.12	330	5.2	19.0	8.02	Clayey loam
C ₂	42–65	7.3	1.41	320	5.5	18.0	11.77	Silty clay
C ₃	65–85	7.5	1.57	340	5.4	21.0	8.56	Silty clay loam
<i>Profile 5</i>								
A _p	0–25	7.3	0.74	285	6.2	18.0	10.70	Clayey loam
C ₁	25–45	7.2	1.50	266	5.0	19.0	12.84	Silty clay loam
C ₂	45–63	7.2	1.08	339	4.3	18.0	8.56	Silty clay loam
C ₃	63–85	7.4	0.88	284	4.4	6.7	5.35	Loam
<i>Profile 6</i>								
A _p	0–25	7.0	0.98	245	5.0	1.6	3.74	Loam
C ₁	25–45	7.5	0.35	380	6.3	19.0	11.23	Silty clay
C ₂	45–75	7.3	0.86	292	5.9	18.0	11.77	Silty clay
C ₃	75–100	7.3	0.26	282	5.2	19.0	12.30	Silt clay

3.2 Available Phase-Soluble and Exchangeable

Tables 2 and 3 showed that cadmium ions concentrations in the soluble and exchangeable phases were in the range of ND to 0.03 $\mu\text{g ml}^{-1}$ and 0.09–0.42 $\mu\text{g g}^{-1}$, respectively. Exception for the soluble cadmium, the element levels in the exchangeable phase are restively low and represent 4.99% of the total cadmium content. The results were compatible with Ma and Rao [29], who did not record any values for dissolved cadmium although some soils contain high levels of total cadmium.

Table 2 Cadmium concentrations bound to soil components

Horizon	Dept. cm	Sol. $\mu\text{g ml}^{-1}$	Exch.	Carb.	Oxid.	OM	Resid.	Total
			$\mu\text{g g}^{-1}$					
<i>Profile 1</i>								
A _p	0–25	ND	0.28	0.56	0.60	1.15	0.60	3.19
C ₁	25–50	ND	0.16	0.44	0.40	1.02	0.50	2.52
C ₂	50–75	ND	0.09	0.08	0.35	0.74	0.07	1.33
<i>Profile 2</i>								
A _p	0–22	0.001	0.35	1.40	1.92	1.90	1.20	6.77
C ₁	22–45	ND	0.42	1.50	3.22	1.66	1.10	7.90
C ₂	45–70	ND	0.21	1.19	2.76	1.65	1.00	6.81
<i>Profile 3</i>								
A _p	0–20	0.003	0.35	1.40	3.38	1.71	1.10	7.94
C ₁	20–50	0.001	0.42	1.40	2.99	1.52	0.90	7.23
C ₂	50–80	0.001	0.35	1.12	1.84	2.09	0.90	6.30
<i>Profile 4</i>								
A _p	0–20	0.003	0.35	1.05	3.22	2.09	1.30	8.01
C ₁	20–42	0.002	0.21	1.33	2.30	2.09	1.10	7.03
C ₂	42–65	0.002	0.28	0.91	2.66	2.28	1.20	7.33
C ₃	65–85	0.001	0.28	1.12	3.22	1.90	0.80	7.32
<i>Profile 5</i>								
A _p	0–25	0.001	0.25	1.00	1.81	1.56	0.70	5.32
C ₁	25–45	ND	0.20	1.10	2.17	1.65	1.00	6.12
C ₂	45–63	ND	0.19	1.00	1.80	1.00	0.80	4.79
C ₃	63–85	ND	0.10	0.90	1.40	0.88	0.50	3.78
<i>Profile 6</i>								
A _p	0–25	ND	0.35	1.00	1.40	0.88	0.60	4.23
C ₁	25–45	ND	0.35	1.40	2.99	1.37	0.90	7.01
C ₂	45–75	ND	0.38	1.30	2.30	1.23	0.80	6.01
C ₃	75–100	ND	0.28	1.20	2.05	1.07	0.70	5.30

When comparing the exchangeable cadmium ions values recorded in the present study with the values in previous studies for different regions of Iraq, they were closed to the values of cadmium extracted by the DTPA solution by Kareem [31], when he examined the soil of the Al-raid project. As well as the results compatible with the results of Sillanpaa and Jansson [32], when they extracted cadmium by EDTA solution from 150 soil samples for different regions of Iraq.

The data of Tables 1 and 2 showed that the distribution of exchangeable cadmium concentrations followed the distribution of the total carbonates content in Profiles 1, 2, and 3. These results were compatible with Sillanpaa and Jansson [32], who

Table 3 Percentage (%) of cadmium concentrations bound to soil components

H	Cd _{EX} /Cd _T	Cd _{Carb} / Cd _T	Cd _{Oxid} / Cd _T	Cd _{OM} / Cd _T	Cd _{Resid} /Cd _T
<i>Profile 1</i>					
A _p	8.70	17.50	18.80	36.05	18.80
C ₁	6.30	17.40	15.80	40.40	19.84
C ₂	6.70	6.00	26.30	55.60	5.20
<i>Profile 2</i>					
A _p	5.10	20.60	28.30	28.00	17.70
C ₁	5.30	18.90	40.70	21.00	13.90
C ₂	3.00	17.40	40.50	24.20	14.60
<i>Profile 3</i>					
A _p	4.40	17.60	42.50	21.50	13.80
C ₁	5.78	19.30	41.30	21.00	12.40
C ₂	5.50	17.70	29.20	33.10	14.20
<i>Profile 4</i>					
A _p	4.30	13.10	40.10	26.00	16.20
C ₁	2.90	18.90	32.70	29.70	15.60
C ₂	3.80	12.40	36.20	31.10	16.30
C ₃	3.80	15.30	43.90	25.90	10.90
<i>Profile 5</i>					
A _p	4.70	18.80	34.00	29.30	13.15
C ₁	3.20	17.97	35.40	26.96	16.30
C ₂	3.90	20.80	37.50	20.80	16.70
C ₃	2.64	23.80	37.00	23.20	13.20
<i>Profile 6</i>					
A _p	8.27	23.60	33.00	20.80	14.20
C ₁	5.00	20.00	42.00	19.50	12.80
C ₂	6.32	21.60	38.20	20.40	13.30
C ₃	5.30	22.60	38.70	20.20	13.20
R	4.99	18.17	34.89	27.36	14.40

noticed that the amount of exchangeable cadmium was directly proportional to the carbonates content in soils. While this distribution differed with the distribution of the total carbonates content in Profiles 4–6. These may be due to the effects of the form of the carbonate minerals that exist in the soils [33].

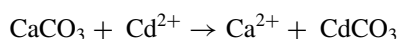
The distribution of cadmium values also differed with the CEC values distribution on unexpected results, because the fact that the values of cation exchange capacity (CEC) can not give a clear prediction of the trace elements adsorption in neutral soils, or the fact that the ion exchange process is not always dominant in the adsorption

process because the additional processes such as precipitation, complexation, and specific adsorption [34, 35].

3.3 *Bound to Carbonates*

Cadmium ions concentrations in the range of 0.08–1.50 $\mu\text{g g}^{-1}$ bound to carbonates of studied soils were partially high compared with concentrations of the element in the previously available phase, representing 18.17% of the total cadmium content (Tables 2 and 3). The present study assumes that cadmium ions might be bound with HCO_3^- ions in an aqueous phase, producing complexes in form of cadmium of bicarbonates CdHCO_3^+ which have a very significant binding coefficient [36]. Alternatively, these ions can be bind with carbonates surface through a sorption reaction.

McBride [33], explained that the affinity of the cadmium ions to the carbonates surfaces is probably due to the large convergence of radius of these ions (0.97 angstroms) with the calcium ions radius (0.99 angstroms), and because of that the cadmium ions replace the calcium ions on the carbonates surfaces according to the following equation



Obviously that the essential issue of the existence of ions in the soil environment and its effects is an available phase determination that represents the weakest phase which is bound to colloidal surfaces [37], and the most hazardous, due to the ease of entering the food chain [38]. Therefore, the assumed phase of the cadmium ions which are bound to carbonates minerals in the present study had a strong affinity for binding the polluted ions (relatively) in the form of carbonate or bicarbonate cadmium complexes.

3.4 *Bound to Oxides*

The data in Table 1 showed that the values of total oxides ranged from 3.4 to 6.3 g Kg^{-1} . These values are low in all soils possibly due to the formative nature and large quantities of salts especially carbonate [39]. The study outcome also referred to distributed nature of these oxides did not take a specific pattern in Profiles for all soils. The results of this fraction agreed with those of Bazini [40], when he studied the distribution of oxides for the sedimentary plain, indicating that the distributed nature of these oxides was not subjected to a particular system within the horizons of the Profiles.

Table 2 showed that the concentrations of cadmium ions that are bound to oxides are higher than those that are bound to other soil components, ranging from 0.35 to

3.38 $\mu\text{g g}^{-1}$ and account for 34.89% of the total element content (Table 3). The high concentrations of cadmium ions that bound with oxides component despite the fact the oxides had a low percentage compared with clay may be attributed to the high specific surface area (especially non-crystalline).

Garcia-Miragaya and Page [41] reported that the non-crystalline iron oxides have a high affinity for cadmium sorption compared with clay due to their high surface area. The high affinity of these oxides to capture large amounts of cadmium ions was confirmed by Tessier et al. [28], who described these components as good scavengers for trace elements, which reflected on the ecological role of the oxides to adsorb a large content of cadmium ions in the soil with a pH above 7 [42].

3.5 Bound to Organic Matter

The results showed the content of organic matter varied from 1.6 to 22.0 g Kg^{-1} (Table 1), noting the distribution of organic matter did not take a uniform pattern in all studying Profiles because of the variation in the effect of the sediments of Diyala and Tigris Rivers in conjunction with the impact of surrounding environmental conditions. It can be noted that the soil content of organic matter is low compared with the other components. However, the role of this component can not be neglected, and this is evident through its clear superiority in the adsorption of cadmium ions. The concentration of cadmium ions bound to organic matter ranged from 0.74 to 2.28 $\mu\text{g g}^{-1}$, and accounted for 27.36% of the total content of the element (Tables 2 and 3).

The high effectiveness of organic matter for attracting cadmium ions may be attributed to the great attraction and preference of this component for cations, particularly M^{2+} [35, 43] because of its high cation exchange capacity (300 Meq/100 g organic matter) [44]. To explain the relationship between the soil amount of organic matter and the amounts of adsorbed cadmium ions, the distribution of these ions showed accordance with organic matter content in Profiles 1 and 5 due to the great attraction between organic matter and cadmium ions. While the distribution of these ions was not appearing to correspond to the content of the organic matter in Profiles 2, 3, 4, and 6 due to the differences in the impact of surrounding conditions on organic matter or as a result of the presence of a relationship between organic colloids and precipitation of minerals [44, 45], which can be interpreted according to two expectations. Firstly, the high proportion of montmorillonite in soils can decrease the decay of organic matter [46], which affects adversely the provision of new charged organic surfaces. Secondly, the creation of interferences between organic matter and clays and oxides colloids can create the closure of available exchangeable sites on colloidal surfaces that lead to the difference in CEC values for those colloids.

3.6 *Bound to Residue*

The results of Table 2 showed that the concentrations of cadmium ions bound to the residue fraction (clay, silt, and sand) especially clay component especially clay, which is the important component that controls physio-chemical reactions in the soil [44, 47, 48] are low compared to the element ions bound to other soil constituents (carbonates, oxides, and organic matter). The concentrations of these ions bound to this fraction ranged from 0.07 to 1.3 $\mu\text{g g}$ and constituted a percentage of 14.40% of the total content of the element (Tables 2 and 3).

The decrease in the amount of cadmium ions associated with the residue fraction may be due to the intense competition that cadmium faced by calcium ions available in the soil solution to occupy the exchangeable sites. McBride [33] explained that the competition process between calcium ion and cadmium to occupy exchangeable sites is controlled by both radiuses of the ions and their concentration within the soil solution. However, the nature of the calcareous soil makes the concentration of calcium ions more than cadmium ions in the soil solution and thus removes it from the surfaces of the exchangeable sites. The results presented above confirm the dominance of the ion concentration effect, which reduced the amount of cadmium ions, bound to clay surfaces and increased their movement in the soil [49].

3.7 *Total Concentration of Cadmium Ions*

The total concentration of cadmium ions, available and that bound with carbonates, oxides, organic matter, and residue represent total cadmium ions concentration in each horizon of Profiles. The results of Table 2 and Fig. 1 showed that total cadmium concentrations ranged from 1.33 to 8.01 $\mu\text{g g}^{-1}$, indicated a significant increase in their values in Profiles 2, 3, 4, and 6, possibly due to their proximity to pollution sources like wastewater, industrial, agricultural and rainwater in the areas of Al-Fadhiliyah, Rustomia, and Sumadia. In addition, the phenomenon of reverse flow of the waters of the Diyala River at unspecified periods of the year due to the rise in the water levels of the Tigris River increased the concentrations of these polluting ions. Sillanpaa and Jansson [32] also reported that the use of phosphate fertilizers can add high values of cadmium ions to Iraqi soils.

The data indicated that there are no clear variances between values of total cadmium ions recorded in Profiles 2, 3, and 4, which could be attributed to the common effect of the conditions prevailing on the physio-chemical behavior of cadmium ions at those Profiles. As for the values of total cadmium ions recorded in Profiles 1 and 5, the results refer to the presence of a significant decrease in their values in Profile 1, which may result from the location of this Profile away from the pollution sources mentioned above. While the results of Profile 5 were another, although this Profile is located far from the sources of pollution, its relatively high values suggest that it may be affected by other sources of pollution.

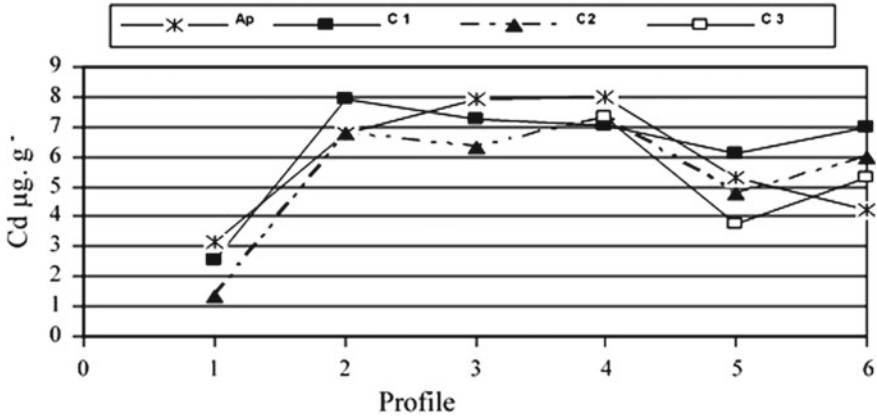


Fig. 1 Horizontal distribution of total cadmium in Profiles

3.8 *Physio-chemical Pathway of Cadmium Ions in Soil*

Table 2 and Figs. 2, 3, 4, 5, and 6 showed the concentrations of cadmium ions that bound to the main soil components followed the following order:

Oxides > Organic matter > Carbonates > Residue > Exchangeable > Soluble

To clarify the dynamics of cadmium ions binding with the soil components, this study suggested the next physio-chemical mobility for these ions:

At the point when the cadmium ions reach the soil body from different sources such as wind deposits and solid and liquid discharges, these ions become under the influences of varying compulsory forces between weak attraction powers and strong

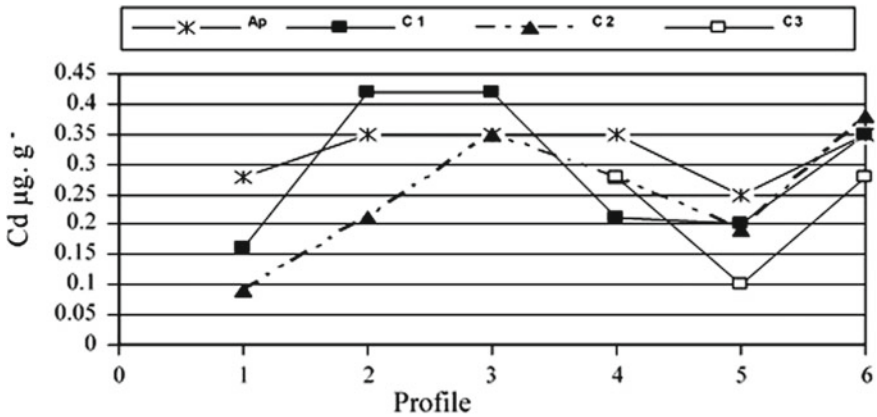


Fig. 2 Horizontal distribution of exchangeable cadmium in Profiles

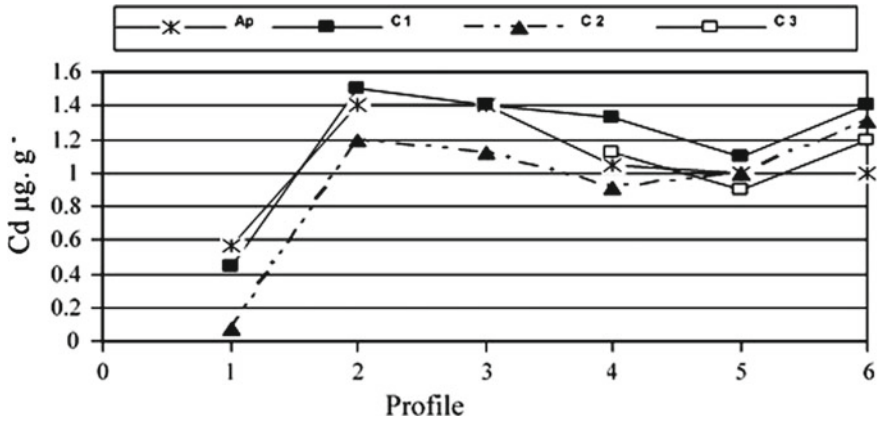


Fig. 3 Horizontal distribution of cadmium bound to carbonates in Profiles

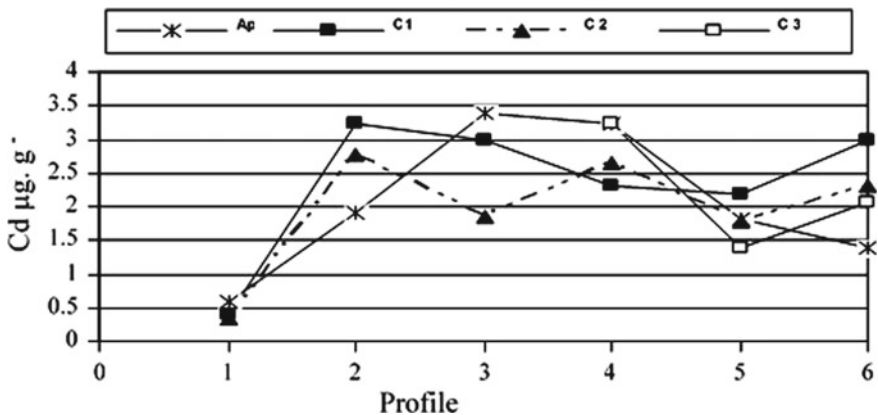


Fig. 4 Horizontal distribution of cadmium bound to oxides in Profiles

chemical bonds with the ions of the soil solution from one viewpoint, or with negative charges on the colloidal surfaces of carbonates, oxides, organic matter, and clay on other hand. These chemical bonds rely on numerous effects, concentration, ionic strength, equivalence, ion volume, substitution capacity, pH, and type and density of negative charges of colloidal surfaces.

Because the studied soils are calcareous, calcium and bicarbonates ions are definitely, available in high concentrations in the soil solution, which can control the chemical reactions that occur in the medium. Thus, the high-concentration of Ca^{2+} ions must compete with the cadmium ions found at colloidal surfaces, which are highest on the surfaces of clay minerals due to most of them have permanent charges compared with non-permanent charges that found on the surfaces of other soil components (oxides and organic matter). Hence, the negative charges on the clay surfaces

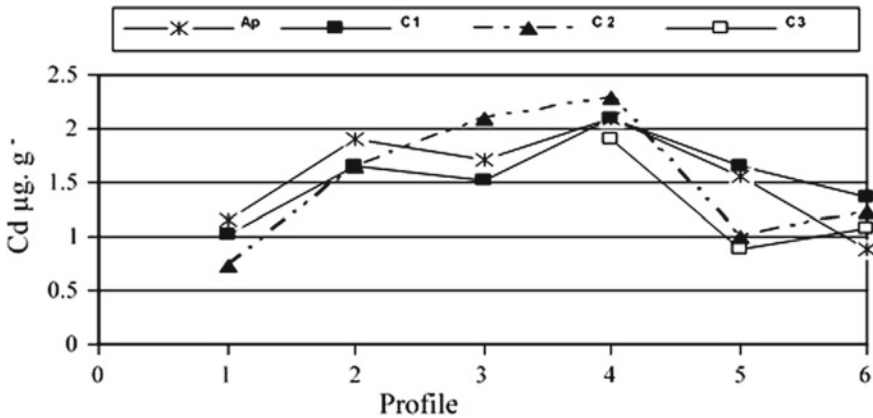


Fig. 5 Horizontal distribution of cadmium bound to OM in Profiles

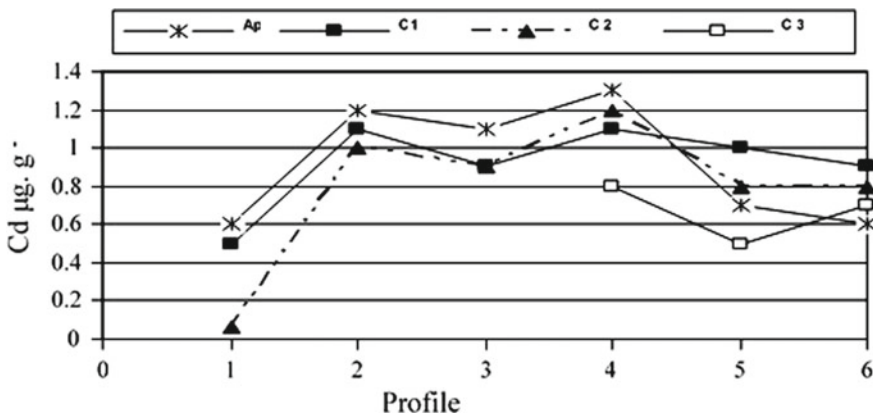


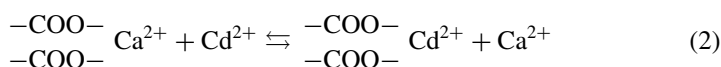
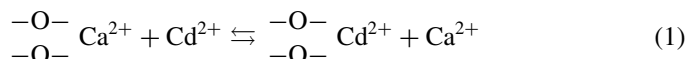
Fig. 6 Horizontal distribution of cadmium bound to residue in Profiles

are quicker and stronger than those on the surfaces of oxides and organic matter, so the reaction of calcium ions with clay surfaces is quicker in the first time of the process than their adsorption by surfaces of oxides and organic matter, may accelerate the mobility of cadmium ions through soil constituents [49].

This assumption is further improved by decreasing cadmium ions bound to the clay particles compared with other soil components. Tessier et al. [28] had shown that oxides and OM have a great ability to capture trace elements and act as scavengers. The above assumption can be seen in the results of Table 2 which confirm that oxides had the largest share in capturing cadmium ions compared to other soil components. The percentage of ions (Table 3) bound with oxides was 34.89%, ranking first in capturing cadmium ions due to their high surface area. Organic matter had an important and influential role similar to the role of oxides in capturing cadmium ions. The results

showed that ions bound by that component formed a percentage of 27.36% of the total element content, taking the second rank in the capture of cadmium ions after oxides.

Adsorption of cadmium ions by charged organic matter surfaces resulting from dissociation and ionization of carboxylic groups and functional phenols [35, 44, 50–53] arises at $\text{pH} < 6$ [54], which is the most pronounced at the neutral conditions of the $\text{pH} 7.0\text{--}7.5$ [55]. Although the mechanism for the bound of ions by the functional groups has not been clearly defined [52], the current study explains it based on the following two equations proposed by Abd-Elfattah and Wada [54].



In addition to the physical, chemical, and biological conditions of the natural environment, particularly the plant roots exuding, organic, inorganic proteins, and ions and their alteration of medium acidity [34, 56], the difference of concentrations of cadmium ions from one component to another depends primarily on the added amount of this pollutant to ecosystems [57]. It is clear that the physio-chemical pathway of cadmium ions is a result of physical, chemical, and biological influences on the ecosystems in which the element is present and which in turn affects its biogeochemical cycle in these systems, as shown in Fig. 7.

4 Conclusions

It can be concluded from the outcome of the present study, that all studied soils have been affected by various concentrations of polluted cadmium ions ranging from concentrations that did not exceed critical limits and concentrations that exceeded these limits as follow:

1. Soils near the pollutants discharge sites in Kargholia, Rustomia, and Sumadia (Profiles 3, 2, and 4) were affected by high concentrations of cadmium ions and exceeded the critical limits of cadmium ions in soils.
2. An increase in the concentrations of cadmium ions in the soil of AL-Jadiria (Profile 5) exceeding the critical limits, indicates that they can be affected by other pollution sources.
3. The soil of the AL-Boiatha Profile 6 was also clearly affected by the water of the Diyala River.
4. The recorded concentrations of cadmium ions, although somewhat low in the soil north Baquba city (Profile1), are a sign that the source of pollution of these ions is the used irrigation water.

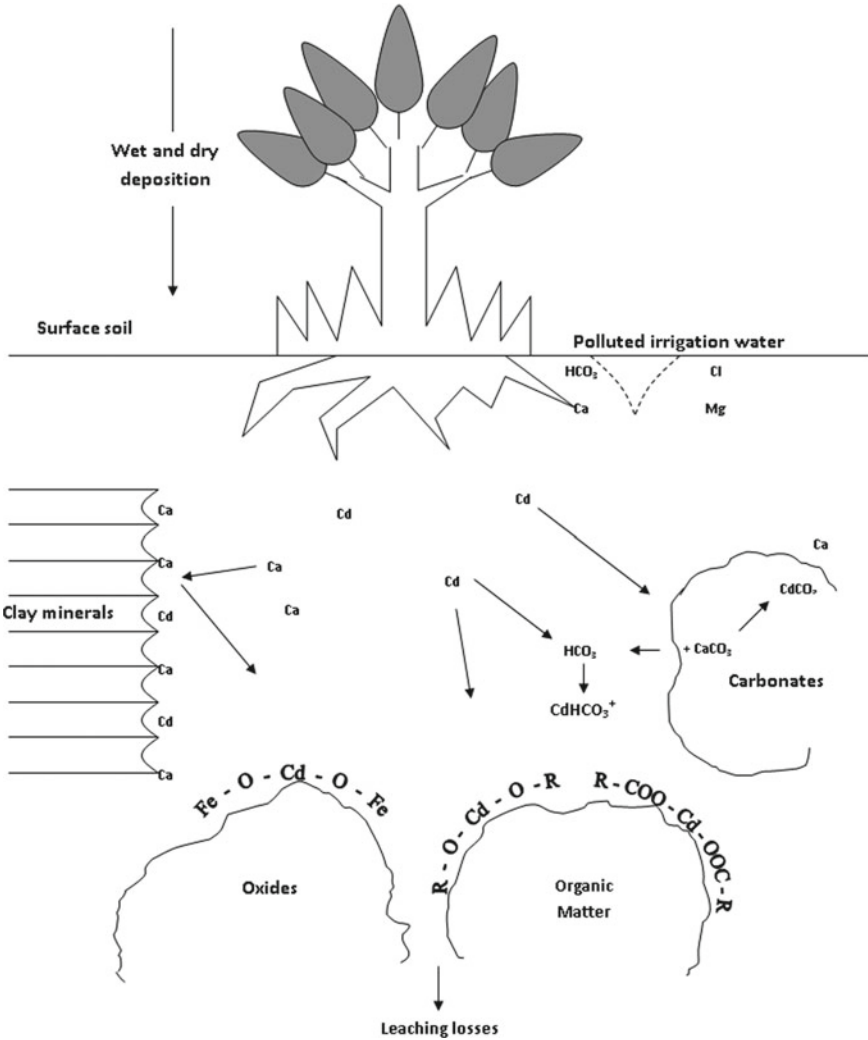


Fig. 7 The expected mechanisms of the association of cadmium ions with soil components [58]

5. The high percentage of cadmium ions has been concentrated in solid soil components, which means that these components are a potential source of pollution, which can be re-released from polluted ions when environmental conditions change.
6. The values of cadmium ions were distributed according to the following order.

Oxides > Organic matter > Carbonates > Residue
> Exchangeable > Soluble.

5 Recommendations

The current study recommends the followings:

1. Do not use the water of the Diyala River in its southern part for drinking purposes and use it carefully for irrigation purposes.
2. Using Tessier's method in the studies of environmental soils pollution with heavy elements because it gives a clear picture of heavy element mobility and its behavior from one component to another in the soils, and then know the degree of its binds to those components and thus assess the status of pollution.
3. Work together with environmental research centers to monitor the environmental impacts of irresponsible discharge of untreated wastewater into rivers.

References

1. Micó C, Recatalá L, Peris M, Sánchez J (2006) Assessing heavy metal sources in agricultural soils of an European Mediterranean area by multivariate analysis. *Chemosphere* 65:863–872
2. Mirsal Ibrahim A (2008) Soil pollution, origin, monitoring and remediation, 2nd edn. Springer, Berlin Heidelberg
3. Tiller KG (1989) Heavy metals in soil and their environmental significance. *Adv Soil Sci* 9:113–142
4. Fadigas FS, Sobrinho NMBA, Anjos LHCD, Mazur N (2006) Estimation of reference values for cadmium, cobalt, chromium, copper, nickel, lead, and zinc in Brazilian soils. *Commun Soil Sci Plant Anal* 37:945–959
5. Li C, Zhou K, Qin W, Tian C, Qi M, Yan X (2019) A review on heavy metals contamination in soil: effects, sources, and remediation techniques. *Soil Sediment Contam Int J* 28(4):380–394
6. Hossain MB, Jahiruddin M, Panaullah GM, Loeppert RH, Islam MR, Duxbury JM (2008) Spatial variability of arsenic concentration in soils and plants, and its relationship with iron, manganese and phosphorus. *Environ Pollut* 156:739–744
7. Elhussien ME, Adwok BA (2018) Determination of Heavy metals in fish and water of White Nile during watery diarrhea outbreak from June to July, 2017, Gezira Aba-Sudan. *Sci J Anal Chem* 6(1):1–6
8. Ramírez R (2013) The gastropod *Osilinus atrata* as a bioindicator of Cd, Cu, Pb and Zn contamination in the coastal waters of the Canary Islands. 29(3):208–220
9. Jović M, Onjia A, Stanković S (2012) Toxic metal health risk by mussel consumption. *Environ Chem Lett* 10(1):69–77
10. Rahim M, Ullah I, Khan A, Haris MRHM (2016) Health risk from heavy metals via consumption of food crops in the vicinity of District Shangla. *J Chem Soc Pak* 38(1):177–185
11. Turkmen M, Turkmen A, Tepe Y, Tore Y, Ates A (2009) Determination of metals in fish species from Aegean and Mediterranean seas. *Food Chem* 113(1):233–237
12. Barakat MA (2011) New trends in removing heavy metals from industrial wastewater. *Arab J Chem* 4(4):361–377
13. Tchounwou PB, Yedjou CG, Patlolla AK (2012) Heavy metals toxicity and the environment. *Exp Suppl* 101:133–164
14. Saunders JE, Jastrzemski BG, Buckley JC (2013) Hearing loss and heavy metal toxicity in a Nicaraguan mining community: audiological results and case reports. *Audiol Neurotol* 18(2):101–113
15. Yadav LGR, Malik RS, Yadav S (2019) Depth wise distribution of heavy metals in different soil series of Northwestern India. *Int J Curr Microbiol App Sci* 8(2):2817–2826

16. Sharma A, Katnoria JK, Nagpal AK (2016) Heavy metals in vegetables: screening health risks involved in cultivation along wastewater drain and irrigating with wastewater. *Spring Plus* 5:488
17. Su C, Jiang LQ, Zhang WJ (2014) A review on heavy metal contamination in the soil worldwide: situation, impact and remediation techniques. *Environ Skept Crit* 3(2):24–38
18. Ugya AY, Imam TS (2017) Temporal heavy metals variation in vegetables sampled at kasuwan mata, kaduna metropolis, Nigeria. *Malaysian J Sci* 36(2):63–73
19. Kubier A, Wilkin RT, Pichler T (2019) Cadmium in soils and groundwater: a review. *Appl Geochem* 108:104388
20. Koleli N, Eker S, Cakmak I (2004) Effect of zinc supply on cadmium toxicity in durum and bread wheat grown in zinc-deficient soil. *Environ Pollut* 131:453–459
21. Santona L, Castaldi P, Melis P (2006) Evaluation of the interaction mechanisms between redmuds and heavy metals. *J Hazard Mater* 136:324–329
22. Wu W, Wu P, Yang F, Sun DL, Zhang DX, Zhou YK (2018) Assessment of heavy metal pollution and human health risks in urban soils around an electronics manufacturing facility. *Sci Total Environ* 630:53–61
23. Day PR (1965) Particle fractionation and particle—size analysis. In: Black AC, Evans DD, Ensminger LE, White JL, Clark FE (eds) *Methods of soil analysis. Part 1. American Society of Agronomy, Madison, Wisconsin, USA*, pp 545–566
24. Richards LA (1954) Diagnosis and improvement of saline alkali soils, agriculture, 160, handbook 60. US Department of Agriculture, Washington, DC
25. Black AC, Evans DD, Ensminger LE, White JL, Clark FE (eds) (1965) *Methods of soil analysis. Part 1. American Society of Agronomy, Madison, Wisconsin, USA*, pp 545–566
26. Mehra OP, Jackson ML (1960) Iron oxide removal from soils and clay by dithionite-citrate system, buffered with sodium bicarbonate. In: *Proceeding of 17th national conference on clay and clay minerals*, pp 317–327
27. Savant NK (1994) Simplified methylene blue method rapid determination of cation exchange capacity of mineral soils. *Commun Soil Sci Plant Anal* 25(19 and 20):3357–3364
28. Tessier A, Campbell PGC, Bisson M (1979) Sequential extraction procedure for the speciation of particulate trace metals. *Analyt Chem* 51:844–850
29. Ma LQ, Rao GN (1997) Chemical fractionation of cadmium, copper, Nickel, and Zinc in contaminated soils. *J Environ Qual* 26:259–264
30. Ure AM (1995) *Methods of analysis for heavy metals in soil*. In: Alloway BJ (ed) *Heavy metals in soil*, 2nd edn. Blackie Academic and Professional, London-C.F., pp 58–95
31. Kareem BM (1985) Effect of treated wastewater on the growth of maize and environmental pollution. Master thesis, College of Agriculture, University of Baghdad
32. Sillanpaa M, Jansson H (1992) Status of cadmium, lead, cobalt and plants of thirty countries. *FAO Soil Bulletin* 65
33. McBride MB (1980) Chemisorption of Cd on calcite surfaces. *Soil Sci Soc Am J* 44:26
34. Rieuwerts JS, Thornton I, Farago ME, Ashmore MR (1998) Factors influencing metal bioavailability in soils: preliminary investigation for the development of a critical loads approach for metals. *Chem Speciat Bioavailab* 10(2):61–75
35. Adriano DC, Bolan NS, Koo B-J, Naid R, Vander LD, Vangronsveld J, Wenzel W (2002) Natural remediation processes: bioavailability interaction in contamination soils. 17th WCSS, Thailand, paper no. 501
36. Hirsch D, Nir S, Banin A (1989) Prediction of cadmium complexation in solution and adsorption to montmorillonite. *Soil Sci Soc Am J* 53:716–721
37. Evans LJ (1989) Chemistry of metal retention by soils. *Environ Sci Technol* 23:1045–1056
38. Lahucky L, Vollmannava A, Kulich J, Tomas J (2001) Mobility of cadmium in various soil types/subtypes. *J Central Eur Agric* 2:235–240
39. AL-Mashhadani ASM (1994) Survey and classification of soils. Dar Al Kuttab for Printing and Publishing. University of Mosul, Iraq
40. Bazini DRA (1999) Nature and distribution of free oxides and their relation to soil development. MSc, College of Agriculture. Baghdad University

41. Garcia-Miragaya J, Page AL (1978) Sorption of trace quantities of Cd by soils with different chemical and mineralogical composition. *Water Air Soil Pollut* 9:289–299
42. Bolt KA, Evans LJ (1996) Cadmium adsorption capacity of selected Ontario soils. *Can J Soil Sci* 76:183–189
43. Bloom PR (1981) Metal—organic matter interactions in soil. In: Dowdy et al (ed) *Chemistry in the soil environment*. ASA Special Publication No 40, Soil Science Society of America, Madison, WI
44. Awad KM (1986) *Principles of soil chemistry*. Ministry of Higher Education and Scientific Research, University of Basrah
45. Watts RJ (1998) *Hazardous wastes: sources, pathways, receptors*. Wiley, NY
46. Alexander M (1961) *Introduction to soil microbiology*. Wiley, NY and London
47. AL-Naimi SNA (1999) *Fertilizers and soil fertility*. Dar Al-Kuttab for Printing and Publishing, University of Mosul, Iraq
48. Bolt GM, Bruggenwert MGM, Kamphorst A (1976) Adsorption of cations by soil. In: Bolt GH, Bruggenwert MGM (eds) *Form soil chemistry, a basic elements*
49. McLean JE, Bledsoe BE (1992) Behavior of metals in soils. EPA. *Ground Water Issue*, 540, S—92, 018
50. AL-Rawi AAH, Al-Zubaidi AH, Nazema Q (1986) *Soil chemistry*, Ministry of Higher Education and Scientific Research, Faculty of Agriculture. Baghdad University
51. Krishnan KA, Anirudhan TS (2003) Removal of cadmium (II) from aqueous solution by steam—activated sulphurised carbon prepared from sugar—cane bagasse pith: kinetics and equilibrium studies. *Water SA* 29:147–156
52. Kyziol J, Twardowska I (2003) Physico-chemical properties of Law-Moor peats VS their binding capacity for heavy metals. *Zezyt* 22:133–135
53. Pena-Mendez Eladia M, Havel J, Patoka J (2004) Humic substances-compounds of still unknown structure: application in agriculture, industry, Environment, and biomedicine. *J Appl Biomed* 3. ISSN 1214-0287
54. Abd-Elfattah A, Wada K (1981) Adsorption of lead, copper, zinc, cobalt, and cadmium by soils that differ in cation-exchange materials. *J Soil Sci* 32:271–283
55. Evans LJ, Sendy B, Lumsdon DG, Stanbury DA (2003) Cadmium adsorption by an organic soil: a comparison of some humic-metals complexation models. *Chem Speciat Bioavailab* 15(4):93–100
56. Collins RN, Merrington G, McLaughlin MJ, Jean-Louis M (2003) Organic ligand and pH effects on isotopically exchangeable cadmium in polluted soils. *Soil Sci Soc Am J* 67:112–121
57. Vrbek B, Ivan P, Dunja N (2002) Heavy metals in forest soils in the Mediterranean Karst of Croatia. 17th WCSS, Thailand, paper no. 1147
58. Hamza HA (2005) Pollution of some soils and water of Diyala River with cadmium. Master thesis, College of Agriculture, University of Baghdad

Land Degradation Due to MSW Dumping and Sanitary Landfilling: Iraq as a Case Study



Salah Farhan A. Sharif

Abstract Municipal Solid Waste (MSW) constitutes a major dilemma in all countries of the world because of the environmental and economic problems it requires and the complex and costly techniques needed to manage and dispose of it. In this chapter, one of the most important environmental impacts of waste was studied even after being treated with a sanitary landfill, which is the depletion of lands. Results showed that vast areas were depleted and their properties changed due to random landfills and sanitary landfills for domestic and industrial waste of all kinds. After presenting the types of waste, sanitary landfill methods and techniques used in calculating the depleted lands, it was noted that there is a close correlation between the depleted lands area and the population census. The study showed that the percentage of land that the sanitary landfills will cover to the total area of the city of Baghdad over the 15 years of preparing this study reaches 0.169%, while this percentage increases to 24% after 100 years due to the huge population growth of the province of Baghdad with the limited area of the province. And so for the rest of the provinces, where the percentage decreases when the area of the province is larger, as is evident in the provinces of Anbar, Muthanna and Najaf.

Keywords Land degradation · Municipal solid waste · Solid waste dumping · Sanitary land filling

1 Introduction

Solid waste is the useless and undesirable solid material that results from household, industrial, commercial and agricultural activities in a specific area. Solid waste can be classified according to its sources, such as domestic, industrial, commercial, construction, or agricultural. It can be, also, classified according to its contents of solid materials or the resulting harmful liquids or gases, such as organic materials, paper, plastic, glass, minerals. Another classification could be presented according

S. F. A. Sharif (✉)
College of Engineering Technology, Al-Kitab University, Kirkuk, Iraq
e-mail: salahfarhan@uoalkitab.edu.iq; dr.salahfarhan@gmail.com

© The Author(s), under exclusive license to Springer Nature Switzerland AG 2022
A. M. F. Al-Quraishi et al. (eds.), *Environmental Degradation in Asia*,
Earth and Environmental Sciences Library,
https://doi.org/10.1007/978-3-031-12112-8_13

257

to the possible risk of mismanagement of these wastes, such as being toxic, non-toxic, radioactive, flammable, or conducive to transmitting a pathological infection. Efficient management of solid waste can reduce or eliminate negative impacts on the environment and human health in addition to helping achieve economic and social life development. The municipality can manage waste based on efficient measures such as awareness, monitoring, reducing waste, efficient collection, proper transportation, proper treatment, recycling, and sanitary landfill.

The general arrangement for solid waste management acceptable to industrialized countries can be shown by Fig. 1 and summarized in the following order:

- Reducing waste
- Reuse of waste
- Recycling waste
- Recovering waste for use after converting it to other useful materials
- Fermentation of waste and turning it into fertilizers
- Burning waste to get rid of it or produce energy
- Ground burial or sanitary landfill.

Unfortunately, in Iraq, so as many other countries, there is not yet, good waste management. Most Iraqi cities still adopt indiscriminate landfills, sanitary landfills, and indiscriminate burning to dispose of all kinds of waste. It is worth noting that some individuals, in Iraq and most of developing countries, a manual isolation of materials that can be reused such as plastics, aluminum, wood, paper, and iron scrap.



Fig. 1 Waste management hierarchy shows the waste management measures order

Unfortunately, this is done manually and in very primitive ways, either during waste collection or when it is thrown into landfills. This method of waste disposal causes the exhaustion of vast areas of agricultural and vacant lands that can be turned into residential, industrial, or agricultural lands.

The main objectives of this study are to find out the rate of lands degradation due to open dumping and landfilling of solid waste in the short and long term, the social and environmental impacts, and the measures that could be taken to stop this tragedy and land rehabilitation on the long term.

2 Sanitary Landfill

2.1 Identifications

A landfill is simply defined as a final control measure of waste disposal on or inland and sometimes practiced as free or open dumping. Landfills could be categorized according to the waste source, such as sanitary landfills, industrial landfills and municipal solid waste landfills. It could be, also categorized according to the waste characteristics, such as liquid or solid waste landfill, hazardous or non-hazardous waste landfill, degradable or non-degradable waste landfill and toxic or nontoxic waste landfill [1].

A sanitary landfill is a type with the protected bottom where trash is buried in layers and compacted to make it more solid and less volume. There are several definitions of landfills in the publications, including what was mentioned by the American Society of Civil Engineers, that a sanitary landfill is a way to dispose of waste without causing damage or risks to public health or safety. This can be achieved, for example, by reducing the volume, and covering it with a layer of earth after each daily operation [2]. This leads to the truth that “a true sanitary landfill is not an open dump”.

The main purpose of a sanitary landfill is to ensure waste is safe by reducing the negative impacts caused by accumulated waste and decomposition. Toxic gases such as methane are produced from waste decomposition, which can be collected from sanitary landfills and transferred to energy instead of being released into the atmosphere such as in open dumping. Clay liner or plastic sheets are used to isolate the trash and resulting leachate from the underground water. Moreover, it involves well-designed engineering methods to protect the environment from contamination by solid or liquid wastes.

When land used as a sanitary landfill is full, a clay layer is used to cover it and then that area could be used for other purposes if that is confirmed that it is safe. In other words, sanitary landfill could be conserve of energy for future.

Solid waste simply used to be dumped in large stacks before 1935. These garbage stacks produce many air pollutants such as methane, which is dangerous because a build-up of methane could cause an unwanted nuisance and expected explosion.

Moreover, water pollution that leaches through waste could pollute groundwater. Systems of sanitary landfills were developed in Fresno—California, in 1935, and today more than 55% of international solid waste ends up in sanitary landfills [3]. However, the sanitary landfill system still causes severe environmental hazards.

2.2 Comparison Between Open Dumping and Sanitary Landfilling

An open dump can be defined as a pile of waste or garbage that has accumulated or is left at a collection site or a specific place where it is not supposed to be. Open dumps are illegal, and the person or group that causes the waste to be dumped in this way may be held accountable. Although such dumpsites directly and indirectly negatively impact health and the environment, many people still use this method because of the simple costs. These methods can pose many and very severe risks to health and the environment due to the intrusion of toxic substances into the air, water, and soil, Fig. 2. Typically, land sites prone to open dumps are roadsides, secluded areas, trenches, and often close to settlements. Because of this dumping, the site becomes attractive to mosquitoes, insects, disease-causing viruses, various harmful animals and emits foul odors. It also affects the quality of soil and groundwater, and in doing so, it will pose a major threat to public health [4].

Unhealthy landfills pose a great danger to health and the environment in the short and long term, which leads to the need for great attention to design healthy landfills according to accurate specifications subject to strict legislation and continuous monitoring to avoid emissions of any liquid or gaseous pollutants. Investigations of the long-term behavior of landfills show that it is necessary also to reduce the landfill's emission potential during the operation and post-operation phase and cap the landfill only when this goal has been reached [3].

The traditional sanitary landfills follow a scientific, well-planned, and monitored waste management process, while open dumps are piles of garbage accumulated in an undefined location.

Sanitary landfill can be considered a safer and more organized system or method for managing waste, which governments usually manage and supervise their implementation according to strict laws, regulations, and advanced treatment systems.

The traditional landfill system was first established in 1935, in Fresno, California. The land site is designed to absorb waste by burying layers of compacted waste and covering it with layers of soil. The system consists of a large hole in the ground, with a thick plastic liner over which a compact earth lining is placed. At the bottom of the pit, a thick liner is placed that helps prevent the leakage of liquid waste (which often oozes from solid waste, especially if rainwater floods the landfill) as it can contaminate water supplies and groundwater. This liquid waste that is collected is called leachate. Then the waste is added to the landfill in the form of organized layers

Fig. 2 Current status of landfilling and waste dumping in Iraqi areas



(layers of waste alternating with layers of soil). This is done to get rid of unpleasant odors and speed up the process of rotting or decomposition. When the dumpsite is completely covered, it is sealed with a layer of compressed clay. Moreover, methane gas produced from the decomposition of organic waste is often collected using a special system to collect and pump it for consumption in power generation. It is worth noting that if the methane collection system is not managed accurately and effectively, it could lead to an explosion and fire that may cause a rise in the release of greenhouse gases.

The following comparison between Sanitary Landfill and Open Dump helps to recognize between them:

- Sanitary Landfills Indicates the location of the land selected and designed for waste management. Whereas, random or open dumps indicate the location of a specific land in which piles of garbage accumulate, even though they are not designated for this purpose.
- A sanitary landfill is much bigger in area and volume than that of the random and open dump. This leads to a higher capacity of sanitary landfills.
- Sanitary Landfills are an organized way of disposal of waste and are regulated by the specified authority. Whereas, random or open dumps are an unorganized, improper, and illegal way of disposing of waste.
- Sanitary landfills have less danger to the health and environment, while random open dumps are very dangerous to the community health and environment.
- Sanitary landfills include tight control systems to avoid unpleasant odors, insects and other harmful animals, while open random landfills are an attractive environment such as rodents, flies, insects and all other harmful pests in addition to unpleasant and harmful odors.
- Sanitary landfilling includes gas and Leachate collection and treatment systems, protection liners, firefighting, and safety measures while all are not included in the random open dumping.
- Finally, the selection of sanitary landfill sites is subject to many specific factors according to special specifications and legislation, such as the distance between the landfill and residential areas and the nature of the geographical area. Whereas, random open dumps are located anywhere, even if it is close to residential areas, without considering any limitations or controls.

Although sanitary landfills are superior to open dumps, due to their many advantages, there are some disadvantages associated with sanitary landfills as well. Here are some of these disadvantages:

1. Building and maintaining a landfill requires a large amount of money and labor. Even so, it only protects public health if it is managed well and meticulously.
2. Failure to take the necessary control measures may lead to problems in the lining systems, which inevitably leads to the risk of groundwater contamination.
3. It has been observed that over time, landfills may generate toxic gases that are released into the environment and this may happen because some wastes do not rot especially inorganic wastes.

4. Sometimes, methane may be released even though the landfill is covered with clay soil and the land is reused by covering it with greenery. One indication that this is happening is circular spots of dead grass, and this could be very dangerous as explosions and fires could occur.
5. There may occasionally be collapses of the surface soil of old dumps, especially if they are used for urban purposes such as buildings and roads, causing huge material and human losses.
6. The most important drawback is that sanitary landfills and random piles of waste are one of the main causes of **land destruction and depletion**, especially in large cities and dense residential communities.

Although sanitary landfills also have their own drawbacks and alternatives are being contemplated, they are better than large piles of open garbage accumulations.

2.3 Types of Sanitary Landfills

There are three general types of Landfilling Systems: (A) Area System, (B) Trench System, and (C) Ramp, or Slope System [5];

- (a) The area system is best suited for flat or slightly sloped areas where some lower lands may exist as shown in Fig. 3. Waste is leveled with a thickness of 50–80 cm and then compacted appropriately and then covered with excavation materials for the same landfill or suitable soil is drawn from neighboring areas.
- (b) The trench system consists of a natural or excavated trench into which the solid wastes are spread, compacted and covered, as shown in Fig. 4. The trench system is more convenient for nearly level land where the water table is not near the surface (deep). Usually the soil excavated from the trench is used again as a covering material. High attention is paid for the under lining, clay or plastic, to protect underground water as shown in Fig. 4.

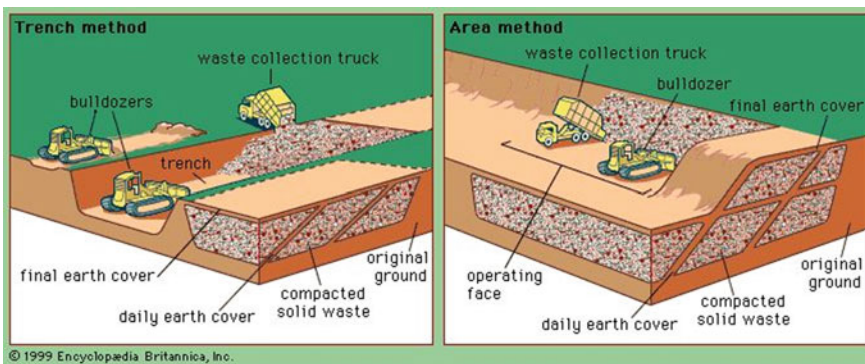


Fig. 3 Flat area and trench landfill types [6]

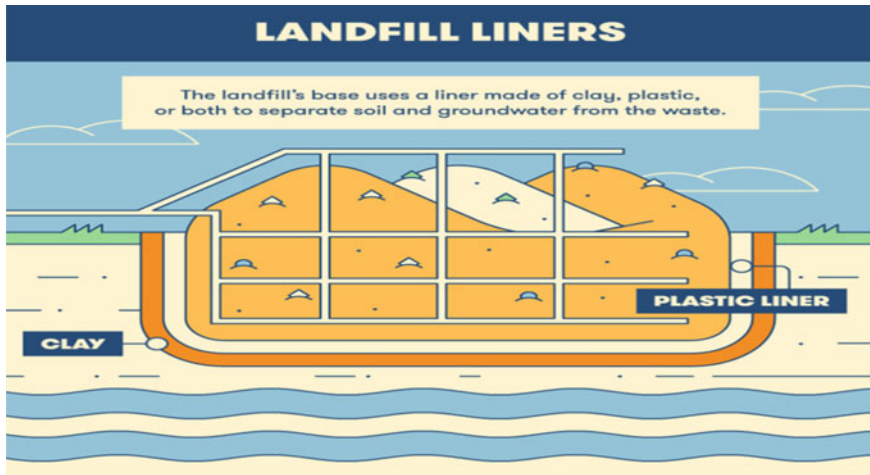


Fig. 4 Trench landfill lining [6]

- (c) In uneven areas that include slopes and low-level areas, waste is spread on the slope, compacted and covered with material usually brought from areas close to the work site. The difference of slopes from flat areas may be positive in the waste leaching systems, in addition to exploiting depressions without the need for excavation.

The landfill method can be adapted to suit many other circumstances, but there is usually one selected method for any specific land and certain waste type.

2.4 Waste Stabilization in Landfills

Historically, municipal solid waste sanitary landfills have been designed and operated as storage facilities with suboptimal degradation under anaerobic conditions resulting in slow waste stabilization, gaseous emissions and leachate formation [7]. Previous designs of landfills required extended maintenance after closure. Increasing strict regulations and shrinking availability of suitable sites for landfills may compel the designer to consider some new technologies that can accelerate the stability of solid waste. Stabilization is achieved through the degradation of sediment wastes, mainly through decomposition, which reduces the size of the landfill which inevitably leads to surface subsidence and the resulting harmful collapses. Landfill designs usually offer two options: dry or sealed landfill; Wet landfills are as follows:

Dry landfills are designed to isolate solid waste to minimize leachate production, thus reducing the potential for leachate to seep out of the landfill system. Studies have shown that the decomposition of solid waste is very limited with the dry system. Due to the tight sealing of the waste, where air and water cannot reach it, this prevented

the waste from decomposing in the long term. Although this method may require low maintenance costs, it may require maintenance for a long period of up to decades.

Wet landfill, the present studies indicated that in wet systems, or landfills that use leachate recycling to accelerate decomposition; it has become the preferred option when considering solid waste stabilization as a landfill's main objective. The complex interactions of bacteria cells result in the decomposition of most biological materials present in the waste, so "sanitary landfills" may also require the addition of air as well as the recycling of leachate to obtain aerobic decomposition in addition to the anaerobic decomposition that inevitably occurs in places where air does not reach. Tightly lined designs of landfills preserve leachate (which also contains organic matter) while minimizing the risk of leakage into the groundwater.

The emission of organic gases, the most important of which is methane, is a major environmental and safety problem in some landfills. Therefore, the designer must take tight measures to prevent gas leakage out of the system. The economics of methane extraction as an energy source makes methane gas production from wet landfills very beneficial and thus may require the designer to make the containment, collection, and recovery of methane an important part of the landfill design.

Time required for reactions, the main advantage of a wet landfill is to increase the stability rate of solid waste in the landfill. Studies indicate that the leachate recycling process can accelerate the rate of reaction and decomposition of waste. The studies show that biological reactions in dry landfills may last for 50 years or more, while it may range from 5 to 10 years only for a wet landfill, and this confirms the speed of reaction in wet dumps [5]. Long-term financial savings through eliminated or reduced maintenance and long-term monitoring in dry landfills may outweigh the initial start-up costs and leachate recycling requirements in wet dumps. Therefore, the designer should consider this.

2.5 Planning and Operation

As long as the sanitary landfill is a pure engineering project, it is very necessary to pay high attention to the preliminary planning that must be carried out by a competent designer who is well versed in the characteristics of the waste. The climatic and geological conditions of the specified area, and the required designs and operational plan to ensure the success of the sanitary landfill on near and far terms.

Technical and economic feasibility of the sanitary landfill: The feasibility study report for a new sanitary landfill should be prepared by engineers and professional experts in order to achieve the factors discussed above, and the report should include the advantages and costs of recycling waste, volume reduction, and waste reduction. The options for the new landfill must also be investigated. These options include extending the life of the landfill with minimal environmental impacts, alternative disposal methods, and the use of regional or private facilities. Suppose a decision to construct a sanitary landfill is reached. In that case, comprehensive plans should be submitted that clarify the current and final conditions, the topography of the

landfill site, the surface drainage, the amount and location of the cover material, the requirements of the supporting facility, and the recommended operational procedures. In most countries, there are country-specific procedures to document the economic and technical feasibility of the landfill project and site.

Operational data for planning: Possible efforts should be made to ensure that the designer's directives are implemented during the operation of the landfill. The operational data and instructions prepared by the designer should include a detailed description of the mechanical equipment that will be used to treat the waste and operate the landfill, and the methods of laying the solid waste that will be used with all the details.

Waste properties, data provided to the planner and designer should include a complete analysis of the solid waste to be disposed of, its types, contents, quantities and changes in delivery rates. The analysis should also be performed by the facility on which the project will be placed, or by another specialized facility. For new, non-existing projects, analysis can be performed theoretically based on the population to be served and other major sources of solid waste. Based on numerous studies, the daily amount of solid waste per person can be considered from 2 to 3 kg of combined waste and garbage.

Operating equipment, detailed information should be provided about the equipment to be used, including transportation, assembly, delivery, and landfill operation. This should also include any planned changes to equipment due to aging and weather conditions. The efficiency and capabilities of this equipment must be taken into account when assessing operating conditions such as access roads, levels, fluid discharge, and operation in severe climates.

Methods of operation, as mentioned earlier, there are two traditional methods of operating a landfill that are the most common: the flat or zigzag area method and the trench method. The choice of the most appropriate method depends on several conditions in the area, including the nature of the land, the size and composition of the waste, the availability of land ... etc. In the area method, waste is placed in large open pits, stretched and compacted, and then covered with suitable material. As for the trench method, its name illustrates that the waste is disposed of in a trench and then covered with materials from the trench digging. Typical survey and trench operations are shown in Figs. 3 and 4. When considering the costs of lining the side slopes, and others in general, the trench method is less desirable than the area method. More details about the design of both methods will be explained in the following sections.

2.6 Design and Site Selection of Sanitary Landfilling

The appropriate and accurate design of the landfill will inevitably lead to the successful operation of the landfill, regardless of the nature of the sites chosen. The design includes a review of all technological alternatives that meet the requirements of the proposed landfill. The design should also result in a landfill capable

of accepting specific solid waste materials for disposal with minimal environmental and economic impacts. The design is mainly based on survey data and analysis of the types and quantities of waste expected to be disposed of in the landfill.

Site Selection

Landfill site selection is the first and most important part of the design process and can be considered the most important step in setting up a landfill disposal facility. When choosing a landfill site, consideration must be taken of the balance between reducing the distances for transporting waste from its sources, which affects the economics of the landfill, and keeping the landfill away from residential areas, inhabited buildings, and other sites that are not suitable for the landfill. Large apartment complexes may require more than one landfill when the savings justify this from lower transportation distances. An initial landfill closure plan should be formulated and submitted prior to site selection to ensure closure scheduling and selection of alternative sites are considered. There are many uses for properly closed landfill sites with minimal damage to health, environment, and economics. This includes many areas of importance to the facility, such as amusement parks, exhibition lands, car parks, etc. [8].

Land depletion and land degradation in the region are important points that deserve attention when choosing the appropriate site and designs, especially in countries with overcrowded populations and limited lands.

Other important considerations must be taken into account when selecting landfill sites, such as ground and surface water conditions, seismic impact areas, fault areas, geology, soil, topographic characteristics, types and quantities of solid and hazardous wastes, geographical factors, and environmental impacts. Also, wetlands and floodplains should be avoided for a period of at least 100 years. Endangered areas and single source aquifer recharge areas should be avoided as potential sites for landfill disposal facilities [9].

These areas may require a thorough site study with regard to environmentally sensitive conditions.

Sit selection considerations of a sanitary landfill can be summarized in the following points:

1. Disturbances—Although landfilling may be satisfactory in terms of appearance, some inherent inconveniences require consideration when preparing designs, such as traffic to and from the site, mechanical equipment noise, and dust.
2. Accessibility—landfill sites must be accessed easily and passage through residential areas should be avoided. For the purpose of business continuity, there must be adequate roads in all weather conditions. Alternative methods should be provided in the event that the route is temporarily closed to ensure the continuity of collection and delivery of waste for disposal. The site represents two-thirds of the total cost of a landfill, and this percentage may increase depending on the availability of land in that area. The location close to the source of the waste is the most economically desirable site and may not be environmentally as well.
3. Community and region development—When preparing designs, consideration should be given to the expected population and urban growth of the area in the

short and long term, and the consequent change in the nature and density of municipal, commercial and industrial wastes.

4. All local laws related to land division must be reviewed and observed to assess the legal aspects related to the project to ensure the legality of constructing the landfill.
5. Utilities services—A well-operated and accurate sanitary landfill requires many services according to the size of the landfill and the flow of waste. This includes: water supply for sanitary purposes, washing equipment, dust control, fire protection, as well as electrical power for lighting, equipment, electrical equipment, telephone or wireless communications, and Sanitation services. All these services fall under one administration called “utility services”.
6. Land requirements—The land area required for a sanitary landfill depends on several factors such as: the amount and characteristics of solid waste, filling depth, pressure efficiency, desired life and the plan for the landfill. Generally speaking, about 15 acres of area or size are needed per year per 10,000 inhabitants []. Cover material requirements account for about 20 percent of the volume of compressed waste and should be readily available, either on or near the landfill site.
7. Soil Information—Soils with good specification and practicality are desirable for landfill sites. Well-graded sandy loam soil conducive to good and necessary operation and compacting. It is also worth noting that the covering material should not crack when it becomes dry due to its high content of clay material. In other words, CH (Very heavy, sticky, plastic clays) soils are highly undesirable as covering material. The suitability of the existing soil for cover material should be determined based on engineering tests and evaluations [10].
8. Land end-use—The end-use of land is an important indicator that greatly influences design and site selection. The final uses of the landfill, after completion, are numerous, including parks, playgrounds, industrial estates, and agriculture.
9. Climate—Climate is an important factor when designing and operating landfills as digging trenches preparing and transporting cover materials may become a problem in the winter months. Wind (intensity and directions) and rain (intensity and times) are all important factors to consider when designing.
10. Geology—Before the final design of the landfill, a geological investigation of the site should be carried out as this helps to reduce the potential for ground and surface water contamination. The elements to consider are in this area:
 - a. Determine the location of the landfill at a safe distance from streams, lakes, wells, and other water sources,
 - b. Avoid choosing sites that are located above the aquifer with high permeability because of the type of structure or cracks they contain, which will lead to the penetration of sap from the landfill to water sources, such as crushed limestone and others,
 - c. Rising groundwater levels must be taken into account
 - d. Use a ground cover that is as impervious as possible,

- e. It is necessary to provide suitable drainage ditches to transport surface water and rain water away from the site, and the depth of drainage should be not less than 3 m under the minimum planned height for the operation of the landfill.
11. Seismic impact areas—areas of high seismic activity should be avoided. No part of the landfill should be in a seismic impact zone unless designed to withstand the corresponding pressure.
12. Unstable areas—karst terrain will be avoided. Before a landfill is implemented in a geologically unstable area, it must be demonstrated to the relevant government agency that the planned landfill will not disrupt the integrity of the liner system and other structural components.
13. Existing site facilities for the area—Sites traversed by pipes or underground channels (for sewage, rainwater, power cables, etc.) should be avoided unless moving them is possible.
14. Airports—It can never be any part of the landfill <3000 m from the end of the runway used by turboprops or <1500 m from the end of the runway used by the piston-engine aircraft [6].

2.7 Estimation of Capacity, Volume, Area and Decomposition Rate

It is very useful to take a look at the methods used in the world to calculate the size, capacity and area required for landfills, as many methods have been proposed in academic research [11] to make these calculations. All methods are based on the following indicators.

1. The volume of waste discharged from the city or the region, where its volume is estimated by the amount of waste disposed per capita and multiplied by the population of the city or region. Very different numbers have appeared, as this depends on many factors, the most important of which are the standard of living, climate, local laws, and the extent of the country's development in which that city is located, as will be mentioned later.
2. The topography of the area, water table and the nature of the land directly affects the design of the landfill in terms of dimensions, size of soil layers used for burial, density of waste compression and so on.
3. One of the most important factors affecting the estimation of the areas needed for dumps is the availability of land and the estimated age of dumps, which are also affected by the techniques used to develop and maintain dumps.

Below, the simplest methods will be presented to estimate the areas required for dumpsites, and then they will be applied to one of the Iraqi cities for the current period. The lands that will be depleted throughout Iraq due to sanitary dumps will also be estimated, as the number can double if the dumps are unsanitary.

Estimation Method (I)

This method depends on the following assumptions and derived equations [12]:

- Assume the current Waste generation per year = W (tons per year)
- Increase (or decrease) waste generation rate per year = x (%), should be estimated. If data of waste generation growth rate not available, then population growth rate can be used.
- Proposed life of landfill (in years) = n (years) [9, 13, 14]
- Waste generation after (n) years = W_n

$$W_n = W (1 + x/100)^n \text{ (tons per year)} \quad (1)$$

- Total waste generation in (n) years = (T) in (tons)

$$T = 1/2 [W + W (1 + x/100)^n] n \text{ (tons)} \quad (2)$$

- Efficiency of collection and compaction of solid waste ζ (assumed 0.80) should be considered for safety. Then total waste generation in (n) years (T) in (tons) must be divided by 0.8.
- Total volume of waste in (n) years is (V_w) (on the assumption of the density of waste = 0.85 tons/cubic meter)

$$V_w = T/0.85 \text{ (m}^3\text{)} \quad (3)$$

- Total volume of daily cover in (n) years is (V_{dc}) (on the basis of 15 cm soil cover on top and sides for lift height of 1.5–2 m)

$$V_{dc} = 0.1 V_w \text{ (m}^3\text{)} \quad (4)$$

- Total volume required for components of liner system and of cover system, on the assumption of 1.5 m thick liner system (including leachate collection layer) and 1.0 m thick cover system (including gas collection layer)

$$V_c = k V_w \text{ (m}^3\text{)} \quad (5)$$

Assume (k) = 0.25 for 10 m high landfill, 0.125 for 20 m high landfill and 0.08 for 30 m high landfill. This is valid for landfills where width of landfill is significantly larger than the height)

- Volume of landfill will be shrink within 10 years due to settlement and biodegradation which likely becomes (V_s):

$$V_s = m V_w \text{ (m}^3\text{)} \quad (6)$$

Assume $(m) = 0.1$ for biodegradable waste, while (m) could be less than 0.05 for incinerated and inert wastes) [12]. In this study (m) will be considered as 0.12 instead of 0.1, because of the hot weather in the Iraqi summer, which will enhance the degradation rate.

- Total estimated landfill capacity (C_i)

$$C_i = V_w + V_d + V_c - V_s \text{ (m}^3\text{)} \tag{7}$$

- The shape of the landfill in plan and section will be highly dependent, as mentioned before, on the topography of area, depth to the ground water table and other design factors such as; area type, trench type, slope rate, valley type, combination.
- Estimation of landfill height and **area**:

- (a) *For Restricted available area* $A_r \text{ (m}^3\text{)}$

Area required for infrastructural facilities = $0.15 A_r \text{ (m}^3\text{)}$

Area available for landfilling = $0.85 A_r \text{ (m}^3\text{)}$

Average landfill height required H_i (first estimate) above base level is:

$$H_i = C_i / 0.9 A_r \text{ (m)} \tag{8}$$

(Depending on the landfill type and area)

- (b) *No limitation on Area*

Possible maximum average landfill Height (H_i), typically between heights 10–20 m, rarely above 30 m.

Area required for landfilling separations:

$$A_i = C_i / H_i \text{ (m}^2\text{)} \tag{9}$$

Depending on the landfill type and area

Total area required A_T (including infrastructural facilities)

$$A_T = 1.15 A_i \text{ (m}^2\text{)} \tag{10}$$

- Estimates of the landfill’s capacity, height, and area can be improved after making the initial estimates. The daily cover size and the size of the lining system and the cover system can be changed, taking into account the final shape of the landfill. And also on the basis of whether the daily cover materials, the linear system and the cover system will be excavated from inside the landfill site or from other sites, causing their destruction as well.
- After considering these revised values, landfill capacity, length, and area estimates can be improved.

- However it should be noted that the values of the landfill's capacity will be subject to review and scrutiny during the operation of the landfill when the quantities of waste received at the site differ from the quantities estimated before the start of the implementation of the landfill.

Estimation Method (II)

This method is, simply, used to estimate the required volume of landfills using a recommended formula for estimating the required annual volume [13]. The method requires knowledge of the amount of waste dumped from the population and its density before landfill and after compression, as the volume of waste varies significantly from one city to another for many reasons, as mentioned earlier.

$$V_{LF} = (P \times E \times C) / D_c \quad (11)$$

where V_{LF} = Volume of landfills (m^3),

P = population,

E = ratio of cover (soil) to compacted fill, then:

$$E = (V_{sw} + V_c) / V_{sw} \quad (12)$$

where V_c = volume of cover (m^3).

V_{sw} = volume of solid waste (m^3).

C = average mass of solid waste collected per capita per year (kg/person).

D_c = density of compacted fill (kg/m^3).

Estimation Method (III)

Another formula has been developed to calculate the Volume of Sanitary Landfill per capita per year (V_1), which includes specific solid waste production rate, volumetric weight and compacting ratio. This formula can be briefed as follows:

$$V_1 = d[R/w + C_V] \quad (13)$$

where V_1 = required landfill volume per one person per year (m^3 /capita-year).

R = specific solid waste production rate, as an example (1 kg/capita-day).

w = volumetric weight of compacted solid waste, as an example ($800 kg/m^3$).

C_V = specific required volume for isolation layer at the bottom, covering layers between solid waste beds and final upper covering layer, as an example ($0.0004 m^3$ /capita-day).

d = number of day in one year (assumed 365 day/year).

ξ = efficiency of collection and compaction of solid waste (assumed 0.80).

D_c = settlement and decomposition factor (assumed 0.8).

Equation 13 can be written in another form when the efficiency of collection and compaction of the SW should be considered, as follows:

$$V_1 = d \times [(R/w) \times + CV] \times D_c \tag{14}$$

The required landfill volume per year V_{year} , for population (N) and settlement/decomposition factor (D_c) can be calculated by Eq. (15) as follows:

$$V_{year} = V_1 \times N \times D_c \tag{15}$$

Estimation Method (IV)

Potential or existing sanitary landfill sites should have a great capacity to meet the community’s needs for several years to come. This enables local officials to prepare structured plans for land acquisition and use and improve other components of the solid waste management system (such as collection, transportation, and treatment) to achieve greater efficiency.

Calculating the required capacity of a sanitary landfill is an essential planning step to know, acquire and use land and improve other components of a solid waste management system.

A monograph has been developed to facilitate calculations of this kind as shown in Fig. 5, which is often used in the United States of America [9]. By using this Monograph, it is possible to calculate the size of the landfill that corresponds to the data given about the city or region such as the population and the amount of waste produced by the individual.

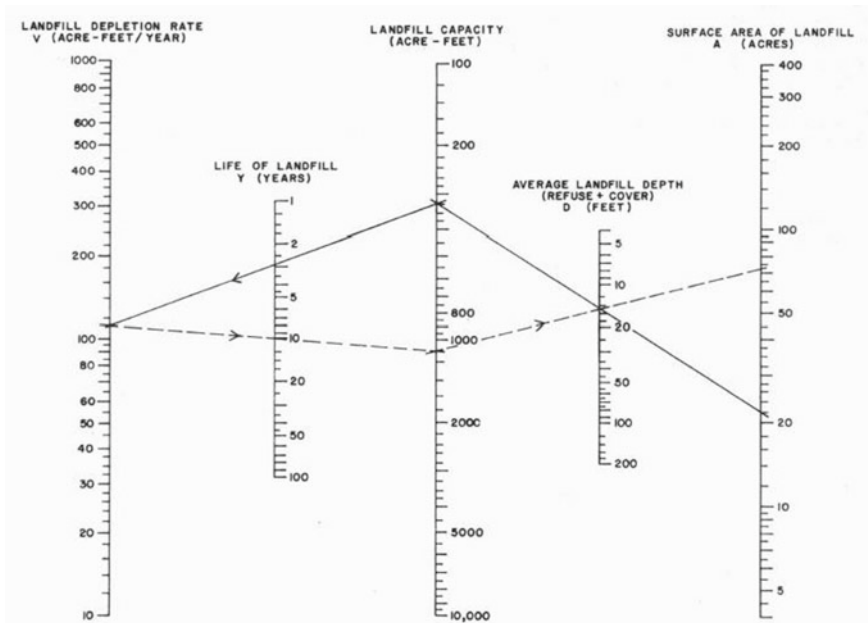


Fig. 5 Monograph for computing landfill area requirements and remaining site life [12]

2.8 *Estimation of Required Land Areas for Existing and Proposed Landfills in Iraq*

There are many methods for calculating the size and capacity of landfills and the area required to implement them. A section of them has been presented for the definition, as there are many other methods.

As long as the main objective of this article is to focus on lands that may be depleted due to random landfill and sanitary landfill of waste, the applied calculations will deal with the calculation of the area of land required to meet the needs of landfills for all Iraqi cities, as a case study, without addressing the design details of dumps.

In Tables 1, 2 and 3, the total volume and areas required for landfills (including infrastructural facilities) in the Iraqi governorates were calculated according to the *Estimation Method (I)*. Table 3 shows the estimated areas of dumps in the Iraqi governorates and the whole of Iraq and the percentage of depleted areas relative to the total area in the short and long term.

The following conditions, design factors, and assumptions will be considered in the calculations of the landfill capacities:

1. The population census for 2018 was approved for the Iraqi governorates to be used in calculations, which was taken from the Population Statistics for Countries, as shown in Table 1 [19].
2. The Central *Statistical Organization (CSO)* has stated, at 22/4/2021, that the average, per capita, generation of solid waste is 1.4 kg/day [20], while Alsamawi et al. (2009) were studied the estimation of MSW generated in Baghdad for the period 2006–2010 and reported that waste generation rates were 0.63 (kg/capita/day) in 2006 and 0.74 (kg/capita, day) in 2010. Al-Rawi and Al-Tayyar (2012) explored that the generation of solid waste in Mosul city was 0.647 (kg/capita, day) in 2010, and it could be increased to reach 1.1 (kg/capita, day) in 2028. It can be concluded from the above studies and other's that the average Iraqi per capita generation of waste in all cities ranges between 0.74 and 1.40 (kg/capita, day) for the current year 2021. As a matter of precaution, the rate will be adopted as (1.07) (kg/capita, day) in this study's calculations.
3. Total days per year will be considered as 365 days for all calculations.
4. Population annual growth in Iraq is 2.35% at 2018, as shown in Fig. 6 [21]. This growth percent will be considered the solid waste growth rate (x) for all calculations because there is no data available about solid the growth rate of solid waste.
5. Proposed life of landfill (n) (in years) will be taken as 15 years.
6. Total volume of daily cover in (n) years (V_{dc}) (on the basis of 15 cm soil cover on top and sides for lift height of 1.5–2 m) [14].
7. Total volume required for components of liner system and cover system (on the assumption of 1.5 m thick liner system (including leachate collection layer) and 1.0 m thick cover system (including gas collection layer). Height of landfills will be taken as 10 m because most of Iraqi lands topography is flat area. Then $k = 0.25$ for 10 m high landfill [12].

Table 1 The population of the Governorates of Iraq and estimated generated solid waste [By author]

Province Name	Abbr.	Capital	Whole Land Area A-L (km ²)	Population Estimate (E)** 2018-07-01 (capita)	Total** Generated Solid waste Weight W (Tons/y) x10 ⁶
Iraq (Total) *	IRQ	Baghdad	435,050	38,124,182	14.889
1. Al-anbar	ANB	Al-ramadi	135,000	1,771,656	0.692
2. Al-Başrah [Basra]	BSR	Al-Başrah	19,070	2,908,491	1.136
3. Al-Muthannā	MTN	As-Samāwah	51,740	814,371	0.318
4. Al-Qādisiyah	QAD	Ad-Dīwāniyah	8,150	1,291,048	0.504
5. An-Najaf	NJF	An-Najaf	28,820	1,471,592	0.575
6. Arbīl [Erbil]	ARB	Arbīl	12,000	1,854,778	0.724
7. As-Sulaymāniyah	SLM	Sulaymāniyah	20,000	2,053,305	0.802
8. Bābil [Babylon]	BAB	Al-Ḥillah	5,800	2,065,042	0.807
9. Baghdād	BGD	Baghdād	5,200	8,126,755	3.174
10. Dahūk [Dohuk]	DHK	Dahūk	10,000	1,292,535	0.505
11. Dhī Qār [Theqar]	DHI	An-Nāşiriya	12,900	2,095,172	0.818
12. Diyālā	DYL	Ba'qūbah	14,700	1,637,226	0.639
13. Ḥalabjah [Halabja]	HLB	Ḥalabjah	880	108,974	0.043
14. Karbalā' [Karbala]	KRB	Karbalā'	5,030	1,218,732	0.476
15. Kirkūk	KRK	Kirkūk	10,500	1,597,876	0.624
16. Maysān	MYS	Al-'Amārah	16,070	1,112,673	0.435
17. Nīnawā [Nineveh]	NIN	Al-Mawşil	36,700	3,729,998	1.457
18. Şalāḥ ad-Dīn [Saladin]	SLD	Tikrīt	26,000	1,595,235	0.623
19. Wasīt	WST	Al-Kūt	17,150	1,378,723	0.539

* The mid-2020 total population is projected as **40,150,200**. ** After; Central Organization for Statistics and Information Technology (web), <https://www.citypopulation.de/en/iraq/cities/> (2018).

** Population × (1.07) kg/capita, day × 365 [15, 16]

Table 2 The estimated landfills volumes according to estimation method (I) [By author]

Area Name	A	B	C	D	E	F	J
	Total Generated Waste Weight W (Tons/year) $\times 10^6$	Total Generated Waste after 15 Years (T) (Tons) $\times 10^6$	Total Volume after 15 Years V_w (m^3) $\times 10^6$	Total Volume of Daily Cover V_{dc} (m^3) $\times 10^6$	Volume of Liner and Cover System V_c (m^3) $\times 10^6$	Volume of settlement and Degradation V_s (m^3) $\times 10^6$	Estimated Landfills Volume Method (I) C_i (m^3) $\times 10^6$
		(Eq.2) /0.8*	B/0.85#	C x 0.1	C x 0.25	C x 0.12	C + D + E - F
Iraq (Total)	14.889	303.317	356.844	35.684	8.921	42.821	358.628
1. Al-Anbār	0.692	14.097	16.585	1.658	0.415	1.990	16.668
2. Al-Basrah [Basra]	1.136	23.143	27.227	2.723	0.681	3.267	27.363
3. Al-Muthannā	0.318	6.478	7.621	0.762	0.191	0.915	7.659
4. Al-Qādisiyah	0.504	10.267	12.079	1.208	0.302	1.449	12.139
5. An-Najaf	0.575	11.714	13.781	1.378	0.345	1.654	13.850
6. Arbīl [Erbil]	0.724	14.749	17.352	1.735	0.434	2.082	17.439
7. As-Sulaymāniyah	0.802	16.338	19.221	1.922	0.481	2.307	19.317
8. Bābil [Babylon]	0.807	16.440	19.341	1.934	0.484	2.321	19.438
9. Baghdād	3.174	64.660	76.071	7.607	1.902	9.128	76.451
10. Dahūk [Dohuk]	0.505	10.288	12.104	1.210	0.303	1.452	12.164
11. Dhi-Qar [Theqar]	0.818	16.664	19.605	1.960	0.490	2.353	19.703
12. Diyālā	0.639	13.018	15.315	1.532	0.383	1.838	15.392
13. Ḥalabjah [Halabja]	0.043	0.876	1.031	0.103	0.026	0.124	1.036
14. Karbalā' [Karbala]	0.476	9.697	11.408	1.141	0.285	1.369	11.465
15. Kirkūk	0.624	12.712	14.955	1.496	0.374	1.795	15.030
16. Maysān	0.435	8.862	10.426	1.043	0.261	1.251	10.478
17. Nīnawā [Nineveh]	1.457	29.682	34.920	3.492	0.873	4.190	35.095
18. Ṣalāḥ ad-Dīn [Saladin]	0.623	12.692	14.932	1.493	0.373	1.792	15.006
19. Wasīṭ	0.539	10.980	12.918	1.292	0.323	1.550	12.982

* Efficiency of waste collection and compaction, # Density of compacted solid waste

Table 3 Estimated landfills area according to methods (I) and land depletion ratio [By author]

Area Name	A	B	C	D	E	F	J
	The Whole Land Area (km ²)	Estimated Landfills Volume Method (I) C _i (m ³) x10 ⁶	Estimated Landfills Area (A _i) Method (I) (m ²) x10 ⁶	Total Est. Landfills Area (A _T) # Method (I) (m ²) x10 ⁶	Total Est. Landfills Area (A _T) (km ²)	Land Depletion Ratio Dew to Landfills After 15 years (%)	Land Depletion Ratio Dew to Landfills After 100 years (%)
	Table (2)	Table (3)	B/10*	C x 1.15	D/10 ⁶	(D/A)x100	Recalculat e
Iraq (Total)	435,050	358.628	35.863	41.242	41.242	0.009	1.4
1. Al-Anbār	135,000	16.668	1.667	1.917	1.917	0.001	0.2
2. Al-Başrah [Basra]	19,070	27.363	2.736	3.147	3.147	0.017	2.4
3. Al-Muthannā	51,740	7.659	0.766	0.881	0.881	0.002	0.2
4. Al-Qādisiyah	8,150	12.139	1.214	1.396	1.396	0.017	2.5
5. An-Najaf	28,820	13.850	1.385	1.593	1.593	0.006	0.8
6. Arbīl [Erbil]	12,000	17.439	1.744	2.005	2.005	0.017	2.4
7. As-Sulaymāniyah	20,000	19.317	1.932	2.221	2.221	0.011	1.6
8. Bābīl [Babylon]	5,800	19.438	1.944	2.235	2.235	0.039	5.5
9. Baghdād	5,200	76.451	7.645	8.792	8.792	0.169	24.3
10. Dahūk [Dohuk]	10,000	12.164	1.216	1.399	1.399	0.014	2.0
11. Dhī Qār [Theqar]	12,900	19.703	1.970	2.266	2.266	0.018	2.5
12. Diyālā	14,700	15.392	1.539	1.770	1.770	0.012	1.7
13. Ḥalabjah [Halabja]	880	1.036	0.104	0.119	0.119	0.014	1.9
14. Karbalā' [Karbala]	5,030	11.465	1.147	1.318	1.318	0.026	3.8
15. Kirkūk	10,500	15.030	1.503	1.728	1.728	0.016	2.4
16. Maysān	16,070	10.478	1.048	1.205	1.205	0.007	1.1
17. Nīnawā [Nineveh]	36,700	35.095	3.510	4.036	4.036	0.011	1.6
18. Şalāḥ ad- Dīn [Saladin]	26,000	15.006	1.501	1.726	1.726	0.007	1.0
19. Wasīṭ	17,150	12.982	1.298	1.493	1.493	0.009	1.3

* Landfills considered 10 m depth, # including landfills infrastructure [17, 18]

8. Volume of landfill most likely will be shrink within 10 years due to the settlement and biodegradation of waste then shrink factor $m = 0.10$ for biodegradable waste while it will be less than 0.05 for inert and incinerated wastes.
9. Efficiency of waste collection and compaction through the landfill life time will be considered as 80%.

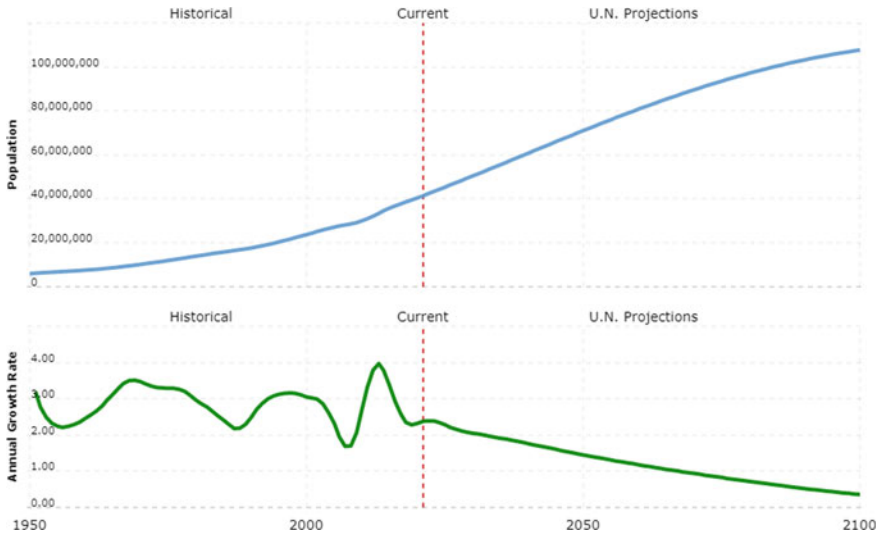


Fig. 6 Population annual growth rate in Iraq [21]

10. Degradation and settlement factor (m) will be considered as 0.12 instead of 0.1, because of the hot weather in Iraq, which leads to higher degradation rate.

2.9 Analysis of Estimated Areas Used for Existing and Future Landfills in Iraq

When reviewing the results that were reached in Table 3, one can imagine the size of the big problem that results from the huge areas that can be depleted due to the waste dumping and sanitary landfill. Table 3 and Figs. 7 and 8 shows that, the percentage of depleted lands versus whole land areas are proportional to the populations and inversely to the total area of each governorate. The tables and drawings clearly show that the governorates with small areas and high population are more vulnerable to land depletion due to waste dumps such as Baghdad, Basra and Nineveh. Whereas in the governorates with large areas, the percentage of land depletion relative to the total areas is small, as in Anbar, Muthanna, Najaf and Sulaymania. Likewise, in Table 3 and Fig. 8, the frightening increase of lands that will be depleted in the long run, as the figure shows depletion after 15 and 100 years, as the high percentage appears clearly in cities with high populations, such as Baghdad, Babylon, Basra, Qadisiyah, Karbala and Erbil.

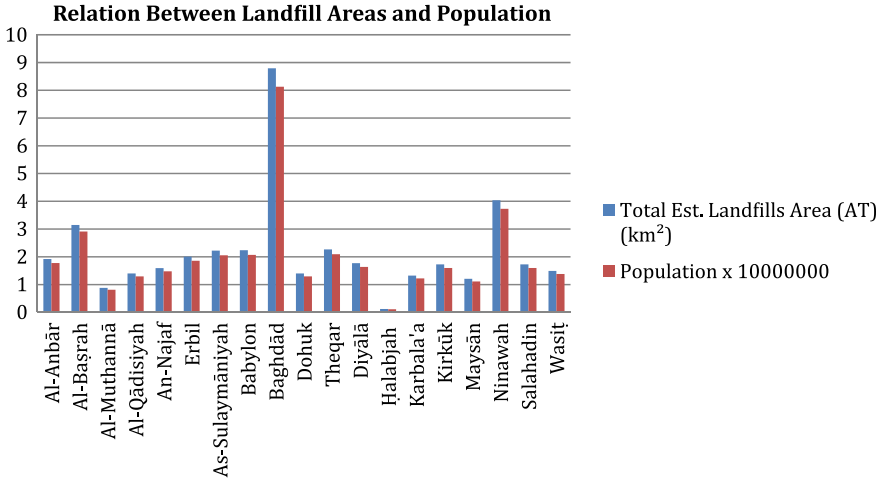


Fig. 7 Population and related land depletion dew to solid waste landfilling in Iraqi Provinces [By author]

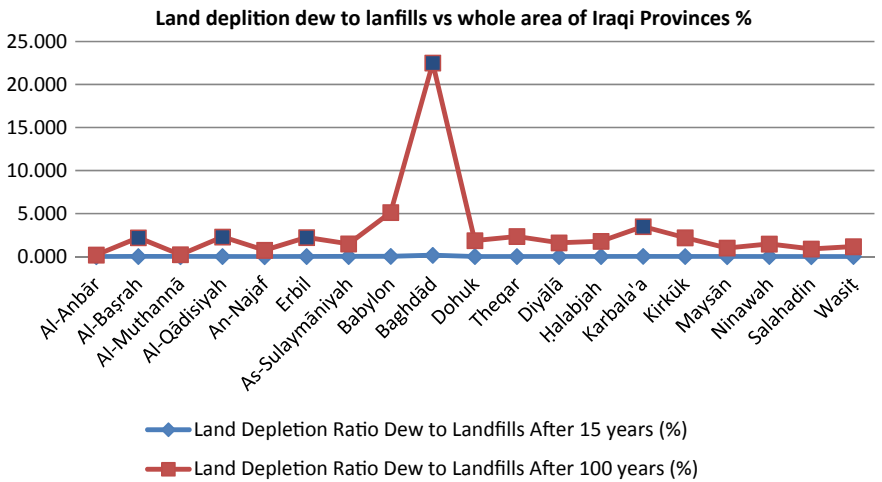


Fig. 8 Short term and long term land depletion ratios of Iraqi Provinces (%) [By author]

2.10 Landfills Impacts

As a result of landfilling, whether sanitary or random dumping, in addition to the depletion of land, many environmental, health and social impacts result, the most important of which are briefly mentioned below. Extensive academic studies and research detail the various environmental and health impacts of random dumpsites

and sanitary landfills [22, 17]. There is no room for details here, but the most important pollutants, sources, and environmental and health impacts will be presented.

The main sources of emissions released from landfills and related activities are:

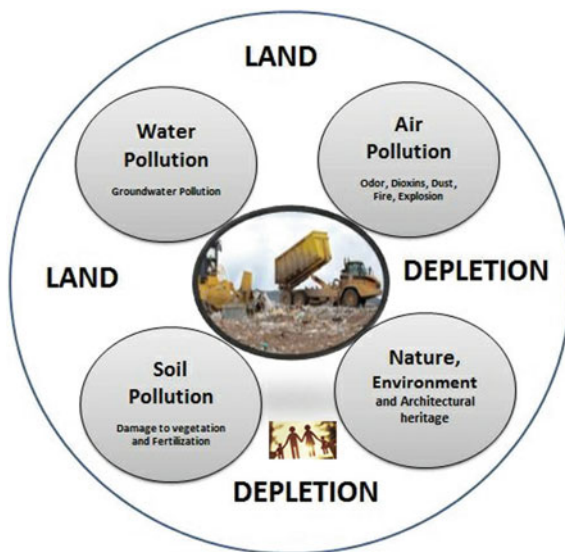
1. Heavy equipment and trucks that collect waste and transport it to landfill sites is an important source of pollution and noise.
2. The equipment that digs, receives, distributes and compresses waste in the landfill and backfills it with soil is also another source of dust, pollution and noise.
3. Waste and dust flying off due to the winds are a source for spreading many pollutants to the neighboring areas.
4. The gases released from the decomposition of waste in the landfill and its burning in some cases is a dangerous source of toxic and suffocating gases such as methane, ethane, ammonia, sulfur dioxide, carbon dioxide, dioxin, trace metals and other dangerous pollutants.
5. The leachate released from the waste is an important source of dangerous pollutants that may cause contamination of groundwater and surface water.
6. Complex chemicals that may be released from waste in the form of solid and liquid substances that lead to soil pollution and spoilage in terms of germination capacity and degradation of fertility.
7. Dumpsites can spoil landscapes, archaeological and heritage sites, and this is in addition to the depletion of a huge amount of usable land to turn into lands unsuitable for agriculture, housing and infrastructure.
8. In the absence of proper systems for collecting gases generated from decomposition of organic waste or poor performance of these systems due to the lack of programmed maintenance, the landfill is exposed to explosion or fire that may cause unforeseen disasters.
9. The landfill can be a source of the spread of rodents, insects and harmful animals, which can cause the spread of dangerous diseases in the area, which may be cumulative and carcinogenic diseases that do not appear in the short term.

It can be said that landfills are mainly designed to store and reduce the volume of waste, as this process results in many potential risks, including what results from the migration of polluted leachate, gases and odors generated from chemical reactions and organic decomposition. Therefore, the environmental impacts of the many landfills located around the world cannot be ignored, as shown in Fig. 9.

Suppose local solid waste is disposed of in a landfill without prior treatment. In that case, it results in major emissions (leachate and biogas) largely due to the anaerobic biological processes that take place in it, and emissions develop and may increase during the landfill operation and for a long period, even after the landfill is closed.

Residents, who live within 5–10 km from the landfill site, are at grave risk to their health. Hydrogen sulfide is the most dangerous gas in terms of rapid injury from other emitted gases and death from lung cancer, death, and hospitalization from respiratory diseases. When the landfill reaches its capacity, the waste is covered with a clay layer or another plastic shield, and all this does not prevent the mentioned dangers, especially in hot climates [24].

Fig. 9 Major impacts of land filling [23]



3 Published Literature and Research Works on Landfilling

Despite the development of solid waste management in a number of countries of the world, especially the developed industrial countries, sanitary and random landfills remained the prevailing method of waste management with the growing quantities of waste in most of the world and especially in developing countries [25]. With the negative effects of landfilling, the number of researchers in universities, academic institutions, and relevant departments is increasing in studying ways to dispose of waste at the lowest costs and minimize the environmental and health impacts. Therefore, we find a huge number of books, surveying studies and research works on sanitary landfill, their types, and methods of design, implementation, and maintenance, the environmental impacts of landfills in the short and long term, and the special cases for each country, according to the geographical nature and climate.

4 Up-to-Date Technologies of Waste Management and Treatment

According to European Legislation, the advanced approach to waste management based on principle “waste hierarchy” [26, 27] which introduce the order of the priorities of solid waste management, as mentioned before (Fig. 1).

Waste minimization can be briefed as the process of reducing the amount of waste produced by a person or a society. Reuse, simply means using an item more than once. This includes traditional reuse where the item is used again for the same function or

re-used for a new function [26]. An example of this is the use of aluminum recycled from soft drink cans for several times after throwing them in the waste either for cans again or other products. So as happens for plastic, iron, wood, paper and other valuable materials. Another examples, waste concrete rejected from industry or demolition can be used after crashing as a base for roads or concrete aggregates.

Recycling and composting are processes of material waste recovery. Recycling means obtaining substances from waste, as a secondary raw materials, and their utilization as a substitution of the primary raw materials. Composting can be briefed as a biochemical decomposition of organic substances found in the waste to produce different types of fertilizer [28].

Energy recovery technologies are widely used to reduce waste volume and energy recovery, but high attention should be paid to properly disposing of residues, discarded and discharged materials according to local environmental legislation, guidelines, or laws.

Accurate and comprehensive waste management techniques, are in short, the processes of recovering and generating energy from waste in its various forms. Waste-To-Energy (WTE) is nowadays one of the preferred methods for managing all waste in a sustainable manner [29, 30].

5 Conclusions

1. *The most important conclusion reached through this article is the clear and important fact: the landfilling of all kinds of waste inevitably leads to land depletion.*
2. Unfortunately, in Iraq, there is not yet good waste management, as in many other countries, as most Iraqi cities still adopt indiscriminate landfills, sanitary landfill, and indiscriminate burning to dispose of all kinds of waste. It should be noted that some individuals doing manual isolation of materials that can be reused such as woods, plastics, aluminum, copper, and iron scrap for their own benefit.
3. The appropriate and accurate design of the landfill will inevitably lead to the successful operation of the landfill, regardless of the nature of the sites chosen.
4. Choosing a landfill site is the essential and very important part of the design stage, and it can be considered the most important step in establishing a successful sanitary landfill in the short and long term.
5. The study showed that the lands used for sanitary landfills will *not be suitable* for civil and urban activities for a long period of time, not to mention the environmental and health effects of those landfills.
6. Using various methods to estimate the land needed by landfill operations, it was found that the depletion of land in Iraqi cities is clearly related to the population census and the land area of those cities. The results of this study confirmed that the city's most depleting the land are the big cities such as Baghdad, Basra and Mosul. The results also indicate that about 25% of Baghdad's land area will be depleted during the next 100 years.

7. From the researcher's point of view, converting waste into fertilizers, through aerobic fermentation techniques, may be the most suitable option for the Iraqi conditions, as Iraq is considered one of the arable countries and was historically called "the land of blackness". In addition, Iraq has large reserves of oil and gas and it may be unfeasible to use the waste-to-energy (WTE) method, although it is considered one of the best ways, in many countries, to solve the problem of waste management in a sustainable manner, as mentioned above.

6 Recommendations

The author's recommendations are twofold:

1. *It* is directed to the Iraqi government agencies as well as in other developing countries, which are responsible for planning and waste management. They should give the utmost attention to waste management and not resort to sanitary or unsanitary landfills, which are easier and less expensive in the short term. But, in the same time, it will simply cause more depletion and destruction of lands, which is considered the most absolutely expensive in the short and long term.
2. It is directed to universities and research institutions to direct more research and studies that help solve and simplify waste management systems of all kinds in Iraqi cities and cities of other developing countries. We also recommend using modern planning and monitoring systems using remote sensing and GIS systems to avoid burying waste in the lands, causing further depletion of the lands.

Acknowledgements I am pleased to extend my great thanks and appreciation to my dear friend Prof. Dr. Ayad Yassin Al-Quraishi and Prof. Dr. Abdul-Azim Al-Najm for their encouragement and continuous support and for giving me the opportunity to write this article.

References

1. Bell JM. Sanitary landfill method of solid waste disposal. School of Civil Engineering, Purdue University. <https://docs.lib.purdue.edu/cgi/viewcontent.cgi?article=3292&context=roadschool>
2. USDA, Natural Resources Conservation Service, Kansas Environment Technical Note KS-2, September 15, 1971. https://www.nrcs.usda.gov/wps/portal/nrcs/detail/ks/people/employees/?cid=nrcs142p2_033385
3. Bookter TJ (1982) Stabilization of solid waste in landfills. *J Environ Eng Div* 108(6):1089–1100
4. Stegmann R (2005) Discussion of different landfill concepts from open dump to MBP landfill, January 2005. Institute of Waste Management, Hamburg University of Technology, Hamburg
5. Paul Guyer J (2009) Introduction to sanitary landfills. Continuing Education and Development, Inc., Course No: C02-018, Credit: 2 PDH
6. Jaramillo J (2003) Guidelines for the design, construction and operation of manual sanitary landfills. PAHO/CEPIS/PUB/03.108, Original: Spanish

7. El Fadel M, Fayad W, Hashisho J (2012) Enhanced solid waste stabilization in aerobic landfills using low aeration rates and high density compaction, August 9, 2012. <https://doi.org/10.1177/0734242X12457118>
8. Sahu B, Singh RV. Site selection and estimation of a sanitary landfill in BIT Sindri, Dhanbad Bidisha Sahu
9. Sweeten JM. Computing sanitary landfill capacities. <https://core.ac.uk/download/pdf/141471593.pdf>
10. Atkinson J. Soil description and classification. University of Waste of England, London, Based on part of the Geotechnical reference package, by Prof. John Atkinson, City University, London. <https://environment.uwe.ac.uk/geocal/SoilMech/classification/default.htm>
11. Macklin Y, Kibble A, Pollitt F (2011) Impacts on health of emissions from landfill sites. Health Protection Agency. ISBN 978-0-85951-704-1
12. Nafae TM, Al-Najar HA et al (2017) Design of municipal solid waste landfill for Baghdad City. WSN 90:1–10. EISSN 2392-2192. www.worldscientificnews.com
13. Davis ML, Cornwell DA (1991) Introduction to environmental engineering. Mc-Graw Hill, Inc
14. Sarmah P, Dutta TT, Sen S (2015) Design of a combination of compost plant and landfill for municipal solid waste management of Guwahati city. Int J Civ Struct Environ Infrastruct Eng Res Dev (IJCSEIERD) 5(4):45–52. ISSN (P): 2249-6866; ISSN (E): 2249-7978
15. Al-Rawe SM, AL-Tayyar TA (2012) Two decades comparison of solid waste composition and generation in Mosul City. Tikrit J Eng Sci 19(1):25–43
16. Alsamawi AA, Ziboon ART, Alnakeeb A (2008) Estimation of Baghdad municipal solid waste generation rate, January 2009. Eng Tech J 27(1)
17. Chabuk A et al (2018) Application of the help model for landfill design in arid areas: case study Babylon Governorate, Iraq. J Civ Eng Archit 12:848–879. <https://doi.org/10.17265/1934-7359/2018.12.003>
18. Iraq National Population Commission (INPC), Iraq population situation analysis report 2012. <https://iraq.unfpa.org/sites/default/files/pub-pdf/PSA%20English%202012.pdf>
19. City population, population statistics for countries, administrative divisions, cities, urban areas and agglomerations—interactive maps and charts. <https://www.citypopulation.de/en/iraq/cities/>
20. Central Statistical Organization Iraq (CSO), 22/4/2021. <http://www.cosit.gov.iq/ar/env-ind>
21. Macrotrends, Iraq population growth rate 1950–2022. <https://www.macrotrends.net/countries/IRQ/iraq/population-growth-rate>
22. Danthurebandara M et al (2012) Environmental and socio-economic impacts of landfills. Linnaeus ECO-TECH 2012, Kalmar, Sweden, November 26–28, 2012
23. Mishra P et al (2020) Landfill emissions and their impact on the environment. Int J Eng Res Technol (IJERT) 9(8). ISSN: 2278-0181. IJERTV9IS080187. www.ijert.org
24. Vaverková MD (2019) Landfill impacts on the environment—review. Geosci Open Access J 9(10):431; Mendel University in Brno, 613 00 Brno, Czech Republic. <https://doi.org/10.3390/geosciences9100431>
25. Hemidat S, Achouri O, El Fels L, Elagroudy S, Hafidi M, Chaouki B, Ahmed M, Hodgkinson I, Guo J (2022) Solid waste management in the context of a circular economy in the MENA region. Sustainability 14:480. <https://doi.org/10.3390/su14010480>. Academic Editors: Abu-Qdais H, Kurbatova A, Picuno C. Received: 23 Nov 2021. Accepted: 30 Dec 2021. Published: 3 Jan 2022. file:///C:/Users/Salah/Downloads/sustainability-14-00480.pdf
26. Golomeova S, Srebrenkoska V, Krsteva S, Spasova S (2013) Solid waste treatment technologies. Faculty of Technology, University “Goce Delcev”, Stip, R. Macedonia, Scientific proceedings x international congress “Machines, technologies, materials”. ISSN 1310-394
27. Al-Ghouti MA, Khan M, Nasser MS, Al-Saad K, Heng OE (2021) Recent advances and applications of municipal solid wastes bottom and fly ashes: insights into sustainable management and conservation of resources. Environ Technol Innov 21:101267. <https://doi.org/10.1016/j.eti.2020.101267>. ISSN 2352-1864. <https://www.sciencedirect.com/science/article/pii/S2352186420315674>

28. Zupančič M, Možic V, Može M, Cimerman F, Golobič I (1823) Current status and review of waste-to-biogas conversion for selected European countries and worldwide. *Sustainability* 2022:14. <https://doi.org/10.3390/su14031823>
29. Zaman AU (2010) Comparative study of municipal solid waste treatment technologies using life cycle assessment method. *Int J Environ Sci Technol* 7:225–234. <https://doi.org/10.1007/BF03326132>
30. US Department of Energy, Office of Energy Efficiency and Renewable Energy and Report. Waste-to-energy from municipal solid wastes, August 2019. <https://www.energy.gov/sites/prod/files/2019/08/f66/BETO--Waste-to-Energy-Report-August--2019.pdf>
31. Park HI, Park B, Lee SR (2007) Analysis of longterm settlement of municipal solid waste landfills as determined by various settlement estimation methods. *J Air Waste Manag Assoc* 57(2):243–251. <https://doi.org/10.1080/10473289.2007.10465318>

RUSLE Model in the Northwest Part of the Zagros Mountain Belt



Arsalan Ahmed Othman, Ahmed K. Obaid, Varoujan K. Sissakian, Ahmed F. Al- Maamar, and Ahmed T. Shihab

Abstract Besides several causes, the researchers believed that erosion is a vital reason of land degradation. Therefore, understanding the nature and type of land erosion processes will benefit many sectors of society in a concerned region. The current study estimated the mean annual loss of soil in Al-Khabur River Basin (KhRB) in the northwest side of the western Zagros Range (Kurdistan Region/ Iraq). KhRB is a main tributary of the Tigris River. We have used DEM-SRTM, TRMM, the HWSD, and Landsat imagery having 30 m pixel resolution to apply the RUSLE model. We have calculated six factors, which are the factor of rainfall and runoff erosivity (R), the factor of soil erodibility (K), the factor of slope length (L), the factor of slope-steepness (S), the factor of cover and management (C), and the factor of support practice related to slope direction (P). Results of RUSLE show that the minimum and the maximum values of the annual soil losses were zero $t^{-1} \cdot ha^{-1} \cdot y^{-1}$ and $\sim 3618 t^{-1} \cdot ha^{-1} \cdot y^{-1}$, respectively. The sum of the annual soil losses for the KhRB was $317,273,283.4 t^{-1} \cdot ha^{-1} \cdot y^{-1}$ with an average $\sim 75.79 t^{-1} \cdot ha^{-1} \cdot y^{-1}$. The

A. A. Othman (✉) · A. F. A.-. Maamar · A. T. Shihab
Iraq Geological Survey, Al-Andalus Square, Baghdad 10068, Iraq
e-mail: arsalan.aljaf@geosurviraq.iq; arsalan.aljaf@komar.edu.iq

A. F. A.-. Maamar
e-mail: ahmedryaman@gmail.com; ahmed.f@geosurviraq.iq

A. T. Shihab
e-mail: ahdsat1975@gmail.com; ahmedshihab@geosurviraq.iq

A. A. Othman
Komar University of Science and Technology, Sulaymaniyah 46001, Iraq

A. K. Obaid
Department of Earth Sciences, University of Durham, Durham DH1 3LE, UK
e-mail: ahmed.k.obaid@durham.ac.uk; ahmedobaid@uobaghdad.edu.iq

Department of Geology, University of Baghdad, Al-Jadriyh Street, Baghdad, Iraq

V. K. Sissakian
Department of Natural Resource Engineering and Management, University of Kurdistan Hewler, KRG, Hewler, Iraq
e-mail: f.khajeek@ukh.edu.krd

southern and northeastern parts of the KhRB exhibit low and very low annual loss of soil ($<10 \text{ t}^{-1} \cdot \text{ha}^{-1} \cdot \text{y}^{-1}$), while the central and northern parts of the KhRB exhibit high and very high annual loss of soil ($>10 \text{ t}^{-1} \cdot \text{ha}^{-1} \cdot \text{y}^{-1}$). Around 19% of the KhRB holds very high value of the annual soil losses ($>50 \text{ t}^{-1} \cdot \text{ha}^{-1} \cdot \text{y}^{-1}$). The study has found that the main factors that dominate the annual soil losses in the KhRB are LS, derived from the slope gradient and flow accumulation, and R factor, which is related to the precipitation. The most vulnerable areas to soil erosion are rough terrain, steep inclines, heavy precipitation, and low plant cover. Implementing the RUSLE model and anticipating soil loss distribution in the KhRB will help in potential land use and watershed management in Iraq.

Keywords RUSLE · Erosion · Iraq · Kurdistan Region

Abbreviations

ρ	Reflectance
C	Cover and Management Factor
CAS	Chinese Academy of Sciences
DEM	Digital Elevation Model
E	Energy
ENVI	Environment for Visualizing Images
EROS	Earth Resources Observation and Science
FA	Flow Accumulation
FAO	Food and Agriculture Organization of the United Nations
FLAASH	Fast Line-of-Sight Atmospheric Analysis of Spectral Hypercubes
HWSD	Harmonized World Soil Database
I30	30-Minute intensity
IDW	Inverse Distance Weighting
ISRIC	International Soil Reference and Information Centre
IIASA	International Institute for Applied Systems Analysis
JAXA	Japan Aerospace Exploration Agency
JRC	Joint Research Centre of the European Commission
K	Soil Erodibility Factor
KhRB	Al-Khabur River Basin
L	Slope Length factor
LS	Slope Length and Slope-Steepness Factor
NDVI	Normalized Difference Vegetation Index
NetCDF	Network Common Data Form
OC	Soil Organic Carbon
OM	Soil Organic Matter
P	Support Practice Factor Related to Slope Direction
S	Slope Steepness Factor
SoL	Soil Loss

SRTM	Shuttle Radar Topography Mission
R	Rainfall and Runoff Erosivity Factor
R ²	Coefficient of determination
RUSLE	Revised Universal Soil Loss Equation
TRMM	Tropical Rainfall Measuring Mission
USGS	United States Geological Survey
USLE	Universal Soil Loss Equation
UTM	Universal Transverse Mercator
VC	Vegetation Cover

1 Introduction

In the last decades, huge researches have been done to quantify and understand the relation between tectonics and erosion. These two competing forces (i.e., tectonic and erosion) build and lower the topography [1]. The erosion is an action that is motivated by tectonic forces through the process of mountains building, creating instability within the earth's surface. Thus, erosion is redistributing masses from the higher to the lower altitudes ending with the achievement of the equilibrium state; however, not in all cases, equilibrium can be achieved; therefore, many slopes still suffer from stability problems.

Erosion is a geomorphic and natural process forced directly by rainfall intensity [2] and causes land degradation, which is responsible for about 84% of land degradation worldwide [3, 4]. It has a serious impact on soil fertility, sustainable agriculture, quality of the water, efficiency of the reservoir, and environmental health of the aquatic system [5]. Soil erosion exhibits huge fluctuation spatially and temporally across the world. Principally, this is because of the fluctuations in rainfall, soil type, human impact, land cover, and physiography of the area [6]. Moreover, economic, social, institutional, and political factors impact the intensity of soil erosion [7]. The rate of erosion controlling the sustainable soil and management of the land use [2]. The durability of soil and the depth of soil horizons are correlated with the soil erosion amount [8].

The Iraqi Kurdistan Region is characterized by a prolonged dry season followed by a season of heavy rain [9–13]. This situation motivated the erosion process, which will be worse in the higher slope regions [14], as in the Kurdistan Region [9–11]. Understanding erosional processes in this region are of importance for soil conservation. Thus, to deduce and evaluate the range and magnitude of soil erosion require quantitative estimation of the amount of soil loss to accomplish effective management planning. Moreover, results from [15] show that the average of the siltation that comes from the upstream region of the Mosul Dam is $\sim 780 \text{ tons km}^{-2} \text{ year}^{-1}$. Therefore, there is an urgent need to investigate sediment yield in the upstream area of the Mosul Dam (i.e., Al-Khabur River Basin, as inside the Iraqi territory is concerned). This may be vital when considering the problems of cavities, which occur in the

foundation of the Mosul Dam [12] and the recent earthquake activity in the nearby area [16]. Then, this investigation will be necessary to suggest mitigations and span life of the Mosul Dam, where Mosul Dam, which impounds the Tigris River, suffers from different problems, is siltation [17].

Soil degradation has been determined as a critical problem regionally, locally, and globally [18, 19], which give on to thinking seriously about soil fertility as the main resource of food security to sustain mankind. Therefore, an investigation of the soil erosion by water and is wind very important to define the essential threat of soil [20]. In the last century, estimation has shown that ~56% of the global land has been deteriorated, and ~40% exploited for agricultural activity [21, 22].

Two well-known models allow the use of data for fluctuating accuracy. Regardless of their multiple insufficiencies, weaknesses, and limitations, the USLE suggested by [23] and the RUSLE by [24]; up to the present time they are the most considerably used models of erosion [25, 26].

2 Case Study

The area of interest is the fifth-order KhRB located between the coordinates 36°55'28"–37°47'01"N latitudes and 42°34'44"–43°29'5"E longitudes, along the border between Iraq and Turkey. It encompasses an area of 3500 km² includes the Zakho city and Sarsing and Batufa towns (Fig. 1). Al-Khabur River and its tributaries store significant precipitation and feed the Mosul Reservoir to the southwest.

The KhRB suffers from considerable seasonal differences in rainfall, evaporation, and temperature. It experiencing dry summer and rainy winter. Data from the Zakho meteorological station (2002–2007) shows that about 586 mm falls, yearly. It occurs between October and May. The maximum average monthly rainfall having an average amount of 134.3 mm, occurs in January. July's maximum average monthly evaporation rate is recorded (354.7 mm). The monthly average temperature varies from 8.47 °C to 33.96 °C in January and July, respectively. The maximum monthly temperature in average of 41.31 °C was registered in July and the minimum average monthly temperature was measured in January (4.17 °C; Fig. 2).

3 Methodology

3.1 Data and Software

We mosaicked four scenes of DEM collected by SRTM, having 1 arc-second global (~30 m) resolution [28]. The use of SRTM allows multiple dataset comparisons through geocoding (orthorectification) [12]. The neighborhood resampling method was used to resample the DEM after the reprojection to UTM coordinate system.

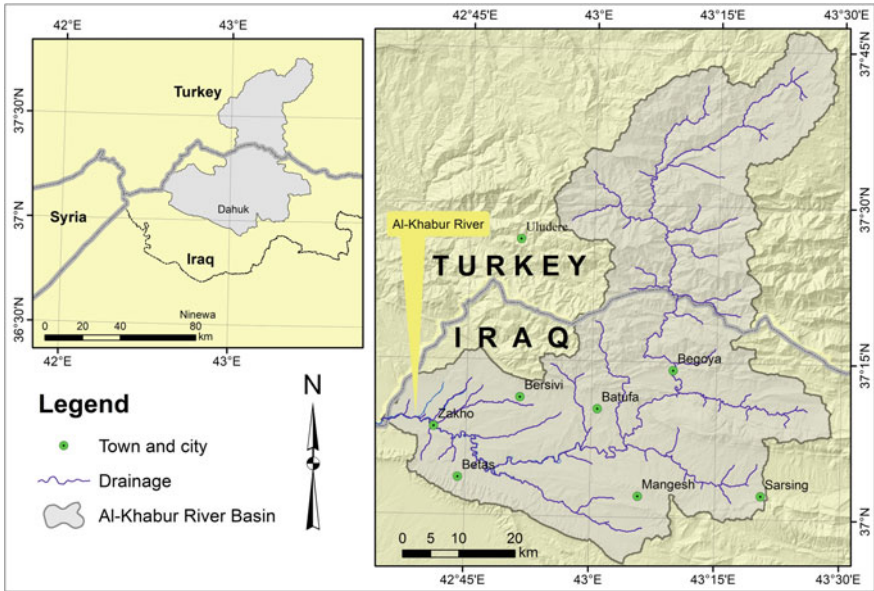


Fig. 1 Location of the KhRB

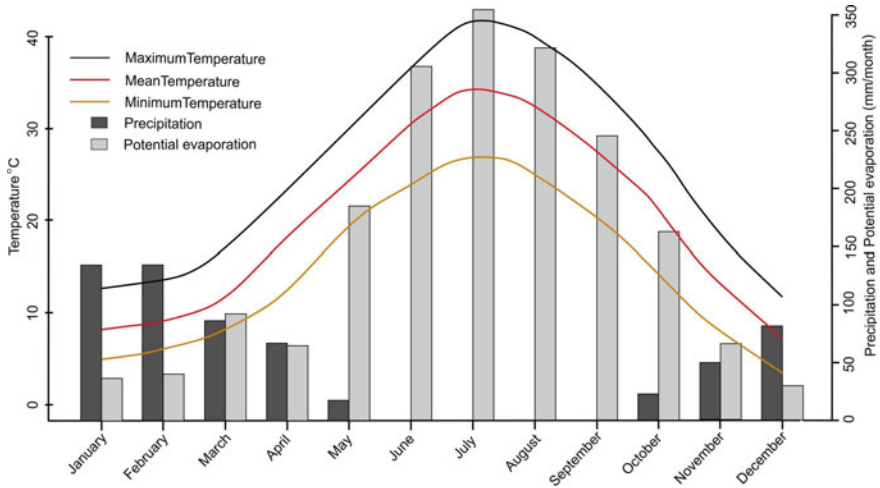


Fig. 2 The variation in climate parameters (rainfall, evaporation, temperature in the Zakho meteorological station collected from 2002 to 2007 [27])

The DEM is utilized to calculate the slope gradient, FA, and drainage network. The drainage network is delineated within TecDEM 2.2, a MATLAB based toolbox. Besides the stream order and delineating the catchment area, TecDEM can extract the geomorphological indices [29–31].

We used 3B43-V7 of the TRMM data to prepare the precipitation map of the KhRB. The TRMM [32] was a shared space project between NASA and the JAXA. TRMM (3B43-V7) collects monthly rainfall with a $0.25^\circ \times 0.25^\circ$ resolution [33].

The HWSO is the outcome of a collaboration between the FAO, CAS, IASA, ISRIC, and JRC. The HWSO [34] is used to prepare K factor. Its pixel size is 30 arc-second (~ 1 km). We resampled all spatial resolutions of each input raster to be 30 m.

Landsat image having a spatial resolution of 30 m, acquired on August 26, 2019, from the USGS is obtained without any charge from the EROS center. We selected one scene with excellent quality and less than 12.5% cloud cover for this study. These Landsat imageries (Level 1 T format) used in this research are geo-referenced and orthorectified. The KhRB is located in the Zone 38 N. All input parameters are of UTM projection and WGS 1984 datum.

We have used GIS and remote sensing to perform the RUSLE model by estimating the soil erosion process in KhRB due to their capability to deal with enormous data from different sources [35]. All GIS functions (e.g., slope, interpolation, convert TRMM “NetCDF” to tiff extension, map algebra, and built base map, and final maps) were conducted using ArcGIS 10.6 [36]. Landsat data were processed using ENVI software for data processing (data preparation, Boolean algebra, radiometric calibration, and unsupervised classification (NDVI)). Finally, statistical processes were made applying the Rstudio scripts.

3.2 RUSLE Model Description

The RUSLE has been broadly utilized to assess the yearly SoL [37, 38]. It is one of the robust, efficient, and simple models that addresses erosion problems through inserting the improved methods for calculating the soil erosion factors [37, 39]. The RUSLE is calculated by Eq. 1 [24]:

$$AE = R.K.LS.C.P \quad (1)$$

where, AE is the actual erosion (yearly rate of the SoL ($t^{-1} \cdot ha^{-1} \cdot y^{-1}$)), R is rainfall erosivity factor ($MJ \cdot mm \cdot ha^{-1} \cdot ha^{-1} \cdot y^{-1}$), K is the soil erodibility factor ($MJ \cdot mm \cdot ha^{-1} \cdot ha^{-1} \cdot y^{-1}$). LS is the slope length and slope-steepness factor (dimensionless). C is the cover management factor (dimensionless) and P is the support practice factor (dimensionless). The used data are obtained from various resolutions and sources within raster formats. The SoL and its parameters were estimated utilizing

raster formats within a GIS environment. The adapted methodology is explained as follows.

3.2.1 Rainfall and Runoff Erosivity I Factor

The R factor indicates the ability of precipitation to induce soil erosion [40]. Detailed and continuous rainfall data is needed to assess the R factor [23, 38]. The R factor quantifies the influence of the precipitation on soil erosion [41] as there is a direct relationship between precipitation and soil detachment [42].

This chapter used annual mean rainfall (mm) of the TRMM to investigate the R factor. Until now, the TRMM is the most satellite data of the precipitation applied to estimate the R factor; because of its appropriated spatial and temporal resolution compared with other satellite-borne data [43]. Therefore, we computed the annual rainfall mean applying the TRMM 3B43-V7 data collected monthly between September 2002 and August 2017. Thirty cells have been appointed covering the KhrB areas. These pixels have been converted to vector (points), thereafter, interpolated applying an IDW technique obtaining continuous coverage.

Several investigations have been tried to estimate the precipitation erosivity factor using long-term data. [44] suggested an Eq. (2) to calculate the precipitation erosivity depends on the linear relationships between the annual precipitation and the computed E of the storm multiplied by its maximum I30 for Damodar valley area [45].

$$R = 81.5 + 0.38P_A \tag{2}$$

where the *R* is the runoff erosivity factor in MJ. Mm. ha⁻¹. Ha⁻¹. Y⁻¹ and *P_A* is the average annual precipitation in mm.

3.2.2 Soil Erodibility (K) Factor

Water-borne erosion has different influences on various types of soil. The K factor is described as the potential soil sensitivity to the erosion caused by precipitation and runoff [43, 46]. Wide ranges of chemical and physical properties of soil affect soil susceptibility, all should be considered when applying the RUSLE equation. These properties of the soil could be determined quantitatively at laboratories [47]. K factor depends mostly on soil texture and the OM, which has an inverse relationship with the soil erodibility. Increasing OM reduces soil susceptibility to detachment [48]. The soil texture information within the HWS dataset were used to compute the OM in a certain region. Table 1 [49] was used to compute the K- factors. According to [50], we converted the K factor in Table 1 from US Customary to S1 Units by multiplying the K factor by 0.131.

Table 1 Estimating soil erodibility (k) based on the content of the soil texture and organic material (modified after [49])

Textural class	Soil Composition %			Mean K (based on % organic material)	
	Sand	Silt	Clay	< 2%	≥ 2%
Clay	0–45	0–40	40–100	0.03144	0.02751
Sandy clay	45–65	0–20	35–55	0.0262	0.0262
Silty clay	0–20	40–60	40–60	0.03537	0.03406
Sand	86–100	0–14	0–10	0.00393	0.00131
Sandy loam	50–7–	0–50	0–20	0.01834	0.01572
Clay loam	20–45	15–52	27–40	0.04323	0.03668
Loam	23–52	28–50	7–27	0.04454	0.03406
Loamy sand	70–86	0–30	0–15	0.00655	0.00524
Sandy clay loam	45–80	0–28	20–35	0.0262	0.0262
Silty clay loam	0–20	40–73	27–40	0.04585	0.0393
Silt	0–20	88–100	0–12	0.05371	0.04847
Silty loam	20–50	74–88	0–27	0.05371	0.04847

[51] concluded that the OM includes 58% of carbon; therefore, the common factor has been estimated by applying the factor of 1.724, to the OC content (Eq. 3).

$$OM = 1.724 * OC \tag{3}$$

3.2.3 Slope Length and Slope-Steepness Factor (LS)

The LS factor reflects the vulnerability of erosion in soil to local topography. It is used to determine a landscape with different topography relief. It is represented by the combination of L and S factors and classified as the most difficult factors of the RUSLE [52, 53]. Several techniques have been suggested to estimate LS factor, such as [6, 23, 48, 54–57], which are summarized by [43]. We have used the L factor equation suggested by [54], according to the Eqs. (4–6).

We created the LS factor using the slope map (in percent) and the FA. We classified the slope catchment into four groups, which are < 1%, 1% –3%, 3% –5%, and ≥ 5% using ArcGIS.

$$L = \left(\frac{\lambda}{22.12848}\right)^m \tag{4}$$

$$m = \begin{cases} 0.2\theta < 1\% \\ 0.31\% \leq \theta < 3\% \\ 0.43\% \leq \theta < 5\% \\ 0.5\theta \geq 5\% \end{cases} \quad (5)$$

$$\lambda = FA * Ps \quad (6)$$

where L is normalized to the amount of the soil erosion on the slope length of 22.12848 m, λ is the L, FA is flow accumulation, Ps is the pixel size of DEM, m is a variable length-slope exponent, and θ represents the slope in percent.

We calculated the S factor by classifying the slope gradient (in percent) of the KhRB into three classes, less than 9%, 9% –18%, and greater than or equal to 18% (Eq. 7). We used Eq. (8) to estimate the LS factor.

$$S = \begin{cases} 10.8.\sin\theta + 0.03\theta < 9\% \\ 16.8.\sin\theta - 0.059\% \leq \theta < 18\% \\ 21.9.\sin\theta - 0.96\theta \geq 18\% \end{cases} \quad (7)$$

$$LS = L * S \quad (8)$$

where S represents the slope-steepness factor, θ represents the slope in percent, and LS represents the slope length and slope-steepness factor [58].

3.2.4 Cover and Management Factor (C)

The C factor is a significant dimensionless factor in the RUSLE model. It refers to the soil erosion amount associated with the VC. Therefore, the estimation of the VC is recognized as the most responsible aspect for evaluating the C factor [59].

In this research, we have used NDVI to characterize the C factor. To do that, the radiometric and atmospheric corrections were performed by applying the FLAASH model. The FLAASH model depends on a MODTRAN4 method to reduce the molecular absorption and particulate scattering, absorption, and adjacency effects to retrieve reflectance (at-surface) values (ρ) [60, 61]. We used the FLAASH model [62] to obtain the surface reflectance by performing Eq. (9).

$$\rho = \pi * L_{\lambda} * D^2 * (E_{sun,\lambda} * \cos(\theta))^{-1} \quad (9)$$

where L_{λ} -the radiance (at sensor), DN-the data digital number, ρ -the reflectance (from 0 to 1), D- sun-earth distance, θ - the solar zenith angle and $E_{sun,\lambda}$ - the solar spectral irradiance.

We computed the NDVI [63] after the converted DN of Landsat OLI imagery to ρ (Eq. 10). Then, the NDVI was applied to estimate the C factor by employing Eq. 11

[64–66].

$$NDVI = \frac{NIR - Red}{NIR + Red} \quad (10)$$

where *Red* and *NIR* of the Landsat-8 OLI are the reflectance of the interval 0.636 μm –0.673 μm (band 4) and the interval 0.851 μm –0.879 μm (band 5), respectively.

$$C = \text{Exp}\left[-\alpha * \frac{NDVI}{(\beta - NDVI)}\right] \quad (11)$$

where α , β are constants, which define the shape of the NDVI–C curve. We considered α , β to be equal to 2 and 1, respectively [64, 65].

3.2.5 Support Practice Factor Related to Slope Direction (P)

This factor represents the proportion of the SoL by a specific support practice to the corresponding loss with up and downslope [6, 37]. Due to the rare field data of the conservation practices in Al-KhRB, we have used the modified Eq. (12) suggested by [67] to estimate the amount of the P factor.

$$P = 0.2 + 0.003 * \theta \quad (12)$$

where, *P* is the Support practice factor, θ is the slope gradient in percent. By implementing the [67] equation, the P factor of flat pixels ($\theta = 0$) was found to be 0.2 (i.e., $P = 0.2 + 0.003 * 0$), and for the highest slope angle pixels ($\theta = 100$) it was 1 (i.e., $P = 0.2 + 0.003 * 100$).

For Using the natural breaks method, the RUSLE value model and its factors were divided into five groups (only the K factor was classified into three groups because the KhRB includes only three types of soil). The natural break method is one of the best used to classify the data within multi-ranges. It permits to decrease the within classes variance and maximizes the between classes variance [68]. Therefore, this method is helpful when the RUSLE and its factors histogram show distinct breaks.

4 Estimation of RUSLE and Its Parameters

4.1 R Factor

We evaluated the appropriateness of TRMM data in the KhRB. We compared the in-situ rainfall collected by the Zakho meteorological station and the corresponding pixel

of the TRMM data. The rainfall data for sixty-two months were used, as measured between September 2002 and December 2007. A strong linear relationship has been shown in Fig. 3 between the monthly in-situ rainfall and TRMM dataset, where the R^2 is 0.853, and the p-value is rejecting the null hypothesis. Rainfall ranges between $562.85 \text{ mm yr}^{-1}$ and 785 mm yr^{-1} for the southern and the northern parts of the KhRB, respectively.

The amount of the R factor in the KhRB ranges between 2965.8 and 393 $\text{MJ. mm. ha}^{-1} \cdot \text{ha}^{-1} \cdot \text{y}^{-1}$, while the mean value of the factor was $354 \text{ MJ. mm. ha}^{-1} \cdot \text{ha}^{-1} \cdot \text{y}^{-1}$. Figure 4A shows the R factor map in the KhRB. The map is classified into five classes.

It is noted that the R factor in the southern part of the KhRB are lower than those in the northern part, where the area is mountainous.

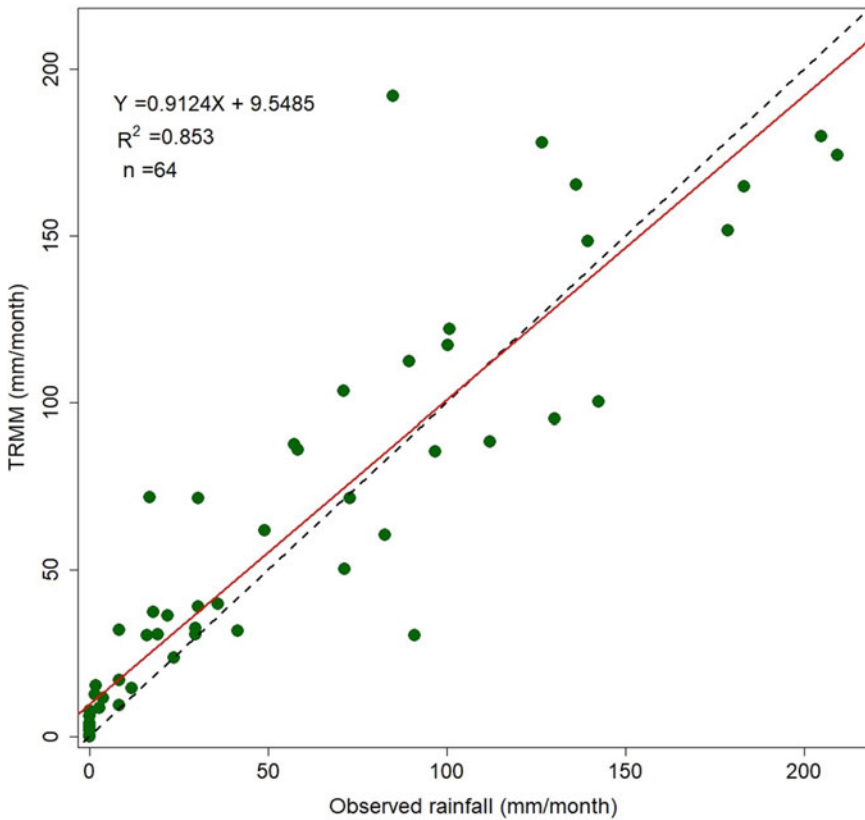


Fig. 3 Comparison between the in-situ rainfall data Zakho meteorological station and the corresponding pixel of the TRMM data between September 2002- December 2007

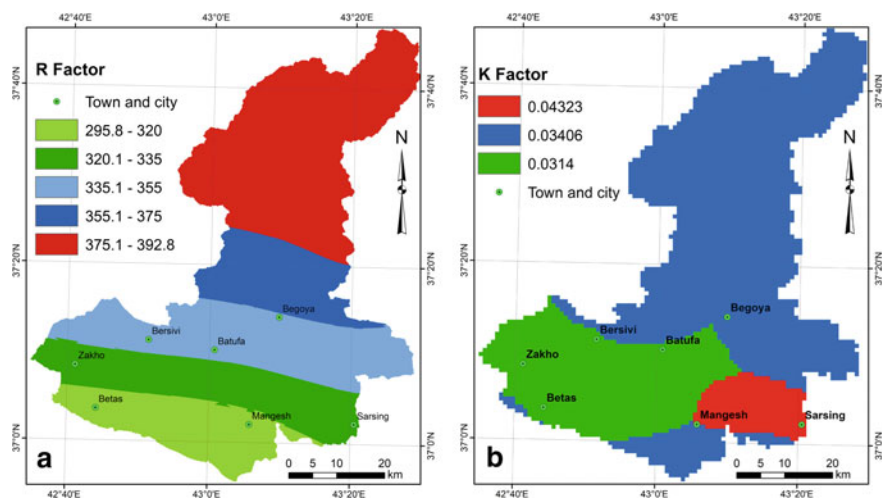


Fig. 4 (A) R factor, and (B) K factor maps

Table 2 Soil type, soil texture, organic material content, and estimated K factor

Soil type	Texture class	Sand %	Silt %	Clay %	OC %	OM	K factor
Lithosols	Loam	43	34	23	1.4	2.4136	0.03406
Calcic Xerosols	Clay loam	40	37	23	0.56	0.96544	0.04323
Chromic Vertisols	Clay	16	29	55	0.75	1.293	0.03144

4.2 K Factor

The K factor map in the KhRB is shown in Fig. 4B. The minimum soil erodibility is $0.023 \text{ t}\cdot\text{ha}\cdot\text{h}\cdot\text{ha}^{-1}\cdot\text{MJ}^{-1}\cdot\text{mm}^{-1}$ in the southwestern part of the KhRB, while the maximum soil erodibility is $0.063 \text{ t}\cdot\text{ha}\cdot\text{h}\cdot\text{ha}^{-1}\cdot\text{MJ}^{-1}\cdot\text{mm}^{-1}$ in the northern and south-eastern parts of the KhRB. Three soil groups are present in the study area: Lithosols, Calcic Xerosols, and Chromic Vertisols. The texture description and the K factor for these types of soils are presented in Table 2 and Fig. 4B.

4.3 LS Factor

Al-Khabur River Basin includes steep slopes where the highest slope is 77° , and the average slope is 17.5° . Almost all of the high slopes are located in the midstream and upstream of the KhRB. As a result of the differences in FA and slope gradient distribution, the LS factor ranges between 0 and 1619.6. The average value is 12.05, and a standard deviation is 12.74 (Fig. 5A). The KhRB, exhibited moderate LS factor

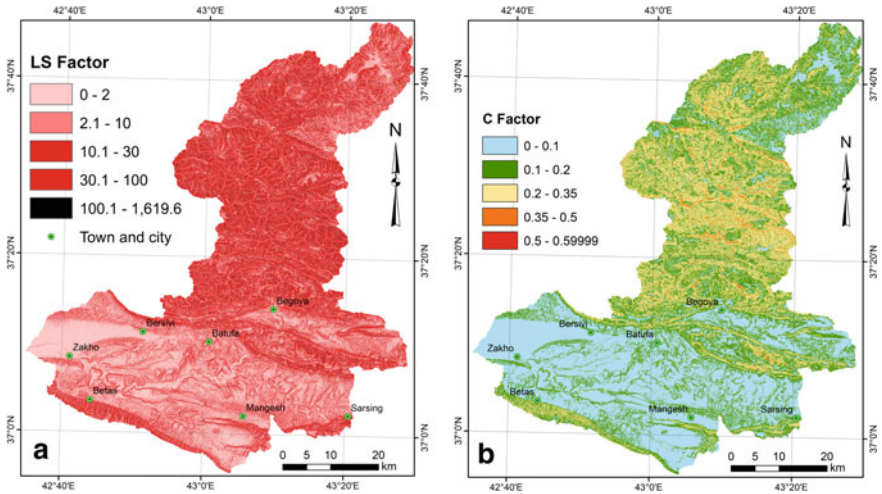


Fig. 5 (A) the LS factor map, and (B) the C factor maps-

values, however these values drop to less than 10 in the areas near the downstream of the KhRB.

4.4 C Factor

We classified the values of the C factor range between 0.0 and 0.5999 (Fig. 5 B) and into five classes with frequency levels of 0.2, 0.28, 0.35, 0.45, 0.55, and 0.87. The VC value of the KhRB is < 10%, mainly existed in the southern part of the KhRB. Therefore, the very low (<0.1) values of the C factor (Fig. 5B) are dominant. On the other hand, the very high (>0.5) values of the C factor mostly exist in the central part of the KhRB. [69] stated that the regions with high C factor values, usually, are represented by exposed rocks, where the NDVI values are comparatively low.

4.5 P Factor

The values of the P factor in the KhRB range between 0 and 1 (Fig. 6 A). The low values of the P factor represent good conservation practice, whereas the high values represent poor conservation practice [38]. The P factor has been classified into five classes. The thresholds of these classes are 0, 0.12, 0.22, 0.35, 0.5, and 1. The high and very high (0.35–1) values of P factor mostly exist in the central part of the KhRB. Whereas the low and very low values (0–0.22) of the P factor mainly exist in the southern and northern parts of the KhRB (Fig. 6 A).

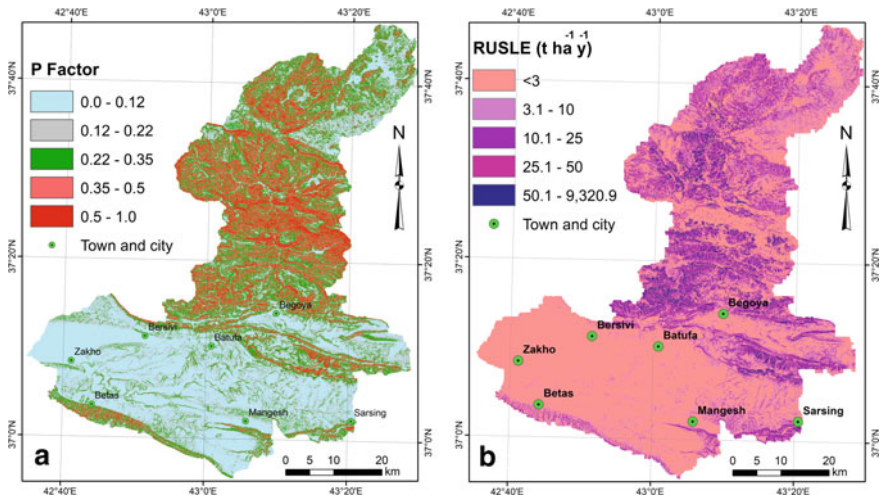


Fig. 6 (A) the P factor map, and (B) the soil erosion map of the KhRB in $t^{-1} \cdot ha^{-1} \cdot y^{-1}$

4.6 Prediction of Soil Erosion

We integrated the parameters of the RUSLE equation in ArcGIS for the estimation of the mean annual SoL in the KhRB (Fig. 6B). The SoL for each pixel has been computed (in $t^{-1} \cdot ha^{-1} \cdot y^{-1}$) by multiplying all RUSLE parameters. Generally, it is difficult to validate spatial soil loss estimation [70]. Few researches have been done to assess the accuracy of the SoL estimation. Furthermore, according to [71], almost all offered results are outlet based, such as sediments deposited in the reservoirs or those load by rivers. The estimated average of the annual SoL in the KhRB was $11.16 t^{-1} \cdot ha^{-1} \cdot y^{-1}$. The maximum and minimum annual SoL were $0 t^{-1} \cdot ha^{-1} \cdot y^{-1}$ and $3617.6 t^{-1} \cdot ha^{-1} \cdot y^{-1}$, respectively. The sum of the annual SoL was $31,237,283.358 t^{-1} \cdot ha^{-1} \cdot y^{-1}$. The low and very low ($<10 t^{-1} \cdot ha^{-1} \cdot y^{-1}$) values of the annual SoL mainly exist in the southern and northeastern of the KhRB. The high and very high ($>10 t^{-1} \cdot ha^{-1} \cdot y^{-1}$) values of the annual SoL mainly exist in the central and northern zones of the KhRB (Fig. 6B). Less than 6.19% of the KhRB suffers from very high annual SoL ($>50 t^{-1} \cdot ha^{-1} \cdot y^{-1}$). In fact, the main factor that controls the annual SoL is the LS factor, which means that the main proxy is the slope gradient [14] (Fig. 5A). The second factor affecting the annual SoL is the R factor related to the precipitation (Fig. 4A). Therefore, the annual SoL values are increased in rugged areas in the central and northern zones of the KhRB.

The suggested dams might be influenced by siltation from the upstream areas leading to decreased planned life. The suggested check dams will prolong the lives of proposed dams (Fig. 7) and increase the Mosul dam's useful life to the southwest of the KhRB. [72] have performed a study to select suitable dam sites in the KhRB. These dam sites will be affected by sediment accumulation from the upstream where there is no dam constructed. We suggested a dam site to reduce the SoL in the

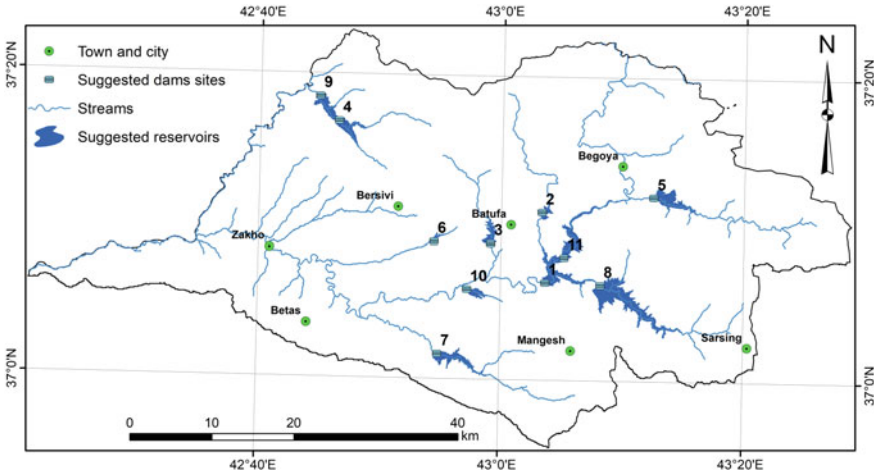


Fig. 7 Suggested dam sites in the KhRB (after [72])

upstream area (Fig. 8). Annually, this check dam will reduce ~80.53% of the total amounts of the annual SoL in the KhRB. The suggested check dam will definitely reduce the planned age of the selected dams' numbers 1 and 11(Fig. 7), in addition to the Mosul dam. Thus, the RUSLE model application results will help in the dam's conservation and developing methods to reduce soil erosion in this area.

5 Conclusions

This chapter is a robust example of integrating remote sensing imageries and GIS for the prediction of erosion in soils and degradation in lands. We selected the KhRB, that is one of the Tigris River tributaries to compute the RUSLE equation aiming to estimate the amount of the annual SoL. For the RUSLE model production, several parameters have been used: Factor of R, factor of K, factor of L, factor of S, factor of C, and factor of P. Results show that the average of the annual SoL within the KhRB was $\sim 11.16 \text{ t}^{-1} \cdot \text{ha}^{-1} \cdot \text{y}^{-1}$. The most influential factors to increase the soil loss are LS and C. These factors represent a vital and dominant role in showing the distribution pattern of the soil erosion areas, particularly those highly affected by the soil erosion. The minimum rate of the soil erosion values is concentrated in the southern and northeastern zones of the KhRB, while the maximum rate of the soil erosion values is located in the central and northern zones of the KhRB, which shows a clear correlation with the areas of steep and rugged topography and the increase of annual rainfall in addition to the areas with decreased VC values. There is an area with higher elevation, higher LS factor and higher precipitation; this area is more vulnerable to the soil erosion. The implementation of the RUSLE equation and the

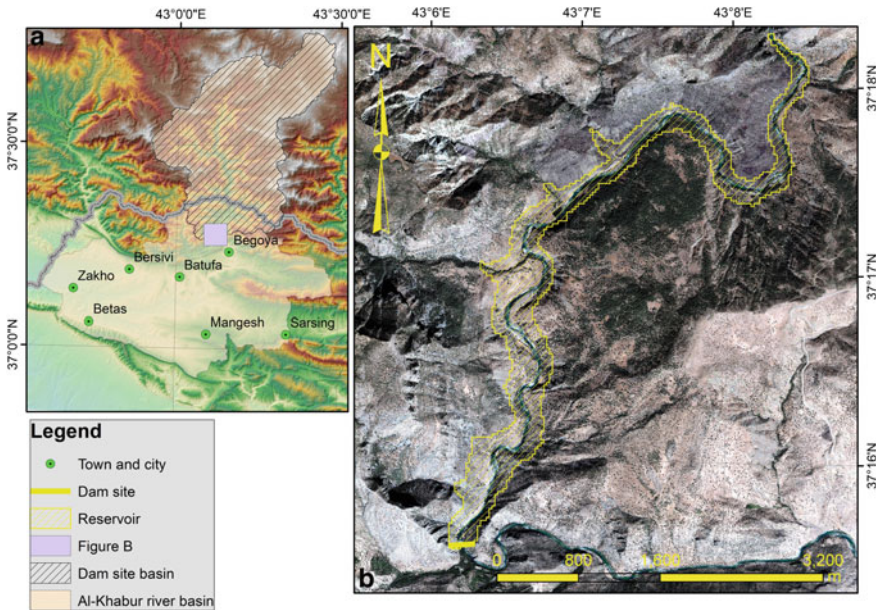


Fig. 8 Suggested dam for the upstream area of the KhRB; note the dam’s location and the depth of the valley that serve dam construction

prediction of the SoL map are fundamental steps in the management and perspective for sustainable land use of watersheds.

6 Recommendations

The acquired valuable and significant data from this study, encourage further studies to ensure the safety of the existing dams in Iraq. First, as the siltation problem is concerned, we recommended studying the annual SoL that will reach the planned dams in Iraq (which were recommended by the previous works) to secure their construction efficiency for the future. The future studies might include preparing a study to measure the total amount of the siltation that will affect dams’ planned life and accordingly to select the most suitable locations for dams. To maintain the Mosul Dam’s safety, we highly recommend studying the annual SoL within the Tigris River, apart from the current study considering the limits of the basin starting from the last constructed embankment on the river within Turkey. However, it is worth estimating the annual SoL for the big reservoirs in Iraq, where most of the existing dams were built more than 40 years ago. The annual SoL in the Greater Zab River and the Lower Zab River downstream from Dukan Dam is important to be investigated to keep the safety of Samarra Dam that is constructed on the Tigris

River downstream from the merging point of both mentioned rivers with the Tigris River. In addition, estimating the annual SoL in the Lower Zab, Sirwan (Diyala), and Euphrates rivers in order to keep the safety of Dukan, Derbendikhan and Himreen, and Hadith, dams, respectively. The same study will enhance the performance of the constructed barrages on the Tigris and Euphrates rivers, such as Kut Barrage, and Al-Hindiya Barrage, both barrages exist on the southern parts of the Tigris and Euphrates rivers.

Acknowledgements We highly appreciate the USGS in providing Landsat images and DEM. We are very thankful to the General Survey Authority and Ministry of Planning/Iraq for providing the used data in the current research. Assistance provided by FAO, CAS, IIASA, ISRIC, and JRC for supplying Harmonized world soil database (HWSD) is greatly appreciated. A big thanks to NASA and the JAXA for providing TRMM data. The second author would like to thank CARA for supporting his research.

References

1. Press F, Siever R, Grotzinger J, Jordan TH (2004) *Understanding earth*, Freeman WH, ISBN 9780716796176
2. Roy P (2019) Application of USLE in a GIS environment to estimate soil erosion in the Irga watershed, Jharkhand, India. *Phys Geogr*40, 361–383, <https://doi.org/10.1080/02723646.2018.1550301>
3. Blanco-Canqui H, Lal R (2008) *Principles of soil conservation and management*; Springer Netherlands, ISBN 9781402087097
4. Toy TJ, Foster GR, Renard KG (2002) *Soil erosion: Processes, Prediction, Measurement, and Control*; Wiley, ISBN 9780471383697
5. Montanarella L, Pennock D, McKenzie N, Badraoui M, Chude V, Baptista I, Mamo T, Yemefack M, Aulakh M, Yagi K, et al.(2016) World's soils are under threat. 2, <https://doi.org/10.5194/soild-2-1263-2015>
6. Renard KG, Foster GR, Weesies GA, McCool DK, Yoder DC (1997) *Others predicting soil erosion by water: a guide to conservation planning with the revised universal soil loss equation (RUSLE)*; United States Department of Agriculture Washington, DC, Vol. 703
7. Webster R, Morgan RPC (2005) *Soil erosion and conservation*, 3rd edition. Blackwell Publishing, Oxford, 2005. x + 304 pp. £29.95, paperback. ISBN 1–4051–1781–8. *Eur J Soil Sci* 56, 686, <https://doi.org/10.1111/j.1365-2389.2005.0756f.x>
8. Kumar S (2019) Geospatial approach in modeling soil erosion processes in predicting soil erosion and nutrient loss in hilly and mountainous landscape. pp. 355–380 ISBN 978–981–13–2127–6
9. Obaid AK, Allen MB (2019) Landscape expressions of tectonics in the Zagros fold-and-thrust belt. *Tectonophysics*
10. Othman AA, Gloaguen R (2013) River courses affected by landslides and implications for hazard assessment: A high resolution remote sensing case study in ne iraq-w iran. *Remote Sens* 5:1024–1044. <https://doi.org/10.3390/rs5031024>
11. Othman AA, Gloaguen R (2013) River courses affected by landslides and implications for hazard assessment: A high resolution remote sensing case study in NE Iraq–W Iran. *Remote Sens* 5:1024–1044. <https://doi.org/10.3390/rs5031024>
12. Othman AA, Al- Maamar AF, Al-Manmi DAM, Liesenberg V, Hasan S, Al-Saady YI, Shihab AT, Khwedim K (2019) Application of DInSAR-PSI technology for deformation monitoring of the mosul dam, Iraq. *Remote Sens*

13. Al-Saady Y, Al-Suhail Q, Al-Tawash B, Othman A (2016) Drainage network extraction and morphometric analysis using remote sensing and GIS mapping techniques (Lesser Zab River Basin, Iraq and Iran). *Environ earth Sci*, 75
14. Thornes JB (2007) Modelling soil erosion by grazing: recent developments and new approaches. *Geogr Res* 45:13–26. <https://doi.org/10.1111/j.1745-5871.2007.00426.x>
15. Issa I (2015) Sedimentological and hydrological investigation of mosul dam reservoir, lulea university of technology
16. Nissen E, Ghods A, Karasözen E, Elliott JR, Barnhart WD, Bergman EA, Hayes GP, Jamal-Reyhani M, Nematı M, Tan F, et al. (2019) The 12 November 2017 M w 7.3 Ezgeleh-Sarpolzahab (Iran) earthquake and active tectonics of the lurestan Arc. *J Geophys Res Solid Earth*, 124, 2124–2152, <https://doi.org/10.1029/2018JB016221>.
17. Issa IE, Al-Ansari N, Knutsson S, (2013) Sedimentation and new operational curves for Mosul Dam, Iraq. *Hydrol Sci J*, 58, 1456–1466, <https://doi.org/10.1080/00262667.2013.789138>
18. Keizer J, Djuma H, Prasuhn V (2016) Soil erosion by water. In: Stolte et al. (eds.), *Soil threats in europe—status, methods, drivers and effects on ecosystem services*. Luxembourg
19. Borrelli P, Robinson DA, Fleischer LR, Lugato E, Ballabio C, Alewell C, Meusburger K, Modugno S, Schütt B, Ferro V, et al. (2017) An assessment of the global impact of 21st century land use change on soil erosion. *Nat Commun*, 8, <https://doi.org/10.1038/s41467-017-02142-7>
20. Amundson R, Berhe AA, Hoppmans JW, Olson C, Szein AE, Sparks DL (2015) Soil and human security in the 21st century. *Science*, (80) 348, 1261071
21. Foley, J (2017) Living by the lessons of the planet. *Science* (80), 356, 251–252, <https://doi.org/10.1126/science.aal4863>
22. Oldeman LR (1992) Global extent of soil degradation. The Netherlands
23. Wischmeier WH, Smith DD (1978) Predicting rainfall erosion losses: a guide to conservation planning [USA]. United States Dept Agric Agric Handb
24. Renard KG, Foster GR, Weesies GA, Porter JP (1991) RUSLE: revised universal soil loss equation. *J Soil Water Conserv* 46:30–33
25. Boardman J (2006) Soil erosion science: Reflections on the limitations of current approaches. *CATENA* 68:73–86
26. Benavidez R, Jackson B, Maxwell D, Norton K (2018) A review of the (Revised) Universal Soil Loss Equation ((R) USLE): with a view to increasing its global applicability and improving soil loss estimates. *Hydrol Earth Syst Sci* 22:6059–6086
27. General-Directorate-of-Research-and-Agricultural-Extension Climate data. 2016
28. Rabus B, Eineder M, Roth A, Bamler R (2003) The shuttle radar topography mission - A new class of digital elevation models acquired by spaceborne radar. *ISPRS J Photogramm Remote Sens* 57:241–262. [https://doi.org/10.1016/S0924-2716\(02\)00124-7](https://doi.org/10.1016/S0924-2716(02)00124-7)
29. Andreani L, Gloaguen R, Shahzad FA (2014) New set of MATLAB functions (TecDEM toolbox) to analyze erosional stages in landscapes and base-level changes in river profiles. *Geophys. Res. Abstr.* 16
30. Shahzad F, Gloaguen R (2011) TecDEM: A MATLAB based toolbox for tectonic geomorphology, Part 2: Surface dynamics and basin analysis. *Comput Geosci* 37:261–271. <https://doi.org/10.1016/j.cageo.2010.06.009>
31. Shahzad F, Gloaguen R (2011) TecDEM: A MATLAB based toolbox for tectonic geomorphology, Part 1: Drainage network preprocessing and stream profile analysis. *Comput Geosci* 37:250–260. <https://doi.org/10.1016/j.cageo.2010.06.008>
32. GSFC_DAAC Tropical Rainfall Measurement Mission Project (TRMM ;3B43 V7)
33. Kummerow C, Barnes W, Kozu T, Shiue J, Simpson J (1998) The tropical rainfall measuring mission (TRMM) sensor package. *J Atmos Ocean Technol* 15:809–817. [https://doi.org/10.1175/1520-0426\(1998\)015%3c0809:TTRMMT%3e2.0.CO;2](https://doi.org/10.1175/1520-0426(1998)015%3c0809:TTRMMT%3e2.0.CO;2)
34. Nachtergaele F, van Velthuizen H, van Engelen V, Fischer G, Jones A, Montanarella L, Petri M, Prieler S, Teixeira E, Shi X (2012) Harmonized world soil database (version 1.2). Fao, Rome, Italy Iiasa, Laxenburg, Austria, 1–50
35. Akintorinwa OJ, Okoro OV (2019) Combine electrical resistivity method and multi-criteria GIS-based modeling for landfill site selection in the Southwestern Nigeria. *Environ Earth Sci*, 78, <https://doi.org/10.1007/s12665-019-8153-z>

36. ESRI ArcGIS Desktop: Release 10 2011
37. Prasannakumar V, Vijith H, Abinod S, Geetha N (2012) Estimation of soil erosion risk within a small mountainous sub-watershed in Kerala, India, using Revised Universal Soil Loss Equation (RUSLE) and geo-information technology. *Geosci Front* 3:209–215. <https://doi.org/10.1016/j.gsf.2011.11.003>
38. Ganasri BP, Ramesh H (2016) Assessment of soil erosion by RUSLE model using remote sensing and GIS—A case study of Nethravathi Basin. *Geosci Front* 7:953–961. <https://doi.org/10.1016/j.gsf.2015.10.007>
39. Mondal A, Khare D, Kundu S, Mukherjee S, Mukhopadhyay A, Mondal S (2017) Uncertainty of soil erosion modelling using open source high resolution and aggregated DEMs. *Geosci Front* 8:425–436. <https://doi.org/10.1016/j.gsf.2016.03.004>
40. Zeng C, Wang S, Bai X, Li Y, Tian Y, Li Y, Wu L, Luo G (2017) Soil erosion evolution and spatial correlation analysis in a typical karst geomorphology using RUSLE with GIS. *Solid Earth* 8:721–736. <https://doi.org/10.5194/se-8-721-2017>
41. Kayet N, Pathak K, Chakrabarty A, Sahoo S (2018) Evaluation of soil loss estimation using the RUSLE model and SCS-CN method in hillslope mining areas. *Int Soil Water Conserv Res* 6:31–42. <https://doi.org/10.1016/j.iswcr.2017.11.002>
42. Ma X, He Y, Xu J, Noordwijk M, Lu X (2014) Spatial and temporal variation in rainfall erosivity in a Himalayan watershed. *CATENA* 121:248–259
43. Phinzi K, Ngetar NS (2019) The assessment of water-borne erosion at catchment level using GIS-based RUSLE and remote sensing: A review. *Int Soil Water Conserv Res* 7:27–46. <https://doi.org/10.1016/j.iswcr.2018.12.002>
44. Babu R, Dhyani BL, Kumar N (2004) Assessment of erodibility status and refined iso-erodent map of India. *Indian J Soil Conserv* 32:171–177
45. Karan SK, Ghosh S, Samadder SR (2019) Identification of spatially distributed hotspots for soil loss and erosion potential in mining areas of Upper Damodar Basin—India. *CATENA* 182:104144. <https://doi.org/10.1016/j.catena.2019.104144>
46. Thomas J (2017) *Frontispiece BT—Nineteenth-Century Illustration and the Digital: Studies in Word and Image*. In: Thomas J, Ed. Springer International Publishing: Cham, pp. 1–14 ISBN 978-3-319-58148-4.
47. Ge Y, Thomasson JA, Sui R (2011) Remote sensing of soil properties in precision agriculture: A review. *Front Earth Sci* 5:229–238. <https://doi.org/10.1007/s11707-011-0175-0>
48. Zerihun M, Mohammedyasin MS, Sewnet D, Adem AA, Lakew M (2018) Assessment of soil erosion using RUSLE, GIS and remote sensing in NW Ethiopia. *Geoderma Reg* 12:83–90. <https://doi.org/10.1016/j.geodrs.2018.01.002>
49. Stewart BA, Woolhiser DA, Wischmeier WH, Caro JH, Frere MH (1975) Control of water pollution from cropland. Washington, DC
50. Foster GR, McCool DK, Renard KG, Moldenhauer WC (1981) Conversion of the universal soil loss equation to SI metric units. *J Soil Water Conserv*, 36, 355 LP–359
51. Pribyl DW (2010) A critical review of the conventional SOC to SOM conversion factor. *Geoderma* 156:75–83. <https://doi.org/10.1016/j.geoderma.2010.02.003>
52. Bircher P, Liniger HP, Prasuhn V (2019) Comparing different multiple flow algorithms to calculate RUSLE factors of slope length (L) and slope steepness (S) in Switzerland. *Geomorphology* 346:106850. <https://doi.org/10.1016/j.geomorph.2019.106850>
53. Nasir N, Selvakumar R (2018) Influence of land use changes on spatial erosion pattern, a time series analysis using RUSLE and GIS: The cases of Ambuliyar sub-basin, India. *Acta Geophys*, 66, 1121–1130, <https://doi.org/10.1007/s11600-018-0186-2>
54. Moore ID, Burch GJ (1986) Physical Basis of the Length-slope Factor in the Universal Soil Loss Equation I. *Soil Sci Soc Am J* 50:1294–1298. <https://doi.org/10.2136/sssaj1986.03615995005000050042x>
55. Desmet PJJ, Govers G (1996) A GIS procedure for automatically calculating the USLE LS factor on topographically complex landscape units. *J Soil Water Conserv* 51:427–433
56. Mitasova H, Hofierka J, Zlocha M, Iverson LR (1996) Modelling topographic potential for erosion and deposition using GIS. *Int J Geogr Inf Syst* 10:629–641. <https://doi.org/10.1080/02693799608902101>

57. Wilson JP, Gallant JC (2000) *Terrain Analysis: Principles and Applications* 4:479
58. Li Y, Qi S, Liang B, Ma J, Cheng B, Ma C, Qiu Y, Chen Q (2019) Dangerous degree forecast of soil loss on highway slopes in mountainous areas of the Yunnan-Guizhou Plateau (China) using the Revised Universal Soil Loss Equation. *Nat Hazards Earth Syst Sci* 19:757–774. <https://doi.org/10.5194/nhess-19-757-2019>
59. Pal SC, Chakraborty R (2019) Simulating the impact of climate change on soil erosion in subtropical monsoon dominated watershed based on RUSLE, SCS runoff and MIROC5 climatic model. *Adv Sp Res* 64:352–377. <https://doi.org/10.1016/j.asr.2019.04.033>
60. Felde GW, Anderson GP, Cooley TW, Matthew MW, Adler-Golden SM, Berk A, Lee J (2003) Analysis of Hyperion data with the FLAASH atmospheric correction algorithm. In *Proceedings of the Geoscience and Remote Sensing Symposium, 2003. IGARSS '03. Proceedings. 2003 IEEE International; 2003; Vol. 1*, pp. 90–92
61. Liesenberg V, Gloaguen R (2013) Evaluating SAR polarization modes at L-band for forest classification purposes in Eastern Amazon, Brazil. *Int J Appl Earth Obs Geoinf* 21:122–135. <https://doi.org/10.1016/j.jag.2012.08.016>
62. Abrams M, Hook S (2002) *ASTER User Handbook; Version 2.*; Jet Propulsion Laboratory/California Institute of Technology: Pasadena, CA 91109
63. Rouse JW, Haas RH, Schelle JA, Deering DW (1974) NASA/GSFC Monitoring the vernal advancement or retrogradation of natural vegetation; Greenbelt, MD
64. Chandramani L, Oinam B (2020) Soil loss assessment in imphal river watershed, Manipur, North-East India: A Spatio-Temporal approach BT—Advances in water resources engineering and management. AlKhaddar R, Singh RK, Dutta S, Kumari M, Eds. Springer Singapore: Singapore, pp. 81–101
65. Durigon VL, Carvalho DF, Antunes MAH, Oliveira PTS, Fernandes MM (2014) NDVI time series for monitoring RUSLE cover management factor in a tropical watershed. *Int J Remote Sens* 35:441–453. <https://doi.org/10.1080/01431161.2013.871081>
66. Nyeshheja EM, Chen X, El-Tantawi AM, Karamage F, Mupenzi C, Nsengiyumva JB (2019) Soil erosion assessment using RUSLE model in the Congo Nile Ridge region of Rwanda. *Phys Geogr* 40:339–360. <https://doi.org/10.1080/02723646.2018.1541706>
67. Othman AA, Obaid AK, Amin Al-Manmi DAM, Al-Maamar AF, Hasan SE, Liesenberg V, Shihab AT, Al-Saady YI (2021) New insight on soil loss estimation in the northwestern region of the Zagros fold and Thrust Belt. *ISPRS Int J Geo-Information*, 10, 1–24, <https://doi.org/10.3390/ijgi10020059>
68. Jenks GF (1967) The data model concept in statistical mapping. *Int Yearb Cartogr* 7:186–190
69. Thomas J, Joseph S, Thirivikramji KP (2018) Assessment of soil erosion in a tropical mountain river basin of the southern Western Ghats, India using RUSLE and GIS. *Geosci Front* 9:893–906. <https://doi.org/10.1016/j.gsf.2017.05.011>
70. Gobin A, Jones R, Kirkby M, Campling P, Govers G, Kosmas C, Gentile AR (2004) Indicators for pan-European assessment and monitoring of soil erosion by water. *Environ Sci Policy* 7:25–38. <https://doi.org/10.1016/j.envsci.2003.09.004>
71. Prasuhn V, Liniger H, Gisler S, Herweg K, Candinas A, Clément J-P (2013) A high-resolution soil erosion risk map of Switzerland as strategic policy support system. *Land Use Policy* 32:281–291. <https://doi.org/10.1016/j.landusepol.2012.11.006>
72. Othman AA, Al-Maamar AF, Al-Manmi DAM, Veraldo L, Hasan SE, Obaid AK, Al-Quraishi AMF (2020) GIS-based modeling for selection of dam sites in the Kurdistan Region, Iraq. *ISPRS Int. J. Geo-Information*

Changes in the Water Quality of Large Rivers in the Asian Part of Russia from the Standpoint of Achieving Sustainable Development Goals



Alesya O. Danilenko, Lyudmila S. Kosmenko, Olga S. Reshetnyak, Maria Yu. Kondakova, and Mikhail M. Trofimchuk

Abstract Among other Sustainable Development Goals (SDGs) for the period till 2030, a special position belongs to Goal 6: provision of presence and rational use of water resources and sanitation for all. Its priority objective 6.3 is: “By 2030, [to] improve water quality by reducing pollution”. This can be monitored by gathering different countries’ reports on various indicators, including Indicator 6.3.2: “Share of natural clean water bodies”. These responsibilities are entrusted to the UN Environmental Programme (UNEP). At present, the record of this indicator is not assigned to any office in the Russian Federation. As a result, despite a well-developed surface water pollution national monitoring system that includes more than 1,800 monitoring stations located at practically 1,200 water bodies, Russia is not taking part in the global data gathering regarding Indicator SDG 6.3.2. This research is the first one to adapt the application of Indicator SDG 6.3.2 in the Russian approaches to the quality evaluation of surface waters. We have studied the interim tendencies in water quality in the large rivers of the Asian part of Russia applying Indicator SDG 6.3.2 methodology. The primary objective was to choose the so-called target values characterizing good water quality. In Level 1 evaluation, we used national water quality standards, those recommended by UNEP, and individual target values for each region under discussion. The obtained results speak for the high informational content of

A. O. Danilenko (✉) · L. S. Kosmenko · O. S. Reshetnyak · M. Yu. Kondakova · M. M. Trofimchuk

Hydrochemical Institute, Stachki ave, 198, Rostov-on-Don 344090, Russian Federation
e-mail: a.danilenko@gidrohim.com

L. S. Kosmenko
e-mail: l.kosmenko@gidrohim.com

M. Yu. Kondakova
e-mail: m.kondakova@gidrohim.com

M. M. Trofimchuk
e-mail: m.trofimchuk@gidrohim.com

O. S. Reshetnyak
Institute for Earth Sciences, Southern Federal University, R. Zorge St., 40,
Rostov-on-Don 344090, Russian Federation
e-mail: o.reshetnyak@mail.ru

Level 1 evaluation based on systemic integral indicators (acidity, salinity, oxygenation and biogene content). Meanwhile, the national evaluations (Level 2 evaluations) serve as an effective test instrument enabling not just to reveal the fact of “not good” state, but also its reasons.

Keywords Sustainable development goals · Target values · Water quality · Large rivers · UNEP · Asian part of Russia

1 Introduction

One of the priority problems of today in the conservation of the environment and sustainable development of territories is adequate evaluation of the state of water resources, water quality variability and ecological state of aquatic ecosystems with account taken of the peculiarities of their functioning, as well as detecting the possible consequences of harmful external effects. The state of the natural ecosystems of any region is of paramount importance for the territory’s sustainable environmental and economic development. In September 2015, during the session of the UN Summit, enacted were 17 basic Sustainable Development Goals aimed at optimum utilization of limited resources and application of environment-oriented saving technologies, preservation of the stability of social and cultural systems, provision of integrity of biological and physical natural systems. Implementation of these goals should improve the quality of people’s lives and the “recovery” of the planet [1].

In accordance with the adopted UN Declarations, water is a resource that is making a basis of human life and activities [2]. Earth freshwater resources are limited, and the questions of their preservation and purity have been lately especially acute. Hence evaluation and forecast for the surface water quality changes are basic elements of efficient management of water resources. To prevent aquatic ecosystems from degradation, stabilize the ecological situation, improve the quality of water resources, water economy politics and water resources management should be based upon unbiased information on the quality of the surface waters.

Water quality improvement is mentioned in SDG 6.3, which reads: “By 2030, [to] improve water quality by reducing pollution, eliminating dumping and minimizing release of hazardous chemicals and materials, halving the proportion of untreated wastewater and substantially increasing recycling and safe reuse globally” [3]. To evaluate the effectiveness of the measures aimed at water quality improvement in the countries much different in their monitoring programs, Indicator SDG 6.3.2 was developed. The central success element of this indicator application is a balance in comparing values at the global level and the national level. This is attained through obligatory measurements of the basic standard components (Level 1) at sufficient flexibility of methodology towards national and local conditions (Level 2) [3].

Record of Indicator SDG 6.3.2 is not yet assigned to any office in the Russian Federation. At the same time, the comparability of national water quality evaluations to global ones has always been relevant. We have compared approaches applied in the

Russian Federation to those proposed by the United Nations Environment Program (UNEP), and the results of different evaluation systems using the example of the outlets of the largest rivers of the Asian part of Russia.

1.1 Global and National Approaches to Water Quality Evaluation Within the Context of Sustainable Development Goals Achievement

As recommended by UNEP, while evaluating water quality (Level 1 monitoring data) used are, the simple properties of water characterizing its mineralization, acidity, the content of dissolved oxygen and biogenic substances—nitrogen and phosphorus compounds [4]. In most cases, this evaluation fails to reveal all the peculiarities of the qualitative composition of surface waters and their pollution. However, these relatively simple characteristics might be measured directly in the field and are used by the monitoring schemes in most countries. This provides a possibility to compare evaluations obtained in various regions differing in their natural and climatic conditions and the nature of the human-induced impact.

The water quality dynamics in the large rivers of the Asian part of Russia, according to the Level 1 monitoring data, will be viewed in detail in Sect. 3. On the other hand, Level 1 is limited in the volume of information; hence, providing positive data fails to reflect all freshwater quality indicators. Level 2 gets beyond this and enables different countries to apply while evaluating water quality, national approaches, methods and indices. Level 2 is required due to heterogeneity of the chemical composition of water bodies located at various territories both within one country and in different countries [3]. The distribution of chemical elements in natural waters is defined by the type of the natural system, elemental properties and generally complies with the basic geochemical regularities [5].

Currently, a content of more than 1,300 compounds is considered a norm in the water medium. No analysis of such a great number of chemicals is possible: it would be too wasteful, expensive and long. Besides, water quality evaluation involving a large number of ingredients causes definite difficulties linked with the need to consider significant number groups. These difficulties can be overcome by a complex evaluation in which the outcome indicator is a scalar value functionally associated with quite a number of values of the ingredients under consideration [6].

Countries with developed monitoring programs pay much attention to creating and applying those integral evaluations indicating a high formalization degree (see Fig. 1). These countries aggregate hydro chemical information using various techniques in observed and relative indicators [6–9].

Since the 1980s the Soviet Union (later the Russian Federation), in official water quality evaluations, has used indicators developed by Hydrochemical Institute (water pollution index or WPI and later DCWPI) and Ministry of Natural Resources and

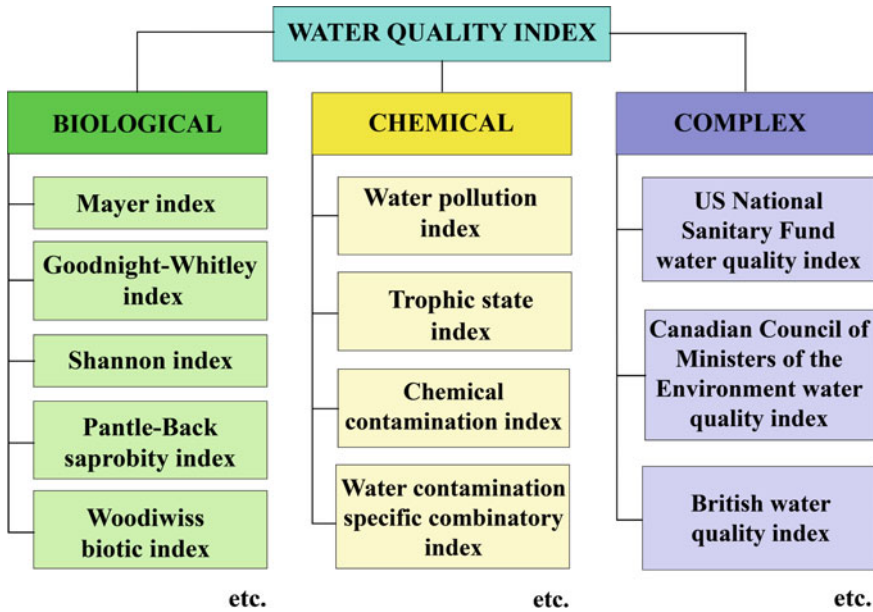


Fig. 1 Integral water quality indicators (from [7] with additions and modifications)

Ecology of the RF (chemical contamination index or CCI-10; is only used to reveal environmental disaster areas and zones of ecological disorders).

Calculations of these criteria are based upon the measured concentration to standard value ratio. These indices are calculated upon a fixed number of indicators. Thus, DCWPI is calculated upon 15 indicators, CCI upon 10, and WPI upon 6. Standard are the maximum allowable concentrations (MAC) of hazardous substances for commercial fishery waters, drinking and household waters or cultural and social waters [9–11]. For DCWPI, the complexity of evaluations can also be reached by way of taking into account both the repeatability and the frequency of MAC exceedance [12]. The obligatory list of indices can be seen in Table 1.

The Federal Service on Hydrometeorology and Monitoring of the Environment (Rosgidromet) currently uses DCWPI as the principal index for water quality evaluations. Hydrochemical Institute (a research institution referred to Rosgidromet) annually publishes information on the level of pollution in the surface waters of the Russian Federation.

The water quality classification made up based on DCWPI values, permits to subdivide surface waters into 5 classes depending on the level of their contamination rate [12]: Class 1—process water; Class 2—slightly polluted; Class 3—polluted or highly polluted; Class 4—dirty or highly dirty; Class 5—extremely dirty. In national evaluations, water quality dynamics in the large rivers of the Asian part of Russia is considered Sect. 3 (Results).

Table 1 Water quality indicators used in the Russian Federation to evaluate water quality, and the reasons of their inclusion in the evaluation

Group of parameters	Parameter	Reason for inclusion in the complex evaluation
1. Oxygen (oxygenation)	Water oxygen	Oxygen deficiency level
	Biochemical oxygen demand in 5 days	Organic pollution level
	Chemical oxygen demand	
2. Contaminants	Phenols	Organic pollutants
	Oil derivatives	
3. Nitrogen	Nitrite ions	Nutrient pollution level
	Nitrite ions	
	Ammonium ion	
4. Metals	Total ferrum	Biologically active double genesis substances
	Copper compounds	
	Zinc compounds	
	Nickel compounds	
	Manganese compounds	
5. Salinity	Chlorides	Water salinity level. Help characterize the water body
	Sulfates	

2 Materials and Methods

The principal question in the use of the Level 1 monitoring data in the evaluation of surface waters quality is a choice of a border whose violation may signify transition from good quality to bad quality. In terms of indicator SDG 6.3.2, a border of the kind is named “target value” (TV). Target values are specific for each water quality parameter; they define concentrations that promote the preservation of ecosystems or their return to the natural or close-to-natural state [3, 13].

Firstly, national water quality standards may be used as such borders. In the Russian Federation, MAC for commercial fishery waters are the most stringent water quality standards. One of the basic objections in applying joint Russian MAC standards (national water quality standards) is the failure to consider the natural climatic peculiarities of formation of the chemical composition and quality of water in large river basins. For example, northern rivers are much less mineralized against southern rivers, containing less biogenic substances.

Secondly, UNEP recommended target values may also be applied. These were defined on the basis of the analysis of the data collected from a large number of objects, yet mainly on the territory of Europe. Still, due to significant differences in the natural factors of formation of the Asian rivers of the Arctic Ocean basin and European rivers, these borders might fail to objectively show a transition from bad state to good state and the other way round.

Thirdly (and this seems most reasonable and environmentally appropriate), individual target values may be defined for each stretch under discussion in each parameter supported by the information concerning the natural or initial state of water. The latter variant is rather rare due to the uncertainty of the methodology of defining such individual borders.

In general, according to UNEP recommendations, standards may be both national and specific for each definite water body or its stretch. The more definite are the water quality standards, the better they reveal potential pollution problems [4]. This investigation demonstrates the results of evaluations of the surface waters quality dynamics based on the three approaches listed above.

In the Russian Federation, Order of the Ministry of Agriculture No 552 dated 13.12.2016 “Approval of Water Quality Standards for Commercial Fishery Water Bodies, Including Standards of Maximum Allowable Concentrations of Hazardous Substances in Commercial Fishery Water Bodies” [14] is a document defining the strictest water quality borders. Recommended MACs for commercial fishery water bodies defined by this document, are shown in Table 2.

However, this Order does not contain all basic values for the evaluation of indicator 6.3.2. Thus, it neither standardize salinity surface waters nor gives definite instructions concerning the borders of standard pH variability. These two indicators

Table 2 Target values for defining the water quality according to the national standards of the Russian Federation and UNEP recommendations

Parameter group	Source of target values	
	National documents of the Russian Federation [14, 15]	Based on GEMS/Water “Optional Target Value” [13]
1. Oxygenation	Dissolved oxygen >6,0 mg l ⁻¹	% saturation 80–120% or dissolved oxygen >8,0 mg l ⁻¹
2. Acidification	pH 6,5–8,5	pH 6–9
3. Salinity	Mineralization 1000 mg l ⁻¹	Electrical conductivity 500 μS cm ⁻¹
4. Nitrogen	N-NO ₃ : 9000 μg N l ⁻¹ N-NO ₂ : 20 μg N l ⁻¹ N-NH ₄ : 400 μg N l ⁻¹	Total nitrogen: 700 μg N l ⁻¹ Oxidized nitrogen: 250 μg N l ⁻¹ Or using Pan European WaterBase Data—40% percentile derived from all available data for the respective parameters in Waterbase over the entire time period (1992–2018) N-NO ₃ : 1,039 mg l ⁻¹
5. Phosphorus	Orthophosphate: depending on the water body trophicity: 50 μg P l ⁻¹ —oligotrophic, 150 μg P l ⁻¹ —mesotrophic, 200 μg P l ⁻¹ —eutrophic	Total phosphorus: 20 μg P l ⁻¹ Orthophosphate: 10 μg P l ⁻¹ Or using Pan European WaterBase Data—0% percentile derived from all available data for TRP (TDP) in Waterbase over the entire time period (1992–2018) Total phosphorus: 33 μg P l ⁻¹

are standardized not so strictly and are mentioned by another national document, Sanitary Rules and Norms 1.2.3685-21 [15]. Table 2 also shows UNEP target values.

The first factor leading to significant differences in the Level 1 monitoring evaluations is target values for biogenic compounds, especially oxidized nitrogen forms (nitrite ions). Besides, Russia has comparatively “elastic” borders in phosphate ion content water quality evaluations, even in terms of oligotrophic waters only.

Still another problem in evaluating the quality of surface waters of the large rivers in the Asian part of Russia in the context of SDG 6.3.2 achievement is a discrepancy of approaches to measuring the salinity indicator. So UNEP recommends using the information on specific conductivity, while in the Russian Federation, they most frequently measure the sum of ions (mineralization). These indicators are functionally related, yet no direct conversion between them is possible due to the different conductivity of solutions of various salts and the temperature impact on this indicator.

In this chapter, we have to take, as an inevitable condition, the use of the factor of conversion between these two parameters: 0.5 (in other words, $500 \mu\text{Scm}^{-1}$ roughly corresponds to salt concentration in natural water 250mg l^{-1}). Such mineralization allows referring these waters to fresh ($200\text{--}500 \text{mg l}^{-1}$), which corresponds to the natural factors of formation of the rivers in the Far North.

The methodology of finding individual target values (hereinafter referred to as I-TV) presents an original approach, which deserves a more detailed description. The natural concentration of chemical substances in rivers may be viewed as systemic parameters whose variability, within certain limits, guarantees a steady-state of an aquatic ecosystem [16]. A rational method enabling to find steady states of dynamic systems, aquatic ecosystems too, is the analysis of their phase pictures. A phase space used to construct a dynamic phase picture is a plane whose coordinate axes contain variables characterizing the state of the ecosystem. At this moment of time, the system’s state is characterized by a point in the phase space named “a describing point”. As the state changes, the describing point draws some curve called “a phase path” in the phase space. A set of phase paths is “a phase picture of the system”. An attractive set that embraces a number of points is named “an attractor” [17]. A phase picture might have one or several attractors. Examples of phase pictures can be seen in Figs. 3–8.

The phase picture analysis used here is focused on the study of the path of describing point in C and dC/dt coordinates, where C is the empirically measured mass concentration of a substance, and dC/dt is its change rate.

To construct a phase picture, one needs data taken with definite time discreteness. The discrete interval is defined by the dynamic properties of the system. It must be less than the time of its reconstruction in response to the impact, yet long enough to diffuse the effects of accidental and seasonal fluctuations. That is why it would be reasonable to take one year as a time unit, while the resulting concentration would be 80% percentile of yearly data since this is a threshold offered by the methodology of water quality evaluations for indicator SDG 6.3.2.

An empirical phase picture thus constructed has a shape of an ellipse and is characterized by greater or lesser density of points, availability of loops, number of attractors

and other features essential for its further visual analysis. The disadvantage of phase pictures in visualizing the dynamics of this or that water quality parameter, is in the absence of a formalized algorithm of its analysis. However, one apparent advantage is its visual expression. Evaluations of surface water quality were carried out with the use of the monitoring data obtained by Rosgidromet subdivisions. Chosen were some outlets of the large rivers in the Asian part of the Russian Federation (see Fig. 2). Such outlets restrict the river basin, hence their water quality in a sense characterizes the state of this basin. It should be noted though that one must not simply extrapolate outlet water quality to the whole basin of such large rivers.

We chose six flows and correspondingly six observation points: (a) the Yenisey near the city of Igarka, (b) the Ob near the city of Salekhard, (c) the Lena near village Kusur, (d) the Yana near-polar station Yubileynaya, (e) the Indigirka near village Chokurdakh, and (f) the Kolyma near village Kolymskoe. All these places are located within the extent of harsh continental climate and the spread of perennially frozen rocks. The local ecosystems are extremely sensitive to both man's impact and the climatic changes that have presently begun to show. We studied the dynamics of surface waters quality evaluations calculated according to the mass results of observations collected between the years 2000 and 2019. There were 4–12 water sample collections with further analyses of their composition.



Fig. 2 The schematic map of the observation points location in outlets of large rivers in the Asian part of Russia

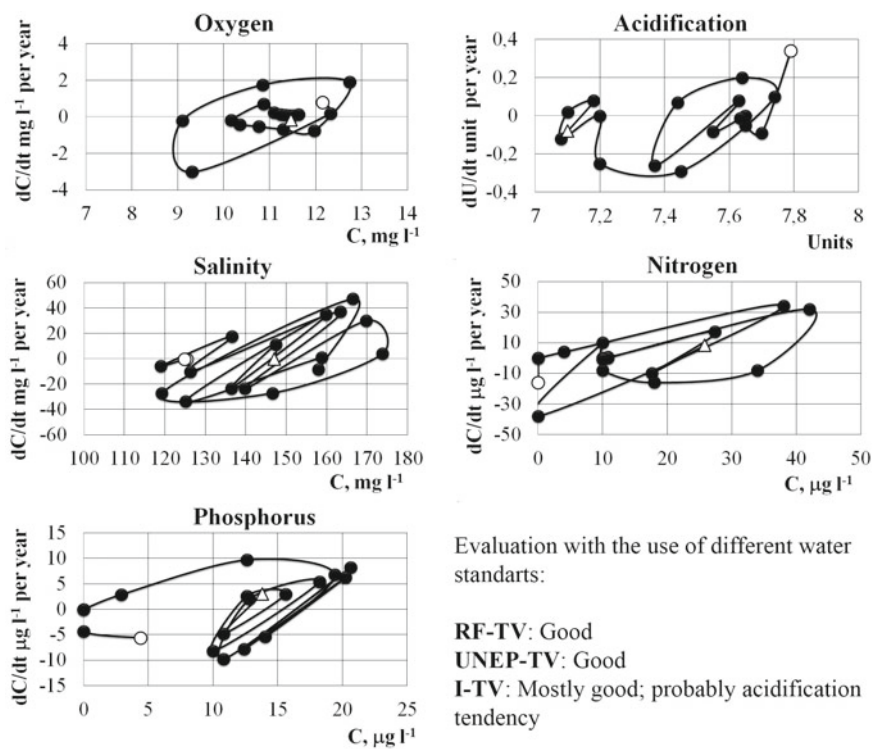


Fig. 3 Phase pictures of the Yenisey river (Igarka) stretch in general water quality parameters and water quality evaluation with the use of target values of various specificity levels. *Note* the path starts with an empty circle and finishes with an empty triangle

3 Results

Application of national target values (hereinafter referred to as RF-TV), as well as those recommended by UNEP (UNEP-TV), even in perennial dynamics, virtually does not reveal problems (see Table 3). Generally speaking, all the outlets of the large rivers of Russia are characterized by high-quality water. Exceptions are the Ob due to comparatively high concentrations of inorganic phosphorus and, in occasional years, the Lena (in mineralization), the Yana and the Indigirka (also in inorganic phosphorus concentrations). However, in our opinion, the specificity of target values RF-TV and UNEP-TV is insufficient to consider the natural variety of water objects and their areas. UNEP recommendations state that if there is information of a monitoring station level, it is better to develop I-TV for it [13].

That is all the more reasonable for those rivers discussed in this paper because their waters occupy large territories and may be located within several contrasting natural and climatic zones.

Table 3 Ranges of 80% percentile data between 2000 and 2019

River, monitoring location	Parameter				
	Oxygen, mg l ⁻¹	Acidification, Units pH	Salinity, mg l ⁻¹	Nitrogen (of NO ₃ ⁻), µg l ⁻¹	Phosphorus (of PO ₄ ³⁻), µg l ⁻¹
Yenisey, Igarka	9.1–12.7	7.1–7.8	119–174	<42	<26
Ob, Salekhard	8.5–13.7	7.2–8.6	134–567	75–278	28–188
Lena, Kususur	10.9–15.7	6.9–7.6	67–256	5–144	6–15
Yana, Yubileynaya	9.4–13.7	6.3–8.1	71–194	24–122	3–23
Indigirka, Chokurdakh	9.5–13.0	6.4–7.6	75–143	20–286	<59
Kolyma, Kolymskoe	11.0–13.1	7.0–8.0	71–137	58–544	<18

I-TV calculation methodology is not strictly drawn. We used a combination of two approaches: statistic analysis of hydrochemical data and visual analysis of phase pictures.

The first stage was the calculation of 80 percentile for each year. These figures made independent samples which we later processed. The following distribution quartiles were calculated:

- (1) for salinity, nitrogen and phosphorus: the 95th available data distribution quartile permitting to obtain a parameter value which, with a probability of 95%, will not exceed 80% of yearly data;
- (2) for acidification: range of values between the 5th and 95th available data distribution quartiles;
- (3) for oxygen: the 5th available data distribution quartile permits obtaining a parameter value that, with a probability of 95%, will not exceed 80% of yearly data.

Calculating distribution quartiles, we took into account the character of the phase path of the describing point. Thus, while calculating I-TV for pH at a stretch of the river Yenisey near the city of Dudinka (see Fig. 2), one should not use recent data (since 2014), making a separate attractor in the phase picture. Then we describe all cases of the use of the phase picture visual analysis while correcting the I-TV statistical calculation. Combining these two approaches, we obtained the following individual target values for the outlet of the Yenisey and other rivers (see Table 4).

The formation of an additional attractor in the Yenisey phase picture in the acidification parameter may indicate some negative quality tendencies (Fig. 2). In the Far North, where the stretches of these rivers are located, pH level is typically close to neutral, off-centered towards the weakly alkaline section due to the local limestone soil. Precipitation of air sulfur-containing and nitrogen-containing compounds might result in surface waters acidification, especially in the areas where water, due

Table 4 Individual target values proposed for the studied river stretches

River, monitoring location	Parameter				
	Oxygen, mg l ⁻¹	Acidification, Units pH	Salinity, mg l ⁻¹	Nitrogen (of NO ₃ ⁻), μg l ⁻¹	Phosphorus (of PO ₄ ³⁻), μg l ⁻¹
Yenisey, Igarka	9.3	7.4–7.8	170	38	20
Ob, Salekhard	10.1	7.3–7.9	244	253	89
Lena, Kususur	13.3	7.0–7.5	256	72	13
Yana, Yubileynaya	9.9	6.8–8.0	118	47	21
Indigirka, Chokurdakh	9.7	6.7–7.2	128	189	20
Kolyma, Kolymskoe	11.1	7.0–7.8	127	115	8

to natural reasons, is characterized by low hardness and alkalinity. For the acidification parameter, RF-TV and UNEP-TV of the rivers under discussion are of a too large scale. Generally, natural fluctuations stay within the range of 7–8 pH units.

The path of the phase picture describing point in oxygenized nitrogen concentration is also worth noting (see Fig. 3). It is formed by a number of loops whose centers are mutually shifted to the right. This might be caused by forming a positive trend in oxygenized nitrogen forms concentrations, and it is an ecologically adverse event. Although nitrogen is a vitally important nutrient, its supply from man-made sources exceeding natural levels might adversely affect the health of a fragile water ecosystem. This tendency is possibly linked with the appearance of an additional attractor in the phase picture in the acidification parameter in the area of lower pH values.

It should be emphasized, for further discussion too, that nitrate-nitrogen was chosen for water quality evaluations in compliance with UNEP recommendations [13]. Any nitrogen forms can be used (total nitrogen, mineral nitrogen, oxidized nitrogen, Kjeldahl nitrogen), yet the total oxidized nitrogen is more effective for evaluating indicator 6.3.2 as it is easier to be analytically measured. The share of nitrates in surface waters is typically extremely small (less than 1% from the total) and it is of the same little importance for practical purposes.

The path of the describing point phase picture in inorganic phosphorus concentration is noteworthy for a big loop in the low concentration area (up to 4 μg l⁻¹), this loop being formed by the data collected between 2000 and 2005 (see Fig. 3). Although since 2006 the describing points have been lying in the higher concentration area, yet the amplitude of their fluctuations gradually falls, which may speak for the fact that the system is approaching steady state condition in this parameter (in

a steady-state this parameter change rate equals zero). In calculating Yenisey I-TV (phosphorus) the points making this loop were excluded from the sample.

The Ob differs from the other studied water bodies by the fact that the quality of its water, even according to the Level 1 monitoring data, complies with neither national standards, nor UNEP due to phosphates high concentration. As is nitrogen, phosphorus is a vitally important nutrient present in water in a number of forms: orthophosphate ions, particle-bound phosphorus, organic particle-bound phosphorus, within dissolved organic forms. Orthophosphates are the form most accessible for use by aquatic vegetation. Since most fresh water ecosystems in their natural state have phosphorus as a limiting factor for gross crop, then even its insignificant increase might result in a notable growth of algae [13].

However, a visual analysis of the phase picture suggests a steady state condition of a stretch in this parameter despite relatively high concentrations (see Fig. 4). The Ob river basin is enormous. In the southern part, it flows across regions of intensive agricultural reclamation, including the countries neighboring Russia. Hence phosphate (and oxidized nitrogen) concentrations in the Ob might be higher than in other rivers of Siberia, mainly flowing across the territories of perennially frozen rocks. That is why orthophosphate I-TV for Ob (Salekhard) appeared to be higher than national.

The phase pictures of the salinity and acidification parameters demonstrate big loops (see Fig. 4). The points entering such a loop may characterize the limits that have been actually reached, which limits the water body can still get back to its steady-state. However, it would make sense to exclude such points from the calculation of individual target values.

In the last few years, the water of this river stretch is characterized by higher oxygen concentrations and close to such concentrations in other rivers, which was taken into account during the calculation of the individual target value for the water oxygen (see Fig. 4; Table 4).

In recent years, the Lena (Kusur) water oxygen concentration has gone down (see Fig. 5). Meanwhile, in absolute terms these concentrations still remain rather high. Such high dissolved oxygen concentrations are of exceptional significance for the health of ecosystems since they support aerobic respiration of all of their trophic levels. Dissolved oxygen weakening should be referred to as a negative phenomenon. Hence the later years' data were excluded from the I-TV calculation.

Another parameter where the phase picture visual analysis lets partially exclude some data from the I-TV calculation is nitrogen. This picture's loop is formed by one value, which denotes a limit that has been actually reached, yet after which the system may get back to its steady-state; however, this limit is not desirable for reaching.

The Yana outlet is notable because its general water quality parameters have separate loops characterizing episodic water quality impairment (see Fig. 6). In this connection, corresponding percentiles were calculated with the exception of loop forming points. As with the outlet of the Lena, recent years have also shown a lower concentration of dissolved oxygen here. Yet in absolute terms concentrations also remain above average. While calculating I-TV for oxygen, we excluded the data of the last 7 years.

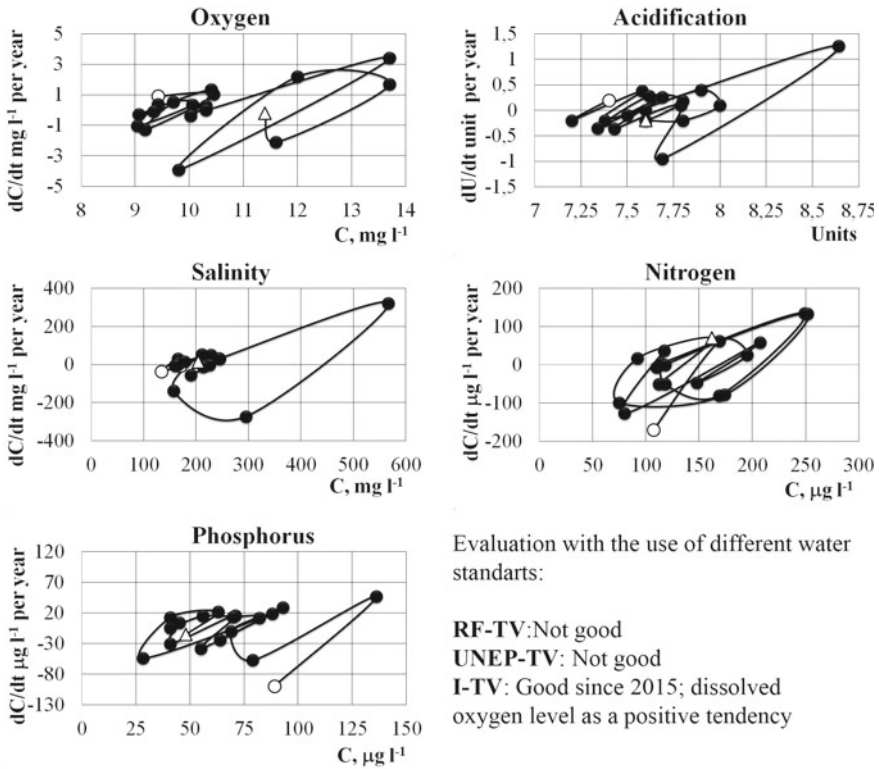


Fig. 4 Phase pictures of the Ob river (Salekhard) stretch in general water quality parameters and water quality evaluation with the use of target values of various specificity levels. *Note* the path starts with an empty circle and finishes with an empty triangle

General quality parameters in the outlet of the river Indigirka also speak for a predominantly steady state of the water body (see Fig. 7). This is with the exception of nitrogen, which with the use of UNEP-TV and with some periodicity, is responsible for water quality impairment. In the phase picture, this is also reflected as a number of loops to the right of the main major mass of points (attractor). With respect to this asymmetry of the phase picture, those points forming such loops were excluded from the I-TV calculation for oxidized nitrogen.

Since 2003, the Kolyma river has been showing significant changes in biogenic substances concentration. During the whole period of studies, nitrogen oxidized forms have steadily gone down. In the phase picture plane this looks like a “stretched spring” whose diameter narrows in the area of lower concentrations. Phosphate concentrations also go down in time after their fast growth of 2009–2011. In absolute terms this “boost” was not too great (reaching 18.4 μg l⁻¹); however this river stretch showed in 2003–2008 phosphate concentrations that were lower than their determination limit (see Fig. 8).

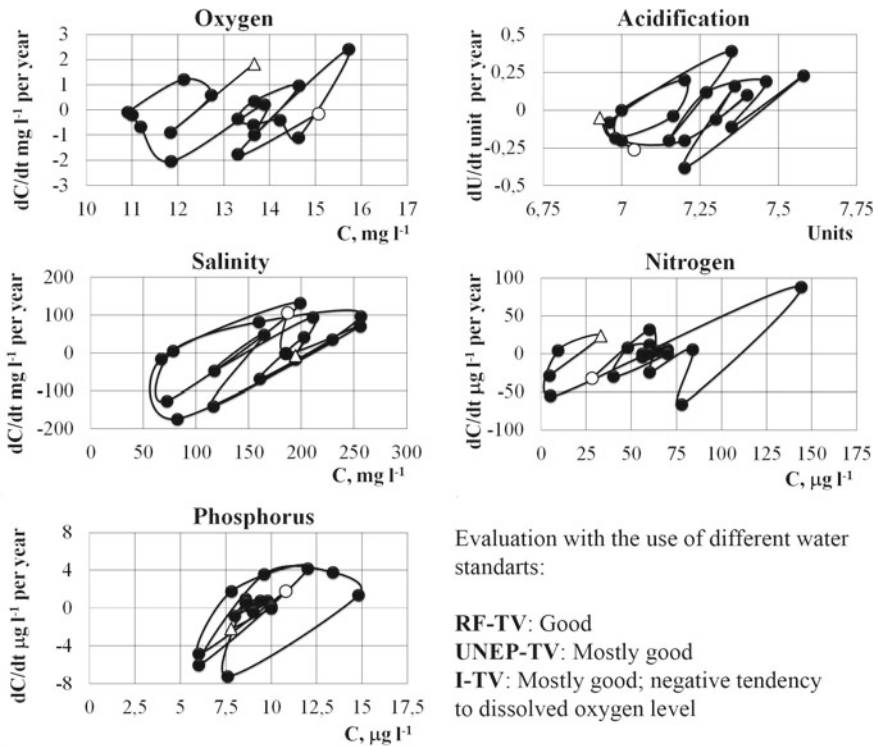
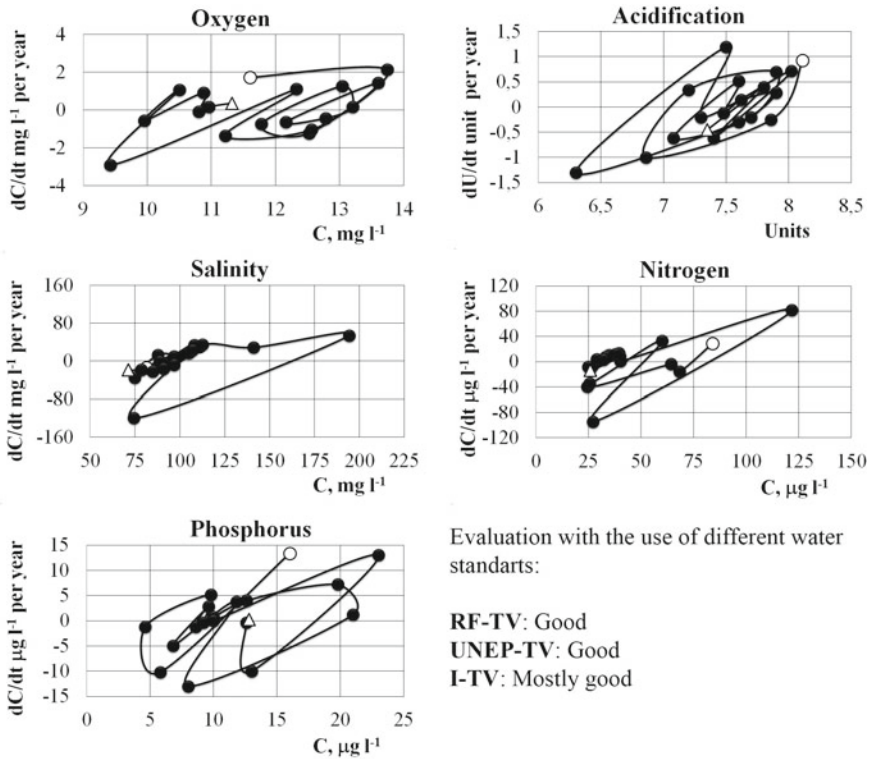


Fig. 5 Phase pictures of the Lena river (Kusur) stretch in general water quality parameters and water quality evaluation with the use of target values of various specificity levels. *Note* the path starts with an empty circle and finishes with an empty triangle

Thus, in this part of our work we defined water quality in the outlets of the large rivers of the Asian part of Russia applying global approaches offered by UNEP. Water quality evaluation using RF-TV and UNEP-TV by the Level 1 monitoring data does not reveal any significant problems with water bodies, except the Ob, whose water is steadily polluted with phosphates. I-TV application reveals new risks: some pH reduction in the Yenisey against an increase in content of oxidized nitrogen forms, periodic water quality impairment in the Indigirka in biogenic elements content, potential water quality impairment in the Kolyma in nonorganic phosphates and oxidized nitrogen content. Besides, the obtained evaluations fail to embrace all significant water quality indicators, that is why we proceeded with the analysis of the perennial dynamics of national quality evaluations (DCWPI) taking into account not less than 15 obligatory indicators (Table 1).



Evaluation with the use of different water standards:

- RF-TV: Good
- UNEP-TV: Good
- I-TV: Mostly good

Fig. 6 Phase pictures of the Yana river (Yubileynaya) stretch in general water quality parameters and water quality evaluation with the use of target values of various specificity levels. *Note* the path starts with an empty circle and finishes with an empty triangle

4 Discussion

Are the water quality dynamics in the large rivers of the Asian part of Russia According to the Level 2 Monitoring Data consistent to the Level 1 Monitoring Data? Recent investigations have shown that long and ongoing anthropogenic impact on the river ecosystems of the Arctic Regions of Russia resulted in an anthropogenic transformation of their environmental position. This above all happens due to a higher level of water medium pollution and enhanced host processes of ecological regression. The latter gives rise to the possibility of oppressed development of particular communities of aquatic organisms, even perhaps their extinction. Greater becomes an ecological risk of ecosystems' degradation [18–21]. Noted is also enhancement of man-induced processes in the water bodies of the Arctic area [22–24]. Toxic pollution of waters, eutrophication, acidulation and other negative processes lead to the disturbance of a delicate balance in the Arctic ecosystems.

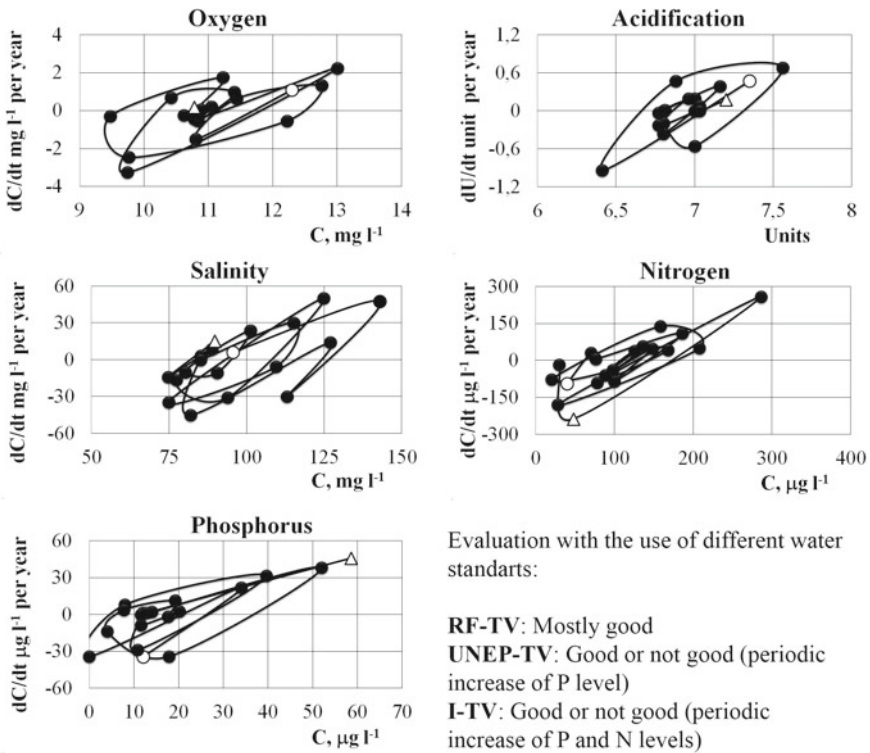


Fig. 7 Phase pictures of the Indigirka river (Chokurdakh) stretch in general water quality parameters and water quality evaluation with the use of target values of various specificity levels. *Note* the path starts with an empty circle and finishes with an empty triangle

In this context, it is most important and topical to study the long dynamics of Arctic water quality formed under harsh natural and climatic conditions at a low potential for self-purification of river ecosystems.

Complex evaluation of water quality in the large rivers of the Asian part of Russia for a long time was carried out using DCWPI [12], a complex relative index of the degree of pollution of surface waters in hydrochemical indicators. DCWPI value may vary in the waters of pollution degree ranging from 1 to 16. The greater is the index value, the worse is water quality in various outlets, points, etc. A DCWPI water quality rate scale permitting to divide surface waters into 5 classes depending on the degree of their pollution, is shown in Table 5.

Quality and degree of pollution in the outlets of the Arctic rivers of the Asian part of Russia are shown between the years 2000 and 2019 (see Fig. 9). In general, the quality of water in the rivers of the studied part of the Arctic zone changes during many years within the range of the 3rd and 4th quality classes. In occasional years there was deterioration reaching the 5th class.

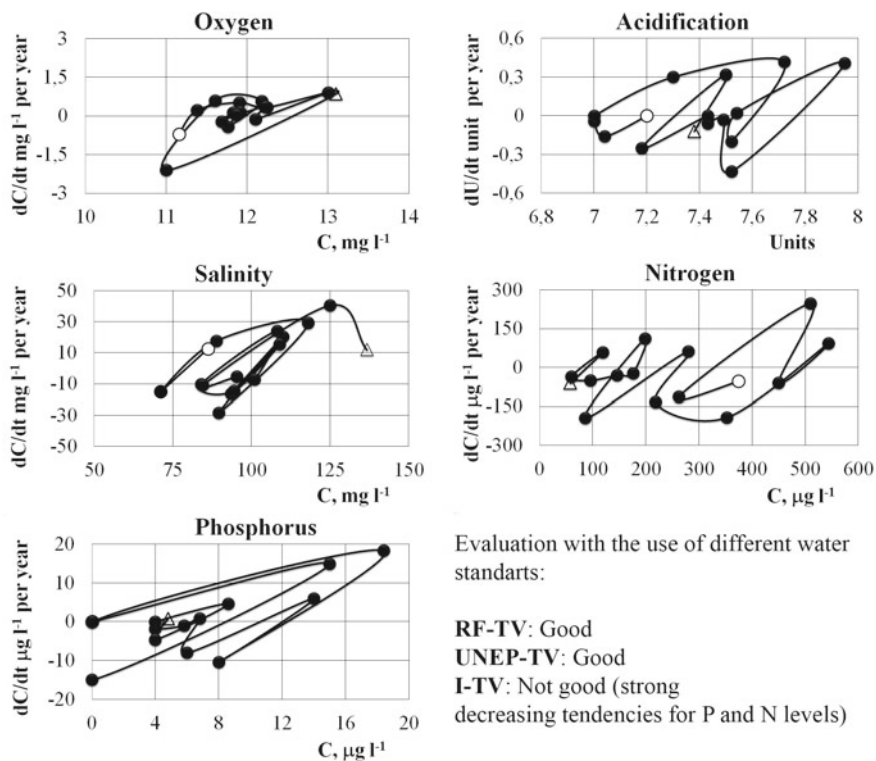


Fig. 8 Phase pictures of the Kolyma river (Kolymskoye) stretch in general water quality parameters and water quality evaluation with the use of target values of various specificity levels. Note: the path starts with an empty circle and finishes with an empty triangle

Table 5 Water quality rate scale according to hydrochemical indicators (from [12] with additions)

Water quality class		Water pollution degree	DCWPI value	Water quality category
Class 1		Process water	lower than 1.0	Good
Class 2		Slightly polluted	(1.0; 2.0]	Good
Class 3	Subclass a	Polluted	(2.0; 3.0]	Good
	Subclass b	Highly polluted	(3.0; 4.0]	Good
Class 4	Subclasses a and b	Dirty	(4.0; 8.0]	Not good
	Subclasses c and d	Highly dirty	(8.0; 11.0]	Not good
Class 5		Extremely dirty	over 11.0	Not good

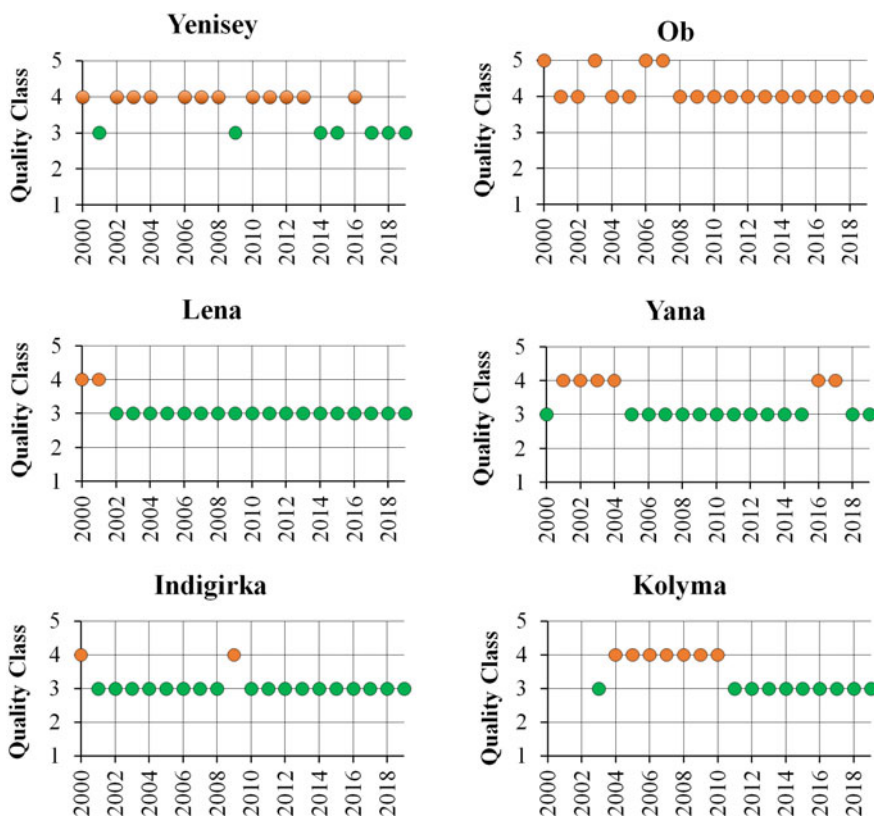


Fig. 9 Dynamics of water quality in the rivers of the Asian part of the Arctic zone of the RF during many years

The most polluted river stretches are located in the western segment of the Asian part of the Russian Arctic zone. In the 80 s, their water pollution degree corresponded to the 4th (“dirty” and “very dirty”) and 5th quality classes (“extremely dirty”). A slight improvement in water quality has been observed in recent years [25, 26].

During many years, tendencies to water quality changes in the studied large Arctic rivers are multidirectional. In the last years (2000–2019) notable were the following basic tendencies in the quality of water and degree of its pollution [21]:

- (1) improvement of water quality from class 4 to class 3 (from ‘not good’ to ‘good’) characteristic of the stretches of the Yenisey, the Kolyma and the Yana;
- (2) stabilization of water quality at the 3rd class level can be observed at the outlets of the Lena and the Indigirka;
- (3) even at the most polluted stretches of the rivers of the Asian part of the Arctic zone there is slight water quality improvement from class 5 to class 4 (the Ob).

At last we carried out generalization of the results of water quality evaluations in the rivers of the Asian part of the Arctic zone of Russia and water quality classification with 'good' or 'bad' scaling. To accomplish this, we accepted the following: if the water quality class at a definite river stretch shows correspondence between classes 1 and 3, then water quality is deemed good; if it is between classes 4 and 5, then water quality is deemed bad. A long period of observations provides us with 20 values of the quality class, and to define good or bad water quality we used a threshold at which 80% of cases and more correspond to standards [3]. Hence, if water quality was characterized as good in 80% and more years (cases), then the outcome evaluation was classified as good quality.

The results of compilation in what concerns water quality with the use of the national system of water quality evaluations are mentioned in Table 6.

Thus, this section of our work defines water quality in the outlets of the large rivers of the Asian part of Russia with the use of the national approaches of the Russian Federation with adaptation to the UNEP scale (good/not good water quality). As with the use of Level 1 monitoring data, bad water quality has long typical for the outlet of the Ob, while good water quality for the Lena. Both evaluation kinds can also reveal episodic water quality impairments in the Indigirka and the Kolyma. Apparent discrepancy of results was noted for the Yenisey. Systemic parameters indicate that the latter ecosystem is in a good state, but with an allowance for additional factors (mainly exceedance of concentrations of iron, copper, zinc, manganese compounds against statutory values) evaluation goes down. The said discrepancy of results might occur because natural elements can form elevated concentrations of these substances. Indirectly it was confirmed by the fact that production level, freshwater intake and waste water discharge have decreased; however, this has not led to any improvement in surface water quality [27].

Table 6 Classification of water quality in the large rivers of the Asian part of the Arctic zone of the RF during many years (according the Level 1 and Level 2 monitoring data)

№	River	Monitoring location	Level 1			Level 2
			RF-TV	UNEP-TV	I-TV	
1	Yenisey	Igarka	Good	Good	Mostly good	Mostly not good
2	Ob	Salekhard	Not good	Not good	Not good	Not good
3	Lena	Kusur	Good	Mostly Good	Mostly good	Good
4	Yana	Yubileynaya	Good	Good	Mostly good	Mostly good
5	Indigirka	Chokurdakh	Mostly good	Fluctuations between good and Not good	Fluctuations between good and Not good	Good
6	Kolyma	Kolymskoe	Good	Good	Not good	Mostly good

5 Conclusions

We have analyzed the results of water quality evaluations in the large rivers in the Asian part of Russia with regard to reaching SDG 6.3.2. With the use of Level 1 monitoring data, in spite of significant differences in the target values accepted by UNEP and in the RF, evaluations appear very close and denote low quality of water in the Ob near Salekhard. However, the use of the target values that are individual for the stretch enables to reveal new possible tendencies towards water quality deterioration, although these tendencies do not yet show themselves in the so-called simple water quality index [4].

Being deceptively unsophisticated, this evaluation is nevertheless truly helpful and informative as it is supported by systemic integral indicators of surface waters quality. At this level, effective is screening of violations of good water quality without revelation of the root causes of the phenomenon. The said evaluation for those trans-border water bodies that need some common standards and universal classification for surface waters quality is even more useful.

National evaluation is based upon regard for a set of quality indicators, and it acts as a diagnostic test revealing definite problems of pollution of a water body. It has generally confirmed the conclusions made on Level 1. Bad water quality can be observed in the Ob outlet. East Siberian rivers are only characterized by episodic water quality deterioration, although at times this deterioration may be rather long like in the outlet of the Kolyma. As we think, there is a discrepancy between the evaluations of Level 1 and Level 2 for the Yenisey results from the natural factors of its water formation. This permits us to make the following assumption. Level 2 water quality evaluations should not use national water quality standards, but, like with Level 1, individual target values oriented towards the natural state of the water body. It is evident that the more specific are the standards for a definite water body or its stretch, the better they reveal possible problems leading to its pollution or change of its state.

6 Recommendation

The Arctic zone intensive development and economic activity in the large rivers basins of the Russian Asian part can violate ecological well-being in vulnerable Arctic ecosystems. This, in turn, will lead to ecosystems degradation and violation of the sustainable development principle of these territories.

The Arctic rivers water quality research is important as the regional level, as the global scale. To achieve sustainable development goals in part of water resources conservation, it is necessary to work out environmentally well-founded water protection activity, reduce the anthropogenic pressure level on the Arctic rivers estuaries, and provide ecological safety in the region as a whole.

The results obtained can be used to solve the above issues, as well as in the preparation of predictive assessments of the arctic rivers water quality in conditions of current climate change and the development of regional criteria for assessing water quality and the aquatic ecosystems state Arctic rivers.

Acknowledgements The Russian Foundation for Basic Research partly supported this investigation under scientific Project No 18-05-60165.

References

1. Sustainable Development Goals. Trade Union Reference Manual on the 2030 Agenda for Sustainable Development (2017) International Training Centre of the ILO, Turin, Italy, p 102. http://www.oit.org/actrav/pubs/WCMS_553141/lang--en/index.htm
2. The Right to Water. Fakt Sheet No 35 (2010). <https://www.ohchr.org/Documents/Publications/FactSheet35ru.pdf>
3. Methodology 6.3.2. (2020) An Introduction to SDG Indicator 6.3.2, version 20200211. <https://communities.unep.org/display/sdg632/Documents+and+Materials>
4. An Introduction to SDG Indicator 6.3.2 (2020) Proportion of bodies of water with good ambient water quality I, version 20200211. <https://communities.unep.org/>
5. Yanin EP, Kuzmich VN, Ivanitskiy OM (2016) Regionalnaya prirodnyaya neodnorodnost khimicheskogo sostava poverkhnostnykh vod sushi i neobkhodimost ee ucheta pri otsenke ikh ekologicheskogo sostoyaniya i intensivnosti tekhnogennogo zagryazneniya. Probl Okruz Sredy I Prir Resur 6:3–72
6. Gagarina OV (2012) Otsenka i normirovanie kachestva prirodnykh vod: kriterii, metody, sushchestvuyushchie problemy: Uchebno-metodicheskoe posobie. Izdatelstvo Udmurtskiy Universitet, Izhevsk, p 199
7. Kimstach VA (1993) Klassifikatsiya kachestva poverkhnostnykh vod v stranakh Evropeyskogo ekonomicheskogo soobshchestva. Gidrometeoizdat, St. Petersburg, p 48
8. Nikanorov AM (2005) Nauchnye osnovy monitoringa kachestva vod. Gidrometeoizdat, St. Petersburg, p 576
9. Dryupina EY (2014) Metodicheskie osnovy rascheta dopustimyykh kontsentratsiy zagryaznyayushchikh veshchestv v stochnykh vodakh predpriyatii pri organizatsii gorodskikh sistem vodootvedeniya na primere g. Barnaula. Diss. na soiskanie uch. stepeni kandidata tekhnicheskikh nauk po specialnosti 25.00.27. Barnaul, p 131
10. Zubarev VA (2014) Gidrokhimicheskie indeksy oysenki kachestva poverkhnostnykh vod Regionalnye problem 17(2):71–77
11. Gagarina OV (2009) Kompleksnaya otsenka stepeni zagryazneniya (kachestva) vody v normativnykh dokumentakh RF. Vestnik Udmurtskogo universiteta. Ser Biologiya Nauki o Zemle 2:3–12
12. RD 52.24.643-2002 (2002) Metodicheskie ukazaniya. Metod kompleksnoy otsenki stepeni zagryaznenosti poverkhnostnykh vod sushi po gidrokhimicheskim pokazatelyam. Gidrometeoizdat, St. Petersburg, pp 49
13. SDG Indicator 6.3.2 Technical Guidance Document No 2. Target values (2020). <https://communities.unep.org/display/sdg632/Documents+and+Materials#DocumentsandMaterials-Intro>
14. Prikaz Ministerstva selskogo khozyajstva No. 552 (2016) Ob utverzhdenii normativov kachestva vody vodnykh obyektov rybokhozyaystvennogo znacheniya, v tom chisle normativov predelno dopustimyykh kontsentratsiy vrednykh veshchestv v vodakh vodnykh obyektov rybokhozyaystvennogo znacheniya (version 13.12.2016). http://www.consultant.ru/document/cons_doc_LAW_211155/

15. SanPiN 1.2.3685-21 (2021) Gigienicheskie normativy i trebovaniya k obespecheniyu bezopasnosti i (ili) bezvrednosti dlya cheloveka faktorov sredy obitaniya. http://www.consultant.ru/document/cons_doc_LAW_375839/
16. Danilenko AO et al (2019) Local aspects of water quality assessment as the basis for regional sustainable development. In: Sustainability perspectives: science, policy and practice. Springer, Cham, pp 155–173
17. Trofimchuk MM (2019) Sustainability of water ecosystems: from theory to practice. In: Sustainability perspectives: science, policy and practice. Springer, Cham, pp 63–94
18. Nikanorov AM, Bryzgalo VA, Reshetnyak OS (2012) Reki Rossii v usloviyakh chrezvychaynykh ekologicheskikh situatsiy. Izd-vo “NOK”, Rostov-na-Donu, p 310
19. Bryzgalo VA et al (2015) Usteviye ekosistemy krupnykh rek Rossii: antropogennaya nagruzka i ekologicheskoe sostoyanie. Izdatelstvo YuFU, Rostov-na-Donu, p 164
20. Chernogaeva GM, Likhacheva EA, Koshkarev AV, Shirokova VA, Chesnokova IV (2019) Potentsialnye ekologicheskie riski v arkticheskoy zone RF v usloviyakh izmenyayushchegosya klimata/Astrakhanskiy vestnik ekologicheskogo obrazovaniya 1(49):4–13
21. Kachestvo poverhnostnykh vod Rossijskoj Federacii za 2019 (2020). Meteoagentstvo Rosgidrometa, Rostov-na-Donu, p 556
22. Moiseenko TI (2018) Antropogenno-indutsirovannyye processy v vodakh sushi arkticheskikh regionov i kriterii ikh otsenki. Vodnye Resursy 45(4):421–432
23. Drake TW, Tank SE, Zhulidov AV, Holmas RM, Gurtovaya T, Spencer RGM (2018) Increasing alkalinity export from large Russian Arctic rivers. Environ Sci Technol 52:8302–8308
24. Moskovchenko DV, Babushkin AG, Yurtaev AA (2020) The impact of the Russian oil industry on surface water quality (a case study of the Agan river catchment, West Siberia). Environ Earth Sci 79(14):1–16
25. Reshetnyak OS, Kosmenko LS, Danilenko AO, Kondakova MY, Reshetnyak VN, Kovalenko AA (2019) Reki arkticheskoy zony Rossiyskoj Federatsii: mnogoletnie tendentsii kachestva i stepeni zagryaznennosti rechnykh vod. Trudy III Vserossiyskoj konferentsii “Gidrometeorologiya i ekologiya: dostizheniya i perspektivy razvitiya”. KHIMIZDAT, St. Petersburg, pp 735–738
26. Reshetnyak OS et al (2019) Prostranstvenno-vremennaya izmenchivost stepeni zagryaznennosti vody i sostoyaniya rechnykh ekosistem razlichnykh shirotnykh zon Sibiri. Voda: khimiya i ekologiya 1–2:126–137
27. Shaparev NY, Andrianova AV (2018) The Yenisei river in terms of sustainable water management. Geogr Nat Resour 39(4):47–56

A Sustainable Way for Fish Health Management by Replacement of Chemical and Drugs by Earthworm



Rahul Kumar, Renu Yadav, Rajender Kumar Gupta, and Pooja

Abstract Now a day population is drastically increasing. So, there is a challenging task to provide food for an increasing population. Fish culture is an alternative method to provide food but the Fish diseases have become a major problem for their culturing. It is well known that the farmed fishes are more vulnerable to disease causing agents than the fishes found in their wild conditions due to presence of artificial conditions in intensive farming. There is no doubt that the use of chemicals and drugs to cure fish diseases is effective, but it results in residual effects in fish organs. In this direction, antibiotics are used at a lower concentration to minimize effect but pathogens become resistant that has been responsible for further spreading of diseases. Due to the residual effect of chemicals and drugs may cause bio-magnification and bioaccumulation effects in higher tropic levels; simultaneously, these chemicals also cause water pollution. The residual effect of used chemicals, drugs and antibiotics, become the major cause of antimicrobial resistance. Therefore, there is a need of a sustainable way for fish health management and earthworms play a key role in this approach. In China, Vietnam and other Asian countries, earthworms have been used as medicinal sources to cure various diseases for many centuries. Earthworms (*Eisenia fetida*, *Eudrilus eugeniae* and *Pherethima posthuma*) have the potential for antimicrobial properties against pathogenic microbes which could cure many fish diseases. Earthworm extract/paste has anti-inflammatory, antipyretic, antioxidant, antibacterial and antifungal properties. *Aeromonas hydrophila* and *Bacillus megaterium* were demonstrated to be sensitive to the coelomic fluid of the earthworm. This chapter highlighted the potential use of earthworms to cure fish diseases.

Keywords Bioaccumulation · Bio-magnification · Earthworms · Fish disease · Health

R. Kumar (✉) · R. Yadav · R. Kumar Gupta
Department of Zoology and Aquaculture, Chaudhary Charan Singh Haryana Agricultural University, Hisar, Haryana 125004, India
e-mail: rahulrohila01@gmail.com

Pooja
Department of Chemistry, Chaudhary Charan Singh Haryana Agricultural University, Hisar, Haryana 125004, India

Abbreviations

AVPF	Antibacterial Vermi-Peptides Family
CAT	Catalase
EE	Earthworm extract
EFE	Earthworm fibrinolytic enzyme
GPx	Glutathione peroxidase
GSH	Glutathione
IL	Interleukin
LK	Lumbrokinase
MAS	Motile Aeromonas Septicaemia
MMP	Matrix Metalloproteinase
PAGE	Poly Acrylamide Gel Electrophoresis
RNA	Ribo Nucleic Acid
SDS	Sodium Dodecyl Sulphate
SOD	Super Oxide Dismutase
TGF	Transforming Growth Factor
TNF	Tumor Necrosis Factor
VHS	Viral Hemorrhagic Septicaemia

1 Introduction

As the world population increases day by day, it puts pressure on the animal food industry. So, in the past few decades, this food industry evolved expeditiously. As a result of the high level of human interference, many fish health-related problems arise [1–4].

Although aquaculture progresses, the intensification and commercialization of aquaculture lead to risk and spread of new fish diseases, which finally causes environmental degradation, leading to stress on cultured fishes. The frequent incidence of disease outbreaks in aquaculture is primarily due to intensive cultural practices for higher economic gain [2, 5]. In aquaculture, under different stress factors like over stoking, nutritionally deficient diet, low water quality and high microbial load, opportunistic agents become pathogenic which may cause severe damage in fishes [6]. One reason for microbial infection and stressful conditions in fish farming may be the development of intensification of cultured fishes [7]. Fish health management is a management practice in aquaculture to prevent fish diseases [8].

Asian countries contribute almost 90% to world aquaculture production. In these countries, fishes are used as protein source among animal food sources. Nevertheless, the fish disease becomes a major challenge to fulfillment of requirements [9, 10]. Worldwide, the main constraints for fishes' growth, survival, reproduction, and disease resistance are disease infection and malnutrition. There is no doubt that chemicals, drugs and antibiotics are used to cure fish diseases. But their residues are

noticed in fish organs. Now people are aware that the drugs, chemicals and antibiotics used to cure fish diseases leads to residual effect in their body. These chemical residue may cause bio-magnification and bioaccumulation in the different organisms (birds, human) and familiarise the severe threat to environment and public health [11, 12].

After the bio-magnification and bioaccumulation, the second most concern is microbial resistance against the residue of chemicals, drugs, and antibiotics in fishes. The pathogenic microorganism of fish develops antimicrobial resistance with time and which may affect human and environmental health directly or indirectly [9, 12, 13]. So, people are demanding those fishes which are free from residual effects. Therefore, there is a need for sustainable ways to cure diseased fishes that are economically cheap, safe to consume in the long term and cause no side effects.

In Asian countries, different earthworm species have been used as therapeutic drugs to cure diseases by using different earthworm forms like powder, extract, paste, and whole live earthworm. In addition, to control disease outbreaks, earthworms also accomplish the nutritious necessities for fishes' immune system so that the quality of fish is maintained for a long time. Earthworms are also used as a protein diet to enhance the growth of fishes [4, 11, 14]. The researchers have done several studies to evaluate the various therapeutic properties of earthworm powder, extract, coelomocyte, paste. But the almost negligible attempt has been carried for its extra-ordinary medicinal properties to cure diseased fishes. Therefore, this chapter describes a sustainable way of replacing chemicals and drugs by earthworms for fish health management (Fig. 1).

2 Causative Agent for Fish Diseases

2.1 Bacterial Diseases

In fishes, bacterial disease is the most common disease and is most often internal, but these can also be external. The causative bacteria generally saprophytic in nature and become pathogenic in poor nutritional diet, non-optimal water, physiological unbalanced fishes. These stressed conditions allow the opportunistic bacterial infection to spread in cultured fish farming. Different symptoms like fluid-filled abdomen, haemorrhagic spot or ulcer on body wall and protruded eye were observed in these diseases.

In general, there are four types of bacterial infections.

1. **Fin Rot:** It generally results from undesirable environmental condition
2. **Bacterial Gill Disease:** gill of fish are damaged
3. **Bacterial Ulceration:** Fish bodies have shallow to deep lesions are developed
4. **The Systematic Infective Bacterial Disease:** This disease is caused by invading bacteria inside the body and affecting the internal organ [8, 15].

Some important bacterial diseases are discussed here.

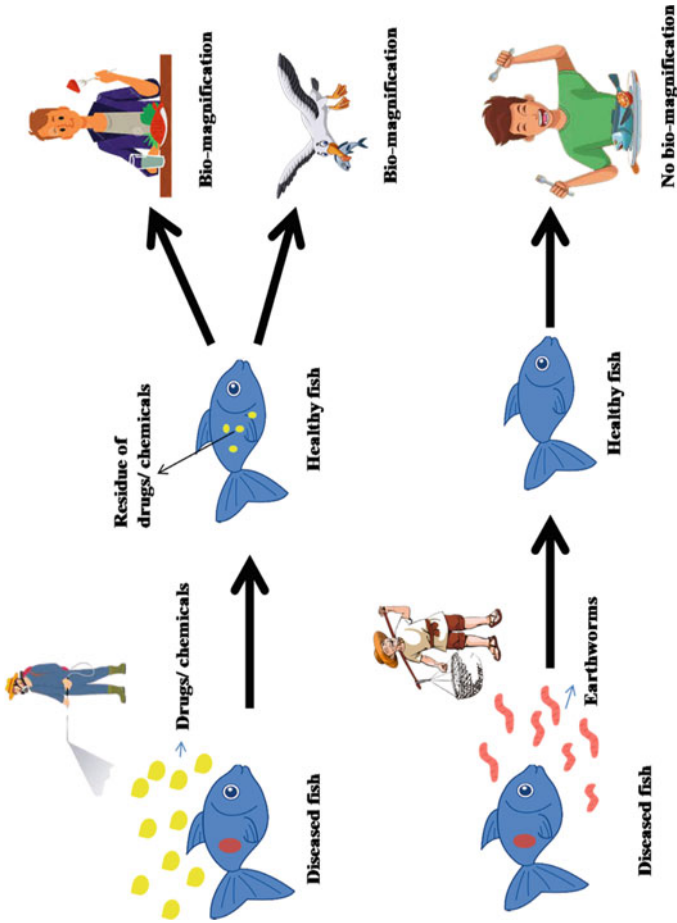


Fig. 1 Diagrammatic representation of Sustainable way of Fish Health Management by Earthworm

1. **Columnaris Disease:** This disease is caused by the external bacteria *Flavobacterium columnare* that affects cultured and wild fishes. This bacterium causes skin lesions, gills necrosis and fin infection. It may be occurred due to rough handling. Small whitish pale discoloration surrounded by radish tinge type lesion is developed on head or back resembling saddle-back. Therefore, also known as a saddle-back disease [2, 16].
2. **Motile Aeromonas Septicaemia (MAS):** This disease mainly caused by *Aeromonas hydrophila*, *A. veronii* and *A. caviae*. This disease was reported worldwide especially in brackish and freshwater fishes. This disease is also known as “red disease” because red patches develop on the body, reddened fin, diffuse haemorrhage on the skin. These bacteria also affect the internal part like the intestine, connective tissue, kidney, spleen etc. Sometimes sudden death is reported that causes high economic loss in cultured freshwater fish [2, 17].

2.2 Fungal Diseases of Fish

Mainly fungi have economic value because they use debris. But if fish are under stressed conditions (maybe due to disease, injury, poor nutritional diet, poor environmental condition), fungi may infect the fish [2, 17]. Some important fungal diseases are discussed here.

1. **Saprolegniasis:** This fungal disease is mainly caused by *Saprolegnia* species known as “Water molds”. This disease occurs in both brackish and freshwater due to poor environmental conditions and injured fish. These water molds are visible as cottony white, grey, greenish or brownish-red masses on fish’s gills and skin [18, 19].
2. **Branchiomycosis:** This disease is also known as “gill rot”. Infections are mainly caused by *Branchiomyces sanguinis* and *B. demigrans*. They affect the gill of fish and cause respiratory distress. Fish may become lethargic and gills appear striated or marbled with pale areas. This disease may cause high economic loss [19, 20].

2.3 Viral Diseases of Fish

The viral disease cannot be cured by medication because the virus uses the host machinery. Therefore, need to provide good nursing care so that fish own immune system can cure viral disease. Some important viral diseases are discussed here.

1. **Viral Hemorrhagic Septicaemia (VHS):** This disease caused by Novirhabdovirus (VHS virus) belongs to Rhabdoviridae family. It is a fatal disease for fish responsible for high economic loss. The virus genome has single-stranded RNA [21]. Rainbow trout is most susceptible to this disease. Clinical symptoms are, damage to endothelial lining of the internal body part, discolouration of the gills,

darkening of the body. Over the year, its host range has expanded and it transfers its genetic material by a horizontal gene transfer mechanism [22, 23].

2. **Lymphocystis:** It is caused by a lymphocystis virus identified as iridovirus. Its distribution is the cosmopolitan effect of the fresh, brackish and marine water fishes. It is the oldest known virus in fish. These viruses are large icosahedral viral particles having diameter 120 to 340 nm [23, 24]. Hypertrophy of fibroblastic cells in the dermis of connective tissue is a characteristic feature of this disease. Infected fish have a small cream-coloured nodular lesion on the skin and fin [24, 25].

2.4 Parasitic Diseases of Fish

Parasites that cause disease in fish belong to diverse groups. Parasites that flourish mainly include protozoan, cestodes, copepods, crustaceans, leeches, monogeneans, nematodes, acanthocephalans, pentastomes, trematodes and tubellarians. Fish may serve as host at any stage of the parasite life cycle [26, 27]. Some important parasitic diseases are discussed here.

1. **White Spot Disease:** It is also known as “Ich” and is caused by ciliated protozoan *Ichthyophthirius multifiliis*. “Ich” is an obligate parasite and capable of causing 100% motility. They develop white, raised nodules up to 1 mm on the body wall and/or fins. This disease was reported in freshwater fishes. If the infection is only limited to gills, no white spot will be visible. Gills will appear swollen with thick mucus covering [27, 28].
2. **Blue Slime Disease:** This is caused by a very small-sized flagellate parasite *Ichthyobodo* (formerly known as *Costia*) and difficult to identify. They can be located on the skin, gills and fins. Infected freshwater fishes secrete huge amounts of mucus. Therefore, the farmers called it “blue slime disease” [26, 28]. In this disease fry, young and stressed fishes have greater mortality. Fishes face respiratory problems and become lethargic. Immediate death may occur before any clinical symptoms were seen [27, 28].

3 Drugs or Chemicals Used to Cure Fish Diseases

A variety of drugs and antibiotics are utilized in aquaculture for fish health management. These are commonly administered by prolonged immersion or mixing into their diet [10]. The most commonly used antibiotics are Florfenicol, Oxytetracycline, Enrofloxacin, Chloramphenicol, Erythromycin, Trimethoprim + Sulfametoxazol [7].

4 Impact of Drugs/Chemicals

With the tremendous expansion of aquaculture, the use of chemicals, antibiotics and aqua drugs are increasing.

4.1 *Bio-Magnification*

The chemicals or drugs used for the treatment of diseases may bio-accumulate in fishes. Bio-magnification occurs when other organisms including humans eat these fishes. This is a major concern because due to persistence of these drugs in fish may affect human and environmental health. Bio-magnification affects the survival of organisms directly or indirectly and may cause the extinction of any species from that particular ecosystem. So, there is the risk of exposure of fish to different drugs [29, 30].

4.2 *Adverse Effects of Antibiotics*

Among the drugs used in fish health management, antibiotics are the severest environmental pollutants. The input of antibiotics into the aquatic environment may lead to the evolution of antibiotic-resistant genes in pathogenic bacterial species [13, 30–32]. Consequently, over time, excessive use of antibiotics in aquaculture contributes to spreading disease-resistant bacteria in consuming organisms like birds and humans. Another problem arises due to excessive use of antibiotics is its residue in different water bodies like ponds, water sediments and in different fish products which leads to undetected consumption of antibiotics by fish consumers. These residues in food items may cause allergy and toxicity to its consumers. Suppose we used sewage treated water for culturing of fish. There is no doubt that the residue of antibiotics remains in this treated water, which affects fish physiology and biochemical functioning [10, 33, 34].

5 Therapeutic Properties of Earthworms

For many centuries, earthworms have been used as a source of food in Ayurveda, Traditional Chinese Medicine (TCM), and other Asian countries like Japan, Vietnam, and Korea. But gradually there is research evidence and renewed efforts through bioprospecting to understand the mechanism of action; whether earthworms are used as food and/or as a source of potential therapeutic products [4, 35, 36].

Since 1340 AD they have been exploited in medicine to treat a variety of diseases. However, the research on the therapeutic properties of earthworms has been started after the development of biochemical technologies [37–39]. Several bioactive molecules that can be used as a potential drug have been found in earthworms during the research. These bioactive molecules showed diverse activities, like anti-microbial, fibrinolytic, anti-coagulative and anticancer. Therefore, they can be exploited to treat various diseases [4, 39, 40].

Earthworms species that are usually used in natural medicine are *Lumbricus rubellus*, *Lampito mauritii*, *Eisenia fetida* and *Pheretima* sp [36]. Earthworm *L. mauritii*, which is found throughout India, especially south India, have antiulcer, anti-inflammatory, antimicrobial and antioxidative properties [4, 41, 42]. Earthworms are appreciated and used for the treatment of a variety of ailments in most eastern and Southeast Asian countries. In China, Vietnam, Korea, and most South East Asia, earthworms have been known as “Earth Dragons” and used for their therapeutic properties and recognized in oriental medicine [43]. In Korea, earthworms are used to prevent a wide array of ailments and to boost general health [9, 44]. In India, various tribes and people from remote villages have been used earthworms to cure various types of diseases [9]. In Iran, they are believed to reduce bladder stones when baked and consumed with bread. Similarly, earthworms have been regarded as a potent and effective therapeutic agent in other Asian countries like Japan, Burma, Laos and Taiwan [40].

5.1 Earthworms as a Source of Biologically Active Molecules

The coelomic fluid and tissue homogenate of earthworms act as a valuable mixture of bio-active molecules, which exhibit potential therapeutic properties and could be very useful in veterinary and human medicine. Some of the bioactive molecules which have been extracted from earthworms include glycoproteins, polysaccharides, peptides, amino acids, glutathione, fibrinolytic enzymes, vitamins, lumbrofebrin, lumbritin, purine, choline, microelements, fatty acids, terrestrolumbrolysin and cholestrin [45, 46]. These bioactive molecules target the cellular host and foreign proteins which are essential for the progression of the disease and play a vital role in the maintaining homeostasis, wound healing and induction of proliferation [47].

Thus, the earthworms could be a useful and economical source of biologically active molecules, which have the biomedical potential to cure a variety of diseases. Extraction and use of bioactive molecules from earthworms have been carried out by local communities worldwide, especially in Asian countries like China, India, Korea, Vietnam and Myanmar [9, 48].

5.2 Anticarcinogenic Property

Earthworm tissue and coelomic fluid contain active molecules which are involved in antitumor and cytotoxic activities. The anticarcinogenic property of these active ingredients from earthworms has been observed in several in vitro and in vivo experiments. Proteases and earthworm fibrinolytic enzyme (EFE) present in earthworm extract (EE) show remarkable anticarcinogenic activity in heptoma cells. Matrix Metalloproteinase-2 (MMP-2) involves in invasion and metastasis of cancer cells. Earthworm fibrinolytic enzyme (EFE) suppresses this enzyme and thus protect the cell [37, 39]. EE prevents the excess uptake of glucose and thus shows anticarcinogenic properties. In earthworms' coelomic fluid, the atumorilytic factor analogous to the vertebrate "cytokine tumor necrosis factor" was identified by SDS-PAGE analysis [49].

5.3 Skin Wound Healing

Skin wound healing is a complicated biological process, which involves various phases like, inflammation, new tissue formation, hemostasis, proliferation, granulation, production of matrix and remodelling [50, 51]. The coelomic fluid of earthworms contains some proteins which aid in skin wound healing by increasing the expression of growth factors and stimulating the proliferation and differentiation of epithelial cells and fibroblasts [52]. Different preparations from earthworms, *L. rubellus* and *E. fetida* shortened the time of healing and promoted wound healing by increasing granulation, epithelization and collagen synthesis [39].

• Mode of action Earthworm Extract (EE) in wound healing [53]

1. The EE accelerates the secretion of hydroxyproline and transforming growth factor- β (TGF- β), which increases collagen synthesis, promotes and expands the blood capillaries, and the proliferation of fibroblasts.
2. Expanded blood capillaries increase the permeability of local blood capillaries, circulation of blood, transportation of nutrients, stimulating the secretion of different cytokines, and inducing cells to enter injured tissue.
3. It accelerates the formation of white blood cells, platelets, and interleukin-6, speeding up the elimination of foreign particles and necrotic tissue.
4. Accelerated white blood cells, granulocytes and platelets promote angiogenesis, enhance the metabolism rate of injured tissue, reduce inflammation injury and boost the local circulation of the wound.
5. It also promotes the repair of injured endothelial cells, which provide nutrition to the new granulation tissue and plays an essential role in hyperplasia by assisting the proliferation of platelets.
6. Thus EE promotes wound healing, reduces infection risk and improves immunity.

5.4 Antipyretic Property

Earthworms contain antipyretic substances (substances that can lower body temperature and inhibit bacterial growth) such as arachidonic acid, antipurin, anti-toxins and vitamins. They also have antibacterial compounds that inhibit the growth of pathogenic bacteria [14]. The elevated body temperature may also be suppressed by anti-inflammatory effects of earthworm extract [54].

5.5 Antioxidative Property

Antioxidants are biomolecules that protect cells from free radical damage and some other oxygen species in the body of organisms. Earthworm extract has been found to show extremely high antioxidative properties due to the presence of high concentrations of antioxidants such as superoxide dismutase (SOD), catalase (CAT), glutathione peroxidase (GPX) and glutathione (GSH) [55]. It also contains a large concentration of phenolic compounds which neutralize the free radicals, due to the presence of the hydroxyl group [41].

5.6 Antiulcer Property

Earthworm paste reduces the quantity of gastric juice, acidity and gastric ulcer index, distinctly indicating its efficacy in reducing these factors, which lead to ulcers. Its highly proteinaceous nature and polyphenolic compounds are responsible for reducing gastric secretions and inhibiting histamine receptors, respectively. The main mechanism that results in ulcer formation is lipid peroxidation. It destroys the cell membrane by releasing intracellular constituents such as lysosomal enzymes, leading to further tissue damage. But the administration of earthworm paste increases the levels of anti-oxidant enzymes. It lowers the peroxidation index, indicating the scavenging of free radicals and reducing lipid peroxidation [42]. Earthworms have a high amount of bio-copper, which has a strong inhibitory effect on gastric secretions. It can be given orally and effectively to treat peptic ulcers, especially gastric ulcers [55, 56].

5.7 Anti-Inflammatory Property

Earthworm extract has anti-transductive, anti-proliferative, and anti-histaminic activities responsible for inhibiting inflammation mediators like Tumor necrosis factor (TNF- α) [38, 54]. TNF- α is a cytokine, which mediates different functions involved

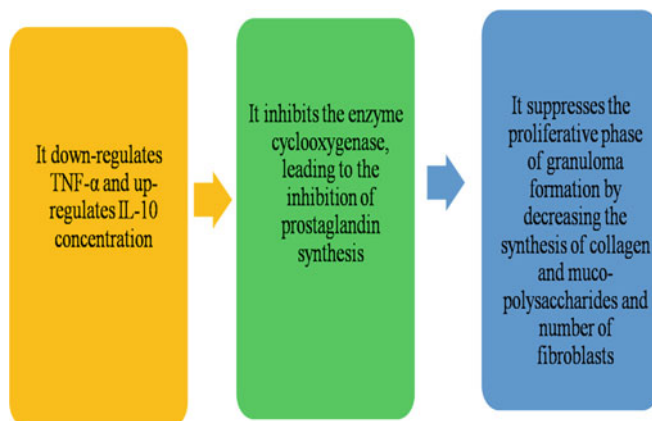


Fig. 2 Mechanism of action of Earthworm Extract as an Anti-inflammatory agent

in systemic inflammation like the stimulation of acute-phase reaction, fever induction, death of apoptotic cells, inflammation, inhibition of tumorigenesis and viral replication etc. A large concentration of TNF is released by various types of cells such as cardiac myocytes, fibroblasts, lymphoid cells, endothelial cells, mast cells, neurons and adipose tissue in response to inflammatory agents like lipopolysaccharide, carrageenan, bacterial products and Interleukin (IL)-1etc. IL-10 is also a cytokine, which down-regulates the inflammatory reactions and its concentration increases during the suppression of inflammation as mentioned in the mechanism of action [57] in Fig. 2.

5.8 Hepato-Protective Property

Hepatotoxic chemicals and several types of drugs cause damage to liver cells primarily by lipid peroxidation and other oxidative damages. The particular damage in liver cells is indicated by decreased liver antioxidants and increased activities of serum enzymes, like Alkaline phosphatase (ALP), Aspartate aminotransferase (AST), Alanine aminotransferase (ALT), Thiobarbituric acid reactive substances (TBARS) and bilirubin [55]. When treated with earthworm extract, these effects get reversed. The earthworm extract acts as a hepatoprotective agent as it increases the activities of the liver by enhancement in the activities and amount of liver antioxidants (GSH, SOD, GP_x, and CAT) and decreases the activities and amounts of serum enzymes (AST, ALP, ALT, TBARS and bilirubin). The mechanism of action of earthworm extract (Fig. 3) modulates the genes involved in the synthesis of antioxidant enzymes in liver tissue prevents the formation of the reactive oxygen species [41].

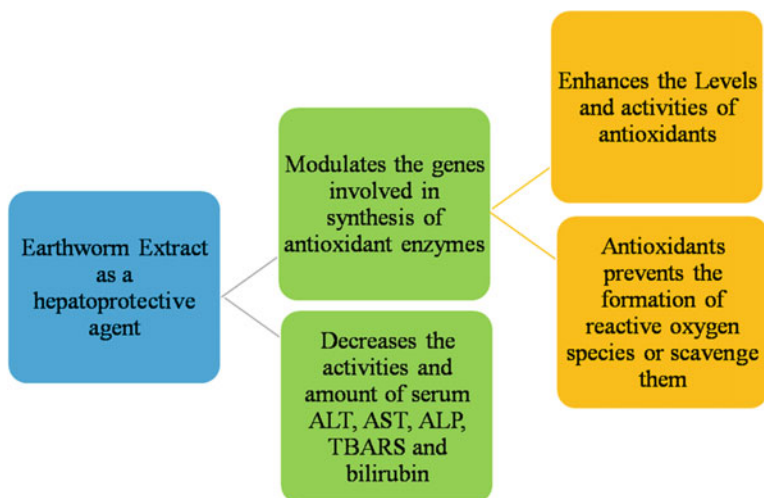


Fig. 3 Mechanism of action of earthworm extract in the damaged liver

5.9 Analgesic Properties

Important analgesic properties of earthworms are.

1. Earthworm extract increases the pain threshold and exhibits peripheral but not central analgesic effects.
2. In addition, it decreases serum neural transmitters, such as nitric oxide synthase (NOS), nor-epinephrine (NE) and 5-hydroxytryptamine (5-HT) concentration like other analgesic drugs e.g. aspirin and morphine.
3. Therefore, EE could be used as a promising peripheral analgesic drug [58].

5.9.1 Anticoagulative or Fibrinolytic Property

In biological systems, the development of fibrin clot and its lysis are usually well balanced, but if fibrin is not hydrolyzed due to some disorder, thrombosis can occur. In blood clot formation, fibrin is the chief protein constituent which is formed from fibrinogen by thrombin [47].

Earthworms act as an attractive source of the fibrinolytic enzymes, urokinase, tissue plasminogen activator (t-PA), physiologically active compounds, such as serine peptidases (eg. peptidase PI and PII) and cytotoxic components (coelomic cytolytic factor—eiseniapore). These biomolecules have very strong anticoagulant and fibrinolytic properties [47, 52]. Urokinase-type plasminogen activators (u-PA) are usually known as lumbrokinase (LK). They convert plasminogen into plasmin by stimulating the activity of endogenous t-PA activity or dissolve the fibrin clots itself. This reaction indirectly lengthens the time of clotting and helps in fibrinolysis. LK has been used to dissolve clots, bring down blood viscosity, and lower platelet aggregation

Table 1 Some of the antimicrobial peptides identified from earthworms are

Sr. No	Earthworm species	Antimicrobial peptides	References
1	<i>Pheretima tschiliensis</i> and <i>Eisenia fetida</i>	Two, (PP1 and OEP3121)	[63]
2	<i>Pheretima guillelmi</i>	lumbricin-PG from skin secretions	[64]
3	<i>E. fetida</i>	Six, antibacterial vermipeptides family (AVPF) from coelomic fluid and tissue homogenate	[62]
4	<i>Lumbricus rubellus</i>	Lumbricin I	[65]

[47]. The anticoagulants found in earthworms particularly interfere in the intrinsic pathway of the blood clotting cascade [59, 60]. In China, earthworm protein extracts and lumbricinase have been studied extensively and have been used to maintain a healthier blood state [36].

5.9.2 Antibacterial Properties

The coelomic fluid and extracts of earthworms are known to have potential enzymes exhibiting antibacterial properties that can inhibit the growth of gram-positive and gram-negative pathogenic bacteria [61]. This antibacterial activity is ascribed to some proteins, such as fetidins, lysozymes, haemolytic factors and coelomic cytolytic factors [32]. Earthworms also have lumbricin (a Group of antimicrobial proteins) which are produced in response to pathogen invasion [14]. Their molecular weight was generally below 10 kDa and can either perform direct antibacterial functions or indirect functions as a signal peptide [62] (Table 1).

5.9.3 Benefits of Earthworm as a Natural Medicine

1. Earthworm extracts are naturally found and rarely exert side effects.
2. Safe for all ages
3. Safe for continuous and long-term consumption
4. It can be used in conjunction with other medications and it also enhances the other drugs work [36].

6 Immune System of Earthworm

Earthworms lack anticipatory, specific and lymphocyte based immune mechanisms and rely on natural, nonspecific and innate immune mechanisms [66] (Fig. 4) which are based on pattern recognition receptors (PRRs) [67]. So far three types of PRRs

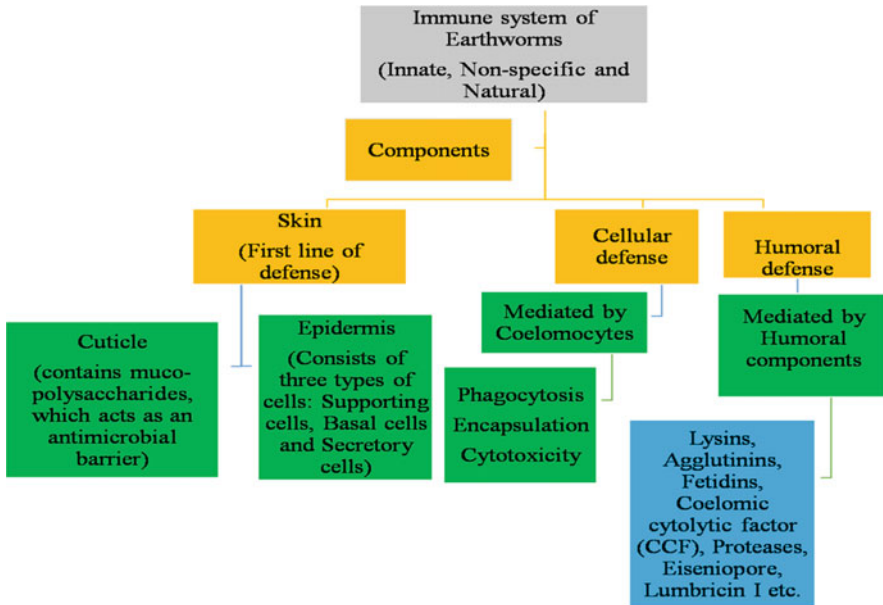


Fig. 4 Components of the immune system of Earthworms

(Coelomic cytolytic factor CCF, lipopolysaccharide-binding protein EaLBI/BPI, Toll-like receptor EaTLR) have been described in earthworms [67–69].

6.1 First Line of Defense

Skin: The earthworm’s skin, combined with mucus membrane, provides the first line of defense as it acts as the non-specific protective barrier against invasion by microbes or parasites. It covers the entire body of the earthworm and formed of the epidermis and a thin layer of cuticle. The cuticle contains antimicrobial mucopolysaccharides [66, 70] and the epidermis contains single-layer epithelium formed of three different cells:

1. **Supportive Cells**
2. **Basal Cells:** These cells are involved in graft rejection, wound healing and exhibit phagocytic activity
3. **Secretory Cells:** They secrete mucus having mucopolysaccharide-lipid-protein complex and several antibacterial factors [66, 71].

The earthworm’s skin cannot properly prevent the microbes from entering the coelomic cavity as it possesses a dorsal pore in every segment of the coelomic cavity [72]. Consequently, some microbes penetrate the earthworm’s first line of defense and enter the coelomic cavity, where they encounter soluble and membrane-bound

pattern recognition receptors (PRRs), that identify pathogen-associated molecular patterns (PAMPs). After this recognition, pathogens are attacked by coelomocytes (cellular defense) and a variety of humoral factors (humoral defense) secreted by coelomocytes [66].

6.2 Cellular Defense Mechanism

Cellular defense mechanism mainly involves the activity of various types of coelomocytes, which are very important for building the innate immunity of earthworms. Based on functional and morphological behaviour, they are differentiated into three different types of immune cells such as granulocytes, eleocytes and amoebocytes [73].

1. **Eleocytes:** They are derived from chloragogen cells found around the intestinal area and exert excretory, trophic and immunological functions by synthesizing and secreting agglutinins, opsonins, cytotoxic and antimicrobial factors in coelomic fluid [74–76]. They resemble the invertebrate liver cells in certain functions, e.g. they transport nutrients by circulation into coelomic fluid and other organs and cells. They are also associated with the metabolism and storage of lipids and glycogen [77].
2. **Amoebocytes:** They originate from the mesenchymal layer around the coelom and characterized by the comparatively large eccentric nucleus and several pseudopodia [76]. They perform cellular immune functions such as phagocytosis and cytotoxicity (NK cell-like activity) [78–81]. In addition, they fight with multicellular invaders, like nematodes through encapsulation (brown body development) [76].
3. **Granulocytes:** These are spherical, acidophilic and composed of centrally located nuclei. They produce humoral factors due to the presence of eosinophilic granules and various vacuoles [73, 82].

The coelomocytes are involved in innate cellular mechanisms, such as encapsulation, phagocytosis, and cytotoxicity, to fight pathogenic microorganisms [83, 84]. These coelomocytic elementary processes can be regulated by opsonins or humoral factors covering foreign bodies and facilitating their encapsulation and phagocytosis [73, 81] as mentioned in Fig. 5.

Encapsulation: It is a cellular immune function used for foreign objects which are not phagocytosed due to their large size [85]. The encapsulated cellular capsule can also be called a “brown body” due to the presence of melanin pigments, which are produced by the activation of the prophenoloxidase cascade [72, 86]. Moreover, some coelomocytes possess cytotoxic activity like natural killer cells [66]. The mechanism of encapsulation [86] is shown in Fig. 6.

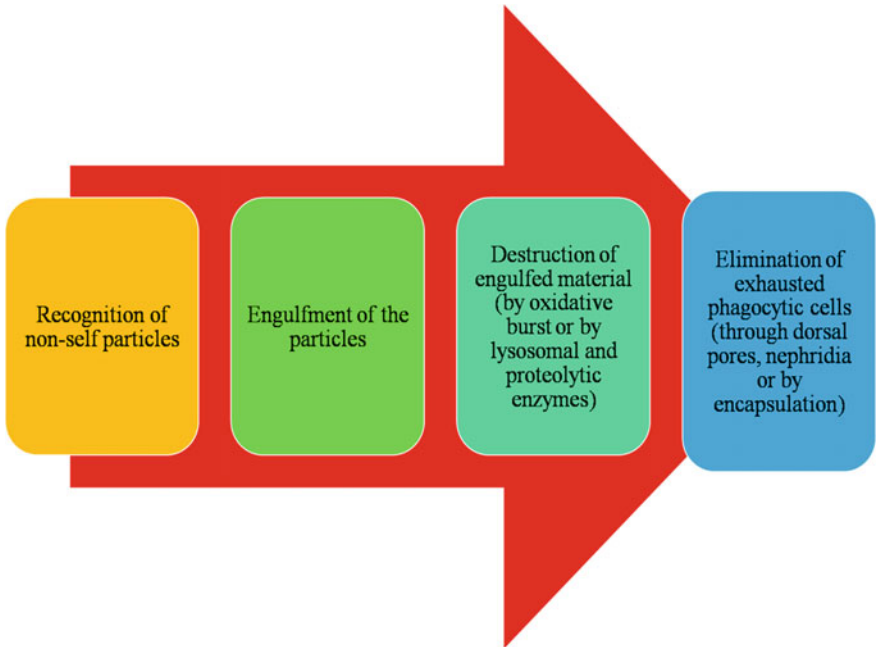


Fig. 5 Mechanism of Phagocytosis

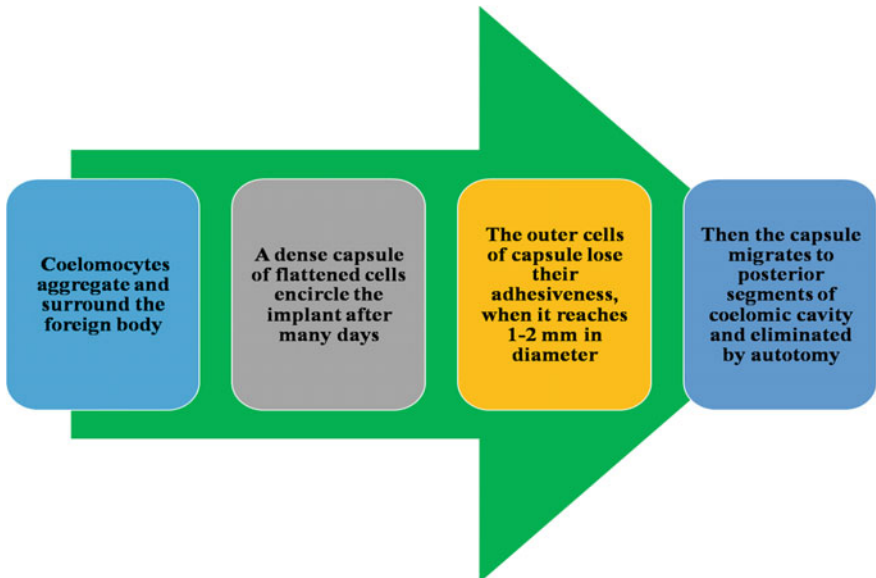


Fig. 6 Mechanism of encapsulation

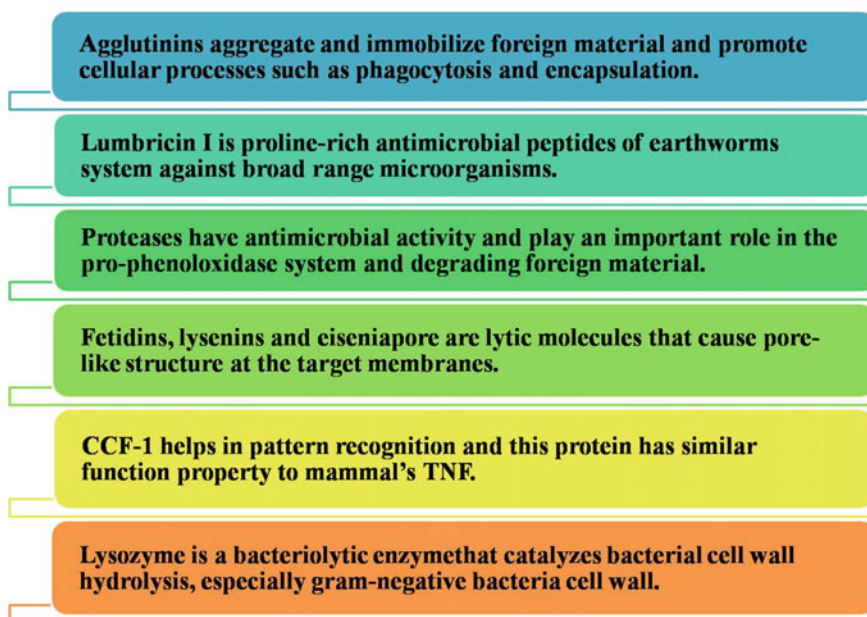


Fig. 7 Functions of some of the humoral components of coelomic fluid [72, 81, 85, 88, 91, 92]

6.3 Humoral Defense Mechanism

Earthworms' coelomic fluid comprises humoral immunity components (examples; agglutinins, lysins, proteases, fetidin, CCF, lumbricin I and eiseniapore) that are synthesized by coelomocytes. These humoral components are responsible for agglutination, opsonisation, lysis of non-self-bodies, clotting, and phenoloxidase cascade reaction [87–89]. In earthworms Lysis cause by fetidins, CCF-1, lysenin and eiseniapore, whereas agglutination and lysis caused by H1, H2 and H3 molecules [90] (Fig. 7).

7 Role of Earthworm to Control Fish Diseases

As we discussed earthworm coelomic fluid have different immunogenic component having important biological properties like antimicrobial, proteolysis, cytolysis and mitogenic. The coelomic fluid of different earthworms has the potential to control a range of fish diseases especially bacterial diseases. Earthworms can also be used to treat fish diseases resistant to antimicrobial drugs, and the results were significant [9, 11].

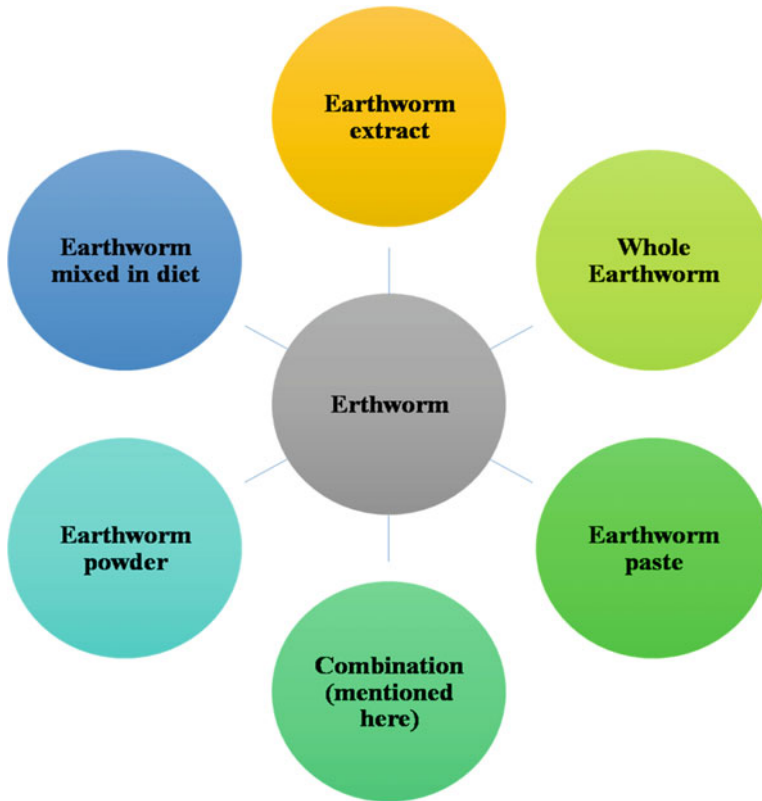


Fig. 8 Different forms of earthworm use

8 Different Method/Strategies to Use Earthworm

Due to the different beneficial attributes of earthworms (which we already studied above), they are used in a different form [4] (Fig. 8). Their activity differs in different solvents like acetone, ethanol etc. [11, 93–95].

9 Comparative Study of Treated and Untreated Fish

1. Morphological Changes

Perionyx excavatus diet significantly increased the growth of mirror carp (*Cyprinus carpio*) [11]. Increased growth performance, survivability, and length of *C. carpio* were observed when earthworm extract was used in combination with fish diets

compared to control fish [9]. *E. fetida* extract enhances *Caspian roach* growth performance [94]. Limited substitution of earthworm meal (*Libyodrilus violaceus*) also enhances African catfish (*Clarias gariepinus*) growth [96].

2. Haemato-Immunological Studies

Extracts from the different earthworm species significantly affect RBC count and haemoglobin value than the control fish. Bansal [9] observed a rise in RBC count, leukocyte count, and packed cell volume in fish after using earthworm extract of *E. fetida* in *C. carpio*. Similarly, Rawling et al. [11] also noticed a rise in haemoglobin but decrement of total leukocyte level in mirror carp (*C. carpio*) when given earthworm (*Perionyx excavatus*) meal as compared to soyabean meal. But, Rufchaei et al. [94] observed *E. fetida* extract positively affect the innate response in the *C. roach*. So, we can say that earthworms can increase the haematological parameters in fishes.

10 Conclusions

As the world population increases, food security is becoming a major problem. This put pressure on agricultural land and fish farming. As a result, many fish disease is being reported. Drugs, antibiotics, and chemicals used to treat fish diseases finally causes bio-magnification and bio-accumulation. Thus, earthworm provides the alternative and sustainable way to cure fish disease. Mainly fish bacterial diseases can be cured by different earthworm products like its extract, powder either individual or in combination with fish diet at different doses. So, we can conclude from this chapter that the earthworms play a vital role to cure fish diseases sustainably.

11 Future Prospective

There is no doubt that modern practices through the use of chemicals, drugs and antibiotics cure fish diseases. But the persistence of these chemicals has an ill effect on the environment as well as on human health along with its effects on water quality. Now a day, people are not only concerned about their health but also the environment and other organism's health. Therefore, these practices become questionable. This chapter highlights the different sustainable ways to cure fish diseases. There is also a need to find some new methods and strategies for an efficient way to cure fish diseases by the use of earthworms. A challenge for the future is developing socio-economically, genetically modified disease-resistant fish through sustainable ways, either by using earthworms or another suitable organism.

Recommendations

Further research needs to find out active compounds from different species of earthworms that can be used to cure diseases in fish and other animals. At large scale commercial products can be formed by using earthworms.

Acknowledgements Authors are thankful to Department of Zoology and Aquaculture, Chaudhary Charan Singh Haryana Agricultural University, Hisar, Haryana, India for prompt provision of all the necessary facilities timely.

References

1. Waite R, Beveridge M, Brummett R, Castine S, Chaiyawannakarn N, Kaushik S, Mungkung R, Nawapakpilai S, Phillips M (2014) Improving productivity and environmental performance of aquaculture. WorldFish
2. Mishra SS, Rakesh D, Dhiman M, Choudhary P, Debbarma J, Sahoo SN, Barua A, Giri BS, Ramesh R, Ananda K, Mishra CK (2017) Present status of fish disease management in freshwater aquaculture in India: state-of-the-art-review. J Aquac Fish 1(003). <https://doi.org/10.24966/AAF-5523/100003>
3. Samson JS, Choresca CH, Quiazon KMA (2020) Selection and screening of bacteria from African nightcrawler, *Eudrilus eugeniae* (Kinberg, 1867) as potential probiotics in aquaculture. World J Microbiol Biotechnol 36(1):16
4. Kumar R, Sharma P, Gupta RK, Kumar S, Sharma MM, Singh S, Pradhan G (2020) Earthworms for eco-friendly resource efficient agriculture. In: Resources use efficiency in agriculture. Springer, Singapore, pp 47–84. https://doi.org/10.1007/978-981-15-6953-1_2
5. Walker PJ, Winton JR (2010) Emerging viral diseases of fish and shrimp. Vet Res 41:51
6. Mishra SS, Dhiman M, Swain P, Das BK (2015) Fish diseases and health management issues in aquaculture. ICAR-CIFA training manual No. 18, Central Institute of Freshwater Aquaculture, Bhubaneswar, India
7. Kumar V, Roy S (2017) Aquaculture drugs: sources, active ingredients, pharmaceutical preparations and methods of administration. J Aquac Res Develop 8:510. <https://doi.org/10.4172/2155-9546.1000510>
8. Francis-Floyd R (1991) Introduction to fish health management. Institute of Food and Agricultural Sciences, University of Florida, Florida Cooperative Extension Service
9. Bansal (2013). Utilization of vermi extract for health management in common carp (*Cyprinus carpio* Linn.) for sustainable aquaculture. Doctoral dissertation, CCSHAU
10. Banerjee S, Kumar V, Pathak AN (2014) Drug effects on aquaculture and its remediation. J Drug Deliv Ther 4(1):117–122
11. Rawling MD, Merrifield DL, Snellgrove DL, Kuhlwein H, Adams A, Davies SJ (2012) Haemato-immunological and growth response of mirror carp (*Cyprinus carpio*) fed a tropical earthworm meal in experimental diets. Fish Shellfish Immunol 32(6):1002–1007
12. Pareja L, Heinzen H, Cesio MV, Colazzo M, Pérez-Parada A (2021). Determination of pesticide residues in fish. Sustain Agric Rev 47(1–46). Springer, Cham. https://doi.org/10.1007/978-030-54712-7_1
13. Yang C, Song G, Lim W (2020) A review of the toxicity in fish exposed to antibiotics. Comp Biochem Physiol Part C Toxicol Pharmacol 108840
14. Waluyo J, Wahyuni D, Nuri N (2019) Antipyretic effects of dried earthworm (*Pheretima javanica* K.) in male white rat (*Rattus Norvegicus*) with typhoid fever. Int J Sci Technol Res 8(08)

15. Sandeep P, Chamundeswari Devi B, Kumar KP (2016) Present status of parasitic and bacterial diseases in fresh water fish seed farms in East Godavari District, Andhra Pradesh. *Int J Appl Pure Sci Agric* 2:117–121
16. Declercq AM, Haesebrouck F, Van den Broeck W, Bossier P, Decostere A (2013) Columnaris disease in fish: a review with emphasis on bacterium-host interactions. *Vet Res* 44(1):1–17
17. Mohanty BR, Sahoo PK (2007) Edwardsiellosis in fish: a brief review. *J Biosci* 32:1331–1344
18. Klinger RE, Francis-Floyd R (1996) Fungal diseases of fish. VM (USA). <http://edis.ifas.ufl.edu/VM033>
19. Yanong RP (2003) Fungal diseases of fish. *Vet Clin Exotic Anim Pract* 6(2):377–400
20. Khoo L (2000) Fungal diseases in fish. In *Seminars in Avian and exotic pet medicine*. WB Saunders 9(2):102–111
21. Chinchilla B, Encinas P, Coll JM, Gomez-Casado E (2020) Differential immune transcriptome and modulated signalling pathways in rainbow trout infected with Viral Haemorrhagic Septicaemia Virus (VHSV) and its derivative Non-Virion (NV) gene deleted. *Vaccines* 1:58
22. Skall HF, Olesen NJ, Mellergaard S (2005) Viral haemorrhagic septicaemia virus in marine fish and its implications for fish farming—a review. *J Fish Dis* 28(9):509–529
23. Öztürk RÇ, Altınok İ (2014) Bacterial and viral fish diseases in Turkey. *Turk J Fish Aquat Sci* 14(1):275–297
24. Borrego JJ, Valverde EJ, Labella AM, Castro D (2017) Lymphocystis disease virus: its importance in aquaculture. *Rev Aquac* 9(2):179–193
25. Leiva-RebolloR LAM, Valverde EJ, Castro D, Borrego JJ (2020) Persistence of Lymphocystis Disease Virus (LCDV) in seawater. *Food Environ Virol* 21:1–6
26. Yanong R (2004) Fish health management considerations in recirculating aquaculture systems—part 2: pathogens. *EDIS* 2004(1)
27. Roberts HE, Palmeiro B, Weber ES III (2009) Bacterial and parasitic diseases of pet fish. *Vet Clin North Am Exotic Anim Pract* 12(3):609–638
28. Klinger RE, Floyd RF (1998) *Introduction to freshwater fish parasites*. Gainesville (FL): University of Florida Cooperative Extension Service, Institute of Food and Agriculture Sciences, EDIS
29. Daughton CG (2003) Chemicals from pharmaceuticals and personal care product. In: Julius Dasch E (ed) *Water: science and issues*. Macmillan Reference USA, New York, pp 158–164
30. Sandor ZJ, Papp ZG, Kosaros TJ, Hegedus R, Csengeri I (2012) Potential effects of pharmaceuticals and their residues in aquatic environment. *Studia Universitatis VasileGoldisSeriaSti-inteleVietii (Life Sci Ser)* 22(2)
31. Liu M, Zhang Y, Yang M, Tian Z, Ren L, Zhang S (2012) Abundance and distribution of tetracycline resistance genes and mobile elements in an oxytetracycline production wastewater treatment system. *Environ Sci Technol* 46(14):7551–7557
32. Akiba M, Sekizuka T, Yamashita A, Kuroda M, Fujii Y, Murata M, Lee K, Joshua DI, Balakrishna K, Bairy I, Subramanian K, Krishnan P, Munuswamy N, Sinha RK, Iwata T, Kusumoto M, Guruge KS (2016) Distribution and relationships of antimicrobial resistance determinants among extended-spectrum-cephalosporin-resistant or carbapenem-resistant *Escherichia coli* isolates from rivers and sewage treatment plants in India. *Antimicrob Agents Chemother* 60(5):2972–2980
33. Straub JO, Gysel D, Kastl U, Klemmer J, Sonderegger M, Studer M (2012) Environmental risk assessment for ancillary substances in biotechnological production of pharmaceuticals. *Environ Toxicol Chem* 31(3):681–687
34. Sinthuchai D, Boontanon SK, Boontanon N, Polprasert C (2016) Evaluation of removal efficiency of human antibiotics in wastewater treatment plants in Bangkok, Thailand. *Water Sci Technol* 73(1):182–191
35. Cooper EL, Roch P (2003) Earthworm immunity: a model of immune competence. *Pedobiologia* 47:676–688
36. Lakshmi Prabha M, Shathya S (2014) Earthworm—an alternative approach to biomedicine. *Int J Curr Sci* 13:E6–8

37. Chen H, Takahashi S, Imamura M, Okutani E, Zhang ZG, Chayama K, Chen BA (2007) Earthworm fibrinolytic enzyme: anti-tumor activity on human hepatoma cells in vitro and in vivo. *Chin Med J* 120(20):898–904
38. Omar HM, Ibraheim ZZ, EL-Shimy NA, Ali RS (2012) Anti-inflammatory, antipyretic and antioxidant activities of the earthworm extract. *J Biol Earth Sci* 2(1)
39. Grdisa M (2013) Therapeutic properties of earthworms. *Bioremediat Biodivers Bioavailab* 7(1):1–5
40. Cooper EL, Balamurugan M, Huang CY, Tsao CR, Heredia J, Tommaseo-Ponzetta M, Paoletti MG (2012) Earthworms dilong: ancient, inexpensive, noncontroversial models may help clarify approaches to integrated medicine emphasizing neuroimmune systems. *Evid-Based Complement Altern Med* 1–12
41. Balamurugan M, Parthasarathi K, Cooper EL, Ranganathan LS (2007) Earthworm paste (*Lampito mauritii*, Kinberg) alters inflammatory, oxidative, haematological and serum biochemical indices of inflamed rat. *Eur Rev Med Pharmacol Sci* 11(1):77–90
42. Prakash M, Balamurugan M, Parthasarathi K, Gunasekaran G, Cooper EL, Ranganathan LS (2007) Anti-ulceral and anti-oxidative properties of “earthworm paste” of *Lampito mauritii* (Kinberg) on *Rattus Norvegicus*. *Eur Rev Med Pharmacol Sci* 11(1):9–15
43. Lourdumary AJB, Uma K (2014) Antimicrobial activity of earthworm powder (*Lampito mauritii*). *Int J Curr Microbiol Appl Sci* 3(1):437–443
44. El-Kamali HH (2000) Folk medicinal use of some animal products in Central Sudan. *J Ethnopharm* 72:279–289
45. Zhang M, Li X, Liu Y, Ye F, Qiu G (2006) Effects of extract of dilong (pheretima) on the scalded skin in rats. *J Tradit Chin Med* 26:68–71
46. Jamshidzadeh A, Dabagh F, Farshad O, Ommat MM, Mahdavinia A, Azarpira N, Shahbazi M, Najibi A, Heidari R (2018) Hepatoprotective properties of the glycolipoprotein extract from *Eisenia foetida*. *Trends Pharm Sci* 4(3):149–160
47. Grdisa M, Mikecin AM, Hrzenjak TM (2009) Earthworms as a source of bioactive molecules. *Curr Bioact Compd* 5(2):155–159
48. Ranganathan LS (2006) Vermibiotechnology: from soil health to human health. *Agrobios (India)*
49. Mohamed Jaabir MS, Shamsheerali L, Yasar MD, Senthil Kumar S (2011) Evaluation of the cell-free coelomic fluid of the earthworm *Eudrilus euginiae* to induce apoptosis in SiHa cell line. *J Pharm Res* 4:3417–3420
50. Guo S, Dipietro LA (2010) Factors affecting wound healing. *J Dent Res* 89:219–229. <https://doi.org/10.1177/0022034509359125>
51. Reinke JM, Sorg H (2012) Wound repair and regeneration. *Eur Surg Res* 49:35–43. <https://doi.org/10.1159/000339613>
52. Metausic-Pisl M, Cupic H, Kasuba V, Mikecin AM, Grdisa M (2010) Gliko-lipoprotein extract (G-90) from *Eisenia foetida* accelerated the rats wound healing. *Eur Rev Med Pharm Sci* 14:177–184
53. Deng ZH, Yin JJ, Luo W, Kotian RN, Gao SS, Yi ZQ, Xiao WF, Li WP, Li YS (2018) The effect of earthworm extract on promoting skin wound healing. *Biosci Rep* 38(2). <https://doi.org/10.1042/BSR20171366>
54. Balamurugan M, Parthasarathi K, Cooper EL, Ranganathan LS (2009) Anti-inflammatory and anti-pyretic activities of earthworm extract *Lampito mauritii* (Kinberg). *J Ethnopharmacol* 121(2):330–332
55. Singh K, Bhartiya DK (2018) Review on therapeutic use of earthworms. *Int J Basic Appl Res*
56. Dan Z, Ying W, Ying W, Jing-jing Z (2009) Analysis of trace elements in earthworm. *J Shenyang Normal Univ (Natural Science Edition)*
57. Chauhan PS, Tomar J, Prasad GBKS, Agrawal OP (2018) Evaluation of anti-inflammatory activity of earthworm (*Eudrilus euginiae*) extract through animal models. *Int J Adv Res Develop* 3(1):283–292
58. Luo W, Deng ZH, Li R, Cheng G, Kotian RN, Li YS, Li WP (2018) Study of analgesic effect of earthworm extract. *Biosci Rep* 38(1). <https://doi.org/10.1042/BSR20171554>

59. Woo J, Bank YK, Yu KH, Paik SR, Chang CS (1996) Mechanism of blood coagulation. *J Biochem Mol Biol* 29:500
60. Mathur A, Verma SK, Singh SK, Prakash A, Prasad GBKS, Dua VK (2011) Anti-inflammatory activity of earthworm extracts. *Int J Pharm Sci Res* 2(2):278
61. Foekh NP, Sukrama IDM, Lestari AAW (2019) The ability of earthworm *Lumbricus rubellus* extract in slowing down the activation of NF κ B and TNF- α in lipopolysaccharide-induced *Rattus norvegicus*. *Bali Med J* 8(2):347–352
62. Wang C, Sun Z, Liu Y, Zhang X, Xu G (2007) A novel antimicrobial vermin-peptide family from earthworm *Eisenia foetida*. *Eur J Soil Biol* 43:S127–S134
63. Wang X, Wang XX, Zhang Y (2003) An antimicrobial peptide of the earthworm *Pheretima tschiliensis*: cDNA cloning, expression and immunolocalization. *Biotechnol Lett* 25:1317–1323
64. Li W, Li S, Zhong J, Zhu Z, Liu J, Wang W (2011) A novel antimicrobial peptide from skin secretions of the earthworm, *Pheretima guillelmi* (Michaelsen). *Peptides* 32:1146–1150
65. Cho JH, Park CB, Yoon YG et al (1998) Lumbricin I, a novel proline-rich antimicrobial peptide from the earthworm: purification, cDNA cloning and molecular characterization. *Biochim Biophys Acta* 1408:67–76
66. Roubalova R, Prochazkova P, Dvorak J, Skanta F, Bilej M (2015) The role of earthworm defense mechanisms in ecotoxicity studies. *Invertebr Surviv J* 12(1):203–213
67. Prochazkova P, Roubalova R, Skanta F, Dvorak J, Pacheco NIN, Kolarik M, Bilej M (2019) Developmental and immune role of a novel multiple cysteine cluster TLR from *Eisenia andrei* earthworms. *Front Immunol* 10:1277. <https://doi.org/10.3389/fimmu.2019.01277>
68. Bilej M, Rossmann P, Sinkora M, Hanusova R, Beschin A, Raes G et al (1998) Cellular expression of the cytolytic factor in earthworms *Eisenia foetida*. *Immunol Lett* 60:23–29. [https://doi.org/10.1016/S0165-2478\(97\)00127-2](https://doi.org/10.1016/S0165-2478(97)00127-2)
69. Skanta F, Roubalova R, Dvorak J, Prochazkova P, Bilej M (2013) Molecular cloning and expression of TLR in the *Eisenia andrei* earthworm. *Dev Comp Immunol* 41:694–702. <https://doi.org/10.1016/j.dci.2013.08.009>
70. Rahemtulla F, Lovtrup S (1974) The comparative biochemistry of invertebrate mucopolysaccharides II. Nematoda; Annelida. *Comp Biochem Physiol* 49B:639–646
71. Valembois P, Roch P, Lassegues M (1986) Antibacterial molecules in annelids. In: *Immunity in invertebrates*. Springer, Berlin, Heidelberg, pp 74–93
72. Bilej M, Prochazkova P, Silerova M, Jaskova R (2010) Earthworm immunity. In: Soderhall K (ed) *Invertebrate immunity*. Springer, New York, pp 66–79
73. Gupta S, Yadav S (2016) Immuno-defense strategy in earthworms: a review article. *Int J Curr Microbiol Appl Sci* 5:1022–1035
74. Valembois P, Lassegues M, Roch P, Vaillier J (1985) Scanning electron-microscopic study of the involvement of coelomic cells in earthworm antibacterial defense. *Cell Tissue Res* 240(2):479–484
75. Opper B, Bognar A, Heidt D, Nemeth P, Engelmann P (2013) Revising lysenin expression of earthworm coelomocytes. *Dev Comp Immunol* 39(3):214–218
76. Engelmann P, Hayashi Y, Bodo K, Ernszt D, Somogyi I, Steib A, Orban J, Pollak E, Nyitrai M, Nemeth P, Molnar L (2016) Phenotypic and functional characterization of earthworm coelomocyte subsets: linking light scatter-based cell typing and imaging of the sorted populations. *Dev Comp Immunol* 65:41–52
77. Cholewa J, Feeney GP, O'Reilly M, Stazrzenbaum SR, Morgan AJ, Plytycz B (2006) Autofluorescence in eleocytes of some earthworm species. *Folia Histochem Cytobiol* 44(1):65–71
78. Valembois P, Lassègues M (1995) In vitro generation of reactive oxygen species by free coelomic cells of the annelid *Eisenia fetida* andr: an analysis by chemiluminescence and nitro blue tetrazolium reduction. *Dev Comp Immunol* 19(3):195–204
79. Cossarizza A, Cooper EL, Suzuki MM, Salvioli S, Capri M, Gri G, Quaglini D, Franceschi C (1996) Earthworm leukocytes that are not phagocytic and cross-react with several human epitopes can kill human tumor cell lines. *Exp Cell Res* 224:174–182

80. Homa J, Zorska A, Wesolowski D, Chadzinska M (2013) Dermal exposure to immunostimulants induces changes in activity and proliferation of coelomocytes of *Eisenia andrei*. *J Comp Physiol B* 183:313–322
81. Homa J (2018) Earthworm coelomocyte extracellular traps: structural and functional similarities with neutrophil NETs. *Cell Tissue Res* 371(3):407–414
82. Adamowicz A, Wojtaszek J (2001) Morphology and phagocytolytic activity of coelomocytes in *Dendrobaena veneta* (Lumbricidae). *Zoologica Poloniae* 46:91–104
83. Cooper EL, Kauschke E, Cossarizza A (2001) Annelid humoral immunity: Cell lysis in earthworms. *Adv Exp Med Biol* 484:169–183
84. Patil R, Biradar M (2017) Earthworm's coelomic fluid: extraction and importance. *Int J Adv Sci Res* 2(2):1–4
85. Valembois P, Seymour J, Lassegues M (1994) Evidence of lipofuscin and melanin in the brown body of the earthworm *Eisenia fetida andrei*. *Cell Tissue Res* 227:183–188
86. Bilej M, De Baetselier P, Beschin A (2000) Antimicrobial defense of the earthworm. *Folia Microbiol* 45(4):283
87. Hamed SS, Kauschke E, Cooper EL (2005) Cytochemical properties of earthworm coelomocytes enriched by Percoll. *Int J Zool Res* 1(1):74–83
88. Engelmann P, Cooper EL, Nemeth P (2005) Anticipating innate immunity without a Toll. *Mol Immunol* 42(8):931–942
89. Tahseen Q (2009) Coelomocytes: biology and possible immune functions in invertebrates with special remarks on nematodes. *Int J Zool* 2009:13. <https://doi.org/10.1155/2009/218197>
90. Koenig S, Wagner F, Kauschke E, Peter-Katalinic J, Cooper EL, Eue I (2003) Mass spectrometric analyses of CL39, CL41 and H1, H2, H3 confirm identity with fetidin and lysenin produced by earthworm leukocytes. *Dev Comp Immun* 27:513–520
91. Kauschke E, Mohrig W, Cooper EL (2007) Coelomic fluid proteins as basic components of innate immunity in earthworms. *Eur J Soil Biol* 43:S110–S115
92. Beschin A, Bilej M, Brys L, Torreele E, Lucas R, Magez S, De Baetselier P (1999) Convergent evolution of cytokines. *Nature* 400(6745):627–628
93. Shen Y (2010) Earthworms in traditional Chinese medicine (Oligochaeta: Lumbricidae, Megascolecidae). In: *Advances of the 4th international oligochaeta taxonomy meeting*
94. Rufchaei R, Hoseinifar SH, Nedaei S, Bagheri T, Ashouri G, Van Doan H (2019) Non-specific immune responses, stress resistance and growth performance of Caspian roach (*Rutilus caspicus*) fed diet supplemented with earthworm (*Eisenia foetida*) extract. *Aquaculture* 511:734275
95. Musyoka SN, Liti DM, Ogello E, Waidbacher H (2019) Utilization of the earthworm, *Eisenia fetida* (Savigny, 1826) as an alternative protein source in fish feeds processing: a review. *Aquac Res* 50(9):2301–2315
96. Dedek GA, Owa SO, Olurin KB, Akinfe AO, Awotedu OO (2013) Partial replacement of fish meal by earthworm meal (*Libyodrilus violaceus*) in diets for African catfish, *Clarias gariepinus*. *Int J Fish Aquac* 5(9):229–233

Climate Change and Human Activities in Nine Chapters

Integration of Field Investigation and Geoinformatics for Urban Environmental Quality Appraisal of Bankura Town, West Bengal, India



Abira Dutta Roy, Jaya Gorai, Rinku Dey, Sujata Pal, and Sunipa Mandal

Abstract The urbanization process has been inflicting detrimental environmental conditions across urban centres irrespective of their size and shape globally. Bankura municipality, a town of West Bengal, India, with a population of only 137,386, according to the Census of 2011, is also a victim of the ill effects of urbanization. In order to facilitate sustainable urban planning of a budding developmental epicentre, this chapter helps in highlighting the wards with poorer environmental quality. Landsat 8 OLI of 2019 was used to assess the biophysical condition such as Land Surface Temperature (LST), Normalized Differential Vegetation Index (NDVI), Normalised Difference Water Index (NDWI) and Normalised Differential Built-up Index (NDBI). Field investigations to identify the level of noise pollution and water pollution, aided with a portable sound meter, pH meter, DO meter, EC/TDS meter and turbidity meter was done. Air quality assessment was carried out from the data of the Central Pollution Control Board's monitoring stations. Vehicular frequency assessment and noise pollution measurements were also conducted during off-peak and rush hours at major road intersections. The monitored data were spatially interpolated using Inverse Distance Weighted Method (IDW) for air pollution as well as transport flow and Kriging for noise pollution. Principal Component Analysis (PCA) was carried out using these indicators and ward level Urban Environmental Quality Index (UEQI) was mapped. The wards identified with the worst environmental quality were 2, 12, and 17, with localities such as College More, Tamliband, Machantala and Panchbaga being the most affected ones. The main problems in these wards were honking near hospitals, schools, and colleges; narrow road intersections with high vehicular frequencies; high air pollution, poor surface water quality sites and congested built-up. An increase in vegetation cover, grassing of footpaths, effective solid waste management, intelligent traffic regulation systems were suggested in this study for improvement of the urban environmental condition of Bankura municipal area.

A. D. Roy (✉) · J. Gorai · R. Dey · S. Pal · S. Mandal
Department of Geography, Bankura Zilla Saradamani Mahila Mahavidyapith, Bankura University,
Bankura, West Bengal 722101, India
e-mail: abira6520@bzsmcollege.org

Keywords Bankura · Urban environmental quality index · Inverse distance weighted method · Principal component analysis

1 Introduction

The term urban and the process of urbanisation have diverse meanings [1, 2]. The selection of definition of urban can shape the level and rate of urbanization in a country [3]. In March 2020, in order to categorise urban and rural areas through various statistical parameters, the United Nations Statistical Commission devised a method that also enabled comprehension of the degree of urbanisation [4]. According to this new method, sustainability indicators were considered, such as public transport, poverty, access to green space, air pollution, noise pollution, population density, and many more. Contrastingly in India, the Census defines an urban area as any municipality, corporation, cantonment board, notified town area, and any other places with over 5000 population and 75% male working in the non-agricultural sector and a population density of 400 persons/sq. km. As a result, cities in India and upcoming towns severely lack the required facilities and infrastructure to become sustainable. More over these cities have sprawled in an unplanned and uneven manner [5–9] resulting in degraded environmental quality. According to Chiu [10] the basic environmental qualities necessary for sustaining human habitats are those which guarantee a hygienic and healthy living environment. Clean water, clean air, and clean internal and external environments are the primary requirements. These parameters are comparable to those essential for sustainable cities as well.

Studies on Indian cities have unconnectedly looked into the condition of air pollution [11–14] water pollution [15–19], water depletion [20–22], noise pollution [23, 24], solid waste management [25–28], urban heat island [29–35], vehicular congestion [36–38], housing conditions and availability of various other infrastructure facilities and pressures on them. According to these studies, most Indian cities have poor air quality, depleted water quality with water logging problems, improper drainage system, unmanaged solid waste, slum problems and high noise pollution. Pieces of literature have tried to identify the correlation between heat island formation and pollution [39], noise pollution and vehicular density [23, 24, 40]. But very few studies in India have holistically looked into the environmental quality [41, 42]. This research endeavour thus attempts to look into all the parameters required for a sustainable Bankura town and assesses the environmental quality to address policy initiatives.

2 Study Area

The Bankura district is an archaeological hub with relics dating back to the chalcolithic age. It is a place where proto-Dravidian and proto-australoids have once

inhabited. Several dynasties have also ruled this land since seventh century AD. The district headquarter, Bankura Municipality is one of the oldest towns in the western region of the state of West Bengal in India. The Bankura Municipality was constituted in 1865. An area of 18.65 sq. km extends from 87° 1' 30" East to 87° 4' 30" East and 23° 12' North to 23° 15' 30" North. It is divided into 24 municipal wards. It is surrounded by agrarian landscape and located in one of the most economically backward regions of the country [43, 44]. With the centralised facility of employment opportunities in various service sectors, business enterprises, better education through schools and colleges, and better health facilities, Bankura municipality draws people from all around the district and neighbouring districts. According to Census of India, Bankura municipality saw a steady rise in population. In 1981 there were 94,954 persons, 1991 (114,927 persons), 2001 (128,811 persons) and in 2011 (137,386 persons). Though the decadal growth rate has slowed down, with pre-existing urban settlements since the British rule, the increasing population has created pressure on the town's carrying capacity, leading to unplanned growth both horizontally and vertically.

The Gandheswari River flanks in the north and Darakeshwar River in the south. The climate here is tropical, sub-humid and dry with an annual rainfall of 1420 mm and summer temperatures ranging to 45 °C maximum during June and 9 °C minimum during January. Connected by State Highway No. 9 and National Highway No. 60 and 60A, south eastern railway, Bankura attracts many floating and immigrant population. Figure 1 shows the administrative location of Bankura Municipality.

3 Materials and Methods

Knowledge of environmental quality in the administrative units of cities allows prioritization of intervention in areas with higher environmental conflicts [45]. It also enables improved zoning, which is one of several tools that urban planners use to control the city's physical characteristics [46]. Studies on environmental quality in Indian cities have been rare but quite a few studies have been carried out in cities of North America [47–49] and South America Escobar [50, 51]. In these research works, socio-economic indicators such as population density, housing density, and income and proxy variables such as size and rent of houses were used. Literacy, electricity, water supply were also considered in addition to ecological indicators such as tree density, availability of open space, sewage and drainage facility, waste management, nearness of landfills, traffic density, etc. These parameters are regulators of sustainable cities. High building density, low vegetation cover and depleted water bodies often lead to high LST, thus creating urban heat islands [52–54]. The increased air pollution further aggravates the problems because of traffic congestions [39, 55–58]. Other than degrading the environmental quality, these factors have serious human health implications [59–64].

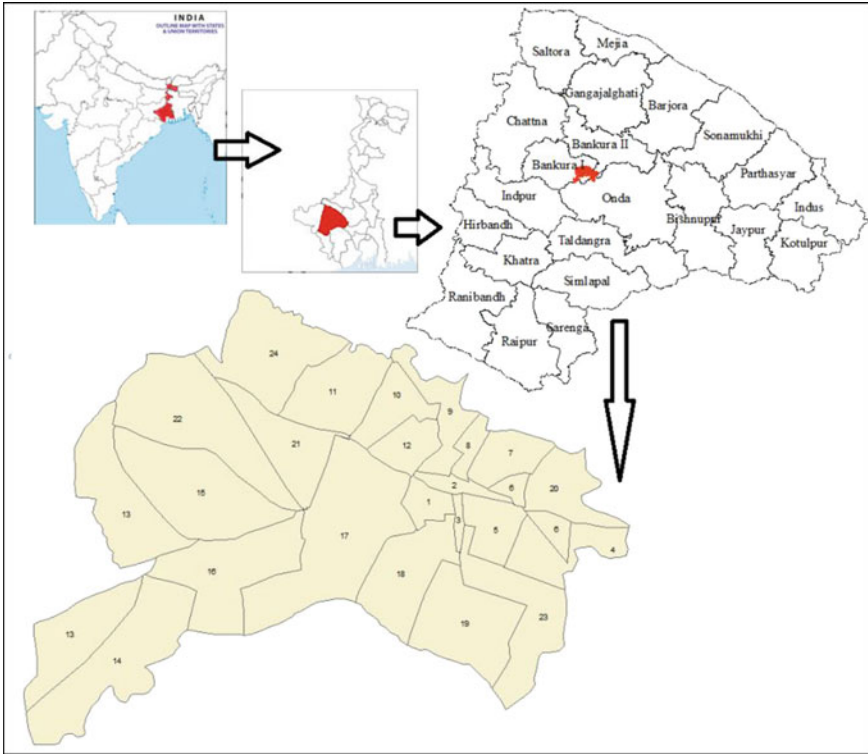


Fig. 1 Location map of Bankura municipality along with ward boundaries

Higher population density and poverty among the residents of the cities make them even more vulnerable. Bankura being remotely located, lacks well distributed monitoring sites for measuring environmental data. Moreover, very coarse data on socio-economic conditions are available at the ward level through a census. Considering these factors to identify the most environmentally degraded ward, which requires special planning initiatives, this study undertook a geospatial analysis with where integration of remote sensing. Secondary data and field observations have been carried out to assess the environmental quality of the wards in Bankura. So, proxy biophysical parameters such as NDWI (Normalised Difference Water Index), NDBI (Normalised Difference Built up Index), NDVI (Normalised Difference Vegetation Index), LST (Land Surface Temperature) derived from remotely sensed images were also taken into account. These indices would represent water quality issues, building density, vegetation quality and thermal environment, respectively [65, 66]. Figure 2 provides a schematic representation of the research methodology undertaken for carrying out this study.

This chapter looked into the current situation of the different environmental aspects and hence did not deal with temporal data purposively. Firstly the ward

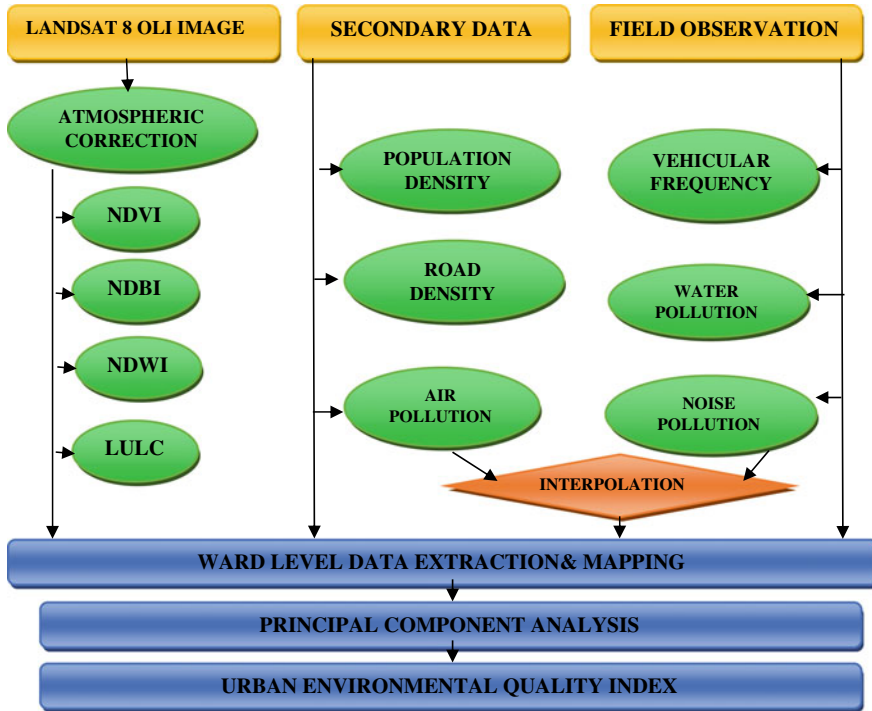


Fig. 2 Methodological flow chart for assessment of urban environmental quality

map which was procured from the Bankura municipality office was scanned, georeferenced and digitized. The Landsat 8OLI of 27th April 2019 was downloaded from <https://earthexplorer.usgs.gov/>. The path and row number were 139 and 044, respectively. Atmospheric correction, radiometric correction and sun angle rectification for each of the bands in the images were carried out in Erdas 2014 following [67]. Equation 1 shows the software’s background algorithm to perform radiometric correction on each band of the Landsat-8 image.

$$p\lambda' = mpQcal + Ap \tag{1}$$

TOA reflectance with a correction for the sun angle was then conducted using Eq. 2

$$p\lambda' = \frac{p\lambda}{\cos(\theta_{sz})} = \frac{p\lambda}{\sin(\theta_{SE})} \tag{2}$$

where,

$p\lambda'$ = TOA planetary reflectance, without correction for solar angle.

mp = Band-specific multiplication rescaling factor from the metadata (REFLECTANCE_MULT_BAND_X, where 'X' is the band number).

Ap = Band-specific additive rescaling factor from the metadata (REFLECTANCE_ADD_BAND_X, where 'X' is the band number).

Q_{cal} = Quantized and calibrated standard product pixel values (DN).

SE = Solar Elevation.

These atmospherically corrected bands were used to produce NDWI, NDVI, NDBI and LST using the band ratio techniques given in Eqs. 2, 3, 4, 5 and 6, respectively [52, 68].

$$NDWI = \frac{NIR - SWIR}{NIR + SWIR} \quad (3)$$

$$NDVI = \frac{NIR - RED}{NIR + RED} \quad (4)$$

$$NDBI = \frac{SWIR - NIR}{SWIR + NIR} \quad (5)$$

$$LST = \frac{T_B}{1 + \left(\lambda * \frac{T_B}{\rho} \right) * \ln \varepsilon} \quad (6)$$

where NIR is near-infrared band, SWIR is the shortwave infrared band and Red is the band itself. T_B is the total brightness value of the pixel, λ is the wavelength of emitted radiance (m), ε is surface emissivity, ρ is hc/K (1.438×10^{-2} mK), h is equal to the Planck's constant (6.26×10^{-34} J see), c —velocity of light (2.998×10^8 m/sec).

The land use land cover (LULC) map was generated from georectified high-resolution Google earth image. In ENVI 5.3, software object-based classification technique was applied for accurate classification of LULC. The population density was computed at the ward level from population data obtained from the census, divided by the area of the wards obtained from the digitized map in GIS environment.

The road networks were digitized in ArcGIS 10.4.1 from the georectified high-resolution Google Earth image. The length of the roads within each ward was computed and divided by the area of the ward as shown in Eq. 7 to obtain a map of ward level road density [69].

$$\text{ROAD DENSITY} = \frac{\text{TOTAL LENGTH OF THE ROAD INSIDE A WARD}}{\text{AREA OF THE MUNICIPALITY WARD}} \quad (7)$$

In order to assess the level of air pollution in the Bankura town, data on SO_2 , NO_2 and PM_{10} monitored by the West Bengal Pollution Control Board (WBPCB) was used. The data is monitored on a bi-weekly basis from January 2016 onward. For this study data of annual average data 2019 was used. Inverse distance weighted (IDW)

interpolation method was applied to map the pre pandemic/lockdown scenario’s average concentration [39, 70]. As Bankura has only one monitoring station, the data for the nearest 8 more stations were included in the computation which is also sparsely situated. The stations included are Purulia town (23.3322° N, 86.3616° E), Barjora (23.4259° N, 87.2855° E), Asansol (23.6889° N, 86.9661° E), Benachity (23.5569° N, 87.2768° E), Bidhan Nagar (23.5178° N, 87.3460° E), Jamuria (23.7061° N, 87.0774° E), PCBL more (23.505639° N, 87.317552° E) and Raniganj (23.6234° N, 87.1143° E). The pollution concentration value at point i (N_0) is calculated through the formula shown in Eq. 8, where N_i ; represents the number of measurement points, N_i ; represents the pollutant value at position i , P_i ; the weight of the pollutant value at i position. P_i weights are calculated using Eq. 9, which shows that it is a function of the distance between the reference point and the interpolation point according to the idea that the effect of the closer points are higher than distant ones and k is the power of the distance. d_i is the horizontal distance between the interpolation point at (x_0, y_0) and the reference points at (x_i, y_i) and is calculated by Eq. 10 [39].

$$N_0 = \frac{\sum_{i=1}^n N_i P_i}{\sum_{i=1}^n N_i} \tag{8}$$

$$P_i = \frac{1}{d_i^k} \tag{9}$$

$$d_i = \sqrt{((x_i - x_0)^2) + (y_i - y_0)^2} \tag{10}$$

WBPCB also monitors water quality for two surface water bodies in Bankura town. One monitoring site located at a lake near Sati Ghat and another near the water intake point on the River Darakeshwar. The parameters measured by WBPCB for water quality assessment are ammonia, BOD, conductivity, Dissolved Oxygen (DO), Fecal Coliform, Fecal Streptococci, Nitrate—N, pH, Temperature (Water), Total Coliform, Boron, Calcium, Chloride, COD, Fluoride, Magnesium, Phosphate—P, Potassium, Sodium, Sulphate, Total Alkalinity, Total Dissolved Solids (TDS), Total Fixed Solids (TFS), Total Hardness as CaCO₃, Total Suspended Solids (TSS), Turbidity. The data were monitored on an approximately quarterly basis from 2010 onwards. The rivers would represent the pollutant load contributed from the entire catchment and not exclusively of the Bankura town, though the town drains most of its effluents into the river. There are high probabilities of non-point source pollution from the agrarian land within the rivers’ watershed would be contributing significantly to pollution. Analysis of the water quality data of these two WBPCB won’t represent the ward level water pollution too and was thus not considered for this study. Figure 3a shows the polluted Gandeshwari River at Sati Ghat and Fig. 3b shows Darakeshwar River.

Bankura municipality is strewn with a large number of big and small water bodies as shown in Fig. 4. So to get an overview of the water quality at ward levels, randomly selected ponds were tested for quality parameters at every ward. In-situ measurement

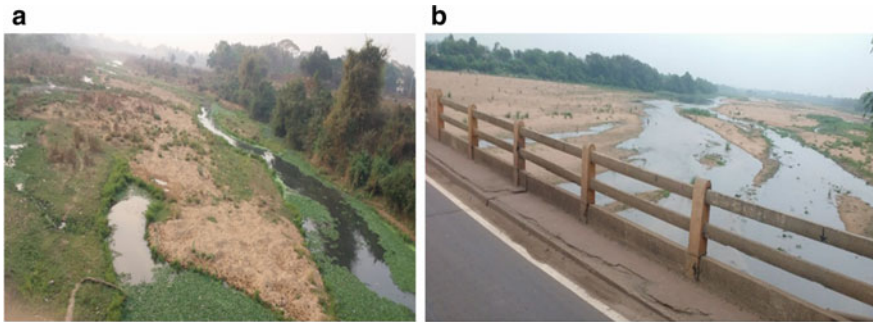


Fig. 3 a Sati Ghat on Gandeshwari river. b Water intake point at Darakeshwar river near Bankura

of temperature and pH of the water samples were carried out using a pH meter (model HI 98130 HANNA, Mauritius, IramacSdn. Bhd.). With the help of three standard solutions (pH 4.0, 7.0, and 10.0) the pH meter was calibrated.

Prior to the measurement of Electrical conductivity (EC), the probe of the Electrical conductivity meter (model HI 98130 HANNA, Mauritius, IramacSdn. Bhd.) was calibrated using a standard solution of a known conductivity. To measure the EC of the collected samples, the probe was submerged in the water samples until the stability indicator on the screen disappeared. Before measuring each sample, the probe was rinsed with deionized water [71]. Total dissolved solids (TDS), were examined by the Aquasol Digital Water proof Hand-held Tester, dissolve oxygen (DO) was tested by the Digital Meter of Lutron DO-5510, and Turbidity by NOVA LYNX 270-WQ730 Turbidity Sensor. The test's quality verification and assessment were guaranteed following the instruments' standard operating protocol (SOP). Repeated

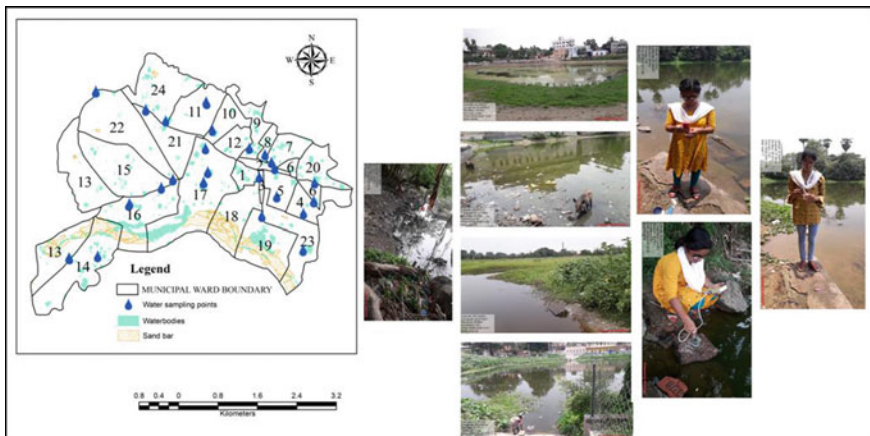


Fig. 4 Water bodies in and around Bankura municipality and in-situ water sample quality measurements

instrument calibrations were carried out. Figure 4 shows the location of ponds from where the water samples were tested. Some of the geo-tagged photographs of highly polluted water bodies and the process of in-situ measurements at field have also been shown alongside. On the basis of these sampled water bodies through the composite index (ranking method) of the pollutants, the most polluted water body was identified, keeping in mind the designated best use water quality criteria of CPCB, standard values set by the World Health Organization (WHO), local standards set by National Drinking Water Quality Standard (NDWQS). Those pollutants exceeding the permissible limit were ranked 2 and those within permissible limit was ranked 1. The average ranks for all the parameters were computed except temperature. The results were extrapolated at ward levels. From the photographs of the water bodies it is explicit that they are mainly dumping grounds of solid waste and are subjected to eutrophication.

Apart from the water sampling, traffic density and sound pollution were estimated at 15 major road intersections. According to HCM, 2000, traffic density is considered as the primary measure for quantifying congestion of roadways other than signalized. Traffic density is computed as the number of vehicles occupying a given length of roadway [72]. For calculating traffic density, two ways are broadly adopted in literatures: one is through traffic survey and the other is estimation method on the basis of fixed detectors data. Traffic surveys can be done through in-out traffic flow surveys and also through high altitude photographs, but the traffic surveys are pricey and hence are often avoided. May [73] writes that aerial photography is the direct method for field measurement of traffic density, which is very difficult to implement in the field. Before the 1950s only photographic techniques were employed.

Measuring traffic density is complex; hence indirect methods have been adopted in literature such as flow, speed or occupancy [72]. During early 1960s, three approaches were being undertaken in parallel: one was calculation of traffic density from input-output counts, the second method was an estimation of traffic density from measured speed and flow, and the third was the measurement of percent occupancy of the streets. Video filming was also been used for estimating macroscopic density from an elevated vantage point from which the highway section under study can be observed [74]. Al Kherret et al. [75] discussed about the automatic extraction techniques of traffic density characteristics carried out from video images using detection and tracking. In Biswas et al.'s study [76] used traffic cameras, which were previously integrated to the traffic infrastructure. Biswas et al. [77] also did a lane-wise car counting to estimate the density with respect to time using traffic cameras. In modern developed nations, magnetic loop detectors and surveillance cameras are also widely used for traffic density estimation. The hardware specific technique like Magnetic loop detectors demands a lot of physical work and is very costly to install and maintain. Wireless vehicle sensors and speed guns are also used [78, 79]. The paper by Al-Sobky and Mousa [80] presents an approach for the utilization of smartphones in measuring temporal and spatial macroscopic traffic density on road networks. Following Al-Sobky and Mousa [80], the vehicular frequencies were monitored twice in their study. One measurement was done around 9.45 to 10 am and the other was done during the evening 5.15 to 5.30 pm at the major road intersections. This time was chosen

as the rush to reach schools and workplaces was the highest between 9.30 and 10 am. Even local trains are scheduled to reach Bankura town during this time to help floating populating and daily commuters reach their respective work places from neighbouring blocks and districts. Similarly, in the evening, the time around 5.15 to 5.30 pm was considered for observation as the office hour's end at this time.

Due to lack of CCTV footage or other monitoring devices video recordings via smart phones were done at the major road intersections shown in Fig. 5, for the flowing traffics and the vehicles were later counted from the videos. The vehicular frequencies were calculated for non-polluting two-wheelers and three-wheelers like bicycle, cycle rickshaws, cycle vans, CNG (Compressed Natural Gas) operated auto-rickshaws and battery operated auto-rickshaws also known as toto. The number of polluting two-wheelers such as motor bikes and scooters [81–83], three wheelers such as motor vans and four-wheelers such as cars, trucks, buses and other utility vehicles [84–86] were also counted. The average numbers of vehicles were then calculated from the two survey periods based on their categories. In order to represent the vehicular frequency, transport flow maps of the different polluting two and four-wheelers were used using IDW interpolation method. The total polluting traffic density at these major road intersections were then extrapolated to the wards in which they were located. To avoid reverberation, in order to show the proportion of different vehicles at a particular road intersection, the representation was done through pie graphs. Figure 5 shows the road intersections where the traffic flow was monitored.

Simultaneously using a digital sound meter during these durations at these road intersections, noise pollution was also monitored. The average values in decibels were mapped and interpolation was carried out using the kriging interpolation technique. Research papers by Aumond et al. [87], Mehrjardi Taghizadeh et al. [88] and Harman et al. [89] showed that kriging is one of the best interpolation techniques used for mapping noise pollution. Kriging uses the following formula (Eq. 11)

$$\hat{Z}(S_0) = \sum_{i=1}^N \lambda_i Z(S_i) \quad (11)$$

where $Z(S_i)$ = the measured value at the i th location, λ_i = an unknown weight for the measured value at the i th location, S_0 = the prediction location, N = the number of measured values.

In ArcGIS 10.4.1 using the zonal statistics arctool, the wards' average noise pollution concentration values were mapped. Using this very technique ward level maps were also made with average NDWI, NDVI, NDBI, LST, road density, vehicular frequency, air pollution, water pollution values. According to the database procured from the municipality office solid waste management is equally bad in all the wards. 75 tons per day (TPD) of waste are generated. There are no segregation, no landfill site, and very little door-to-door collection system. Hence this parameter was not considered for the study. In order to classify the wards based on environmental quality using these various bio-physical, environmental and socio-economic parameters, it

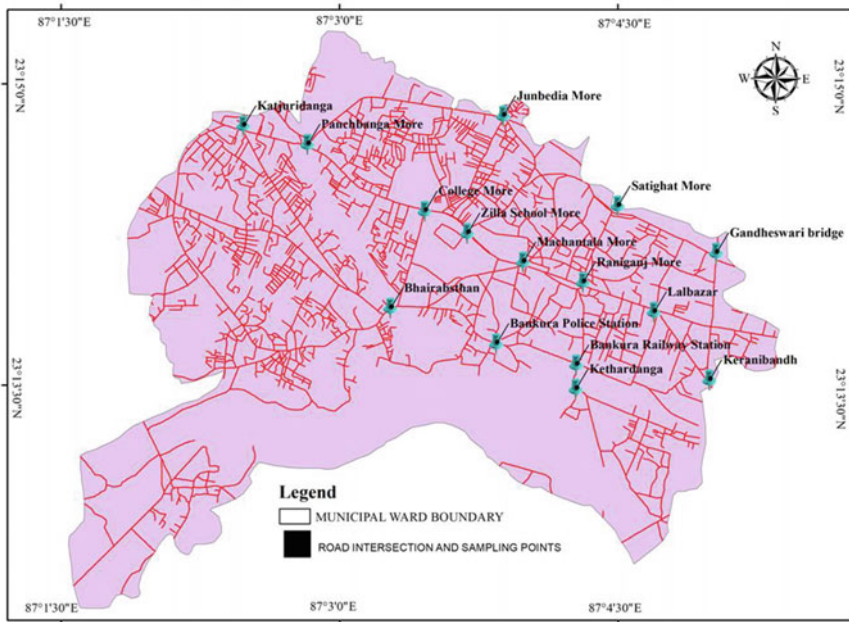


Fig. 5 Road network and intersections for monitoring traffic density as well as noise pollution in Bankura municipality

was imperative to calculate UEQI (Urban Environmental Quality Index) [41, 48]. Multivariate methods and principal component analysis are frequently used to assess UEQI. Other techniques have also been used in literature including weighting score according to the level of importance to obtain a final score or by overlaying values (summed) using the vector map of each indicator in a geographic information system [45]. PCA technique has been preferred in this study because all eigen values and eigen vectors are calculated and sorted in PCA. Then, the top most eigen vectors are selected to project the input data. By projecting the input data into the chosen eigen vectors, the dimension of the input data is, practically, reduced [90]. PCA is a data transformation technique that transforms many correlated input variables into a smaller number of uncorrelated components latent dimensions that explain the input information [47, 91]. Jolliffe and Cadima [92] has researched and given a detailed description of PCA well.

The integration of values derived from band ratio images, census, WBPCB and field survey at ward level were performed by principal component analysis (PCA), using SPSS v.19 software. Before performing PCA, the Pearson's correlations among all the 9 indicators were computed, to inspect the relationships among these indicators [93]. Kaiser–Meyer–Olkin sampling adequacy test and Bartlett's sphericity tests were also conducted. As the first component explains most of the variance in the data the derived components with eigen values greater than 1 were reserved [94]. To acquire

the UEQI, the scores of the larger generated components were combined with the variance of each one using a linear model [48]. Equation 12 explains the process.

$$UEQI = \sum_1^n f_i w_i \quad (12)$$

where n is the number of components extracted, f_i is the component score and w_i is the percentage of variance explained by component i maps of the components. The UEQI were created to depict the spatial expression of each component and the environmental quality at a ward level. The values of UEQI were grouped into categories, which will enable planning authorities to monitor the environmental quality.

4 Results and Discussion

The LULC map was generated from Google Earth images through object-based classification (Fig. 6). Built-up comprised of 82% of the total area, 13% of the area was occupied by vegetation, 3% by the sand bars and open spaces, while the rest of the LULC was under water bodies. The percentage area occupied by each of the LULC at a ward level also plays a pivotal role in determining its environmental quality. So, indices such as NDBI, NDVI, and NDWI which act as substitutes for building density, vegetation quality and extension of water bodies respectively were used. The NDBI is used to understand the extent and density of built up from remote sensing images. For quick mapping of built up areas NDBI is an excellent alternative [95]. The values more than 0 are considered to be categorised as built up, but often presence of sand in the building material and sand in the soil leads to categorisation in one group. In Fig. 7a the NDBI values in Bankura Municipality are seen to have ranged from 0.22 to -0.260 . The highest values are present in the sand bars of the Darakeshwar River flowing south of the study area. The negative NDBI values mainly occupied the vegetated patches and water bodies. The juxtaposition of Figs. 6 and 7a visually speaks about the building density in the wards and rationalises the spatial variation of NDBI values. The building density in Bankura municipality can thus be considered as semi dense because the wards are scattered with vegetation along the roads, along the river banks, in open spaces and recreational parks. The wards have large number of ponds and lakes as well. The average NDBI values when extrapolated to the wards and choropleth was done showed negative values, which indicated lack of dense or compact built up area. In Fig. 7b, the ward 2, 3, 13, 14, 19 and 24 have higher but negative NDBI values. Ward 2, 3 primarily have compact built up. Ward 13, 14 and 24 have more fallow agricultural land. In ward 19 open space or barren land and sand bars are occupying major portions. These LULCs share similar spectral properties with that of built up and henceforth have higher NDBI values [96].

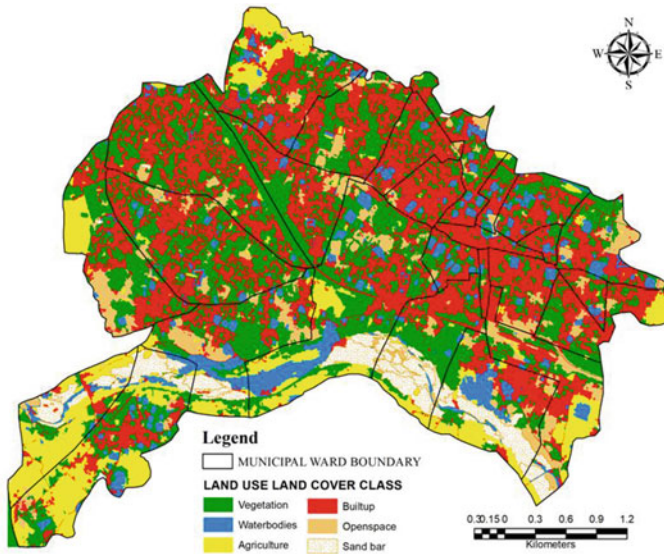


Fig. 6 Land use land cover map of Bankura municipality

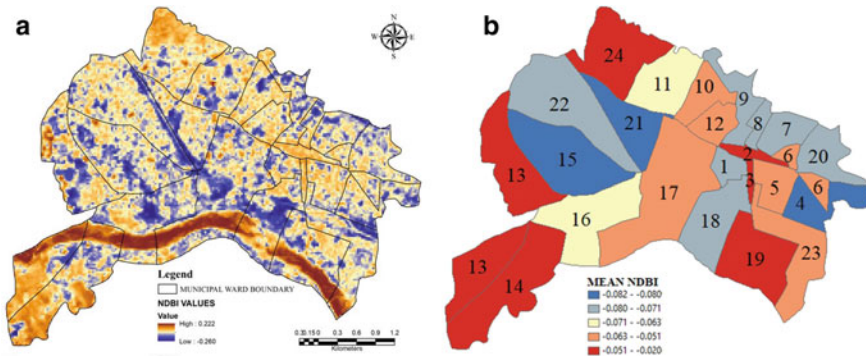


Fig. 7 a NDBI of Bankura municipality **b** Mean NDBI at different wards in Bankura municipality

NDBI often do not therefore present an accurate picture because of spectral mixing between built up and other LULCs. Ward number 4, 15 and 21 have a higher percentage of area covered by vegetation and water bodies and hence belonged to the category of wards with lower NDBI values and are environmentally better-off than the other wards. Presence of vegetation and water bodies act as a coolant against higher LST [52, 97–99]. These wards with higher NDBI values would have higher LST values (Fig. 10).

NDVI values represent the quality and density of vegetation. The healthy vegetation has low red-light reflectance and high near-infrared reflectance, producing

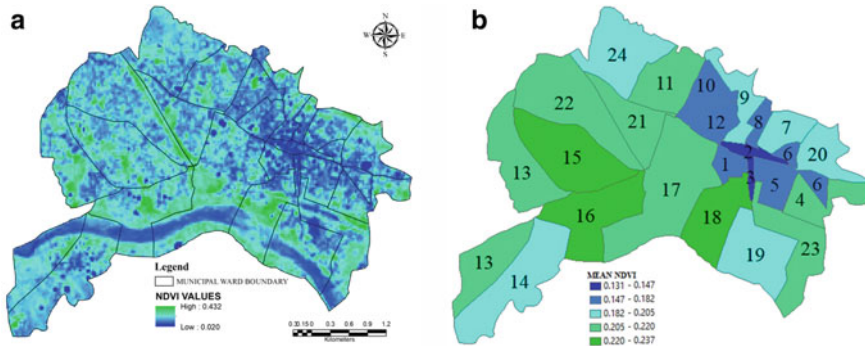


Fig. 8 a NDVI of Bankura municipality. b Mean NDVI at different wards in Bankura municipality

high NDVI values [100]. NDVI values range from +1.0 to -1.0 . Land cover such as barren rock, sand, or snow show very low NDVI values (0.1 or less). Scrubby vegetation, shrubs, grasslands or croplands show moderate NDVI values (ranging from 0.2 to 0.5). High NDVI values (0.6 to 0.9) can be associated with areas of dense vegetation especially temperate and tropical forests or even crops during their peak growth stage [101]. In Bankura as shown in Fig. 8a the NDVI values range from 0.02 to 0.432. The lower NDVI values coincide with the areas of built up, water bodies and current fallow lands. The vegetation here is mostly scattered trees, shrubs, some croplands and grasses. The mean NDVI values generated from Zonal statistics in ArcGIS were then extrapolated to the ward map which is shown in Fig. 8b.

It can be visualised that ward number 15, 16 and 18 has the highest NDVI values (0.22–0.23). Though the areal extent of the vegetation patches is not that significant in ward number 15, 16, yet the vegetation's density and good health have impacted the high values. More houses have large trees, herbs, and shrubs planted in their backyards and gardens, contributing to low NDBI but high NDVI values in many wards. These wards have large trees, like sal, mango, jackfruit, neem etc. Ward number 4, 11, 13, 17, 21, 22 and 23, covered with trees lining the roads, parks boundaries and open abandoned spaces. Ward number 1, 2, 3, 5, 6, 8, 10, 12 are fully concretised with impervious surface dominating the LULC in these wards. There is lack of vegetation cover and hence the NDVI values are the least here.

The NDWI is also dimensionless like any other band ratio indices whose value varies from -1 to $+1$. Water features have positive values, whereas soil and terrestrial vegetation features have zero or negative values [65]. NDWI helps delineate water bodies and assess the water content in vegetation canopies [102].

The vegetation quality has been very poor in most parts of the study area. The NDWI values have ranged from 0.028 to -0.382 (Fig. 9a). The vegetated areas, shown in green colour in Fig. 8a show very little moisture content, especially because the satellite image belongs to the summer month of April. Low NDVI and low NDWI have created environmental stress in the area. The mean NDWI values extrapolated to the ward map have shown negative values for all the wards (Fig. 9b). The wards

16 and 18 had relatively higher NDVI values, but the presence of sand bars, built-up areas, and open space has counter balanced or negated the impact of vegetation. Similar results are seen in ward 4, 11, 16, 15, 19, 21, 22, 23.

NDBI, NDVI, NDWI, which all act as a representative biophysical parameter to determine the environmental health of a region, has an enormous impact on the LST of that region. Research has identified a positive correlation between NDBI and LST and a negative correlation between NDVI and NDWI with LST [52, 54]. The indices NDBI, NDVI and NDWI showed predictably results of high LST values across the different wards in Bankura. The LST ranged from 35.98 to 28.47 °C because of summer temperatures (Fig. 10a). The spatially averaged values in each ward represented that ward 3 and 19 had the highest LST. The reasons responsible were high NDBI and low NDVI values dominated by built up in the LULCof ward number 3 and 19, (Fig. 10b). The high NDBI values in ward 19 have resulted from the reflectance properties of sand bars that equally dominate the LULC of the ward beside the built up. The lowest LST have been identified in ward number 9, 11, 15 and 22

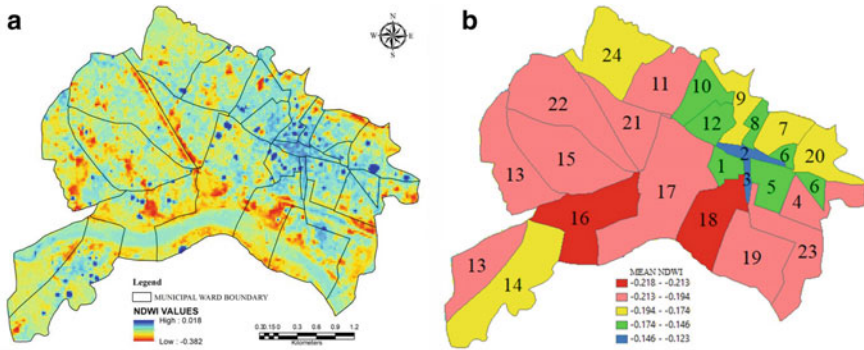


Fig. 9 a NDWI of Bankura municipality. b Mean NDWI at different wards in Bankura municipality

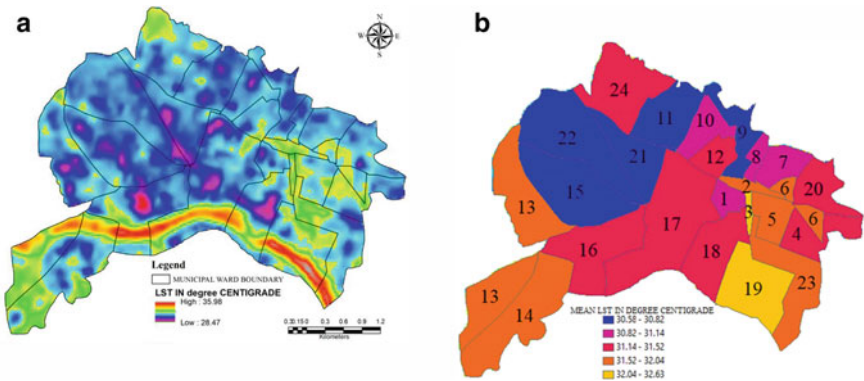


Fig. 10 a LST of Bankura municipality b Mean LST at different wards in Bankura municipality

where vegetation cover, presence of sparsely distributed settlements, and relatively higher NDWI values can be seen. The presence of vegetation cover and low density built up had resulted in lower LST values. Rest all the other wards too experienced high LST ranging from 30.82 to 32.04 °C. On 27th April 2019 the recorded maximum air temperature was 29.1 °C (India Meteorological Department). The LST and air temperature often rises above 40 °C (India Meteorological Department, Kolkata), which being higher than the comfort level of human tolerance [103] may often have serious human health implications [104, 105].

After the analysis of ward wise variation of the biophysical parameters derived from the remote sensing images, a field based investigation to assess the physico-chemical characteristics of water sample from random water bodies from each and every ward was done. Table 1 shows the parameters that were tested for the water bodies and its values. The values were categorised into two classes based on being within permissible limit or exceeding permissible limit of drinking and bathing water as per NDWQS, CPCB and WHO norms. According to WHO, the permissible limit of conductivity is 1000 $\mu\text{S}/\text{cm}$ as per NDWQS, pH between 6.5 and 8.5 as per CPCB, turbidity of 5NTU and TDS of 500–1200 mg/l according to WHO, The ranks were averaged and a choropleth map was produced from the generated index as shown in Fig. 11.

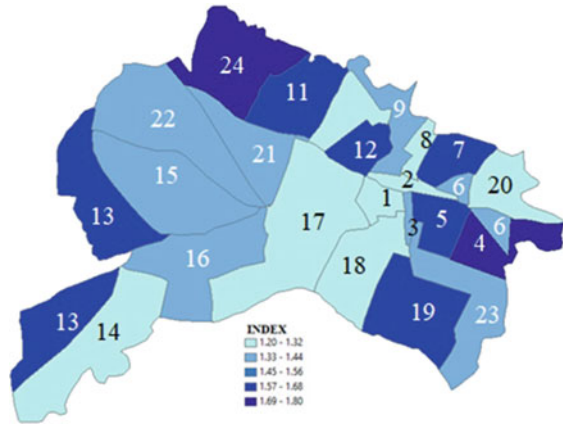
It was observed that the water body from ward 4, 13 and 24 were in the worst condition. Though the DO level was high in the water bodies and TDS was within the permissible limits but the pH level, turbidity, EC were much beyond the permissible limit of drinking water. The wards 1, 2, 8, 14, 18, 20 had relatively better water quality though it been violated the standards in some of the parameters. Overall the odor and color of the water too suggested that it was not suitable for drinking. Few other chemical analyses could have strengthened the claims and remains a limitation in this paper.

Some other field investigations that were carried out included surveying of traffic density and noise pollution at major road intersections in Bankura municipality. The location of the major road intersections are mapped in Fig. 5. The buses and heavy vehicles that connect the town with other neighbouring areas have their entry at Keranibandh through Lalbazar, Bankura Railway station, Machantala, Bhairabsthan and then to the bus depots located at Katjurianga. The exit route of these vehicles is different. It initiates from Katjuridanga through Panchbaga, Junbedia, Sati Ghat, and Gandheswari Bridge. The road networks were first mapped and a network density computed. The network density is shown in Fig. 12a. Ward 2, 8, 10, 11, 15, 21, 22 have high density of road networks. While ward number 13, 14, 17, 18, 19 are larger in size and have longer but fewer roads leading them to be wards with low road density. The almost straight road joining Kathjuridanga and Keranibandh is one of the most frequented by vehicles in the study area. Along the roads are major market centers, schools, colleges, offices. Katjuridanga, the bus depot as can be seen in juxtaposition with Figs. 5 and 12b has government and private run buses picking and dropping passenger from neighbouring blocks and districts. Moreover many other vehicles such as toto, auto, bikes and scooters congregate here to pick and drop people within the municipal boundaries. A 15 min observation was done on

Table 1 Water quality parameters from different ponds in each of the wards of Bankura municipality

Ward number	pH	Temp (°C)	TDS (mg/l)	Turbidity (in NTU)	DO (mg/l)	EC (µS/cm)	Ward number	pH	Temp (°C)	TDS (mg/l)	Turbidity (in NTU)	DO (mg/l)	EC (µS/cm)
1	7.5	32.0	606	10	8.3	1250	13	8.6	31.0	306	15	8.2	1854
2	8.1	31.6	562	52	8.6	1321	14	8.2	31.5	547	32	8.0	244
3	8.1	33.7	410	116	7.3	1306	15	8.3	31.2	235	09	10.0	20
4	8.7	30.6	485	105	8.4	1125	16	7.8	30.6	303	146	4.1	1261
5	8.3	31.4	381	10	8.0	1702	17	7.9	30.4	186	07	11.3	1601
6	8.4	32.0	370	25	7.8	1311	18	8.2	31.3	415	32	8.2	70
7	8.2	31.6	433	35	7.6	1263	19	8.4	31.6	216	16	8.1	1058
8	7.7	31.4	486	10	6.8	2028	20	8.0	32.0	498	30	8	1227
9	7.7	30.4	540	19	8.3	2031	21	7.8	31.4	252	144	9.0	1821
10	7.3	30.5	311	15	6.7	657	22	8.4	30.7	371	140	4.2	487
11	7.6	31.0	586	83	7.2	789	23	7.2	30.9	178	115	6.6	621
12	7.6	29.7	311	15	12.3	222	24	9.2	29.5	324	145	10.6	1145

Fig. 11 Water quality status of ponds in different wards of Bankura municipality



25th April, 2019 during morning and evening hours. Figure 12b through the IDW represents that about 1150 polluting vehicle passed through the intersection. Of the total vehicle load, 22% were non-polluting cycles, totos/e-rickshaws and rickshaws. 70% included scooters and motor bikes and 8% were buses and cars.

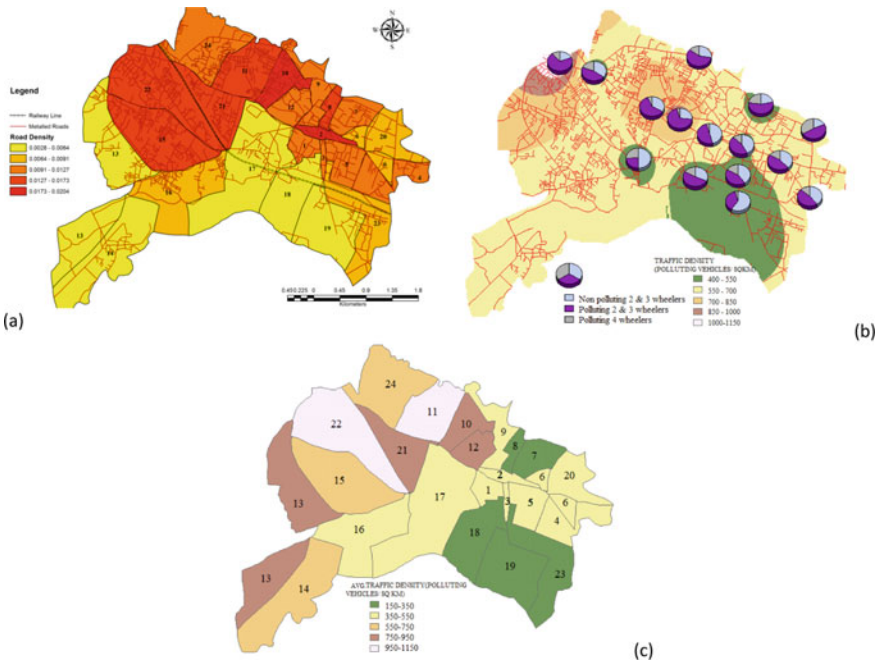


Fig. 12 a Road density map of Bankura municipality, **b** Traffic composition at various road intersections **c** Traffic density at ward level in Bankura municipality

The very next bus stop Panchbaga, from where the larger and heavier vehicles exit out of Bankura town and smaller vehicles move inside showed that of the vehicle count, 30% were non-polluting vehicles, 40% comprised of motorbikes and scooters while the rest included the buses, cars and trucks. The railway crossing near Panchbaga often created long halting time for the vehicles leading to traffic jams. The road that diverged into the Bankura town crossing College More, Bankura Zilla School More and Machantala is also one of the busiest. The road here is lined by important educational institutes like Christian College, Bankura Saradamani Mahila Mahavidyapith, Bankura Mission Girls High School and various other government offices where people flock with their vehicles during the hours of observation (Fig. 13c). 700–1000 polluting vehicles passed through these intersections during the 15 min of observation (averaged).

These polluting two wheelers comprised 75% of the total load of vehicles, 20% included cycles and totos that are non-polluting and 5% included cars. Buses are not permitted through this road excepting one or two school buses. The road further links Machantala, the central market area of the town. There are shops, stores,

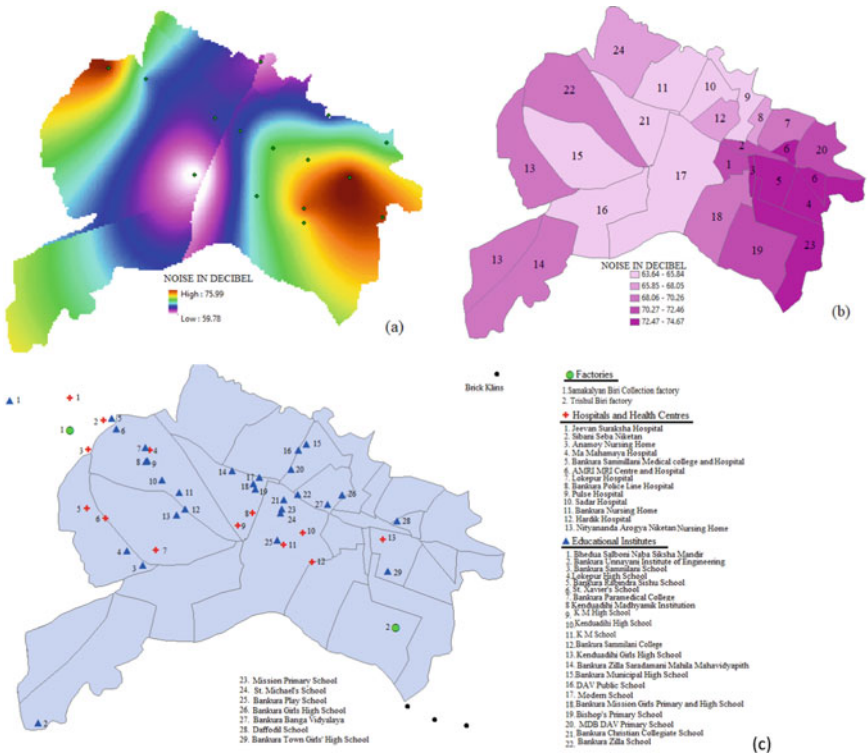


Fig. 13 a Noise pollution level in Bankura municipality, b Noise level in different wards in Bankura Municipality c Location of educational institutes, factories and hospitals on Bankura municipality

houses, banks, ATMs, post office and various other service providers at Machantala. Around 700 polluting vehicles cross this intersection. Of the total vehicular load 45% belonged to cycles and totos, 45% belonged to scooters and bikes and 10% of the vehicles were mostly small vans used to transport various goods to the shops.

Bankura railway stations, Lalbazar too are busy because through these routes, large vehicles such as buses and trucks enter into Bankura. The ward map derived the mean values of the total polluting vehicles on the basis of spatial joining from the interpolated map. From Fig. 12c it can be visualised that ward number 11, 22 had the maximum traffic density followed by ward number 10, 12, 13 and 21. The least vehicular density can be observed in ward number 7, 8, 18, 19, 23. Here the road density (Fig. 12a), population density (Fig. 15) is also less, dominated by agricultural land, water bodies, and vegetated areas, leading to lower vehicular frequency.

Higher traffic density mostly causes noise pollution. Studies by [106, 107] show that noise level is closely related to the number and composition of road traffic. A noise pollution monitoring was carried out at similar road intersections where vehicular frequency was monitored for 15 min during morning and evening hours. The data was averaged and then interpolated using Kriging. The noise recorded at different places throughout the Bankura town ranged from 59.78 to 75.99 decibels (Fig. 13a). The road intersection at Bhairabsthan bus stop recorded the least noise. The maximum noise was recorded at Bankura railway station, Lalbazar and Katjuriganga bus depot. Throughout the town the noise levels are seen to have exceeded the permissible limit of 45 dB at residential zones set by CPCB. More over the maximum noise is found to be near Jeeban Suraksha Hospital, Anamoy Nursing Home and Ma Mahamaya Hospital which are just 750 and 550 m away from Katjuridanga as shown in Fig. 13c. Moreover several other hospitals and health centres are situated in the vicinity of Bankura railway station. Even the various educational institutes that are located along the roads face severe noise pollution.

The average noise pollution value allotted spatially from the interpolated map to the wards 3, 4, 5, 6 and 23 had the highest noise pollution. Following which ward 1, 2, 7, 13, 14, 18, 19 were also facing high noise pollution.

Besides the noise pollution, air pollution is also contributed to the study area by the vehicles, adjacent industries, brick kilns, Hindu cremation grounds and stone crushers located at a radius of 1 km as shown Fig. 13c. Industrial belts and commercial hubs located in adjacent districts of Bankura too greatly influence on the spatial distribution of air pollution here [108, 109]. Therefore, the air quality of those CPCB monitoring stations was also considered within this study. The IDW used for interpolation and mapping of pollutants distribution are shown in Fig. 14. The PM₁₀, SO₂ and NO₂ are shown in Fig. 14a–e respectively. The maps show that the PM₁₀ concentration is high near the western part of Bankura municipality (112.51 $\mu\text{g}/\text{m}^3$). These are the regions with highest road and traffic density. The east of Bankura Municipality areas has relatively low PM₁₀ concentration (97.9451 $\mu\text{g}/\text{m}^3$), but these values were also slightly higher than the permissible limit set by the CPCB (100 $\mu\text{g}/\text{m}^3$). The extrapolated map in Fig. 14b showed that the most polluted wards are 13, 14, 15 and 22. The areas near the colleges, schools and market places within ward number 11,

17 and 21 have comparatively less PM10 concentration, though slightly higher than the required CPCB norms.

Following similar spatial distribution to PM10, the NO₂ and SO₂ are also concentrated towards the western part of Bankura municipality and decreases towards the east. Both NO₂ and SO₂ are within the permissible limits stated by CPCB, which are 80 and 100 µg/m³ respectively. As can be seen in Fig. 14c the SO₂ concentration ranged from 2.12 to 3.57 µg/m³, whereas the concentration of NO₂ varied from 20.10 to 22.61 µg/m³ as can be seen in Fig. 14e. The Fig. 14d and f shows the ward level distribution of the mean SO₂ and NO₂ concentrations respectively.

The various pollutant levels and other environmental quality aspects affect the well being of residents of that particular region [110–112]. Moreover, a study by [113]

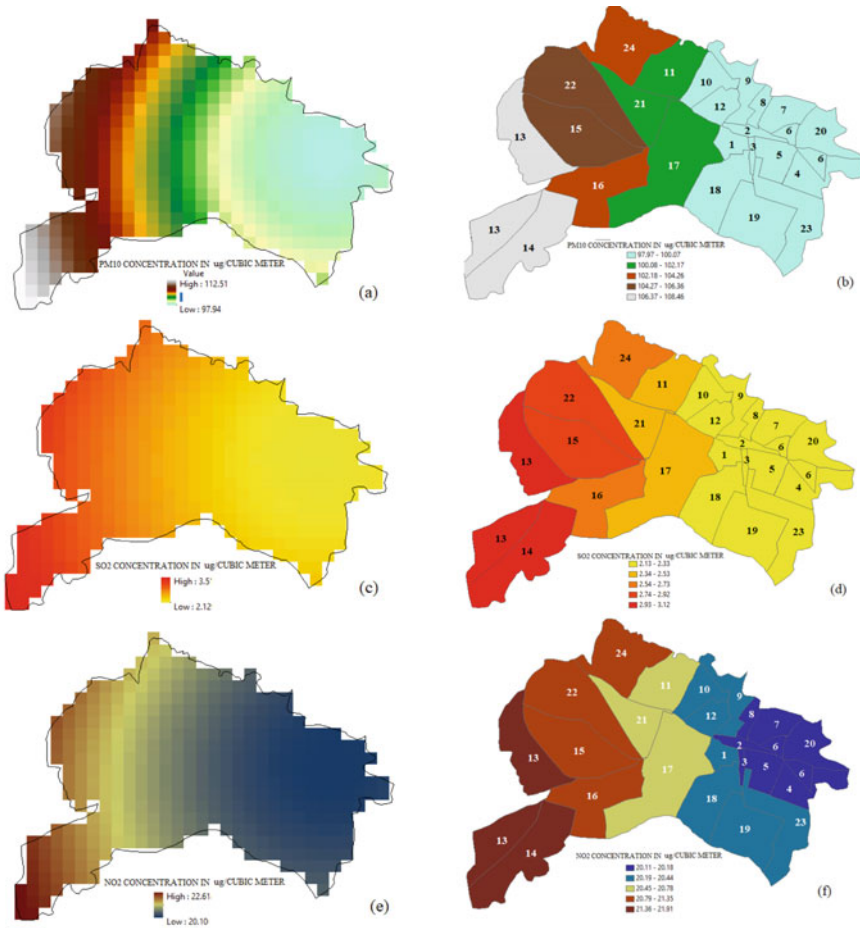


Fig. 14 Air pollution concentration in Bankura municipality a PM10, b PM10 at ward level, c SO₂, d SO₂ at ward level, e NO₂, f NO₂ at ward level

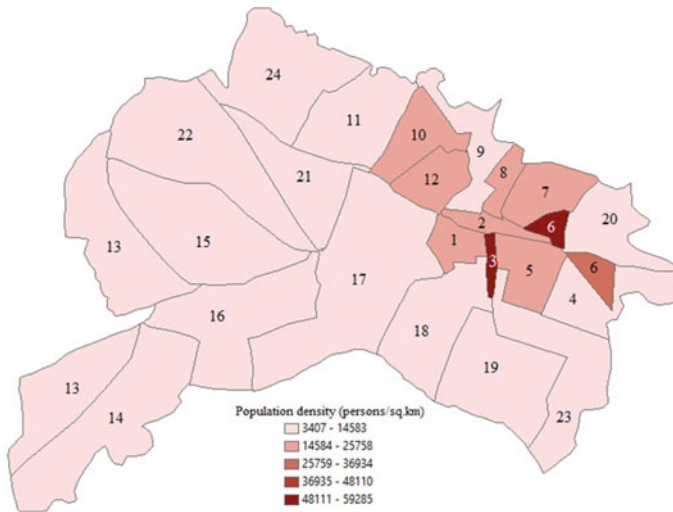


Fig. 15 Population density distribution at ward level in Bankura Municipality

has established that higher population density can lead to higher LST. The higher and denser the population of an area, the more pressure is created on the natural resources of that region, if not sustainably utilised [114, 115]. Hence it becomes crucial to know the population density of the wards with different pollution levels and environmental stressors. This would provide an overview of the wards where there is acute pressure on its resources and it also illustrates the number of people vulnerable to the impacts of environmental degradation. Thus mapped in Fig. 15, the population density shows that ward number 3 and 6 are the most densely populated because of their smaller areal extent. The population density on a ward level is comparable to some of the wards of large metropolitan cities of India, such as Delhi [113] and Kolkata [116, 117]. But the infrastructural facilities here lag far behind of those of the metro cities, presenting a grim scenario.

Besides identifying the different wards with degraded environmental conditions for various parameters, it is essential to understand the overall condition in terms of all environmental stressors cumulatively. This approach would provide a holistic scenario of the wards, for prioritising policy interventions. Henceforth a principal component analysis was carried out. In the principal component analysis, the correlation matrix was first computed between the 12 variables taken into consideration for the study. Principal component analysis was used to identify the meaningful dimensions, i.e., uncorrelated components that account for most of the variance in the original indicators [118].

The communality among variables and the Kaiser–Meyer–Olkin measure of sampling adequacy and Bartlett’s Test of sphericity (based on a probability model chi-square) was carried out to assess the partial correlations of data arrays. Tables 2 and 3 show the correlation matrix between the variables used and the KMO and

Bartlett's test. Strong negative correlation can be seen between the air pollutants, NDVI and NDWI. Moderately strong positive correlation is found between NDBI and LST (0.767). The test result of KMO was 0.633 and statistical significance was 0.000. These facts prove that principal component analysis can be performed among the variables chosen in this study.

Table 4 shows the results of the derived initial eigen values. On the basis of these eigen values which were greater than 1, the 12 variables considered in this study have been reduced to four components using the Kaiser criteria [94]. Figure 16 also shows steep breaks in the slope of the scree plot at four different points, which also signifies formation of four components. The percentage variance of the four components cumulatively showed 89.813% variance of the input data. Excepting the variables noise pollution (NOISE) and population density (POPDEN), the other variables accounted for more than 95% of the total communality. To obtain a better interpretation these components were then rotated using Varimax methods [118]. As shown in Table 5 the component loadings help in establishing a relationship between components and the variables used. Component 1 showed very strong positive loadings (correlation) with the pollutants considered for the study (PM10, NO₂, SO₂) and moderate correlation with traffic density (TRAFDEN) which are responsible for the pollution to a large extent. Component 2 showed a strong negative correlation with NDVI and positive correlation with NDWI. Population density (POPDEN) and road network density (ROADDEN) showed moderate positive correlation with component 2. Component 3 demonstrated strong positive correlation with LST and moderate positive relation with NOISE and NDBI, whereas moderate negative correlation with TRAFDEN and ROADDEN. The last component 4 shows very high correlation with the water quality Index (WQI). Higher scores of the components with adverse effects on the environment signify degraded environmental quality.

The scores derived from each component for the 24 wards in Bankura municipality are shown in Table 6. The different dimensions of environmental quality have been depicted.

The four components have been mapped in Fig. 17a–d. From Fig. 17a it can be concluded that component 1 which predominantly considers traffic density and its resultant pollutant, has affected ward number 4, 7, 18 and 20 the most. Component 2 mapped in Fig. 17b shows that in terms of bio-physical indicators like NDBI, NDWI and NDVI, ward number 16 and 18 are the worst affected. Component 3 which has clubbed together the building density and its ensuing land surface temperature in combination with road density, traffic density and their effect on noise pollution show ward number 8, 10, 11, 15, 21 and 22 to be in an environmentally critical condition. Component 4, where water quality aspects have been emphasised, portrays ward number 1, 2, 8, 10, 14, 17, 18 and 20 to have depleted surface water quality.

These four components represent different aspects of urban environmental quality (air quality, water quality, built up and vegetation quality and living condition), the scores of these components were further used to generate an overall urban environmental quality index (UEQI) and identify the wards which required immediate attention. Due to the lack of available criteria for weighting the components, authors [48, 93] proposed to use the percentage of variance obtained in the analysis as the

Table 2 Correlation matrix between the variables used (ROADDEN: Road Network Density, NDBI: Normalized Difference Built up Index, NDVI: Normalized Difference Vegetation Index, NDWI: Normalized Difference Water Index, LST1: 1Land Surface Temperature, NOISE: Noise Pollution, WQI: Water Quality Index, NO₂: Nitrogen Dioxide, SO₂: Sulphur Dioxide, PM10: Particulate Matter, TRAFDEN: Traffic Density, POPDEN: Population Density)

	ROADDEN	NDBI	NDVI	NDWI	LST	NOISE	WQI	NO ₂	SO ₂	PM10	TRAFDEN	POPDEN
Correlation	ROADDEN	1.000										
	NDBI		1.000									
	NDVI			1.000	0.767	0.244	0.062	0.257	0.257	0.255	-0.083	0.220
	NDWI					0.415	0.197	0.481	0.481	0.483	0.261	-0.738
	LST			1.000	0.226	0.389	-0.225	-0.531	-0.531	-0.533	-0.261	0.755
	NOISE				1.000	0.644	0.078	-0.103	-0.104	-0.106	-0.570	0.318
	WQI					1.000	0.139	-0.406	-0.406	-0.410	-0.552	0.506
	NO ₂						1.000	0.136	0.136	0.136	0.173	-0.091
	SO ₂							1.000	1.000	1.000	0.627	-0.526
	PM10								1.000	1.000	0.627	-0.526
	TRAFDEN									1.000	0.629	-0.528
	POPDEN										1.000	1.000

Table 3 Results of the KMO sampling adequacy test and Bartlett’s sphericity

KMO and Bartlett’s test		
Kaiser–Meyer–Olkin measure of sampling adequacy		0.632
Bartlett’s test of sphericity	Approx. chi-square	860.766
	df	66
	Sig	0.000

Table 4 Initial eigen values, variance and communalities

Component	Initial Eigenvalues			Communality
	Total	% of variance	Cumulative %	
ROADDEN	5.269	43.910	43.910	0.836
NDBI	2.563	21.357	65.267	0.895
NDVI	1.916	15.966	81.233	0.965
NDWI	1.030	8.580	89.813	0.959
LST	0.477	3.972	93.785	0.951
NOISE	0.329	2.745	96.530	0.722
WQI	0.228	1.902	98.432	0.960
NO ₂	0.168	1.400	99.832	0.972
SO ₂	0.017	0.139	99.971	0.972
PM10	0.003	0.029	100.000	0.973
TRAFDEN	0.000	0.000	100.000	0.854
POPDEN	0.000	0.000	100.000	0.717

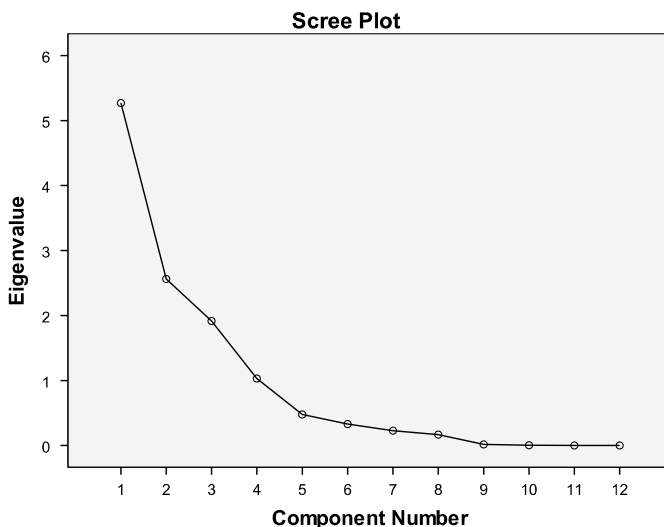


Fig. 16 Scree plot of principal component analysis showing the Eigen values and their respective components

Table 5 Rotated components loading matrix

Variables	Component			
	1	2	3	4
PM10	0.945	-0.280	0.004	0.032
NO ₂	0.945	-0.279	0.007	0.032
SO ₂	0.945	-0.279	0.006	0.032
TRAFDEN	0.684	-0.012	-0.591	0.191
NDVI	0.226	-0.943	-0.126	0.096
NDWI	-0.291	0.928	0.036	-0.112
POPDEN	-0.385	0.730	0.183	0.047
LST	-0.027	0.233	0.945	0.047
ROADDEN	-0.061	0.535	-0.739	0.020
NDBI	0.464	0.500	0.655	-0.003
NOISE	-0.413	0.293	0.625	0.276
WQI	0.092	-0.112	0.058	0.967

weights. All the components make a negative contribution to environment quality and it was therefore necessary to square the products and sum them up in order to get a positive value followed by normalization which was done by finally dividing the result by 100 to have values between 0 and 1 [45]. The map shown in Fig. 18 represents the urban environmental quality index for each ward. The classification was performed using five classes to express the environmental quality: very poor (UEQI values 0.11–0.14), poor (0.15–0.31), moderate (0.32–0.43) good (0.44–0.60), and very good (0.61–1). The map of the environmental quality index for Bankura municipality reflects that, in general, the city's environmental quality is bad. Of 24 wards, 9 have been categorised under very poor and poor classes. While only two wards (13, 14) have very good environmental quality. Ward number 2, 12 and 17 need immediate policy intervention such as reducing noise pollution, green roofing, cleaning and restoration of ponds.

5 Conclusions

Apposite biophysical, air quality, water quality, noise and traffic density as well as and population density parameters were used to understand the environmental quality of Bankura town at ward level. Remote sensing images used to derive band ratios and field investigation were done to collect water quality, noise, and traffic density data. Secondary database was used to procure information on air quality and population density. Interpolation and extrapolation of data were done to map these environmental parameters at ward level. The principal component analysis and an

Table 6 Component scores for the wards of Bankura municipality

Ward no	Component1	Component2	Component3	Component4
1	-0.751	0.457	-0.291	-1.059
2	0.111	2.453	0.411	-1.063
3	-0.350	2.165	1.125	0.096
4	-1.284	-0.824	-0.089	2.294
5	-0.776	0.615	0.484	1.100
6	-0.765	1.025	0.686	0.308
6	-0.745	0.768	0.674	0.208
7	-1.098	-0.449	-0.395	0.796
8	-0.848	0.426	-0.956	-1.124
9	-0.540	-0.089	-0.934	-0.340
10	0.323	1.092	-1.638	-0.957
11	0.364	-0.011	-1.506	0.967
12	-0.071	0.827	-0.500	0.832
13	1.865	-0.307	0.736	0.730
13	1.862	-0.274	0.737	0.743
14	2.302	-0.047	1.419	-1.458
15	0.709	-0.649	-1.357	-0.091
16	0.479	-1.216	-0.050	-0.546
17	-0.014	-1.004	0.267	-1.534
18	-1.036	-2.002	0.852	-1.302
19	-0.447	-0.660	1.997	0.559
20	-0.951	-0.598	0.080	-0.961
21	0.137	-0.634	-1.675	-0.132
22	1.212	-0.177	-1.221	0.347
23	-0.782	-0.902	1.065	-0.036
24	1.093	0.014	0.077	1.622

UEQI map were generated to assess the most vulnerable wards that need urgent planning intervention to improve environmental quality. Intervention such as increased green patches, regulated traffic flow and noise pollution, recovery of polluted water bodies, appropriate solid waste management would improve the overall environmental quality of the wards. Various other techniques and parameters can also be used based on data availability. Periodic assessments are also needed using these techniques to understand the impacts of various interventions and improvements made.

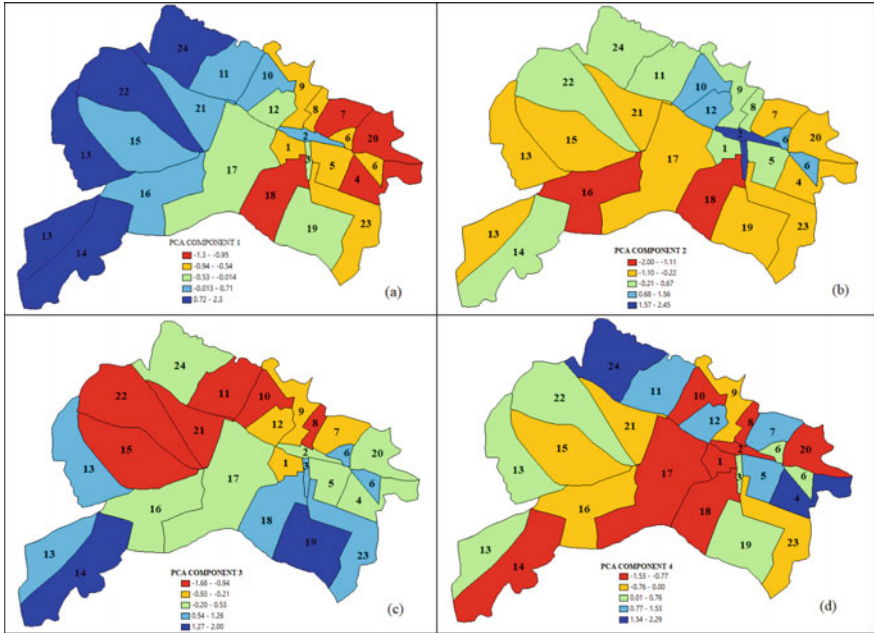


Fig. 17 a Map of the scores for component 1, b Map of the scores for component 2, c Map of the scores for component 3, d Map of the scores for component 4

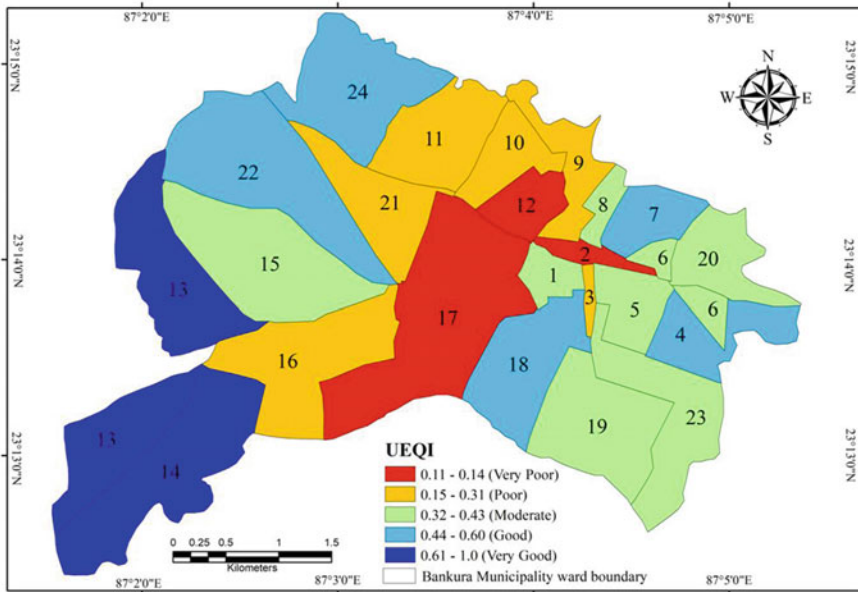


Fig. 18 Map of urban environmental quality index at ward level of Bankura municipality

6 Recommendations

The use of UEQI and various other weighted analyses, Analytic Hierarchic Process (AHP) and other urban models can prove to be extremely useful for understanding micro level environmental problems in urban areas, especially those that are upcoming ones. It would result in better decision making and sustainable developmental processes. In order to address the urban environmental problems remote sensing data of high resolution, detailed survey data, people's perception survey and public participation in mapping their environment would increase the efficiency towards problem solving. Poverty reduction, improved waste management system, sanitation facilities are a must have in urban areas. Waste water treatment and reuse should be initiated, and low-cost alternatives must be identified. To reduce air pollution usage of public vehicles, solar or battery operated vehicles, green technologies in adjacent industries should be promoted. Noise pollution regulations should be strictly implemented. Increased vegetated patches and clean water bodies in urban centres would improve the environmental quality.

References

1. Montgomery MR, Sren R, Cohen B, Reed HE (2013) Panel on urban population dynamics. Urban population dynamics, pp 108–154. http://www.nap.edu/catalog.php?record_id=10693
2. UN Statistics Division (2013) Final draft—principles and recommendations for a vital statistics system, revision 3. http://unstats.un.org/unsd/demographic/standmeth/principles/unedited_M19Rev3en.pdf
3. Wineman A, Alia DY, Anderson CL (2020) Definitions of “rural” and “urban” and understandings of economic transformation: evidence from Tanzania. *J Rural Stud* 79:254–268. ISSN 0743-0167. <https://doi.org/10.1016/j.jrurstud.2020.08.014>
4. Dijkstra L, Florczyk AJ, Freire S, Kemper T, Melchiorri M, Pesaresi M, Schiavina M (2020) Applying the degree of urbanisation to the globe: a new harmonised definition reveals a different picture of global urbanisation. *J Urban Econ* 103312. ISSN 0094-1190. <https://doi.org/10.1016/j.jue.2020.103312>
5. Bhatta B, Saraswati S, Bandyopadhyay D (2010) Urban sprawl measurement from remote sensing data. *Appl Geogr* 30(4):731–740. ISSN 0143-6228. <https://doi.org/10.1016/j.apgeog.2010.02.002>
6. Nengroo ZRA, Bhat MS, Kuchay NRA (2017) Measuring urban sprawl of Srinagar city, Jammu and Kashmir, India. *J Urban Manag* 6(Issue 2):45–55. ISSN 2226-5856. <https://doi.org/10.1016/j.jum.2017.08.001>
7. Roy B, Kasemi N (2021) Monitoring urban growth dynamics using remote sensing and GIS techniques of Raiganj Urban Agglomeration, India. *Egypt J Remote Sens Space Sci* 24(2):221–230. ISSN 1110-9823. <https://doi.org/10.1016/j.ejrs.2021.02.001>
8. Vaz E, Taubenböck H, Kotha M, Arsanjani JJ (2017) Urban change in Goa, India. *Habitat Int* 68:24–29. ISSN 0197-3975. <https://doi.org/10.1016/j.habitatint.2017.07.010>
9. Shukla A, Jain K (2021) Analyzing the impact of changing landscape pattern and dynamics on land surface temperature in Lucknow city, India. *Urban For Urban Green* 58:126877. ISSN 1618-8667. <https://doi.org/10.1016/j.ufug.2020.126877>
10. Chiu RLH (2012) International encyclopedia of housing and home. Elsevier, pp 91–96. ISBN 9780080471716. <https://doi.org/10.1016/B978-0-08-047163-1.00688-3>

11. Lawrence A, Fatima N (2014) Urban air pollution & its assessment in Lucknow City—the second largest city of North India. *Sci Total Environ* 488–489:447–455. <https://doi.org/10.1016/j.scitotenv.2013.10.106>
12. Ghosh S, Rabha R, Chowdhury M, Padhy PK (2018) Source and chemical species characterization of PM10 and human health risk assessment of semi-urban, urban and industrial areas of West Bengal, India. *Chemosphere* 207:626–636. ISSN 0045-6535. <https://doi.org/10.1016/j.chemosphere.2018.05.133>
13. Agrawal G, Mohan D, Rahman H (2021) Ambient air pollution in selected small cities in India: observed trends and future challenges. *IATSS Res* 45(1):19–30. ISSN 0386-1112. <https://doi.org/10.1016/j.iatssr.2021.03.004>
14. Prashanth GP (2021) India's air pollution: the need for city-centric plans and regulations. *Lancet Planet Health* 5(4):e185. ISSN 2542-5196. [https://doi.org/10.1016/S2542-5196\(21\)00032-2](https://doi.org/10.1016/S2542-5196(21)00032-2)
15. Pandit DN, Kumari R, Shitanshu SK (2020) A comparative assessment of the status of Surajkund and Rani Pond, Aurangabad, Bihar, India using overall index of pollution and water quality index. *Acta Ecol Sin*. ISSN 1872-2032. <https://doi.org/10.1016/j.chnaes.2020.11.009>
16. Kumar M, Ram B, Honda R, Poopipattana C, Canh VD, Chaminda T, Furumai H (2019) Concurrence of antibiotic resistant bacteria (ARB), viruses, pharmaceuticals and personal care products (PPCPs) in ambient waters of Guwahati, India: Urban vulnerability and resilience perspective. *Sci Total Environ* 693:133640. ISSN 0048-9697. <https://doi.org/10.1016/j.scitotenv.2019.133640>
17. Jyothi SN, Thomas GM, RV RR, Masetti A, Tammana A, Motheram M, Gutlapalli NC (2021). Assessment of water quality Index and study of the impact of pollution on the rivers of Kerala. *Mater Today Proc*. ISSN 2214-7853. <https://doi.org/10.1016/j.matpr.2020.09.084>
18. Mishra R, Singh D (2020) Impact of pollution on Kelo River of Raigarh District. *Mater Today Proc* 29(Part 2):310–315. ISSN 2214-7853. <https://doi.org/10.1016/j.matpr.2020.07.280>
19. Suthar S, Nema AK, Chabukdhara M, Gupta SK (2009) Assessment of metals in water and sediments of Hindon River, India: impact of industrial and urban discharges. *J Hazard Mater* 171(Issues 1–3):1088–1095. ISSN 0304-3894. <https://doi.org/10.1016/j.jhazmat.2009.06.109>
20. Singh S, Hariteja N, Renuka Prasad TJ, Janardhana NR, Ramakrishna Ch (2020) Impact assessment of faecal sludge on groundwater and river water quality in Lucknow environs, Uttar Pradesh, India. *Groundw Sustain Dev* 11:100461. ISSN 2352-801X. <https://doi.org/10.1016/j.gsd.2020.100461>
21. Ghosh S, Majumder S, Roy CT (2019) Assessment of the effect of urban pollution on surface water-groundwater system of Adi Ganga, a historical outlet of river Ganga. *Chemosphere* 237:124507. ISSN 0045-6535. <https://doi.org/10.1016/j.chemosphere.2019.124507>
22. Ahmad S, Mazhar SN (2020) Hydro chemical characteristics, groundwater quality and sources of solute in the Ramganga Aquifer, Central Ganga Plain, Bareilly District, Uttar Pradesh. *J Geol Soc India* 95(6):616–625. <https://doi.org/10.1007/s12594-020-1488-y>
23. Hunashal RB, Yogesh PB (2012) Assessment of noise pollution indices in the City of Kolhapur, India. *Proc Soc Behav Sci* 37:448–457. ISSN 1877-0428. <https://doi.org/10.1016/j.sbspro.2012.03.310>
24. Das P, Talukdar S, Ziaul Sk, Das S, Pal S (2019) Noise mapping and assessing vulnerability in meso level urban environment of Eastern India. *Sustain Cities Soc* 46:101416. ISSN 2210-6707. <https://doi.org/10.1016/j.scs.2019.01.001>
25. De Shaoli, Debnath B (2016) Prevalence of health hazards associated with solid waste disposal—a case study of Kolkata, India. *Proc Environ Sci* 35:201–208. ISSN 1878-0296. <https://doi.org/10.1016/j.proenv.2016.07.081>
26. Gautam S, Brema J, Dhasarathan R (2020) Spatio-temporal estimates of solid waste disposal in an urban city of India: a remote sensing and GIS approach. *Environ Technol Innov* 18:100650. ISSN 2352-1864. <https://doi.org/10.1016/j.eti.2020.100650>
27. Sudhir V, Muraleedharan VR, Srinivasan G (1996) Integrated solid waste management in Urban India: a critical operational research framework. *Socio-Econ Plan Sci* 30(Issue 3):163–181. ISSN 0038-0121. [https://doi.org/10.1016/0038-0121\(96\)00012-2](https://doi.org/10.1016/0038-0121(96)00012-2)

28. Kumar A, Agrawal A (2020) Recent trends in solid waste management status, challenges, and potential for the future Indian cities—a review. *Curr Res Environ Sustain* 2:100011. <https://doi.org/10.1016/j.crsust.2020.100011>
29. Mohan M, Sati AP, Bhati S (2020) Urban sprawl during five decadal period over National Capital Region of India: impact on urban heat island and thermal comfort. *Urban Clim* 33:100647. ISSN 2212-0955. <https://doi.org/10.1016/j.uclim.2020.100647>
30. Dutta I, Das A (2020) Exploring the spatio-temporal pattern of regional heat island (RHI) in an urban agglomeration of secondary cities in Eastern India. *Urban Clim* 34:100679. ISSN 2212-0955. <https://doi.org/10.1016/j.uclim.2020.100679>
31. Raj S, Paul SK, Chakraborty A, Kuttippurath J (2020) Anthropogenic forcing exacerbating the urban heat islands in India. *J Environ Manag* 257:110006. ISSN 0301-4797. <https://doi.org/10.1016/j.jenvman.2019.110006>
32. Mathew A, Khandelwal S, Kaul N (2016) Spatial and temporal variations of urban heat island effect and the effect of percentage impervious surface area and elevation on land surface temperature: study of Chandigarh city, India. *Sustain Cities Soc* 26:264–277. ISSN 2210-6707. <https://doi.org/10.1016/j.scs.2016.06.018>
33. Thomas G, Sherin AP, Ansar S, Zachariah EJ (2014) Analysis of urban heat island in Kochi, India, using a modified local climate zone classification. *Proc Environ Sci* 21:3–13. ISSN 1878-0296. <https://doi.org/10.1016/j.proenv.2014.09.002>
34. Kikon N, Singh P, Singh SK, Vyas A (2016) Assessment of urban heat islands (UHI) of Noida City, India using multi-temporal satellite data. *Sustain Cities Soc* 22:19–28. ISSN 2210-6707. <https://doi.org/10.1016/j.scs.2016.01.005>
35. Borbora J, Das AK (2014) Summer time urban heat island study for Guwahati city, India. *Sustain Cities Soc* 11:61–66. ISSN 2210-6707. <https://doi.org/10.1016/j.scs.2013.12.001>
36. Muneera CP, Krishnamurthy K (2020) Economic evaluation of traffic congestion at intersection: case study from an Indian City. *Transp Res Proc* 48:1766–1777. ISSN 2352-1465. <https://doi.org/10.1016/j.trpro.2020.08.212>
37. Lal G, Divya LG, Nithin KJ, Mathew S, Kuriakose B (2016) Sustainable traffic improvement for urban road intersections of developing countries: a case study of Ettumanoor, India. *Proc Technol* 25:115–121. ISSN 2212-0173. <https://doi.org/10.1016/j.protcy.2016.08.088>
38. Padma S, Velmurugan S, Kalsi N, Ravinder K, Erramapalli M, Kannan S (2020) Traffic impact assessment for sustainable development in urban areas. *Transp Res Proc* 48:3173–3187. ISSN 2352-1465. <https://doi.org/10.1016/j.trpro.2020.08.165>
39. Dutta Roy A, Parial MD, Mukherjee K (2020) Synergy between air quality, various urban forms, and land surface temperature: a case study of Kolkata metropolitan area. In: *Handbook of research on resource management for pollution and waste treatment*. IGI Global, pp 576–609. ISBN 9781799803690. <https://doi.org/10.4018/978-1-7998-0369-0.ch024>
40. Firdaus G, Ahmad A (2010) Noise pollution and human health: a case study of Municipal Corporation of Delhi. *Indoor Built Environ* 19(6):648–656
41. Rao KRM, Kant Y, Gahlaut N, Roy PS (2012) Assessment of quality of life in Uttarakhand, India using geospatial techniques. *Geocarto Int* 27(4):315–328. <https://doi.org/10.1080/10106049.2011.627470>
42. Sruthi KV, Mohammed FC (2020) Regional urban environmental quality assessment and spatial analysis. *J Urban Manag* 9(Issue 2):191–204. ISSN 2226-5856. <https://doi.org/10.1016/j.jum.2020.03.001>
43. Shamim Md (2002) Regional disparities in socioeconomic development in West Bengal. Aligarh Muslim University, Aligarh
44. Government of West Bengal (2007) West Bengal human development report. Development and Planning Department
45. Musse MA, Barona DA, Rodriguez LMS (2018) Urban environmental quality assessment using remote sensing and census data. *Int J Appl Earth Observ Geoinf* 71:95–108. ISSN 0303-2434. <https://doi.org/10.1016/j.jag.2018.05.010>

46. Wilson JS, Clay M, Martin E, Stuckey D, Vedder-Risch K (2003) Evaluating environmental influences of zoning in urban ecosystems with remote sensing. *Remote Sens Environ* 86(3):303–321. [https://doi.org/10.1016/S0034-4257\(03\)00084-1](https://doi.org/10.1016/S0034-4257(03)00084-1)
47. Lo CP (1997) Application of Landsat TM data for quality of life assessment in an urban environment. *Comput Environ Urban Syst* 21(3):259–276
48. Li G, Weng Q (2007) Measuring the quality of life in city of Indianapolis by integration of remote sensing and census data. *Int J Remote Sens* 28(2):249–267. <https://doi.org/10.1080/01431160600735624>
49. Ogneva-Himmelberger Y, Rakshit R, Pearsall H (2012) Examining the impact of environmental factors on quality of life across Massachusetts. *Prof Geogr* 65(2):187–204. <https://doi.org/10.1080/00330124.2011.639631>
50. Escobar Jaramillo LA (2010) El valor económico de la calidad ambiental urbana. Universidad del Valle, Cali, Colombia, p 306
51. Santana LM, Escobar JLA, Capote PA (2010) Estimación de un índice de calidad ambiental urbano, a partir de imágenes. *Revista de Geografía Norte Grande* 45:77–95
52. Dutta Roy A, Parial MD (2019) Estimating the relationship between land use land cover and surface temperature: a case study of Kolkata Metropolitan Area. *Int J Integr Res Dev* 2:189–207
53. Alqasemi AS, Hereher ME, Al-Quraishi AMF, Saibi H, Aldahan A, Abuelgasim A (2020) Retrieval of monthly maximum and minimum air temperature using MODIS Aqua land surface temperature data over the United Arab Emirates (UAE). *Geocarto Int.* <https://doi.org/10.1080/10106049.2020.1837261>
54. Das N, Mondal P, Sutradhar S, Ghosh R (2021) Assessment of variation of land use/land cover and its impact on land surface temperature of Asansol subdivision. *Egypt J Remote Sens Space Sci* 24(Issue 1):131–149. ISSN 1110-9823. <https://doi.org/10.1016/j.ejrs.2020.05.001>
55. Liang Z, Huang J, Wang Y, Wei F, Wu S, Jiang H, Zhang X, Li S (2021) The mediating effect of air pollution in the impacts of urban form on night time urban heat island intensity. *Sustain Cities Soc* 102985. ISSN 2210-6707. <https://doi.org/10.1016/j.scs.2021.102985>
56. Alqasemi AS, Hereher ME, Kaplan G, Al-Quraishi AMF, Saibi H (2021) Impact of COVID-19 lockdown upon the air quality and surface urban heat island intensity over the United Arab Emirates. *Sci Total Environ* 767:144330
57. Wan L, Wang H (2021) Control of urban river water pollution is studied based on SMS. *Environ Technol Innov* 22:101468. ISSN 2352-1864
58. Yan R, Gao Y, Li L, Gao J (2019) Estimation of water environmental capacity and pollution load reduction for urban lakeside of Lake Taihu, eastern China. *Ecol Eng* 139:105587. ISSN 0925-8574. <https://doi.org/10.1016/j.ecoleng.2019.105587>
59. Singh N, Singh S, Mall RK (2020) Urban ecology and human health: implications of urban heat island, air pollution and climate change nexus, chap. 17, pp 317–334. ISBN 9780128207307. <https://doi.org/10.1016/B978-0-12-820730-7.00017-3>
60. Wong LP, Alias H, Aghamohammadi N, Aghazadeh S, Sulaiman NMN (2017) Urban heat island experience, control measures and health impact: a survey among working community in the city of Kuala Lumpur. *Sustain Cities Soc* 35:660–668. ISSN 2210-6707. <https://doi.org/10.1016/j.scs.2017.09.026>
61. Khwarahm NR, Qader S, Ararat K, Al-Quraishi AMF (2021) Predicting and mapping land cover/land use changes in Erbil/Iraq using CA-Markov synergy model. *Earth Sci Inf* 14:393–406
62. Mohamed AMO, Paleologos EK, Howari FM (2021) Noise pollution and its impact on human health and the environment. In: *Pollution assessment for sustainable practices in applied sciences and engineering*. Butterworth-Heinemann, pp 975–1026. ISBN 9780128095829. <https://doi.org/10.1016/B978-0-12-809582-9.00019-0>
63. Nadrian H, Taghdisi MH, Pouyesh K, Khazae-Pool M, Babazadeh T (2019) “I am sick and tired of this congestion”: perceptions of Sanandaj inhabitants on the family mental health impacts of urban traffic jam. *J Transp Health* 14:100587. ISSN 2214-1405. <https://doi.org/10.1016/j.jth.2019.100587>

64. Dasgupta S, Lall S, Wheeler D (2021) Spatiotemporal analysis of traffic congestion, air pollution, and exposure vulnerability in Tanzania. *Sci Total Environ* 147114. ISSN 0048-9697. <https://doi.org/10.1016/j.scitotenv.2021.147114>
65. Tucker CJ (1979) Red and photographic infrared linear combinations for monitoring vegetation. *Remote Sens Environ* 8:127–150
66. McFeeters SK (1996) The use of the normalized difference water index (NDWI) in the delineation of open water features. *Int J Remote Sens* 17:1425–1432
67. KC A, Chalise A, Parajuli D, Dhital N, Shrestha S, Kandel T (2019) Surface water quality assessment using remote sensing, GIS and artificial intelligence. *Tech J* 1(1):113–122. ISSN: 2676-1416. <https://doi.org/10.3126/tj.v1i1.27709>
68. Guha S, Govil H, Gill N, Dey A (2020) Analytical study on the relationship between land surface temperature and land use/land cover indices. *Ann GIS* 26(2):201–216. <https://doi.org/10.1080/19475683.2020.1754291>
69. Wan L, Jiang B (2013) Road density analysis algorithm and optimization based on constrained D-TIN. *Inf Technol J* 12:5147–5153
70. Yu X, Ivey C, Huang Z, Gurrum S, Sivaraman V, Shen H, Eluru N, Hasan S, Henneman L, Shi G, Zhang H, Yu H, Zheng J (2020) Quantifying the impact of daily mobility on errors in air pollution exposure estimation using mobile phone location data. *Environ Int* 141:105772. ISSN 0160-4120 <https://doi.org/10.1016/j.envint.2020.105772>
71. Rahmanian N, Ali SHB, Homayoonfard M, Ali JN, Rehan M, Sadeif Y, Nizami SA (2015) Analysis of physiochemical parameters to evaluate the drinking water quality in the state of Perak, Malaysia. *J Chem* 2015:10p, Article ID 716125. <https://doi.org/10.1155/2015/716125>
72. Raj J, Bahuleyan H, Vanajakshi L (2016) Application of data mining techniques for traffic density estimation and prediction. *Transp Res Proc* 17:321–330. <https://doi.org/10.1016/j.trpro.2016.11.102>
73. May AD (1990) *Traffic flow fundamentals*. Prentice Hall Inc., Englewood Cliffs
74. Thabet O (2010) *Modeling and macroscopic simulation of traffic streams on multi-lane highways* (Master thesis). Cairo University, Giza
75. Al Kherret AR, Al Sobky A, Mousa R (2015) Video-based detection and tracking model for traffic surveillance. Presented at the 94th TRB annual meeting, Washington, DC (No. 15-1465)
76. Biswas D, Su H, Wang C, Stevanovic A, Wang W (2019) An automatic traffic density estimation using single shot detection (SSD) and MobileNet-SSD. *Phys Chem Earth Parts A/B/C* 110:176–184. <https://doi.org/10.1016/j.pce.2018.12.001>
77. Biswas D, Su H, Wang C, Blankenship J, Stevanovic A (2017) An automatic car counting system using OverFeat framework. *Sensors* 17(7):1535
78. Morarescu IC, Canudas-de CW (2011) Highway traffic model-based density estimation. In: American control conference (ACC), pp 2012–2017
79. Tabibiazar A, Basir O (2011) Kernel-based optimization for traffic density estimation. In: IEEE vehicular technology conference (VTC Fall), pp 1–5
80. Al-Sobky ASA, Mousa RM (2016) Traffic density determination and its applications using smartphone. *Alex Eng J* 55(1):513–523. ISSN 1110-0168. <https://doi.org/10.1016/j.aej.2015.12.010>
81. Voinov A, Morales J, Hogenkamp H (2019) Analyzing the social impacts of scooters with geo-spatial methods. *J Environ Manag* 242:529–538.4797. <https://doi.org/10.1016/j.jenvman.2019.04.114>
82. Platt S, Haddad I, Pieber S et al (2014) Two-stroke scooters are a dominant source of air pollution in many cities. *Nat Commun* 5:3749. <https://doi.org/10.1038/ncomms4749>
83. Kamalan MSH (2005) Air quality deterioration in Tehran due to motorcycles. *J Environ Health Sci Eng* 2(3):145–152
84. Affek HP, Eiler JM (2006) Abundance of mass 47 CO₂ in urban air, car exhaust, and human breath. *Geo Chim Cosmo Chim Acta* 70(1):1–12. ISSN 0016–7037. <https://doi.org/10.1016/j.gca.2005.08.021>

85. Faiz A, Gautam S, Burki E (1995) Air pollution from motor vehicles: issues and options for Latin American countries. *Sci Total Environ* 169(1–3):303–310. ISSN 0048–9697. [https://doi.org/10.1016/0048-9697\(95\)04662-K](https://doi.org/10.1016/0048-9697(95)04662-K)
86. Palmgren F, Berkowicz R, Ziv A, Hertel O (1999) Actual car fleet emissions estimated from urban air quality measurements and street pollution models. *Sci Total Environ* 235(1–3):101–109. ISSN 0048-9697. [https://doi.org/10.1016/S0048-9697\(99\)00196-5](https://doi.org/10.1016/S0048-9697(99)00196-5)
87. Aumond P, Can A, Mallet V, De Coensel B, Ribeiro C, Botteldooren D, Lavandier C (2018) Kriging-based spatial interpolation from measurements for sound level mapping in urban areas. *J Acoust Soc Am* 143(5):2847–2857
88. Mehrjardi Taghizadeh R, Zare M, Zare S (2013) Mapping of noise pollution by different interpolation methods in recovery section of Ghandi telecommunication cables company. *J Occup Health Epidemiol* 2(1):1–11
89. Harman BI, Koseoglu H, Yigit CO (2016) Performance evaluation of IDW, Kriging and multiquadric interpolation methods in producing noise mapping: a case study at the city of Isparta, Turkey. *Appl Acoust* 112:147–157
90. Damavandinejadmonfared S, Mobarakeh AK, Azmin SS, Affendi RB (2012) Evaluate and determine the most appropriate method to identify finger vein. *Proc Eng* 41:516–521. ISSN 1877-7058. <https://doi.org/10.1016/j.proeng.2012.07.206>
91. Torbick N, Becker B (2009) Evaluating principal components analysis for identifying optimal bands using wetland hyperspectral measurements from the Great Lakes, USA. *Remote Sens*. 1(3):408–417. <https://doi.org/10.3390/rs1030408>
92. Jolliffe IT, Cadima J (2016) Principal component analysis: a review and recent developments. *Philos Trans R Soc* 374201502022015020. <https://doi.org/10.1098/rsta.2015.0202>
93. Liang B, Weng Q (2011) Assessing urban environmental quality change of Indianapolis, United States, by the remote sensing and GIS integration. *IEEE J Sel Top Appl Earth Obs Remote Sens* 4(1):43–55. <https://doi.org/10.1109/JSTARS.2010.2060316>
94. Kaiser HF (1960) The application of electronic computers to factor analysis. *Educ Psychol Measur* 20:141–151
95. Zha Y, Gao J, Ni S (2003) Use of normalized difference built-up index in automatically mapping urban areas from TM imagery. *Int J Remote Sens* 24:583–594. <https://doi.org/10.1080/01431160304987>
96. Bhatti SS, Tripathi NK (2014) Built-up area extraction using Landsat 8 OLI imagery. *GIS Remote Sens* 51(4):445–446. <https://doi.org/10.1080/15481603.2014.939539>
97. Guha S, Govil H, Diwan P (2020) Monitoring LST-NDVI relationship using premonsoon landsat datasets. *Adv Meteorol* 2020:15p. <https://doi.org/10.1155/2020/4539684>
98. Guha S, Govil H (2021) An assessment on the relationship between land surface temperature and normalized difference vegetation index. *Environ Dev Sustain* 23:1944–1963. <https://doi.org/10.1007/s10668-020-00657-6>
99. Gorgani SA, Panahi M, Rezaie F (2013) The relationship between NDVI and LST in the urban area of Mashhad, Iran. In: International conference on civil engineering architecture & urban sustainable development
100. Saravanan S, Jegankumar R, Selvaraj A, Jennifer JJ, Parthasarathy KSS (2019) Utility of landsat data for assessing mangrove degradation in Muthupet Lagoon, South India, Chapter 20, pp 471–484. ISBN 9780128143506. <https://doi.org/10.1016/B978-0-12-814350-6.00020-3>
101. <https://www.usgs.gov/landsat-missions/landsat-enhanced-vegetation-index>
102. Serrano J, Shahidian S, Marques Da Silva J (2019) Evaluation of normalized difference water index as a tool for monitoring pasture seasonal and inter-annual variability in a mediterranean agro-silvo-pastoral system. *Water* 11:62. <https://doi.org/10.3390/w11010062>
103. Nag PK, Ashtekar SP, Nag A, Kothari D, Bandyopadhyay P, Desai H (1997) Human heat tolerance in simulated environment. *Indian J Med Res* 105:226–234
104. Heaviside C, Macintyre H, Vardoulakis S (2017) The urban heat island: implications for health in a changing environment. *Curr Environ Health Rep* 4(3):296–305. <https://doi.org/10.1007/s40572-017-0150-3>

105. Mirzaei M, Verrelst J, Arbabi M, Shaklabadi Z, Lotfizadeh M (2020) Urban heat island monitoring and impacts on citizen's general health status in Isfahan Metropolis: a remote sensing and field survey approach. *Remote Sens* 12:1–17. <https://doi.org/10.3390/rs12081350>
106. Manea L, Manea A, Florea D, Tarulescu S (2017) Road traffic noise pollution analysis for Cernavoda city. In: IOP conference series: materials science and engineering, vol 252, No. 1. IOP Publishing, p 012057
107. Pal D, Bhattacharya D (2012) Effect of road traffic noise pollution on human work efficiency in government offices, private organizations, and commercial business centres in Agartala City using fuzzy expert system: a case study. *Adv Fuzzy Syst* 2012:9. <https://doi.org/10.1155/2012/828593>
108. Reddy GS, Ruj B (2003) Ambient air quality status in Raniganj-Asansol area, India. *Environ Monit Assess* 89(2):153–163. <https://doi.org/10.1023/a:1026070506481>
109. West Bengal Pollution Control Board and The energy and Resource Institute (2004) Air quality status of West Bengal. A state environment Report, New Delhi
110. Speldewinde CP, Cook A, Davies P, Weinstein P (2009) A relationship between environmental degradation and mental health in rural Western Australia. *Health Place* 15(Issue 3):880–887. ISSN 1353-8292. <https://doi.org/10.1016/j.healthplace.2009.02.011>
111. Archana DC, Tiwari P (2016) Impact of environmental degradation on human health. *Int Res J Manag IT Soc Sci* 3(1):1–6. <https://sloap.org/journals/index.php/irjmis/article/view/341>
112. Gwangndi MI, Muhammad YA, Tagi SM (2016) The impact of environmental degradation on human health and its relevance to the right to health under international law. *Eur Sci J* 12(10):485. <https://doi.org/10.19044/esj.2016.v12n10p485>
113. Mallick J, Rahman A (2012) Impact of population density on the surface temperature and micro-climate of Delhi. *Curr Sci* 102:1708–1713
114. Leblois A (2018) Remote-sensing evidence about national deforestation rates in developing countries: what can be learned from the last decade. Reference module in earth systems and environmental sciences. ISBN 9780124095489. <https://doi.org/10.1016/B978-0-12-409548-9.10871-1>
115. Shrestha Nanda R (1982) A preliminary report on population pressure and land resources in Nepal. *J Dev Areas* 16(2):197–212. <http://www.jstor.org/stable/4191001>
116. Nath B, Majumder S, Rahman MM, Sen J (2020) Dealing with Covid-19 infections in Kolkata, India: a GIS based risk analysis and implications for future scenarios. *GeoHealth* 5(4). <https://doi.org/10.1101/2020.08.31.20185215>
117. Ali SA, Ahmad A (2018) Using analytic hierarchy process with GIS for Dengue risk mapping in Kolkata Municipal Corporation, West Bengal, India. *Spat Inf Res* 26(4):449–469. <https://doi.org/10.1007/s41324-018-0187-x>
118. Musse MA, Barona DA, Rodriguez LMS (2018) Urban environmental quality assessment using remote sensing and census data. *Int J Appl Earth Observ Geoinf* 71:95–108. ISSN 0303-2434. <https://doi.org/10.1016/j.jag.2018.05.010>

Urban Heat Island Under the Background of Urbanization: A Case Study in Nan Jing City, China



Zhanya Xu, Xiao Liu, Xiangang Luo, Shuang Zhu, Ning Zhang, and Qi Guo

Abstract Since the beginning of the twenty-first century, urban heat island (UHI) has become a problem of the urban ecological environment. Land Surface Temperature (LST) is one of the most effective methods to study UHI. Taking Nanjing, Jiangsu province, China, as an example, we identified and discussed the changes of urban heat island associated with the nature of the underlying surface of the city. Besides the potential driving forces in Nanjing from 2000 to 2015 using GIS (geographic information system), RS (remote sensing) technologies, and statistical methods. The results showed that Nanjing experienced rapid urbanization from 2000 to 2015, which caused dramatic changes in land cover types. A large amount of cultivated land was converted into construction land. The global spatial autocorrelation and local spatial autocorrelation results showed that LST has obvious agglomeration characteristics (Moran's $I > 0.22$). This agglomeration characteristic gradually weakens with the development of the city and finally stabilizes. In addition, according to correlation analysis and stepwise regression analysis, LULC and social economy have a significant correlation with LST, and the construction land is the main cause of the UHI ($r > 0.6$). The correlation coefficient between most landscape metrics and LST is low, meaning that landscape metrics have little effect on LST, but its impact on LST gradually increases with urbanization. Furthermore, Topography, including DEM

Z. Xu · X. Liu · X. Luo · S. Zhu (✉) · N. Zhang
School of Geography and Information Engineering, China University of Geosciences, Wuhan,
People's Republic of China
e-mail: zhushuang19@126.com

Z. Xu
e-mail: xuzhanya@cug.edu.cn

N. Zhang
e-mail: ningzhang@cug.edu.cn

Z. Xu · X. Luo
National Engineering Research Center for Geographic Information System, Wuhan, China

Q. Guo
Hubei Tianhong Detection and Technology Group (Stock) Co., Ltd, Wuhan, China
e-mail: guoqjwh@163.com

and slope, has no impact on LST in a small-scale area without significant relief. These findings can provide city planners with practical measures to alleviate UHI.

Keywords Urban heat island (UHI) · Land surface temperature (LST) · Driving factors · Spatiotemporal variations · Nanjing city

1 Introduction

The proportion of the urban population in the total population increased from 30% in 1950 to 55% in 2018 and is predicted to increase to 65% [1], with the rapid progress of urbanization. This unprecedented rapid urbanization has caused a large number of natural surfaces to be converted into impervious surfaces and permanently changed the properties of the surface and the way the energy exchanges between the surface and the atmosphere [2, 3]. These changes resulted in many problems, including the destruction of the ecological environment and biodiversity and local climate changes, which have attracted more and more people's attention [4–6]. The most significant impact on daily human life is the urban heat island (UHI), a phenomenon first discovered by British climatologist Lake Howard [7–9].

UHI means that the surface temperature of the urban center is higher than the surface temperature of the surrounding non-urban areas and has caused many problems. On the one hand, UHI profoundly affects urban biodiversity, climatic conditions, water resources and air quality, and energy consumption [10–13]. On the other hand, it has many negative effects on urban residents' physical and mental health and well-being, such as increasing the risk of illness and death [14, 15]. Therefore, a better understanding of the UHI effect has an important guiding role in providing decision-making agencies with measures to alleviate the urban heat island effect and improve residents' happiness [16, 17].

At present, there are two main types of urban heat islands based on the previous research. The first type is canopy heat islands, often calculated using temperature data from monitoring stations distributed in cities and rural areas [18]. The second is the surface heat island retrieved from various remote sensing images through band calculations [19]. Due to the scattered distribution of ground meteorological monitoring stations, it is difficult to rely solely on ground monitoring data to accurately and quantitatively describe UHI [20–22]. With the development of remote sensing technology in recent years, remote sensing data has been widely used in urban surface heat island research [23, 24] and has gradually become a main method for studying UHI. At the same time, remote sensing data is easy to obtain and can provide different resolutions for research [25, 26]. As a result, we use remote sensing images to explore UHI effects in this article.

In order to understand the Spatiotemporal changes of urban heat island and the leading driving factors in the process of urbanization, this chapter takes Nanjing City, Jiangsu Province, China as the research area, and global autocorrelation, local

autocorrelation, correlation analysis, and stepwise regression methods are comprehensively used to provide policymaker practical suggestions and measures to alleviate UHI, optimize urban spatial patterns, and improve the sustainable development of cities. This study aims to: (1) explore the LULC change and development model of Nanjing during the urbanization process from 2000 to 2015. (2) Explore the temporal and spatial changes of the spatial distribution of surface temperature density and its spatial autocorrelation. (3) Use correlation analysis and stepwise regression to explore the correlation between each driving factor and LST and the dominant driving factors leading to the change of LST in the process of urbanization.

2 The Surface Heat Island

Although remote sensing data can effectively help researchers describe the spatial distribution pattern of surface temperature, it is difficult to propose measures to mitigate urban heat islands only through the spatial distribution of surface temperature [27]. The interaction between surface temperature and influencing factors leads to the difference in surface temperature distribution. Therefore, in the previous thermal environment research, the quantitative relationship between various influencing factors and LST has been widely studied [28]. The type of land cover and land use (LULC) significantly influences the surface temperature, and different types of LULC have different surface temperatures [29]. The surface temperature of the impervious surface, the leading cause of UHI, is often high, while the temperature in areas covered by much vegetation is relatively low [30, 31].

Therefore, the transformation of a large amount of forest land and arable land into the impervious surface in the process of urbanization aggravated the heat island effect to a certain extent [32]. Several studies confirmed that the normalized building index (NDBI) [33, 34] and the normalized vegetation index (NDVI) [33, 35, 36] have a good linear relationship with LST. In addition, landscape metrics (including landscape configuration, composition, and diversity) [37, 38] and socio-economic [39, 40] have also been confirmed to be correlated with LST.

Although existing studies have shown that LULC, landscape metrics, and social-economic impact the change of LST, most studies only consider the effect of one or several factors on LST and few studies comprehensively consider all of them. Peng Jian et al. [27] used OLS and stepwise regression methods to clarify the correlation between LULC, landscape metrics, and socio-economic driving factors, and LST in summer, winter, and transitional seasons. It fails to effectively explain the spatial distribution of LST and the spatiotemporal non-stationary of each driving factor. Therefore, this study comprehensively combines topography, LULC, landscape metrics, social economy, and other driving factors to explain LST's temporal and spatial evolution. Furthermore, it establishes a comprehensive driving factor system, determines the dominant influencing factors of LST, and then analyzes the spatial heterogeneity and Mechanism.

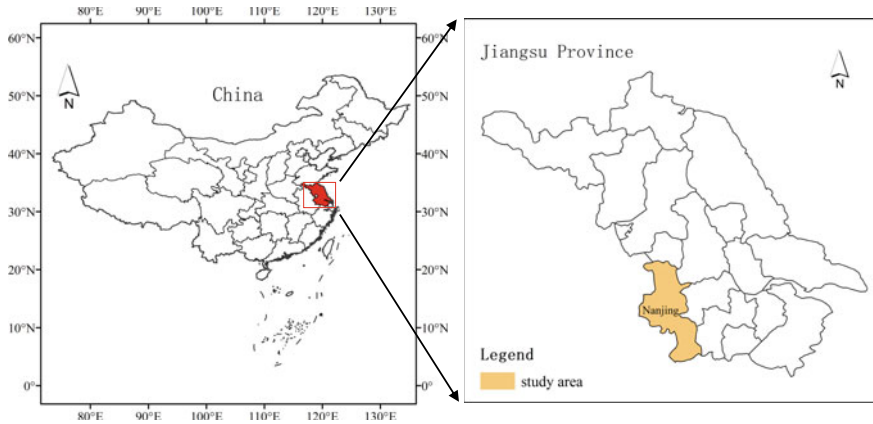


Fig. 1 Location of the study (the red area represents Hubei province)

3 Materials and Methods

3.1 Study Area

Nanjing ($118^{\circ}22' \sim 119^{\circ}14' \text{ E}$, $31^{\circ}14' \sim 32^{\circ}37' \text{ N}$), the capital of Jiangsu Province, is located in the middle and lower reaches of the Yangtze River in eastern China (shown in Fig. 1). It is the only megacity in the Yangtze River Delta and East China and is sited in the humid foothills of the North subtropical zone, with an average annual rainfall of 1200 mm and an average annual temperature of 15.4°C . The urbanization rate of Nanjing has increased substantially in recent years. The total population of Nanjing has increased from 6.14 million in 2000 to 8.43 million, and the proportion of the urban population has increased from 56.8 to 82.5%.

3.2 Materials and Preprocessing

In order to obtain the annual difference in surface temperature, we selected an 8-day composite land surface temperature data MOD11A2 in 2000, 2005, 2010, and 2015, with an image resolution of 1 km. MOD11A2 data includes night surface temperature data (observation time at 22:30) and daytime surface temperature data (observation time at 10:30). Wan et al. (2008) compared MODIS V5 LST with measured data from the ground monitoring station and found that the two are consistent (root mean square error is less than 0.7 k). The result shows that the MOD11A2 data has high accuracy in representing the surface thermal properties of LULC. In this study, the study used daytime data. To reflect the LST changes in different years, we combine the data of July and August based on the average value of the pixels at the same

location. All original MODIS data were geo-corrected, reprojected and combined to generate spatial mosaic LST datasets within the study area.

The LULC data used in this article comes from the Resource and Environmental Science Data Center of the Chinese Academy of Sciences (<http://www.resdc.cn>). The data includes 6 first-level classes and 25 s-level classes and the date of data are consistent with the MOD11A2 datasets. Liu et al. [41] found that the overall classification accuracy of the first-level class of land cover data exceeded 94.3%, and the overall classification accuracy of the second-level classes also reached more than 91.2% in their study [41, 42]. In order to better distinguish the type of the LULC and show the changes in land cover between years, we merged the original LULC types into six categories: farmland (including paddy fields and dry land), forest land (including the land with natural forests, plantations and urban trees, grassland (including natural grassland and managed grassland), water bodies (Including rivers, natural lakes, and artificial lakes), construction land (including buildings, streets and other artificial surfaces), and unutilized land (including bare land and wasteland).

The population and GDP data are also from the Resource and Environmental Science Data Center of the Chinese Academy of Sciences (<http://www.resdc.cn>), with a resolution of 1 km and the data date is synchronized with the surface temperature data. This study used SRTM DEM data from the geospatial data cloud (<http://www.gscloud.cn/>) with a resolution of 90 m to obtain terrain factors. All data have been reprojected and resampled to 1000 * 1000 m resolution. All remote sensing data preprocessing is carried out in the ArcGis 10.2 platform [13].

3.3 Study Methods

3.3.1 LST Retrieval

Due to the existence of the deviation, the MOD11A2 data cannot be directly expressed as the surface temperature, and it needs to be transformed through a certain relationship. This conversion relationship is shown in the formula (1) [43]:

$$T_i = DN_i * 0.02 - 273.15 \quad (1)$$

DN_i represents the brightness value of pixel i , and DN_i represents the real surface temperature ($^{\circ}\text{C}$) of pixel i after conversion.

3.3.2 The Classification of First Zones

There are many methods for the classification of LST zones. This chapter adopts the mean-standard deviation method [32] to classify surface temperature due to the atmospheric and sunshine conditions are different in different years. Besides quantitatively comparing the changes of LST zone in different years and their response

Table 1 The classification of LST zones

Classification	LST zones
$T_S < \mu - std$	Low
$\mu - std < T_S \leq \mu - 0.5 std$	Sub-low
$\mu - 0.5 std < T_S \leq \mu + 0.5 std$	Medium
$\mu + 0.5 std < T_S \leq \mu + std$	Sub-high
$T_S > \mu + std$	High

mechanisms to changes in land cover types, the obtained surface temperature needs to be normalized. The normalization rule is shown in formula (2). Then, the surface temperature is divided into six levels according to the mean and standard value, as shown in Table 1 below.

$$T_S = \frac{T_i - T_{min}}{T_{max}} \quad (2)$$

T_{max} , T_{min} , T_s represent the minimum surface temperature value, the maximum surface temperature value, the normalized surface temperature value, respectively.

3.3.3 Selection of the Driving Factors

In order to comprehensively analyze the driving factors of LST change, we selected 15 influencing factors and divided them into 4-factor layers, including land cover, socio-economic, topographic and landscape metrics. The landscape metrics include three levels: patch level, class level and landscape level. This study selected eight landscape-level indices to describe the landscape's composition, shape, and spatial arrangement. The details of the impact factors are shown in Table 2. We use a 4 km * 4 km grid to cut the data and then calculate the landscape metrics of each grid in the FRAG STATS 4.2 software package. The average value of each indicator and LST in each grid was counted to analyze the relationship between LST and driving factors. Based on the previous studies [32, 44], this study used Pearson correlations and stepwise regression to determine the impacts of different driving factors on the UHI. All statistical analyses are performed in SPSS 25 [45].

3.3.4 Spatial Autocorrelation Analysis

Spatial autocorrelation analysis [48–50] has the function of identifying spatial agglomeration, which can determine whether a variable is spatially correlated and its degree of correlation. There are many statistics for spatial autocorrelation analysis. This article chooses Moran's I index to reflect the overall characteristics of the spatial agglomeration pattern of surface temperature. The calculation formula of

Table 2 Influencing factors of land surface temperature (LST) used in this study

Categories	Variables	Meaning of variables
LULC	Ecological land	Percentage of ecological land
	Construction land	Percentage of construction land
	Farmland	Percentage of farmland
Landscape metrics	PD	Patch density
	LPI	Largest patch index
	ED	Edge density
	LSI	Landscape shape index
	MSI	Mean shape index
	CONTAG	Contagion
	SHDI	Shannon’s diversity index
	AI	Aggregation index
Socio-economic	GDP	GDP density in the spatial unit
	POP	Population density in the spatial unit
Topography	DEM	Average altitude of the spatial unit
	Slope	Average slope of the spatial unit

Note Ecological land [46, 47] includes forest land, grassland and water body

global Moran’s I is as follows (3). The value range of the global Moran’s I index is [-1, 1]. When Moran’s I is close to 0, there is no spatial autocorrelation. The observations are randomly arranged in space. However, if Moran’s I > 0 or < 0, it means that there is a positive or negative correlation between the observations.

$$Moran's\ I = \frac{n \sum_{i=1}^n \sum_{j=1}^n w_{ij} (x_i - \underline{x})(x_j - \underline{x})}{\sum_{i=1}^n \sum_{j=1}^n w_{ij} \sum_{i=1}^n (x_i - \underline{x})^2} \tag{3}$$

The calculation formula of local Moran’s I [51] is as follows (4):

$$Moran's\ I_i = \frac{x_i - \underline{x}}{S^2} \sum_{j=1}^n w_{ij} (x_j - \underline{x}) \tag{4}$$

$$S^2 = \frac{1}{n} \sum_{i=1}^n (x_j - \underline{x})^2$$

$$\bar{x} = \frac{1}{n} \sum_{i=1}^n x_i$$

n represents the total number of units involved in the analysis; x_i and x_j are the attribute values at positions i and j , respectively; \bar{x} is the average value of attribute values at all positions; w_{ij} is the spatial weight; S is the standard deviation.

4 Results

4.1 Urbanization Process and Land Cover Changes in Nanjing

Figure 2 shows that with the development of the economy and under the guidance of relevant policies, the urban scale of Nanjing has continued to expand and the built-up area has increased significantly. The results revealed that from 2000 to 2005, the overall development direction of Nanjing was southeast, south and northwest, and the development in the south and southeast is the most significant. The expansion is mainly based on the city center, expanding to the periphery and suburbs of the original city center. From 2005 to 2010, several main development directions of the city include northwest, southwest, and northeast. The development direction was relatively scattered and there was no obvious core. Driven by policies, the areas along the Yangtze River and some satellite towns have developed rapidly. In contrast, the extent of development on the urban fringe has dropped significantly compared with the previous period. From 2010 to 2015, the development speed of the city was relatively slower, the change was small, there was no clear direction, and the expansion in all directions was small.

With the advancement of urbanization, the types of LULC have undergone significant changes with human activities for the needs of urban expansion and functions. Figure 3 shows the statistics of the dynamic changes of LULC in Nanjing. The outcomes showed that the farmland and construction land area changed most significantly. The area of construction land increased from 1017 to 1435 km² in 2000–2015 and the growth rate reached 41.1%. In contrast, the area of farmland decreased from 4116 km² in 2000 to 3613 km² in 2015 and the net loss reached 12.2%. With the implementation of the policy of returning farmland to forest and people's awareness of environmental protection, planners have paid more and more attention to protecting forest land and grassland in the process of urban development. This is why the minor changes of forest land and grassland in Nanjing from 2000 to 2015. The water body area varies with the inter-annual rainfall, but overall there is no significant change. The above analysis indicated that in the rapid urbanization process, a large amount of farmland in the city's surrounding areas had been transformed into an impervious

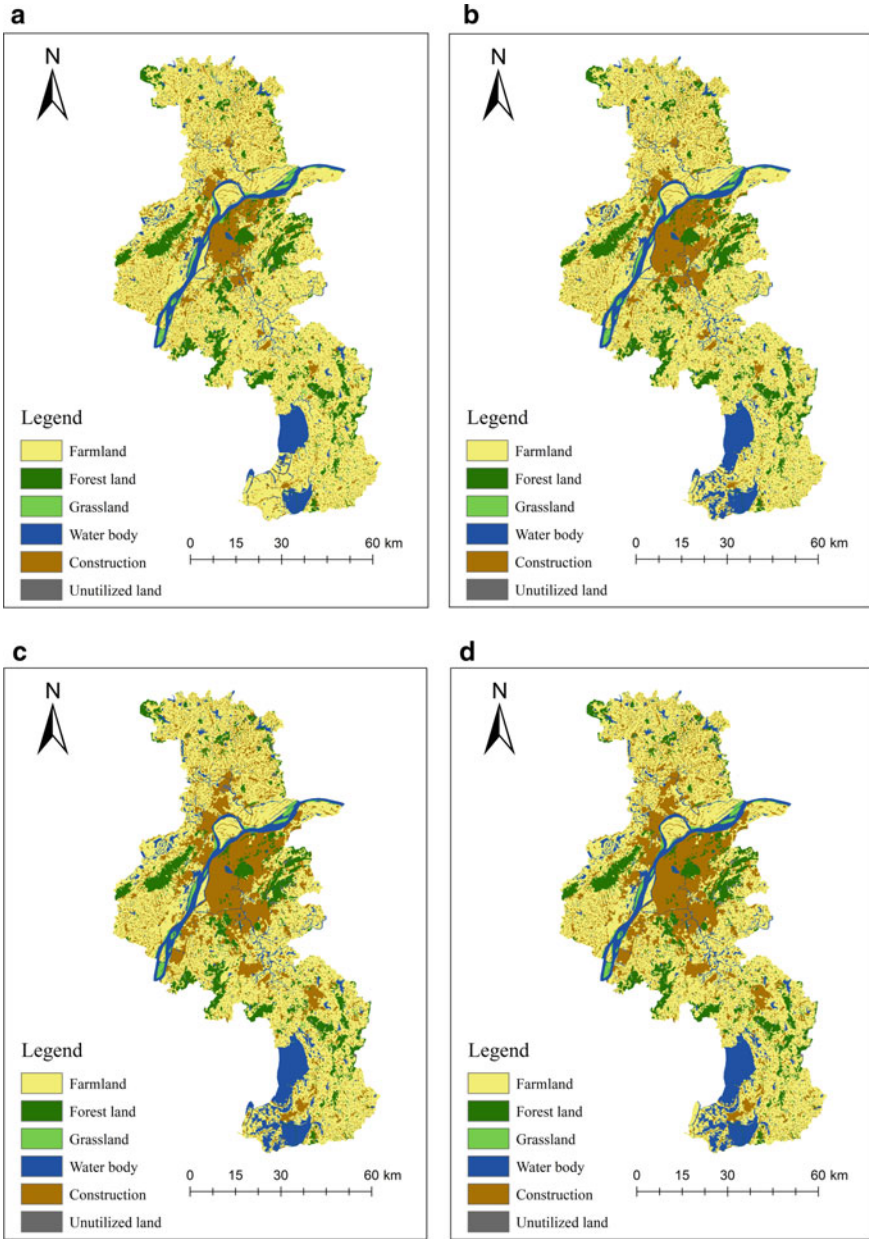


Fig. 2 LULC maps of Zhengzhou City in **a** 2000, **b** 2005, **c** 2010, and **d** 2015

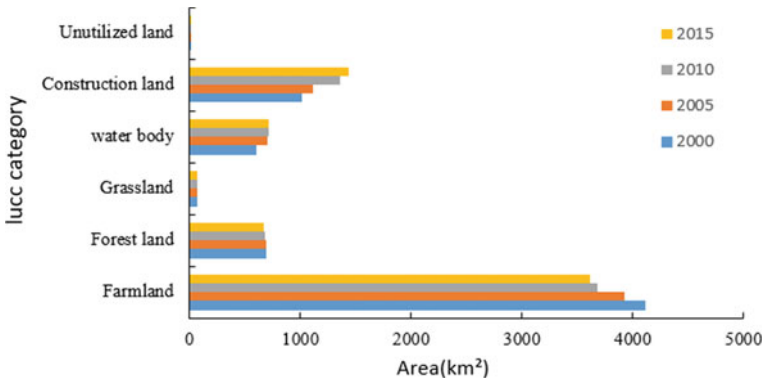


Fig. 3 Area change for the LULC categories from 2000 to 2015

surface because of the needs of urban development and woodland occupation, and grassland is relatively small.

4.2 The Variation of LST Zones

According to Eq. (1), we get the annual LST in Nanjing. According to the calculation results, the average temperature in Nanjing increased from 29.42 °C in 2000 to 30.82 °C in 2015, an increase of 1.4 °C. Meanwhile, the lowest temperature, 20.08 °C appeared in 2005, and the highest temperature was 37.13 °C, appeared in 2000.

This study calculated the average temperature by six land cover types from 2000 to 2018, as shown in Table 3. The results reflected that the surface temperature of water bodies, forest land and grassland is low. On the contrary, the surface temperature of construction land is the highest. Because construction land is composed of various impervious surfaces, such as roads, buildings, factories, etc., these ground objects have the characteristics of small specific heat capacity and rapid heating. However, due to the influence of agricultural work, the surface temperature of the farmland is relatively high. Similarly, on account of lack of vegetation cover, unutilized land also has a relatively high surface temperature. In general, the difference in the thermal properties of the surface of the different LULC results in the different surface temperatures of different LULC.

As shown in Fig. 4, the spatial distribution of surface temperature showed that the surface temperature in urban areas during 2000–2015 was significantly higher than that in surrounding areas. High and sub-high temperature zones are mainly distributed in cities. Some larger satellite towns full of buildings, commercial areas and roads, and sub-high temperatures are always distributed around high-temperature areas, indicating that the existence of high temperatures has a certain impact on the surrounding environment. The low-temperature zones and sub-low-temperature

Table 3 Mean surface temperature (°C) of different LULC

LULC categories	2000	2005	2010	2015
Farmland	31.56 ± 1.49	31.06 ± 1.41	32.64 ± 1.65	33.39 ± 1.43
Forest land	31.9 ± 1.53	31.17 ± 1.41	32.47 ± 1.5	32.98 ± 1.43
Grassland	29.73 ± 1.71	29.6 ± 1.39	30.51 ± 1.85	31.75 ± 1.96
Water body	29.86 ± 1.87	29.81 ± 1.79	31.09 ± 2.05	31.91 ± 1.98
Construction land	32.62 ± 2.25	32.78 ± 2.66	34.5 ± 2.58	35.09 ± 2.18
Unutilized land	32.43 ± 1.48	30.66 ± 0.49	32.5 ± 0.74	33.28 ± 1.18

Note Mean ± standard deviation

zones are mainly distributed in areas covered by vegetation or water. At the same time, the results (as shown in Fig. 5) reflected that with the development of cities, the area of high-temperature zones was increasing year by year, while the areas of medium-temperature and sub-high temperature zones continued to decrease. The possible reason for this phenomenon is that the farmland around the city is converted into construction land, which leads to the transition of the medium temperature Zone and sub-high temperature zone to high-temperature zone.

4.3 Spatial Autocorrelation of LST Zones

Through the spatial analysis of the global autocorrelation, as shown in Table 4, Moran's I index of the LST zones from 2000 to 2015 are all positive, and the P value is less than 0.001. Indicating that the Nanjing heat island has a significant spatial positive correlation, meaning the high values or low values have obvious aggregation. And we can see that the Moran's I index from 2000 to 2015 is gradually decreasing. The possible reason is that a large number of natural landscapes have turned into impervious surfaces and urban landscape patterns have become more scattered with the process of urbanization. As a result, the correlation of spatial autocorrelation between heat island regions is weakened.

The local spatial autocorrelation of urban heat island intensity reflects the spatial agglomeration characteristics of urban heat island intensity. Figure 6 shows that the "high-high" type, high urban heat island intensity clusters, are mainly concentrated in urban built-up areas and some satellite towns, and with the progress of urbanization, the area of "high-high" clusters has increased significantly, Basically consistent with the development of the city. The "low-low" type, low-temperature areas, are mainly distributed in water and forest coverage areas, and the spatial distribution of low-low clusters varies greatly in different years.

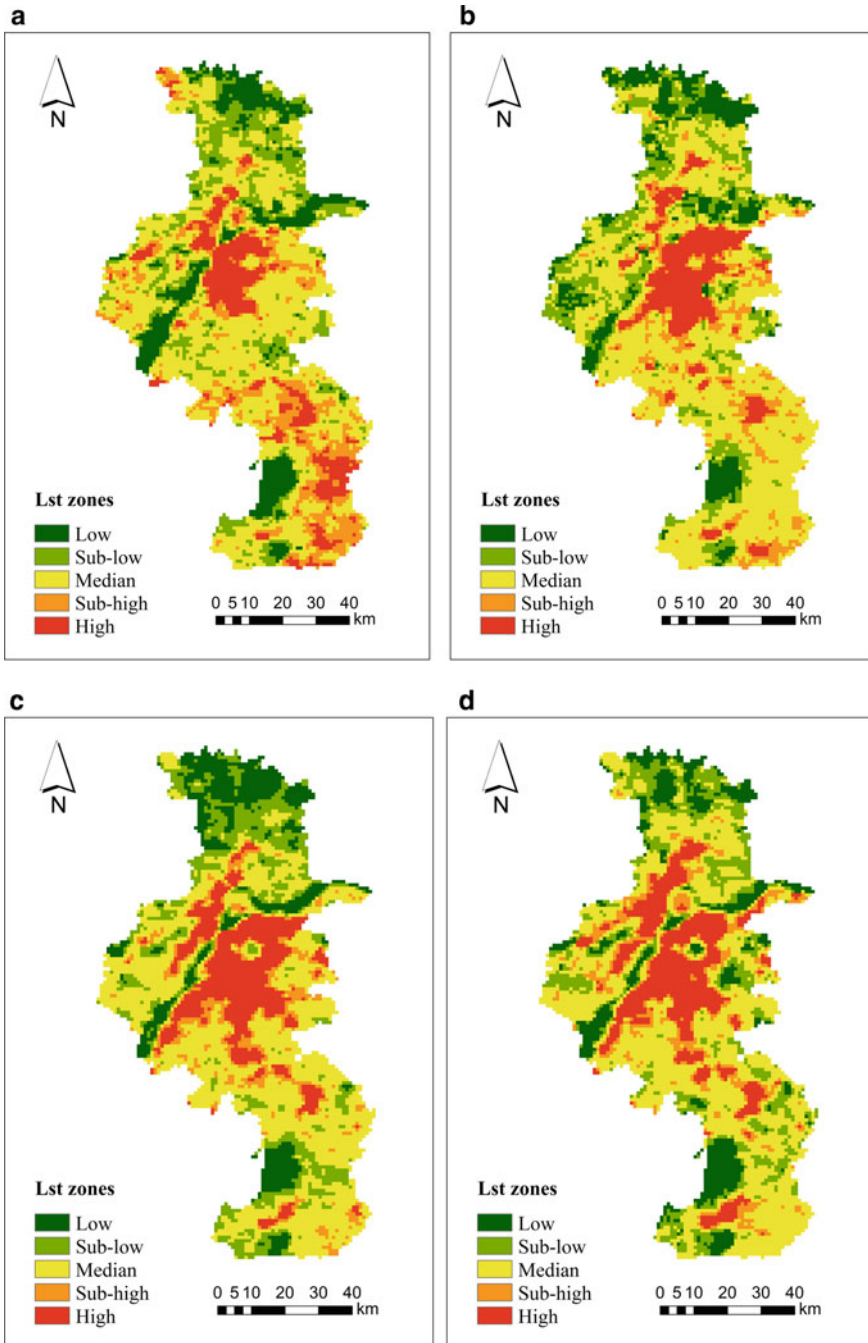


Fig. 4 Spatial pattern of LST zones from 2000 to 2015. a 2000. b 2005. c 2010. d 2015

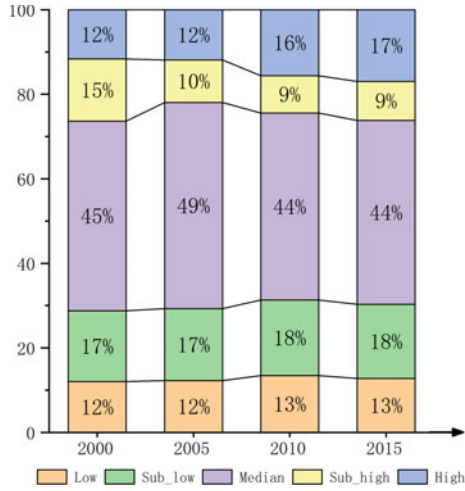


Fig. 5 Changes in the area of LST zones

Table 4 Global autocorrelation coefficient from 2000 to 2015

index	2000	2005	2010	2015
Moran's I	0.300498	0.268810	0.233196	0.226416
Z scores	14.150906	17.896740	11.316172	11.120972
P value	<0.001	<0.001	<0.001	<0.001

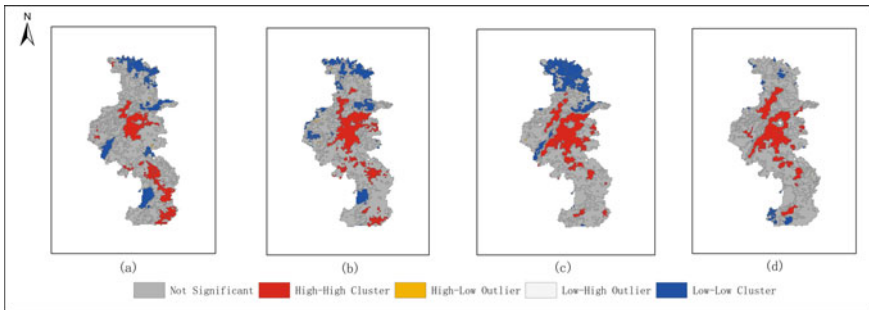


Fig. 6 Local spatial autocorrelation distribution map

4.4 Driving Factors Analysis

4.4.1 The Relationship Between Driving Factors and LST

As shown in Table 5, we calculated the Pearson correlation coefficients between 15 driving factors of 4 factor layers and LST. The three driving factors of the LULC have the highest correlation with LST. All have passed the 0.01 level of a significance test. There is a significant positive correlation between construction land and LST ($r > 0.6$), indicating that construction land is an important cause of UHI. In addition, there is a significant negative correlation between the proportion of ecological land ($r < -0.3$) and farmland ($r < -0.2$) and surface temperature, revealing that green vegetation and water bodies can alleviate the heat island effect to a certain extent. Secondly, there is a significant correlation between socio-economic and LST.

The results show that population density and GDP have a significant positive correlation with LST and the correlation coefficient r is greater than 0.15 and 0.2, respectively. With the urbanization process, the correlation between GDP and LST is getting higher and higher, and the correlation between population density and LST is getting weaker. The correlation between each factor and LST is not stable for the landscape metrics. In general, with urbanization, the correlation between most landscape metrics (eg LSI, MSI, and SHDI) and LST has gradually increased. However, their correlation is relatively weak compared with LULC and socio-economic indicators. As for the terrain factor index, there is no significant correlation between DEM and slope and LST and the correlation coefficient r is close to 0. The results reflect that the topography has little influence on LST change in the region with a small regional range and small topographic relief.

4.4.2 Analysis of Leading Factors

The results of stepwise regression analysis of driving factors and LST of each factor layer are shown in Table 4. Each year, the land cover has the highest degree of explanation for LST ($R^2 = 0.512$ in 2000, $R^2 = 0.563$ in 2005, $R^2 = 0.643$ in 2010, $R^2 = 0.694$ in 2015). All factors have entered the stepwise regression equation, indicating that land cover is the main reason for LST change. At the same time, the results of correlation analysis show that construction land will aggravate urban heat islands. On the other hand, ecological land (forest land, grassland, water bodies, etc.) and farmland can alleviate the UHI to varying degrees. The GDP and population density of economic indicators have also entered the stepwise regression equation ($R^2 > 0.2$), showing that economic indicators are an important factor leading to urban heat islands in the process of urbanization.

For the urban landscape metrics, its explanation for the changes in LST is relatively low. However, with urbanization, the degree of interpretation of the landscape metrics for the change of LST gradually increases (from 0.017 in 2000 to 0.14 in 2015), because the shape and proportion of the urban landscape pattern are caused by

Table 5 Results of correlation analysis and stepwise regression analysis

Categories	Driving factors	2001		2005		2010		2015	
		r	R ²	r	R ²	r	R ²	r	R ²
Landscape metrics	PD	0.001 (/)	0.017	-0.130*	0.06	-0.284**	0.123	-0.258**	0.14
	LPI	-0.032		-0.038		-0.027		-0.04	
	ED	0.04 (/)		-0.099 (/)		-0.220** (/)		-0.144** (/)	
	LSI	0.04 (/)		-0.099 (/)		-0.220** (/)		-0.144** (/)	
	MSI	-0.002 (/)		0.078 (/)		-0.175** (/)		-0.224** (/)	
	CONTAG	0.142*		0.151**		0.121*		0.092	
Socio-economic	SHDI	0.03 (/)		0.006 (/)		-0.115*		-0.117*	
	AI	-0.037 (/)		-0.105 (/)		-0.218** (/)		-0.137*	
	GDP	0.211**	0.286	0.249**	0.312	0.257**	0.337	0.343**	0.136
	POP	0.191**		0.186**		0.161**		0.117**	
	Ecology Land	-0.278**	0.512	-0.349**	0.563	-0.381**	0.643	-0.520**	0.694
	Construct Land	0.626**		0.751**		0.794**		0.790**	
Topography	Farmland	-0.165**		-0.253**		-0.366**		-0.250**	
	DEM	0.101 (/)	-	0 (/)	-	-0.042 (/)	-	-0.159 (/)	-
	SLOPE	0.113 (/)		0.044 (/)		0.009 (/)		-0.103 (/)	

Note ** and * represent the significance level of 0.01 and 0.05 respectively; r represents the correlation coefficient between LST and each factor and R² represents the stepwise regression analysis results of each factor layer and LST, indicating the degree of interpretation of the factor layer to LST. “/” indicates that the variable has not entered the stepwise regression equation

urbanization have changed significantly. For terrain factors, DEM and slope did not enter the regression equation in all years, which shows that terrain cannot effectively explain the change of LST on a small scale. In general, land cover and economic indicators have the strongest impact on LST, and land cover can most effectively explain the change of LST, which is the main reason for the formation of UHI.

5 Discussions

Based on the results of the temporal and spatial dynamics of LULC and heat island regions, this study analyzed the impact of some important features of LULC on UHI in the process of urbanization and discussed the impact of various factors on surface temperature. First, Nanjing's construction land increased significantly from 2000 to 2015, indicating that Nanjing has experienced rapid urbanization. This result is similar to the results of other studies [32, 51]. In addition, urbanization has led to huge changes in land cover. Due to development needs, a large amount of farmland around the city has been converted into construction land. Secondly, changes in LULC led to dramatic changes in the urban thermal environment. High-temperature areas continued to increase from 2000 to 2015. At the same time, it can be found that high-temperature areas and sub-high-temperature areas are mainly located in construction land, while low-temperature areas are mainly located in vegetation coverage areas and water areas. This finding is consistent with the research results of others [32].

We have also analyzed the spatial distribution of different levels of surface temperature areas in the process of urbanization. The results show significant spatial clustering characteristics in surface temperature regions, and this clustering feature gradually weakens and stabilizes with the urbanization process. The results also showed that the drastic changes in LULC in urbanization lead to more urban landscape fragmentation, which weakens the spatial autocorrelation between heat island regions. The correlation analysis and LSR analysis results show that land cover and economic indicators are the leading causes of urban heat islands. However, compared to other research results [37, 52], this article's urban landscape index has a lower degree of explanation for LST. The reason may be that rapid Urbanization urbanization leads to an increase in artificial surface area. The corresponding artificial green space will also increase, making the urban landscape pattern more fragmented, resulting in LST being affected by multiple interaction factors.

In addition, our research also provides some suggestions for urban planners to alleviate urban heat islands. For example, the results show that high-density construction land will aggravate urban heat islands, and lower vegetation and water temperature can alleviate urban heat islands. Therefore, vegetation and water areas should be appropriately increased in urban development, such as building parks and artificial lakes. At the same time, the results show that optimizing the urban internal spatial structure and increasing the pattern of green vegetation patches are effective means to alleviate the urban heat island.

6 Conclusions

We use RS and GIS technology to comprehensively explore the temporal and spatial changes of urban heat islands in this study. At the same time, we explore the impact of various driving factors, including LULC, socio-economic, landscape metrics, and topography, on the urban heat island in the process of urbanization.

From this study, we mainly concluded: (1) From 2000 to 2015, Nanjing experienced rapid urbanization. Urbanization has caused drastic changes in LULC, and a large amount of farmland has been converted into construction land. (2) High-temperature areas are mainly located in city business districts and satellite towns, while low-temperature areas are mainly located in vegetation coverage areas and waters. LULC has a significant impact on urban heat island. The area of high-temperature areas has increased year by year with urbanization. (3) The LST zones have a noticeable agglomeration effect (high-high clustering and low-low clustering) in spatial distribution. This agglomeration effect gradually weakens with the urbanization process and will eventually stabilize. (4) LULC and socio-economic index are the main factors affecting urban heat islands.

The results show that construction land is the most important cause of urban heat islands. At the same time, GDP and population density also aggravate the heat island effect, while ecological land (woodland, grassland, and water) can effectively alleviate the heat island effect. In addition, the results reveal that the urban landscape configuration has a small impact on the urban heat island, and this impact gradually increases with the process of urbanization. Therefore, in the process of urban construction, we can take some measures (such as increasing vegetation coverage and water areas, adjusting the spatial distribution of different landscapes) to alleviate the urban heat island effect.

This study reveals the influence and changes of LULC, socio-economy, topography, and landscape metrics on land surface temperature in urbanization. With the rapid development of remote sensing technology, we can more accurately explore the impact of various LULC on the surface temperature at a finer scale. In addition, this study did not consider the impact of human behavior, climate conditions, seasonal changes, and the interaction of various driving factors on the surface temperature at different scales.

7 Recommendations

In the future, we should pay more attention to mitigating the effects of UHI by optimizing spatial patterns of all kinds of driving factors, especially LULC, combined with understanding the formation mechanism of urban heat islands. Decision-makers should consider optimizing the urban spatial pattern and increasing the green area reasonably to mitigate the urban heat island and improve the residents' happiness.

Acknowledgements Thanks to all the collaborators for their efforts in this study, including downloading data, processing data, and determining the experimental plan.

References

1. United Nations (2012) World urbanization prospects: the 2014 revision. CD-ROM Edition
2. Yonghong H, Meiting H, Gensuo J, Chunlei Z, Xiaojun Z, Yanhua X (2019) Comparison of surface and canopy urban heat islands within megacities of eastern China. *ISPRS J Photogramm Remote Sens* 156:160–168
3. Jie T, De Y, Qiang L, Xuelan T, Weijun Z (2020) Spatial relationship between land-use/land-cover change and land surface temperature in the Dongting Lake area, China. *Sci Rep* 10:1–9
4. Morabito M, Crisci A, Guerri G, Messeri A, Congedo L, Munafò M (2021) Surface urban heat islands in Italian metropolitan cities: tree cover and impervious surface influences. *Sci Total Environ* 751:142334
5. Kim SW, Brown RD (2021) Urban heat island (UHI) intensity and magnitude estimations: a systematic literature review. *Sci Total Environ* 146389
6. Jun Y, Weiling L, Yonghua L, Xueming L, Quansheng G (2018) Simulating intraurban land use dynamics under multiple scenarios based on fuzzy cellular automata: a case study of Jinzhou district, Dalian. *Complexity*
7. Tim RO (1988) The urban energy balance. *Prog Phys Geogr* 12:471–508
8. Shushi P, Shilong P, Philippe C, Pierre F, Catherine O, François-Marie B, Huijuan N, Liming Z, Ranga BM (2012) Surface urban heat island across 419 global big cities'. *Environ Sci Technol* 46:696–703
9. Xu L, Wang J, Xiao F, Sherif EB, Awed A (2021) Potential strategies to mitigate the heat island impacts of highway pavement on megacities with considerations of energy uses. *Appl Energy* 281:116077
10. Chaobin Y, Xingyuan H, Fengqin Y, Lingxue Y, Kun B, Jiuchun Y, Liping C, Shuwen Z (2017) Mapping the influence of land use/land cover changes on the urban heat island effect—a case study of Changchun, China. *Sustainability* 9:312
11. Die H, Qingyan M, Linlin Z, Ying Z (2020) Spatial quantitative analysis of the potential driving factors of land surface temperature in different “Centers” of polycentric cities: a case study in Tianjin, China. *Sci Total Environ* 706:135244
12. Nidhi S, Saumya S, Mall RK (2020) Urban ecology and human health: implications of urban heat island, air pollution and climate change nexus. In: *Urban ecology*. Elsevier
13. Hari S, Seema B (2016) Spatial data analysis with ArcGIS and MapReduce. In: 2016 international conference on computing, communication and automation (ICCCA). IEEE, pp 45–49
14. Li X, Stringer LC, Chapman S, Dallimer M (2021) How urbanisation alters the intensity of the urban heat island in a tropical African city. *PLoS ONE* 16(7):e0254371
15. Scott AL (2016) An energy and mortality impact assessment of the urban heat island in the US. *Environ Impact Assess Rev* 56:139–144
16. Decheng Z, Shuqing Z, Shuguang L, Liangxia Z, Hao Z (2014) Surface urban heat island in China's 32 major cities: spatial patterns and drivers. *Remote Sens Environ* 152:51–61
17. Marie Luise B, Frieder L, Thomas P (2018) Urban river recovery inspired by nature-based solutions and biophilic design in Albufeira, Portugal. *Land* 7:141
18. Ian DS, Tim RO (2012) Local climate zones for urban temperature studies. *Bull Am Meteor Soc* 93:1879–1900
19. Gordana K, Ugur A, Zehra YA (2018) Urban heat island analysis using the landsat 8 satellite data: a case study in Skopje, Macedonia. In: *Multidisciplinary digital publishing institute proceedings*, p 358

20. Dewan A, Kiselev G, Botje D (2021) Diurnal and seasonal trends and associated determinants of surface urban heat islands in large Bangladesh cities. *Appl Geogr* 135:102533
21. Kai W, XiuQun Y (2013) Urbanization and heterogeneous surface warming in eastern China. *Chin Sci Bull* 58:1363–1373
22. Byambakhuu G, Falin W, Battsengel V, Enkhjargal D, Baasandolgor T, Uyanga M, Yan Z (2019) Implication of urban heat island (UHI) related to human activities: a case study in Mongolia. In: *Remote sensing technologies and applications in urban environments IV*, 111570V. International Society for Optics and Photonics
23. Xin H, Ying W (2019) Investigating the effects of 3D urban morphology on the surface urban heat island effect in urban functional zones by using high-resolution remote sensing data: A case study of Wuhan, Central China. *ISPRS J Photogramm Remote Sens* 152:119–131
24. Alqasemi AS, Hereher ME, Al-Quraishi AMF, Saibi H, Aldahan A, Abuelgasim A (2020) Retrieval of monthly maximum and minimum air temperature using MODIS Aqua land surface temperature data over the United Arab Emirates (UAE). *Geocarto Int.* <https://doi.org/10.1080/10106049.2020.1837261>
25. Nicholas C, Peng G (2013) MODIS detected surface urban heat islands and sinks: Global locations and controls. *Remote Sens Environ* 134:294–304
26. Yuzhou Z, Jie C (2019) Spatio-temporal analysis of urban heat island using multisource remote sensing data: a case study in Hangzhou, China. *IEEE J Selected Topics Appl Earth Observ Remote Sens* 12:3317–3326
27. Jian P, Jinglei J, Yanxu L, Huilei L, Jiansheng W (2018) Seasonal contrast of the dominant factors for spatial distribution of land surface temperature in urban areas. *Remote Sens Environ* 215:255–267
28. Yuxia L, Chaoyang W, Dailiang P, Shiguang X, Alemu G, Rachhpal SJ, Altaf A, Linlin L, Bin F, Jing MC (2016) Improved modeling of land surface phenology using MODIS land surface reflectance and temperature at evergreen needleleaf forests of central North America. *Remote Sens Environ* 176:152–162
29. Lu Y, Yue W, Liu Y, Huang Y (2021) Investigating the spatiotemporal non-stationary relationships between urban spatial forms and land surface temperature: a case study in Wuhan, China. *Sustain Cities Soc* 103070
30. Cheng H, Ligu Z, Youru Y, Weichun M, Patrick LK (2020) Estimating spatial effects of anthropogenic heat emissions upon the urban thermal environment in an urban agglomeration area in East China. *Sustain Cities Soc* 57:102046
31. Khudair DA, Al-Quraishi AMF, Hasan AA (2019) Spatiotemporal monitoring and modeling of urban sprawl using remote sensing and GIS: a case study Al-Karkh, Baghdad, Iraq. *JARDCS* 11(6):1691–1698
32. Hongbo Z, Juntao T, Zhibin R, Zheyue W (2020) Spatiotemporal characteristics of urban surface temperature and its relationship with landscape metrics and vegetation cover in rapid urbanization region. *Complexity*
33. Guha S, Govil H, Gill N, Dey A (2021) A long-term seasonal analysis on the relationship between LST and NDBI using Landsat data. *Quatern Int* 575:249–258
34. Paul M, Florian S (2017) Comparison of NDBI and NDVI as indicators of surface urban heat island effect in landsat 8 imagery: a case study of Iasi. *Present Environ Sustain Develop* 141–150
35. Yan L, Maosheng Z, David J M, Safa M, Qiaozhen M, Eugenia K, Fang Z, Shuangcheng L, Kaicun W (2016) Potential and actual impacts of deforestation and afforestation on land surface temperature. *J Geophys Res Atmos* 121:14,372–14,386
36. Fadhil AM (2011) Drought mapping using Geoinformation technology for some sites in the Iraqi Kurdistan region. *Int J Digit Earth* 4:239–257
37. Shihong D, Ziqian X, Yichen W, Luo G (2016) Quantifying the multilevel effects of landscape composition and configuration on land surface temperature. *Remote Sens Environ* 178:84–92
38. Saha S, Saha A, Das M, Saha A, Sarkar R, Das A (2021) Analyzing spatial relationship between land use/land cover (LULC) and land surface temperature (LST) of three urban agglomerations (UAs) of Eastern India. *Remote Sens Appl Soc Environ* 22:100507

39. Ganlin H, Cadenasso ML (2016) People, landscape, and urban heat island: dynamics among neighborhood social conditions, land cover and surface temperatures. *Landscape Ecol* 31:2507–2515
40. Dengsheng L, Guiying L, Emilio M, Scott H (2013) Spatiotemporal analysis of land-use and land-cover change in the Brazilian Amazon. *Int J Remote Sens* 34:5953–5978
41. Jiyuan L, Wenhui K, Zengxiang Z, Xinliang X, Yuanwei Q, Jia N, Wancun Z, Shuwen Z, Rendong L, Changzhen Y (2014) Spatiotemporal characteristics, patterns, and causes of land-use changes in China since the late 1980s. *J Geog Sci* 24:195–210
42. Xinliang X, Jiyuan L, Dafang Z (2012) Remote sensing monitoring methods of land use/cover change in national scale. *J Anhui Agric Sci* 4
43. Zhengming W (2007) Collection-5 MODIS land surface temperature products users' guide. University of California, Santa Barbara, ICES
44. Ali A, Bahman JA, Yousef S (2015) Assessing the effect of green cover spatial patterns on urban land surface temperature using landscape metrics approach. *Urban Ecosyst* 18:209–222
45. Paul M (2018) IBM SPSS statistics 25 step by step: a simple guide and reference. Routledge
46. Jing C, Peijun S (2005) Discussion on functional land use classification system. *J-Beijing Normal Univ Nat Sci Edition* 41:536
47. Hongqi Z, Lixin W, Baoquan J (2004) A conception of ecological land use and its function classification in arid area in Northwest China. *Chin J Eco-Agric* 12:5–8
48. Bian HY, Ren ZY (2011) Spatial autocorrelation of land carrying capacity in the guanzhong tianshui areas. *J Ningxia Teachers Univ* 32:56–59
49. Andrew David C, J Keith O (1981) *Spatial processes: models & applications*. Taylor & Francis
50. Yantun S, Shixiao Y, Nan L (2007) Spatial structure of the surface temperature in Shenzhen, China. *Acta Ecol Sin* 27:1489–1498
51. Luc A (1995) Local indicators of spatial association—LISA. *Geogr Anal* 27:93–115
52. Ruci W, Hao H, Yuji M, Ahmed D (2020) Spatiotemporal analysis of land use/cover patterns and their relationship with land surface temperature in Nanjing, China. *Remote Sens* 12:440

Optimization of Ecological Environment Sensor Network Sites with Multiple Monitoring Targets



Xiangang Luo, Kai Luo, Yangchun Li, Fukun Zhu, Libo Zhou, and Bei Xu

Abstract Regular monitoring is essential for understanding the ecological and hydrological processes at the basin scale. There are complex trade-offs in the layout and optimization of more than one ecological environment index monitoring network. This article introduces an optimization method that uses the universal cokriging (UCK) model to establish multiple monitoring target variables in the watershed. After establishing a multivariate linear model, the spatial trend of the target variable is eliminated, and the Linear Model of Coregionalization (LMC) is used to fit the cross-variation function and regression residual variance. The weighted average of the mean regression kriging variance (MRKV) of multiple target variables is used as the objective function. The spatial simulated annealing algorithm (SSA) is used for sampling optimization. The optimized sample is combined with Pareto's method to make the final optimization sample. This paper takes the establishment of a multi-objective wireless monitoring network for surface temperature, soil moisture, and rainfall in the Jinsha River Basin as the research object. The results show that the multi-objective optimization design based on the UCK model can well show the spatial variability of the target variables. It can also better solve other multi-objective optimization trade-offs such as economic maintenance based on entropy other than

X. Luo · K. Luo

School of Geography and Information Engineering, China University of Geosciences,
Wuhan 430074, China
e-mail: BillLxg@126.com

K. Luo

e-mail: luokai@cug.edu.cn

National Engineering Research Center of Geographic Information System, Wuhan 430074, China

Y. Li (✉)

Chengdu University of Technology, Chengdu 610059, China
e-mail: 82066240@qq.com

Geological Hazard Technical Service Center of Guizhou Province, Guiyang 550004, China

F. Zhu · L. Zhou · B. Xu

Wuhan Zhongdi Yunshen Technology Co. LTD, Wuhan 430074, China

non-target monitoring variables. The final result realizes the dual multi-objective site optimization of multi-objective variables and multi-objective benefits.

Keywords Spatial simulated annealing · Multi-objective · Regression kriging · Entropy · Site optimization

1 Introduction

Obtaining baseline data to assess the impact and protection of regional ecosystems, and developing and validating ecological hydrological models is a vital [1–4]. In general practice, the ecological hydrological observations of a river basin are mainly through fixed-point ground stations or satellite remote sensing data. Although remote sensing data can quickly obtain massive large-area dynamic and comprehensive observational data. Some relevant verification studies have shown that these products may be biased, and the accuracy of the data needs to be verified by ground observation data [5]. Relatively speaking, a fixed-point observation station on the ground can obtain more accurate observation data. The original sites are often sparse in spatial distribution. A site needs to monitor a large spatial range, which makes it difficult to ensure the accuracy of the monitored values. High-density site deployment often consumes a lot of manpower and material resources [6, 7]. Developing a complete set of program software for deploying and optimizing a multi-objective ecological, hydrological site monitoring network is vital to establishing a future hydrological and ecological integrated monitoring network.

In most cases, ecological hydrological variables are spatially autocorrelated. Therefore, methods based on geostatistical models can be used to optimize WSN sampling locations [6]. According to the spatial correlation, the model may be established with the difference between isotropy and anisotropy. The optimization methods for ecological hydrological sites can be summarized as traditional mathematical statistics [6, 8], network optimization methods [9, 10], information entropy methods [11–14], and geostatistical methods [15–18]. Many studies have focused on its optimization criteria, such as choosing the smallest mean regression kriging prediction variance (MRKV) as the sampling model to obtain the best sampling sample. So far, the optimized SSA (Spatial Simulated Annealing) algorithm [19] for sampling a single target has been widely used in the ecological environment.

The monitoring station of multiple target variables often involves the spatial distribution of multiple variables, and multi-target variables always have a close relationship [6]. Such as precipitation, soil moisture and surface temperature have a spatial correlation in a certain area. A spatial sampling method with multiple target variables is proposed and applied to soil sampling. This method can better consider the spatial correlation of multiple target variables. Multi-objective optimization algorithms are widely used in multi-objective problems in ecological environment, such as SA (simulated annealing) algorithm [20], genetic algorithm (GA) [21, 22], particle swarm algorithm (PSO) [23], and their various variant algorithms [24–29].

In practical applications, the number of points is huge, which means that the search is extremely time-consuming. It is particularly important to use an effective search algorithm to find a combination with the smallest MRKV value. Among them, the space simulated annealing algorithm (SSA), which is developed from the simulated annealing algorithm to solve the problem of spatial location optimization, can help find the global optimum [19]. SSA can say that the mean regression kriging variance (MRKV) of ordinary kriging (OK) is minimized, which will lead to the distribution of the sample to the entire area. The experimental results of [19] show that the optimized spatial sampling sample is essentially a compromise between geographic space and feature space.

The problem of multi-objective combination optimization problem (MOCOP) has also received extensive attention from various industries [29–31]. A multi-objective algorithm is used to obtain the Pareto solution set by establishing multiple objective functions. Find a set of optimal solutions in the Pareto solution set as the final optimization result. Many new multi-objective algorithms have been applied to spatial sampling and layout optimization [18, 32–34].

Optimization of the maximum space coverage and multi-objective optimization of the comprehensive benefits of a single variable. Both are just a single consideration of space coverage or comprehensive economics. In reality, we often need to consider both. In this chapter, we elaborated a sampling optimization methodology for multi-objective factors. In addition to considering the spatial coverage, we also consider the need for information redundancy and economic efficiency. We planned a two-stage site design and layout plan. The goal of the first phase was to show the spatial relationship between precipitation, land surface temperature, soil moisture, etc. and environmental covariates, and get their spatial trends. The goal of second phase was to reflect the relationship between precipitation, surface temperature and soil moisture and other constraints. The final site distribution can consider the influence of the spatial trend (i.e. variograms) and the sampling constraints and information redundancy of the sites.

2 Study Area and Data

2.1 Study Area

The Jinsha River basin is located in the upper reaches of the Yangtze River Basin (Fig. 1). It is the collective name for the upper reaches of the Yangtze River from the source to the Xiangjiaba reservoir in Yibin city. The JinSha River basin has an about area of 340,000 km² with a longitude range 90 °E–105 °E and latitude 24 °N–36 °N. The altitude ranges from 500 to 5000 m. The Jinsha River Basin is rich in hydropower resources. The water resources in this area account for nearly 40% and 15% of the entire Yangtze River Basin and China, respectively. The Jinsha River basin

has obvious spatial heterogeneity, affected by vegetation, climate, hydrology, topography, etc. Most of the Jinsha River basin is located in mountainous areas, and the topography varies greatly. The topography and topography will significantly impact the basin's forest ecosystem and hydrological processes. These factors determine that there are also many climate types in the Jinsha River basin, such as monsoon climate, vertical climate, and plateau climate [35, 36].

2.2 Data Description

The data of the study area mainly includes basic geographic data and auxiliary environmental data. This study used data from 31 existing weather stations in the study area. The 31 stations are roughly scattered in the west and densely distributed in the east. Basic geographic data includes Jinsha River basin boundary data, water system data, DEM data, road data, etc. The target variable data is related to the prior data of the multi-target site data that needs to be monitored, such as Land Surface Temperature (LST), precipitation, and soil moisture. Environmental covariate data includes altitude, slope, aspect, longitude, and latitude. Due to the difference in the data, this research uniformly rasterizes the target variable data and environmental covariate data into a spatial resolution of $1 \text{ km} \times 1 \text{ km}$.

2.2.1 Basic Geographic Data

The basic geographic data describes the natural geographic environmental conditions in the Jinsha River basin, including basin boundary, river, existing weather station, slope, aspect and Digital Elevation Model (DEM). The slope and aspect data are extracted from the DEM data downloaded from the Geospatial Data Cloud (<http://www.gscloud.cn/>) (Fig. 2). The basin boundary and river system data are extracted from DEM data using the ArcSWAT model [37].

2.2.2 Environmental Auxiliary Data

Environmental auxiliary data were used to provide as prior information about mainly ecohydrology variables. In view of the fact that there is no observation data of the three target variables before the monitoring site is deployed. Therefore, these data are needed as a priori knowledge of annual average precipitation, land surface temperature (LST), and soil moisture (Fig. 3).

1. Precipitation data

Precipitation data were obtained from the website of WorldClim.org. The website provides the global precipitation data obtained by spatial interpolation of more than

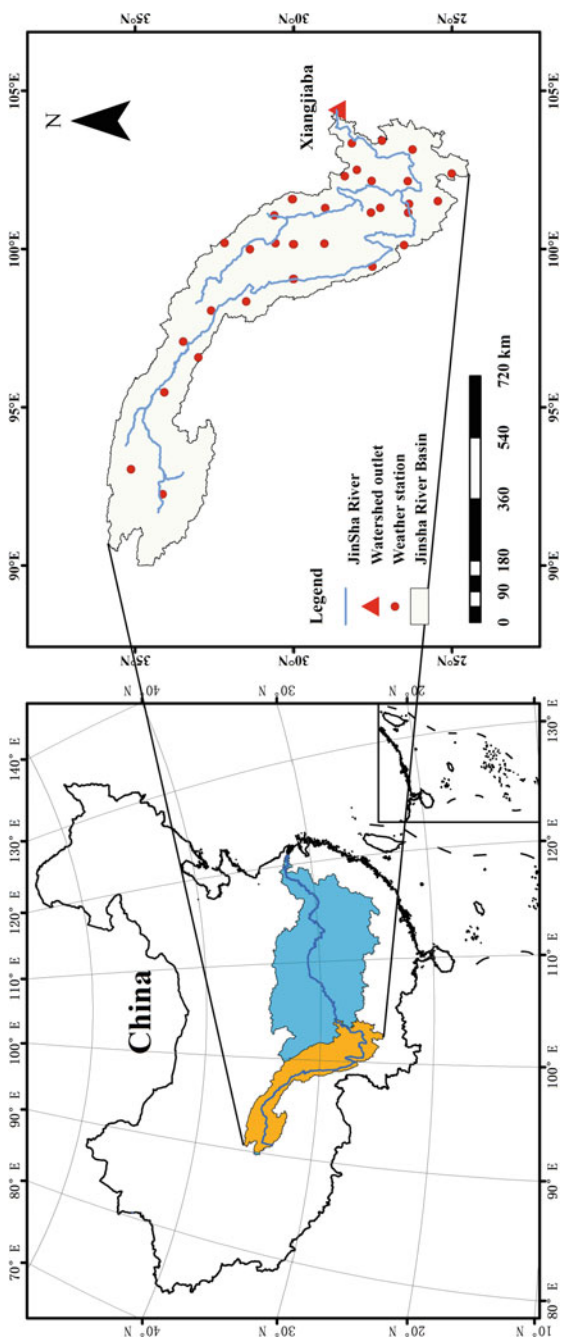


Fig. 1 The location of the Jinsha River basin on YangZi River and China

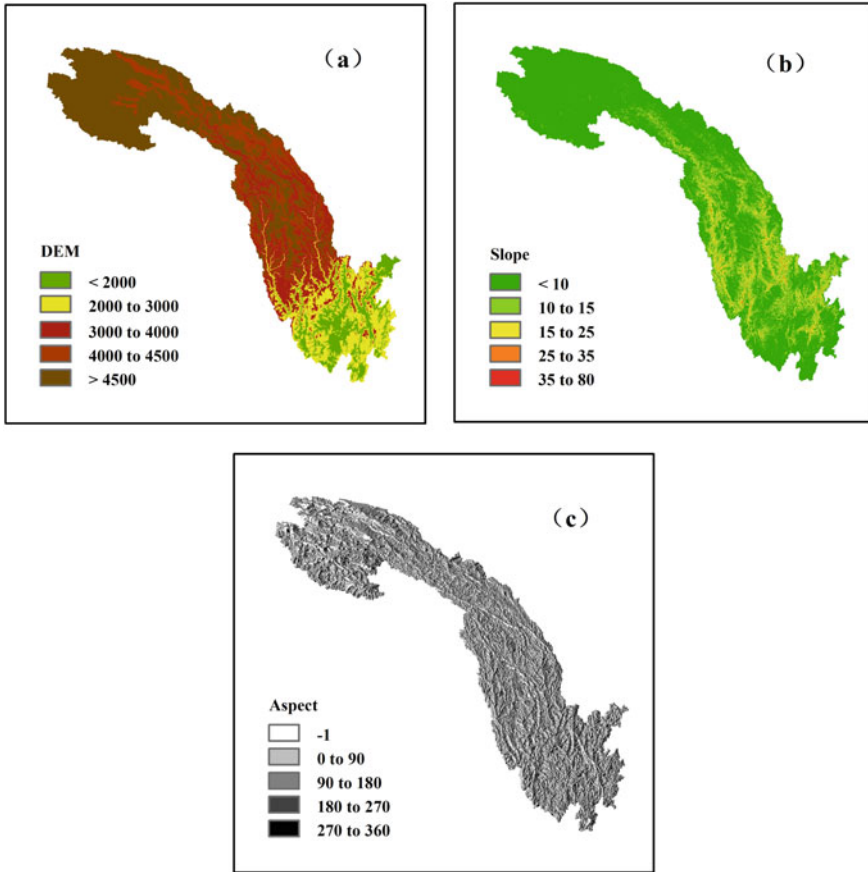


Fig. 2 Basic geographic data **a** elevation **b** slope **c** aspect

15,000 weather stations worldwide [38]. We used the 2019 precipitation data as the prior precipitation information, with the spatial resolution 1 km.

2. LST

Annual average data of LST was obtained from the Moderate Resolution Imaging Spectroradiometer (MODIS). The data comes from the MOD11A2 data retrieved from the Earthdata website of the National Geological Survey, with a spatial resolution of 1 km and a temporal resolution of 8 days [39–41]. By performing pixel-based weight overlap addition on 46 scenes of image data in a year, MODIS data has missing values at some pixels because clouds cover it. The weighted overlap addition based on pixels can solve the overlap calculation of missing values very well. When calculating the average, record the number of non-missing values as weight for each pixel in all layers. After overlay analysis, divide by the weight value corresponding to

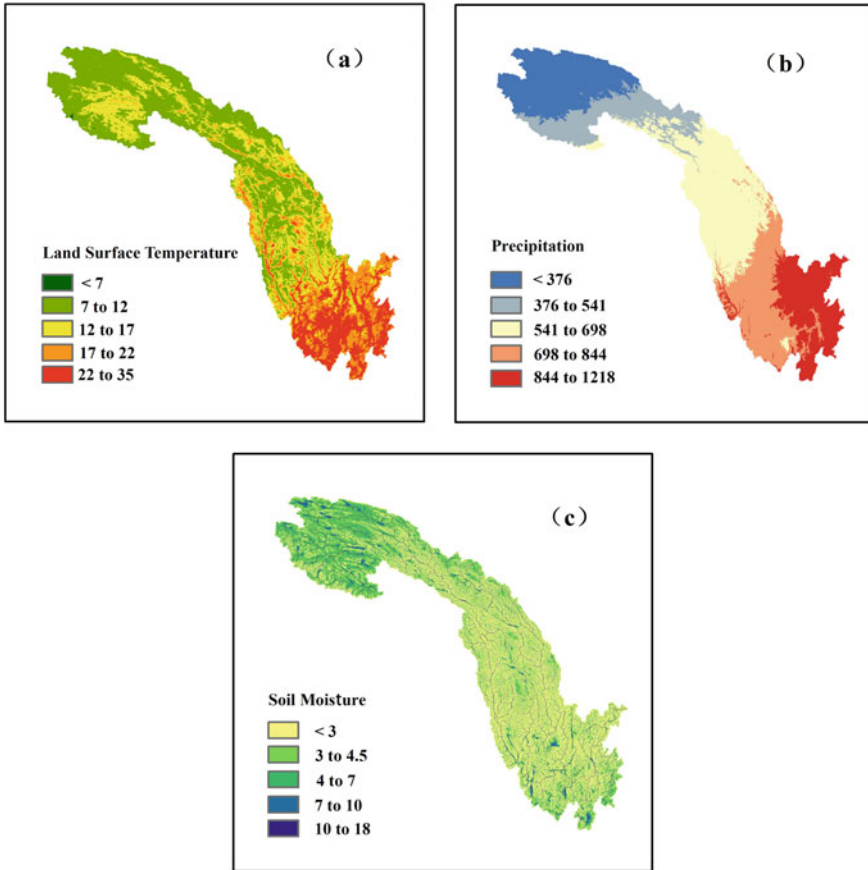


Fig. 3 Environmental auxiliary data. **a** Annual average MODIS land surface temperature product. **b** Annual mean precipitation product. **c** Topographic wetness index calculated from DEM data to represent soil moisture

each pixel to get the average value. This method can ensure that the average value of pixels with missing values is not too large or too small.

3. Soil moisture data

The spatial resolution of the existing product data of commonly used soil moisture is 0.25° . As the resolution accuracy is low, it is not suitable for the use of this research. Therefore, the soil moisture data is calculated based on the TWI (topographic wetness index) [42, 43] calculated from DEM products. Based on DEM, TWI reflects the spatial distribution characteristics of soil moisture by quantitatively describing the catchment area and slope of the upslope of the basin. This method is simple to calculate, easy to obtain parameters, and comprehensively considers topography, soil and other factors, which can better simulate the spatial distribution pattern of water, and

thus has been widely used. TWI calculated with the multiple-flow direction algorithm (FD8) [44, 45].

4. The latitude and longitude data

The latitude and longitude data is a grid of 1 km * 1 km. The information exists in each raster dataset.

3 Methodology

The site optimization of this research is a two-phase optimization. The first phase (Spatial trend optimization): establish a regression relationship between multiple target variables based on UCK trend modeling, and use the weighted average (WA) regression kriging variance of the three variables as the objective function. The spatial simulated annealing algorithm obtains the distribution of stations. The second phase (combine objective optimization): a multi-objective solution function for WA, joint information entropy ratio, and information redundancy is established through information entropy theory. The multi-objective function selects and adjusts the stations added in the first step to obtain the final station distribution. The main optimization process is shown in Fig. 4.

3.1 Trend Modeling

The optimization objectives of this study are three target variables: soil moisture, precipitation, and soil temperature. A multiple linear regression model establishes the relationship between the target variable and environmental covariates and simulates the target variable's spatial trend. As shown in Fig. 4 (matrix table of correlation between each other), it can be seen from the correlation matrix that elevation has a correlation with surface temperature, precipitation, and soil moisture, especially a strong correlation with surface temperature and precipitation. The slope also correlates with the target variable, indicating that the method of predicting the target variable employing environmental covariates is reliable. There is also a strong correlation between surface temperature and precipitation ($r = 0.72$). There is a weak correlation between soil moisture and surface temperature ($r = 0.24$). The surface temperature and latitude and longitude also have a strong correlation. Regression models of target variables are established from environment variables with strong correlations.

We used stepwise regression to model the multivariate linear model, and the Akaike information criterion (AIC) to filter the corresponding explanatory variables of the respective target variables. It can be seen from stepwise regression modeling that surface temperature has a regression relationship with longitude, latitude, elevation, and slope. In contrast, precipitation has a regression relationship with longitude,

Fig. 4 The main optimization steps of the study

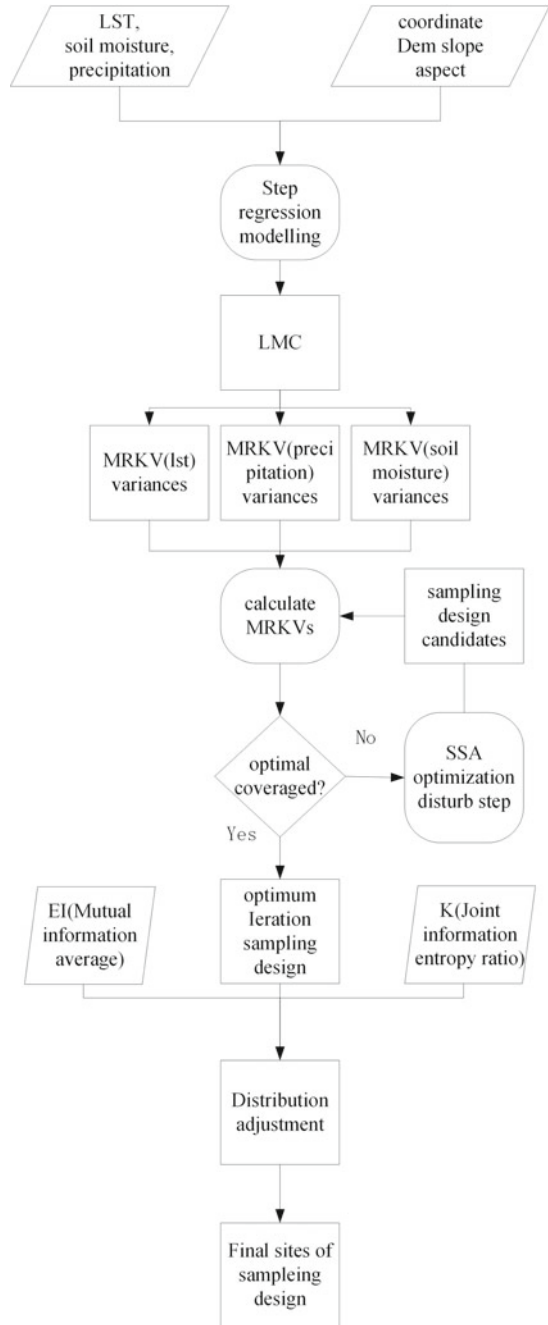


Table 1 Trend parameters of object variances

Variable	Trend variances
LST	Longitude, latitude, slope, aspect, elevation, b
Precipitation	Longitude, latitude, aspect, elevation, b
Soil moisture (TWI)	Longitude, latitude, slope, elevation, b

Note b = intercept

Table 2 Shapes and parameters of the LMC fitted to experimental variograms

Variable	Shape	Psill	Nugget	Sill	Nugget to sill ratio (%)	Range (m)
LST	Spherical	4.4146	6.7062	11.1208	60.30%	300,000
Precipitation	Spherical	28.3865	0.5291	28.9156	18.30%	300,000
Soil moisture	Spherical	0.4041	3.8253	4.2294	90.45%	300,000

latitude, elevation, and slope, and soil moisture has a regression relationship with longitude, latitude, slope, elevation, and aspect.

There are spatial differences between multiple target variables, and a single variogram fitting separately becomes unsuitable. It is not simple to use cross-variation function and self-variation function to describe the geostatistical covariates of multiple target variables. We can fit a LMC model to meet the constraints of various constraints. The R language *gstat* package [46] is used to fit the semi-variogram according to the Linear Model of Coregionalization (LMC) modeling. LMC uses the same variograms to describe the spatial dependence of LST, precipitation and soil moisture. LMC parameters are listed in Tables 1 and 2 (Fig. 5).

3.2 Optimize the Target

In this chapter, mean regression kriging variance (MRKV) is used as the target function of a single target variable. The final objective function WA is defined as the weighted average of multiple MRKVs.

3.2.1 Univariate Prediction

In this section, single target variable in UCK model is defined as:

$$Z(s) = \sum_{j=0}^m \beta_j \chi_j(s) + \xi(s) \tag{1}$$

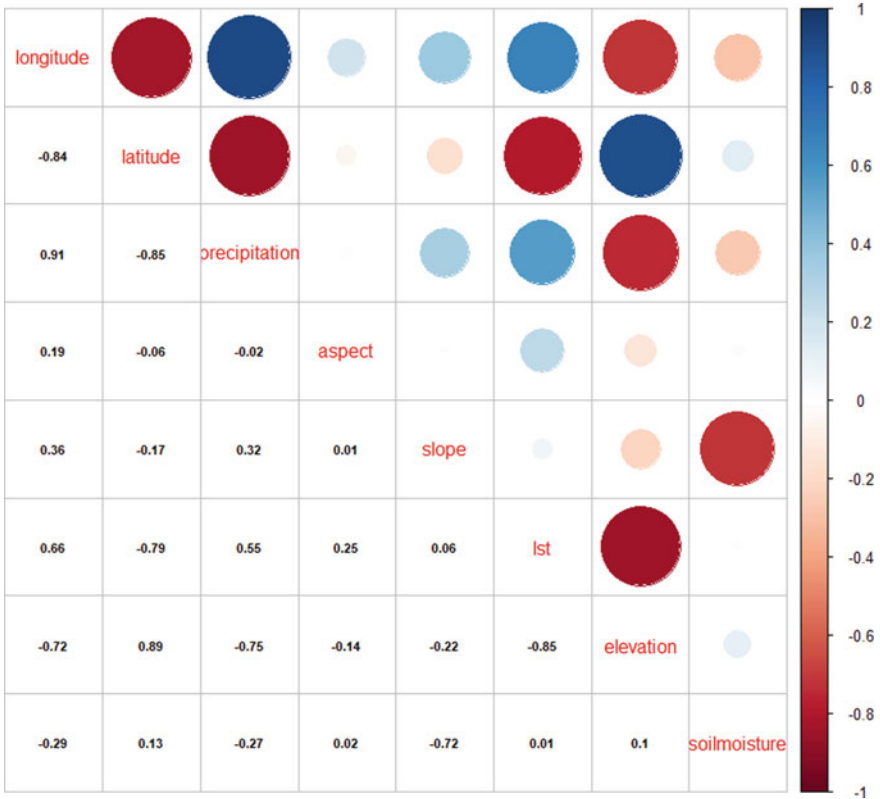


Fig. 5 Correlation coefficient matrix of object variances (LST, precipitation, soil moisture) and covariate data (longitude, latitude, aspect, slope, elevation)

Z(s) is the target environmental variable, here is precipitation, soil humidity or surface temperature, $\chi(s)$ is m environmental covariates (such as elevation, slope, aspect, etc.), $s = (x, y)$ means Two-dimensional space coordinates, β is the regression coefficient to be estimated, and $\xi(s)$ is the residual term after the regression of the target variable and the oblique variable, which obeys a normal distribution with a mean of 0. The spatial autocorrelation of $\xi(s)$ can thus be quantitatively expressed by the covariance function or the variogram. Written in matrix form:

$$Z(s) = x'(s)\beta + \xi(s) \tag{2}$$

where x and β are column vectors of m + 1 covariates and m + 1 regression coefficients, respectively. Which is expressed as:

$$z^{\wedge}(s_0) = m^{\wedge}(s_0) + e^{\wedge}(s_0) = \sum_{k=0}^p \beta^{\wedge}_k \cdot q_k(s_0) + \sum_{i=1}^n \lambda_i \cdot e(s_i) \tag{3}$$

$m^\wedge(s_0)$ is the drift value of the fitting, $e^\wedge(s_0)$ is the inserted residual, β^\wedge_k is the regression coefficient of multiple linear regression, which is divided into (OLS) β^\wedge_{OLS} and (GLS) β^\wedge_{GLS} .

From the multiple linear regression of ordinary least squares (OLS), the regression coefficient β^\wedge_{OLS} is:

$$\beta^\wedge_{OLS} = (q^T \cdot q)^{-1} \cdot q^T \cdot Z(s) \tag{4}$$

However, in geographic statistics, multiple linear regression using generalized least squares (GLS) is more reliable than the ordinary least squares regression. Then the regression coefficient β^\wedge_{GLS} is:

$$\beta^\wedge_{GLS} = (X'CX)^{-1} X' CZ(s) \tag{5}$$

C is the covariance matrix of $n \times n$ residuals. X is the predictor matrix of $n \times (m + 1)$ as the sampling position.

Thus, the best linear unbiased estimation (BLUE) value at any point can be obtained. The general kriging prediction of the unobserved position s_0 from n observations $Z(s_i)$ is given by:

$$z^\wedge(s_0) = x_0 \cdot \beta^\wedge_{GLS} + \lambda_0^T \cdot (z - x \cdot \beta^\wedge_{GLS}) \tag{6}$$

Formula (6) has two parts, the first half is the vector of the trend item or regression term x_0^T is the value of the covariate at the point to be estimated, and the residual item in the second half is the covariance established by OLS. The function is inversely solved. λ_0^T is $(Cov(Z(s_0), Z(s_1)), \dots, Cov(Z(s_0), Z(s_n)))$ which is the vector of kriging weights. Bring β^\wedge_{GLS} in (5) into formula (6).

$$\begin{aligned} \sigma_{RK}^2(s_0) &= (C_0 + C_1) - c_0^T \cdot C^{-1} \cdot c_0(x_0 - X^T \cdot C^{-1} \cdot x_0)^T \\ &\cdot (X^T + C^{-1} \cdot X)^{-1} \cdot (x_0 - X^T \cdot C^{-1} \cdot c_0) \end{aligned} \tag{7}$$

For regression kriging, the variance consists of two parts: the variance of the residual prediction error, and the other is the variance of the estimated error of the trend term. $(C_0 + C_1) = c(0) = Var(Z(s_0))$ is the sill value (sill = Nugget + Partial sill), x_0 is the vector [14] formed by the covariance between the sample point and the point to be estimated 2007. C and c_0 can be obtained from the variation diagram of the residual.

3.2.2 Multivariable Prediction

Multivariate prediction includes the joint prediction of multiple spatial and covariate related variables. For n variances, Let $\{Z_i(s), X_i, \beta_i, \varepsilon_i, x_i(s_0), c_i, C_i\}$ equivalent to

$\{Z(s), X, \beta, \varepsilon, x(s_0), c, C\}$. So that the i variance is let $Z(s) = (Z_1(s)', \dots, Z_n(s)')$, $\beta(s) = (\beta^1', \dots, \beta^n')$, $\varepsilon(s) = (\varepsilon_1(s)', \dots, \varepsilon_n(s)')$.

It can be seen from formula (7) that the variance of regression kriging is irrelevant with the predicted value but is only related to the geographic location of the sample, environmental covariates, and the variance function of the residual. This makes it possible to calculate the average regression Kriging variance of the points to be estimated in the study area before the data is collected at the Iwamoto point. The minimum variance of mean regression kriging is used as the objective function of optimization. The variograms and cross-variation function fitted by LMC are shown in Fig. 6 and Table 2.

Optimizing a single objective in geographic space often uses an optimization criterion of mean regression kriging variance (MRKV) minimization [15, 47, 48]. The prediction error variance depends tightly on the sampling location, and the known environmental variables can be exhausted through the variance–covariance matrix.

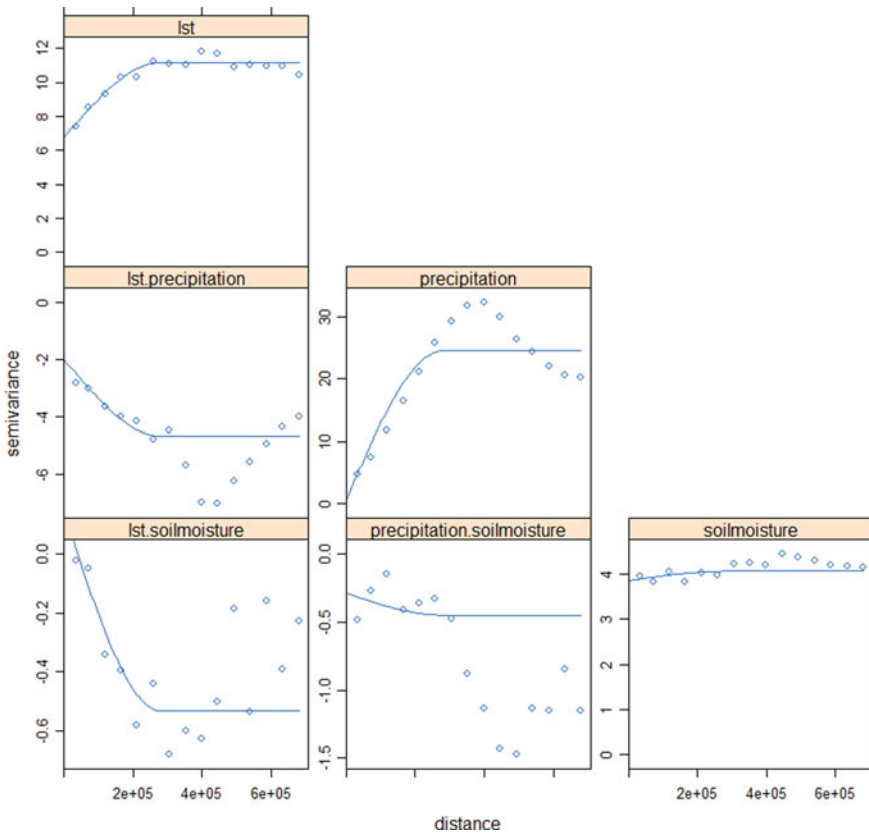


Fig. 6 Direct variograms (diagonal) and cross-variograms (off-diagonal) for LST, precipitation and soil moisture variables fitted with LMC

The observed value of the target variable is used to calculate the prediction error variance, which allows the error variance to be estimated before the observations are collected. Therefore, for optimizing the three target variables LST, precipitation, and soil moisture, the optimization criterion can be selected as the weighted average of the MKV values of the three target variables.

$$WA = \frac{M_1}{S_1} * w_1 + \frac{M_2}{S_2} * w_2 + \frac{M_3}{S_3} * w_3 \quad (8)$$

WA is the weighted sum of three single goals. M_i are the MRKV values of the three target variables, and S_i are the sill values of the corresponding variograms of the target variables. M/S can unify the three target variables into a quantified scale [17]. w_i is the weight, and we set three target variables here to be equally important. The calculation of WA is based on the *intamapInteractive* package (a package of R language), and the target variable function script is redefined based on its code to meet the needs of this research.

3.3 Sampling Method

The current sampling methods are mainly based on probability sampling, geometry-based sampling, and model-based sampling. Model-based sampling methods are usually more effective when the target variable has a significant spatial structure. In this study, the three target variables have obvious spatial structure. We use a universal cokriging (UCK) model to optimize the sampling of multi-objective variables. Experiments in the Babao River Basin show that the UCK model is significantly better than simple random sampling model (SRS) and simple coverage sampling model (SCS) [6]. The sampling based on geostatistical models is usually the best sample. The mean regression kriging variance (MRKV) of the sample is required to be minimum. The best linear unbiased estimator (BLUE) can use the zoom method to convert the observation value of a certain index of WSN to a grid format covering the entire watershed. Inverse distance weighting (IDW) is used when there is auxiliary data, and Kriging is better when there is no auxiliary data. Ecological hydrological wireless sensor network (EHWSN), highly non-average data, must introduce related auxiliary data.

To determine the appropriate number of sites, it is necessary to obtain the relationship between the number of sites and the corresponding minimum standard. According to the corresponding analysis, as the number of stations increases, the WA value will decrease, but when a certain value is reached, the WA value will no longer change significantly. This inflection point value is regarded as the appropriate number of stations.

3.4 Optimization Algorithm

A brief introduction to the spatial simulated annealing algorithm will be given below. For a more detailed description, please refer to [47, 48]. (1) Initialization of control parameters, sampling correlation coefficient; (2) Determine the auxiliary grid required for the objective function; (3) Calculate the initial objective function value according to the weighted objective function value, and regard it as the current optimal solution; (4) Randomly select a sample point and move it in a random direction between lhl and max . When the objective function value obtained after moving a point is less than or equal to the minimum objective function value encountered initially, then this disturbance is accepted as The new initial value. And record the optimal objective function value at this time, and the coordinate value of each point at this time. Otherwise, accept it as the new initial position with a certain probability. Repeat the disturbance process. (5) The optimal solution obtained at this time is closest to the optimal solution of the objective function.

Several parameters need to be defined for simulated annealing, such as the initial annealing temperature, the maximum number of iterations, the average probability of accepting the deteriorating design, and the maximum allowable number is 200 of Markov chains. The stopping criterion of the optimization process is a key parameter to avoid excessive optimization time.

$$P(D_i \rightarrow D_{i+1}) = \begin{cases} 1, & \text{if } \Phi(D_{i+1}) \leq \Phi(D_i) \\ \exp\left(\frac{\Phi(D_i) - \Phi(D_{i+1})}{c}\right), & \text{if } \Phi(D_{i+1}) > \Phi(D_i) \end{cases} \quad (9)$$

where D_i and D_{i+1} are the previous and the new combination, c is the positive control parameter (so-called “system temperature”, which is lowered as optimization progresses) and $\Phi(\cdot)$ is the quality measure (objective function).

3.5 Entropy

In ecological site monitoring, each site can be regarded as an information source, and the information volume of LST, precipitation and soil moisture contained in each site can be represented by information entropy $H(X)$. Divide into s groups according to the observation sequence, count the number of each group, p_i is the probability of each group [11, 12, 49, 50].

$$H(X) = \sum_{i=1}^s p_i \log_2 \frac{1}{p_i} \quad (10)$$

When there are N sites (X_1, X_2, \dots, X_n) in the monitoring network, the total amount of information contained in the sites can be combined by information

entropy $H(X_1, X_2, \dots, X_n)$, $p_1 \dots p_n$ represents variables (X_1, X_2, \dots, X_n) joint probability density function.

$$H(X_1, X_2, \dots, X_n) = - \sum_{i_1=1}^{N_1} \sum_{i_2=1}^{N_2} \dots \sum_{i_n=1}^{N_n} p_{i_1} \dots p_{i_n} \log[p_{i_1} \dots p_{i_n}] \quad (11)$$

The redundancy information (also called mutual information) between two sites can be expressed by $I(X; Y)$, where $H(X)$ and $H(Y)$ are X and Y respectively. The information entropy of each site, $H(X; Y)$ is the joint information entropy between X and Y .

$$I(X; Y) = H(X) + H(Y) - H(X; Y) \quad (12)$$

3.6 Distribution Adjustment

The precipitation, surface temperature, and soil moisture of each site are taken as observations of random variables, and the information entropy $H(x_i)$ of each observation is calculated, and the point with the largest information entropy is taken as the first point x_1 of the site selection. The remaining $(n - 1)$ sites take the point x_i with the smallest mutual information with x_1 as the second site x_2 , and so on, select the remaining sites to determine the order of all sites.

$$F(X) = \begin{cases} F_1(x) = WA \\ F_2(x) = K = \frac{H(x_1, x_2, \dots, x_m)}{H(x_1, x_2, \dots, x_m, \dots, x_n)} \\ F_3(x) = EI = \frac{\sum_{i=1}^{n-1} \sum_{j=i+1}^n I(x_i, x_j)}{c_n^2} \end{cases} \quad (13)$$

$F_1(x)$ is the WA value optimized in the first step, and $F_2(x)$ is the current m sites to the joint information entropy of all n sites. $F_3(x)$ is the average value of the mutual information between the two stations, which represents the amount of information redundancy between the stations, or the degree of information redundancy. The larger the value, the greater the degree of redundancy.

For the multi-objective solution, the ideal point method is used. Calculate the sum of square deviations $S(x)$ between the general point and the ideal solution. The formula of the ideal point method is as follows:

$$S(x) = \sqrt{\sum_{i=1}^3 [F_i(x) - F_i^*]^2} \quad (14)$$

WA is the weighted mean regression kriging variance after the first step optimization, reflecting the site's coverage. K is the current ratio of joint information entropy of m sites to n sites. K reflects the current total size of information. If K is too small, the selected site combination cannot fully reflect the information of all sites, such as surface temperature, precipitation, and soil moisture. If K is too large, it means that the selected site combination has enough information. This may cause information redundancy. EI is the average value of mutual information between two sites, indicating the degree of information overlap between sites or information redundancy. The larger the value, the greater the information redundancy.

4 Results and Discussion

4.1 Number of Optimization Sites

Based on the original existing 31 sites, the sites in the study area are encrypted. Based on the objective function of WA, as we add more stations, the value of the objective function will become smaller. But based on economy and reality, we need to determine a more appropriate number of sites. As shown in Fig. 7, when the number of stations keeps increasing, the value of WA will gradually become smaller. When the number of stations is 81, the value of WA will no longer decrease significantly but become stable. Therefore, 81 is determined as the most suitable number of stations in the study area.

4.2 Spatial Trend Optimization

50 new sites are optimized through SSA algorithm, and the final value of WA is 0.37428. The optimized site's location was then obtained. In Fig. 8a, Black points represent the original site locations, and Green points represent the 50 new site locations. As shown in Fig. 9, the sample distributions of LST, precipitation, soil moisture, DEM, slope and aspect of the 50 newly added stations are basically consistent with the overall distribution of the entire study area. It shows that the 50 newly added sites are very representative.

Only the main slope, aspect, elevation, latitude, and longitude were used as environmental covariates when building the UCK model. The three target variables LST, precipitation, and soil moisture are not affected by these factors, and each will also be affected by other factors. For example, soil moisture is also closely related to vegetation coverage and the transpiration rate. Some factors have no obvious spatial sub-correlation in space, which results in a larger nugget and the ratio of the nugget to the sill of the corresponding variogram (Fig. 6).

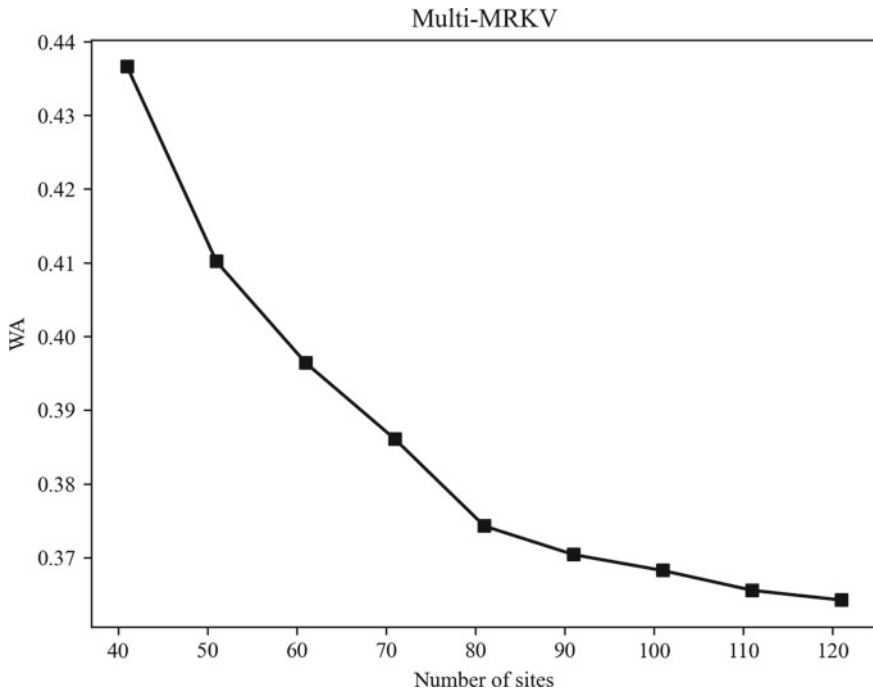


Fig. 7 WA values under different numbers of sites (the number of test intervals is 5)

4.3 Combine Objective Optimization Result

Sort the added 50 sites according to the site ranking rules. Site order and each step MRKV, K and EI are shown in Table 3. Perform site network evaluation based on the MRKV, K and EI values of the three objective functions of the combination of different sites. The resulting line chart is shown in Fig. 10a. The WA value will begin to decrease rapidly with the increase of site data, decreasing steadily. Both K and EI increase with the increase of sites.

Figure 10a shows that after the number of stations is 45, the values of WA, EI and K tend to be stable. Figure 10b also shows that the value of the objective function also tends to be stable, so choose 45–50 to form the Pareto solution set. In the composed Pareto solution set, K reached 98% of the information at 46. It has been able to obtain most of the information. The EI value will become larger and larger, so 46 is selected as the final number of sites. After removing the redundant four sites, the new site distribution is shown in Fig. 8b.

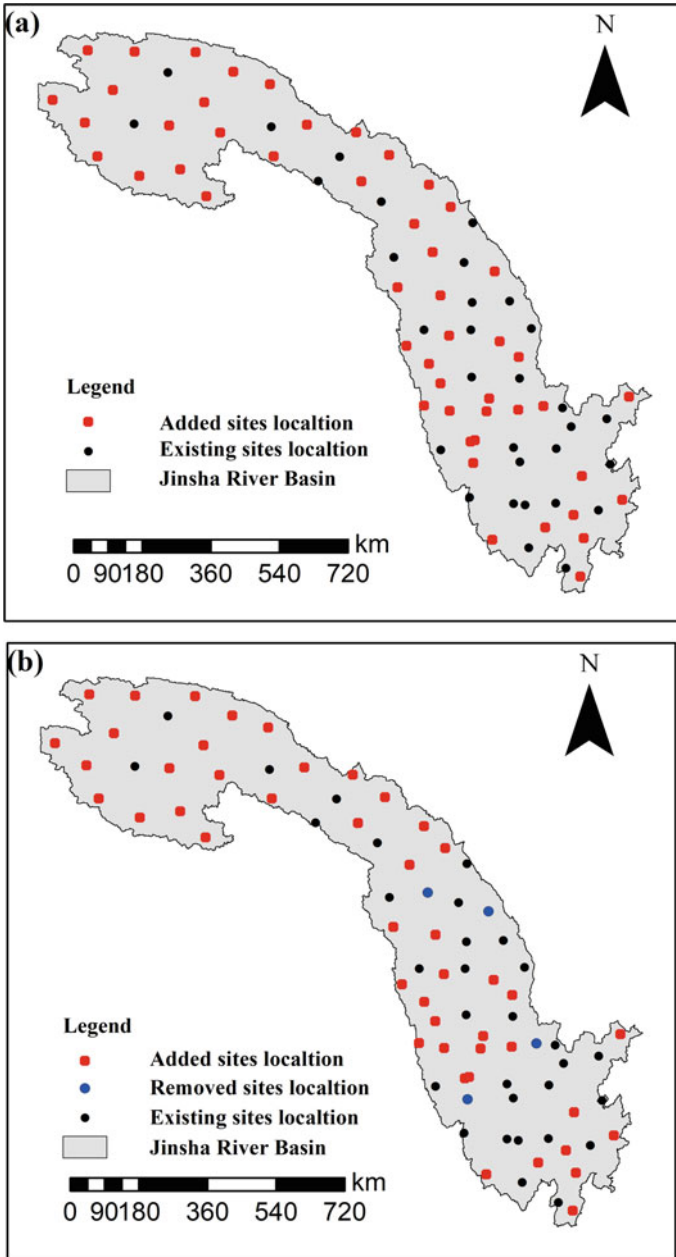


Fig. 8 **a** Spatial trend optimization: distribution of Jinsha River Basin's existing sites location and added sites location (color of black is existing sites (31) and color of red is added sites (50)). **b** Combine objective optimization: distribution of Jinsha River Basin's existing sites location, added sites location and removed sites location (color of black is existing sites (31), color of red is added sites (46) and color of blue is removed redundant sites(4))

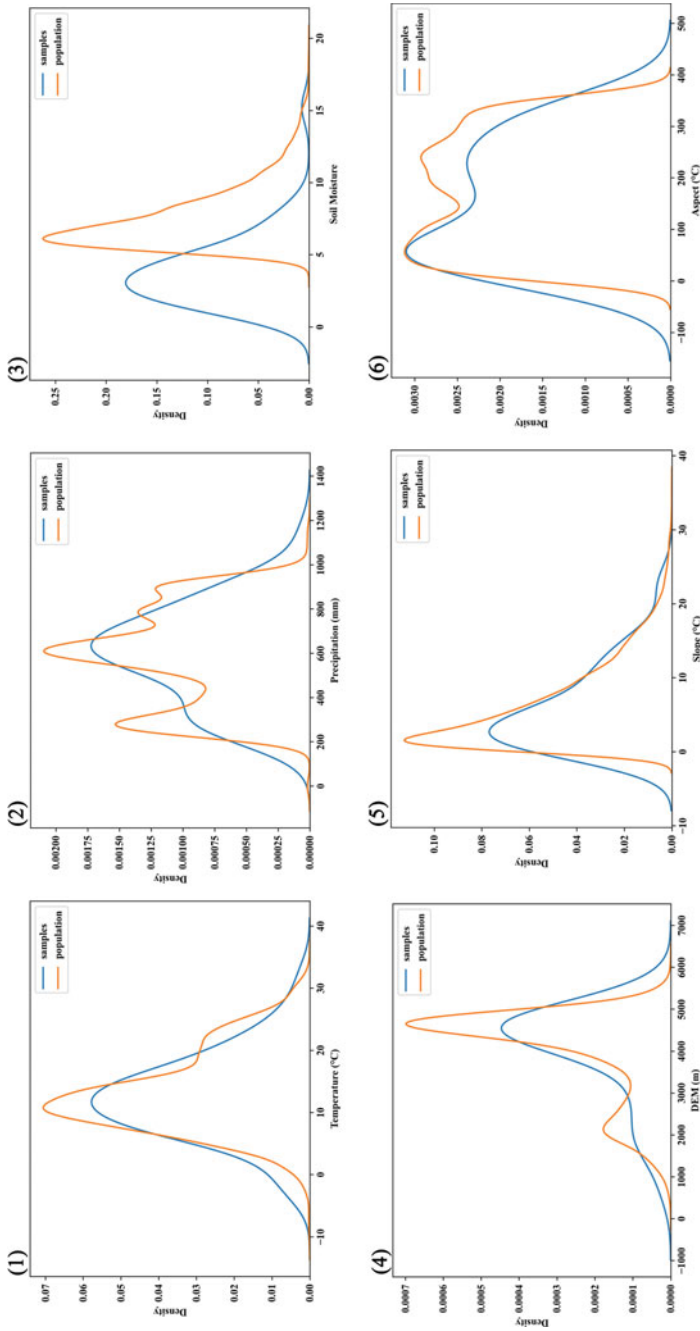


Fig. 9 Comparison of optimized sample attributes density distribution and corresponding population density distribution. (1) LST, (2) precipitation, (3) soil moisture, (4) DEM, (5) slope, (6) aspect

Table 3 Computed result for site order per step of WA, EI and K

Number of sites	Site number	WA	K	EI
1	45	–	0.052	–
2	43	1.15E+16	0.1781	9.28E–07
3	19	5.44E+13	0.2823	7.04E–05
4	1	5.97E+13	0.3562	0.000117
5	15	2.16E+12	0.4135	0.000161
6	14	29.12965	0.4604	0.000207
7	29	8.167191	0.5	0.000254
8	9	4.506026	0.5343	0.000342
9	4	4.068209	0.5646	0.000413
10	25	2.56216	0.5916	0.000531
11	50	2.264591	0.6161	0.00067
12	10	2.175304	0.6385	0.000761
13	11	1.978275	0.6591	0.000847
14	39	1.442543	0.6781	0.000974
15	6	1.363774	0.6958	0.00105
16	27	1.255115	0.7124	0.001131
17	30	1.216104	0.728	0.001208
18	49	1.151726	0.7427	0.001903
19	32	1.134644	0.7566	0.002139
20	5	1.095794	0.7698	0.002459
21	16	0.989437	0.7823	0.003547
22	41	0.925549	0.7942	0.004858
23	18	0.875266	0.8057	0.005945
24	12	0.784524 ara>	0.8166	0.006298
25	33	0.773647	0.8271	0.00739
26	48	0.722451	0.8372	0.007767
27	38	0.699694	0.8469	0.008805
28	28	0.672949	0.8562	0.009402
29	17	0.656272	0.8652	0.009852
30	3	0.640008	0.8739	0.010354
31	37	0.621514	0.8824	0.01089
32	7	0.61631	0.8905	0.011595
33	47	0.607413	0.8984	0.012305
34	20	0.591428	0.9061	0.012776
35	36	0.581399	0.9135	0.01344
36	8	0.574167	0.9208	0.013938

(continued)

Table 3 (continued)

Number of sites	Site number	WA	K	EI
37	31	0.565574	0.9278	0.014358
38	23	0.560299	0.9347	0.014827
39	26	0.54557	0.9413	0.015246
40	40	0.543173	0.9479	0.015878
41	35	0.538307	0.9542	0.016296
42	46	0.533193	0.9604	0.016754
43	22	0.528777	0.9664	0.017209
44	34	0.524761	0.9723	0.017735
45	44	0.518171	0.9781	0.018781
46	2	0.512587	0.9838	0.019214
47	21	0.503627	0.9893	0.020214
48	13	0.498755	0.9947	0.020671
49	42	0.495222	1	0.021177
50	24	0.490566	1	0.023039

4.4 Sampling Comparison of SRS, SCS and UCK

Figure 11 shows that the WA value of the UCK-based sampling mode is less than the WA value of SRS and SCS in most cases. This shows that the sampling method of UCK-based trend modeling in the Jinsha River Basin is significantly better than the sampling methods of SRS and SCS, and its sample points can better represent the spatial characteristics of the study area.

4.5 Discussion

The Jinsha River basin's LST, precipitation, and soil moisture have different spatial distribution patterns. Precipitation and LST have a relatively obvious continuous spatial distribution, and their spatial distribution is closely related to elevation (Figs. 2 and 3). The soil moisture does not have strong spatial continuity in space (Fig. 3). The proportion of soil moisture nugget to sill ratio value is as high as 90.45%, showing that its spatial autocorrelation is not strong. The LST nugget accounts for 60.30% of the sill value, indicating that the LST has a moderate spatial autocorrelation in this area. The precipitation has a strong spatial autocorrelation due to 18.30% of the nugget to sill ratio. In this study, the contribution of LST, precipitation and soil moisture to the WA value was 39.7%, 12.2%, and 48.1%, respectively. This shows that the spatial changes of soil moisture and surface temperature greatly affect the spatial distribution of the site.

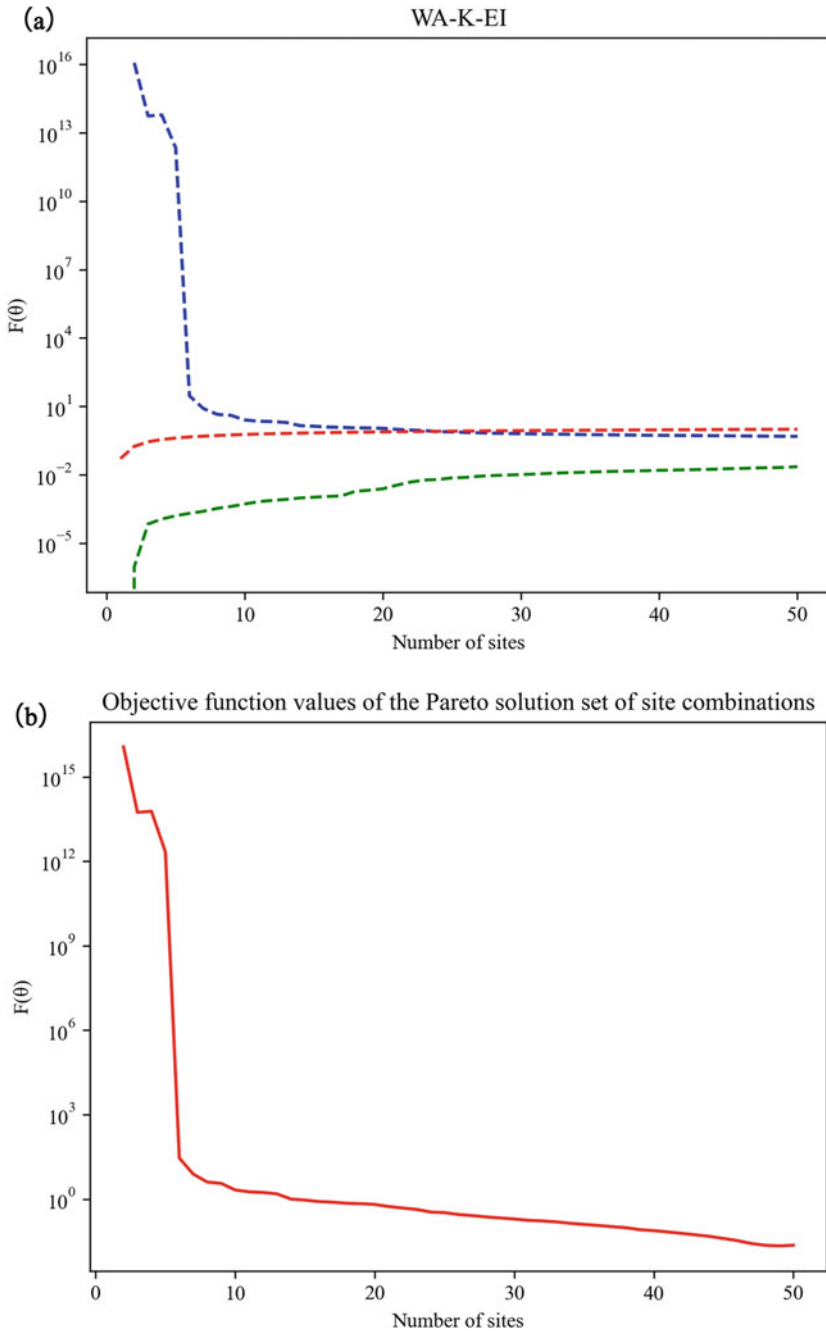


Fig. 10 **a** The relationship of WA, K (joint entropy ratio), EI (average mutual information) and the number of sites. **b** Objective function values of the Pareto solution set of site combinations

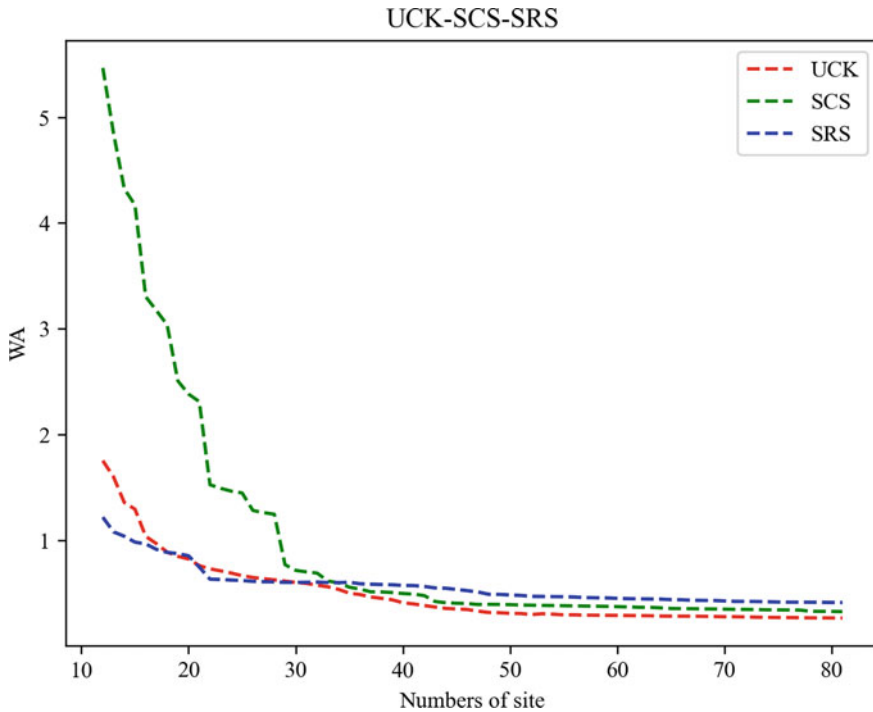


Fig. 11 Comparison of WA values of SRS, SCS and UCK sampling methods

In the upper reaches of the Jinsha River Basin, the terrain is not very undulating, and the precipitation and LST are relatively evenly distributed. Therefore, when there are fewer existing sites, the distribution of add sites tends to be regular. In the downstream area, there are many existing sites. After adding new sites, the probability of site information redundancy is greater, so the four removed sites are all in the downstream area.

This research is based on spatial research and does not consider the time factor. In addition to the influence of spatial factors such as topography, latitude, and longitude, and slope aspect, soil moisture, precipitation, and the land surface temperature will also have obvious time differences. This study selected only the data of soil moisture, precipitation, and surface temperature in a single year, without considering the temporal and spatial variability of the target variables in long-term years.

The soil moisture data is replaced by TWI (topographic wetness index), but in actual operation, using TWI data instead of soil moisture data has some obvious disadvantages. For some of the more vulgar areas, its uniqueness cannot be well displayed. Due to spatial resolution constraints, soil moisture data with a resolution of 0.25° is not directly used. Besides, the soil moisture data is divided into multiple monitoring levels in monitoring, such as 0–10 cm, 10–20 cm, etc. In addition, other

factors such as transpiration, vegetation coverage, precipitation, etc. These error factors will directly lead to the fitting of the LMC trend.

5 Conclusions

The research results of this article show that the site layout of the newly-added multi-target wireless monitoring network in the river basin can be more evenly distributed in the study area. Through UCK-based trend modeling, the layout optimization of new sites with multiple goals is established. The spatial trend is determined by multiple linear regression, and the variance map and the cross variance map of the calculated residuals are obtained, and the LMC method is used for fitting prediction. The first phase uses the weighted MRKV value of multiple targets as the objective function and uses the spatial simulated annealing algorithm SSA to optimize the sampling. In the second phase, the optimization results of the previous step and other factors (roads, costs) are normalized to an objective function using the idea of Pareto, and the final sample sampling is obtained by obtaining the minimum objective function value.

Through the two-phase optimization process, it is possible to consider the balance of spatial heterogeneity of multiple targets and consider the economic benefits of multiple cost factors. The final site distribution is significantly better than the ordinary sampling optimization distribution. The spatial trend distribution can be highly correlated with the study area, and some optimizations have been made in terms of site redundancy.

Recommendations

- Establish a multi-object real-time wireless monitoring network in the Jinsha River Basin.
- Combine more new multi-objective algorithms to optimize the ecological environment multi-objective sites.

References

1. Njue N, Stenfert Kroese J, Gräf J, Jacobs SR, Weeser B, Breuer L, Rufino MC (2019) Citizen science in hydrological monitoring and ecosystem services management: state of the art and future prospects. *Sci Total Environ* 693:133531
2. Brierley G, Reid H, Fryirs K, Trahan N (2010) What are we monitoring and why? Using geomorphic principles to frame eco-hydrological assessments of river condition. *Sci Total Environ* 408:2025–2033
3. Rodero C, Olmedo E, Bardají R, Píera J (2021) New radiometric approaches to compute underwater irradiances: potential applications for high-resolution and citizen science-based water quality monitoring programs. *Sensors* 21:5537

4. Fryirs K, Hancock F, Healey M, Mould S, Dobbs L, Riches M, Raine A, Brierley G (2021) Things we can do now that we could not do before: developing and using a cross-scalar, state-wide database to support geomorphologically-informed river management. *PLOS ONE* 16
5. Turner DP, Ritts WD, Cohen WB, Gower ST, Running SW, Zhao M, Costa MH, Kirschbaum AA, Ham JM, Saleska SR (2006) Evaluation of MODIS NPP and GPP products across multiple biomes. *Remote Sens Environ* 102:282–292
6. Ge Y, Wang JH, Heuvelink GBM, Jin R, Li X, Wang JF (2015) Sampling design optimization of a wireless sensor network for monitoring ecohydrological processes in the Babao River basin, China. *Int J Geogr Inf Sci* 29:92–110
7. Ayadi A, Ghorbel O, BenSalah MS, Abid M (2020) Spatio-temporal correlations for damages identification and localization in water pipeline systems based on WSNs. *Comput Netw* 171:107134
8. Lark RM, Papritz A (2003) Fitting a linear model of coregionalization for soil properties using simulated annealing. *Geoderma* 115:245–260
9. Hosseini M, Kerachian R (2017) A data fusion-based methodology for optimal redesign of groundwater monitoring networks. *J Hydrol* 552:267–282
10. Maymandi N, Kerachian R, Nikoo MR (2018) Optimal spatio-temporal design of water quality monitoring networks for reservoirs: application of the concept of value of information. *J Hydrol* 558:328–340
11. Alfonso L, Lobbrecht A, Price R (2010) Optimization of water level monitoring network in polder systems using information theory. *Water Resour Res* 46
12. Vigneaux JP (2019) Topology of statistical systems: a cohomological approach to information theory. *Université Sorbonne Paris Cité*
13. Wang W, Wang D, Singh VP et al (2020) Information theory-based multi-objective design of rainfall network for streamflow simulation. *Adv Water Resour* 135:103476
14. Li H, Wang D, Singh VP et al (2020) Developing a dual entropy-transinformation criterion for hydrometric network optimization based on information theory and copulas. *Environ Res* 180:108813
15. Brus DJ, Heuvelink GBM (2007) Optimization of sample patterns for universal kriging of environmental variables. *Geoderma* 138:86–95
16. Hengl T, Heuvelink GBM, Rossiter DG (2007) About regression-kriging: from equations to case studies. *Comput Geosci* 33:1301–1315
17. Vašát R, Heuvelink GBM, Borůvka L (2010) Sampling design optimization for multivariate soil mapping. *Geoderma* 155:147–153
18. Lark RM (2016) Multi-objective optimization of spatial sampling. *Spat Stat* 18:412–430
19. van Groenigen JW, Siderius W, Stein A (1999) Constrained optimisation of soil sampling for minimisation of the kriging variance
20. Kirkpatrick S, Gelatt CD, Vecchi MP (1983) Optimization by simulated annealing. *Science* 220:671–680
21. Whitley D (1994) A genetic algorithm tutorial. *Stat Comput* 4:65–85
22. Israeli A, Emmerich M, Iggy Litaor M, Shir OM (2019) Statistical learning in soil sampling design aided by pareto optimization. In: Genetic and evolutionary computation conference
23. Kennedy J, Eberhart RC (1997) A discrete binary version of the particle swarm algorithm. In: 1997 IEEE International conference on systems, man, and cybernetics. Computational cybernetics and simulation. IEEE, pp 4104–4108
24. Cunha M, Marques J (2020) A new multiobjective simulated annealing algorithm—MOSA-GR: application to the optimal design of water distribution networks. *Water Resour Res* 56(3):e2019WR025852
25. Bandyopadhyay S, Saha S, Maulik U, Deb K (2008) A simulated annealing-based multiobjective optimization algorithm: AMOSA. *IEEE Trans Evol Comput* 12:269–283
26. Li H, Zhang Q (2008) Multiobjective optimization problems with complicated Pareto sets, MOEA/D and NSGA-II. *IEEE Trans Evolut Comput* 13:284–302

27. Li X, Parrott L (2016) An improved genetic algorithm for spatial optimization of multi-objective and multi-site land use allocation. *Comput Environ Urban Syst* 59:184–194
28. Zhang Y, Wang G-G, Li K, Yeh W-C, Jian M, Dong J (2020) Enhancing MOEA/D with information feedback models for large-scale many-objective optimization. *Inf Sci*
29. Li X, Gao B, Bai Z, Pan Y, Gao Y (2020) An improved parallelized multi-objective optimization method for complex geographical spatial sampling: AMOSA-II. *ISPRS Int J Geo Inf* 9:236
30. Ngatchou P, Zarei A, El-Sharkawi A (2005) Pareto multi objective optimization. In: *Proceedings of the 13th international conference on intelligent systems application to power systems*, pp 84–91
31. Marler RT, Arora JS (2010) The weighted sum method for multi-objective optimization: new insights. *Struct Multidiscip Optim* 41:853–862
32. Tavakoli-Someh S, Rezvani MH (2019) Multi-objective virtual network function placement using NSGA-II meta-heuristic approach. *J Supercomput* 75:6451–6487
33. Saadatpour M, Afshar A, Khoshkam H (2019) Multi-objective multi-pollutant waste load allocation model for rivers using coupled archived simulated annealing algorithm with QUAL2Kw. *J Hydroinf* 21:397–410
34. Pang J, Zhou H, Tsai Y-C, Chou F-D (2018) A scatter simulated annealing algorithm for the bi-objective scheduling problem for the wet station of semiconductor manufacturing. *Comput Ind Eng* 123:54–66
35. Wang GX, Zeng XF, Zhao N, He QF, Bai YR, Zhang RY (2018) Potential relationships between the river discharge and the precipitation in the Jinsha River basin, China. In: *International conference on energy engineering and environmental protection*
36. Chao N, Chen G, Li J, Xiang L, Wang Z, Tian K (2020) Groundwater storage change in the Jinsha River basin from GRACE, hydrologic models, and in situ data. *Groundwater* 58:735–748
37. Winchell M, Srinivasan R, Di Luzio M, Arnold J (2007) ArcSWAT interface for SWAT2005 user's guide. USDA Agricultural Research Service and Texas A&M Blackland Research Center, Temple, Texas
38. Fick SE, Hijmans RJ (2017) WorldClim 2: new 1-km spatial resolution climate surfaces for global land areas. *Int J Climatol* 37:4302–4315
39. Duan S-B, Li Z-L, Tang B-H, Wu H, Tang R (2014) Generation of a time-consistent land surface temperature product from MODIS data. *Remote Sens Environ* 140:339–349
40. Lu L, Zhou XM (2021) A four-parameter model for estimating diurnal temperature cycle from MODIS land surface temperature product. *J Geophys Res* 126
41. Wan Z, Zhang Y, Zhang Q, Li Z-L (2004) Quality assessment and validation of the MODIS global land surface temperature. *Int J Remote Sens* 25:261–274
42. Sorensen R, Zinko U, Seibert J (2006) On the calculation of the topographic wetness index: evaluation of different methods based on field observations. *Hydrol Earth Syst Sci* 10:101–112
43. Yıldırım Ü (2021) Identification of groundwater potential zones using GIS and multi-criteria decision-making techniques: a case study Upper Coruh River Basin (NE Turkey). *ISPRS Int J Geo Inf* 10:396
44. Kopecký M, Čížková Š (2010) Using topographic wetness index in vegetation ecology: does the algorithm matter? *Appl Veg Sci* 13:450–459
45. Kopecký M, Macek M, Wild J (2021) Topographic Wetness Index calculation guidelines based on measured soil moisture and plant species composition. *Sci Total Environ* 757:143785
46. Pebesma E (2004) Multivariable geostatistics in S: the gstat package. *Comput Geosci* 30:683–691
47. van Groenigen J-W (1999) Constrained optimisation of spatial sampling: a geostatistical approach (`[sn]`)
48. van Groenigen JW, Stein A (1998) Constrained optimization of spatial sampling using continuous simulated annealing. *J Environ Qual* 27:1078–1086
49. Bayat B, Nasserli M, Hosseini K, Karami H (2021) Nested augmentation of rainfall monitoring network: proposing a hybrid implementation of block kriging and entropy theory. *Water Resour Manag*

50. Zhou S, Wang Y, Li Z, Chang J, Guo A (2021) Quantifying the uncertainty interaction between the model input and structure on hydrological processes. *Water Resour Manag* 1–21

The Influence of Large Scales of Reservoir Construction in the Upper Yangtze River Basin on Regional Precipitation



Shuang Zhu, Jianan Wei, Jiang Li, Yuying Wang, and Siwen Cao

Abstract The interaction between human activities and climate change has made the global climate change trend to unstable in the past 10 years. Extreme floods and droughts have occurred frequently. Large-scale reservoir construction in the Chinese Upper Yangtze River Basin has huge flood control and beneficial benefits. However, its impact on regional ecological changes cannot be ignored for its contribution to the changes of land use types and destruction of the natural runoff rhythm. Therefore, the focus of this study is to explore the temporal and spatial trend of precipitation for the Upper Yangtze River Basin (UYRB) during 2001–2019 and the impact of reservoir construction in UYRB on precipitation changes for the first time. In order to better study the spatial feature of precipitation change, this study uses multi-satellite precipitation datasets as the research data. The estimation accuracy of IMERG and TMPA products was evaluated. Then the Mann–Kendall test, spatial analysis, and probability analysis were implemented to search the impact of reservoir construction on annual and monthly average precipitation changes and extreme daily precipitation. The results indicated that: (1) the monthly and annual precipitation in the Jialing River Basin showed an obvious upward trend, and the precipitation in the southern part of Jinsha River Basin showed a clear downward trend. These are places where reservoirs are densely built. (2) In the Reservoir Affected Area (RAA), the maximum daily precipitation shows an unstable trend, and its upward and downward trends are more obvious than that in the Non-Reservoir Affected Area (N-RAA). (3) The impact increased as the total storage capacity of the reservoir increased. It was found that

S. Zhu · J. Wei

School of Geography and Information Engineering, China University of Geosciences, Wuhan 430074, China

e-mail: zhushuang@cug.edu.cn

National Engineering Research Center of Geographic Information System, Wuhan 430074, China

J. Li (✉)

Information Center, Department of Natural Resources of Hubei Province, Wuhan 430074, China

e-mail: johnlee1124@126.com

Y. Wang · S. Cao

Wuhan Zhongdi Yunshen Technology Co., Ltd, Wuhan 430000, China

© The Author(s), under exclusive license to Springer Nature Switzerland AG 2022

A. M. F. Al-Quraishi et al. (eds.), *Environmental Degradation in Asia*,

Earth and Environmental Sciences Library,

https://doi.org/10.1007/978-3-031-12112-8_20

large-scale reservoir construction has a certain impact on the rising and falling trends of regional precipitation changes, and its impact is related to the total storage capacity, distribution density, and the time of operation of the reservoir.

Keywords IMERG · Extreme precipitation · Impact · Reservoir · Upper Yangtze River Basin

1 Introduction

Climate change has great effects on the ecological environment and agricultural production everywhere in the globe. It has led to increasing events of drought, floods, water scarcity, sea levels rising and crop failures [1–3], and most of these natural phenomes are directly or indirectly related to changes in precipitation pattern [4, 5]. The spatial–temporal evolution of precipitation becomes an important issue of climatological, meteorological and hydrological areas.

A variety of existing methods can be used for precipitation spatial–temporal evolution analysis, such as Mann–Kendall (MK) test, Theil–Sen analysis method (TSA), seasonal Kendall method and Modified MK test (MMK) [6–10]. Yacoub and Tayfur used rain gauge data to study the drought trend in Mauritania over a long time series and obtain historical drought intensity and drought frequency [11]. Toride used rain gauge data to study the historical precipitation trends in the Shasta Dam basin [12], and further analyze the extreme precipitation changes in the area. Generally, ground rain gauge observation is the most reliable surface precipitation data source, which is indispensable in hydrological simulation and climate change research [13–15]. Due to various restricted conditions, especially in cold high-altitude areas and economically underdeveloped areas (Mondal et al. 2018). With the launch of the Tropical Precipitation Measurement Mission (TRMM) satellite [16], satellite precipitation dataset successfully solves the problem of global coverage [17–20].

Gan verified the reliability of precipitation estimation of IMERG V6 in the Nan River Basin [21]. Using a larger study area and a variety of satellite data [22] confirmed the performance of Climate Hazards Group InfraRed Precipitation with Station data (CHIRPS) [23] and TRMM Multi-satellite Precipitation Analysis (TMPA) in Indian precipitation estimation. Yangtze River Basin (YRB) is the first largest river basin in China. Also, it is the third-largest river basin in the world. Its total area is 1.8 million sq. km, accounting for 18.8% of China's land area. Scholars analyzed and evaluated different satellite precipitation estimations in the YRB. TRMM 3B42V6, CHIRPS and TRMM 3B42V7 were proved alternatives for the precipitation temporal and spatial evolution study in the Yangtze River Basin [24].

Furthermore, scholars are eager to explain the driving force of long-term changes of these meteorological and hydrological variables to understand precipitation's temporal and spatial evolution. Urbanization brings a series of adverse effects such as the urban heat island and reduction of bare soil land type, which impact regional

temperature, rainstorm, and waterlogging [25, 26]. However, the situation is more characteristic and complicated for the upper Yangtze River Basin (UYRB). Large-scale reservoirs have been built and put into operation on the mainstream and tributaries, including Jinsha River, Yalong River, Min River, Jialing River and Wu River in the last years. The total water storage capacity is more than 100 billion m^3 ; regulated storage capacity is 46 billion m^3 , flood control storage capacity is 36 billion m^3 , and installed capacity is 76 million kilowatts [27]. The construction of a huge reservoir system widened the river's water surface, expanded the water area, and increased water evaporation. The natural hydrological rhythm of the Yangtze River is also affected due to reservoir action [28–30].

To clarify the hydrological impact of reservoir construction, recently, Wang simulated the regional hydrology process and found that the operation of cascade reservoirs in the UYRB caused the river water temperature to rise in spring [27], drop in autumn and winter. Su and Chen found reservoir is one of the impact factors of nonstationary change of extreme value distribution of streamflow [31]. However, it's important to note that relevant researches were just carried out, and studies on the influence of reservoir construction on precipitation pattern change are relatively rarer. Precipitation is the most direct response to climate change and human activities. Compared with the river flow and river water temperature, precipitation has a more widespread spatial distribution and complicated temporal change, the influence of reservoirs on rainfall is not concentrated in several locations but spatially heterogeneous.

From the above, this chapter aims to reveal the total and local impact of the existing reservoirs on precipitation change in the UYRB using multi-source precipitation data for the first time. To achieve the goal, the accuracy of the satellite precipitation products on each sub-basin and time scales of day, month, and year was evaluated. Then the temporal and spatial changes of precipitation and extreme precipitation in the UYRB were analyzed. Ultimately collect the information of reservoir location and storage capacity, the impact of reservoir construction on extreme precipitation was finally studied using the spatial analysis method. The study work provides a first reference for understanding the relation of regional reservoir planning and precipitation changes.

2 Materials and Methods

2.1 Study Area

Yangtze River Basin is the largest in China, with a total catchment area of about 1.8 million km^2 . It located between $24^\circ 30' - 35^\circ 45' \text{ N}$ and $90^\circ 33' - 122^\circ 25' \text{ E}$, plays a leading role in China's climate evolution. UYRB covers an area of 1.3 million km^2 from Tanggula Mountain in Tibet to Yichang in Hubei Province. It is mainly composed of mainstream and Jinsha River Basin (JSRB), Jialing River Basin (JLRB),

Min River Basin (MRB) and Wu River Basin (WRB). The JSRB is the largest sub-basin of UYRB. Its entire elevation is high in the west and low in the east, and the climate is complex and diverse. It is composed of a typical plateau climate, an abrupt climate, and a monsoon climate [32, 33]. The JLRB has a subtropical monsoon climate. Affected by that, the seasonal precipitation varies greatly. Precipitation is mainly concentrated in the rainy season from May to September, accounting for 70–90% of the annual precipitation [34–36]. The MRB has a complex topography, with a maximum elevation drop of nearly 6000 m in the entire basin [37]. Compared with the other basins, the elevation of WRB is relatively low, and the subtropical monsoon climate makes WRB have a mild climate and abundant rainfall.

The topography and climate of the four sub-basins in UYRB show significant differences. In this study, the performance of satellite precipitation datasets was respectively evaluated for four sub-basins. Figure 1 shows the location of UYRB and the 88 national rain gauges. Figure 1a shows the latitude and longitude of China and the location map of UYRB in China, Fig. 1b shows the location of the UYRB sub-basins, Fig. 1c shows the DEM distribution of UYRB, Fig. 1d shows the distribution of UYRB surface rain gauge stations.

2.2 *Satellite Datasets*

Considering the different available time periods of the multi-satellite precipitation products, this study uses the IMERG-Final (IMERG-F) and TMPA-3B42 V7 and daily precipitation data sets from 2001 to 2019. IMERG is a global (90° S–90° N, 60° S–60° N is the complete coverage) multi-satellite precipitation dataset, which is the third-level product of the GPM mission [38]. The algorithm adopted in TRMM satellite precipitation products is version 7 TRMM multi-satellite precipitation analysis, called TMPA [2]. TMPA is a quasi-global (60° S–60° N) precipitation dataset. It is one of the best multi-satellite precipitation datasets in the TRMM era. The time resolution of two satellite precipitation datasets has 3 h, daily and monthly.

2.3 *Ground-Based Dataset*

The rain gauge observation daily data comes from the Chinese Meteorological Department (CMD). Eighty-eight national rain gauge stations are located in the UYRB, including 35 rain gauge stations in the JSRB, 14 rain gauge stations in the JLRB, 13 Rain gauge stations in the MRB, and 13 rain gauge stations in the WRB. Monthly and annual data are obtained through daily data accumulation.

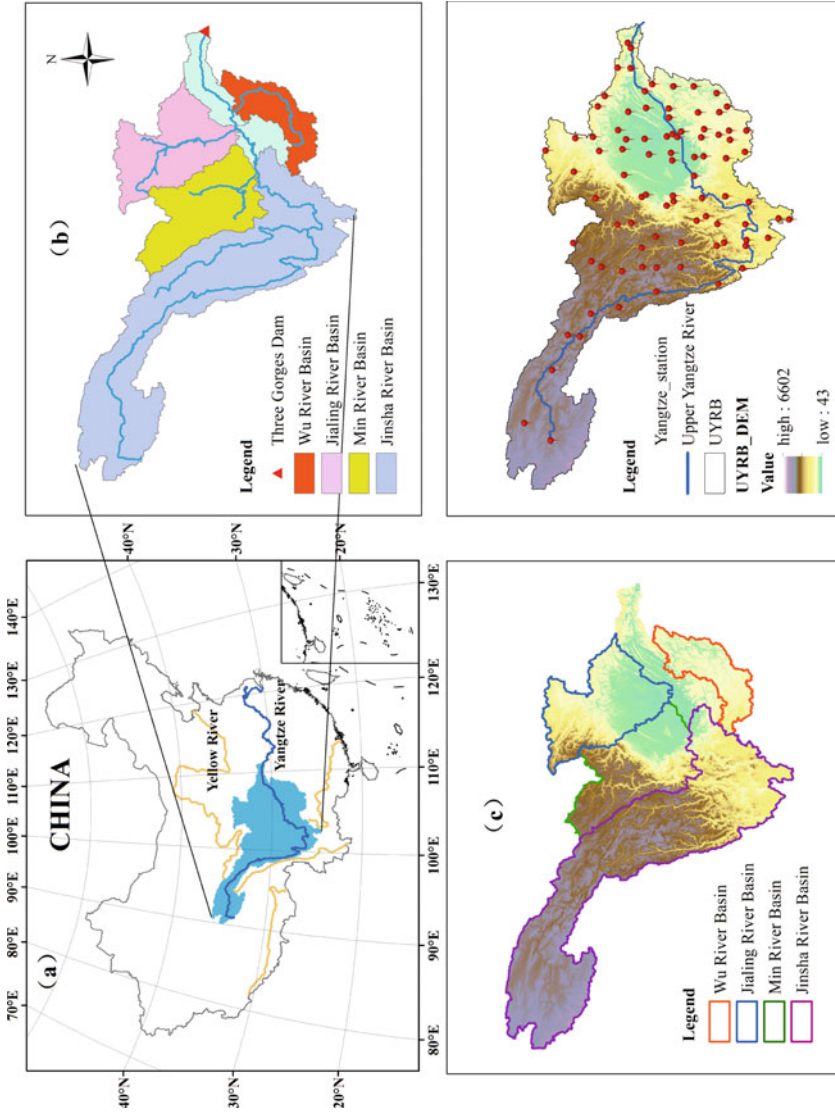


Fig. 1 Study Area, **a** is the latitude and longitude of China and the location map of UYRB in China, **b** is the location map of the UYRB sub-basin, **c** is the DEM distribution map in the four sub-basins of UYRB **d** shows the distribution of UYRB ground rain gauge stations and UYRB DEM

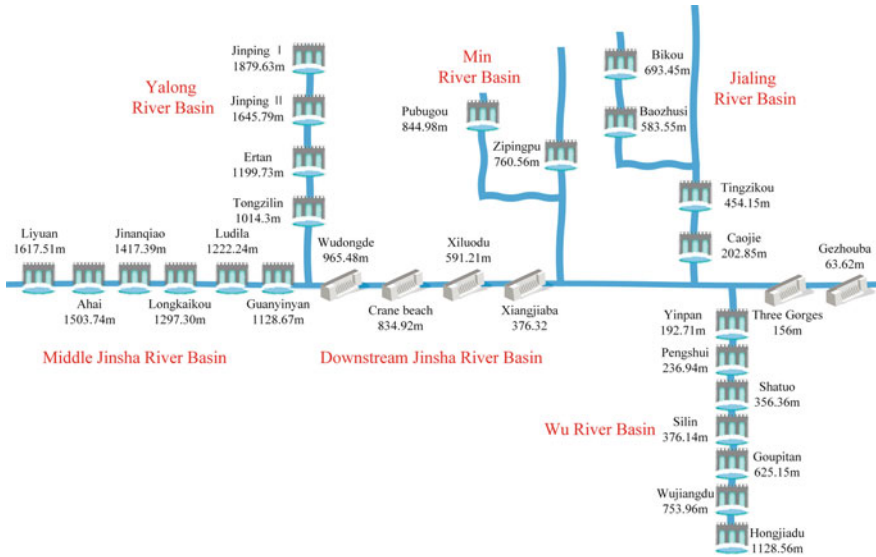


Fig. 2 Schematic diagram of the spatial distribution of the medium and large reservoirs in the UYRB

2.4 UYRB Reservoir Data

There are a large number of reservoirs in the UYRB. Figure 2 is a schematic diagram of the spatial distribution of medium and large reservoirs. The Three Gorges Project is located nearly in the outlet of the UYRB and was put into use in 2003. The Three Gorges hydropower station and the Gezhouba hydropower stations not far downstream have formed a cascade dispatching power station. It is the largest hydropower station globally in terms of flood control, drought resistance, shipping and power generation. It is also the largest engineering project ever built in China. The middle reaches of the JSRB have a large elevation drop, and the distribution of reservoirs is relatively dense. The Yalong River flows into the lower reaches of JSRB reservoirs' total storage capacity. The total storage capacity of reservoirs downstream of the JSRB is larger than that in the middle reaches. The storage capacity of the reservoirs built in the MRB is relatively small. In the JRB and WRB, the distribution of reservoirs is relatively even, and the storage capacity of the reservoirs is relatively large.

2.5 Accuracy Assessment of Satellite Precipitation Estimation

The accuracy of the satellite precipitation dataset is evaluated based on the ground rain gauge data [39]. In this study, the UYRB is divided into JSRB, JLRB, MRB

and WRB. Each sub-basin is assessed separately. With the point-to-point extraction of the satellite precipitation estimation data at the rain gauge location, the obtained observed precipitation data and the estimated precipitation data are used to calculate the Bias and RMSE. The accuracy of the satellite precipitation dataset is evaluated at three kinds of time resolutions, including day, month and year. The formulas of Bias and RMSE are as follows:

$$Bias = \frac{\sum_{i=1}^n P_i - G_i}{n} \tag{1}$$

$$RMSE = \sqrt{\frac{\sum_{i=1}^n (P_i - G_i)^2}{n}} \tag{2}$$

where P_i and G_i respectively represent the satellite precipitation estimation value and the station precipitation observation value at time i .

2.6 Mann–Kendall Trend Analysis

Mann–Kendall test is widely used in the trend analysis of meteorological and hydrological variables. It is a non-parametric test, and does not make strict assumptions about the overall distribution of variables of interest [40]. The calculation formula is [41, 42]:

$$Z = \begin{cases} \frac{S-1}{\sqrt{\text{var}(S)}}, & S > 0 \\ 0, & S = 0 \\ \frac{S+1}{\sqrt{\text{var}(S)}}, & S < 0 \end{cases} \tag{3}$$

The positive or negative sign of Z can be used to indicate the rising or falling trend of precipitation time series, and the absolute value of Z can be used to evaluate its significance. Where

$$S = \sum_{i=1}^{n-1} \sum_{k=i+1}^n \text{sgn}(x_k - x_i) \tag{4}$$

$$\text{sgn}(\theta) = \begin{cases} 1, & \theta > 0 \\ 0, & \theta = 0 \\ -1, & \theta < 0 \end{cases} \tag{5}$$

$$\text{var}[S] = \frac{[n(n-1)(2n+5) - \sum_t t(t-1)(2t+5)]}{18} \tag{6}$$

x_k represents the value of the variable x at the time k , n is the sample number of the time series, and t is the year or month in this study.

The index to measure the trend of MK test results is expressed by β :

$$\beta = \text{Median}\left(\frac{x_i - x_j}{i - j}\right), \forall j < i \quad (7)$$

where $0 < j < i < n$, when $\beta > 0$, it means that the time series shows an upward trend, when $\beta < 0$, it shows a downward trend, and the value of β indicates the intensity of the trend.

2.7 Reservoir Affected/Non-affected Area

The impact area of reservoirs should be different according to the water storage scale. In this study, the impact radius of a reservoir with a total storage capacity of 1 billion m^3 is set to 10 km, 5 billion m^3 is set to 50 km, 10 billion m^3 is set to 100 km. Following this trend, each reservoir's impact area can be interpolated calculated according to its storage capacity. For instance, the total storage capacity of Xiluodu reservoir is 12.67 billion m^3 , and the influence radius is set to 130 km. The total storage capacity of Crane Beach reservoir is 20.6 billion m^3 , and the influence radius is set to 210 km. The total storage capacity of Three Gorges is 39.3 billion m^3 , and the influence radius is set to 400 km. Then UYRB can be divided into reservoir affected area (RAA) and Non-reservoir affected area (N-RAA).

2.8 Probability Distribution of Precipitation Evaluation in RAA and NRAA

The probability density function can be used to analyze the overall situation of a variable. It can reflect the probability of a variable being distributed in a certain numerical interval. By comparing the probability distributions of the precipitation trend values in the two regions, whether the construction of the reservoir has a significant impact on precipitation will be clear. In addition, RAA is divided into five levels according to the size of the reservoirs. Reservoirs with a total storage capacity of less than 5 billion m^3 and reservoirs with a total storage capacity of 5–10 billion m^3 are classified as one level. Super-large reservoirs with a total storage capacity of more than 10 billion m^3 are one of its own levels, through the probability distribution of extreme precipitation change trend to judge the impact of different levels of reservoirs on extreme precipitation.

3 Results and Discussion

3.1 Multi-satellite Data Validation Using Ground Gauges

Satellite precipitation data will average the local high-intensity precipitation with the surrounding low-intensity precipitation. Therefore, the difference in rainfall intensity at the location of the rain gauge maybe have a certain impact on the verification results. It means that if local precipitation is high and the surrounding precipitation is relatively low. Satellite precipitation observations maybe underestimate the observed precipitation. On the contrary, satellite precipitation's observed value may overestimate the measured precipitation.

During the 9-year evaluation period from 2001 to 2019, IMERG and TMPA were compared with the rain gauge data. Figure 3 shows that the Bias spatial distribution of satellite precipitation data compares with rain gauge data in the four sub-basins of UYRB. (a) Bias distribution of precipitation for JLRB satellite precipitation products. In JLRB, IMERG data slightly underestimates the measured precipitation. On the contrary, TMPA data overestimate the measured precipitation. From the results of Bias distribution, both satellite precipitation products underestimate the precipitation in the eastern part of JLRB to a certain extent. The upper Bailong River Basin is mostly mountainous and the terrain is complex. Both satellite precipitation products have a certain overestimate compare with measured precipitation. (b) Bias distribution map for JSRB satellite precipitation products. We can observe that both products overestimate the precipitation of JSRB.

Compared with the TMPA data, the estimated performance of IMERG data for JSRB is better than that of TMPA. In the central of JSRB, the spatial distribution of Bias for two satellite precipitation products showed similarity. The observation effect of IMERG showed a certain underestimation in the northwest of JSRB. (c) Bias distribution map for MRB satellite precipitation product. Both satellite precipitation datasets have a certain underestimation of the observed precipitation. The climate of MRB is complex and diverse. Affected by the difference between MRB's southern and northern topography, Bias distribution in southern and northern MRB showed an obvious difference. Both satellite precipitation products have a certain overestimation compared with measured precipitation for the northern MRB. This may be attributed to the complex topographical drop in the northern mountains. The downstream channel of MRB widens and flows into the Sichuan Basin. Mild and humid climate with abundant precipitation. Both satellite precipitation datasets underestimate the observed precipitation in downstream of MRB. In the southeast of Min River, TMPA has a slightly underestimate compared with observed precipitation, while the precipitation estimates of IMERG showed an inevitable overestimation. (d) Bias distribution map for WRB satellite precipitation product. From the distribution results, TMPA has a relatively obvious precipitation underestimation in the southern part of WRB.

Table 2 shows the Bias and RMSE results of two satellite precipitation datasets for the four sub-basins of UYRB, including the average Bias and RMSE values of

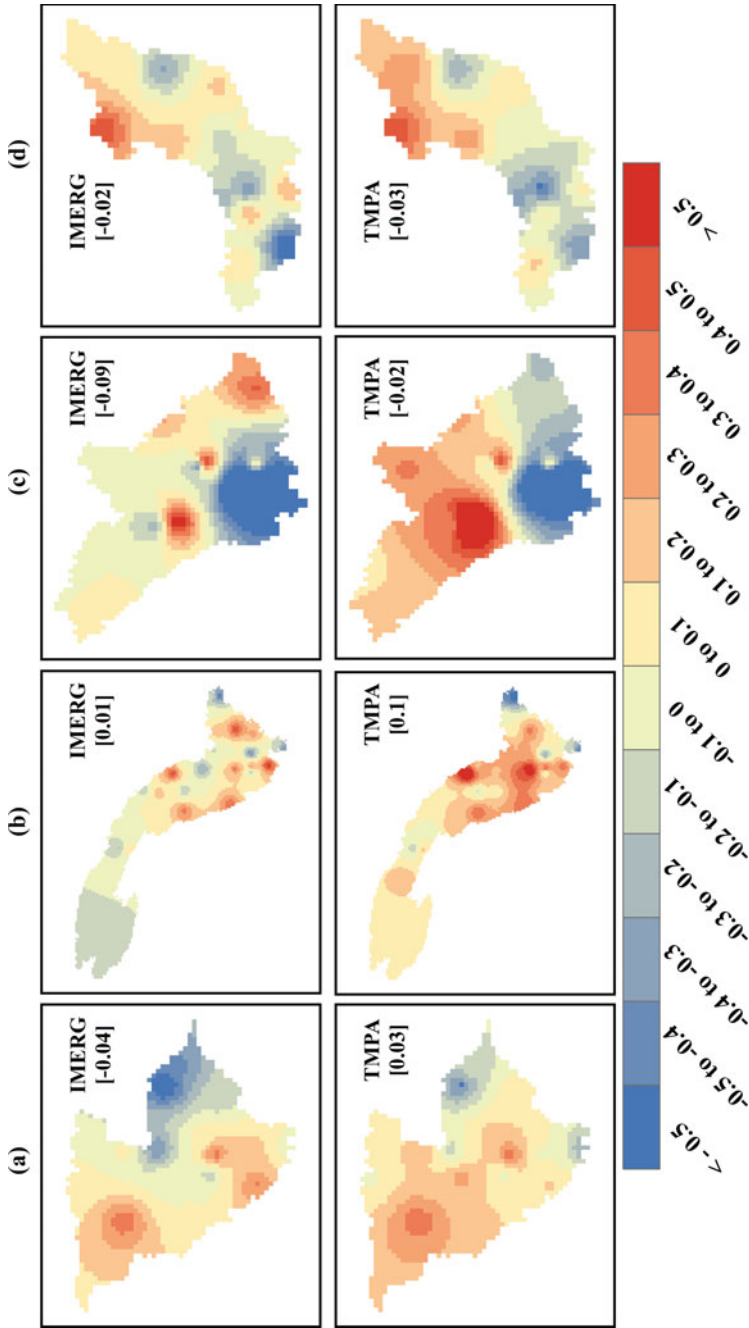


Fig. 3 The Bias distribution of daily precipitation (mm day⁻¹) and average Bias of TMPA and IMERG in the four UYRB sub-basins from 2001 to 2019. **a** Bias distribution of JLRB; **b** Bias distribution of JSRB; **c** Bias distribution of MRB; **d** Bias distribution of WRB

Table 2 Bias and RMSE results of the four UYRB sub-basins

	Datasets	Jialing		Jinsha		Min		Wu	
		Bias	RMSE	Bias	RMSE	Bias	RMSE	Bias	RMSE
Daily	IMERG	-0.04	10.35	0.01	6.69	-0.09	9.69	-0.02	10.48
	TMPA	0.03	11.39	0.1	7.15	-0.02	10.15	-0.03	11.17
Monthly	IMERG	-1.21	33.93	0.11	22.63	-2.81	38.23	-0.89	33.04
	TMPA	0.95	33.98	3.09	26.38	-0.61	42.75	-0.97	36.13
Annual	IMERG	14.56	129.92	1.35	102.74	-33.78	200.33	-10.54	141.65
	TMPA	11.38	126.46	37.02	121.45	-7.26	223.36	-11.59	152.97

three-time scales of daily, monthly and annual. The observation effect of TMPA in JSRB is far inferior to IMERG. In MRB, the effect of precipitation estimation of IMERG is relatively poor. In addition, both the two satellite precipitation datasets showed a good performance in the four sub-basins. As a derived product of TMPA, IMERG data in UYRB showed good observation effects.

3.2 Yearly and Monthly Precipitation Trend Analysis

The accuracy of evaluation results shows that the precipitation estimates of TMPA in JLRB and MRB are better than IMERG. In JSRB and WRB, the precipitation estimates of IMERG are better than TMPA. Therefore, TMPA data is used for the trend analysis of JLRB and MRB, and IMERG data is used for the trend analysis of JSRB and WRB, and the analysis period is 2001–2019.

Check the significance level of the MK test results (Z statistics) by performing MK test on the satellite precipitation data for the four sub-basins from 2001 to 2019 on monthly and annual scales. Figure 4 shows that the spatial distribution of the Z statistics about MK test for satellite precipitation data. Both the annual and monthly precipitation has shown a positive trend. Central and northwestern parts of the JLRB have been observed a positive and significant trend in annual precipitation. The annual precipitation of northern JSRB has also observed a significant positive trend. At the same time, the southwest region of JSRB showed a significant negative trend on both monthly and annual scales. In the southern part of MRB, a negative trend was observed on both monthly and annual scales, although this negative trend seems insignificant. Both the MRB and WRB have not shown significant trends on monthly and annual scales, including the positive and negative trends.

In order to further observe the changing trend of precipitation in the UYRB during the study period, the precipitation trend index β of monthly and annual precipitation for four sub-basins of UYRB during the study period was calculated. Figure 5 shows the spatial distribution of precipitation change trend on the annual scale for four sub-basins of UYRB from 2001 to 2019. The value of β expresses size of the trend. According to the results of MK test, in terms of the annual precipitation from 2001 to

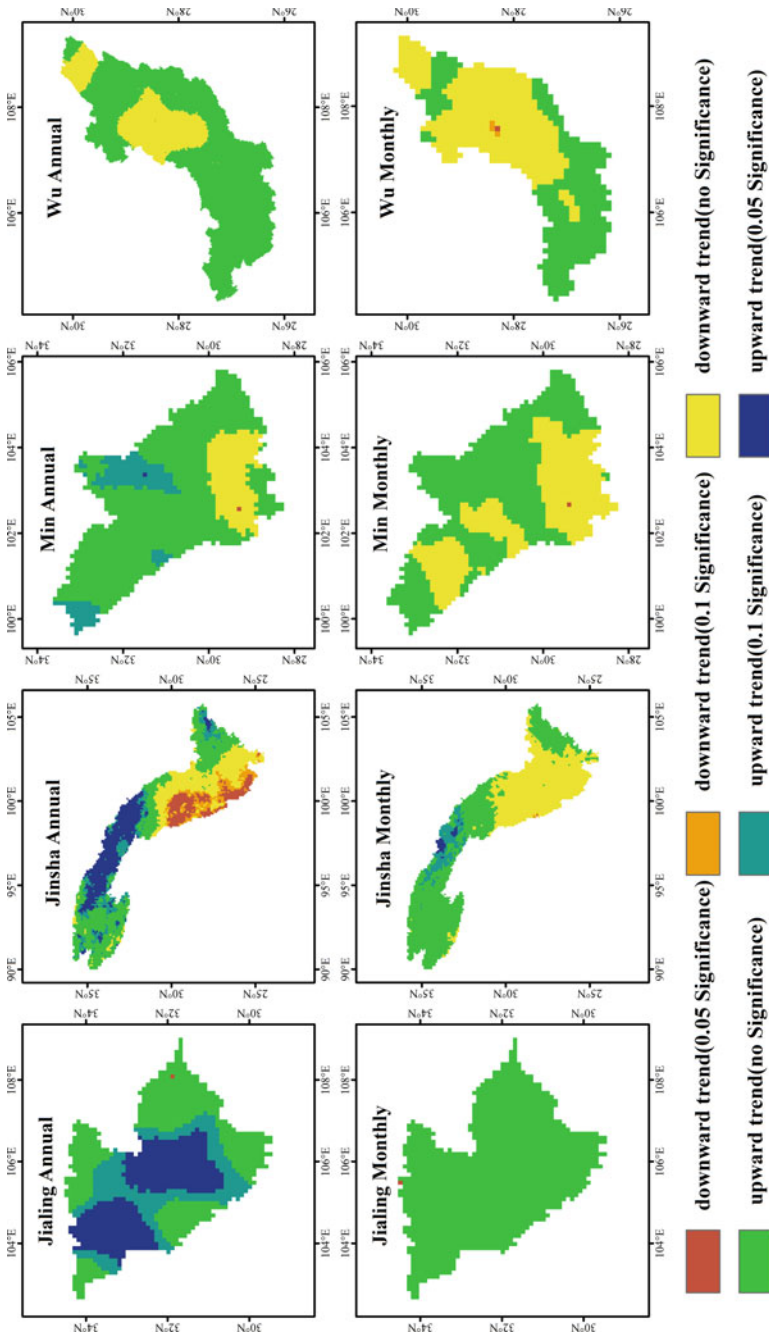


Fig. 4 Spatial distribution of Z-statistical significance at the UYRB sub-basins for period 2001–2019

2019. The annual precipitation for JLRB showed a certain downward trend. Except for a small part of the northwest of JLRB, the annual precipitation of the entire JLRB is basically on the rise. Compared with other regions, the central part of JLRB showed the most obvious upward trend. For JSRB, the annual precipitation of southwestern JSRB showed an obvious downward trend. The annual precipitation for the midstream of JSRB showed a slight upward trend. MRB precipitation was relatively stable from 2001 to 2019, and there was no obvious upward or downward trend for annual precipitation. Compared with the other three sub-basins of UYRB, precipitation for most areas of WRB showed a downward trend, which the downward trend was more obvious in the northern part of WRB, while the southern part showed a slight upward trend.

In addition, by analyzing the relationship between the location of reservoirs and the change in the trend of annual precipitation, it can be observed that the distribution of reservoirs seems to be related to the changing trend of regional precipitation. In the area around the reservoirs of the Upper-JLRB, annual precipitation showed an obvious upward trend. The Tingzikou reservoir and Baozhusi reservoir were put into use in 2012 and 1996, respectively. In the southern part of JLRB, annual precipitation also showed a certain upward trend, and the area is also the RAA. On the contrary, In the south of JSRB and downstream of WRB, reservoirs in these two regions are more densely distributed. The operation time of reservoirs was late. The total storage capacity is relatively small, affected by the diversion of the rivers during the construction of cascade dams. The trend of annual precipitation showed an obvious downward trend. The Zipingpu reservoir with a total storage capacity of more than 1 billion m^3 was put into use in 2005. In the RAA of Zipingpu, annual precipitation also had a certain upward trend during the study period.

Figure 6 shows the spatial distribution of the monthly precipitation change trend for the four sub-basins of UYRB from 2001 to 2019. In view of the small trend value of monthly precipitation during the study period, this study divided the size of the trend into five levels, named downward, downward (not obvious), no obvious trend, upward (not obvious) and upward. The monthly precipitation for MRB generally shows an upward trend, and the upward trend in the northeast of MRB is more obvious. The monthly precipitation for the southern part of WRB also showed an obvious upward trend. In addition, monthly precipitation is relatively stable for most areas of the other two basins. In the central part of WRB, monthly precipitation showed a slight downward trend.

By observing the relationship between the location distribution of reservoirs and the spatial distribution of the monthly precipitation change trend, the monthly precipitation of JLRB and JSRB does not seem to be significantly affected by reservoirs. However, in the southern part of JSRB and downstream of WRB, monthly precipitation also showed a certain downward trend like that the trend of annual precipitation. Zipingpu reservoir is located upstream of MRB. The reservoir was put into use in 2005, with a total storage capacity of more than 1 billion m^3 . Affected by the upstream catchment of Zipingpu reservoir, monthly precipitation showed a visible upward trend.

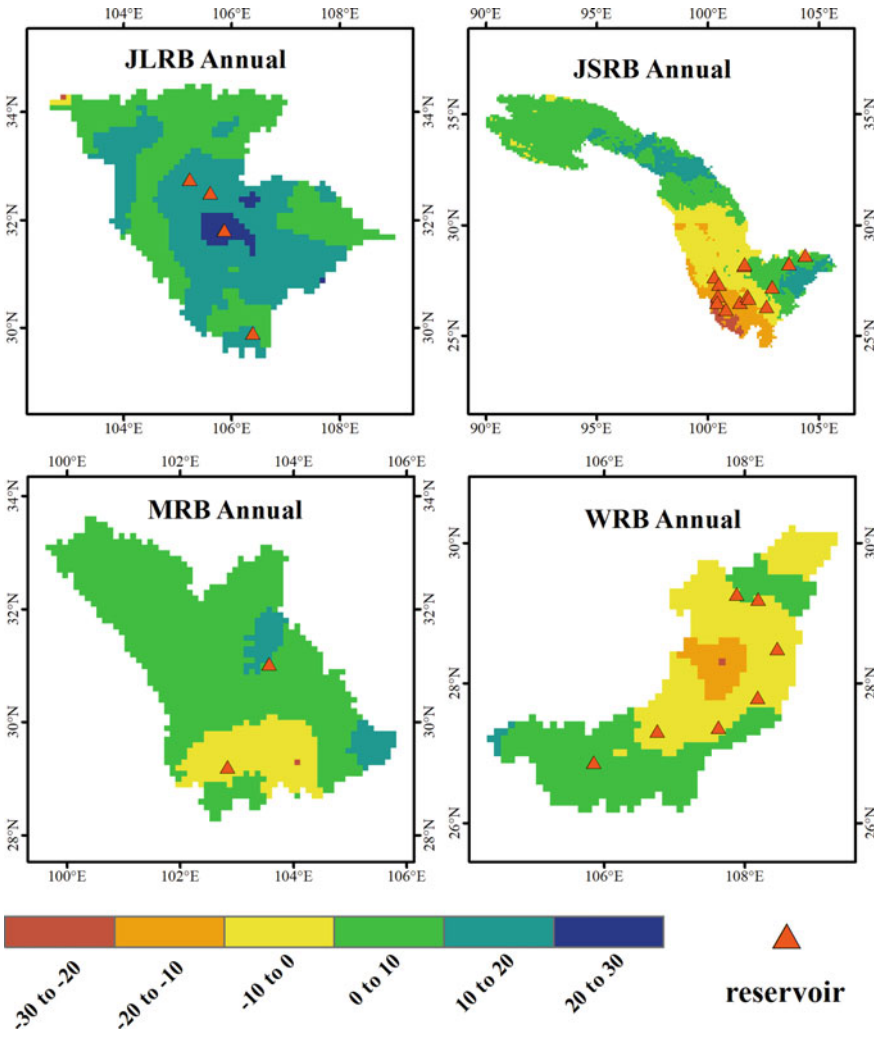


Fig. 5 Spatial distribution of annual precipitation trends in UYRB sub-basins from 2001 to 2019

3.3 Precipitation Extreme Value Trend Analysis

The annual maximum 1/3-day precipitation can reflect the level of heavy precipitation and continuous heavy precipitation in the study area. This study finally used IMERG data to analyze the extreme precipitation change trend for UYRB from 2001 to 2019 and analyzes the changing trend of extreme precipitation within the UYRB during the study period by changing the annual maximum 1/3-day precipitation over time series.

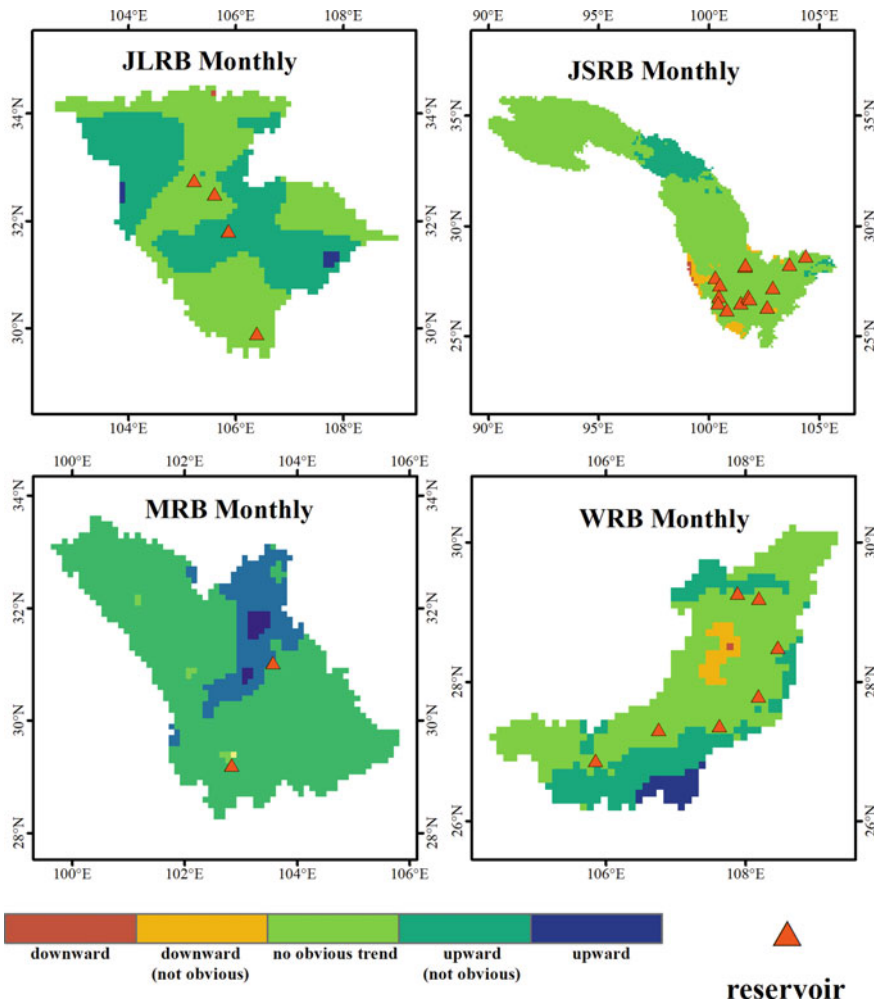


Fig. 6 Spatial distribution of monthly precipitation trends in UYRB sub-basins from 2001 to 2019

Figure 7 shows the results of the MK test using the UYRB satellite precipitation dataset for the extreme (1 day) precipitation. (a) Spatial distribution of Z statistics for UYRB extreme (1 day) precipitation from 2001 to 2019. Figure 7 shows a significant upward trend of extreme (1 day) precipitation in the northern JSRB.. On the contrary, the downward trend of extreme (1 day) precipitation in the southwestern JSRB is somewhat significant. On the whole, UYRB has a significant upward trend in precipitation on extreme (1-day) precipitation. (b) Spatial distribution of β for UYRB extreme (1 day) precipitation from 2001 to 2019. An inevitable upward trend has been observed from Fig. 7 for the extreme (1 day) precipitation upstream of JSRB. At the same time, the junction of the middle reaches of JSRB and the downstream

of Yalong River shows a relatively obvious downward trend. In the downstream of the three basins of MRB, JLRB, and WRB near the mainstream of the Yangtze River (Middle area of UYRB), extreme (1 day) precipitation has shown an obvious upward trend. In the upper reaches of these three sub-basins (MRB, JLRB and WRB), the extreme (1 day) precipitation all showed a partial downward trend.

Figure 8 shows the UYRB extreme (3 days) precipitation trend analysis results. The results show that the spatial distribution of extreme (3 days) precipitation upward and downward is consistent with the extreme (3 days) precipitation trend. The upward trend of extreme (3 days) precipitation upstream of JSRB is more significant than extreme (1 day) precipitation. According to the spatial distribution of extreme (3 days) precipitation trend, it can be observed that the precipitation change trend in the north and south of UYRB showed obvious differences. Except for the upstream of JLRB, the northern part of UYRB has a certain upward trend. The extreme (3 days) precipitation has the most obvious upward trend in the central part of UYRB.

3.4 The Influence of Reservoirs on Extreme Daily Precipitation

In order to further explore the influence of reservoirs on extreme precipitation (1 day/3 days), Fig. 9 shows the spatial distribution map of RAA and N-RAA extreme (1 day) precipitation. One phenomenon is observed in Fig. 9: the extreme (1 day) precipitation has a relatively obvious upward trend in areas with more reservoirs downstream of the JLRB and WRB. Affected by the Three Gorges Dam and some reservoirs downstream of JLRB, the annual maximum daily precipitation in the eastern part of RAA has a significant upward trend. On the contrary, the annual maximum daily precipitation in parts of the RAA downstream in JSRB has a significant downward trend. In addition, the annual maximum daily precipitation in the lower reaches of MRB and JLRB near the mainstream of the Yangtze River has a clear upward trend.

Figure 10 shows that the spatial distribution of extreme (3 days) precipitation in RAA and N-RAA. Its distribution is basically consistent with the spatial distribution of the extreme (1-day) precipitation change trend. Compared with the annual maximum 1-day precipitation trend spatial distribution, the annual maximum 3-day precipitation change trend is more significant in NRAA. This trend is mainly manifested in downstream of MRB. On the contrary, the trend of extreme (3 days) precipitation in the middle of JSRB has a relatively small upward trend.

Divide UYRB into two regions, RAA and N-RAA, and analyze the changing trend of the extreme (1/3-day) precipitation in the two regions. Figure 11 shows the probability distribution of extreme precipitation trends in the two regions. Figure 11's upper part shows the probability distribution of the extreme (1 day) precipitation in RAA and N-RAA. Figure 11 shows that the changing trend of the extreme (1 day) precipitation in N-RAA is concentrated between 0 and 1.

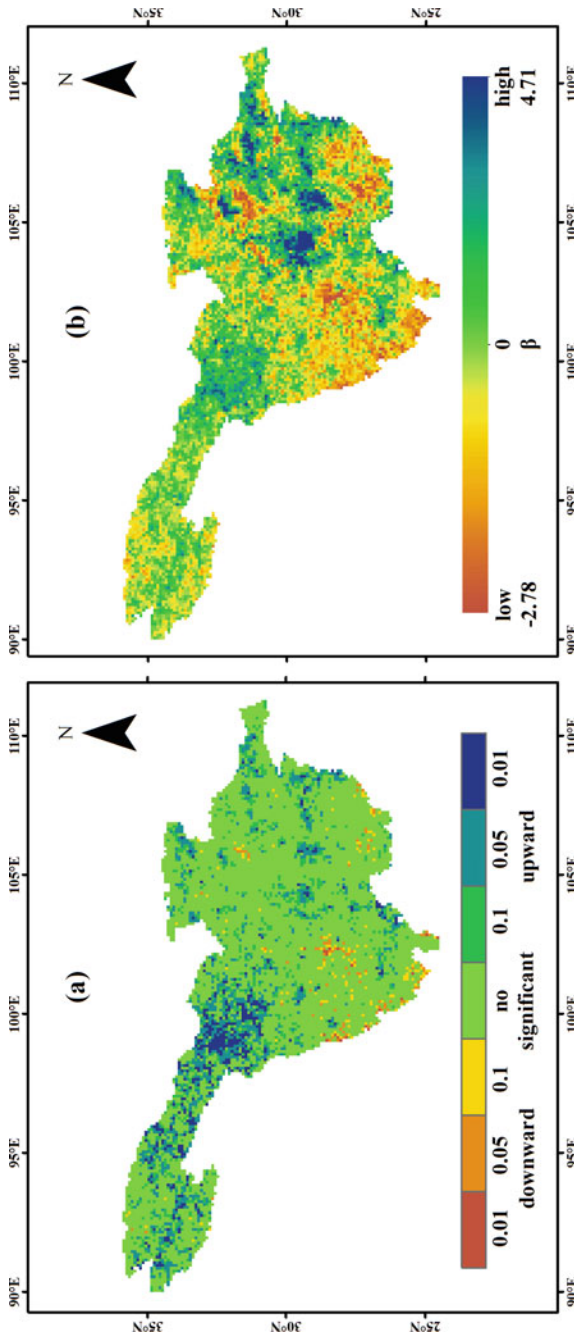


Fig. 7 UYRB 2001–2019 IMERG data extreme (1 day) precipitation trend analysis significance and spatial distribution. **a** Significance spatial distribution of MK test trend analysis results; **b** MK test trend analysis trend size (β) spatial distribution

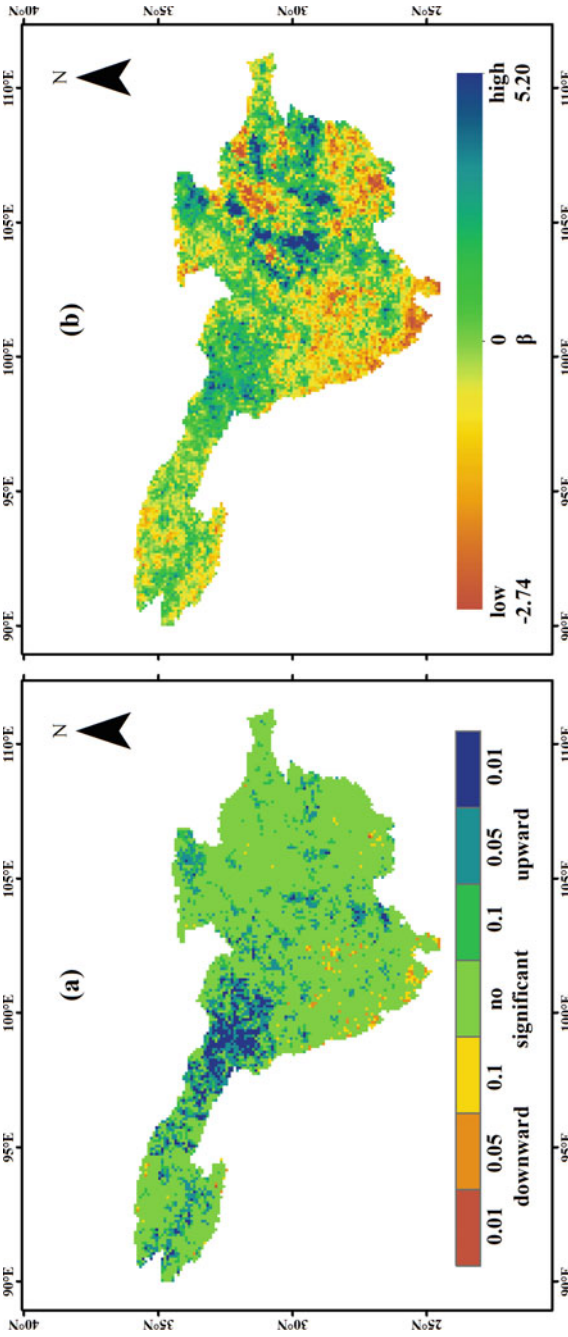


Fig. 8 UYRB 2001–2019 IMERG data extreme (3-day) precipitation trend analysis significance and spatial distribution. **a** Significance spatial distribution of MK test trend analysis results; **b** MK test trend analysis trend size (β) spatial distribution

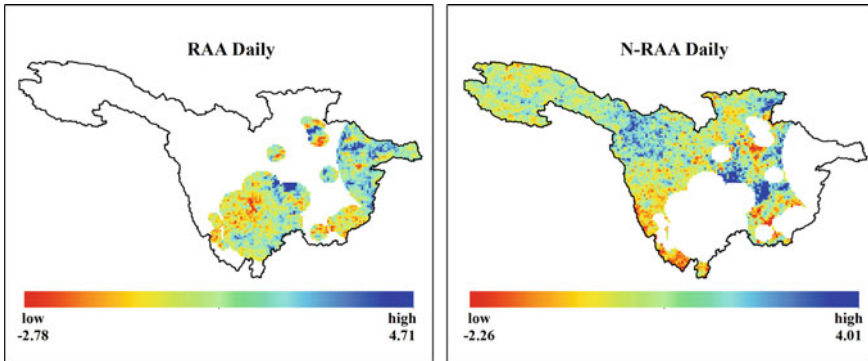


Fig. 9 Spatial distribution of the extreme (1 day) precipitation change trend in RAA and N-RAA from 2001 to 2019

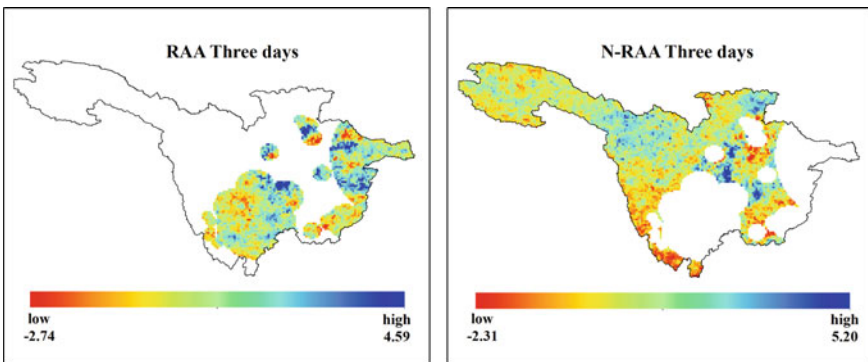


Fig. 10 Spatial distribution of the extreme (3 days) precipitation change trend in RAA and N-RAA from 2001 to 2019

The probability at $x = 0.5$ is as high as 0.65, and the overall change trend is small. In RAA, the extreme (1 day) precipitation change trend is more distributed far away from $x = 0$, which is in obvious contrast with the N-RAA region between -2 and -0.5 and between 1 and 3 . The lower part shows the probability distribution of the extreme (3 days) precipitation in RAA and N-RAA. Compared with the extreme (1 day) precipitation change trend distribution, the downward trend in RAA and N-RAA is relatively close, and there is no obvious difference between $x = 0$ and $x = 1.5$. The distribution of N-RAA is significantly higher than that of RAA. In the region of $x > 2$, RAA showed a more obvious upward trend. According to the probability distribution function, the reservoir had a certain impact on UYRB extreme precipitation (1 day/3 days). The upward trend of the extreme (3 days) precipitation is more affected than the downward trend.

The RAA is divided into five areas according to the size of reservoirs. Figure 12 shows the probability distribution of the extreme (1 day/3 days) precipitation trend

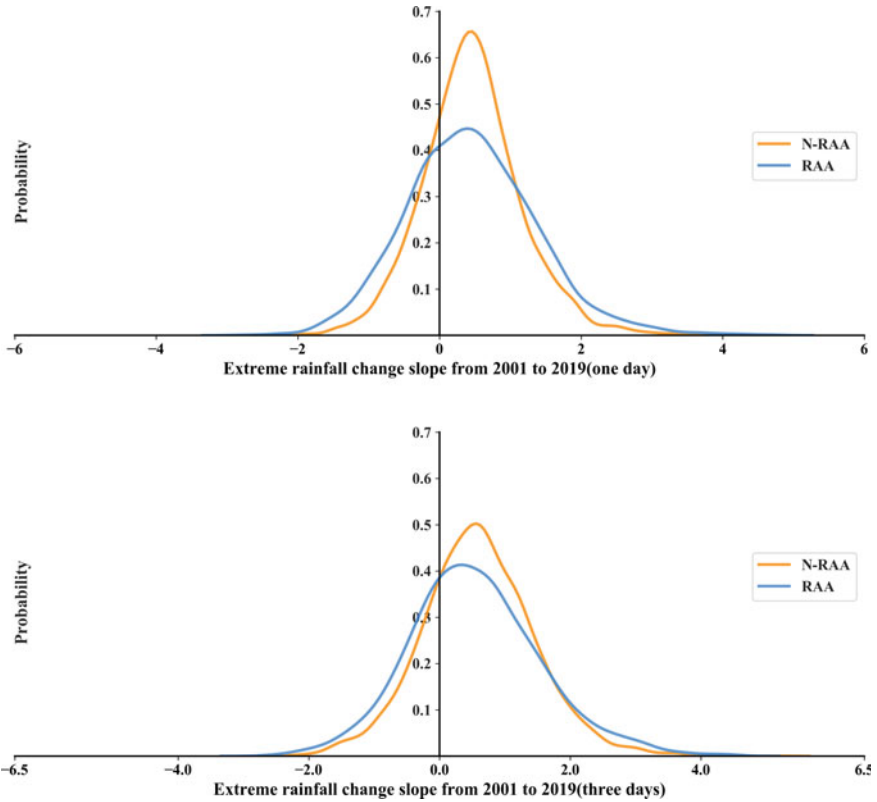


Fig. 11 The probability distribution function of extreme precipitation changes over RAA and N-RAA from 2001 to 2019

in the five sub-regions of RAA. The upper part of Fig. 12 showed the probability distribution about extreme (1 day) precipitation trends in five sub-regions. From Fig. 12, it can be observed that the precipitation trend of Three Gorges RAA is totally different from the other regions. The annual maximum daily precipitation has a clear upward trend in Three Gorges RAA. The probability distribution of the other four regions is basically the same in the upward and downward trends. In RAA, with a total storage capacity of less than 5 billion m³, the annual maximum daily precipitation also changes significantly. The change is mainly manifested as a downward trend. The lower part of Fig. 12 showed the probability distribution of the extreme (3 days) precipitation trend in the five sub-regions of RAA. Compared with the changing trend of the annual maximum 1-day precipitation, the 3-day maximum annual precipitation change trend is more affected by the grade of reservoirs. The probability distribution of the five sub-regions of RAA all has a deviation in the direction of $x > 0$. The probability distribution of the annual maximum 3-day precipitation trend in the RAA of different grades of reservoirs is also showed more differences.

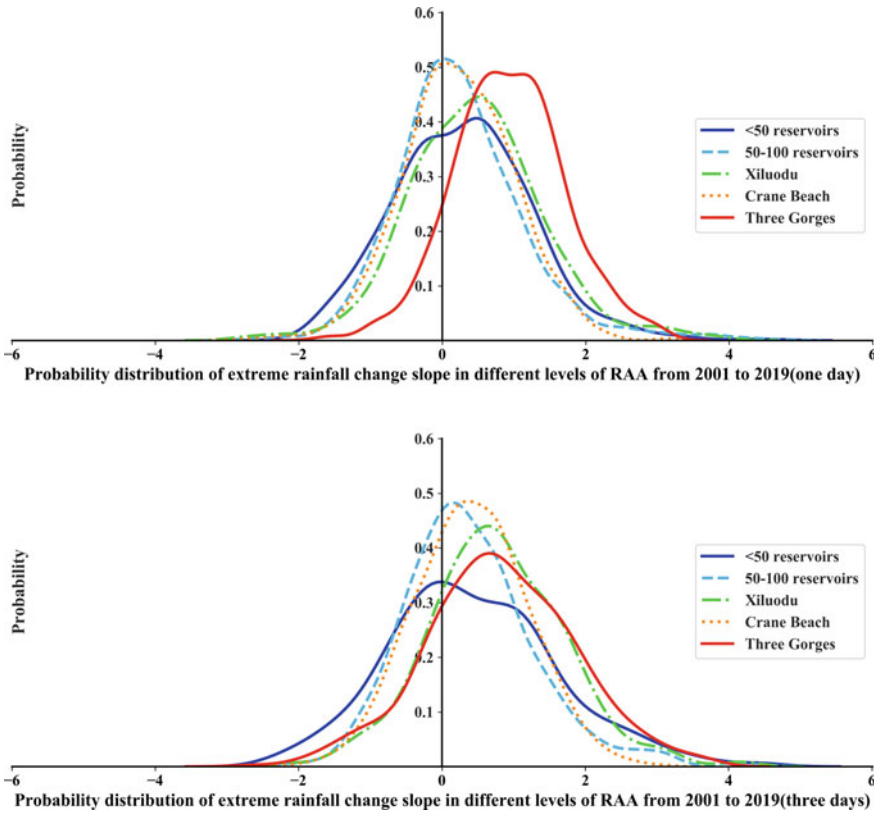


Fig. 12 Probability distribution of extreme rainfall change trend of different scales of RAA from 2001 to 2019

3.5 Influence of the Construction Year and Storage Capacity of the Reservoirs

From the perspective of the operation time and the total storage capacity of reservoirs, mostly reservoirs in the middle reaches of JSRB were completed around 2015. The capacity of these reservoirs was all less than 1 billion m³, which has not caused a significant impact on the upward trend of extreme (1 day/3 days) precipitation during 2001–2019. At the downstream of JSRB and MRB, Pubugou, Xiluodu and Xiangjiaba were put into operation in 2009, 2013, and 2012 respectively, and the total storage capacity of the reservoir was all above 5 billion m³. Within the range of influence of these reservoirs, extreme precipitation has shown a relatively obvious upward trend.

In the RAA of four reservoirs in the central of WRB (Wujiangdu, Goupitan, Silin, Shatuo), extreme precipitation has a certain degree of a downward trend. However, its downward trend is relatively small compared with the surrounding N-RAA area. Most

of the reservoirs in downstream of WRB were put into operation before 2010. Within the range of influence of these reservoirs, extreme precipitation had a relatively obvious upward trend during 2001–2019. Three Gorges was put into use in 2003. Within the RAA of Three Gorges, the extreme (1 day) precipitation upward trend point accounted for 89.07% of the total area. The extreme (3 days) precipitation upward trend point accounted for 78.56% of the total area. Compared with other scales, RAA has a more obvious upward trend.

4 Conclusions

This study evaluated the precipitation performance of IMERG and TMPA in UYRB based on observations during 2005–2013. It also focuses on the impact of large-scale reservoir construction on the temporal and spatial trends of regional precipitation from 2001 to 2019. The main conclusions are summarized below:

- (1) As the derivative product of TMPA, precipitation estimates of IMERG show acceptable observation effects in UYRB.
- (2) From 2001 to 2019, the upward trend of annual precipitation in the central part of JSRB and the northern part of JLRB showed strong significance. The annual precipitation in the southern part of JSRB showed a significant downward trend. The spatial distribution of the annual precipitation trend is the same as that of the reservoir.
- (3) The monthly and annual precipitation from 2001 to 2019 showed an obvious upward trend in the central part of UYRB, while the precipitation in the southwest part of UYRB showed a clear downward trend.
- (4) Compared with the annual maximum 3-day precipitation, the impact of reservoir construction on the annual maximum 1-day precipitation is more prominent. In Three Gorges RAA, extreme precipitation showed the most obvious upward trend.

This paper studies the impact of reservoir construction on precipitation and found that large-scale reservoirs have a significant impact on regional annual precipitation and extreme precipitation changes. In subsequent studies, more methods such as hydrological models and more data sources will be introduced to analyze the impact of reservoirs on the whole water cycle and find the main driving factors that cause temporal and spatial changes in regional climate.

5 Recommendations

Based on the study results, it can be recommended the following points:

- It is advised to apply multi-source fusion precipitation products to hydrological research.
- Comprehensive research can be carried out by combining climate influencing factors such as temperature and air pressure with precipitation.
- It is advised to evaluate the accuracy of satellite precipitation products through hydrological simulation.

Acknowledgements This work was supported by the National Natural Science Foundation of China (No. 51809242).

References

1. Li G, Yu Z, Wang W, Ju Q, Chen X (2020) Analysis of the spatial distribution of precipitation and topography with GPM data in the Tibetan Plateau. *Atmos Res* 247:105259
2. Ma Q, Li Y (2020) Performance evaluation and correction of precipitation data using the 20-year IMERG and TMPA precipitation products in diverse subregions of China. *Atmos Res* 249:105304
3. Wang R, Chen J, Chen X, Wang Y (2017) Variability of precipitation extremes and dryness/wetness over the southeast coastal region of China, 1960–2014. *Int J Climatol* 37:4656–4669
4. Sun F, Roderick ML, Farquhar GD (2018) Rainfall statistics, stationarity, and climate change. *Proc Natl Acad Sci* 115:2305–2310
5. Wang Y, Xu Y (2020) Innovative trend analysis of annual and seasonal rainfall in the Yangtze River Delta, eastern China. *Atmos Res* 231:104673
6. Mondal A, Lakshmi V, Hashemi H (2018) Intercomparison of trend analysis of multisatellite monthly precipitation products and gauge measurements for river basins of India. *J Hydrol* 565:779–790
7. Sonali P, Kumar DN (2013) Review of trend detection methods and their application to detect temperature changes in India. *J Hydrol* 476:212–227
8. Tabari H, Marofi S, Ahmadi M (2011) Long-term variations of water quality parameters in the Maroon River, Iran. *Environ Monit Assess* 177:273–287
9. Wang Y, Xu Y (2016) Spatio-temporal characteristics of precipitation and dryness/wetness in Yangtze River Delta, eastern China, during 1960–2012. *Atmos Res* 172:196–205
10. Sun W, Song X (2016) Changes in extreme temperature and precipitation events in the Loess Plateau (China) during 1960–2013 under global warming. *Atmos Res* 168:33–48
11. Yacoub E, Tayfur G (2020) Spatial and temporal of variation of meteorological drought and precipitation trend analysis over whole Mauritania. *J Afr Earth Sci* 163:103761
12. Toride K, Cawthorne DL, Ishida K, Kavvas ML, Anderson ML (2018) Long-term trend analysis on total and extreme precipitation over Shasta Dam watershed. *Sci Total Environ* 626:244–254
13. Güçlü YS (2020) Improved visualization for trend analysis by comparing with classical Mann-Kendall test and ITA. *J Hydrol* 584:124674
14. Li L, Ngongondo CS, Xu CY, Gong L (2013) Comparison of the global TRMM and WFD precipitation datasets in driving a large-scale hydrological model in southern Africa. *Hydrol Res* 44:770–788
15. Collins M (2013) Observational challenges in evaluating climate models. *Nat Clim Chang* 3:940–941
16. Huffman GJ, Adler RF, Bolvin DT, Nelkin EJ (2010) The TRMM multi-satellite precipitation analysis (TMPA). Springer, Satellite rainfall applications for surface hydrology, pp 3–22

17. Wang W, Lin H, Chen N, Chen Z (2021) Evaluation of multi-source precipitation products over the Yangtze River Basin. *Atmos Res* 249:105287
18. Adler RF, Gu G, Sapiano M, Wang J-J, Huffman GJ (2017) Global precipitation: means, variations and trends during the satellite era (1979–2014). *Surv Geophys* 38:679–699
19. Kucera PA (2013) Precipitation from space: advancing earth system science. *Bull Am Meteor Soc* 94:365–375
20. Sun Q, Miao C (2018) A review of global precipitation data sets: data sources, estimation, and intercomparisons. *Rev Geophys* 56:79–107
21. Gan F, Gao Y, Xiao L (2021) Comprehensive validation of the latest IMERG V06 precipitation estimates over a basin coupled with coastal locations, tropical climate and hill-karst combined landform. *Atmos Res* 249:105293
22. Prakash S (2019) Performance assessment of CHIRPS, MSWEP, SM2RAIN-CCI, and TMPA precipitation products across India. *J Hydrol* 571:50–59
23. Funk C (2015) The climate hazards infrared precipitation with stations—a new environmental record for monitoring extremes. *Sci Data* 2:1–21
24. Lu X, Wang L, Pan M, Kaseke KF, Li B (2016) A multi-scale analysis of Namibian rainfall over the recent decade—comparing TMPA satellite estimates and ground observations. *J Hydrol Reg Stud* 8:59–68
25. Lu M, Xu Y (2019) Effect of urbanisation on extreme precipitation based on nonstationary models in the Yangtze River Delta metropolitan region. *Sci Total Environ* 673:64–73
26. Pei F, Liu X (2018) Detection and attribution of extreme precipitation changes from 1961 to 2012 in the Yangtze River Delta in China. *CATENA* 169:183–194
27. Wang Y, Zhang N, Wang D, Wu J (2020) Impacts of cascade reservoirs on Yangtze River water temperature: assessment and ecological implications. *J Hydrol* 590:125240
28. Ban X, Chen S, Pan BZ (2017) The eco-hydrologic influence of the three Gorges Reservoir on the abundance of larval fish of four carp species in the Yangtze River, China. *Ecohydrology* 10:e1763
29. Wang Y, Rhoads BL, Wang D (2016) Assessment of the flow regime alterations in the middle reach of the Yangtze River associated with dam construction: potential ecological implications. *Hydrol Process* 30:3949–3966
30. Wang Y, Zhang N, Wang D, Wu J, Zhang X (2018) Investigating the impacts of cascade hydropower development on the natural flow regime in the Yangtze River, China. *Sci Total Environ* 624:1187–1194
31. Su C, Chen X (2019) Assessing the effects of reservoirs on extreme flows using nonstationary flood frequency models with the modified reservoir index as a covariate. *Adv Water Resour* 124:29–40
32. Meng-Bo S, Tai-Xing L, Ji-qin (2012) Preliminary analysis of precipitation runoff features in the Jinsha River Basin. *Proc Eng* 28:688–695
33. Wang G (2018) Potential relationships between the river discharge and the precipitation in the Jinsha River basin, China. *E&ES* 121:052011
34. Wu L, Long T-Y, Liu X, Guo JS (2012) Impacts of climate and land-use changes on the migration of non-point source nitrogen and phosphorus during rainfall-runoff in the Jialing River Watershed, China. *J Hydrol* 475:26–41
35. Zhang S, Liu Y, Wang T (2014) How land use change contributes to reducing soil erosion in the Jialing River Basin, China. *Agric Water Manag* 133:65–73
36. Zhou Y, Li D (2020) Distinguishing the multiple controls on the decreased sediment flux in the Jialing River basin of the Yangtze River, Southwestern China. *Catena* 193:104593
37. Zhang L, Liu S (2016) Using DEM to predict *Abies faxoniana* and *Quercus aquifolioides* distributions in the upstream catchment basin of the Min River in southwest China. *Ecol Ind* 69:91–99
38. Su J, Li H, Zhu Y, Cui Y, Wang X (2019) Evaluating the hydrological utility of latest IMERG products over the Upper Huaihe River Basin, China. *Atmos Res* 225:17–29
39. Bowman KP (2005) Comparison of TRMM precipitation retrievals with rain gauge data from ocean buoys. *J Clim* 18:178–190

40. Da Silva RM, Santos CA (2015) Rainfall and river flow trends using Mann-Kendall and Sen's slope estimator statistical tests in the Cobres River basin. *Nat Hazards* 77:1205–1221
41. Kendall M, Gibbons J (1990) Rank correlation methods. Oxford University Press, London
42. Mann HB (1945) Nonparametric tests against trend. *Econ J Econ Soc* 245–259

Impact of Climate Changes and Landuse/Land Cover Changes on Water Resources in Malaysia



Hadi Hamaaziz Muhammed, Nuraddeen Mukhtar Nasidi,
and Aimrun Wayayok

Abstract This study explored various research conducted on the impact of climate change, land use, and cover change (LULC) on Malaysia's availability of water resources. The country has abundant surface water reservoirs with adequate annual rainfall, which has been projected to be higher in the future. However, climate change and LULC have been global issues with consequences on water resources everywhere. The rate of rainfall erosivity in Malaysia was increased considerably as climate change continued increase caused by global warming. Several parts of the country have reported cases of increasing flash floods and soil degradations such as soil erosion and sedimentation. Moreover, the LULC has shown a serious effect on water availability for domestic uses in several regions of the country. For instance, Selangor has consumed the largest volume of water in excess of about 4,000 MLD, which has been increasing on an annual basis. However, the supply has no longer meet the water demand with occasional interruptions due to sudden water pollution. This phenomenon has been attributed to variation in climate parameters, leading to frequent occurrences of flash flood, severe soil erosion, and sedimentation. Ultimately, the domestic water supplies are affected which depend mainly on river water resources and thus, changes in climate will indirectly influence the resident and industrial water supplies. Additionally, LULC has indicated that more lands are highly becoming erosion potentials by surface exposure due to conversion of forestlands to other forms of land use such as agriculture and developments. The combined effect of climate change and LULC is undoubtedly increasing soil erosion and sedimentation

H. H. Muhammed (✉)

Faculty of Agricultural Sciences and Landscape Architecture, Osnabrück University of Applied Sciences, 49076 Osnabrück, Germany
e-mail: h.muhammed@hs-osnabrueck.de

N. M. Nasidi

Department of Agricultural and Environmental Engineering, Faculty of Engineering, Bayero University Kano, PMB 3011 Kano, Nigeria

N. M. Nasidi · A. Wayayok

Department of Biological and Agricultural Engineering, Faculty of Engineering, Universiti Putra Malaysia, 43400 Selangor, Malaysia

© The Author(s), under exclusive license to Springer Nature Switzerland AG 2022

465

A. M. F. Al-Quraishi et al. (eds.), *Environmental Degradation in Asia*,
Earth and Environmental Sciences Library,
https://doi.org/10.1007/978-3-031-12112-8_21

of water reservoirs. Thereby, causing water quality deterioration and reducing water storage volumes by reducing water reservoirs' carrying capacities.

Keywords Flash flood · Climate change · Water quality · Lan use change · Sedimentation · Water availability

1 Introduction

Climate change and land-use change are among the significant factors influencing water resources and the regional hydrological cycle. Change of land use affects water resources quality, availability and hydrological processes by changing surface roughness, canopy cover, soil properties, and rate of evapotranspiration, whereas change in climate alters main components of hydrological cycle such as evaporation, precipitation, groundwater availability, soil moisture, quantity and timing of runoff [1]. Understanding the possible implications of land use change and climate change on water quantity and quality on a regional scale is critical for long-term water resource management and planning. Land use and climate change's hydrological implications have received growing attention from water resources experts and decision-makers as water scarcity, droughts, and floods have become more common [2]. Alteration in the local and regional hydrological cycle may increase intensity and frequency of storms, floods, and droughts [3]. It is critical to dynamically evaluate the simultaneous hydrological effects of land use change and climate change in order to optimally manage the quantity and quality of water resources in response to development and population growth. This will further help to optimally manage quantity and quality of water resources in response to development and population growth.

In a worldwide setting, there is a growing interest in understanding how land use change and climate change affect water supplies, including in Malaysia. Malaysia is a country in Southeast Asia that is divided into two regions: Malaysian Borneo and Peninsular Malaysia. In 2017, the country's population was predicted to be over 32 million people, with a total land area of 330, 803 km² [4]. Because of anthropogenic activities such as urbanization, agricultural growth, and deforestation, Malaysia has seen significant land use and cover changes. Furthermore, the country has an equatorial climate characterized by hot and humid weather throughout the year, as well as rainfall inconsistencies in recent decades. As a result, various research on the effects of land use change, climate change, and both land use change and climate change on water resources in Malaysia have been done Tang [3] and Tan et al. [4]. According to Nainar et al. [5], the forest catchment converted to oil palm catchment exhibited highly variable discharge, quick reactions during storm events, but extremely low baseflow at all times. According to the study, the primary forests also supported the highest stream baseflow and good runoff control. Another study by Saadatkah et al. [6] found that the increase in severe water flow in the Kelantan River basin is a result of urbanization and the conversion of forest lands to low-canopy

plantations like oil palm, rubber, and mixed agriculture. Malaysian rivers have also been contaminated as a result of increased industrial growth, forest degradation, and agricultural expansion, resulting in unregulated and uncontrollable LULC. As a result, ongoing developments have resulted in a worsening of water quality [7]. According to Camara et al. [8], agricultural and logging activities had a greater impact on water quality due to their significant positive correlation with chemical and physical indicators of water quality, whereas urbanization had a greater impact on water quality due to changes in hydrological processes such as erosion and runoff. In addition to the effects of land use change and climate change, studies of the combined effects of land use and climate change on Malaysia's water resources have been conducted. Tan et al. [3] investigated the effects of land use change and climate change on the hydrological components of the Johor River basin. The authors determined that the combined effects of land use and climate change cause an increase of 4.4 and 1.2% in annual streamflow and evaporation, respectively. Adnan and Atkinson [9] discovered that climate and land use change enhanced streamflow in the wet season and lowered streamflow in the dry season in the Kelantan River basin.

The fundamental motivation for this research is that climate change and anthropogenic activities such as deforestation, agricultural development, and urbanization have continually worsened the state of Malaysia's lands and water resources throughout the country. Despite the fact that there has been a lot of study done to address the issues described above, this review was important to incorporate the major findings of the previous studies to help policymakers identify specific basins that need to be improved and prioritized. As a result, this review aims to highlight the most recent trends and potential impacts of land use change, climate change, and combined land use and climate change impacts on water quantity and quality in various parts of Malaysia and identify the major sources of water resource degradation. Based on the current study's findings, the review also suggests mitigation and adaptation strategies for managing water resources.

2 Impact of Climate Changes on Malaysian Water Resources

2.1 Introduction to Climate Change

The climate system results from a complex interrelation of atmosphere, ocean, land surfaces, cryosphere, biosphere and lithosphere [10, 11]. The cryosphere comprises land surface covered by ices (ice shelves and glaciers), snow and sea ice. The biosphere refers to all living organisms on the planet that spread throughout the ocean and land surfaces. The role of land surfaces as a climate system component is more pronounced by major impacts of green vegetation. The solid earth portion is regarded as lithosphere which facilitates the distribution of ocean basins, mountain ranges, including the incidence of volcanic eruption [12]. The chemical composition

in the atmosphere can be considered as component of climate change. Both internal undercurrent and external factors influence climate system. The forcing mechanisms usually refer to external factors, including natural phenomena such as volcanic eruptions, solar variations, and human-induced factors. Human factors include continuous burning of fossil fuels and the depleting natural vegetation cover, both actions lead to changes in atmospheric composition. The amount of solar radiation entering the earth's atmosphere and surface has been in balance with the amount of energy emitted. The latter is made up of shortwave and longwave components in each case. Meanwhile, the earth's surface absorbs roughly half of the incoming radiation; this energy is transported back to the atmosphere, warming the air in contact with the surface (sensitivity heat), evaporating water (latent heat), or absorbed by clouds and green gases. Long wave energy is eventually radiated back to the planet as well as out into space by the atmosphere [13].

Nowadays, climate change is one of the most severe challenges facing humanity around the world [14, 15]. This problem drew the attention of international and multidisciplinary researchers and organizations to direct their efforts towards global environmental sustainability. Among these organizations are Intergovernmental Panel for Climate Change (IPCC), United Nation Environment Program (UNEP) and World Metrological Organization (WMO). The main objective of establishing these organizations was to provide the world with clear idea of current knowledge on climate change and its potential impact on the environment and global socioeconomic activities. Both global and regional climate changes are complex phenomenon which human activities are the major influencing factors for their changes [10]. The studies conducted by IPCC working groups show that, change in climate have indicated positive and negative consequences in future. However, the negative effect will prevail with large rates of climate change to be observed globally. Among the anticipated adverse impacts of climate change are excessive changes in extreme rainfall and temperature events [16]. Moreover, the patterns in some climate system variables were expected to include more hot days and heat waves in some regions, while in other regions, there were fewer cold days and cold waves. Eventually, it may lead to rise in global precipitation, a greater number of severe events (flood and drought) and a catastrophic overall ecosystem [12]. There are clear convictions that the global environment is already changing and that more changes are inevitable. For example, the average global temperature rose by about 0.74 °C over the last century from 1906 to 2005 [16].

The IPCC recently released studies that showed solid evidence of rising global average sea level. The melting of snow cover and mountain glaciers is thought to have caused a total worldwide mean sea level rise of 12.22 cm during the twentieth century [17]. It was also discovered that there have been changes in the amount, intensity, frequency, and types of precipitation over the last century [18]. Furthermore, it was predicted that by the year 2100, the earth's surface temperature is expected to rise by 1.1–6.4 °C. Latest evidence has revealed that the climate system has been steadily heating since the 1950s, with more spectacular observable changes spanning decades to millennia.

Similarly, increased warming has been observed in both temperature and ocean water while the amount of snow and ice have reduced and both sea level and concentration of GHG have increased. In addition, the earth has been successively warmer in each of the last three decades at the surface of the earth than any preceding decade since the year 1850. Energy stored in the climate system has been dominated by ocean warming, accounting for more than 90% of the energy accumulated between the year 1971 and the year 2010 [19]. Recent studies have shown that, there have been reductions in the mass of the Greenland and Antarctica ice sheets during the last two decades. This indicates a worldwide shrinkage of glacier with both Arctic Sea ice and Northern Hemisphere spring snow cover have continued to reduce in sizes. Similarly, the rate of sea level rise since the mid-nineteenth century has been larger than the mean rate during the two previous millennia.

Carbon dioxide (CO₂), methane (CH₄), and nitrogenous oxide (NO₂) concentrations in the atmosphere have also surged to levels not seen in at least 800,000 years. Carbon dioxide concentrations have risen by 40% from pre-industrial times, owing largely to fossil fuel emissions. Although the ocean absorbed around 30% of the produced anthropogenic carbon dioxide, the alterations have triggered land use emissions changes, leading to ocean acidification [20]. Natural and manufactured chemicals and processes that modify the earth's energy budget are main component climate change drivers [14]. According to Nasidi et al. [21], climate drivers are the elements that contribute to GHG emissions directly or indirectly. Interaction of the climate system components can lead to important climate processes. This may lead to a possible imbalance in the earth ecosystem with a global consequence requiring other components to respond accordingly.

2.2 Impact of Climate Change on Water Resources in Malaysia

Several studies were conducted with respect to climate change, land use/cover change (LULC), and available water resources. These studies have revealed changes in climate variables, increased rainfall frequency and expansion of surface water storage. For example, Amin et al. [22] reported an increase in future temperature of Malaysia by 36.3% from baseline condition for the twenty-first century with a corresponding change in precipitation of 45.4% due to climate change. This agrees with Tan and Nying [23] where high temperature and precipitation are projected to occur due to climate change at Pahang in 2069 period. The study also highlighted the need to follow management control guidelines to curtail erosion and landslide problems that affect water resources quality. Moreover, earlier studies have reported the significance of restricting any unsustainable agriculture practice because of its severe impacts on the environment, wildlife, tourism, and humans. Their impacts are further impinging on quality and quantity of water supplies from upstream down to the surrounding lowlands regions of Malaysia. Similarly, Razali et al. [24] conducted

review on land use change in highlands and its impact on river water quality and reported considerable water quality deterioration due to change of land use which largely caused by development and agriculture activities.

2.3 Water Quality and Quantity Changes Due to Climate Change

Peninsular Malaysia has a rich network of rivers and streams that produce approximately 150 major river basins. The Pahang River is the longest, running for 434 km before reaching the South China Sea. The drainage catchment area is approximately 29,000 km². The Kelantan, Terengganu, Dungun, Endau, and Sedili rivers all drain into the South China Sea in a similar manner [25]. The major river basins in the east of Malaysia are larger than those in Peninsular Malaysia. The Rajang River in Sarawak, eastern Malaysia, has the longest river in the country at 563 km. The quality and quantity of water in these rivers kept changing over considerable time [26, 27]. Climate change has significantly affected the variability of water received from the atmosphere, consequently influencing environmental sustainability.

Similarly, the quality of available water has been affected considerably that causes intermittent disruption of domestic water supply in several states, for example Selangor and Kedah [28]. Nasidi et al. [18] reported that increased rainfall in most parts of Malaysia is the main reason for increasing water contamination from high inflow of soil erosion and sedimentation. The study has further connected high erosive rainfall with influence of climate change on climate variables. Thus, it leads to increasing contamination of surface water storage such as dams and riverbanks. Consequently, affect the quality of domestic water supply in most towns and cities of Malaysia. Furthermore, Ismail [28] assessed the availability of water resources in Perak which shared a boundary with Pahang from west and correlated it with land degradation. The results showed a clear agreement between the volume of water received and soil erosion. Abdullah et al. [27] has further evaluated the rainfall received in Pahang state of Malaysia and found the average rainfall received has been increased by 26% of the past three decades. The disadvantage of this study is that, since erosivity is reported yearly, two months erosivity is insufficient to conclude soil erosion for a particular study location.

For instance, Nasidi et al. [26] conducted a study on the impact of climate change on erosion severity, water resources, and corresponding area coverage under different emission scenarios (Fig. 1). The study selected two future periods for the impact assessment (2050s and 2080s). The results revealed a progressive increase in degree of erosion which translates into high rate of water contamination. Reference with baseline period (1976–2005), future scenarios indicate more areas to be affected by high soil erosion intensities under each Representative Concentration Pathway (RCP). In addition, high area extent was found to experience more intense soil degradation and water contamination in 2080s than the corresponding period in 2050s.

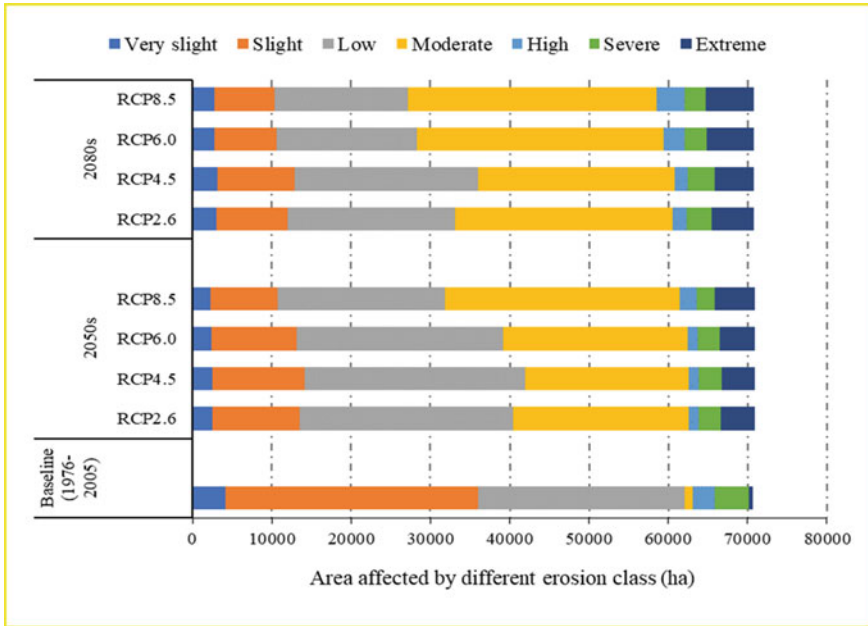


Fig. 1 Soil erosion severity change due to climate change [18]

However, both climate change projection periods have shown considerable increase of soil erosion relative to the baseline condition.

However, the demand for water use in Malaysia rises annually due to a rise in population and economic growth, resulting in a water deficit experienced since 2010. Perlis, Kedah, Pulau Pinang, Selangor, and Melaka are among the states in Peninsular Malaysia that are affected [25]. In 2010, severe water scarcity was recorded in Kedah and Selangor, with deficits of 1,852 Mm³ and 1,278 Mm³, respectively. Water shortfalls are expected to rise until 2050, according to projections. According to the Water Resources Study undertaken for the period 2015–2050, the Northern States, especially Perlis, Kedah, and Penang, have been experiencing water shortages of around 246–221 Mm³. Selangor and Melaka are next, with estimates of over 1,000 Mm³ and about 200–336 Mm³ respectively. Despite the fact that Selangor’s population has been growing over the years, the state faced a water crisis in 2014 due to a drought season that led the dam level to drop. The main factor responsible for this scarcity of water resources was attributed to the climate change. Figure 2 shows change of domestic water consumption in Malaysia in million liters per day (MLD). With the increase in climate variability, these figures might have increased by now and will continue to increase.

Moreover, roughly 360 km³ of the entire annual rainfall volume of 990 km³ is lost to evapotranspiration [25]. Similarly, total surface runoff is 566 km³, and groundwater recharge is about 64 km³ (about 7% of total annual rainfall). Despite this, about 80%

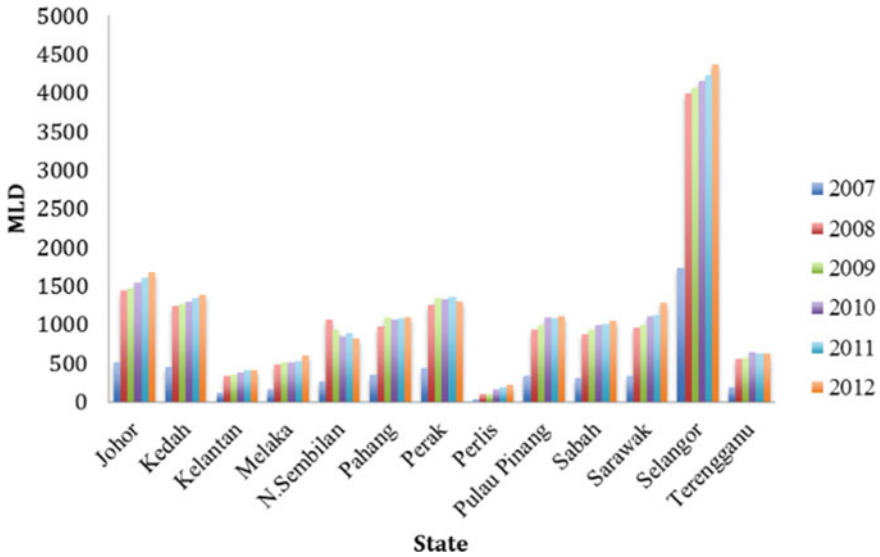


Fig. 2 Water resources in Malaysia from 2007–2012 [25]

of groundwater is returned to rivers and is not considered a separate resource. As a result, Malaysia’s total internal water resources are projected to be 580 km³ per year.

2.4 Factors Affecting Water Demand and Supply in Malaysia

Globally, studies have reported that climate change influences the demand and supply of water e.g. [29–31]. Similarly, according to a Malaysian assessment, climate change is a major contributor to changes in water demand and supply, including reservoir operations, water quality, hydroelectric generation, and navigation [18, 25]. During dry seasons, the demand for water in agriculture activities tends to increase. As a result of climate change, water supplies are becoming increasingly scarce and expensive. Population, affluence, as well as the expansion of the ecology system and recreational usage, all influence water demand. As a result, water consumption efficiency must strike a balance between water supply constraints and rising demand.

3 Land Use Change Impacts on Quality and Quantity of Water

3.1 Land Use Change Trends and Implications

Land use and land cover change (LULC) management is still a major environmental issue that society must solve. LULC is one of the key causes of environmental change, with substantial consequences for human livelihoods, in addition to ecosystem fragility. Hydrological, climatological, and biodiversity responses all show such changes [32]. Over the world, expansion of cropland and urban areas is at the expense of forest and grasslands [33]. LULC change is one of the important driving factors forcing environmental changes at spatiotemporal scales, significantly contributing to earth surface processes and forest fragmentations. In addition, the hydrological response of watershed is notably changed due to LULC alterations [34]. An example of this phenomenon is a study by Gyamfi et al. [35] who reported that groundwater flow is higher and surface runoff is lower in the vegetative lands due to the greater percolation of rainfall into the shallow and deep aquifer. While vegetation is absent in the cleared lands, groundwater flow is lower and surface runoff is higher. Urbanization, deforestation, and other human land use activities can significantly change seasonal and annual distribution of stream flow. Understanding how these changes impact water quantity will enable policymakers and planners to formulate plans towards minimizing the negative effects of projected land use changes on runoff rate and stream flow patterns. The situation is more critical in high rainfall regions like Malaysia [36].

In Malaysia, population growth and human activities have increased pressure on land, forests, and water resources causing misuse of the land use. In the last decades, Malaysia has experienced intensified and rapid urbanization since its independence because of high economic growth [37]. Agricultural productions are still critical to the country's economic development, even though the country's development policy has shifted from the agricultural to the manufacturing sectors since the 1980s [38]. Consequently, most of the forestland has been turned to cropland, especially oil palm and rubber plantations. Furthermore, the development of wood and non-timber resources that provide the country with socio-economic benefits has resulted in the loss of most of Malaysia's forested land (Table 1). The land use change trends of intensified rubber and oil palm crops over the last century have altered the features of Malaysia's landscape. Accordingly, forest land has been converted to rubber and oil palm lands until the mid of 1990s, thereafter not only forest land rather rubber and oil palm plantation areas were converted to urban and built-up areas due to industrialization in the region [39]. These findings revealed that the rapid industrial development remarkably increased the rate of urban and built-up area. Such fragmentation, landscape pattern changes and heterogeneity have affected the integrity of different ecological systems including water quantity and quality. Several studies such as Olaniyi et al. [40] and Pourebrahim et al. [41] have confirmed that land use transition was made in Malaysia mainly due to agricultural productions up to

Table 1 A summary of numerous studies conducted on land use/cover change extent in various parts of Malaysia

Target	Observations/results	Location	Studies
Hydrologic characteristics and land use assessment	Built-up and oil palm area were increased at the expense of forest area	Tasik Chini's Feeder Rivers/Pahang	[36]
Changes in agricultural landscape pattern and its relationship with forestland	(1966–1981) the total area of oil palm was increased 4.7% per year, while total area of forest declined 0.2% per year	Selangor, Peninsular	[38]
Generating insights on the changing process of land use/land cover and landscape pattern	(1966–1995) the total area of oil palm plantation was increased from 866 (ha) to 6967 (ha), while total area of forests was reduced from 2137 (ha) to 2087 (ha)	Selangor State	[42]
Relationship between landscape pattern and landscape type response to changes in land use	Recently, land use conversion has been more associated with urbanization than using to crop lands	Selangor State	[39]
Assessment of Drivers of Coastal Land Use Change	Between (1980–2000) Urbanized area was increased from 26.1% to 33.7% whereas mangrove forested area was increased by 4.6%	Perak State	[40]
Land cover and industrial plantation distribution in The Peatlands of Peninsular Malaysia, Sumatra, and Borneo	Between (2007–2015) deforestation rate of 4.1% per year was performed. Industrial plantation was the major reason for the change	Sarawak State	[43]
Determination of land cover changes in the city of Seremban	Between (1990–2010) non-vegetative land was increased from 3.55 to 7.25%	Negeri Sembilan State	[44]

1990s. Afterward, land cover changes were attributed to urbanization and the industrial sector development. All the studies in the (Table 1) concluded that urbanized area and industrial plantation are the two main driving factors contributing to forest clearance and land use change.

3.2 Water Quantity Response to Land Use Change

When local and regional development rise, land use and land cover shift as well. Such changes are increasingly influencing the hydrological process, resulting in water yields, streamflow, surface runoff, flow regimes, soil moisture, and evapotranspiration [44]. The land will become impervious when the forest takes over and vegetative

sections are converted to built-up areas. Furthermore, forested places differ from barren fields, short crops, and built-up areas in terms of roughness and morphology. Rainfall that falls in urban areas enters waterways quickly, creating stormwater runoff and erosion [45]. Malaysia's economic transformation from an agriculture-based to an industry-based economy has rapidly expanded in developed areas in recent years [46]. For example, in Peninsular Malaysia's peatlands, forest-dominated cover had decreased to 42% by 2007, although forest cutting rates had remained high. Over a quarter of peatlands had been converted to managed land use categories, resulting in lower water table levels (11% small-holder areas and 18% industrial plantations) as reported by Miettinen [43]. As a result, quantity of water resources in Malaysia has undergone remarkable alteration. Uncontrolled urban development has negatively affected Malaysia watershed ecosystems, in particular their capacity to regulate streamflow.

However, majority of the reports indicated that logging activities and conversion of natural forests to agricultural and urban lands are the key factors changing water quantity and increasing flood risks in various parts of Malaysia. As a result, several research on the effects of changing land use and land cover on water quantity and flood events have been done (eg. Saadatkhah et al. [6] and Mansor et al. [47]). The data demonstrated that conversion of forest land to agricultural and built-up areas increased surface runoff and stream flow, trends in water discharge, and upsurges in flood volume at the watershed scale. Groundwater flow and percolation reduced dramatically compared to surface water [3]. The fundamental cause of this phenomena is that forest cover areas have higher interception and infiltration rates than other managed land uses; thus, forest clearing can boost surface flow while decreasing groundwater flow. Based on the findings, it can be concluded that increased surface water flow was recorded in cleared fields and catchments with low-density vegetation, but low surface runoff was observed in basins with forest and secondary jungle. Furthermore, urbanization and deforestation, notably the transfer of forest lands to less densely wooded areas for rubber and oil palm plantations and mixed agriculture, were revealed to be responsible for the rise in surface water flow. Urban soils, on the other hand, have a superior impermeable ground surface due to the lower rate of infiltration and less/loss evapotranspiration, resulting in excess runoff volume [6].

Nevertheless, there are some other contradictory results about the influence of LULC on water quantity. For example, Adnan and Atkinson [9] conducted a study on exploring the impact of land use change on streamflow changes in Kelantan River. They found that deforestation and urbanized area increased streamflow, and consequently increased flood events in the wet season in the downstream catchment but decreased streamflow in the dry season. Furthermore, the findings from small catchments differed from those obtained from moderate and large catchments. Ngah and Reid [48] found that a moderate-sized catchment (1000 km²) is not straightforward and usually contradictory when compared to findings from other experimental catchments. Particularly those studies on impact of land use change on water yield in the Langat River basin in Selangor State and the Linggi River basin in Negeri Sembilan

State. Consequently, it may be deduced that forest area supports good runoff management and stream baseflow. On the other hand, urban and built-up regions enhance surface runoff and flood volume.

3.3 Land Use Change Impacts on Water Quality

Anthropogenic land use change negatively affects the conditions of water quality [7]. Transformation of grasslands and natural forests to croplands and built-up regions, combined with intensive agricultural activities and population increase, is a potential source of toxins from agricultural chemicals, urban sewage disposal, and landfill, all of which affect water quality [49]. Increased nitrate and nitrogen concentrations in surface and subsurface water have been a major source of concern in recent decades. This is because of a rapid agricultural, industrial, and urban development, which revealed a clear link between rising nitrate levels in water resources and increased human activities [50]. Changes in surface water quality are strongly linked to nearby land use, and the types and quantities of contaminants that flow into lakes, rivers, and aquifers are largely determined by the land use pattern [51]. Water quality is defined as a measurement of water utilization for a variety of purposes, including drinking, irrigation, industrial, recreation, and habitat, based on chemical, physical, and biological factors [52]. Water quality is extremely important to all living species on the planet. As a result, many scholars, policymakers, and water resource managers have taken notice of this viewpoint. The quality of water changes based on the time, place, climate, and pollution source. Water resources can be contaminated by point and non-point source (NPS) contamination [8]. Natural processes may cause NPS contamination, which cannot be completely avoided, but synthetic alterations can have a major impact on the rate of pollution at the source.

Pollution of water resources in Malaysia poses a severe threat to public health and the environment. According to a report published by the Department of Irrigation and Drainage in 2001 and quoted by Juahir et al. [52], about 60% of Malaysia's major rivers are regulated for domestic, industrial, and agricultural reasons. According to Rosnani [53], sewage disposal, industrial discharges, land clearance, and earthworks activities harm Malaysian rivers. Similarly, Juahir [52], 42% reported that the river basins were polluted with suspended solids (SS) from uncontrolled land use and land clearing, 30% with biological oxygen demand (BOD) from industrial discharges, and 28% with ammoniacal nitrogen (AN) from husbandry activities and urban sewage disposals in 1999. This finding showed that poorly planned land clearing activities polluted the majority of river basins (42%) the most. Numerous studies have been undertaken to investigate the impacts of land use change on water quality and their association with water quality indicators (Table 2). The findings from (Table 2) revealed that anthropogenic land use change has evidently affected water quality due to the rapid and continuous developments that Malaysia has been undergoing over the last decades. Thus, changes in landscape pattern by human developments are the source of water quality degradation in different water bodies

through different processes. In Malaysia, land use is categorized into three major types namely: dominated forest land use, agricultural land use, and urbanized lands.

Natural forests would have no major negative effects on water quality without anthropogenic activities. It is obvious that trees can help to preserve the quality of

Table 2 Impact of land use change on water quality in different regions of Malaysia

Location	Objectives	Observations/results	Studies
Cameron Highlands, Pahang State	To summarize the impacts of land use change, practices-policy-management of agriculture, and agro-tourism on water quality of the river system network	Outcomes from earlier studies have highlighted that the factors such as soil erosion, agriculture activities, landslides urbanization, and unplanned developments associated with land use change have notably affected the river water quality	[56]
Nerus River, Terengganu State	To assess response of water quality in Nerus River to land use and land cover characteristics	The relationship between water quality and land use change demonstrated that urbanization was a major factor affecting the river water quality, followed by horticultural activities in rural areas close to the rivers	[57]
Malacca River, Malacca State	To determine the connection of LULC changes in contributing to pollutant sources in the Malacca River	Urbanized area significantly polluted the water through E. coli, total coliform, EC, BOD, COD, TSS, Hg, Zn, and Fe, while cropland activities caused EC, TSS, salinity, E. coli, total coliform, arsenic, and Iron pollution	[7]
Pinang River, Keluang River, and Burung River, Penang State	To investigate the interaction of land use change and water quality in rivers in Penang Island and identify the pollution sources along the rivers	The overall results showed that total organic carbon (TOC) increased due to urban sewage in Pinang and Keluang Rivers, while TOC increased due to the paddy fields in Burung River	[58]
Sabah State	To evaluate the effects of various land uses on suspended sediment dynamics	The findings demonstrated that even multiple-logged forests have high value in conserving water quality and reducing erosion in hilly terrain, while oil palm cover requires careful land management	[59]

(continued)

Table 2 (continued)

Location	Objectives	Observations/results	Studies
The states of Kedah, Penang, and Perak	To study water quality status of rivers under different managed land use activities	The rivers with industrial land use setting showed the highest level of pollution, followed by rivers with plantation pollution, while recreational and less distributed rivers recorded the lowest level of pollution	[60]
Tanah Tinggi Lojing, Kelantan State	To discover the relationship between managed land uses and water quality status	The results pointed out that land use developments have affected the water quality parameters in the Tanah Tinggi Lojing area	[61]
Gombak River, Selangor State	To establish a link between water quality and land use characteristics	The findings revealed that as the amount of activity in the river watershed rose, the water quality index (WQI) value declined. Furthermore, the anticipated WQI revealed a steady decline in water quality	[62]

surface water. For example, in a study published by Nainar et al. [50], the rainforest was found to make a few noteworthy contributions to water quality and erosion reduction. Despite their importance in safeguarding water quality, forest areas are shrinking in Malaysia. This is primarily due to the conversion of forest lands to agricultural and urban development uses. As a result, the majority of the studies analyzed in this study focused on the effects of deforestation on Malaysian surface water quality. The association between land use change and water quality characteristics revealed a significant positive relationship between changes in chemical and physical water quality indicators and forest land use.

Furthermore, according to the findings summarized in this review, forest clearance can cause more salinity problems in river basins. Also, the sediment export and organic matter decomposition in streams, which can cause acidity issues in the basin, such as total acidity, low pH, and mobilization of dissolved heavy metals. The correlation analysis revealed a substantial positive link between increasing agricultural lands and physical and chemical water quality parameters in Malaysia. Water quality indicators (physical parameters such as temperature, electrical conductivity (EC), total suspended solids (TSS), turbidity, and total dissolved solids (TDS), as well as chemical parameters such as pH, biochemical oxygen demand (BOD), heavy metals, dissolved oxygen (DO), chemical oxygen demand (COD), and nitrate) have been the focus of major studies in Malaysia to address the impact of land use change on water quality. This is because these criteria are made up of elements used to establish the quality of various water bodies (lakes, rivers, and streams) in Malaysia

using the Malaysian Marine Water Quality Standards and Index, controlled by the Department of Environment [54].

Urbanization is another type of land use which affects water quality. Several researchers have investigated the effects of urbanized land on water quality over the last decade in Malaysia. Thus, urban land use as one of the forcing factors has been the focus of numerous studies (Table 2) in dealing with water quality status in the country. The findings of the reviewed reports in this study stated that the major sources of water quality degradation in built areas involve industrial, residential, and recreational activities. As a result, urban growth has become a key predictor of water quality changes in the water resources of Malaysia. A study by Azyana et al. [55] which was conducted on water quality degradation in the Kinta River, Perak State, the results showed that land development was the best indicator for water quality degradation. The overall results of the reviewed reports illustrated that logging activities and conversion of forest land to urban and agricultural land use are the main sources of water quality degradation in Malaysia. However, comprehending the correlation between land use change and water quality can facilitate viable management of the major sources of water deterioration and the processes involved in assessing water quality status.

4 Conclusions

Malaysia is blessed with a high annual rainfall amount in almost all the regions of the country. However, studies have revealed the considerable impact of climate change on the quantity and quality of the available water resources. The climate change, which is caused by global warming, has limited the water availability for domestic uses in several regions. Many catchments are found to have higher rainfall characteristics with raise in temperatures. These increments in climate variables could lead to extreme events that cause flash flood and severe drought incidents. Since, the domestic water supplies are relying on river water resources, changes in climate will greatly influence the resident and industrial water supplies due to variation of both water quantity and quality. Moreover, land degradation is also bound to occur such as soil erosion at higher rates when rainfall erosivity is higher due to climate change.

Consequently, the higher rates of both erosion and sedimentations will directly affect the quality of river waters. In addition, higher sedimentation will eventually lead to the reduced river carrying capacity and, hence, reduces the river's water quantity or flow rates. Furthermore, this study found that the LULC due to anthropogenic activities has directly contributed to the change in quantity and quality of water resources in Malaysia. Also, the rate of deforestation for residential development showed an increasing trend, affecting the quality of river water.

5 Recommendations

1. Anthropogenic activities (e.g. deforestation, agricultural activities, residential developments, mining, landscape reforming-cutting hills, etc.) are the major causes of climate change. Optimization of these activities and recovery process such as reforestation should be emphasized to overcome the issues of human activities that trigger or induce land use and climate changes.
2. Future LULC requires proper planning, especially on expanding residential area and agricultural land for food production. Any developments should consider a conservative aspect to determine the consequences on the water resources.
3. Enforcement and campaign on the implementation of Best Management Practices (BMPs) for land use and water resources management to all stakeholders are important mechanisms to ensure that they are protected and conserved.
4. Wise management of the land and water resources by all stakeholders including the authorities and societies is necessary to ensure that it does not induce the climate change and interrupt water resources both in terms of flow quantity and river quality.
5. More studies and implementation of Integrated River Basin Management (IRBM) by the relevant authorities could minimize the effect of LULC and climate changes on water quantity and quality.

Acknowledgements This work is fully funded by the Universiti Putra Malaysia grant number UPM/800-4/11/MRUN/2018/5539220.

References

1. Wang S, Zhang Z, McVicar TR, Guo J, Tang Y, Yao A (2013) Isolating the impacts of climate change and land use change on decadal streamflow variation: Assessing three complementary approaches. *J Hydrol* 507(1):63–74
2. McVicar TR (2007) Developing a decision support tool for China's re-vegetation program: simulating regional impacts of afforestation on average annual streamflow in the Loess Plateau. *For Ecol Manage* 251(2):65–81
3. Tan ML, Ibrahim AL, Yusop Z, Duan Z, Ling L (2015) Impacts of land-use and climate variability on hydrological components in the Johor River basin, Malaysia. *Hydrol Sci J* 60(5):873–889
4. Tang KHD (2019) Climate change in Malaysia: trends, contributors, impacts, mitigation and adaptations. *Sci Total Environ* 65(1):1858–1871
5. Nainar A (2018) Hydrological dynamics of tropical streams on a gradient of land-use disturbance and recovery: a multi-catchment experiment. *J Hydrol* 566:581–594
6. Saadatkhah N, Tehrani MH, Mansor S, Khuzaimah Z, Kassim A, Saadatkhah R (2016) Impact assessment of land cover changes on the runoff changes on the extreme flood events in the Kelantan River basin. *Arab J Geosci* 9(17):687
7. Hua AK (2017) Land use land cover changes in detection of water quality: a study based on remote sensing and multivariate statistics. *J Environ Pub Health* 23(1):23p

8. Camara M, Jamil NR, Abdullah AFB (2019) Impact of land uses on water quality in Malaysia: a review. *Ecol Process* 8(1):10
9. Adnan NA, Atkinson PM (2011) Exploring the impact of climate and land use changes on streamflow trends in a monsoon catchment. *Int J Climatol* 31(6):815–831
10. Nasidi NM, Aimrun W, Abdullah AF, Kassim MSK (2020). Dynamics of potential precipitation under climate change scenarios at Cameron highlands, Malaysia. *SN Appl Sci*. Springer Nature
11. Neelin JD (2011) *Climate change and climate modeling*. Cambridge University Press 978-0-521-84157-3
12. Stocker TF (2014) *Climate change—the physical science basis*, vol 9781107057. Cambridge University Press, Cambridge
13. Amirabadizadeh M, Huang YF, Lee TS (2015) Recent trends in temperature and precipitation in the Langat River Basin, Malaysia. *Adv. Meteorol.* 3(2):1–16. <https://doi.org/10.1155/2015/579437>
14. Viola MR, De Mello CR, Chou SC, Yanagi SN, Gomes JL (2015) Assessing climate change impacts on Upper Grande River Basin hydrology. *Southeast Brazil* 1068(1):1054–1068. <https://doi.org/10.1002/joc.4038>
15. Markus M, Angel J, Wang K, Byard G, Mcconkey S, Zaloudek Z (2017) Impacts of potential future climate change on the expected frequency of extreme rainfall events in Cook, DuPage, Lake, Northeastern Illinois
16. IPCC (2014) *Climate change: synthesis report*. In: Contribution of working groups I, II and III to the fifth assessment report of the intergovernmental panel on climate change IPCC, Geneva, Switzerland
17. Azim F, Shakir AS, Habibur-Rehman KA (2016) Impact of climate change on sediment yield for Naran watershed, Pakistan. *Int J Sediment Res* 31(3):212–219. <https://doi.org/10.1016/j.ijsrc.2015.08.002>
18. Nasidi NM, Wayayok A, Abdullah AF, Kassim MSM (2020a) Spatio-temporal dynamics of rainfall erosivity due to climate change in Cameron Highlands, Malaysia, *Model Earth Syst Environ*. <https://doi.org/10.1007/s40808-020-00917-4>
19. Litschert SE, Theobald DM, Brown TC (2014) Effects of climate change and wildfire on soil loss in the Southern Rockies Ecoregion. *CATENA* 18:206–219. <https://doi.org/10.1016/j.catena.01.007>
20. IPCC (2013) Summary for policymakers. In: *Climate change 2013: the physical science basis, contribution of working group I to the fifth assessment report of the intergovernmental panel on climate change*, Cambridge University, UK
21. Nasidi NM, Aimrun W, Abdullah AF, Kassim MSK (2020) Vulnerability of potential soil erosion and risk assessment at hilly farms using InSAR technology. *Algerian J Eng Technol*. <https://doi.org/10.5281/zenodo.3841100>
22. Amin IMZBM, Ercan A, Ishida K, Kavvas ML, Chen ZQ, Jang SH (2019) Impacts of climate change on the hydro-climate of peninsular Malaysia. *Water (Switzerland)* 11(9):1798. <https://doi.org/10.3390/w11091798>
23. Tan KW, Nying LP (2017) Climate change assessment on rainfall and temperature in Cameron Highlands, Malaysia using Regional Climate. *Carpathian J Earth Environ Sci* 12(2):413–421
24. Razali A, Syed Ismail SN, Awang S, Praveena SM, Zainal AE (2018) Land use change in highland area and its impact on river water quality: a review of case studies in Malaysia. *Ecol Process* 7(1):19. <https://doi.org/10.1186/s13717-018-0126-8>
25. Anang Z, Padli J, Kamaludin M, Sathasivam S (2015) The effect of climate change on water resources using panel approach: the case of Malaysia. *Int J Acad Res Bus Soc Sci* 7:11. <https://doi.org/10.6007/ijarbss/v7-i11/3446>
26. Nasidi NM, Aimrun W, Abdullah AF, Kassim MSK (2020) Susceptibility to soil erosion and risk assessment at hilly farms using geospatial techniques. *J Eng Technol Appl Phys* 2(1):6–13. <https://doi.org/10.33093/jetap.2020.x1.2>
27. Abdullah AF, Wayayok A, Nasidi NM, Hazari SAF, Sidek LM, Selamat Z (2019) Modelling erosion and landslides induced by farming activities at hilly farms. *J Teknol* 6:195–204

28. Ismail H, Rowshon MK, Hin LS, Abdullah AFB, Nasidi NM (2020) Assessment of climate change impact on future streamflow at Bernam river basin Malaysia. *IOP Conf Ser Earth Environ Sci* 540:12–40. <https://doi.org/10.1088/1755-1315/540/1/012040>
29. Kang Y, Khan S, Ma X (2009) Climate change impacts on crop yield, crop water productivity and food security. *Prog Nat Sci* 19(12):1665–1674. <https://doi.org/10.1016/j.pnsc.2009.08.001>
30. Shanono NJ, Nasidi NM, Maina MM, Bello MM, Ibrahim A, Umar SI, Usman IMT, Zakari MD (2019) Socio-hydrological study of water users' perceptions on the management of irrigation schemes at Tomas irrigation project. *Kano, Nigeria* 5(2):139–145
31. Chen Y, Zhang Z, Tao F (2018) Impacts of climate change and climate extremes on major crops productivity in China at a global warming of 1.5 and 2.0 °C. *Earth Syst Dyn* 9 (2):543–562. <https://doi.org/10.5194/esd-9-543>
32. Guzha A, Rufino MC, Okoth S, Jacobs S, Nóbrega R (2018) Impacts of land use and land cover change on surface runoff, discharge and low flows: evidence from East Africa. *J Hydrol Reg Stud* 15:49–67
33. Gashaw T, Tulu T, Argaw M, Worqlul AW (2018) Modeling the hydrological impacts of land use/land cover changes in the Andassa watershed. *Blue Nile Basin, Ethiop, Sci Total Environ* 61(9):1394–1408
34. Gebremicael T, Mohamed Y, Betrie G, Van der Zaag P, Teferi E (2013) Trend analysis of runoff and sediment fluxes in the Upper Blue Nile basin: a combined analysis of statistical tests, physically-based models and landuse maps. *J Hydrol* 48(2):57–68
35. Gyamfi C, Ndambuki JM, Salim RW (2016) Hydrological responses to land use/cover changes in the Olifants Basin. *South Africa, Water* 8(12):588–603
36. Mustafa Y, Amin M, Lee T, Shariff A (2012) Evaluation of land development impact on a tropical watershed hydrology using remote sensing and GIS. *J Spat Hydrol* 5(2)
37. Ngah M, Othman Z (2012) Impact of land development on water quantity and water quality in Peninsular Malaysia. *Malays J Environ Manag* 12(1):113–120
38. Abdullah SA, Nakagoshi N (2008) Changes in agricultural landscape pattern and its spatial relationship with forestland in the State of Selangor, Peninsular Malaysia. *Landsc Urban Plan* 87(2):147–155
39. Abdullah SA, Nakagoshi N (2006) Changes in landscape spatial pattern in the highly developing state of Selangor, Peninsular Malaysia. *Landsc Urban Plan* 77(3):263–275
40. Olaniyi A, Abdullah A, Ramli M, Alias M (2012) Assessment of drivers of coastal land use change in Malaysia. *Ocean Coast Manag* 67(1):113–123
41. Pourebrahim S, Hadipour M, Mokhtar MB (2015) Impact assessment of rapid development on land use changes in coastal areas; case of Kuala Langat district, Malaysia. *Environ Dev Sustain* 17(5):1003–1016
42. Abdullah SA, Hezri AA (2008) From forest landscape to agricultural landscape in the developing tropical country of Malaysia: pattern, process, and their significance on policy. *Environ Manage* 42(5):907–917
43. Miettinen J, Shi C, Liew SC (2015) Land cover distribution in the peatlands of Peninsular Malaysia, Sumatra and Borneo in 2015 with changes since 1990. *Glob Ecol Conserv* 6:67–78
44. Aburas MM, Abdullah SH, Ramli MF, Ash'aari ZH, (2015) Measuring land cover change in Seremban, Malaysia using NDVI index. *Procedia Environ Sci* 30:238–243
45. Sikka A, Samra J, Sharda V, Samraj P, Lakshmanan V (2003) Low flow and high flow responses to converting natural grassland into bluegum (*Eucalyptus globulus*) in Nilgiris watersheds of South India. *J Hydrol* 270(2):12–26
46. Nourqolipour R (2015) Multi-objective-based modeling for land use change analysis in the South West of Selangor, Malaysia. *Environ Earth Sci* 74(5):4133–4143
47. Mansor S, Saadatkhah N, Khuzaimah Z, Asmat A, Adnan NA, Adam SN (2018) Regional modelling of rainfall-induced runoff using hydrological model by incorporating plant cover effects: case study in Kelantan. *Malays, Nat Hazards* 93(2):739–764
48. Ngah MS, Reid I (2010) The impact of land use change on water yield: the case study of three selected urbanised and newly urbanised catchments in Peninsular Malaysia, in land degradation and desertification: assessment. *Mitig Remediat* 1:347–354

49. Fletcher TD, Andrieu H, Hamel P (2013) Understanding, management and modelling of urban hydrology and its consequences for receiving waters: a state of the art. *Adv Water Resour* 51:261–279
50. Narany TS, Aris AZ, Sefie A, Keesstra S (2017) Detecting and predicting the impact of land use changes on groundwater quality, a case study in Northern Kelantan. *Malays Sci Total Environ* 599(1):844–853
51. Lee J, Yang J, Kim D, Han M (2010) Relationship between land use and water quality in a small watershed in South Korea. *Water Sci Technol* 62(11):2607–2615
52. Juahir H, Gazzaz NM, Yusoff MK, Ramli MF, Aris AZ (2013) Spatial water quality assessment of Langat River Basin (Malaysia) using environmetric techniques. *Environ Monit Assess* 173(4):625–641
53. Rosnani I (2001) River water quality status in Malaysia. In: National conference on sustainable river basin management in Malaysia, pp 13–14
54. DOE (2019) Malaysian marine water quality standards and index. <https://www.doe.gov.my/portal/v1/wp-content/uploads/2019/04/BOOKLET-BI.pdf>
55. Azyana Y, Na NN, Jannah N (2012) Land use and catchment size/scale on the water quality deterioration of Kinta River. *Perak, Malays MJS* 31(2):121–131
56. Razali A, Ismail SNS, Awang S, Praveena SM, Abidin EZ (2018) Land use change in highland area and its impact on river water quality: a review of case studies in Malaysia. *Ecol Process* 7(1):19
57. Toriman M, Alssgeer H, Gasim M, Kamarudin K, Daw M, Alabyad L (2018) Impacts of land-use changes on water quality by an application of GIS analysis: a case study of Nerus River, Terengganu, Malaysia. *Int J Eng Technol* 7:155–164
58. Yen L, Yang J, Ssu-Yao J, Chyan D, Wang JS (2017) Characteristics of water quality of rivers related to land-use in Penang Island Malaysia. In: AIP conference proceedings, vol 1892, no 1, p 40008. AIP Publishing LLC
59. Nainar A, Bidin K, Walsh RP, Ewers RM, Reynolds G (2017) Effects of different land-use on suspended sediment dynamics in Sabah (Malaysian Borneo)—a view at the event and annual timescales. *Hydrol Res Lett* 11(1):79–84
60. Cheah EH, Hamid SA (2016) Determination of water quality of rivers under various land use activities using physico-chemical parameters and bacterial populations in Northern Peninsular Malaysia 14(6):788–797
61. Wan AY, Mokhtar J, Mohd KAK, Mohd ET (2015) Land exploration study and water quality changes in Tanah Tinggi Lojing, Kelantan, Malaysia. *Malays J Anal Sci* 19(5):951–959
62. Gorashi F, Abdullah A (2008) An integrated approach for the prediction of water quality index based on land use attributes using data generation method and back propagation network algorithm. *Plan Malays* 2(7):1

Impact of Land Use—Land Cover and Socio-economic Changes on Groundwater Availability: A Case Study of Barrackpore-II Block, West Bengal, India



Satabdi Biswas, Satiprasad Sahoo, and Anupam Debsarkar

Abstract Limited access to safe water is a growing crisis for rural areas. Various socio-economic activities are responsible for changing land use and land cover (LULC) and hotspots for water. The present study has been undertaken to unveil the crisis of groundwater scarcity and seek a way out through mixed methods, including recent changes to LULC (2010–2020) and a socio-economic survey carried out for 211 rural households in Barrackpore II block, West Bengal, India. The amalgamation of GIS and statistical techniques showed a drastic increase in the built-up area at the cost of water bodies and vegetation. The LULC study showed the maximum share of the land (73.79%) used for built-up purposes, with the share of existing water bodies being only 4.63%. The study was focused on how water scarcity got influenced by some socio-economic variables of the households. A binary logistic regression of the water scarcity index (WSI) was carried out to explain the level of awareness of rooftop rainwater harvesting (RRWH). The result confirmed 85.4% of the predictability of WSI. Anthropogenic activities are mostly responsible for climate degradation which ultimately has led to environmental degradation and contamination of precious water resources. Finally, the study emphasized regular monitoring of the present trend of diminishing water bodies and other green areas and the relevance of the adoption of urgent planning for RRWH as a safe sustainable water management practice for areas with contaminated groundwater.

Keyword LULC change · Rainwater harvesting · GIS · Binary logistic regression · Socio-economic study

S. Biswas
Department of Geography, Mrinalini Datta Mahavidyapith, Kolkata, West Bengal, India

S. Sahoo (✉)
Geoinformatics Division, International Institute of Geospatial Science and Technology, Kolkata, West Bengal, India
e-mail: satispss@gmail.com

A. Debsarkar
Department of Civil Engineering, Jadavpur University, Kolkata, India

1 Introduction

Water is one of the key resources safeguarding food security and the ecosystem. It underpins economic and human productivity. Many underlying human-induced factors related to water make the local environment more complex [1]. Major water demand is met from groundwater, including different irrigation systems of deep tube well (DTW), shallow tube well (STW), aquaculture, urbanization, industrialization, drinking, and domestic water. Even the surface water supply is also based on pumped groundwater [2]. India has been struggling to manage its water resources effectively. Depleting the water table coupled with the instability of access to clean water, food security, and health ultimately led to social and political unrest [3].

Easy access to groundwater, cheaper boring cost, availability of loans from a bank, subsidized electricity and compelling to need boost 'Boro cultivation' (winter rice) along with other crops are responsible for unethical major share drafting of groundwater common in West Bengal [4]. High drafting causes the gradual appearance of arsenic on the surface as shallow aquifer (20–80 m bgl) is affected by the geological source of arsenic and high level of iron contamination [5].

The arsenic contamination in drinking water has gradually become a worldwide overuse over the last four decades [6, 7]. However, from 2004 villages had experienced a huge growth of STW coming up with the National Policy of Arsenic Mitigation (NPAM) [4]. The arsenic toxicity covers 34,000 km² with 42.4 million people at risk in 37 blocks of West Bengal. The highly affected nine districts are North 24 Parganas, South 24 Parganas, Malda, Murshidabad, Nadia, Kolkata, Howrah, Hoogly, and Bardhaman. Surprisingly, most blocks are situated on the eastern side of the river Bhagirathi [8]. Nearly 98% of water samples of public tube wells of the state were reported to have an arsenic concentration above 0.01 mg/l. Even in some cases, it was noticed as high as 0.135 mg/l [9].

In the district of North 24 Parganas, the level of arsenic was reported in the range of 0.06–2.28 mg/l, causing the suffering of 21,96,158 populations in 2699 affected habitats, which is the worst situation in the state [10, 11]. The rural habitations of the district mostly depend on groundwater with only 4.9% being catered by surface water systems and alternative sources. Thus, groundwater is the only significant source for the piped water supply schemes (PWSS). Out of groundwater-based PWSS, 64% are covered by different small-scale PWSS, each covering nearly 10 habitations. However, this groundwater-based scheme is typically fitted with a bore well and pumps, supplying water to households after disinfection through chlorination [5]. More precisely, 53.4% arsenic contaminated tube wells were found in the North 24 Parganas among which 3.4% had above the level of 300 µg/l. Consuming arsenic-contaminated water over a prolonged period in the form of cooking, drinking, and irrigation, the poison of arsenic has entered the food chain [5]. It is worth mentioning that the BIS level for arsenic is 0.01 mg/l since 2003 [12]. The severity of arsenic calamity causes many health-related sufferings such as skin lesions, diarrhoea, gastrointestinal problems, anemia, renal defect, neurological defects, etc. Arsenic also causes oxidative damage and alters the regulation of DNA repair [7, 8]. The level of urbanization

of the district remained high at 57.6% compared to state and the national average of 31.89 and 31.16%, respectively (Census of India 2011).

Under such circumstances, arsenic contamination puts a huge burden on rural households. It happens in three ways: unpopular Government programs, lack of proper institutional efforts, and ignorance about the socioeconomic and cultural background. To unfold in brief, most government policies are by and large associated with the dependency on a single source, i.e. groundwater for all uses, even for real estate development business, especially in adjoining areas of Kolkata [4]. Arsenicosis is aggravated by malnutrition, poor socioeconomic status, illiteracy, food habit, and regular consumption of contaminated water [5]. The poor socio-economic condition has become a threat for nearly 20% of the state population affected by arsenic contamination [7]. In the technological park at Baruipur, West Bengal, most of the arsenic removal plants were found inoperative because of a lack of awareness of arsenic-related hazards among the affected population, poor sense of belonging, and willingness, user-unfriendliness, etc. [5].

The lack of participation of the highly affected and marginal community in the government's water policy decision-making platform was another reason behind the failure [5, 6]. There are several underlying socio-economic and anthropogenic factors such as poverty, population growth, unawareness of water resources, unscientific and primitive method of groundwater withdrawals, etc. All play a significant role in aggravating water scarcity [11].

To date, the government is yet to provide enough technical support to encounter arsenic calamity in a cost-effective and user-friendly way, while presently available and widely used arsenic mitigation filter systems further damage soil, surface water, and the local ecosystem due to unplanned open disposal [8]. It is necessary to change the present behavior of water use and tap new sources like Rainwater harvesting (RWH) to avoid deadly diseases [8]. However, RWH has been widely practiced in dry areas of Bankura, Birbhum, Darjeeling, Jalpaiguri, and Purulia by different agencies. Artificial recharge plants were developed in some of the arsenic-affected areas like Swarnnagar and Gaighata Blocks, North 24-Parganas, West Bengal [13]. RWH plays a vital role in combatting water scarcity by individuals or governments at a reasonable cost [14].

There have been several studies on analyzing the land use and landcover (LULC) to select a suitable site of RWH [15–17]. No such research has so far been made to combine LULC with the socio-economic aspect. The present study attempts to provide a mixed approach to assess the extent of water scarcity and the feasibility of RWH to overcome the adverse effects of declining groundwater levels. Incorporating the recent (2010–2020) LULC change, we identify the water hotspot, and finally, water scarcity is judged by rural households, which was so far unnoticed, especially in the semi-critical block like Barrackpore II, North 24 Parganas District of West Bengal. Heavy drafting of groundwater by rampant use of shallow, medium capacity, and deep tube wells are very common in the study area to support winter paddy and other crops as well as industrial and domestic purposes. This indiscriminate over-drafting of groundwater is one of the main causes of land degradation, water pollution, and associated environmental problems. A gradual decline of groundwater table with

increasing arsenic-iron contamination caused by various anthropogenic activities is influencing all dimensions of the environment. It is necessary to adopt adequate measures to combat groundwater-related land degradation for the sustainability of the environment. Thus, the present paper helps formulate a potential action plan for augmenting groundwater by the local authority to extract the maximum benefit of RWH. Thus, the objectives of this study can be summarized as:

1. To find out the extent of groundwater scarcity,
2. To identify the change of LULC and hotspots of water,
3. To access the water insufficiency and awareness of rooftop RWH (RRWH) by rural households.

2 Study Area

The present study area is Barrackpore II, North 24 Parganas, West Bengal, India (see Fig. 1). Topographically, this block is a part of the Gangetic delta having an average elevation of 25 m. Geologically it has an alternate layer of sand, silt, dark gray clay of middle and upper Holocene age (<http://wbwridd.gov.in/>). Having deltaic plain with silt types of fertile soil, agriculture is done involving a huge number of DTW and STW mainly for Boro (winter paddy) cultivation. Most of the agricultural lands are used for multi-crop cultivation throughout the year. The clay surface gets poorly drained, thus, facing a flood in every rainy season. The average rainfall is more than 1600 mm, mostly happening during the rainy season.

The questionnaire survey was based on 11 selected villages like Chhota Kanthalia, Bara Kanthaliya, Surjyapur, Iswaripur, Dopere, Bilkanda I, Bilkanda II, Patulia, Sewli, Mohanpur, and Bandipur that covered 7.56% of total households as per the 2011 census (see Table 1). However, the total villages of the block are 15, having 51,874 rural populations with the highest decadal growth rate of 36.73%.

The surveyed area has a historical background that after partition with Bangladesh, many refugees settled here. The proximity of Kolkata and the river Hooghly influenced the urbanization process. Simultaneously, industries like jute, petrochemical, electronics, iron and steel factories, food processing, and information sector have pulled a large section of the rural people of the adjacent blocks. However, at present, though many industries are closed, better amenities attract people from rural areas [18]. Gradually, the agricultural landscape started changing in 2004 mainly in two ways. Firstly, with rapid mushrooming of small-scale dye, textile, glycerine factories abstracting excessive groundwater and secondly, due to disposal of untreated industrial waste degrading the agricultural land, surface water bodies, and shallow aquifer [4]. These industries made huge shifts in labor from agriculture. Our study area is facing quantitative and qualitative water scarcity, which puts underprivileged rural households in a critical situation.

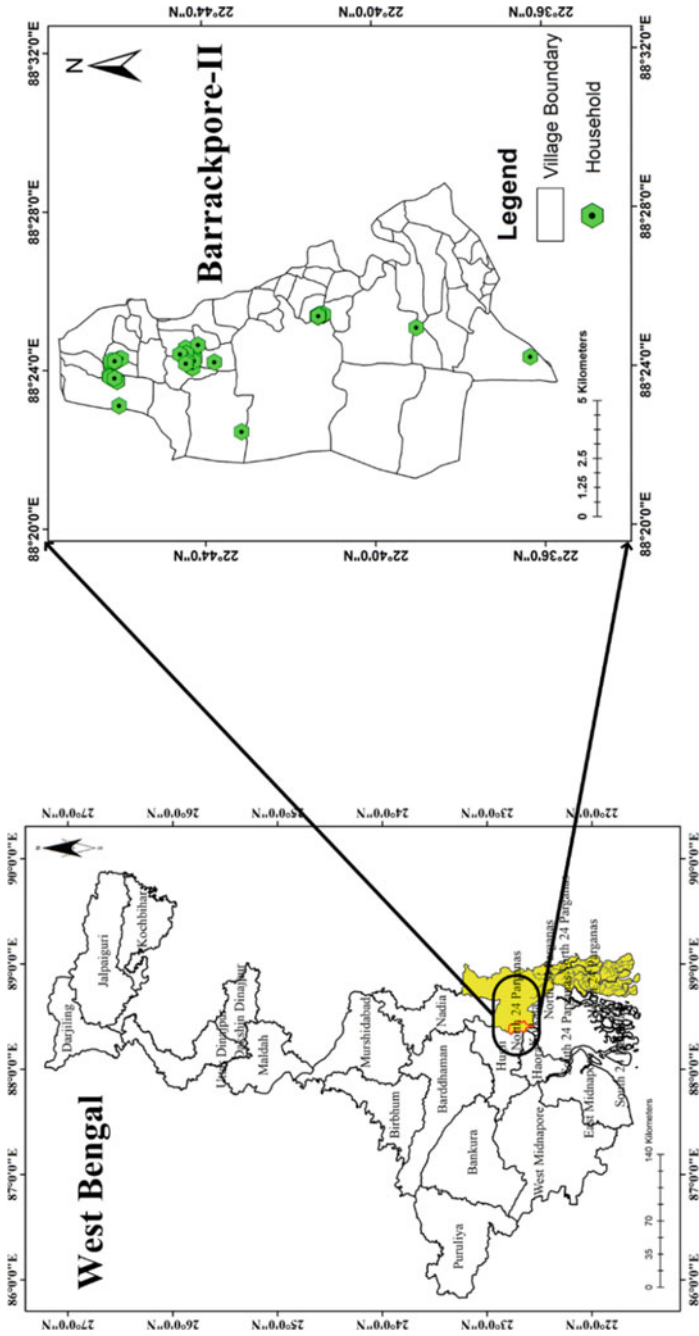


Fig. 1 Study area and location of the households survey

Table 1 Details of the study area: Barrackpore II block

Stage of groundwater development	Surveyed village	Surveyed households	% Samples with Arsenic > 10 ppb	Average rainfall in mm	Average rainy days in monsoon	Driest month with rainfall	Wettest month with rainfall
Semi-critical	11	211(22.9%)	0.32	1570	81	December, 3 mm	August, 306 mm

Source SWID 2018, Census of India 2011 part XIIA, PHED 2018, Primary data 2019

3 Material and Methodology

The methodology consists of three parts viz., data collection, data analysis, and assessment of the significance of RRWH through statistical analysis represented in Fig. 2.

3.1 Data Collection

Satellite images from Landsat 7 ETM+ (Enhanced Thematic Mapper Plus) and American Earth Observation Satellite Landsat 8 OLI/TIRS (Operational Land Imager

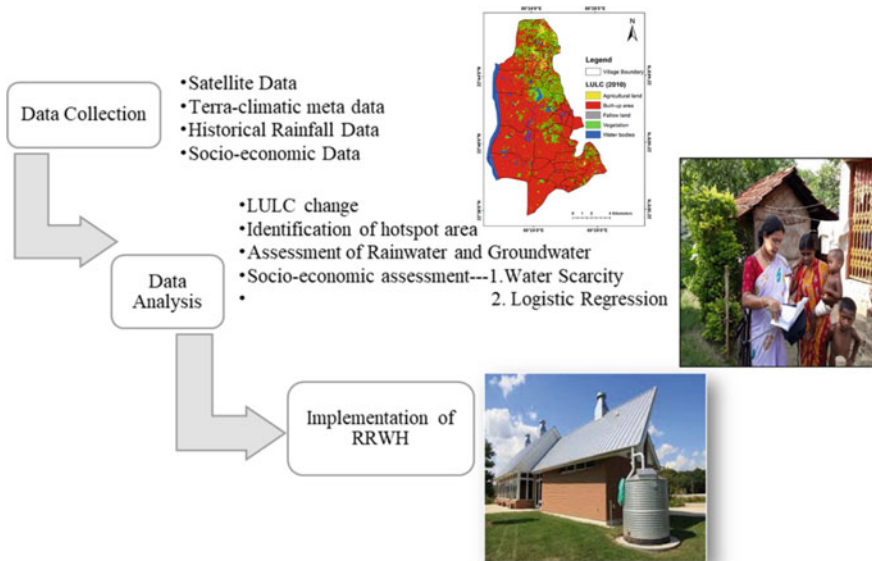


Fig. 2 Graphical representation of methodology

Table 2 Details of satellite data

Satellite data	Path/row	Time	Spatial resolution (m)	Map projection	UTM zone	Datum	No. of bands
Landsat 7 ETM+	138/44	2010/01/29	30	UTM	45° N	WGS84	8
Landsat 8 OLI/TIRS	138/44	2020/01/01	30	UTM	45° N	WGS84	11

(OLI) and Thermal Infrared Sensor (TIRS) were used for preparing LULC. The Terraclimatic metadata having monthly $0.5^\circ \times 0.5^\circ$ grid-wise resolution was collected from (<https://climate.northwestknowledge.net>) to develop a water deficit map. Forty-five years of historical rainfall data (1971–2015) were collected from IMD (Pune). To enquire about the key information of water scarcity and awareness of water, a questionnaire survey was carried out in the rural areas of Barrackpore II block through personal interviews of 211 households during 2018–2019. The questionnaire consisted of three sections: (1) socio-economic characteristics including income of the household, (2) household's perceptions on the water scarcity (3) household awareness about RRWH.

3.2 Methodology of LULC

The LULC was developed in remote sensing (RS) and geographical information system (GIS) platform to predict the changes during 2010–2020 in the study area (Table 2). The field visit was done to verify the latitude and longitude of specific LULC categories by taking an average of 10° latitude and longitude points. Cross-checking was made based on the pixel color tone of the Landsat image using GIS. Layer stacking and haze reduction were done to improve the quality of satellite images for LULC using ERDAS Imagine and Arc GIS software. The LULC changes were analyzed with the 'K-means Clustering unsupervised classification method'. The Google Earth Images were used for selecting and validating the LULC classes. The key categories of the LULC were agricultural land, built-up area, fallow land, vegetation, and water bodies. Among water bodies, we considered a wetland, ponds, other surface water bodies (locally known bills or jhils), etc.

3.3 Calculation of Index with Statistical Analysis

The water scarcity index was calculated based on the responses of the rural households. However, the responses were perception-based judgments made from socio-economic aspects. For this index, we considered a set of 5 questions. However,

the response of each question was converted to an indicator of the index with two values '0' and '1'. '1' was given as the positive contributor of the index and '0' was taken otherwise. The index was obtained by adding the binary values to the related questions, namely the 'water scarcity index' (WSI). Thus, each household had five answers. Suppose the answers to these questions were 0, 0, 1, 1, 1, then we took some of the values of a particular household, and the sum was 3. So, we had a number between 0 to 5 for each household. We took two values as a cut-off value and then considered each household having the sum of the answers to these five questions. Then less than or equal to '2' was given '0' and the households having the sum of more than 2 were given '1'. All five variables showed significant dependency within the index by bivariate tables. All the independent variables were strongly associated with dependent variables in the chi-square test (χ^2). In the second stage, we considered logistic regression to assess the combined effect of some socio-economic variables on the 'water scarcity index' (WSI). The questionnaire was coded with the help of SPSS software.

4 Results

4.1 Assessment of Rainwater and Groundwater

The average rainfall of 45 years for the study area was 1719.91 mm. The average monsoon and post-monsoon rainfalls were 1289.01 mm and 205.62 mm, respectively. The range of monsoon rainfall varied from 921.03 to 1772.14 mm. It indicates a greater scope of natural recharge when soil and other factors are favorable. The results showed huge potentialities for RRWH. The study area was categorized as 'semi-critical' based on the stage of groundwater development and it already has 97.99% development (Table 3). Net groundwater available for future uses showed a negative value ($-12,744.99$ ham), which implies the urgent necessity for artificial recharge and stringent restrictions over further drafting. However, according to the Central Ground Water Board (2017), more than 70% to equal or more than 100% drafting of groundwater was categorized as 'semi-critical'. The aquifer is very near to the surface and thus, a lion's share of groundwater was extracted from the shallow aquifer for all purposes very easily.

The quality of the water is intricately associated with the drafting of groundwater. The falling water level trend was found in both the wells with an average of 0.351 and 0.616 m/years from 2007 to 2017. Barrackpore-II block is one of the highly urbanized blocks of North 24 Parganas. It has the highest negative growth (-25.42%) during 1991–2001 due to the formation of new municipalities (Development and Planning Department 2010). The decadal variation of the population for the block was 58,344 as per the present census. Due to intensive urbanization, the population density and water demand are expected to reach respective values of 9976.14 person/km² and

Table 3 Groundwater profile of Barrackpore II Block*

Block	Net groundwater availability (ha.m)	Existing gross groundwater draft for all uses (ha.m)	Stage of groundwater development in %	Gross groundwater for irrigation (ha.m)	Rainfall recharge in monsoon (ha.m)	Net groundwater available for future (ha.m)	Depth of GWL (m) bgl	Aquifer thickness (m)
Barrackpore II	4702.55	4608.11	97.99	348.60	4043.75	-12,744.99	12.9	35

ha.m = hectare metre, (m) bgl = metre below ground level

*Source State CGWB 2017 and PHEID 2017

Table 4 Percentage of change in the LULC

Year	Barrackpore-II (%)	
	2010	2020
Agricultural land	2.00	1.89
Built-up area	72.1	73.79
Fallow land	1.87	1.47
Vegetation	18.5	18.22
Water bodies	5.53	4.63

2233 m³/day by the year 2031. The water demand of urban North 24 Parganas is expected to be 111.48 MLD (million liters per day) in 2021 [10].

4.2 LULC Change

In our study, rural settlement and impermeable surfaces, including roads, were categorized as ‘built-up area’ while bare land, seasonal bare land, and brick kiln came under ‘fallow land’. Another LULC class was ‘vegetation’, consisting of open fields, grass, forest patch, roadside trees, shrub, scattered trees, kitchen gardens, etc. Areas coming under the river, pond, bills, wetland, and other surface water bodies were classified as ‘water bodies’ and agricultural land. These are the five categories of LULC. The percentage of LULC changes is presented in Table 4. As appears in Fig. 3, the major land use for the study area in 2010 was built-up areas (72.1%) followed by vegetation, water bodies, agricultural land, and fallow land, and the same trend will be observed in 2020.

The built-up area has increased from 72.1 to 73.79%, i.e. by 1.69% over a span of 10 years’. However, in this block, the percentage share of water bodies, vegetation, agricultural land, and fallow land was reduced marginally to the extent of 0.9%, 0.28%, 0.11%, and 1.05%, respectively, over the decade (2010–2020).

4.3 Identification of Hotspot

The water deficit zoning map was developed to identify hotspot zones of water (see Fig. 4). The terra-climatic data included temperature, precipitation, evaporation, vapor pressure, runoff, soil moisture, etc. The water balance model was calculated based on the Thornthwaite-Mather climatic method. As the Barrackpore II block has already been highly urbanized with the less rural area, more than 50% area was under high (45.83–46.14 mm) to very high (46.14–46.64 mm) water deficit, mostly in the east to the south-eastern part of the block. On the contrary very small area was found under low (45.30–45.59 mm) to very low (45.01–45.30 mm) water deficit categories, scattered mostly over the north and western parts of the block.

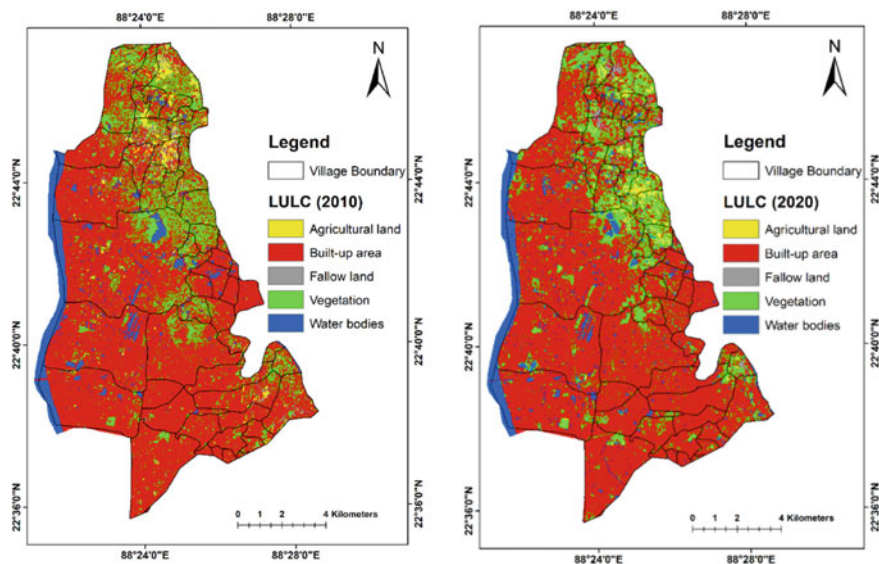


Fig. 3 LULC of Barrackpore-II from 2010 to 2020

4.4 Socio-economic Assessments of Water Scarcity and RRWH

4.4.1 Socio-economic Characteristics of the Households

Water is tied in a complex relationship with the socio-economy and surrounding environment [1]. In the present study, we tried to unfold the water scarcity situation faced by rural households in their daily lives. They were found to be well aware of RRWH to combat the situation.

(a) General Information about the Households

Among the respondents, males and females were 51.2% and 48.8%, respectively. Each household had an average of 4 members (73.5%). Among the households, 18.0% were engaged in agricultural activity. Almost 47% of the household's monthly income was Rs. 10,000. Most of the respondents had attained class X level education (51.7%) and 31.3% of families had at least one educated member in the family. About 27.5% had more than Rs. 10,001 monthly incomes. The rural household used to fetch water from groundwater-based shallow hand tubes as the principal source of water.

(b) Perception of Households about Water Scarcity

As judged by households in the water scarcity index, we found that 52.6% of households complained about acute water shortage in summer. When asked about drinking water sources, 89.1% admitted their dependency on PHE/own shallow tube well

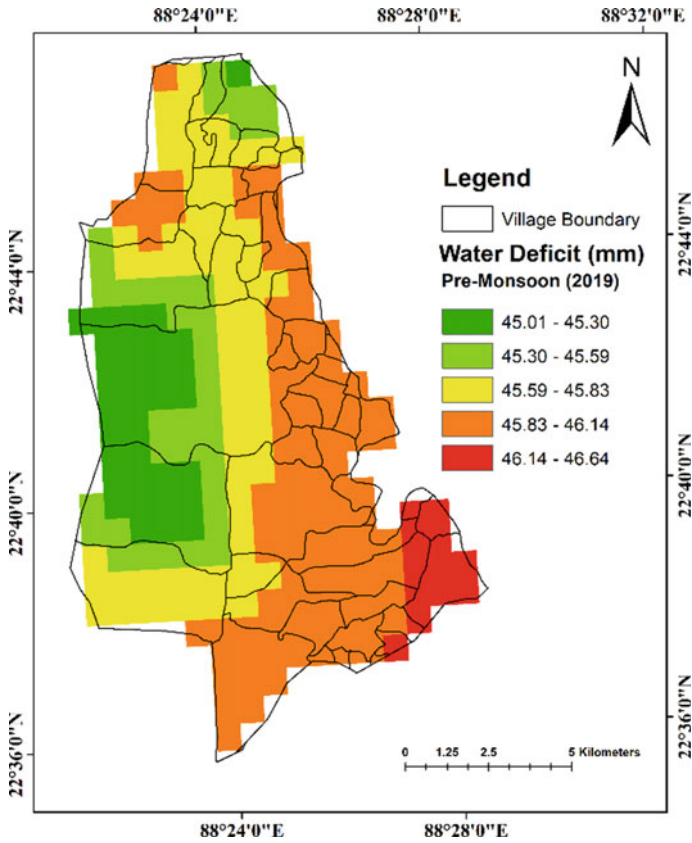


Fig. 4 Water deficit map of Barrackpore-II, 2019

water. Regarding the taste of water, 75.4% of households expressed their water as having ‘good taste’. According to the households, sweet water meant ‘good’ and salty or odorous water ‘not good’. Almost cent percent of households expressed a dislike for water due to its reddish color. The first shallow aquifer of the study block was contaminated with arsenic and iron, having 7.14 ppb and 1.01 ppm, respectively [19]. Thus, rural households suffered a lot from the single dependency on the groundwater.

(c) Water-related Diseases

During the field survey, the percentage of households frequently suffering from water-borne diseases, i.e. dysentery, diarrhea, jaundice, typhoid, was 66.4%. All these five variables were included in WSI. A significant portion of the households (70.1%) had frequently been suffering from combined water and vector-related diseases. Near about 6.6% of the households were suffering from skin lesions, whereas 10.4% were suffering from constipation which implied the quality of supplied water was a matter of concern. The share of pucca houses and land around the household for constructing

a water reservoir was found 93.8% and 86.7%, respectively. However, 24.2% of the households already had their water tank.

4.4.2 Binary Logistic Regression Analysis

The present study intended to find out whether rural households were aware of RRWH as an alternative way of countering groundwater scarcity. The logistic regression was carried out by taking the log-odd ratio of WSI on nine independent socio-economic variables (See Table 5). WSI was taken as a dependent variable (y) given values '0' for low water scarcity and '1', for acute water scarcity. Each of the nine variables was taken as binary with '0' for low and '1' for high.

Data were analyzed with binary logistic regression to assess the extent of water scarcity and awareness of RRWH as judged by the households.

In logistic regression, six variables i.e. 'male member', 'female member', 'large roof area', 'gastrointestinal problem', 'willingness to direct use of RRWH water' and 'other known families to use rainwater' were found to have a statistically significant effect on WSI. The suffering from the gastrointestinal problem, other known families to use rainwater had a positive effect on WSI while roof area and willingness to direct use of RRWH had a negative effect. The reason behind this can be explained that having more male and female members in the family implied a large family size, which further implied increased water demand. We also tried to find out whether

Table 5 Result of Logistic Regression of water scarcity index (WSI) on the Related Independent Variables

	B	S.E	Sig	Exp (B)
Male member	2.343	0.472	0.000***	10.418
Female member	2.060	0.463	0.000***	7.848
Roof area	-1.064	0.442	0.016**	0.345
Known iron	-0.042	0.619	0.946	0.959
Known arsenic	-0.855	0.875	0.329	0.425
Gastro-intestinal problem	1.325	0.478	0.006**	3.762
Collect rain	-0.580	0.671	0.387	0.560
Willingness to direct use of RRWH water	-1.049	0.559	0.060*	0.350
Other known families using rainwater	2.294	0.797	0.004**	9.910

-2 Log likelihood = 167.919, percentage of correct 85.8%,

Dependent Variable (Y) = 'Water Scarcity Index (WSI)',

*: Significant at 10%, **: Significant at 5% & ***: Significant at 1%.

Male member: up to 2 = 0, 3 and more = 1, Female member: up to 2 = 0, 3 and more = 1, Roof area: large = 0, small = 1, Known iron: Yes = 1, No = 0, Known Arsenic: Yes = 1, No = 0, Gastro-intestinal problem: Yes = 1, No = 0, Collect rain: Yes = 1, No = 0, Willing to direct use: Yes = 1, No = 0, Know other families use rainwater: Yes = 1, No = 0.

the water requirement of male and female members was significantly different, and consequently, they were considered separately.

The more male and female members in a family were found to be 26.5 and 25.1% of households respectively. More than 57% of households had been suffering from gastrointestinal problems which implied poor water quality. Thus, 15.2% of sizable households were found to buy water as they felt private packaged bottled water was a reliable source of drinking water. In comparison, only 8.5% of households preferred to treat drinking water by domestic water filter or boiling. This private packaged water might be one possible reason for positive significance. However, bottled water did not maintain the standard of the BIS level. Only 8.1% of households were aware of the fact that their neighbors used to collect rainwater for domestic purposes in the rainy season. Whereas only 38.4% of households had a large roof (more than 400 m²). Nearly 22% of respondents expressed their willingness to use the harvested water for drinking purposes in the future, while 62.6% of respondents were found conditionally willing i.e. expecting incentives.

Surprisingly, 27 and 17.5% of respondents were well aware of iron and arsenic problems. More than 89% of households used the shallow tube well as drinking water without having any alternatives. The Public Health Engineering Department (PHED) is the sole authority for the installation and supply of drinking/domestic water while the local government (Gram Panchayat) has been responsible for its maintenance. DTW and private STW were untreated drinking water sources, and the respondents were compelled to consume the same having no alternative. Thus, these two variables harmed WSI. However, only 19.9% of households occasionally collected rainwater whatever they could collect in their home but none of them used it for drinking purposes but mostly for other domestic purposes.

However, 'households had large family sizes', 'a large roof area', 'suffering from gastrointestinal problems' and 'knowing neighbors collecting rainwater in the locality' had significant influence in the order of at least at 5% level of significance. Only willingness to direct use of RRWH had a 10% level of significance. Overall, the logistic regression could explain 85.8% of the dependent variable.

5 Discussion

The supply of unsafe drinking water in rural North 24 Parganas has a cumulative effect on the households and consequently, they face an enormous amount of risk related to arsenic toxicity. Sometimes skin lesions due to arsenic contamination are mistaken by people as leprosy due to a lack of social awareness. Rural people took it as a curse of God and socially boycott the families suffering from arsenicosis [20].

Agriculture, infrastructure, and other anthropogenic expansions are primarily responsible for the negative impacts of LULC [21]. Thus, groundwater is nearly the source of all critical consumption and has made a tremendous adverse impact in peri-urban villages of North 24 Parganas [4]. Banerjee and Jatav [4] pointed out that institutional negligence and Governmental failure were responsible for water

insufficiency in many ways. Firstly, infrastructural lacuna, erratic supply, poor operation and maintenance, unreliable supply of public stand posts were responsible for water scarcity. This scarcity is supplemented by rampant private informal tube wells and private packaged drinking water. Secondly, private packaged drinking water does not maintain the BIS standard. Thirdly, untreated industrial wastes go into low-lying paddy land or surface watercourses and contaminate them along with shallow aquifers. Over time, those lands become fallow and are being sold to the factories. Thus, agricultural land and water bodies are converted by powerful industrial lobbies. This further aggravates the situation by illegal extraction of groundwater for industries and 'Boro cultivation'. Lastly, the policy of real estate development ruins the groundwater and natural recharge process. The hydro-geochemistry of groundwater is dependent on several factors like soil, lithology of rock, percolations of rainwater, climate, the role of microorganisms, topography and the role of human activities, etc. [22].

Another study [2] identifies the hotspot areas based on LULC change (1990–2017) in North 24 Parganas. Their result showed that the western and northwestern parts of the district experienced huge urbanization with a 22.59% increase in the built-up area due to the development of cities like Rajarhat Newtown-Gopalpur, Barrackpore, Barasat, Bidhannagar. However, this transformation was gained from the agriculture and vegetation area. But over time, a huge number of brick kilns were identified in the surrounding low-lying agricultural land for getting more benefits. Population growth was one of the significant factors directly affecting the existing LULC. According to [23], it was found that the forest land was degraded or fragmented by the pressure population after assessing LULC. Pristine [24] developed a district-wise Spatio-temporal surface model from 2000 to 2014 to assess the groundwater storage changes and stress zones by the GIS platform in West Bengal, India. The result found that the negative attitude of humans towards urbanization blocks infiltration and surface retention. Banerjee and Jatav [4] found that 20% of households complained about the acute water crisis for some reason in the Bodai village under Barrackpore II.

The findings of the Planning Commission of India (2007) recommended RWH as a local solution for providing safe drinking water through ponds with proper planning and motivation of local people. But in this district ponds are heavily used for pisciculture. Kar and Mukherjee [1] suggested introducing RWH with low-cost water treatment technology to ensure water for all including underprivileged rural people in the project. However, the cement factory situated in Sujapur, Barrackpore II estimated annually 2780 m³ or 20% potential harvested storage capacity by RWH [22] but [4] argued and stated that re-cycling wastewater and RWH were hardly taken up in Barrackpore II. However, Das and Angadi [18] suggested that rooftop RWH necessary for Barrackpore II.

Addressing water scarcity calls for integration across different multi-disciplinary approaches among all water-related resources, economic and social welfare, and sustainability of ecosystems without compromise. Simultaneously, it is necessary to overcome the existing wastage of water in agriculture, restore the lack of trust in

governmental activities, minimize corruption, adopt scientific attitudes with traditional producers, and promote such technologies to improve society's quality of life [14].

Rana and Suryanarayana [17] found socio-economic criteria extremely crucial, thus, making the field study necessary to select sites for RWH to avoid land conflict. An increase in awareness levels and education helps stop the consumption of arsenic-contaminated water and introduce RWH [8]. Sarkar [25] found that educated people are more aware of water contamination and related health implications. It was also mentioned that it was the responsibility of the government to supply safe and sufficient water to people as they have been paying taxes. It was suggested [18, 26] to make people aware of the negative impact of the transformation of natural land into the built-up area.

Unlike these studies, the present study found rural households quite educated, had enough roof area, pucca house, homestead land, and had their own water tank but suffering from water-related health hazards and faced water insufficiency in summer. Buying unsafe water puts households in a critical situation. Only 6.2% demanded proper training of RRWH. It was found from the survey that the households did not know the proper know-how of RRWH. It implied households were not aware of RRWH as an alternative water source. But few households occasionally crudely collected rainwater. Thus, unconsciously rainwater was being considered as an alternative source of safe water. However, 33.2% of households suffered from acute water scarcity, which is established by logistic regression.

This study noticed that the built-up area is the giant feature increasing at the cost of vegetation cover, water bodies, fallow land, and agricultural land LULC categories from the year 2010 to 2020. Additionally, the steep water demand would be very challenging to cater safe water to future generations. However, more than 52% of respondents complained about water shortage to lower the water table. In our study, the water deficit zoning maps identified the hot spots in the study area where RWH needs to be introduced with an artificial recharge structure like an injection well.

6 Policy Implication and Recommendations

The need of the hour to have a more effective institutional regulatory work restricts the drafting of groundwater and establishes a balance between development and environment conservation centering socio-economy. First of all, the government should restrict population growth which is the key factor in controlling the negative change of land use. Water, particularly the groundwater needs to be managed as a community resource by the state under public trust doctrine to achieve food, better standard of life, and livelihood security of rural households. Following measures would be suggested for considering the magnitude and extent of the water situation.

- It is necessary to introduce appropriate land use to restrict and penalize illegal construction and landfilling. A region-wise micro-level aquifer mapping, arsenic-iron-based vulnerability maps, and LULC maps should be published in the public domain to make people aware of the quantity-quality status of the aquifer and drastic changes in land use and to share a periodical update.
- The over-withdrawal of groundwater should be minimized by regulating the use of STW and DTW for pumping groundwater for all use.
- The local authority should arrange a water safety plan of RWH to introduce simple technical know-how of rooftop RWH by frequent meetings, training, workshop, increasing the social awareness program among the affected community for social acceptance of scheme and rescue their aquifers for the future generation.
- It is imperative to arrest the decline of groundwater levels in over-exploited areas by improved technologies of artificial recharge. The main focus will be to shift from the construction of a high-cost arsenic treatment plant to RWH. RWH helps to dilute the arsenic-iron concentration of aquifers and plays the role of an alternative source of drinking water.
- An increase in the number of parks with water bodies, provision of injection wells and rooftop RWH with recharge wells for all built-up areas, and re-excavation of the existing wells or ponds may be adopted to avoid valuable land acquisition.

7 Conclusions

Significant reduction in water bodies, fallow land, and vegetation cover indicates the consequences of an indiscriminate increase in built-up areas over the last decade in Barrackpore II block. Inadequate awareness regarding the importance of groundwater among the various stakeholders viz. different governmental agencies, policymakers, households, etc. is to be duly addressed as a part of water conservation. However, the socio-demographic status of rural households plays a significant role in changing the LULC, which so far has been neglected repeatedly. Unsafe drinking water has a collapsing effect in terms of arsenic toxicity, sometimes even to the extent of social exclusion. Arsenic is difficult to be removed overnight but the judicious adoption of RRWH as an alternative safe water supply scheme may combat the age-old problem of water scarcity.

Thus, the proposed mixed approach incorporating assessment of LULC change, identification of water hotspot zone, evaluation of the statistical significance of water scarcity perceived by the rural households, and the implementation of RRWH can be considered as a simple yet effective strategy for addressing the issue of combined qualitative and quantitative water stress for semi-critical, arsenic-iron contaminated areas. This method needs less time and more effective to extract the full advantage of RWH. Thus, an attempt was made to identify the root socio-economic factors associated with groundwater depletion by combining GIS and statistical approaches, which would help the local authority combat the water scarcity for other semi-critical blocks with identical socio-economic and physical conditions. The introduction of RWH

should cater safe water to the affected community and also enhance the groundwater resource.

Acknowledgements We acknowledge the CGWB, PHED, and IMD Pune for providing data to improve the quality of the text.

References

1. Kar S, Sen E, Mukherjee S (2020) A geospatial technique-based site suitability analysis for construction of water reservoirs in Arsha and Balarampur Blocks, Purulia. *World Water Policy* (May). <https://doi.org/10.1002/wwp2.12021>
2. Bera S, Das Chatterjee N (2019) Mapping and monitoring of land-use dynamics with their change hotspot in North 24 Parganas District, India: a geospatial- and statistical-based approach. *Model Earth Syst Environ* 5(4):1529–1551. <https://doi.org/10.1007/s40808-019-00601-2>
3. CWMI-NITI Aayog (2019) Report on Composite Water Management index (Cwmi). <https://niti.gov.in/sites/default/files/2019-08/cwmi-2.0-latest.pdf>
4. Banerjee P, Jatav M (2017) Thematic paper on urbanisation and groundwater use: socio-economic system mapping. In: South Asia consortium for interdisciplinary water resources studies (SaciWATERS). <http://saciwaters.org/shiftinggrounds/pdfs/ThematicReportonUrbanizationandGroundwaterUse.pdf>
5. Planning Commission of India (PCI) (2007) Report of the task force on formulating action plan for removal of Arsenic contamination in West Bengal. In: Government of India planning commission, New Delhi, vol 001. http://planningcommission.gov.in/aboutus/committee/wrkgrp11/tf11_arsenics.pdf
6. Asian Development Bank (ADB) (2020) Guidelines for drinking water safety planning for West Bengal (Issue December)
7. Roy S (2020) Arsenic contamination of groundwater and its socio-economic impacts in West Bengal. 14(6):59–62. <https://doi.org/10.9790/2402-1406045962>
8. Dey TK, Banerjee P, Bakshi M, Kar A, Ghosh S (2014) Groundwater Arsenic contamination in West Bengal: current scenario, effects, and probable ways of mitigation. *Int Lett Nat Sci* 13(August 2015):45–58. <https://doi.org/10.18052/www.scipress.com/ilns.13.45>
9. Asian Development Bank (ADB) (2018) West Bengal drinking water sector improvement project. <https://www.adb.org/sites/default/files/project-documents/49107/49107-006-rrp-en.pdf>
10. Development & Planning Department Government of West Bengal (DPDWB) (2010) District human development report north 24 Parganas. http://wbplan.gov.in/HumanDev/DHDR/24pgs_north.PDF
11. Mukherjee S, Pati S, Dutta RN, Saha K (2009) Groundwater arsenic contamination situation in West Bengal, India: a nineteen year study. *Bhujal News Quart J, India*
12. Chatterjee U (2018) Water scarcity in semi-arid regions of Bankura District, West Bengal, India-problems and prospects. *Khaj: Int Peer Rev J Geogr* 5(1):87. <https://doi.org/10.5958/2455-6963.2018.00007.3>
13. CGWB (2011) Select case studies rain water harvesting and artificial recharge. In: Central ground water board, ministry of water resources. <https://hindi.indiawaterportal.org/content/groundwater-arsenic-contamination-situation-west-bengal-india-nineteen-year-study/content-type-page/53063>
14. Amos CC, Rahman A, Gathenya JM (2016) Economic analysis and feasibility of rainwater harvesting systems in urban and Peri-urban environments: a review of the global situation with a special focus on Australia and Kenya. *Water* (Switzerland), 8(4). <https://doi.org/10.3390/w8040149>

15. Adham A, Sayl KN, Abed R, Abdeladhim MA, Wesseling JG, Riksen M, Ritsema CJ (2018) A GIS-based approach for identifying potential sites for harvesting rainwater in the Western desert of Iraq. *Int Soil Water Conserv Res* 6(4):297–304. <https://doi.org/10.1016/j.iswcr.2018.07.003>
16. Navin S, Loganathan A (2019) Land use land cover change detection using k-means clustering and maximum likelihood classification method in the Javadi Hills, Tamil Nadu, India. *Int J Eng Adv Technol* 9(1S3):51–56. <https://doi.org/10.35940/ijeat.a1011.1291s319>
17. Rana VK, Suryanarayana TMV (2020) GIS-based multi-criteria decision making method to identify potential runoff storage zones within watershed. *Ann GIS* 26(2):149–168. <https://doi.org/10.1080/19475683.2020.1733083>
18. Das S, Angadi DP (2020) Land Use-Land Cover (LULC) transformation and its relation with land surface temperature changes: a case study of Barrackpore subdivision, West Bengal, India. *Remote Sens Appl Soc Environ* 19(July 2019):100322. <https://doi.org/10.1016/j.rsase.2020.100322>
19. CGWB (2020) Groundwater year book of West Bengal and Andaman & Nicobar Islands (Issue 284)
20. Biswas S, Debsarkar A, Pal M (2020) Water insufficiency, health hazards and rainwater harvesting in north 24 Parganas, West Bengal, India: results of a socio-economic survey. *Arthaniti: J Econ Theor Pract* 097674792096339. <https://doi.org/10.1177/0976747920963399>
21. Takala DW, Adugna DT, M. K. (2020) Drivers and implications of land use/land cover dynamics in Finchaa catchment. *Northwest Ethiop Land* 9(113):1–20
22. Islam K, Jashimuddin M, Nath B, Nath TK (2018) Land use classification and change detection by using multi-temporal remotely sensed imagery: the case of Chunati wildlife sanctuary, Bangladesh. *Egypt J Remote Sens Space Sci* 21(1):37–47. <https://doi.org/10.1016/j.ejrs.2016.12.005>
23. Sahoo S, Chakraborty S, Pham QB, Sharifi E, Sammen SS, Vojtek M, Vojteková J, Elkhachy I, Costache R, Linh NTT (2021) Recognition of district-wise groundwater stress zones using the GLDAS-2 catchment land surface model during the lean season in the Indian state of West Bengal. *Acta Geophys* 69(1):175–198. <https://doi.org/10.1007/s11600-020-00509-x>
24. Pristine Cement Pvt. Ltd (PCPL) (2015) Pristine Cement Pvt. Ltd. Retrieved from http://www.wbpcb.gov.in/writereaddata/files/eia_Pristine_Cement.pdf
25. Sarkar SM (2018) Rainwater harvesting technology and water use practices: a study from Purulia district of West Bengal, India. *IMPACT: Int J Res Humanit Arts Lit (IMPACT: IJRHAL)* 6(8):583–596
26. Patra S, Sahoo S, Mishra P, Mahapatra SC, Islam K, Jashimuddin M, Mukherjee S (2018) A geospatial technique-based site suitability analysis for construction of water reservoirs in Arsha and Balarampur blocks, Purulia. *World Water Policy* 7(2):37–47. <https://doi.org/10.35940/ijeat.a1011.1291s319>

Unplanned Urban Sprawl Impact on Cultivable Soil Degradation



Suhad M. Al-Hedny and Qassim A. Talib Alshujairy

Abstract Unplanned urban sprawl reflects the concept of expansion of a built-up area at the expense of agricultural area as a result of the increase in population density. The main environmental impact of land use category changes from agricultural to urbanization is the degradation of cultivable soils and decreasing green spaces in cities and agricultural lands surrounding cities. Landsat image scenes that cover Babil Governorate, Iraq used to determine the percentages of land use/cover classes, namely, built up and bare-soil areas for 2001 and 2018. The Soil Adjusted Vegetation Index (SAVI), Normalized Difference Built-up Index (NDBI), Built-Up Index (UI), Dry Built-Up Index (DBI) and Dry Bare-Soil Index (DBSI) were derived from remotely sensed data to evaluate the rate of the land use/cover changes due to uncontrolled urban sprawl. Moreover, supervised satellite image classification was also performed to identify the study area's vegetated, bare-soil and built-up classes. The spectral indices results showed a noticeable increase in the built-up class from 14.4% in 2001 to 63.5% in 2018, while bare-soils and vegetated areas decreased from 38.7% and 46.9% in 2001 to 14.2% 22.3% in 2018, respectively. Different analyses types through supervised classification for indices composed and RGB images were beneficial to separate the land use/cover categories in this study. The remotely sensed-based indices helped recognize different land use/cover features with an overall accuracy value of 86.55% and a Kappa coefficient rated as substantial with the value of 0.7988. The usage of DBI and DBSI allowed to easily identified the expansion of built-up area by reducing the influence of bare soil and vegetation cover in built-up area detection.

Keywords Soil degradation · Remote Sensing · NDBI · DBI · DBSI · UI · SAVI

S. M. Al-Hedny (✉)

Department of Environment, Faculty of Environmental Science, Al-Qasim Green University, Babil, Iraq

e-mail: suhad.khudair@environ.uoqasim.edu.iq

Q. A. T. Alshujairy

Department of Soil and Water Science, College of Agriculture, University of Muthana, Samawah, Iraq

e-mail: qassimtalib@mu.edu.iq

© The Author(s), under exclusive license to Springer Nature Switzerland AG 2022

505

A. M. F. Al-Quraishi et al. (eds.), *Environmental Degradation in Asia*,

Earth and Environmental Sciences Library,

https://doi.org/10.1007/978-3-031-12112-8_23

1 Introduction

Land cover change has been an essential trend in research worldwide. As a highly complex process with such broad environmental impacts, international programs supported it as a core project and hot topic. Replacing vegetation areas with built-up areas extremely contributes to soil degradation. Soil is an essential natural resource that is as important as air and water. Hence soil is an ecosystem in itself rather than just an element of the ecosystem. Accordingly, soil science specialists studied the criteria and indicators of soil degradation, which are still evolving and developed so far in a few countries [1, 2].

Soil degradation is the loss of cultivatable soil capacity in terms of loss of its fertility, biodiversity, and degradation. It is defined as “a consequence of intensive land use management, which is assumed to be caused by human impact, poverty, and a response to economic opportunities at the global level” [3]. This concept includes all negative changes in the capacity of soil to provide goods and services for its beneficiaries. On a broader scope, soil degradation could be to such an extent that the original use is no longer possible.

Soil quality is the most commonly used index linked to the living and dynamic nature of the soil in relation to the diversity of uses. This emphasizes the importance of viewing the concept of soil quality as a relative rather than an absolute concept. Therefore, each soil has a natural ability to perform a specific function [4]. Soil quality is often used to compare one soil’s capacity to another and assess the suitability of the soil for specific uses. Currently, soil quality is used to assess the degree of degradation according to how the soil changes depending on how it is used. Usage options affect soil organic matter, soil structure, and water and nutrient retention capacity. This vital aspect of soil quality is the focal point for assessing the declining healthy soil resource. Soil quality studies often emphasize biological variable properties, but this does not eliminate or reduce the significance of physical and chemical factors (permanent properties of soil) [5].

In 1992, the United Nations Conference on Environment and Development (UNCED) stressed the principle of an integrated approach to land-use planning and management. In recent years, agricultural land has declined rapidly due to unregulated and unplanned urban sprawl (slums). According to the United Nations, nearly one-third of the cultivatable soils have degraded in the last four decades due to urban expansion and other unsustainable human practices [6]. The Ministry of Planning of Iraq announced that “the number of informal settlements in all Iraqi cities is about 3700 slums”. According to recent statistics, these slums are continuously increasing throughout the country. Baghdad came at the top of Iraqi cities with 1002 slums, followed by Basra and Ninawa with 700 slums. Karbala and Najaf governorates were the least by 98 slums [7].

Land-use change, especially the transformation of land use from agricultural to residential land, led to permanent degradation of land productivity [8]. This shift created serious problems and increased annual rates of land degradation [9].

1.1 Population Growth and Urban Areas in Iraq

Throughout the past 17 years, Iraq has experienced an unrivaled rapid uncontrolled urbanization due to population growth. The most important factors that accelerated the unplanned urbanization (slums) are the de-agriculturalization process and socio-economic transition from villages towards urban villages. The informal settlement is the main consequence of urban policy absent in the rural and semi-rural areas. Many studies considered the regional inequalities, economic activities, population growth, and poverty in rural areas as the main reasons behind unplanned urbanization [10–12]. Population growth is the key factor that directly stimulates land use changing, which leads to negative impacts on soil and the overall environment [13, 14]. The land use pattern remains a personal decision, particularly with the decline in the agricultural sector and the desire to fragmentation farmable land into housing and urban areas [15].

The estimated growth rate of Iraq's population is 2.28% per year, Iraq's population is expected to be 54 million by 2030 [16]. Iraq's most densely populated regions are the alluvial plain and northeast, with a very sparsely inhabited in the desert regions. In 1960, 57% of Iraq's population lived in the rural areas of the country. This number has declined as more people move away to larger urban areas. Agriculture represents the second largest contributor to Iraq's Gross Domestic Product (GDP) and the source of livelihood for 25% of Iraq's population. The decline of the agricultural sector kept rising the loss of arable land and a reduction in agriculture contribution to GDP. Greater frequency and intensity of drought further threaten small-scale farms mostly irrigated, particularly in Babylon, which has decreased agricultural productivity.

Iraqi families prefer housing in independent private houses with their own plots of land. Therefore, Babylon has a horizontal expansion and development similar to all Iraqi cities and Baghdad [17]. This kind of habit is most common in rural and semi-rural regions in comparison to the cities. Al Jarah [18] deemed proposing a strategic urbanism plan as a critical requirement to control the unplanned urban growth in the cities and rural areas.

Urban sprawl on agricultural areas in Baghdad was studied by Kahachi and Jafar [19], taking into consideration the political and socio-economical changes in Iraq from 2003 to 2015. Their results showed that the urban sprawl was at an accelerated speed over all the studied areas. In the first eight years of the study period, from 2002 to 2010 less than 25% of agricultural land was changed into built-up areas. The sprawl was more accelerated for the second period of the study (2010–2015). The same study described the sprawl's pattern, which started as scattered housing units around the agricultural areas and then organized into clusters of housing units near the standard housing units.

Generally, sprawling is entirely related to the availability of cheap agricultural land and disorganized development, particularly in rural and semi-rural regions of Iraq. Slums, informal settlements, low-income housing, and other synonyms of unplanned urban sprawl usually refer to the residential areas characterized by the lack of basic infrastructure services. Most of the unplanned urban areas in Iraq were in high-class

buildings with good finishing materials, which could not be considered temporary poverty housing (closer to stable housing). Almost all areas registered as agricultural land in Iraqi cities are classified as palm orchards and small-scale farms that are mostly surrounded by good infrastructure services. This urbanization system sprawled in acceptance by the community as a good solution for the housing crisis overall Iraqi cities.

1.2 Urban Sprawl Monitoring

Urban sprawl as a human-made spatial phenomenon, remotely sensed indices represent the most effective tools to monitor, describe and measure the urban sprawl rate, speed, and pattern of the expansive. The complexity and variety of required data could be effectively tackled using remote sensing (RS) techniques and Geographic Information Systems (GIS) in most urbanization studies. The following overview includes the most recent studies and the impacts on different fields of study. In Canada, Hathout [20] used GIS to study the impact of population on agricultural land by measuring population changes between 1960 and 1989.

Land use changing pattern was also successfully estimated using GIS, where the increase of population for years 1980, 1990, 2000, 2009, and 2014 led to environmentally affected 10% of Texas state lands [21]. Gong et al. [22] summarized the negative impacts on health due to shifting a rural to an urban society. The results of their study showed that the type of land use changed to built-up areas.

Several researchers studied the land-use changes (vegetation abundance) impacts on the land surface temperature (LST) [23–27]. They found a negative relation between the vegetation cover index (NDVI) and land surface temperature (LST). Rasul and Ibrahim [28]. studied the impacts of land-use changes on the land surface temperature in Duhok city, Kurdistan region of Iraq. They used Landsat 5-TM and Landsat OLI-TIRS-8 for years 1990, 2000, and 2016 to generate NDVI, Normalized Difference Water Index (NDWI), Normalized Difference Built-up Index (NDBI) and LST maps. Their results showed that NDVI and NDWI negatively correlated with high temperatures, while NDBI positively correlated. The same study results proved that rapid and uncontrolled urbanization could lead to hazard impacts on the environment.

The term “urban sprawl” was studied from different points of view in different fields. Almost all these perspectives correlated this term with its impacts, while other studies considered it a controversial term., They intensely focused on the main reasons behind this phenomenon. Al-Hedny et al. [29] identified vegetation cover changes in Babylon governorate for 2000, 2004, 2008, 2012, and 2016. They generated change detection maps for each studied year compared to 2000, which was considered a reference year for their study. They found an extreme decrease in vegetation cover at the east and south-east parts of Babylon governorate. Based on their study, this decline in vegetation cover was the normal consequence of

the fragmentation of farmland into housing and decline in the agricultural sector production.

The timely monitoring of the urban sprawl and its dynamic features represent critical requirements to identify the spatial changes and costs of new infrastructure and facilities needs. Compared with traditional methods, remote sensing-based indices provide a timely and cost-effective depiction of the spatial and temporal variation of the built-up areas at levels ranging from regional to global. NDBI is the most commonly used among these parameters.

Studies of urban patterns changing in rapidly growing urban such as Beijing and Shanghai in China were executed by [30–32], who confirmed the effectiveness of the remotely sensed techniques, particularly in such environments. Many studies used several remote sensing based-indices to evaluate urban expansion and the land-use changes over a limited study period. By combining Landsat ETM+, TM, ASTER, and Spot5 datasets and indices, researchers detected vegetation changes in Al-Madinah, Riyadh and Jeddah. They identified population growth as the key factor driving urban sprawl and vegetation cover declining over all the studied cities [33–36]. NDBI and NDVI are very easy indices to detect the significant land cover and describe the trend and pattern of change.

The combination of NDBI and NDVI through arithmetic manipulation from Landsat images served as a useful method for quickly mapping to monitor built-up changes [37]. To increase the efficiency of these indices, Rasul et al. [38] used dry built-up index (DBI) and dry bare-soil index (DBSI) to map urban areas and bare soil in the city of Erbil in the Kurdistan region of Iraq. Their results showed the suitability of these indices to detect built-up areas in arid and semi-arid regions. Therefore, the appropriate remotely sensed index should be carefully defined according to the study area's climatic region and other conditions.

Although there is much discussion on land-use change, few studies paid attention to the impact of this change on soil characteristics and the damage caused to the environment in general. To this end, this study aims to determine cultivatable soil degradation caused by changing the type of soil use from agricultural to urban (slums). Normalized Difference building Index (NDBI), Built-up Index (UI), were used to assess the decline of the cultivable soils under changing the type of soil use.

2 Materials and Methods

2.1 Study Area

Babil is located in central Iraq between 32° to 33.25° North latitude and 44° to 45° East longitude. The Euphrates river intersects the governorate and splits into two branches: Hindyah and Hilla. Babil has a typical climate with temperatures exceeding 40° in summer and the rainfall is restricted to the period between November and April

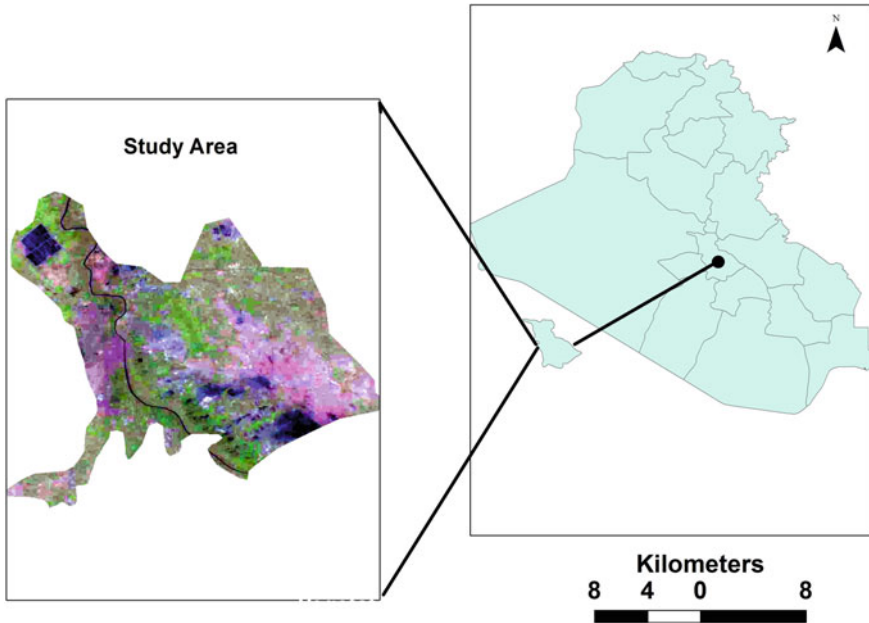


Fig. 1 The study area in Babil Governorate, Iraq

with a minimal amount. The governorate covers 5119 Km² of Iraq, divided into: Al-Musayab, Hilla, Al-Mahawil and Hashimiya. It is the fifth-largest governorate in terms of population estimated to be around 1,728,132 inhabitants in 2015, of which 52.8% is rural and 47.2% is urban population. The district of Hashimiya was selected as the study area because of its rapid urbanization over the past 17 years Fig. 1.

2.2 Remotely Sensed Indices

Landsat scenes were chosen due to their free availability, corrected before delivery for radiometric and distortions, and medium to high spatial resolution (Table 1).

Table 1 The characteristics of Landsat datasets used in this study

Acquisition date	Sensor	Path/Row	Spatial resolution	Cloud (%)	Number of bands	Format
April 2001	Landsat 5 TM	168/38	30	0	7	Geotiff
April 2018	Landsat 8 OLI	168/38	30	0	11	Geotiff

The datasets covering the study area were freely acquired from USGS Earth explorer website (<http://earthexplorer.usgs.gov/>). USGS Level-one terrain- corrected (L1T) Landsat data in WGS84 with UTM map projection provided the primary data to calculate the built-up indices for the study area.

Different remotely sensed indices were used to divide the study area into three major land-use classes: built-up, vegetation, and bare soils. Several indices were derived to well separate of each class of land using. Soil Adjusted Vegetation Index (SAVI) was used instead of the Normalized Difference Vegetation Index (NDVI) to improve the detecting of vegetation area and minimize soil influences. SAVI and NDVI were obtained from formulas (1) and (2) [37, 39, 40].

$$NDVI = \frac{NIR - RED}{NIR + RED} \tag{1}$$

$$SAVI = \frac{(NIR - RED)(1 + k)}{NIR + RED + k} \tag{2}$$

where k is a factor of correction with values range from 0 for very high vegetation cover to 1 for very low vegetation cover area, in this study we chose k to be 0.5. To achieve this study’s purpose, the Dry Built-Up Index (DBI) and Dry Bare-Soil Index (DBSI) were used to map and separate the built-up and bare soil classes. The DBI and DBSI were selected based on their suitability to differentiate between urban and bare soil areas. The formulas for obtaining the DBI and DBSI as proposed by Rasul et al. [38] are shown in formulas (3) and (4):

$$DBI = \frac{\rho_{Blue} - \rho_{TIR1}}{\rho_{Blue} + \rho_{TIR1}} - SAVI \tag{3}$$

$$DBSI = \frac{\rho_{SWIR1} - \rho_{Green}}{\rho_{SWIR1} + \rho_{Green}} - SAVI \tag{4}$$

The current study used SAVI instead of NDVI in the main formulas proposed by Rasul [38] to well separating the built-up area from the bare soil areas within the study area. The Urban Index (UI) and the Normalized Difference Built-up Index (NDBI) were used for rapid mapping of built-up land. The mathematical formulas for the calculation of both urban indices are represented in (5) and (6) [37, 41].

$$UI = \frac{SWIR2 - NIR}{SWIR2 + NIR} \tag{5}$$

$$NDBI = \frac{SWIR1 - NIR}{SWIR1 + NIR} \tag{6}$$

The newly created data set of DBI, DBSI, UI, NDBI and SAVI images were manipulated to simplify separating the three major land-use classes. The maximum likelihood was performed using a supervised classification based on training regions

to calculate the percentages of vegetated, built-up and bare-soil areas during 2001 and 2018.

2.3 Accuracy Assessment

Error matrix is the simplest and most commonly used way to evaluate the accuracy of the LULC classification map. Google earth and the reference ground and Global Positioning System (GPS), were used to collect ground validation data for 2018. Totally 290 ground reference points (Fig. 2) were generated over the study area to assess the accuracy of the classification of each reference point [42].

Overall accuracy and Kappa coefficients were derived from the error matrix using the following formula:

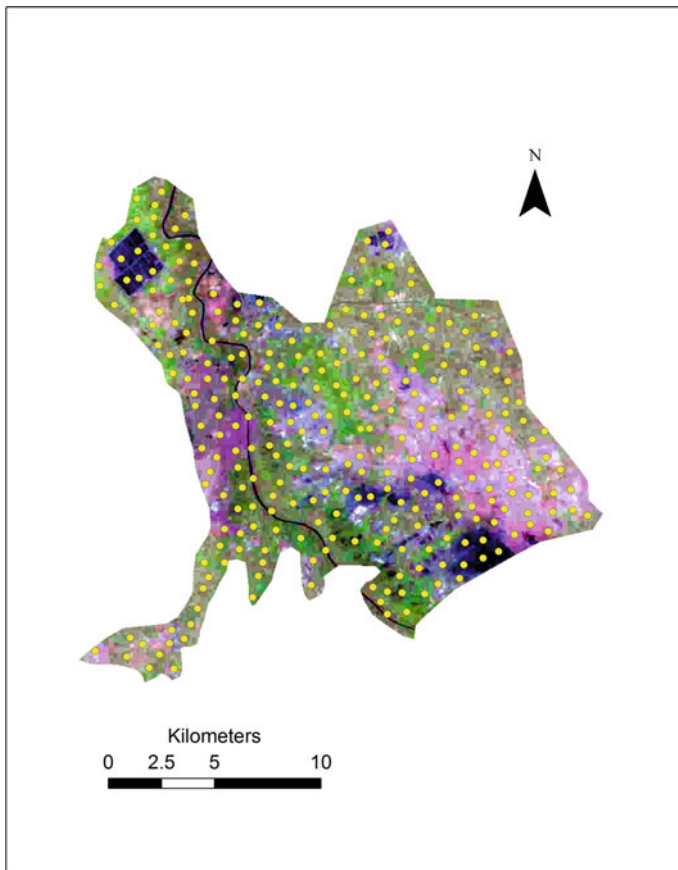


Fig. 2 Classified map of study area covered with 290 random points

$$\text{Kappa coefficient} = \frac{(T \times C) - G}{T^2 - G} \quad (7)$$

where: T is the test pixels, C is the correctly classified pixels, G is the sum of multiplied total value [43]. The overall accuracy is computed using the following formula:

$$T = \frac{\sum D_{ii}}{N} \quad (8)$$

where: T is the overall accuracy, $\sum D_{ii}$ is the total number of correctly classified pixels and N is the total number of pixels in the error matrix [44].

3 Results and Discussion

3.1 Built-Up Area Extension Spatial Pattern

The resulted maps of the indices NDBI, BDI and UI are presented in Fig. 3. The calculated indices showed a noticeably rising in the built-up area in the outskirts and on isolation patterns within the study area. The distribution of the built-up area of 2018 is obviously higher than the year 2001, reflected by higher spectral values.

The parameters: Min, Max, Mean and the standard deviation of the NDBI, DBI and UI for 2001 and 2018 are shown in Table 2. These parameters reflect a higher extent of the built-up area of 2018 than 2001. As can be seen from Table 2, the increase of the built-up areas combined with declining in vegetated and bare soil areas is reflected by decreasing the values of SAVI and DBSI indices during 2018 compared to the year 2001.

The SAVI values (minimum and maximum) for the year 2018 are -0.33 and 0.86 while for the year 2001 are -0.27 and 1.49 , respectively. These values clearly indicate the decline of the vegetated area. The results of maximum NDBI, UI and DBI are 1 , 1 and 1.04 ; respectively, for the year 2018 are quite close to each other. These values proved the suitability of using these indices for urbanization extend across the study area. Diminishing SAVI in the DBI index improved built-up area identification compared to NDBI and UI that are often confused with green areas.

3.2 Land Use/Cover Identification

The Land Use/Cover (LULC) classes, namely, built-up, bare-soil and vegetated areas of the studied area, were extracted based on the spectral response of the land cover

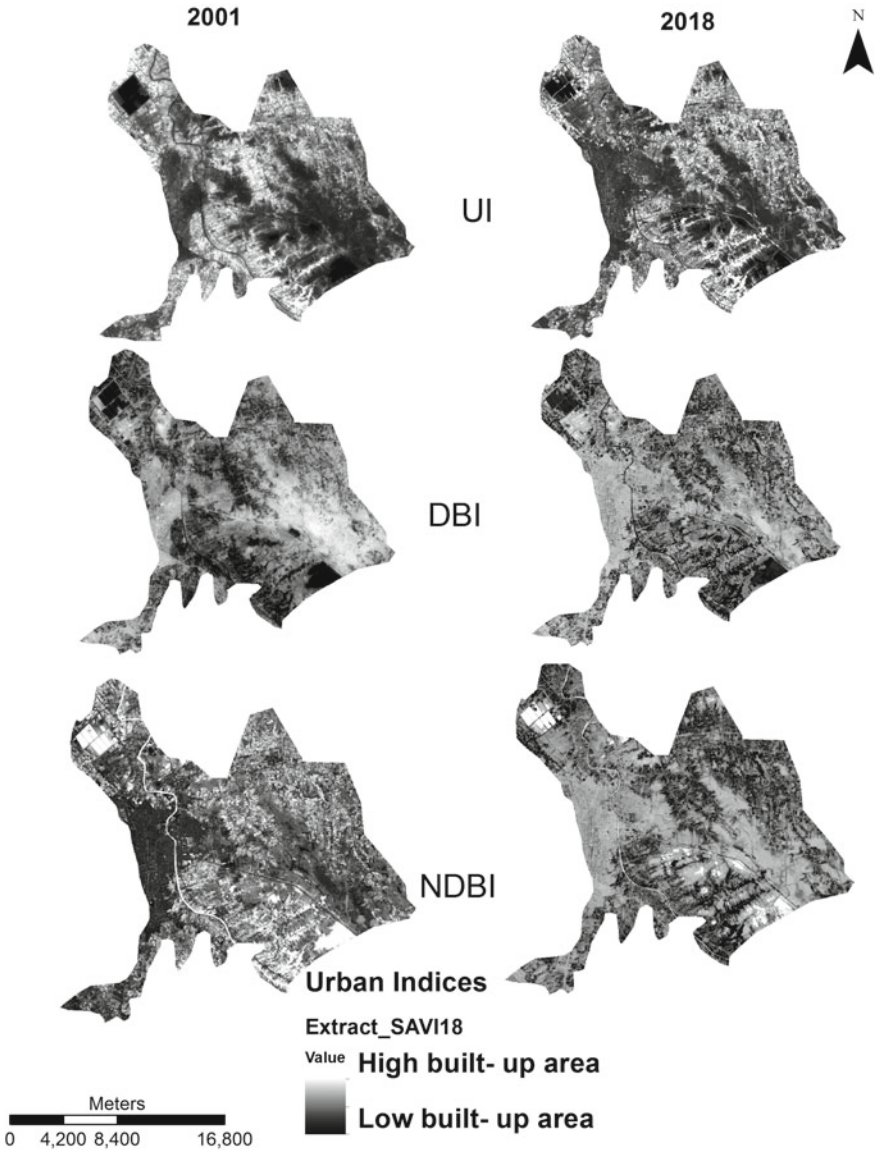


Fig. 3 Maps of NDBI, UI and DBI indices of the study area from Landsat 5 and 8 images for 2001 and 2018

Table 2 Statistical data of NDBI, DBI, UI, SAVI and DBSI indices for 2001 and 2018

Index	Min		Max		Mean		SD	
	2001	2018	2001	2018	2001	2018	2001	2018
SAVI	-0.27	-0.33	1.49	0.86	0.04	0.22	0.08	0.14
NDBI	-0.54	-0.11	0.34	1	-0.13	0.1	0.09	0.05
UI	-0.39	-0.45	0.18	1	-0.05	-0.18	0.06	0.08
DBI	-1.1	-0.35	-0.16	1.04	-0.62	-0.02	0.11	0.28
DBSI	-1.62	-0.41	1.38	0.23	0.25	-0.03	0.18	0.09

features. The classification approach involved two steps: Firstly, supervised classification for land cover based on the training areas for land cover categories from April 2001 and 2018 were derived from RGB composition. Secondly, supervised classification was derived from the NDBI, DBI, UI, DBSI indices composed images. The method based on indices combination noticeably enhanced the reflectance of each element and decreased confusion between urbanization and bare areas.

Figure 4 showed that vegetation and built-up areas characterize the study area. It can be seen that built-up areas increased between 2001 and 2018, while bare-soils and vegetated areas decreased in 2018. The built-up area expansion developed into a randomized pattern in all study area directions Fig. 4. The main expansion was on the borders of the agricultural land and along the paved roads as well as the river. The decline of the vegetated and increasing built-up areas in 2018 is due to the region's political, economic, and social situation. Increasing population, housing crisis, poverty, weakness of legislation and many other factors contributed to increasing urban lands within the study area. These results were also endorsed in different regions of Iraq [19, 38, 45]. This urban area expansion effectively contributed to soil degradation, which is considered the main consequence of human-induced phenomenon. The displacement of the productive soils with bare soils in most areas signifies that the soil degradation is taking place or has occurred.

This study used the area size data extracted from the supervised classification for each year to calculate each LULC class area (%). The results as shown in Fig. 5 quantified the land cover changes, the urban area increased from 14.4% (10.868 Km²) in 2001 to 63.5% (50.883 Km²) in 2018, while bare-soils and vegetated area decreased from 38.7% (29.29 Km²) and 46.9% (35.474 Km²) in 2001 to 14.2% (12.511 Km²) and 22.3% (19.601 Km²) in 2018, respectively. Almost all of the study area was classified/registered as agricultural land. The new or reconstructed households living in the area come from neighboring districts or relocating the new houses in the slum area. The constructed area was classified as a reasonable settlement for building materials and acceptable by the community, which could not be classified as temporary housing. Although this phenomenon is serving to overcome the housing crisis in most Iraqi cities, it has potential impacts on loss of cultivated agricultural land and contributing to many environmental consequences of soil degradation and desertification.

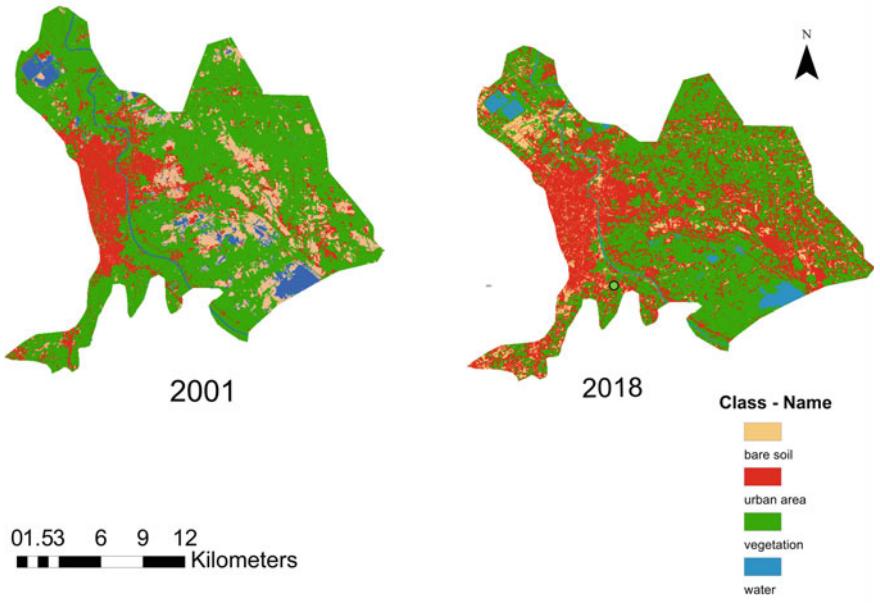


Fig. 4 LULC maps for 2001 and 2018

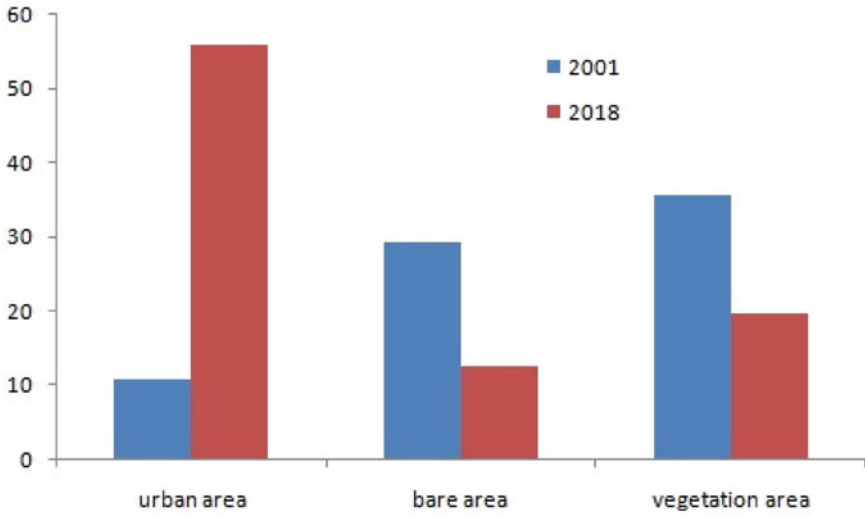


Fig. 5 Area (Km²) of LULC classes in 2001 and 2018

Table 3 Error matrix of LULC classification

Classified	Water	Built-up	Vegetation	Bare soil	Total	Correct sampled
Water	44	3	0	0	47	44
Built up	0	65	3	10	78	65
Vegetation	0	0	127	3	130	127
Bare soil	0	7	2	26	35	26
Total	44	75	132	39	290	251
Overall accuracy	86.55%		Kappa coefficient		0.7988	

3.3 Classification Accuracy Assessment

In order to provide helpful information for applications of urban indices and LULC maps, it is necessary to evaluate the accuracy of the classification map. Table 3 shows the error matrix of LULC classification according to the relationship between classified data and ground reference data. The overall accuracy (total number of correctly classified pixels/number of total reference points) was 86.55%. Statistically, an accuracy level of up to 80% is adequate to verify the feasibility of the LULC classification map [31].

Moreover, this study assessed the accuracy of land cover types classification by using the Kappa coefficient. An estimation of this statistic parameter refers to the strength of agreement. A Kappa value of 1 means perfect agreement, while a value close to zero means a poor agreement [46, 47]. In this study, Kappa was rated as substantial with a value of 0.7988.

The high values of overall accuracy and Kappa coefficient referred to how effectively each pixel was sampled into the correct land cover class. The effectiveness of using DBI and DBSI to mapping built-up and bare-soil areas in arid and semi-arid regions was proved with an overall accuracy of 93% in Erbil, Iraq [38]. The supervised classification was the best technique for classifying LULC of Baghdad Al-Karkh from 1986 to 2017 with an accuracy assessment ranging between 89–95% [35].

4 Conclusions

The main conclusions of this study are:

- (1) The implementation of remotely sensed-based indices were encouraging with the overall accuracy of the LULC classification map with the value of 86.55%. The accuracy of land cover types was rated as substantial with a Kappa coefficient of 0.7988.
- (2) Urbanized areas obviously increased from 14.4% in 2001 to 63.5% in 2018. All of the derived indices were higher in 2018 than in 2001.

- (3) Using SAVI and DBSI instead of NDVI contributed to reducing the spectral confusion between land-use classes.
- (4) Using bands and indices composed images vastly improved the defining training regions and consequently, considerable extraction accuracy of land use features was achieved.

5 Recommendations

LULC use reflects temporal and spatial soil degradation nature under a high-growth population scenario. Therefore, periodically updated maps of LULC change are critical for effective city planning and management. More efforts are needed to study how the different LULC changes will impact and change the soil conditions.

References

1. Carla SSF, Rory PDW, António JDF (2018) Degradation in urban areas. *Curr Opin Environ Sci Health* 5:19–25
2. Seifu W, Elias E (2018) Soil quality attributes and their role in sustainable agriculture: a review. *Int J Plant Soil Sci* 26(3):1–26
3. Lambin EF (2001) The causes of land-use and land-cover change: moving beyond the myths. *Glob Environ Chang* 11:261–269
4. Warkentin BP (1995) The changing concept of soil quality. *J Soil Water Conserv* 50:226–228
5. Bünemann EK, Bongiorno G, Bai Z, Rachel E et al (2018) Soil quality—a critical review. *Soil Biol Biochem* 120:105–125
6. Maximillian J, Matthias AD (2019) *Environmental and pollution science*, 3rd edn
7. Al-Sheikhly B (2018) The Arab weekly. *Global Research*, December 19, 2018, site visit in 27 April 2019
8. Obade DPV, Lal R (2016) Towards a standard technique for soil quality assessment. *Geoderma* 265:96–102
9. Ajami M, Khormali F, Ayoubi S, Omrani RA (2006) Changes in soil quality attributes by conversion of land use on a loess hillslope in Golestan Province, Iran. In: 18th International Soil Meeting (ISM) on soil sustaining life on earth, maintaining soil and technology proceedings, soil science society of Turkey, pp 501–504
10. Liu M, Tang CY, Tang HR, Shi SN (2017) The controlling effects of on newly-increased construction land expansion under general land use planning—a case study of Guiping City, Guangxi. *Guangdong Land Sci.* 16:24–32
11. Faihan SM (2014) Urban policy in Iraq for the period 1970–2012, evaluation study. *J Adv Soc Res* 4:58–76
12. Arsanjani JJ, Helbich M, Vaz EDN (2013) Spatiotemporal simulation of urban growth patterns using agent-based modeling: the case of Tehran. *Cities* 32:33–42
13. Bimal KP, Harun R (2017) Chapter six—land use change and coastal management. In: Paul BK, Rashid H (eds) *Climatic hazards in coastal Bangladesh*, Butterworth-Heinemann, pp 183–207
14. Byomkesh T, Nakagoshi N, Dewan AM (2012) Urbanization and green space dynamics in Greater Dhaka, Bangladesh. *Landsc Ecol Eng* 8:45–58
15. Prasad G, Rajesh R, Arun K (2020) Land use pattern as an indicator of sustainability: a case study. In: *Proceedings of the international conference on industrial engineering and operations management*, Dubai, UAE, March 10–12

16. United Nations, Department of Economic and Social Affairs, Population Division (2019) World population prospects 2019, vol 1: comprehensive tables (ST/ESA/SER.A/426)
17. Hilla City Master Plan (IQ05122) The study includes building up EMM2 traffic model for testing the different road network alternatives proposed for the city Master plan 2007–2008
18. Al Jarah SH, Zhou B, Abdullah RJ, Lu Y, Yu W (2019) URbanization and Urban sprawl issues in city structure: a case of the Sulaymaniah Iraqi Kurdistan region. *Sustainability* 11:485
19. Kahachi HA, Jafar AJ (2015) Urban sprawl on agricultural land in Iraq- The factors and impacts: a study of Karkh area in the city of Baghdad. *Int J Environ Water* 4(2):69–76
20. Hathout S (2002) The use of GIS for monitoring and predicting Urban growth in east and west St. Paul Winnipeg, Manitoba, Canada. *J Environ Manage* 66(3):229–238
21. Kharel G (2010) Impacts of urbanization on environmental resources: a land use planning perspective. Thesis, University of Texas, USA, MSc
22. Gong P, Liang S, Carlton EJ, Jiang Q, Wu J, Wang L, Remais JV (2012) Urbanisation and health in China. *The Lancet* 379(9818):843–852
23. Jiang J, Tian G (2010) Analysis of the impact of Land use/land cover change on land surface temperature with remote sensing. *Proc Environ Sci* 2:571–575
24. Khwarahm NR, Qader S, Ararat K, Al-Quraishi AMF (2021) Predicting and mapping land cover/land use changes in Erbil/Iraq using CA-Markov synergy model. *Earth Sci Inf* 14:393–406
25. Alqasemi AS, Hereher ME, Al-Quraishi AMF, Saibi H, Aldahan A, Abuelgasim A (2020). Retrieval of monthly maximum and minimum air temperature using MODIS Aqua land surface temperature data over the United Arab Emirates (UAE). *Geocarto Int* <https://doi.org/10.1080/10106049.2020.1837261>
26. Divya Y, Gopinathan P, Jayachandran K, Al-Quraishi AMF (2020) Colour slices analysis of land use changes due to urbanization in acity environment of Miami Area, South Florida, USA. *Model Earth Syst Environ*. <https://doi.org/10.1007/s40808-020-00883-x>
27. Alqasemi AS, Hereher ME, Kaplan G, Al-Quraishi AMF, Saibi H (2021) Impact of COVID-19 lockdown upon the air quality and surface urban heat island intensity over the United Arab Emirates. *Sci Total Environ* 767:144330
28. Rasul G, Ibrahim F (2017) Urban land use land cover changes and their effect on land surface temperature: case study using Dohuk city in the Kurdistan region of Iraq. *Climate, MDPI* 5:13
29. Al-Hedny SM, Karkoosh HS, Talib QA (2018) Studying urban sprawl by using Normalized Difference Vegetation Index (NDVI) in Babylon governorate, Iraq. *Int J Agric Stat Res* 14. Supplement 1:117–124
30. Guo L, Wang D, Qiu J, Wang L, Liu Y (2009) Spatio-temporal patterns of land use change along the Bohai Rim in China during 1985–2005. *J Geog Sci* 19(5):568–576
31. Zhou M, Lu L, Guo H, Weng Q, Cao S, Zhang S, Li Q (2021) Urban sprawl and changes in land-use efficiency in the Beijing–Tianjin–Hebei Region, China from 2000 to 2020: a spatiotemporal analysis using earth observation data. *Remote Sens* 13:2850
32. Kim S, Rowe PG (2012) Does large-sized cities’ urbanisation predominantly degrade environmental resources in China? Relationships between urbanisation and resources in the Changjiang Delta Region. *Int J Sust Dev World* 19(4):321–329
33. Al-Harbi KM (2010) Monitoring of agricultural area trend in Tabuk region—Saudi Arabia using Landsat TM and SPOT data. *Egypt J Remote Sens Sp Sci* 13:37–42
34. Al- Gaadi KA, Samdani MS, Patil VC (2011) Assessment of temporal land cover changes in Saudi Arabia using remotely sensed data precision agriculture research chair, college of food and agriculture sciences. *Middle-East J Sci Res* 9:711–717
35. Khudair DA, Al-Quraishi AMF, Hassan AA (2019) Spatiotemporal monitoring and modeling of urban sprawl using remote sensing and GIS: a case study Al-Karkh, Baghdad, Iraq. *J Adv Res Dyn Control Syst* 11(6):1691–1698
36. Deng Y, Qi W, Fu B, Wang K (2020) Geographical transformations of urban sprawl: exploring spatial heterogeneity across cities in China 1992–2015. *Cities* 105:102–415
37. Zha Y, Gao J, Ni S (2003) Use of normalized difference built-up index in automatically mapping urban areas from TM imagery. *Int J Remote Sens* 24(3):583–594

38. Rasul A, Balzter H, Ibrahim GRF, Hameed HM, Wheeler J, Adamu B, Ibrahim S, Najmaddin MP (2018) Applying built-up and bare-soil indices from landsat 8 to cities in dry climate. *J Land* 7:81
39. Kawamura M, Jayamana S, Tsujiko Y (1996) Relation between social and environmental conditions in Colombo Sri Lanka and the Urban Index estimated by satellite remote sensing data. *Int Arch Photogramm Remote Sens* 31:321–326
40. Huete A (1988) A soil-adjusted vegetation index (SAVI). Elsevier: *Remote Sens Environ* 25(3):295–309
41. Lee AJ, Lee SS, Chi HK (2010) Development of an urban classification method using a built-up index. In: Theme paper for the selected topics in power systems and remote sensing, Japan, pp 39–43
42. Ranagalage M, Wang R, Gunarathna MHJP, Dissanayake D, Murayama Y, Simwanda M (2019) Spatial forecasting of the landscape in rapidly urbanizing hill stations of South Asia: a case study of Nuwara Eliya, Sri Lanka (1996–2037). *Remote Sens* 1743(11):2–31
43. Petropoulos GP, Kalivas DP, Georgopoulou IA, Srivastava PK (2015) Urban vegetation cover extraction from hyperspectral imagery and geographic information system spatial analysis techniques: case of Athens, Greece. *J Appl Remote Sens* 9(1):096088
44. Pal S, Ziaul S (2017) Detection of land use and land cover change and land surface temperature in English Bazar urban centre. *J Remote Sens Sp Sci* 20:125–145
45. Kahachi H (2002) State-led low-cost housing in the political and social context: a study of the evolution of state-led low-cost housing initiatives in the post-colonization era through a case os Sadr City in Baghdad, Masters dissertation, school of city and regional planning, Cardiff University in UK
46. Murty PS, Tiwari H (2015) Accuracy assessment of land use classification—a case study of Ken Basin. *J Civ Eng Archit Res* 2:1199–1206
47. Al-Shujairy QA, Al-hedny S, Al-Barakat H (2021) Evaluation of dryness conditions in Babylon governorate using the Stabdarized Precipitation Index (SPI) and the Normalized Difference Water Index (NDWI). In: IOP conference series: earth and environmental science, vol 722, pp 1–14

Variability Analysis of Local Climate Change and Its Association with Urbanization in the Beijing-Tianjin-Hebei Region, China



Saobo Zhong, Min Xu, Chunxiang Cao, and Wei Zhu

Abstract Urbanization has a significant impact on local climate change such as trends and variations of temperature and precipitation. Accurate evaluation on effect of urbanization on local climate change provides guidance for the prevention and control of extreme weather in cities and towns. In this chapter, taking the Beijing-Tianjin-Hebei region as the study area, we investigated the statistical relationship between population, urbanization, land use and cover change (LUCC) and climate change. The Beijing-Tianjin-Hebei is one of China's three major urban agglomerations. Both Pearson's moment correlation and Spearman's rank correlation was used. Moreover, an empirical orthogonal function (EOF) method was selected to decompose a proposed urbanization index and an array of meteorological variables and correlation analysis between the resulting modes. This study can be conclude: (1) the annual cumulative precipitation shows no significant trend in the Beijing-Tianjin-Hebei region while the annual average temperature is increasing, and has a statistical correlation with urban development to some extent, (2) compared with the precipitation variables, the temperature variables show better similarity to the first mode of the urbanization index in the first 10 modes, (3) the residential land and industrial and mining land has a strong impact on climatic factors such as annual average temperature and the impact of residential land on climate is higher than that of industrial and mining land, and (4) green land, water bodies and wetlands have a stabilizing effect on the temperature in the cities, and are negatively correlated with the maximum temperature and positively correlated with the minimum temperature.

S. Zhong · W. Zhu (✉)

Beijing Academy of Science and Technology, Beijing 100035, China

e-mail: zhuweianquan@126.com

M. Xu · C. Cao

State Key Laboratory of Remote Sensing Science, Aerospace Information Research Institute, Chinese Academy of Sciences, Beijing 100101, China

e-mail: xumin@radi.ac.cn

C. Cao

e-mail: caocx@aircas.ac.cn

© The Author(s), under exclusive license to Springer Nature Switzerland AG 2022

A. M. F. Al-Quraishi et al. (eds.), *Environmental Degradation in Asia*,

Earth and Environmental Sciences Library,

https://doi.org/10.1007/978-3-031-12112-8_24

Keywords Urbanization · Climate change · Empirical orthogonal function (EOF) · Pearson's moment correlation · Spearman's rank correlation

1 Introduction

In the past 50 years, greenhouse gas concentrations in the atmosphere have increased significantly. The global warming effect has been remarkable, which has led to the change of climate factors in the world. For example, the Fifth Assessment Report (AR5) of the United Nations Intergovernmental Panel on Climate Change [1] indicates that the temperature increase rate from 1998 to 2012 is estimated to be around $0.004\text{ }^{\circ}\text{C/a}$, one-third to one-half of the trend over the period from 1951 to 2012. Nonetheless, the climate system has very likely continued to accumulate heat since 1998, and the sea level has continued to rise. Plenty of research suggests that the main human activities that affect climate change are industrialization and urbanization. With the rapid development of industrialization and science and technology, urbanization is also rapid. As a result, artificial facilities in built-up areas gradually replace forest, grassland, and farmland. In recent years, high-intensity economic activities and high-density population gradually gather to cities and towns from rural areas.

China is one of the countries with the most prominent global warming characteristics and the fastest urbanization. Over the period 1961–2013, China's temperature increased by $1.44\text{ }^{\circ}\text{C}$ (90% confidence interval $1.22\text{--}1.66\text{ }^{\circ}\text{C}$) [2]. Built-up area increased from $30,406\text{ km}^2$ in 2004 to $52,102\text{ km}^2$ in 2015. The annual compound growth rate is more than 4.59%, much higher than the global average. The Beijing-Tianjin-Hebei region is an urban agglomeration in North China. Its development process is a multidimensional and complex problem for the local climate.

For trend detection of climate change, many researchers have been contributing to global and local climate data series. For example, several methods are proposed and used for long-term meteorological series homogeneity tests [3–6]. At present, the study of the impact of urbanization on climate change mainly focuses on temperature and precipitation. Velazquez-Lozada et al. found that the heat island effect was strengthened in San Juan, Puerto Rico, with urbanization development [7]. Peterson et al. studied the trend of rural climate change in the world and found that rural areas are consistent with warming trends in neighboring urban areas [8]. Hughes et al. studied the impact of urban warming on the temperature trends in South Africa [9]. They found that the increased rate of temperature in the three major cities of South Africa is significantly higher than its suburbs. However, the impact of urbanization on the significance of precipitation is not obvious.

Nie et al. investigated the effect of urbanization on climate change in China's three urban agglomerations: the Beijing-Tianjin-Hebei region, the Yangtze River Delta region, and the Pearl River Delta region through the daily climate data and urban population data [10]. They concluded that urbanization has a more significant impact on the temperature, but the impact of precipitation is not obvious. Niyogi et al.

analyzed the effect of the eastern United States' urbanization on summer rainstorms through satellite remote sensing vegetation data [11]. Lin et al. found that the intensity of heat island effect is significantly associated with the speed of urban infrastructure construction, the change of the underlying surface, and the local climate factors [12].

According to Thanh Hoan et al. for Hanoi City of Vietnam, transforming a chosen area from vegetation to built-up can result in enhanced thermal contrast by 3.3 °C [13]. Climate change also enhances the global threat posed by natural hazards and anthropogenic stress [14]. Some studies also explored the impact of population and land use and cover change (LUCC) on climate change such as temperature, precipitation, greenhouse gas concentrations, and urban heat island effect [15–19]. It can be seen that depending on different regions and scales, the impact extents and patterns are also different. However, universal evidence of association between these factors and climate change has been found in this literature [20–22].

It is a challenging issue to measure the urbanization level. On the one hand, urbanization systems are complex dynamic systems influenced by many indicators or factors. The methods used in urbanization level evaluation (ULE) are various and still under study. On the other hand, ULE is heavily dependent on different development levels and patterns for cities in different countries or regions. Long before, it was found that the urban population of some third world countries increased rapidly. However, the growth of GDP (Gross Domestic Product) and the built-up area was much lower than population, i.e., population growth did not bring “effective” urbanization [23, 24]. What's more, economy development isn't also equal to urbanization.

In China, for example, urbanization lags behind economic development, for which some reasons are analyzed by Jun [25]. Compared with other factors associated with urbanization, the statistics of population data are more perfect. Therefore, in some studies on urbanization, population size and density is used to represent urban scale. For example, when ranking the city level in China, the population size is one of the most important concerning factors. Nonetheless, only demographic data are far from a complete description of urbanization. Therefore, in ULE, researchers generally consider a variety of variables comprehensively. For example, Zhao et al. proposed an indicator system considering urban construction, economic development, social development, etc. [26].

In this chapter, taking four contiguous cities in China's Beijing-Tianjin-Hebei region as the study area, the meteorological, socio-economic, and LUCC data were synthetically used to explore the correlation and variability between urbanization and local climate change. We constructed urbanization indicators based on population size, population density, GDP, built-up area etc., socio-economic data. Several data analysis methods including Pearson's moment correlation, Spearman's rank correlation, and EOF were selected to achieve the goals. The conclusions drawn from our study can help urban planners foresee the potential climate change induced by urbanization to a certain extent, and provide guidance for the prevention and control of extreme weather in cities and towns.

2 Materials and Methods

2.1 Study Area

We chose the Beijing-Tianjin-Hebei region as the study area, which extends from 113°40'E–118°10'E in longitude and 38°20'N–41°10'N in latitude (Fig. 1). The time span is 1980 to 2015, which is also one of the most rapid period of urbanization in the study area. The Beijing-Tianjin-Hebei region is one of China's three major urban agglomerations and one of the largest urban agglomerations in the world. In the past few decades, the study area had rapid urbanization. According to the China Demographic Yearbook data, as of 2014, the population of the Beijing-Tianjin-Hebei region has increased by about 109 million since 1978. The population density is low in the northwest of the Beijing-Tianjin-Hebei region and high in the southeastern. Four densely populated cities: Beijing, Tianjin, Baoding and Langfang are formed during urban development.

In this chapter, the four cities: Beijing, Tianjin, Langfang, and Baoding in the study area were selected as the representative cities, and Langfang and Baoding were used for referents. Langfang is located at the connection between Beijing and Tianjin, and

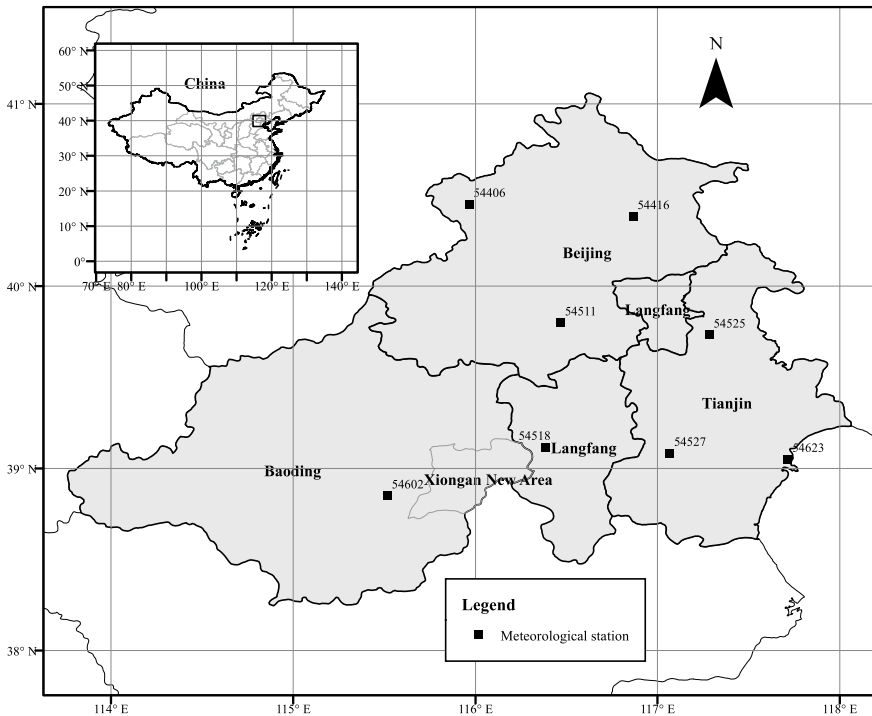


Fig. 1 The geographical extent of the study area and its location in China

the urban development is relatively slower than Beijing and Tianjin. In addition, on April 1, 2017, a notice was issued to set up a new zone called Xiongan New Area, which is supposed to divert Beijing’s non-capital functions to ease the increasing load of the metropolitan city. Urbanization is bound to bring some climate impact in the future development of Xiongan New Area. Baoding and Langfang are located near the new zone and will be accelerated in their development in the future. We expect to provide useful suggestions for constructing the new zone and its neighborhood from this study.

There is a total of 8 surface meteorological stations located within the study area: 3 in Beijing, 3 in Tianjin, 1 in Baoding, and 1 in Langfang. The locations and distribution of these stations can be seen in Fig. 1.

2.2 Methods

2.2.1 Evaluating Urbanization Levels

Based on some studies [27–31], we proposed a composite index to represent the regional comprehensive urbanization level by adding three normalized indices: normalized population density, normalized GDP, and normalized proportion of built-up area, i.e., the composite urbanization level index is expressed as:

$$CI = I^{(1)} + I^{(2)} + I^{(3)} \tag{1}$$

where, $I(i)$, $i = 1, 2, 3$ denotes the i th normalized individual index, which is calculated as follows:

$$I^{(i)} = \frac{x^{(i)} - x_{\min}^{(i)}}{x_{\max}^{(i)} - x_{\min}^{(i)}}, i = 1, 2, 3 \tag{2}$$

where x is the value of the individual index for the current year, x_{\min} and x_{\max} are the minimum and maximum values from all years respectively.

The yearly values of individual indices were collected and calculated from the National Bureau of Statistics Data Center and the Statistical Yearbook of Hebei Province. The original data in some regions of Hebei province changes abruptly because of the administrative area adjustment. For example, Baoding area and Baoding city were merged into a new municipality in December 1994. The new municipality is still called Baoding and directly under the Hebei province government. Dingzhou, previously administered by Baoding, had not been under Baoding by June 2013. This change of administrative division leads to a decrease by 1200,000 in population in the new Baoding. To maintain the consistency of the data, the statistics were consistently made according to the administrative areas of the four cities in

1980. We obtained the permanent resident population, GDP, and built-up area in four cities: Beijing, Tianjin, Baoding, and Langfang from 1980 to 2015. The area of each city was obtained according to its administrative area in 1980. Finally, we calculated the permanent resident population densities, GDP per unit area, and proportion of built-up area through dividing the values by area.

We also used LUC data to evaluate the creditability of the proposed index. The LUC data are from the Chinese Academy of Sciences Resources and Environment Science Data Center (<http://www.resdc.cn/>). The format of the data is raster data. The time span is from 1980 to 2015 and the retrieved time interval is 5 years. The institution produced the data by artificial visual interpretation taking Landsat TM/ETM remote sensing images as the main data source. The land classification standard in the original dataset are derived from “China’s 1:1,000,000 land use map” [32]. According to the standard, the land use types include: (I) farmland, (II) forest land, (III) grass land, (IV) waterbody, (V) rural land, urban land, industrial and mining land, (VI) unused land. We calculated the proportion of type V to reflect the human activity.

2.2.2 Calculating Meteorological Variables

The original meteorological data were obtained from the China Meteorological Information Center, which are the daily observations of the meteorological stations in the study area (there is a total of 8 stations as shown in Fig. 1). The period is from 1980 to 2015. We obtained an array of annual meteorological variables according to the research needs by synthesizing the original data in annual and quarterly time scales. There are a total of 33 variables for each station (including 20 temperature variables and 13 precipitation variables). We referred to the definitions of these meteorological variables by CMDC (China Meteorological Data Service Center, <http://data.cma.cn/en>) and calculated them by developing a Matlab code.

2.2.3 Analyzing Correlation and Variability

(1) Pearson’s moment correlation analysis

The Pearson’s moment correlation coefficient was used to describe the linear correlation between the composite urbanization level index and meteorological variables. It is calculated as:

$$r_{xy} = \frac{\sum x_i y_i - n\bar{x}\bar{y}}{(n-1)s_x s_y} = \frac{n \sum x_i y_i - \sum x_i \sum y_i}{\sqrt{n \sum x_i^2 - (\sum x_i)^2} \sqrt{n \sum y_i^2 - (\sum y_i)^2}} \quad (3)$$

where [xn] and [yn] are observed samples for the two sets of concerned variables, and s_x , s_y are their standard deviation, respectively. Since the Pearson’s moment

correlation coefficient describes the linear relationship between the two variables, its value is not affected when one of the variables has a translation. This is very beneficial in studying the impact of urbanization on climate change, because the impact of urbanization on climate change may lag behind, Pearson’s moment correlation coefficient can avoid this lagging effect very well.

(2) Spearman’s rank correlation analysis

On the other hand, Spearman’s rank correlation was used to investigate the correlation of two variables [33]. Assuming that the sample size is n , the two statistical variables are $[X_n]$ and $[Y_n]$, and they are sorted into hierarchical data $[x_n]$ and $[y_n]$, respectively. The Spearman’s rank correlation coefficient is:

$$\rho = \frac{\sum_i (x_i - \bar{x})(y_i - \bar{y})}{\sqrt{\sum_i (x_i - \bar{x})^2 \sum_i (y_i - \bar{y})^2}} \tag{4}$$

In general, the Spearman’s rank correlation coefficient is applicable for small sample size [34]. In this study, the Spearman’s rank correlation coefficient is selected for the correlation analysis between the LUCC data and the climate variables (since the number of the LUCC data has only 7 periods).

(3) EOF analysis

The EOF analysis method finds EOF by calculating the eigenvalues and eigenvectors of the anomaly covariance matrix of the time series data, and the derived eigenvalues provide a measure of the percentage of the variance explained by each mode. Generally, most variance is included in the first several modes.

In the practical application, the field T in the m space points is assumed to have n observations for each point (i.e., $m \times n$ observation matrix). The EOF analysis transforms the field T into the product of the time function and the space function:

$$T_{ij} = \sum_{q=1}^m d_{iq} t_{qj} \tag{5}$$

where d_{iq} is a spatial function and does not change with time (also called modes), t_{qj} is a time function that is orthogonal to d_{iq} . In general, the variance contribution rate of the temporal functions of the first several modes can reach more than 75%, which explains most of the variance. The calculation of the variance contribution rate of a mode can be referred to [35]. Before performing EOF analysis, each sample time series need be centered (mean subtracted) [36].

3 Results

3.1 Regional Urban Development

Figure 2 shows the permanent resident population densities of the four cities from 1980–2015. The growth rates of the population densities also were plotted. We can see that the population densities in Beijing and Tianjin had a rapid increase in the first decade after 2000. The year of 2002 is the change point of time when the population densities in Tianjin are higher than Beijing before that and lower after that. There is a stable accelerating growth for Beijing and Tianjin during 2001–2008 and an overall slow and stable increase in Baoding and Langfang. Several growth peaks appear at different points of time during the whole study period. The growth rates are generally positive except two cases: Beijing in 1997 and Baoding in 2011, showing negative growths close to zero.

Figure 3 shows the changes of GDP and the built-up area in the four cities during 1980–2015. From the change curves of GDP, Beijing and Tianjin, and Baoding and Langfang have similar increase processes, respectively. However, Beijing and Tianjin's GDP have faster increases than that of Baoding and Langfang, which indicates urbanization of Beijing and Tianjin is far faster than Baoding and Langfang. The acceleration of urbanization in Beijing and Tianjin occurred in 2004 or so. The newly added built-up area in Beijing and Tianjin is significantly larger than Baoding and Langfang from the change curves of built-up area. Tianjin's increase in built-up area is quite stable. Beijing has an obvious increase from 2000 to 2003, and keeps a large and stable increase hereafter.

The LUCC data of each period in the study area were processed in ArcGIS, into 3200×4000 grid ($1 \text{ km} \times 1 \text{ km}$ per grid). The proportion of residential and

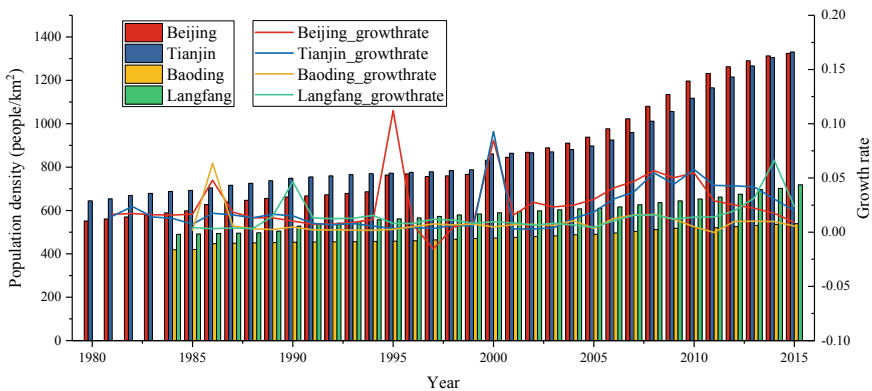


Fig. 2 Population densities and growth rates in Beijing, Tianjin, Baoding, and Langfang in recent decades. The growth rate is calculated based on the population density of the previous year. The population data of Baoding and Langfang before 1984 are not available

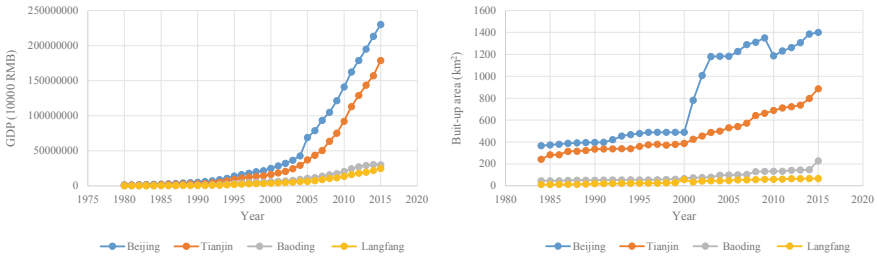
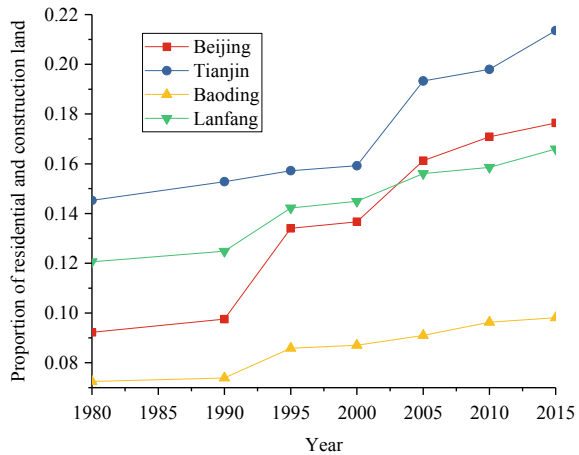


Fig. 3 The change curves of GDP and built-up area in Beijing, Tianjing, Baoding, and Langfang in recent decades

Fig. 4 The proportion of residential and construction land for different period in the four cities during 1980–2015



construction land for different period in the four cities are shown in Fig. 4. The increases of Beijing, Tianjin and Langfang in residential and construction land are a little larger than that in Baoding.

3.2 Local Climate Change

From the changes of the annual average temperature in Fig. 5, it can be seen that yearly temperatures in most stations in the study area have overall dominant increase trends. During 2010–2015, there is an abrupt decrease first and then a rapid increase for all stations under consideration.

Figure 6 shows the annual cumulative precipitation in the study area. We can see that the annual cumulative precipitation shows no obvious trend. Several piecewise trends can be seen in some stations and certain periods, such as from 1999 to 2012 in stations 5411, 54,623 and 54,602. Nonetheless, the global trends for every station are still nonsignificant according to a trend test algorithm of linear regression.

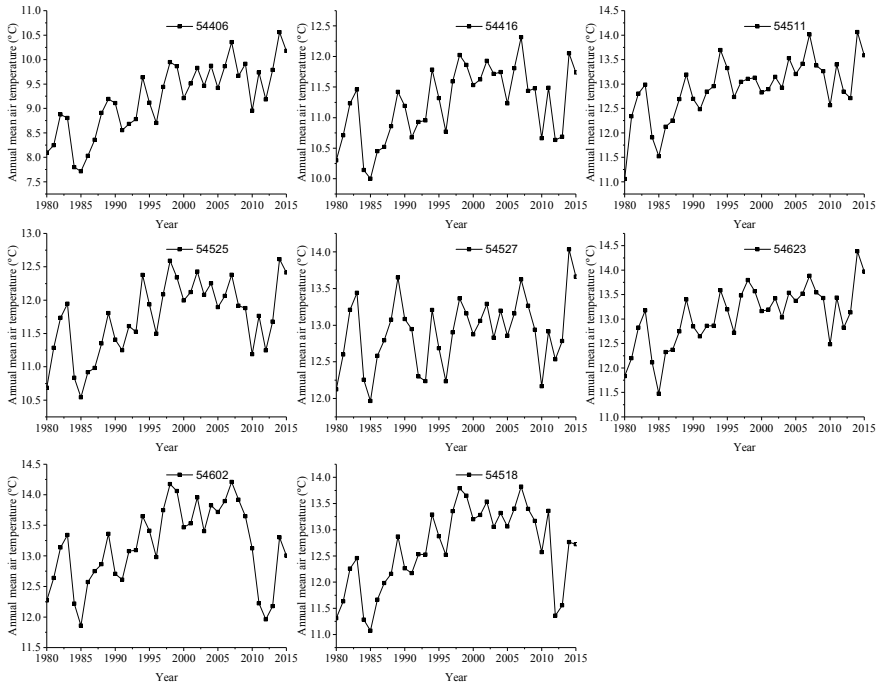


Fig. 5 The annual average temperature profiles in eight meteorological stations in the study area from 1980–2015

3.3 Correlation and Variability

(1) Pearson’s moment correlation analysis between population/urbanization and the annual average temperature/the annual cumulative precipitation. To explore the correlation between urbanization and climate change, we calculated the Pearson’s moment correlation coefficient by making linear regression between population/urbanization and the annual average temperature/the annual cumulative precipitation, respectively. The variance test was performed on the two sets of data before the t-test. The variance of the two sets of data was not the same, so the heterogeneity hypothesis t test was used. Finally, the heteroscedasticity hypothesis with two tails was carried out and the results are shown in Tables 1 and 2.

From Tables 1 and 2, we can see, except Tianjin, there are quite significant linear correlation between annual average temperature and normalized population index/CI in the other three cities. However, there is a relatively weak linear relationship between precipitation and population/urbanization.

(2) Spearman’s rank correlation analysis of climate data and LUCC

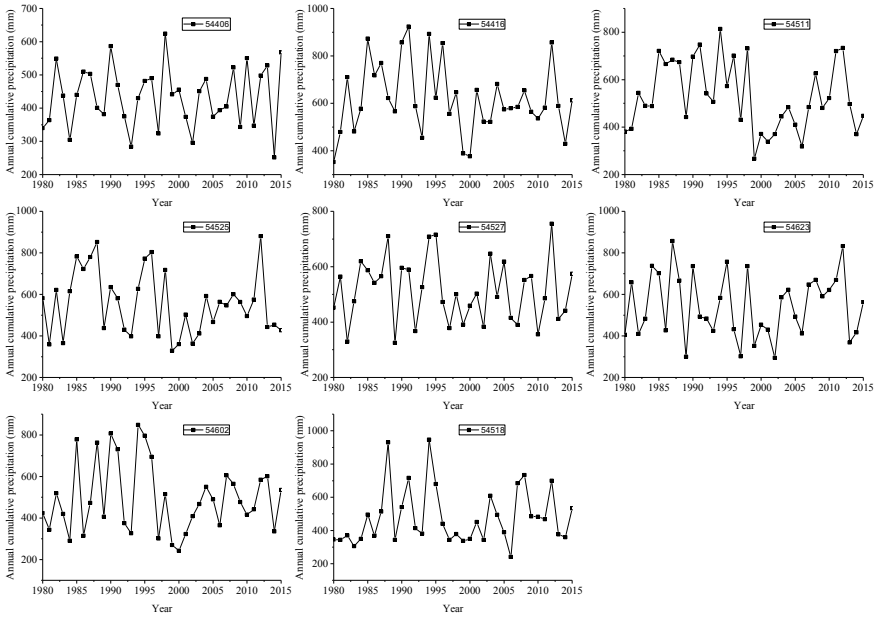


Fig. 6 The annual cumulative precipitation profiles in eight meteorological stations in the study area from 1980–2015

Table 1 Pearson’s moment correlation coefficients between population/urbanization and the annual average temperature

Temperature	Annual average temperature			
	Beijing	Tianjin	Langfang	Baoding
Normalized population index	0.96**	0.75	0.97**	0.91**
CI	0.84*	0.60	0.95**	0.91

**Indicates the significance level is 0.05, * indicates the significance level is 0.10

Table 2 Pearson’s moment correlation coefficients between population/urbanization and the annual cumulative precipitation

Precipitation	Annual cumulative precipitation			
	Beijing	Tianjin	Langfang	Baoding
Normalized population index	0.42	0.23	0.64	0.24
CI	0.50	0.20	0.54	0.31

**Indicates the significance level is 0.05, * indicates the significance level is 0.10

Spearman's rank correlation analysis correlation between the LUCC data of 1980–2015 and the corresponding climatic factors is analyzed. The Spearman's rank correlation coefficients are shown in Tables 3 and 4.

Tables 3 and 4 show that the correlation between residential land and industrial land coverage and each of climatic factors is consistently strong (the correlation is consistently positive or negative). The coverage rate of residential land has a stronger correlation with the average summer temperature, the annual hot days, the annual temperature difference, the annual cumulative precipitation, the cumulative summer precipitation, the annual rainstorm days, and the daily average precipitation of rainstorm. The coverage rate of industrial and mining land has stronger correlation with annual average temperature, annual temperature difference, and annual cumulative precipitation of rainstorms.

Table 3 The Spearman's rank correlation coefficients of temperature and land coverage rate

Temperature		Residential land	Industrial and mining land	Greenland	Waterbody and wetland	Unused land
Annual average	Beijing	+0.18	+0.25	+0.07	-0.11	+0.01
	Tianjin	+0.64	+0.65	-0.06	+0.12	-0.37
	Langfang	-0.11	+0.59	-0.31	+0.00	+0.20
	Baoding	+0.12	+0.30	-0.19	-0.02	-0.01
Summer average	Beijing	+0.75	+0.18	-0.09	-0.01	-0.01
	Tianjin	+0.64	+0.56	-0.26	-0.52	-0.10
	Langfang	+0.76	+0.39	-0.26	-0.22	-0.06
	Baoding	+0.43	++0.20	-0.59	-0.00	+0.01
Winter average	Beijing	-0.31	+0.13	+0.56	+0.33	+0.43
	Tianjin	-0.19	+0.04	+0.18	+0.10	+0.16
	Langfang	-0.22	-0.11	+0.39	+0.16	-0.13
	Baoding	-0.17	+0.18	+0.20	+0.28	-0.09
Annual hot days	Beijing	+0.84	+0.37	-0.23	-0.17	+0.04
	Tianjin	+0.68	+0.27	-0.17	-0.32	+0.00
	Langfang	+0.90	+0.13	-0.32	-0.27	-0.25
	Baoding	+0.59	+0.24	-0.27	+0.02	+0.29
Annual cold days	Beijing	+0.15	-0.04	+0.11	-0.29	-0.04
	Tianjin	-0.25	+0.15	+0.09	+0.43	+0.08
	Langfang	-0.11	+0.01	-0.09	-0.30	+0.14
	Baoding	-0.10	+0.21	+0.08	-0.48	-0.27
Annual difference	Beijing	+0.70	+0.31	-0.23	-0.21	-0.08
	Tianjin	+0.43	+0.62	-0.13	+0.06	+0.16
	Langfang	+0.82	+0.62	-0.12	+0.18	+0.22
	Baoding	+0.64	+0.44	-0.51	-0.11	+0.16

Table 4 The Spearman’s rank correlation coefficients of precipitation and land coverage rate

Precipitation		Residential land	Industrial and mining land	Green land	Waterbody and wetland	Unused land
Annual cumulative	Beijing	+0.74	+0.57	−0.10	−0.16	+0.03
	Tianjin	+0.41	+0.18	+0.17	+0.07	+0.20
	Langfang	+0.85	+0.64	+0.17	−0.06	+0.04
	Baoding	+0.81	+0.44	−0.03	−0.31	+0.04
Summer cumulative	Beijing	+0.76	+0.65	+0.11	+0.06	+0.12
	Tianjin	+0.63	+0.59	−0.01	−0.01	−0.05
	Langfang	+0.85	+0.30	−0.52	−0.01	−0.01
	Baoding	+0.80	+0.32	−0.22	−0.00	−0.13
Annual middle rain days	Beijing	+0.22	+0.23	+0.06	+0.21	−0.14
	Tianjin	−0.04	+0.02	+0.18	−0.04	+0.08
	Langfang	+0.07	+0.28	−0.11	+0.08	−0.09
	Baoding	+0.00	+0.33	+0.03	+0.14	−0.20
Annual heavy rain days	Beijing	+0.22	+0.15	−0.33	−0.16	−0.02
	Tianjin	−0.03	+0.01	−0.18	+0.02	−0.04
	Langfang	+0.08	+0.21	−0.30	−0.18	+0.15
	Baoding	+0.05	+0.28	−0.17	−0.42	+0.01
Annual rainstorm days	Beijing	+0.92	−0.30	+0.07	−0.05	+0.21
	Tianjin	+0.66	+0.43	−0.01	−0.11	−0.04
	Langfang	+0.92	+0.62	−0.13	−0.04	+0.08
	Baoding	+0.88	+0.23	−0.06	−0.02	+0.14
Annual cumulative precipitation of rainstorm	Beijing	+0.84	+0.46	−0.17	+0.27	+0.10
	Tianjin	+0.63	+0.69	+0.09	+0.12	−0.11
	Langfang	+0.94	+0.65	+0.11	−0.11	−0.08
	Baoding	+0.62	+0.50	+0.12	−0.38	+ 0.14

The Spearman’s rank correlation coefficients between Greenland (wetland or water bodies) and annual average temperature (or average summer temperature) in the four cities are basically consistently positive. Those between Greenland (wetland or water bodies) and the average winter temperature are consistently negative. It shows that the two land use types have played a stable role on regulating urban temperature and can help reduce extreme weather.

(3) Variability of EOF analysis of urbanization and climatic factors

After obtaining the meteorological variables from original daily observations and the CI calculated by Eq. (1), we performed the EOF decomposition of the CI, 20 temperature variables, and 13 precipitation variables, respectively. According to the results, the explained variance of the first mode for the urbanization index accounts for

99.28% (Fig. 7). The sum of the variance explanations of the first 10 modes for each of 33 meteorological variables is more than 90%, indicating that the 33 meteorological variables can be explained by their first 10 modes, respectively. Finally, we only chose EOF1 of the CI to represent the urbanization evolution and explored its correlation with the modes for each of those meteorological variables. Specifically, the EOF1 of the CI was compared with the first 10 EOFs for each of the 33 meteorological variables. Correlation coefficients were computed and the ones with the highest correlation were identified. The results were shown in Tables 5 and 6. Figure 8 shows the time series of the EOF1s of the CI, the annual maximum temperature, and the annual hot days. Their variations (mean subtracted) have the strongest correlation among all selected 33 meteorological variables.

It can be seen from Tables 5 and 6 that the first modes of the two temperature variables (the annual maximum temperature and the annual hot days) can correspond to the first mode of the CI. The correlation coefficients are 0.52 and 0.50. The

Table 5 The corresponding EOFs of the temperature variables that have the highest absolute correlation coefficients with the EOF1 of the CI

Temperature		Mode	Correlation coefficient	Variance contribution rate (%)
Average	Annual	2	-0.85	7.74
	Spring	3	+0.52	5.74
	Summer	3	-0.58	7.11
	Autumn	2	-0.61	11.36
	Winter	2	+0.79	7.39
Maximum	Annual	1	+0.52	69.09
	Spring	2	+0.50	5.64
	Summer	7	-0.44	1.59
	Autumn	2	-0.53	9.65
	Winter	3	+0.70	4.74
Minimum	Annual	2	-0.72	11.55
	Spring	2	-0.77	9.69
	Summer	3	-0.52	7.65
	Autumn	2	-0.71	10.42
	Winter	2	-0.68	9.28
Annual difference		2	+0.88	17.93
Extreme annual maximum		1	+0.50	55.06
Extreme annual minimum		3	+0.68	7.44
Annual hot days ^a		None	-	-
Annual cold days ^a		3	+0.58	6.86

^aIt is a hot/cold day if the maximum/minimum temperature in the day is greater than 38°C/-10°C

Table 6 The corresponding EOFs of precipitation variables that have the highest absolute correlation coefficients with the EOF1 of the CI

Precipitation		Mode	Correlation coefficient	Variance contribution rate (%)
Cumulative	Annual	5	0.38	4.98
	Spring	5	0.51	3.22
	Summer	6	0.30	4.95
	Autumn	2	0.40	11.11
	Winter	7	-0.42	2.05
Annual cumulative	Light rain	6	-0.58	5.17
	Moderate rain	5	-0.36	5.81
	Strong rain	None	-	-
	Rainstorm	None	-	-
Annual light rain days		6	0.40	4.21
Annual moderate rain days		5	0.40	6.08
Annual strong rain days		None	-	-
Annual rainstorm days		None	-	-

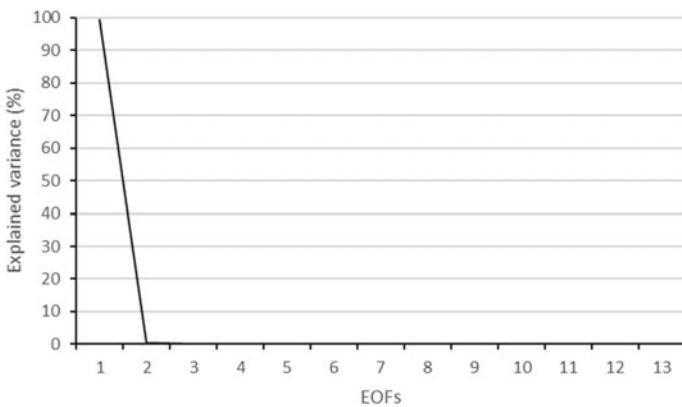


Fig. 7 The variance contribution rates of the EOFs for the CI

variance contribution rates are 69.09% and 55.06%, respectively, indicating that the variability of the above two temperature variables has a high degree of consistency with the variation of urbanization development. By contrast, there is no significant correlation between the first mode of urbanization and the first modes of precipitation variables. Furthermore, the first three modes of most of temperature variables have the highest correlation with the EOF1 of the urbanization index. While few precipitation variables do so. These evidences show the weak association between urbanization and precipitation in the study. However, the underlying mechanism of

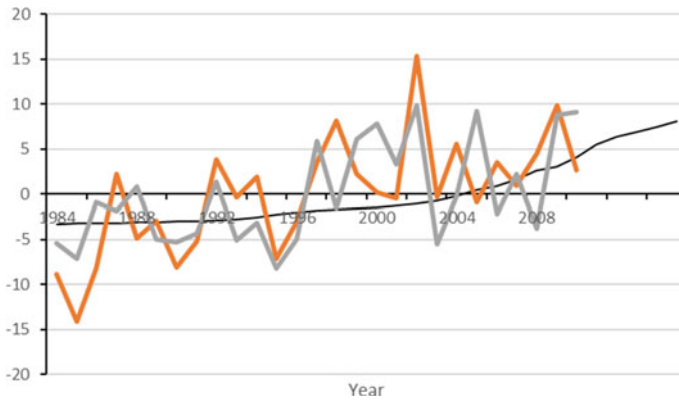


Fig. 8 The time series of the EOF1s of the CI, the annual maximum temperature, and the annual hot days

those kinds of association evidences need to be further investigated in collaboration with theoretical analysis.

4 Discussion

Kalnay and Cai think Urbanization causes the conversion of the land use and changes the thermodynamic properties of the underlying surface. Which results in a general increase of temperature in the built-up areas and those temperature variables appear uneven distribution in space and time [37]. The study also found that green land, water bodies and wetlands have a stabilizing effect on the temperature in the cities. Urbanization changes the land use patterns, and plenty of lands are changed into built-up areas from green areas. On the other hand, more population and economic activities mean more energy consumption and greenhouse gas emission. As a result, the urban heat island effect is getting more obvious with rapid population growth and economic development. Furthermore, it is worth noting that in some rural areas in China, temperature is increasing trend with resident population's decreasing. Factors that may contribute to temperature, as well as factors other than population growth, jointly lead to a gradual increase in temperature in the rural areas. However, these kinds of background patterns are basically fixed for a certain city, and we think they did not affect the correlation analysis between urbanization and climate change for the city.

The effect of urbanization on precipitation is a little more complicated. Some studies thought the influence of urbanization on the wind speed in the urban area changes urban precipitation patterns. Urbanization leads to the increase of the roughness of the urban surface, and the rough urban surface will weaken the wind speed in the stratum. Furthermore, high-rise buildings in cities block airflow and decrease wind speed [38]. The weakening of the wind speed in the urban area leads to the change of the convergence field of water vapor in the rainfall area, thus increases

the occurrence of precipitation. Also some authors thought the uneven temperature distribution caused by the heat island effect also causes the instability of the boundary layer disturbance and the strengthened city convection. As a result, a short period of heavy precipitation occurs more frequently [39]. However, it is not obvious from linear correlation analysis and EOF analysis that urbanization has affected the precipitation patterns in this study. More variables should be used and multi-scale analysis should be performed to find out new evidence.

While population is used as a main (even unique) indicator to classify urban scales and evaluate urban development, some studies showed the urbanization levels in China lag behind the economic development. Furthermore, the built-up area is increasing with urbanization levels increasing since urban development requires plenty of land is changed into residential land and industrial land from green areas. Therefore, a synthetic index considering population, economy, and construction is required to quantify the urbanization level. Nonetheless, the currently existing urbanization indices are a little bit arbitrary anyway, which certainly affects the analysis results. To validate and consolidate the analysis results, well-defined urbanization indices should be exploited and examined. For example, sensitivity analysis and comparison can be done to examine the impact of different urbanization indices on results.

There are global and local contributions to the local climate change. Thus, on studying local climate change, we have to face the confounders from global climate change. Due to global climate change, it is acknowledged that simply examining the association between urbanization and climate may mislead to overestimating the role of urbanization on climate. However, according to existing studies, climate change all over the world is far less than that in the study area. So we thought we can ignore the effect of the global climate change in this study and take the stable constant as the benchmark. Furthermore, in this study, we took several areas including underdeveloped, developing, and developed ones to compare the effect of urbanization on climate change. We assumed that the global climate change has same or similar effect on these different areas. So these kinds of comparisons between different development levels are expected to remove the contribution by global climate change and demonstrate the effect of the local urbanization factors.

We should keep in mind that the association between variables does not mean a causal relationship. At the same time, it provides important clues for further causal investigation. We also have to acknowledge that data are an important limitation to this study though those data used in this study were obtained from either official sources or formal scientific research institutions. For correlation analysis between land use type data and climate variables, we used Spearman's rank correlation analysis (which is applicable for a small size sample) to calculate the correlation coefficient instead. There are 13 cities and 58 meteorological stations in the study area for the EOF analysis, and a time span of more than 30 years. This data volume generally is sufficient for EOF analysis. The inferences obtained by Pearson's moment correlation analysis is limited because Pearson's moment correlation analysis can only analyze the linear correlation of two sets of variables and cannot reflect other

possible correlations. For example, for two sets of variables with a form of $Y = X^2$, Pearson's moment correlation coefficient cannot fully reflect its true correlation.

5 Conclusions

In this chapter, the influence of urbanization on climate change in the Beijing-Tianjin-Hebei region was studied by Pearson's moment correlation analysis, EOF analysis and Spearman's rank correlation analysis by constructing normalized population index and CI. The main conclusions are as follows:

- (1) Since 1980, urbanization has a rapid development, population, GDP and built-up area are generally increasing year by year, and the increasing trend is more stable. In the study area, annual precipitation shows no significant trend while annual average temperature increases and has a certain linear correlation with urban development.
- (2) Compared with the precipitation variables, the first three modes of most meteorological variables show better similarity to the first mode of the CI in the first 10 modes while those of few precipitation variables strongly correlate with the EOF1 of the urbanization index. The correlation between urbanization and temperature variability is stronger than that between urbanization and precipitation.
- (3) The residential land and industrial and mining land in the four selected cities have strong impact on some climatic factors and the impact of residential land on climate is higher than that of industrial and mining land. In addition, green areas, waterbodies, and wetlands stabilize the temperature in these cities and negatively correlate with the annual maximum temperature and the annual minimum temperature.

The methods used in this study are statistical ones. The "significant" correlation in statistics does not necessarily mean that there is a causal relationship between the two sets of statistical variables. In other words, we cannot arbitrarily conclude that "urbanization leads to climate change" before a further investigation is done in collaboration with theoretical analysis. In order to further explore the causal relationship between urbanization and climate change, the subsequent studies include but not limited to the following aspects: correlation analysis with fined grain data (e.g., shorter time interval data, satellite remote sensing data with higher space-time resolution), validation of the causal relationship with some methods such as Granger, and exploration of the correlation between urbanization and climate change through theoretical and dynamic approaches.

6 Recommendations

Our results show urbanization has brought significant increase in air temperature. This is also the well-known urban heat island effect, which is of great concerns in modern cities. In order to reduce the negative effect, in the process of urban planning and governance, attention should be paid to strengthening the rational planning and utilization of land, and optimizing the positive contribution of green space, water body and wetland in reducing urban heat island effect.

It is also imperative to strengthen the research on the effect of different urban land cover types on urban heat island intensity. The results will provide scientific clues for urban governance. For example, urban policy makers can better plan land use to reduce its contribution to the heat island effect such as optimizing space layout of land cover type. We also proposed further strengthening research on the trend of extreme weather events caused by urbanization and its underlying mechanism and providing scientific support for prevention and mitigation of urban meteorological disasters.

Acknowledgements The authors acknowledge support from the National Natural Science Foundation of China (Grant No. 72174031) and the Youth Scholar Program of Beijing Academy of Science and Technology (Contract No. YS202004). We also appreciate the support for this paper from the Beijing Key Laboratory of Operation Safety of Gas, Heating and Underground Pipelines.

References

1. IPCC (2014) Climate change 2014: synthesis report. Contribution of working groups I, II and III to the fifth assessment report of the intergovernmental panel on climate change [Core Writing Team: Pachauri RK, Meyer LA (eds)]. IPCC, Geneva, Switzerland, 151 pp
2. Sun Y, Zhang X, Ren G, Zwiers FW, Hu T (2016) Contribution of urbanization to warming in China. *Nat Clim Change* 6(7):706
3. Siswanto S, Oldenborgh GJ, Schrier G, Jilderda R, Hurk B (2016) Temperature, extreme precipitation, and diurnal rainfall changes in the urbanized Jakarta city during the past 130 years. *Int J Climatol* 36(9):3207–3225
4. Wang XL, Wen QH, Wu Y (2007) Penalized maximal t test for detecting undocumented mean change in climate data series. *J Appl Meteorol Clim* 46(6):916–931
5. Wang XL (2008) Penalized maximal F test for detecting undocumented mean shift without trend change. *J Atmos Ocean Tech* 25(3):368–384
6. Wang XL, Chen H, Wu Y, Feng Y, Pu Q (2010) New techniques for the detection and adjustment of shifts in daily precipitation data series. *J Appl Meteorol Clim* 49(12):2416–2436
7. Velazquez-Lozada A, Gonzalez JE, Winter A (2006) Urban heat island effect analysis for San Juan, Puerto Rico. *Atmos Environ* 40:1731–1741
8. Peterson TC, Gallo KP, Lawrimore J, Owen TW, Huang A, McKittrick DA (1999) Global rural temperature trends. *Geophys Res Lett* 26:329–332
9. Hughes WS, Balling RC (1996) Urban influences on South African temperature trends. *Int J Climatol* 16:935–940
10. Nie AQ, Chen X, Feng ZG (2011) Detection and comparison of effect of urbanization on climate in three megacity agglomerations of China. *J Meteorol Sci* 31:372–383
11. Niyogi D, Lei M, Kishitawal C, Schmid P, Shepherd M (2017) Urbanization impacts on the summer heavy rainfall climatology over the Eastern United States. *Earth Interact*. <https://doi.org/10.1175/EI-D-15-0045.1>
12. Lin XC, Yu SQ, Tang GL (2005) Study of the relationship between urbanization and heat island strength in Beijing, China. *Prog Nat Sci* 15:882–886

13. Thanh Hoan N, Liou YA, Nguyen KA, Sharma RC, Tran DP, Liou CL, Cham DD (2018) Assessing the effects of land-use types in surface urban heat islands for developing comfortable living in Hanoi City. *Remote Sens-Basel* 10(12):1965
14. Nguyen KA, Liou YA (2019) Global mapping of eco-environmental vulnerability from human and nature disturbances. *Sci Total Environ* 664:995–1004
15. Li H, Zhou Y, Jia G et al (2021) Quantifying the response of surface urban heat island to urbanization using the annual temperature cycle model. *Geosci Front* 101141
16. Wang C, Wang ZH, Kaloush KE et al (2021) Perceptions of urban heat island mitigation and implementation strategies: survey and gap analysis. *Sustain Cities Soc* 66:102687
17. Alqasemi AS, Hereher ME, Al-Quraishi AMF, Saibi H, Aldahan A, Abuelgasim A (2020) Retrieval of monthly maximum and minimum air temperature using MODIS Aqua land surface temperature data over the United Arab Emirates (UAE). *Geocarto Int.* <https://doi.org/10.1080/10106049.2020.1837261>
18. Yang J, Wang Y, Xiu C et al (2020) Optimizing local climate zones to mitigate urban heat island effect in human settlements. *J Clean Prod* 275:123767
19. Martilli A, Krayenhoff ES, Nazarian N (2020) Is the urban heat island intensity relevant for heat mitigation studies? *Urban Clim* 31:100541
20. Satterthwaite D (2009) The implications of population growth and urbanization for climate change. *Environ Urban* 21(2):545–567
21. Yao C (2012) The effect mechanism of population dynamics and climate change in the process of urbanization: theoretical framework and co-integration test. *Urban Dev* 10:020
22. Yao X, Wang Z, Wang H (2015) Impact of urbanization and land-use change on surface climate in middle and lower reaches of the Yangtze River, 1988–2008. *Adv Meteorol.* <https://doi.org/10.1155/2015/395094>
23. Gilbert A, Gugler J (1982) Cities poverty and development: urbanization in the third world
24. Khwarahm NR, Qader S, Ararat K, Al-Quraishi AMF (2021) Predicting and mapping land cover/land use changes in Erbil/Iraq using CA-Markov synergy model. *Earth Sci Inf* 14:393–406
25. Jun F (2002) Study on coordination of urbanization and economic development in China. *Urban Stud* 2:004
26. Zhao J, Chai J (2015) A novel approach for urbanization level evaluation based on information entropy principle: a case of Beijing. *Phys A* 430:114–125
27. Zhang GT (1998) Discussion on establishing an indicator system for urbanization level. *Urban Issues* 1:6–9
28. Lin Q (2001) Empirical analysis of urbanization indicator system. *Urban Iss* 4:14–16
29. Du QJ, Wu Q (2006) Research on regional urbanization level based on indicator system. *Urban Dev Res* 13(5):5–8
30. Zhang SY, Zhou JL (2007) Construction and evaluation of urbanization indicator system. *Tech Econ* 26(3):32–37
31. Lv P, Zhou T, Zhang ZF, Tian Z (2008) Building and application of land urbanization and its measurement index system. *China Land Sci* 22(8):24–28
32. Cheng WM, Liu HJ, Zhang Y, Zhou CH (2004) Classification system of land-cover map of 1:1 000 000 in China. *Resour Sci* 26(6):2–8
33. Zar JH (1998) Spearman rank correlation. *Encyclopedia of biostatistics*
34. Myers L, Sirois MJ (2004) Spearman correlation coefficients, differences between. *Wiley*
35. Wang B, An SI (2005) A method for detecting season-dependent modes of climate variability: S-EOF analysis. *Geophys Res Lett* 32(15):291–310
36. Taylor MH, Losch M, Wenzel M, Schröter J (2013) On the sensitivity of field reconstruction and prediction using empirical orthogonal functions derived from Gappy data. *J Climate* 26(22):9194–9205
37. Kalnay E, Cai M (2003) Impact of urbanization and land-use change on climate. *Nature* 423(6939):528
38. Jiang XY, Liu WD (2007) Numerical simulation on impacts of urbanization on heavy rain in Beijing using different land use data. *Acta Meteorol Sin* 21(2):245
39. Zhang DL (2020) Rapid urbanization and more extreme rainfall events. *Sci Bull* 65(7):516–518

Spatial-Environmental Assessment of the Transport System in the Northern Emirates, UAE: Toward Policies and Practices



Robert M. Bridi, Naeema Al Hosani, and Ahmed Al Murshidi

Abstract Environmental degradation that is related to economic growth includes greater consumption of non-renewable resources, increased levels of pollution and carbon dioxide emissions, and natural habitat destruction. The chapter examines the relationship between economic growth, environmental degradation, and transport infrastructure development in the northern emirates, an emerging economic region in the United Arab Emirates (UAE). The main research question is to what extent does economic growth and transport development affect environmental degradation? The objectives are to display the transport infrastructure across the northern emirates, examine the relationship between economic growth and environmental degradation, and recommend policies and practices. Primary data was collected using geographic information systems and interactive interviews with personnel from the Ministry of Energy and Infrastructure. Secondary data was gathered from government publications, global organizations, and other researchers. The findings demonstrate that the northern emirates' economy will continue to expand. Transport development will allow for a booming logistics sector, building on the location of the east–west trade routes and further development of the tourism sector. Furthermore, investment in transport has brought increases in local access to healthcare, education, and non-local job markets. Sustainable development, however, remains a challenge. Infrastructure development has been ad hoc with little planning and proper assessment of the effects on the environment. Proposed policies and practices include the introduction of low emission zones, investment in ecofriendly public transport, a gradual decarbonization of the public and private transport system, and the introduction of walking and cycling paths.

R. M. Bridi (✉) · N. Al Hosani · A. Al Murshidi
Geography and Urban Sustainability Department, College of Humanities and Social Sciences,
United Arab Emirates University, P. O. Box 15551, Al Ain, UAE
e-mail: rmbridi@uaeu.ac.ae

N. Al Hosani
e-mail: naeemam@uaeu.ac.ae

A. Al Murshidi
e-mail: ah.almurshidi@uaeu.ac.ae

Keywords Environmental degradation · Northern emirates · Transport system · Sustainable development · United Arab Emirates

1 Introduction

Environmental degradation broadly refers to any damaging or detrimental change to the environment that results in the deterioration or depletion of resources including air, water, soil; the obliteration of biomes and ecosystems; habitat disturbance and annihilation; species extinction; and pollution [1, 2]. Some of the causes of environmental degradation include population increase, economic growth, resource depletion, and the development of polluting technologies [3–5]. Urban scholars that focus on economic growth refer to “a process of creating and utilizing physical, human, financial, and social assets to generate improved and broadly shared economic well-being and quality of life for a community or region” [6, p. 5]. Economic growth encompasses both quantitative and qualitative measures. Quantitative measures include, for example, gross domestic product (GDP), “the standard measure of the value added [and] created through the production of goods and services in a country during a certain period” [7]. In addition, qualitative measures refer to progressive societal changes that improve the well-being of people and the environment in which they live [8, 9].

The United Arab Emirates (UAE) consists of seven emirates (Abu Dhabi, Dubai, Sharjah, Ajman, Umm al-Quwain, Ras al-Khaimah, and Fujairah) that have witnessed significant economic growth over several decades. The economy is the second largest in the Middle East (following Saudi Arabia), with a GDP of US\$421.077 billion in 2019, which places the UAE on par with leading Western nations. Government expenditures have created employment opportunities and infrastructure expansion with greater private sector holdings. Free trade zones provide 100% foreign ownership with no taxes and attract foreign investors. The UAE has been successful at diversifying its economy; however, currently approximately 30% of GDP comes from the oil and gas sectors. Government plans for the future of the economy include further diversification into global trade and tourism, industrial development, and the creation of employment opportunities [10–12].

The chapter examines the relationship between economic growth, environmental degradation, and infrastructure development in the UAE. The authors bring into focus the development of the transport system in the northern emirates—an emerging economic region in the UAE—and the effects this has had on environmental degradation. Given the continued economic growth in the UAE more generally and the northern emirates more specifically, the authors assess and devise a variety of proposed policies and practices that curb the inevitable environmental degradation associated with the development of the transport system. The chapter is organized in the following manner: Sect. 2 is a review of the relevant academic literature. The authors demonstrate that the existing literature has primarily focused on economic growth and economic degradation as it relates to increases in GDP and associated

carbon dioxide emissions. There is little attention, however, to the development of the transport system in the northern emirates and the policies and practices that seek to ameliorate further environmental degradation. Section 3 includes the primary research question and sub-questions, the objectives of the study, and the hypothesis. Section 4 includes the research design and methodology. The authors draw on existing secondary data to demonstrate the correlation between economic growth and environmental degradation. Primary data was collected that demonstrates the extensive development of the transport system in the northern emirates, and the proposed policies and practices to curb the inevitable environmental degradation in light of such developments. Section 5 is a discussion of the results. The growth of the transport system in the northern emirates is illustrated using geographic imaging systems (GIS) mapping and interviews with personnel from the Ministry of Energy and Infrastructure that provide important insights regarding existing policies that deal with environmental degradation and the transport system as well as future plans and prospects. Section 6 is the conclusions and recommendations from the authors on a way forward in terms of devising policies and practices that ameliorate the effects of economic growth on environmental degradation.

2 Literature Review

The relationship between economic growth and environmental degradation was established by the early work of Kuznets [13], which was then popularized by the development of the Environmental Kuznets Curve (EKC) hypothesis [14]. Scholars that examine the relationship between economic growth and environmental degradation have drawn on the EKC hypothesis. The EKC is an inverted U-shaped curve that postulates an initial rise in environmental degradation followed by a peak and eventual decrease [15]. This is premised on the environmental degradation that occurs during the shifts from the primary to the tertiary sectors in the economy. The primary sector is based on the extraction and processing of raw materials (e.g., agriculture, fishing, coal, logging, petroleum) for subsistence and commercial use. Globally, there has been a decrease of economic activity in the primary sector. For example, in 2019 only 10.9% of employment in the US was related to food and agriculture and only 1.3% was direct on-farm employment [16]. Following the EKC hypothesis, environmental degradation is relatively low during this period of economic growth, but begins to rise gradually.

The shift from the primary to the secondary sector, often referred to as the process of industrialization, results in an intensive increase in environmental degradation, as illustrated by the rise of the EKC to its peak. The secondary sector primarily involves manufacturing. Extracted materials from the primary sector are converted into a variety of products. For example, 48% of China's GDP emanates from industry and construction making China the leading country in the world in industrial output. This includes iron and steel; machine manufacturing (machine tools, electric power

equipment, transportation equipment, metallurgical equipment, electronics); chemicals; building materials; paper; textiles; food processing; and other consumer goods. China's industrial production averaged 11.64% growth from 1990 until 2020 [17, 18]. According to Wu and Edmonds [19], China's environmental degradation includes intensive land use, lack of water resources, deforestation, desertification, pollution, urbanization climate change, marine ecosystem degradation, and toxic waste. China's industrialization period provides a stark example of the intensive rise in environmental degradation to its highest point in the country's history.

The transition from the secondary to tertiary sector, often referred to as the process of deindustrialization, phases out heavy industry and ushers in service-oriented production. The focus becomes the interaction of individuals rather than the transformation of raw materials into physical goods. Services include utilities, wholesale trade, retail trade, transportation and warehousing, information technology, financial activities, professional and business services, educational services, health care and social assistance, leisure and hospitality, government, and other services. A growing portion of people is employed in the tertiary sector in more developed economies. The US was the first country where this shift was witnessed following the Second World War. Production in the secondary sector fell roughly by half while production in the tertiary sector increased to three quarters by 2000 followed by an increase in the employment ratio [20, 21]. As of 2019, 80.3% of the labor force in the US was employed in the tertiary sector [22]. The evolution from the secondary to tertiary sector causes a decrease in environmental degradation due to a shift from manufacturing to services, demand by consumers for more environmentally sustainable policies and practices, and greater political interest in the environment [23] as illustrated by the decrease of the EKC.

Researchers have applied the EKC hypothesis to determine the relationship between economic growth and environmental degradation as it relates to carbon dioxide emissions. Global carbon dioxide emissions have been rising exponentially and are associated with climate change, global warming, extreme weather events, the disturbance of ecosystems, and air pollution, all of which affect human health. Carbon dioxide emissions, however, have been accepted as part of the hazards that come with economic growth. Accordingly, many studies have attempted to understand the economic growth-environmental degradation nexus. Some studies identified economic growth as indicated by GDP per capita as a cause of environmental degradation with the intention of finding effective ways to reduce environmental degradation while maintaining economic growth. These studies demonstrate that a higher GDP per capita leads to an initial increase in carbon dioxide emissions to a peak followed by a decrease as stipulated by the EKC hypothesis [24–28]. While such studies demonstrate a positive impact on the environment that results from an increase in GDP, other studies have demonstrated the opposite effect [29, 30]. The authors point to important issues that impact environmental degradation amidst economic growth that are not factored into the EKC hypothesis such as environmental governance, corruption, and the challenges facing developing economies that lack environmental standards.

Other authors have introduced additional variables into the EKC to explain the relationship between economic growth and environmental degradation. For example, some studies examined energy consumption to understand the relationship between economic growth and pollution emissions [31–35]. These studies demonstrate the positive impact that a shift from reliance on fossil fuels to electrification has on the reduction of harmful pollutants. Other authors have focused on financial development's impact on environmental degradation. Financial development has been identified as an important factor because of its impact on carbon dioxide emissions. In some cases, financial development reduces carbon dioxide emissions as firms and governments invest in research and development and adopt more efficient 'environmentally friendly' technologies [36–38]. Other cases, however, demonstrate the opposite effect. Financial development may increase investment in manufacturing and ultimately have a negative impact on environmental degradation [39–41]. Mixed results have also been identified with issues related to trade openness. Trade openness refers to the relative impact of the sum of imports and export on GDP. It is related to issues such as the globalization of a country's economy. As an economy grows, there is a general increase in trade openness. While some studies have identified a positive outcome on the environment related to trade openness [42–44] other studies have found the opposite [45–47].

Another important variable in the relationship between economic growth and environmental degradation is urbanization. The number of people living in urban areas has been on the rise globally. According to the United Nations [48], in 1950 30% of the world's population was residing in urban areas compared to 55% in 2018 (approximately 4.2 billion) with projections that approximately 68% of the globe's population will be living in urban areas by 2050. As of 2018, approximately 3.4 billion people were living in rural areas, with projections that the number will decrease to approximately 3.1 billion by 2050. India and China have the largest rural populations with approximately 893 million and 578 million, respectively. India, China, and Nigeria are predicted to account for 35% of global urban growth between 2018 and 2050, with approximately 416 million, 255 million, and 189 million urban inhabitants. Leading urbanized regions as of 2018 included: North America (82%), Latin America and the Caribbean (81%), Europe (74%), and Oceania (68%). While Asia is approximately 50% urban, Africa remains mostly rural with 43% of the population residing in urban areas. Given the large influx of urban inhabitants globally, there has been a rise in the number of megacities (more than 10 million residents), with 33 megacities in 2018 and projected 43 megacities by 2030, most of which will be in developing regions. Among the megacities are Tokyo (37 million), Delhi (29 million), and Shanghai (26 million). Mexico City and São Paulo have approximately 22 million inhabitants, while Cairo, Mumbai, Beijing, and Dhaka have approximately 20 million inhabitants. Some cities in Asia and Europe have stagnated or declined in population in recent years due to different factors such as low fertility rates, economic contraction, and environmental disasters [48, 49].

Urbanization is a global phenomenon resulting from a conglomeration of complex processes. This includes both perceived and real benefits associated with the clustering of human activity in areas of close proximity. In particular, urban centers

provide opportunities and advantages associated with employment prospects, infrastructural development such as transport and communications, improved education and health care services, and higher standards of living. Urban dwellers have longer life expectancy, lower infant mortality, and lower fertility rates than rural dwellers. In addition, urban centers are regarded as socially diverse cultural centers, spaces of innovation, and drivers of social change [50–52]. Urban centers, however, also present significant challenges such as social disparity (rise in criminal activity and incarceration), poverty (rise in slum and squatter populations), struggle (civil unrest and protests), and environmental degradation.

Given the higher density in population associated with urbanization, greater energy use has significantly impacted air pollution and human health. Urban centers have higher concentrations of carbon dioxide emissions, larger volumes of uncollected waste, and flash flooding due to thunderstorms, hurricanes, tropical storms, meltwater from ice or snow, and extreme weather events associated with global warming. In addition, urbanization promotes less tree cover, inhibits and/or leads to the extinction of animal species, increases the release of toxic substances, more vehicle congestion, and the loss of habitats and food sources. Such challenges, in developing and developed nations, are often the result of ineffective or unplanned urban diffusion. This results in greater traffic congestion, poor infrastructure maintenance and planning, insufficient affordable housing, significant strain on services such as education and health care, air and water pollution. The effects are experienced unevenly by the majority of the populations living in urban centers that are at or below the poverty line. In cases where people living at or below the poverty line have access to services, often the quality is poor, whereas in other cases specific groups of people have no access at all or are marginalized from any decision-making processes [53–56].

Research that examines urbanization in relation to economic degradation has focused on the effects of urbanization on carbon dioxide emissions. Abdallah and Abugamos [57] examined 20 countries in the MENA region and found the EKC hypothesis did not apply. Energy use and economic growth were identified as primary factors impacting the rise in carbon dioxide emissions. Another study that focused on different levels of urbanization in three regions across 29 provinces in China found that the EKC hypothesis did apply. The results demonstrated different effects depending on the level of urbanization with a general increase in carbon dioxide emissions to a threshold followed by a decrease [58]. There were similar findings by another study that examined the effects of urbanization on carbon dioxide emissions in the OECD (Organization for Economic Co-operation and Development) countries from 1960 to 2010 where energy consumption and per capita GDP had an impact on carbon dioxide emissions [59].

Authors that focus on the UAE examined the effects of economic growth and urbanization on environmental degradation [60–62]. Some authors found that the EKC hypothesis applied among a variety of factors. In general, economic growth in the UAE, sustained mostly by high oil prices, brought an initial rise in environmental degradation to a peak followed by a decline. An increase in urbanization occurred from approximately 54% in 1950 to approximately 87% in 2019 due to rural-to-urban

migration and the inflow of an expatriate population to urban centers. Further, the UAE boasted one of the highest levels of urbanization in the world during the period from 2005 to 2010. Such rapid developments have resulted in a significant impact on environmental degradation. This was followed by a decrease in environmental degradation as the introduction of alternative forms of energy, such as electricity, has resulted in the reduction of carbon dioxide emissions. This has been the result of the UAE reducing its dependence on petroleum and natural gas and the promotion of renewable forms of energy, such as electricity, to satisfy increasing energy demands. This demonstrates that a shift to more energy-efficient technologies lowers the harmful effects of carbon-based energy sources.

A related issue is that of exports. As the UAE adopts more environmentally friendly technologies there is a feedback effect on consumption of energy as it relates to exports. This demonstrates the importance of adopting renewable energy for domestic production, which in turn affects the level of carbon dioxide emissions from exports. In addition, the introduction of financial services, including bonds and securities markets, into the economy has reduced carbon dioxide emissions. An increase in financial services provides more investment in research and development on clean energy technologies. Trade openness also resulted in lower carbon dioxide emissions as technology transfer from more advanced countries allows developing countries to adopt energy friendly technologies. Such technologies promote the electrification of private and public transport, the promotion of online work, and improved water treatment and desalination facilities [63–66].

Some countries have been effective at mitigating the effects of environmental degradation that are caused by economic growth. The UAE, for example, has experienced unprecedented economic growth since its inception in the 1970s and the expansion of its bifurcated economy consisting of the primary sector (mostly extraction based such as petroleum) and tertiary sector (mostly service based such as tourism). This, in part, has included an extensive transport infrastructure such as roads, railways, and airports. Despite such ongoing growth, however, the UAE has been effective at curbing the negative effects on the environment. This is due to effective governance through the management and application of specific policies that, on the one hand, ensure economic growth, but on the other hand, take into consideration critical environmental issues.

Much of the academic literature on the relationship between economic growth and environmental degradation provides a quantitative assessment that draws on the Environmental Kuznets Curve (EKC) hypothesis with mixed and in some cases contradictory results. While the authors draw on the many important findings from these studies to provide secondary data about the relationship between environmental degradation and economic growth, the study builds on the academic literature by using GIS mapping to display the arrangement of the transport infrastructure across the northern emirates, and recommending policies and practices that achieve collective purposes shaped with and through civil society and the market at various stages of the policy process. This approach builds on the contributions of the existing literature and provides a way forward for stakeholders in terms of addressing the nexus

between academic growth and environmental degradation as it relates to the transport sector in the northern emirates and beyond.

3 Research Questions, Objectives, and Hypothesis

The study's main research question is to what extent does economic growth affect environmental degradation in the northern emirates of the UAE? The sub-questions are what is the relationship between the expansion of the transport infrastructure and carbon dioxide emissions in the northern emirates? In what ways has the development of the transport sector affected economic growth and the subsequent rural to urban transition in the northern emirates? What are the protective and/or preventative policies and practices that have been implemented in the northern emirates that curb environmental degradation?

The objectives are first, to display the arrangement of the transport infrastructure across the northern emirates using GIS mapping. Second, to examine the relationship between economic growth and environmental degradation as evidenced from the transportation sector. Third, to recommend policies and practices that achieve collective purposes shaped with and through civil society and the market at various stages of the policy process.

The authors contend that there is a direct relationship between economic growth and environmental degradation. This is due to some of the effects associated with economic growth such as increases in human consumption and the depletion of non-renewable resources, increases in the levels of pollution including carbon dioxide emissions and related phenomenon such as global warming, the destruction of habitats and extinction of species, and so forth. Such outcomes, however, are not the only effects associated with economic growth. In some cases, economic growth amidst the shift from the primary to the tertiary sectors of the economy has followed an inverted U-shaped Kuznets curve where economic degradation decreases during the transition to a post-industrial society. This is due to a variety of factors such as the move from an industrial to a service based economy, investment and improvements in 'cleaner' technologies, less dependence on non-renewable resources and the adoption of renewable resources, and so on. Despite the positive effects that a transition from the primary to the tertiary sector has had on environment, the outcome from studies around the globe have not been conclusive. While in some countries economic growth amidst the transition from the primary to the tertiary sectors of the economy has had a positive effect on the environment, this has not been the case in all countries. In fact, in some countries such a transition has had a negative impact on the environment. The only conclusive finding is that economic growth leads to environmental degradation, however, the question remains to what degree does this occur?

4 Research Design and Methodology

The authors address the research questions and objectives using a combination of “extensive” and “intensive” concrete research designs [67, pp. 242–251]. Extensive research primarily focuses on discovering common properties and general patterns as a whole by employing descriptive and inferential statistics and numerical analysis. The focus is mainly on taxonomic groups that share similar formal attributes, but need not connect or interact with each other. Testing in extensive research determines how general the particular findings are in the wider population (replication). Intensive research primarily focuses on how structural processes work out in specific or different cases. Attention is given to groups and individuals that relate to each other structurally. Intensive research tests determine if the results apply to those individuals studied (corroboration).

The combination of extensive research for understanding macro-level dynamics combined with intensive research for understanding micro-level dynamics provided a comprehensive understanding of the general patterns and causal processes that affect environmental degradation in relation to economic growth more generally and the transport system more specifically. The extensive research method that the researchers employed to collect primary quantitative data was GIS maps that contain data layers and analytics using spatial location. This analysis allowed the researchers to determine the extent of the development of the current transport system in the northern emirates and evaluate its suitability in terms of addressing issues related to economic growth and the effects on environmental degradation. The authors chose GIS maps for several reasons. First, the collection of data using GIS provides a visual illustration of the development of the transport system in the northern emirates that is easily disseminated to other scholars, industry personnel, and policy makers. This allows a wider audience to access the findings of the research by overcoming academic language that may be difficult for the public to decipher. Second, using GIS allowed the researchers to understand the interaction among different phenomena such as economic growth, the transport system, and environmental degradation as well as their impact on different locations such as mountainous regions, urban areas, and city centers. Third, by combining GIS data with other data from secondary sources based on descriptive and inferential statistics and numerical analysis the authors provided a more comprehensive analysis. Maps produced from GIS data can be used to depict relationships and significant areas in a region. This is critical in terms of understanding the relationship between economic growth, transport, and environmental degradation at different interlocking scales from the local to the global. Without a proper assessment, government officials are uninformed, underprepared, and may develop policies and practices that are potentially ineffective and irrelevant.

The primary data that was collected using GIS maps and was combined with secondary data from government entities, global organizations, and other researchers. The secondary data was primarily used to inform the primary data. It provided the

authors with a longitudinal analysis of the relationship between environmental degradation, economic growth, and the transport system. This included large data sets that allowed for an exploration of specific trends and changes of phenomena over time.

The intensive research method that the researchers employed to collect qualitative data was interactive interviews. Interviewing is a complex social interaction in which the researcher and the respondent bring expectations to the interview. This requires a high level of interpersonal skills on the part of the researcher so that the respondent will feel at ease. A rapport must be established with the respondent to develop a trusting relationship [68]. This was accomplished by requesting interviews with personnel from the Ministry of Energy and Infrastructure that were acquainted with one of the researchers.

Interviewing is suited for describing both program processes and outcomes from the target audience's perspective or key stakeholder [69]. This included understanding policies that have been adopted by the Ministry of Energy and Infrastructure which, on the one hand, adhere to the overall development of the infrastructure in the UAE, and on the other hand, take into consideration issues that are related to environmental degradation. Interactive interviews are a less formal, less standardized, and more interactive method of interviewing that gives the researcher an effective manner of learning from the respondents what is significant about the issues raised during the interview [70]. For example, the researchers discussed issues such as economic growth in relation to the development of infrastructure including transport and how such developments impact environmental degradation. This enables the researcher to build upon and refer to knowledge gained about specific issues.

The goal of the interviews was to deeply explore the respondents' points of view, feelings, and perspectives regarding economic growth, transport, and environmental degradation. This allowed the researchers to have discussions with the respondents that explain issues, complexities, and contradictions in order to produce rich and varied data. A set of predetermined questions was created that addressed economic growth, transport, and environmental degradation issues. First, the authors decided what kind of information should be collected and questions posed based on the research questions and the objectives. Second, the authors constructed a first draft of the questions for revision. Third, the questions were edited and the procedures for their use was specified. The way that a question is phrased during an interview can have a large impact on how a respondent answers the question. Accordingly, the researchers prepared an introductory statement that describes the project followed by a lead statement before each question. For example, when questioning a respondent regarding environmental degradation, the lead statement to introduce the question was, 'The United Nations International Strategy for Disaster Reduction characterizes environmental degradation as the lessening of the limit of the earth to meet social and environmental destinations and needs. There are several different techniques that are being used to prevent this, including environmental resource protection and general preventative efforts'. The questions then follow this, 'Are there any protection and/or preventative techniques that have been implemented in the UAE's northern emirates? Are there plans that build upon and extend existing standards?' Further, the researchers also recognized that different individuals, cultures, and languages

can impact the interview. Accordingly, particular care was taken into consideration to be sensitive to differences from one respondent to another, cultural attributes, and languages. In some cases, translation of certain words or phrases from English to Arabic was conducted during the interview to facilitate communication.

5 Results and Discussions

5.1 *The Arabian Gulf, the United Arab Emirates, and the Northern Emirates*

In the 1950s, the Arabian Gulf's economy was mainly based on "nomadic farming, date palm cultivation, fishing, pearling, and seafaring" [11]. Following the discovery of petroleum, the region exemplified a bifurcated economy comprised of the primary sector (mostly resource extraction) and the tertiary sector (mostly service based production). Accordingly, the region did not undergo a sufficient industrialization period (secondary sector) unlike other regions that experienced industrialization as part of their transition to the tertiary sector [71].

The UAE is one of the fastest growing economies in the region and the world. High levels of construction and infrastructural development are attracting large numbers of people to work and live in the country. Following its formation in the early 1970s, the economy has been driven mainly by the primary and tertiary sectors. The primary sector includes the extractive industries such as petroleum and natural gas, which accounted for 29.5% of GDP in 2017. The tertiary sector includes wholesale, retail trade, and vehicle maintenance (11.7%); finance and insurance (8.6%); construction (8.4%); public administration, defense, and social security (5.8%); real estate (5.7%); transport and storage (5.4%); electricity, gas, and water (3.2%); information and communications (2.9%); professional, scientific, and technical services (2.6%); accommodation and food services (2.2%); administrative and support services (1.9%); and other services (3.9%). Accordingly, the tertiary sector comprised 62.3% of GDP in 2017 [11].

Economic growth in the UAE reflects a unique combination of the success in the petroleum and service sectors. The rate of economic growth in the individual emirates of the UAE, however, has varied. Abu Dhabi is most dependent on the petroleum industry and public sector functions. It has seen substantial growth in GDP because of its oil sector. The other emirates have significant growth in the non-oil industries given the diversification of the economy. The emirates reflect a complex mix of spatial governance with several emirates controlling land that is not adjacent and has its own environment and diversity of bioenvironmental habitat such as desert, mountains, and marine life [72].

One of the consequences of the continued growth of the UAE economy is urbanization with a substantial rise in population, driven by both the national population as

families out-migrate, and the expatriate community, as more employment opportunities become available. This level of population growth requires substantial support from public facilities. In the remote areas of the northern emirates, there will be the need for considerable infrastructure enhancement to satisfy the needs of changing populations.

The northern emirates' (Fig. 1) economy will continue to expand. Land, sea, and air transport development will allow for a booming logistics sector, building on the location at the center of the east–west trade routes. The natural beauty of the landscape, appealing environment, and cultural richness will allow further development of the tourism sector, particularly in rural areas.

Rural economies are typically dictated by agriculture, extractive industries, and local service activities. The rural parts of the northern emirates are largely situated in the inland areas, while the major urban (cities) areas are located along the coast. Sustainable rural development is a major challenge. Continued investment in infrastructure, providing access to employment and leisure opportunities and enabling a good quality of life are key drivers of rural development.

The scale of infrastructure development that opened many of the remotest areas has changed the northern emirates' rural dynamics. Governments' significant investment has brought rapid increases in local access to healthcare and education, provisions of basic utilities, and access to non-local job markets. This has been coupled with strong family ties and cultural attachment to local areas that have aided rural development and the resulting standard of living available. As such, the tendency for out-migration from rural areas has been reduced.

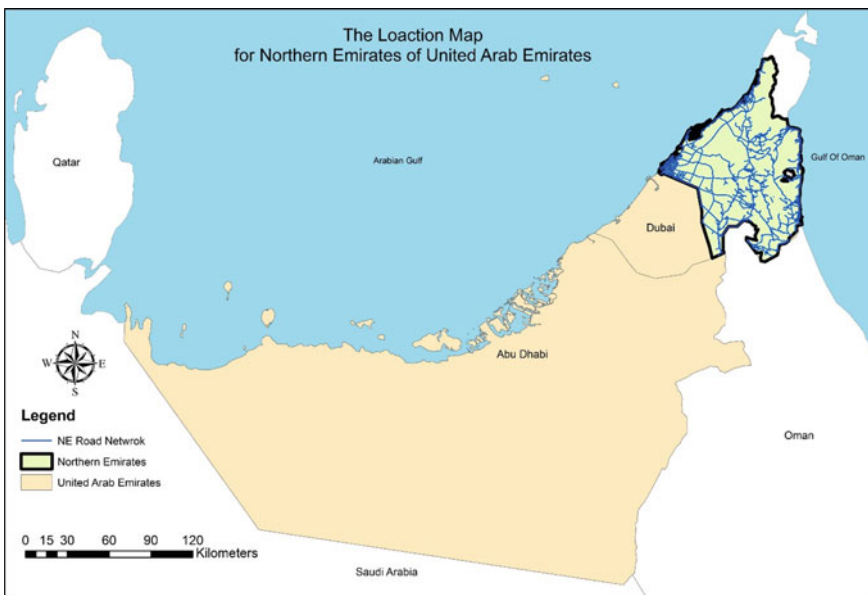


Fig. 1 Location map of the northern emirates of the United Arab Emirates

Continued economic growth and population increase is expected in the northern emirates. Ongoing investment in infrastructure continues to open new areas to development and encourage growth in rural areas; however, much of the development has been ad hoc and a more strategic approach to planning is required in the future because of the impact on the environment. In particular, transport infrastructure is of strategic importance in terms of enabling the future development of the northern emirates. Parts of the northern emirates benefit from excellent links with larger settlements whereas others suffer from relatively poor connectivity. Currently, appropriate roads do not serve some communities in remote parts of the northern emirates. In addition, the northern emirates have very limited public transport, which places greater emphasis on private transport. Major new development proposals should be accompanied by measures and schemes to reduce the reliance on private transport. A reliable public transport will help reduce carbon dioxide emissions from private transport that serves local residents and tourists. A further reduction in trip distances and the need for car journeys through mixed-use planning and establishing dense urban centers between rural areas will bring great benefits to the environment. This will improve accessibility to facilities and services, help to reduce vehicle movements, and encourage trips by more sustainable modes of transport, therefore improving the health and well-being of the population. Moreover, the impact on the natural environment will be reduced compared to creating additional roads between existing natural habitats.

In term of transportation infrastructure, the federal government is responsible for constructing and maintaining the highways and roads that connect major cities in the northern emirates, while the local governments are responsible for internal roads between settlements and collector roads. Figure 2 illustrates the road network of the northern emirates spanning the period from 2010 to 2019. The existing road network throughout the northern emirates links the major cities along the coasts through an expansive highway system. The highway system further extends into the identified mountainous areas and branches into dispersing major and minor road networks, which provide connectivity to the mountainous areas' settlements. The smaller settlements in very remote areas are generally connected by unpaved track roads along the natural terrain.

Figure 3 shows the road network of the northern emirates in 2020, which will significantly improve the connectivity of the northern emirates as well as the mountainous areas settlements. The coastal regions of Sharjah and Ras al-Khaimah are connected via a highway corridor that bypasses Ajman and Umm al-Quwain underneath the developed and congested centers. In addition, a road was recently constructed between the mountains that has five tunnels which provide a new traffic corridor from Sharjah to the Khorfakkan on the east coast and pass the Fujairah downtown area. The existing road network in the mountainous areas is less developed than the network outside of the mountainous areas. Although there are existing major roads and highways in the mountainous areas, several remote settlements are connected to each other and the road network via track roads, which are not paved or levelled. As a result, driving between settlements can be time consuming and dangerous.



Fig. 3 Road network of the northern emirates in 2020

rail and other modes of transport account for the remaining 3%. These figures are expected to increase, therefore raising concerns about identifying alternative energy sources [73]. In the UAE, road transport is primarily based on gasoline cars and diesel trucks and buses. As of 2016, there were approximately 3.4 million registered vehicles in the UAE [74]. Much of the urban landscape and planning is geared toward

automobiles with few alternatives that are being developed. In addition is a car culture that promotes luxury cars and SUVs. The transport sector in the UAE accounts for 22% of the energy consumption and contributes to carbon dioxide emissions [75].

The UAE's road system was ranked seventh globally in the quality index of the 2019 World Economic Forum, with extensive connections throughout all of the emirates. Road density (the ratio of the length of the country's road network to the country's land area) in the UAE has been increasing at an average rate of 136% per year since 2008 [76]. Abu Dhabi alone had approximately 27,000 km of roads in 2019 [77] and Dubai boasted an investment of \$27 billion in roads and transport during the period 2006–2018 [78]. As part of an effort toward energy-saving measures and the reduction of carbon dioxide emissions, the UAE replaced all the federal roads lamps with LED bulbs, which have a longer lifespan and consume 50% less energy. Furthermore, there is a commitment by the Ministry of Infrastructure to continue developing the road system using the most advanced technologies and international environmental standards [79]. For example, the UAE has incorporated a recycling program by reusing asphalt from deteriorated roads to construct new roads.

The interviews with personnel from the Ministry of Energy and Infrastructure regarding the inevitable development of the transport system in the UAE and the northern emirates revealed some interesting findings. The UAE has made significant technical progress in the development of its transport system that resulted in lower carbon dioxide emissions. For example, the Dubai Metro and similar projects are committed to developing the transport system while reducing environmental impact. Public transport has augmented private vehicle transport and decreased vehicle energy consumption. These changes do not necessarily guarantee a solution to the problem of carbon dioxide emissions, but certainly address issues related to decreasing the impact on the environment. One of the challenges that was raised for the future is the continued commitment to reducing environmental impact given the ongoing economic growth that the UAE is experiencing and the northern emirates are projecting. The reduction of road transport emissions will prove to be a challenge and the introduction of technological advancements has limited advantages, therefore effective solutions are required.

While technological advancements and innovations cannot be the solution to environmental degradation, there is significant potential for such technologies to ameliorate the effects on the environment by establishing more sustainable efforts in transport. The UAE has introduced several measures such as location analysis, connectivity of devices, development of networks, and data capturing, analytics, and processing to enhance its transport system. This contributes to land use planning, infrastructure development, road maintenance, and so forth. While such advancements bring significant opportunities toward reducing the impact of transport on the environment, risks and vulnerabilities remain. Various emerging digital solutions and innovations are evolving technologies that require further monitoring, upgrading, and investment. The ongoing development of a digitally supported sustainable transport system would require significant efforts and investment. This in part is due to the undeniable reality that any effective transport system must be reasonably priced to not incur greater costs than necessary on allocated budgets as well as provide sufficient

service to users. Accordingly, a sustainable transport system must strike a balance between understanding the costs associated with developing the infrastructure, the necessary services required, and greater environmental sustainability.

Another important point that was raised during the interviews is the relationship between economic growth, transport activity, and environmental degradation. There is a direct and strong relationship between economic growth and transport activity. Simply stated, as the economy in the UAE grew there has been a significant increase in transport activity. According to Mattar Al Tayer, Director-General and Chairman of the Board of Executive Directors of the Dubai Roads and Transport Authority, “Dubai raised \$46 billion after it invested more than \$27 billion in its roads and transport over 12 years”. Additional benefits include reducing travel time and fuel cost and increasing the share of public transport from 6% in 2006 to 17.5% in 2018 [78]. A similar situation is occurring in the northern emirates. As their economies grow, transport activity’s impact on the environment will be negative and significant. This includes issues such as air quality and noise pollution.

The UAE has made significant adjustments to address these issues. Traffic flow models have been used to improve the transport network. Models have been designed using GIS mapping and data analytics to reduce capacity on specific routes thus effectively managing pollution levels and dispersion. For example, the Darb website in Abu Dhabi uses GIS to “access fast, up-to-date and reliable information on driving directions, car travel maps, bus travel maps (bus routes and bus stops), bus terminals, points of interest (ATMs, petrol stations, hospitals etc.), ferry routes and timings. Darb also provides information on all airports in the UAE, with particular emphasis on details about the airports in the emirate of Abu Dhabi and related facilities such as passenger terminals and parking locations” [79]. Furthermore, the “Roads and Transport Authority (RTA) launched Smart Drive, an on-board route planning and exploration app, which operates without mobile Internet connection. RTA Smart Drive App provides turn-by-turn voice and visual instruction, automatic re-routing and speed limit alerts while displaying points of interest along the drive” [79]. Such efforts are significant and exemplify the impact that financial investment in combination with technological advancements play in mitigating the inevitable environmental degradation associated with economic growth and related development of the transport system.

While the UAE’s transport system remains heavily dependent on burning fossil fuels for energy, which ultimately has a negative impact on the environment, including humans, one cannot underestimate concerns about air pollution. The World Health Organization (WHO) identified air pollution as a major environmental risk to health, which is associated with “stroke, heart disease, lung cancer, and both chronic and acute respiratory diseases, including asthma” [80]. Simply stated, lower levels of air pollution result in better short- and long-term cardiovascular and respiratory health of the population. Most of the ambient (outdoor) air pollution is beyond the control of individuals and requires action by governments at various scales from the local to the international in a variety of sectors that are related to transport, such as energy and urban planning. The UAE has made some progress. For example, there has been significant shifts toward alternative modes of power generation by increasing the use

of low-emissions fuels and renewable combustion-free power sources. This includes solar, wind or hydropower, co-generation of heat and power, and distributed energy generation such as mini-grids and rooftop solar power generation [80].

In terms of urban planning, there has been significant development of energy efficient urban transit systems, walking and cycling networks in cities, as well as plans for inter-emirate rail passenger travel. However, despite such efforts, the UAE's air quality remains 'unsafe'. According to the International Association for Medical Assistance to Travelers, "The most recent data indicates the UAE's annual mean concentration of PM_{2.5} is 41 $\mu\text{g}/\text{m}^3$ which exceeds the recommended maximum of 10 $\mu\text{g}/\text{m}^3$ " [81]. This places the UAE's air pollution level at approximately four times higher than the recommended level by the WHO. The primary factors that contribute to air pollution in the UAE are industrial and vehicle emission; however, among the most polluted are Abu Dhabi and Dubai cities as the country continues to expand its transport network. While data is not available for cities in the northern emirates, one can predict with certainty based on current trends in the UAE, that air pollution levels will indeed rise as the transport network is developed. While many challenges lie ahead, in terms of reversing such trends, stricter air quality guidelines are required that include supportive national policies and legal and regulatory frameworks.

6 Conclusions and Recommendations

The development of the bifurcated economy in the UAE, like other countries in the Arabian Gulf, is comprised mostly of the primary (resource extraction) and tertiary sectors (services). Unprecedented economic growth over several decades has resulted in dramatic increases in the population as well as significant development of the infrastructure including the transport system. In addition, there has been a spillover in such developments to the northern emirates. The northern emirates may be viewed as emerging economies given the ongoing increase in population and greater demand for public facilities. Continued investment in the transport system is essential in terms of providing access to employment, leisure, hospitals, schools, and so forth.

Infrastructure development in the northern emirates has been ad hoc with little in terms of planning and proper assessment of the effects on the environment. The result has been uneven outcomes, where some places benefit from excellent links to larger settlements while others are poorly connected. In addition is the lack of public transport, which results in greater use of private transport and does not provide sufficient transportation options. A reliable public transport is necessary to reduce carbon dioxide emissions, serve local residents and tourists, reduce traffic in the city centers, provide greater accessibility to services, reduce air pollution, and decrease the number of roads required.

Proposed plans will run rail from Abu Dhabi and Dubai and connect Sharjah with Ras al-Khaimah in the north and Fujairah in the east coast. This will provide efficient transport of goods to ports, airports, and major centers of employment thus furthering the opportunities for economic growth in those areas. In addition, the development

of the transport corridors in 2020 significantly improved the connectivity of the northern emirates. This includes roads that connect Sharjah and Ras al-Khaimah, Ajman, Umm al-Quwain, Sharjah, Khorfakkan, and Fujairah; however, the transport system in the mountainous areas is not well developed. Although there are some roads and highways, remote settlements are connected with track roads that are not paved or leveled.

Expected increases in the demand for transport services in the future have raised concerns about the urgency of identifying effective methods of curbing the environmental degradation associated with the transport system. The UAE's transport sector accounts for 22% of energy consumption and is a major contributor to carbon dioxide emissions [75]. In 2016, there were 3.4 million registered vehicles in the UAE and road density has been rising at a rate of 136% per annum since 2008 [76]. Public transport to date is not well developed or in the cases of the northern emirates is non-existent. This has resulted in an automobile centric transport system, a car-oriented infrastructure, and a 'car culture' that promotes luxury cars and SUVs.

Given these challenges, governing bodies in the UAE have made significant efforts at reducing the inevitable environmental degradation associated with the development of the transport sector. For example, the development of the Dubai metro has augmented private vehicle transport and decreased average vehicle energy consumption. This is recognized as part of the solution to reducing environmental degradation; however, some caution is required. The authors contend that the positive impact of public transport is limited. This is due to the ongoing demand in the UAE for private transport despite the fact that the public transport system in Dubai, for example, is among the highest ranking in the world. Accordingly, a balance must be struck in terms of the type of public transport (e.g., metro, light rail, busing) that is most suitable for booming cities such as Abu Dhabi and Dubai as well as the emerging northern emirates.

The authors make three suggestions in this regard: first, decisions must be based on proper assessment of the needs of the public rather than promoting expensive solutions that attract attention. Given the importance of budgeting during the ongoing financial crisis since 2007/2008 and the current effects of the pandemic on the economy, ensuring efficient use of resources is paramount. Inexpensive solutions, such as busing instead of rail, may bring very effective outcomes in terms of covering a larger area and serving more people. Second, more attention is required in the northern emirates where an effective public transport system currently does not exist. This requires more coordinated efforts at both the federal and emirate levels of governments. An effective way forward is for local planners to work with politicians in the development of a plan. The requirements, for example, in one emirate compared to another may be quite different. It is only through the expertise of local personnel that such nuances are revealed and would make for more effective planning. Third, studies are required that identify the impact on the environment of a new public transport system. This may require the development or revision of existing procedures and practices. Much of the existing theoretical framework in the academic literature may be used to understand similar scenarios from around the world as these provide examples from other regions struggling with similar challenges.

The UAE has been very effective at using the most advanced technologies in the development of the transport system by applying location analysis, connectivity of devices, development of networks, and data capturing, analytics, and processing. This has contributed to much more efficient operations. Such technologies, however, require costly and ongoing monitoring, upgrading, and investment. Moreover, while Abu Dhabi and Dubai benefit greatly from such sophisticated infrastructure, the northern emirates have not been integrated. In addition, while the development of roads and transport in Dubai, for example, has cost approximately \$27 billion, \$46 billion was raised following the investment. Additional benefits beyond the economic include reducing travel time and fuel cost, increasing the share of public transport from 6% in 2006 to 17.5% in 2018, the development of traffic flow models using GIS mapping, and data analytics to reduce capacity on specific routes [78]. Such efforts are considerable and have been effective at, on the one hand, justifying the economic costs of such a sophisticated transport system, and on the other hand, effectively reducing the impact on the environment.

While the authors applaud the progress that has been made in the development of the UAE's transport system, the fact remains that a necessary relationship exists among factors such as rapid economic growth, transport development and activity, and environmental degradation. One of the most concerning aspects of the development of the transport system in the UAE is the effects this has had on air pollution. Recent data places the UAE's air pollution level at approximately four times higher than the recommended level by the WHO [81]. Further, the WHO identified air pollution as a major environmental risk to health connected to stroke, heart disease, lung cancer, and chronic and acute respiratory diseases, including asthma [80]. Reducing air pollution requires progressive and integrated policies from both the federal and emirate governments. The authors make several recommendations in this regard: the introduction of low emission zones where access by some vehicles (e.g., large SUVs, trucks, luxury vehicles) is restricted or deterred with the aim of improving air quality, investment in ecofriendly public transport in the northern emirates, a gradual decarbonization of the existing public transport system through the introduction of electric buses, the lowering of speed limits, and the introduction of walking and cycling paths in the northern emirates. Lastly, one cannot overlook the importance of the public. Changes in behavior require nationwide campaigns and continued education about public health risks associated with air pollution. This speaks to the most vulnerable in our society, such as children and the elderly. Making changes is well within the capabilities of the public. It not only requires an understanding of the scientific data, but also the costly toll on public health.

References

1. Johnson DL, Ambrose SH, Bassett TJ, Bowen ML, Crummey DE, Isaacson JS, Winter-Nelson AE et al (1997) Meanings of environmental terms. *J Environ Qual* 26(3):581–589
2. Mitra S (2020) Environmental degradation: bridging the gap in EKC literature. *Econ Dev Clim Chang Environ* 45
3. Chertow MR (2000) The IPAT equation and its variants. *J Ind Ecol* 4(4):13–29
4. Huesemann M, Huesemann J (2011) *Techno-fix: why technology won't save us or the environment*. New Society Publishers
5. Wang J, Dong K (2019) What drives environmental degradation? Evidence from 14 Sub-Saharan African countries. *Sci Total Environ* 656:165–173
6. Seidman KF (2005) *Economic development finance*. Sage
7. OECD [Organisation for Economic Co-operation and Development] Data (2020) Gross domestic product (GDP). [https://data.oecd.org/gdp/gross-domestic-product-gdp.htm#:~:text=Gross%20domestic%20product%20\(GDP\)%20is,and%20services%20\(less%20imports](https://data.oecd.org/gdp/gross-domestic-product-gdp.htm#:~:text=Gross%20domestic%20product%20(GDP)%20is,and%20services%20(less%20imports)
8. Greenwood DT, Holt RP (2014) *Local economic development in the 21st century: quality of life and sustainability: quality of life and sustainability*. Routledge
9. Stock T, Obenaus M, Kunz S, Kohl H (2018) Industry 4.0 as enabler for a sustainable development: a qualitative assessment of its ecological and social potential. *Process Saf Environ Prot* 118:254–267
10. Roukanas SA, Sklias PG (2021) The political economy of UAE branding from marketing to economics and power. In: *Handbook of research on future policies and strategies for nation branding*. IGI Global, pp 1–17
11. The Official Portal of the UAE Government (2020) Economy. <https://u.ae/en/about-the-uae/economy>
12. Vel P, Gomišček B (eds) (2021) *Corporate success stories in the UAE: the key drivers behind their growth*. Emerald Publishing Limited
13. Kuznets S (1955) Economic growth and income inequality. *Am Econ Rev* 45(1):1–28
14. Grossman GM, Krueger AB (1995) Economic growth and the environment. *Q J Econ* 110(2):353–377
15. Naqvi SAA, Shah SAR, Anwar S, Raza H (2021) Renewable energy, economic development, and ecological footprint nexus: fresh evidence of renewable energy environment Kuznets curve (RKC) from income groups. *Environ Sci Pollut Res* 28(2):2031–2051
16. USDA [United States Department of Agriculture] (2020) Ag and food sectors and the economy. <https://www.ers.usda.gov/data-products/ag-and-food-statistics-charting-the-essentials/ag-and-food-sectors-and-the-economy/#:~:text=In%202019%2C%2022.2%20million%20full,1.3%20percent%20of%20U.S.%20employment>
17. Trading Economics (2020) China industrial production. <https://tradingeconomics.com/china/industrial-production>
18. Zhou X, Cai Z, Tan KH, Zhang L, Du J, Song M (2021) Technological innovation and structural change for economic development in China as an emerging market. *Technol Forecast Soc Chang* 167:120671
19. Wu F, Edmonds R (2017) China's three-fold environmental degradation. In: Tubilewicz C (ed) "Environmental degradation" in critical issues in contemporary China, 2nd edn. Routledge
20. Alshehhi Y (2017) Accounting for growth: comparing economic sectors in the UAE. *The Annals of the University of Oradea*, p 270
21. Alshehhi YZ, Oláh J (2017) Sectorial analysis: growth accounting of secondary industries. *Netw Intell Stud* 5(9):39–45
22. U. S. Bureau of Labor Statistics (2020) Employment projections—employment by major industry sector. <https://www.bls.gov/emp/tables/employment-by-major-industry-sector.htm>
23. Dinda S (2004) Environmental Kuznets curve hypothesis: a survey. *Ecol Econ* 49(4):431–455
24. Ali W, Abdullah A, Azam M (2017) Re-visiting the environmental Kuznets curve hypothesis for Malaysia: fresh evidence from ARDL bounds testing approach. *Renew Sustain Energy Rev* 77:990–1000

25. Belaïd F, Zrelli MH (2019) Renewable and non-renewable electricity consumption, environmental degradation and economic development: Evidence from Mediterranean countries. *Energy Policy* 133:110929
26. Boubellouta B, Kusch-Brandt S (2020) Testing the environmental Kuznets Curve hypothesis for E-waste in the EU28+ 2 countries. *J Clean Prod* 277:123371
27. Dogan E, Turkekel B (2016) CO₂ emissions, real output, energy consumption, trade, urbanization and financial development: testing the EKC hypothesis for the USA. *Environ Sci Pollut Res* 23(2):1203–1213
28. Hanif I, Gago-de-Santos P (2017) The importance of population control and macroeconomic stability to reducing environmental degradation: an empirical test of the environmental Kuznets curve for developing countries. *Environ Dev* 23:1–9
29. Dabachi UM, Mahmood S, Ahmad AU, Ismail S, Farouq IS, Jakada AH, Kabiru K (2020) Energy consumption, energy price, energy intensity environmental degradation, and economic growth nexus in African OPEC countries: evidence from simultaneous equations models. *J Environ Treat Tech* 8(1):403–409
30. Ozturk I, Al-Mulali U (2015) Investigating the validity of the environmental Kuznets curve hypothesis in Cambodia. *Ecol Ind* 57:324–330
31. Asumadu-Sarkodie S, Owusu PA (2017) The causal effect of carbon dioxide emissions, electricity consumption, economic growth, and industrialization in Sierra Leone. *Energy Sources Part B* 12(1):32–39
32. Bella G, Massidda C, Mattana P (2014) The relationship among CO₂ emissions, electricity power consumption and GDP in OECD countries. *J Policy Model* 36(6):970–985
33. Farhani S, Shahbaz M (2014) What role of renewable and non-renewable electricity consumption and output is needed to initially mitigate CO₂ emissions in MENA region? *Renew Sustain Energy Rev* 40:80–90
34. Shahbaz M, Uddin GS, Rehman IU, Imran K (2014) Industrialization, electricity consumption and CO₂ emissions in Bangladesh. *Renew Sustain Energy Rev* 31:575–586
35. Tenaw D, Beyene AD (2021) Environmental sustainability and economic development in sub-Saharan Africa: a modified EKC hypothesis. *Renew Sustain Energy Rev* 143:110897
36. Piñeiro Chousa J, Tamazian A, Vadlamannati KC (2017) Does higher economic and financial development lead to environmental degradation: evidence from BRIC countries. *Energy Policy* 37(1):2009
37. Rajpurohit SS, Sharma R (2020) Impact of economic and financial development on carbon emissions: evidence from emerging Asian economies. *Manag Environ Qual Int J*
38. Raza SA, Shah N, Khan KA (2020) Residential energy environmental Kuznets curve in emerging economies: the role of economic growth, renewable energy consumption, and financial development. *Environ Sci Pollut Res* 27(5):5620–5629
39. Jiang C, Ma X (2019) The impact of financial development on carbon emissions: a Global Perspective. *Sustainability* 11(19):5241
40. Khuky MA (2021) The financial development-environmental degradation nexus in Bangladesh: a long-run co-integration approach. *Energy Econ Lett* 8(2):109–121
41. Shahbaz M, Solarin SA, Mahmood H, Arouri M (2013) Does financial development reduce CO₂ emissions in Malaysian economy? A time series analysis. *Econ Model* 35:145–152
42. Ali HS, Law SH, Lin WL, Yusop Z, Chin L, Bare UAA (2019) Financial development and carbon dioxide emissions in Nigeria: evidence from the ARDL bounds approach. *GeoJournal* 84(3):641–655
43. Kasman A, Duman YS (2015) CO₂ emissions, economic growth, energy consumption, trade and urbanization in new EU member and candidate countries: a panel data analysis. *Econ Model* 44:97–103
44. Ozturk I, Acaravci A (2013) The long-run and causal analysis of energy, growth, openness and financial development on carbon emissions in Turkey. *Energy Econ* 36:262–267
45. Cetin M, Ecevit E, Yucel AG (2018) The impact of economic growth, energy consumption, trade openness, and financial development on carbon emissions: empirical evidence from Turkey. *Environ Sci Pollut Res* 25(36):36589–36603

46. Shahbaz M, Hye QMA, Tiwari AK, Leitão NC (2013) Economic growth, energy consumption, financial development, international trade and CO₂ emissions in Indonesia. *Renew Sustain Energy Rev* 25:109–121
47. Siddique HMA (2017) Impact of financial development and energy consumption on CO₂ emissions: evidence from Pakistan. *Bull Bus Econ* 6(2):68–73
48. United Nations (2018) World urbanization prospects: the 2018 revision. <https://population.un.org/wup/Publications/Files/WUP2018-KeyFacts.pdf>
49. Majeed MT, Ozturk I (2020) Environmental degradation and population health outcomes: a global panel data analysis. *Environ Sci Pollut Res* 27(13):15901–15911
50. Ahmad M, Jiang P, Murshed M, Shehzad K, Akram R, Cui L, Khan Z (2021) Modelling the dynamic linkages between eco-innovation, urbanization, economic growth and ecological footprints for G7 countries: does financial globalization matter? *Sustain Cities Soc* 70:102881
51. Henderson V (2002) Urbanization in developing countries. *World Bank Res Obs* 17(1):89–112
52. Hildebrand M, Kanaley T, Roberts B (2013) Sustainable and inclusive urbanization in Asia Pacific (Strategy Paper). UNDP, New York
53. Beall J, Guha-Khasnobis B, Kanbur R (2010) Urbanization and development: multidisciplinary perspectives. OUP/UNU WIDER, Oxford
54. K' Akumu O (2004) Privatization of urban water supply in Kenya: policy options for the poor. *Environ Urban* 16(2):213–222
55. Mitlin D, Satterthwaite D (2012) Urban poverty in the global south: scale and nature. Routledge, Abingdon
56. Satterthwaite D (2015) Urban poverty, urban pollution and environmental management: topic guide. Evidence on Demand
57. Abdallah AA, Abugamos H (2017) A semi-parametric panel data analysis on the urbanisation-carbon emissions nexus for the MENA countries. *Renew Sustain Energy Rev* 78:1350–1356
58. He Z, Xu S, Shen W, Long R, Chen H (2017) Impact of urbanization on energy related CO₂ emission at different development levels: regional difference in China based on panel estimation. *J Clean Prod* 140:1719–1730
59. Wang Y, Zhang X, Kubota J, Zhu X, Lu G (2015) A semi-parametric panel data analysis on the urbanization-carbon emissions nexus for OECD countries. *Renew Sustain Energy Rev* 48:704–709
60. Mahmood H, Maalel N, Hassan MS (2021) Probing the energy-environmental Kuznets curve hypothesis in oil and natural gas consumption models considering urbanization and financial development in middle east countries. *Energies* 14(11):3178
61. Nathaniel S, Anyanwu O, Shah M (2020) Renewable energy, urbanization, and ecological footprint in the Middle East and North Africa region. *Environ Sci Pollut Res* 1–13
62. Shahbaz M, Sbia R, Hamdi H, Ozturk I (2014) Economic growth, electricity consumption, urbanization and environmental degradation relationship in United Arab Emirates. *Ecol Ind* 45:622–631
63. Charfeddine L, Khediri KB (2016) Financial development and environmental quality in UAE: cointegration with structural breaks. *Renew Sustain Energy Rev* 55:1322–1335
64. Khan SH, Agha S (2015) Impact of FDI in UAE over the main elements of sustainable development: economy and environment. *J Emerg Trends Econ Manag Sci* 6(7):263–267
65. Nasir MA, Canh NP, Le TNL (2021) Environmental degradation & role of financialisation, economic development, industrialisation and trade liberalisation. *J Environ Manage* 277:111471
66. Shahbaz M, Haouas I, Sohag K, Ozturk I (2020) The financial development-environmental degradation nexus in the United Arab Emirates: the importance of growth, globalization and structural breaks. *Environ Sci Pollut Res* 1–15
67. Sayer RA (1992) Method in social science: a realist approach. Psychology Press
68. Breakwell GM (2006) Interviewing methods. *Research methods in psychology*. Sage, Los Angeles, pp 232–253
69. Kitchin R, Tate N (2013) Conducting research in human geography: theory, methodology and practice. Routledge

70. Rathbun BC (2008) Interviewing and qualitative field methods: pragmatism and practicalities. In: *The Oxford handbook of political methodology*
71. Malecki EJ, Ewers MC (2007) Labor migration to world cities: with a research agenda for the Arab Gulf. *Prog Hum Geogr* 31(4):467–484
72. Al-mulali U, Che Sab CNB (2018) Energy consumption, CO2 emissions, and development in the UAE. *Energy Sources Part B* 13(4):231–236
73. International Renewable Energy Agency (2020) Reaching zero with renewables. <https://www.irena.org/publications/2020/Sep/Reaching-Zero-with-Renewables>
74. World Health Organization (2018) Global status report on road safety 2018. file:///C:/Users/rmbridi/Downloads/9789241565684-eng.pdf
75. Sushil Jha S, Tandon DJ (2019) A study on the impact of transport and power infrastructure development on the economic growth of United Arab Emirates (UAE). *J Manag* 6(2)
76. World Data Atlas (2020) United Arab Emirates—road density. <https://knoema.com/atlas/United-Arab-Emirates/Road-density>
77. Puri-Mirza E (2020) Length of roads in the Abu Dhabi Emirate in 2019, by region. <https://www.statista.com/statistics/1067710/uae-length-of-roads-in-abu-dhabi-by-region/#:~:text=Road%20length%20in%20the%20Abu%20Dhabi%20Emirate%202019%20by%20region&text=As%20of%202019%2C%20the%20total,was%20almost%2027%20thousand%20kilo meters>
78. White S (2019) Dubai makes \$19bn through road and transport investment. <https://meconstructionnews.com/37479/dubai-makes-19bn-through-road-and-transport-investment#:~:text=Mattar%20Al%20Tayer%2C%20Director%2DGeneral,and%20transport%20over%2012%20years>
79. The Official Portal of the UAE Government (2020) Roadways. https://www.google.com/search?q=length+of+road+system+in+the+UAE&rlz=1C1WPZA_enAE765AE847&oq=length+of+road+system+in+the+UAE&aqs=chrome..69i57.10093j1j7&sourceid=chrome&ie=UTF-8
80. World Health Organization (2018) Ambient (outdoor) air pollution. Retrieved from [https://www.who.int/news-room/fact-sheets/detail/ambient-\(outdoor\)-air-quality-and-health](https://www.who.int/news-room/fact-sheets/detail/ambient-(outdoor)-air-quality-and-health)
81. The World Factbook (2021) United Arab Emirates. <https://www.cia.gov/the-world-factbook/countries/united-arab-emirates/#economy>

Drought, Vegetation Degradation

Influence of Cryogenic Processes and Phenomena on Minimum Runoff in Russia



M. L. Markov, M. V. Georgievsky, and M. A. Mamaeva

Abstract Over large areas of the Asian part of Russia, air temperatures remain below 0° C for a long time, leading to the transition of water from a liquid to a solid state and vice versa. Climate warming gradually leads to a decrease in the role of cold in the heat and moisture circulation of these territories. Permafrost degradation occurs in the permafrost zone. In temperate latitudes, seasonal freezing of soil and grounds decreases or completely stops. All this leads to the beginning of environmental degradation. The purpose of this chapter is to assess the cumulative impact of the main cryogenic phenomena and processes on the underground recharge of Russian rivers and processes that form and occur in river basins: In riverbeds, catchments, swamps and wetlands, soils, fractured and loose rocks. The chapter also presents the authors' reflections on the evolution of stable and unstable structures in a «water flow-ice-channel sediments» system (in annual and multi-year cycles) while air temperature decreases, and also lists the main problems, according to the authors, arising in the assessment of natural groundwater resources based on hydrological data under climate change. As a result of the performed calculations, it was established that air temperature plays a significant role in the formation of almost 20% of the total annual river runoff in the temperate and northern latitudes of Russia with stable winters. The ongoing and forecasted increase in winter air temperature over these territories may gradually weaken cryogenic runoff regulation and noticeable changes in the water regime.

Keywords Minimum winter and summer runoff · Groundwater inflow · Aufeises · River and seasonal underground ice · Swamps · Cryogenic river runoff control · Climate change

M. L. Markov · M. V. Georgievsky (✉) · M. A. Mamaeva
State Hydrological Institute (SHI), 199004 St. Petersburg, Russia
e-mail: mgeorgievsky@hotmail.com

© The Author(s), under exclusive license to Springer Nature Switzerland AG 2022
A. M. F. Al-Quraishi et al. (eds.), *Environmental Degradation in Asia*,
Earth and Environmental Sciences Library,
https://doi.org/10.1007/978-3-031-12112-8_26

567

1 Introduction

Over most of the territory of the Asian part of Russia, negative air temperatures persist for a significant part of the year, and winter lasts more than four months. Such a long cold period leads to the formation of various cryogenic phenomena associated with «water–ice/snow–water» phase transitions: River and lake ice; underground ice, aufeis of various types, soil freezing, etc. All these phenomena affect, to varying degrees, the hydrological regime and the state of the environment. Climate warming is gradually reducing the role of cold in heat and moisture circulation in the gigantic territory of Asian Russia. Permafrost degradation occurs in the permafrost zone. In temperate latitudes, seasonal freezing of soil and grounds decreases or completely stops. These processes lead to the beginning of environmental degradation. As a mobile element of nature, water is an active participant in the accumulation and transfer of thermal energy over territories and plays a significant role in the formation and evolution of the state of the environment. Due to the physical property of water to change its phase state, it can both strengthen the ongoing climate changes and weaken them. This controversial role of water in environmental change is the article's main focus.

Many works have been devoted to assess the impact of certain natural cryogenic phenomena on the formation of river runoff in Russia [1–6]. It was found that their main influence affects the underground feeding of rivers. At the same time, there is still no overall assessment of the impact of cryogenic phenomena on river runoff. Perhaps, such studies were not as relevant until recently as it became in the last 20–30 years due to the climate's recent and expected future warming, especially in winter in the Northern hemisphere. Therefore, the main purpose of this chapter is to assess the cumulative impact on the groundwater recharge of Russian rivers, including rivers located in the Asian part of the country, of many cryogenic phenomena and processes occurring in riverbeds, catchments, swamps and wetlands, soils, fissured and loose rocks.

The general assessment of the impact of cryogenic phenomena on river runoff is still a poorly studied area of hydrology, which causes various discussions. The chapter presents the authors' reflections on the evolution of stable and unstable structures in «water flow–ice–channel sediments» system (in annual and multiyear cycles) as air temperature decreases. Also, according to the authors, it lists the main problems arising in the assessment of minimum runoff and groundwater recharge of rivers under climate change. The evolution of river flow structures is associated with the problem of determining the relationship between the role of randomness and determinism in them. The change in structures also determines the variability of the water regime of rivers in winter.

2 Problems of River Underground Recharge Assessment by Hydrological Data Under Climate Change Conditions

Calculation of underground recharge of rivers and their complete drainage of underground aquifers (assessing natural resources of underground waters) is based on the division of river flow hydrographs into the surface and underground components. There are various schemes for dismembering runoff hydrographs. However, they are all united by the fact that the reference ordinates for determining the underground recharge are the water discharge in the low-water winter and summer periods. The formation of these costs is influenced by hydrogeological conditions and external factors, including changes in meteorological conditions.

Figure 1 shows the factors of the formation of the minimum winter runoff associated with the meteorological conditions of the winter period.

The first and well-studied phenomenon is the accumulation of water in ice. This is especially evident in the area of permafrost distribution. Thick ice cover on rivers 1–2 m thick, ice of different types and seasonal underground ice is formed in these areas in winter [7, 8]. This leads to a decrease in the winter river runoff, and in the warm season it causes an increase in the underground component of the river runoff [9, 10]. The State Hydrological Institute (SHI) has extensive experience in long-term expeditionary work in permafrost regions. As a result of these specialized expeditionary operations, a large amount of information was accumulated. Based on the generalization of this information and theoretical studies, several methods were developed for calculating hydrographs in the presence, inadequacy and absence of

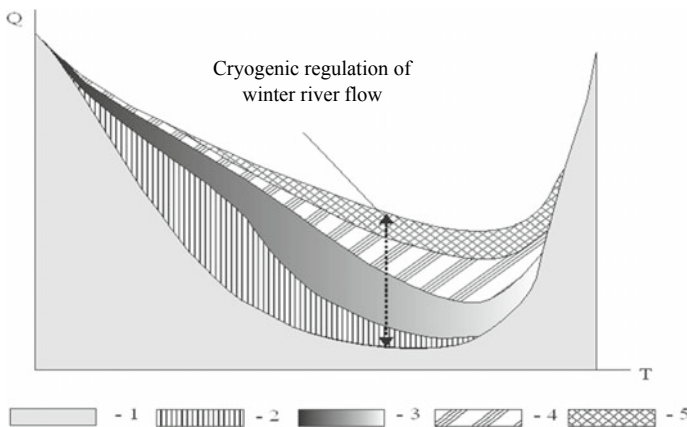


Fig. 1 Schematic hydrograph of winter runoff (1); runoff losses due to water accumulation in the ice cover (2). Reduction of underground recharge of rivers due to: A decrease in the throughput of small river channels under ice (3), migration of unfrozen moisture in the aeration zone to the freezing front of soil (4), the occurrence of low air pressure above groundwater with a decrease in their level due to a decrease in air permeability of the frozen layer (5)

initial information with an accuracy acceptable for practice [11, 12]. These methods can be used in other areas where the winter period lasts more than four months.

The second factor in the influence of climatic conditions on winter runoff is associated with a decrease in the carrying capacity of river channels under the ice. It is known that most of the river runoff in river basins located from the forest zone to the tundra zone is formed by very small rivers less than 10 km long (70–80% of the length of the hydrographic network). With an ice thickness of 0.3–0.5 m, these rivers may freeze over or significantly reduce their cross-section. In the northern regions of the Russian Federation, small rivers freeze over, and medium rivers can dry up if there is no groundwater supply. Suppose the decrease in the underground recharge of the river and the river runoff in winter occurs at a lower intensity than the decrease in the throughput capacity of the river section with intensive ice formation, then on small rivers (where ice is rigidly attached to the banks). In that case, a pressure flow regime under the ice may arise. The realization of the pressure can be expressed either in the destruction of ice, the release of water to its surface and the formation of ice, or in a decrease in the inflow of underground water into the river. On wide rivers, the pressure is compensated for by the free rise or bend of the ice cover [13].

Calculations of ordinates of runoff hydrographs performed according to the method described in [14] showed that the lower air temperature in winter and the thicker ice cover, the faster decrease in runoff in rivers occurs. In less severe winters, we observe a decrease in river ice thickness and persistence in rivers of higher water discharge by the end of winter [15]. An increase in ice thickness, for example, in the basin of the Severnaya Dvina River, by only 10 cm, leads to a decrease in runoff at the end of winter in small streams, almost two times compared with warm winters. For the basin of the Aldan River, the deviation of the average winter air temperature from the long-term average by 2–3 degrees leads to a deviation of the average winter river runoff by 20–30% from the long-term average [16].

The third climatic factor is associated with the migration of unfrozen moisture to the freezing front. A study of the conditions for formation of stored soil moisture in the winter period in the Vyatka River basin, the objects of the Valdai branch of the State Hydrological Institute, showed that the limit values of an increase of stored soil moisture due to migration are:

- about 40 mm with a weak initial freezing (up to 10 cm),
- about 25 mm with a strong initial freezing (20–40 cm) [17].

Accordingly, the groundwater resources may temporarily decrease by these values.

The fourth climatic factor began to be studied relatively recently. However, the influence of changes in atmospheric pressure on the water level in wells, the consumption of healing springs, the operation of water mills, etc., has been known for over three hundred years.

Experimental work is being carried out at the SHI to identify the effect of fluctuations in air pressure in the aeration zone on the mode of discharge of underground water into water bodies [18]. Already the first results showed that the pressure difference in the atmosphere and in the unsaturated soil-ground area during the passage

of atmospheric fronts can be up to 50–100 mm in the equivalent of a water column, and in winter—up to 200 mm or more in the event of a seasonally frozen layer, poorly permeable to air, which is necessary to fill voids with a decrease in the level of groundwater. With the warming of winters, the cessation of freezing of soils and grounds, this physical phenomenon, which keeps the rapid drainage of underground waters, disappears. It is also appropriate to note that the relationship between pressure fluctuations in the aeration zone during the day (by 2–5 mm in the water layer) with the intraday variation of the air temperature at constant atmospheric pressure has been recorded. This is probably due to the intraday dynamics of evaporation from land. According to the study results, a preliminary conclusion has been made that, in addition to the known forces (gravitational, capillary-film, electromagnetic, temperature, etc.), the movement of water in soils is significantly influenced by fluctuations in air pressure. This force can lead to the movement of water even if there is no slope towards the drain (water body), which has a lower air pressure.

The increase in air temperature during the cold period in many regions of the Russian Federation over the past two decades has led to a decrease in the role of the factors described above in the formation of the minimum river runoff [19, 20]. It increased 1.5–2 times [21, 22]. Nevertheless, does this also mean a correspondingly sharp increase in the natural resources of groundwater? The answer is probably no. According to the annual reports of the HMSN Center (website <http://www.geo-monitoring.ru>), there have been no significant changes in the regime of ground and underground water levels over the past 20–30 years.

The discrepancy between the increase in the minimum river flow and the relatively stable state of groundwater levels can be explained as follows.

On the one hand, due to significant warming of winters, a decrease in freezing of soil and grounds, the infiltration of precipitation and recharge of underground aquifers increased. On the other hand, the drainage capacity of the hydrographic network has also increased due to the decrease or complete absence of ice cover on small rivers and streams. Therefore, the increase in underground water recharge in winter is compensated by their more intensive drainage in the upper links of the hydrographic network (underground water recharge zone). As a result, groundwater levels, even if they do rise, are not as strong as the winter underground feeding of rivers.

The question arises as to why the minimum costs in the summer-autumn low-water period also increase. One of the reasons may be as follows. Winter runoff increased, first of all, due to groundwater drainage, a decrease in the regulatory role of other factors described above. In colder winters of the previous climatic period, these waters were discharged less (low drainage capacity of small rivers with ice cover, freezing of underground runoff channels, etc.). The runoff of small rivers decreased. Accordingly, the runoff in the lower links of the hydrographic network also decreased. The water level in them decreased, and the conditions for drainage of groundwater from deeper aquifers improved (their slope towards the river increased). As a result, the runoff of large rivers during this climatic period was formed in winter to a greater extent from deeper aquifers.

In warmer winters, as noted above, the drainage capacity of small rivers increases, the water level in the lower links becomes significantly higher due to the inflow from the upper ones, and their drainage of deep aquifers decreases. That is, the depletion of subsurface water reserves during warm winters is reduced due to more intensive depletion of groundwater. And the underground water accumulated in the river valleys (or not depleted in winter) is redistributed during the summer-autumn low-water period, when the inflow from the upper links of the hydrographic network decreases. Thus, the warming of winters leads to a greater participation in the feeding of rivers in the cold period of the waters of the upper layer, and in the warm period—of the lower layer of the zone of active water exchange in the lithosphere. At the same time, the average annual levels of both groundwater and underground water may not change significantly. From this, the same minimum water discharge in the river can be formed in warm years, to a greater extent due to the upper aquifers, and in cold years—due to deeper ones.

Thus, the reference minimum water discharge used in the hydrological substantiation of the assessment of natural resources of groundwater does not fully reflect them in cold winters. However, in warm winters, it can lead to their unjustified overestimation.

An analysis of the results of experimental studies shows a still poor understanding of the physical process of interaction between river waters and underground water. This continues to restrain the development of sufficiently substantiated (theoretically and physically) blocks of mathematical models that would allow to reproduce this process adequately on models and determine the calculated hydrological characteristics more accurately. Therefore, the SHI plans to continue experimental studies of the underground river recharge formation processes with the involvement of all interested organizations and specialists.

3 About Chaos and Order in Cryogenic Phenomena and River Runoff Forming Processes

Among the features of the hydrological regime of northern rivers, the most important hydrological role belongs to cryogenic processes and phenomena caused by seasonal phase transitions of water with different types' ice, which create seasonal glaciation (SG): River, over-ice, underground. These processes and phenomena are temporary accumulators of natural waters in various forms. They redistribute a significant part of river and underground runoff throughout a year (less often from year to year) and have a noticeable impact on the hydrological regime of rivers. This must be taken into account in engineering and hydrological calculations and forecasts.

The whole set of approaches to the natural ice research and their hydrological role fit into three mutually related directions, (a) these are the physical research of the various types of ice generating processes under the influence of external and internal factors, (b) phenomenological studies aimed at obtaining generalized scientific ideas

about the spatial and temporal patterns of individual components formation of SG, and evolutionary studies of SG, as a single set of its elements, certain forms of organization of matter and energy of the geological cryogenic system in general and river systems in particular, in the interrelation of these elements, the transition of some to others in time and in spatial coordinates.

Until recently, the research in this direction was limited to an attempt to identify only paired relationships: Glaciers-aufeises; glaciers-snowfields-aufeises; river ice-river aufeises; groundwater icings-seasonal ground ice, etc. This level of the research seems to be local. Only after finding out the place of each of the SG components in the evolutionary space–time series of the organization forms' transformations of flows of matter and energy in the river systems of northern regions, on the one hand, and its formation as an aggregate of lower structural forms, on the other hand, we can approach the creation of the foundations theoretical knowledge about the considered cryogenic water bodies with all the ensuing scientific, methodological and practical conclusions.

Over the past forty years, the idea of self-organization and self-regulation of natural and social objects and systems (synergetics) has been developing with increasing intensity in natural science. It was experimentally and theoretically established that with a certain change in the external influence, open systems change into an unstable state (chaos) in relation to small perturbations. In one case, the instability leads to the formation of some new stable structures (order), in the other, to their destruction. These patterns can be observed in the evolution of SG.

Under the influence of gravity, solar and planetary energy, water and energy of a certain changing structure continuously pass through river systems. We can conditionally highlight two structures. The first one reflects a set of stable internal and external relationships of the elements of the river system (RS). This structure is a linear tree-like system with one-way flow of substances (liquid runoff, river and underflow runoff with dissolved and colloidal substances, sediment runoff) and energy (heat flow). The system has a finite number of inputs and one output (river system structure—SRS). The second structure reflects stable internal connections, relationships between the elements of the flow itself (flow structure—FS). The intra-annual cycle of solar energy leads to changes in river systems and flow structures, especially pronounced in the northern regions and the cryolithozone.

In the cold season, ice of various types becomes a limiting factor for the flow of matter and energy. With an increase in its influence, the nature of the interaction between liquid, solid and heat discharge naturally changes in time. In the process of self-organization and spatio-temporal change of local FSs, new structures are created, which provide a balance between the inflow of heat and energy to RS and its outflow. Figure 2 shows the evolution of stable and unstable FSs in time (in annual and long-term cycles) as air temperature decreases in winter.

During the period of a free channel, most rivers are characterized by a dynamic balance (stable structure) between the water flow, sediment runoff and the forms of channel sediments due to self-regulation [23]. At the beginning of winter, when water temperature decreases at a certain point in time, intra-water ice is formed.

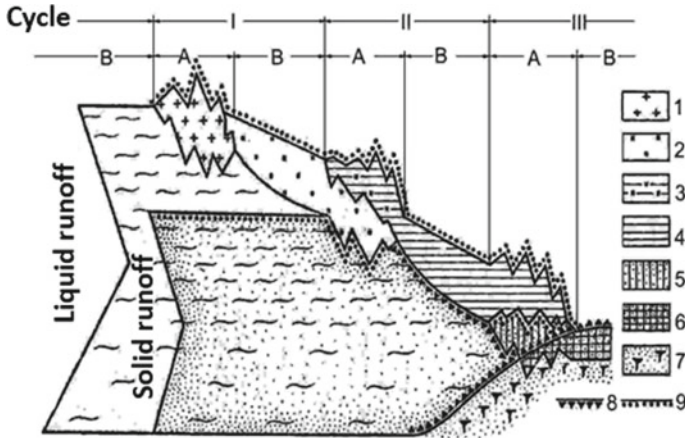


Fig. 2 Evolution cycles of liquid runoff organization forms through a river system with an increase in the negative temperature field. Structures: A-unstable, B-stable; ice formations: 1-intra-water ice, 2-ice cover (river ice), 3-river aufeis, 4-groundwater ice, 5-season underground ice, 6-long-term underground ice; leading transformations of the substance flow: 8-perennial, 9-seasonal

There is additional resistance to water movement in the water flow due to the heterogeneity of its density and an increase in the wetted perimeter. Water refrigeration processes begin to withstand the crystallization heat generation processes, which slow down the system’s cooling during ice formation. With the addition of a new element (slush), the system begins to move from a stable state to an unstable one, becoming extremely sensitive to small changes in external influences. Insignificant weather or flow hydrodynamics fluctuations in local areas (expansion, narrowing of the channel, etc.) may induce significant changes in the ice material density, a particular consequence of which is ice jams. In this case, the scale of changes in the state of the system is completely incommensurate with the external impulse, and the cause-and-effect relationships of the processes are of a random nature. This complicates the development of methods for calculating and predicting ice jams on a deterministic basis.

An ice cover is formed after a certain volume of ice material accumulation. Ice crystals chaotic formation in the flow entire volume acquires an ordered character on the lower surface of the ice cover. The channel capacity is increasing. The flow turns into dynamic equilibrium, a steady state. It is achieved by the fact that any change in external influence is compensated by a change in the ice thickness or ice cover bending, the channel deformation. The system becomes less sensitive to external conditions changes. The cause and effect relationships of the processes take on a deterministic character. According to a finite number of determining factors, not only the ice thickness is calculated quite accurately [24], but also the characteristics of winter runoff.

With a further decrease in air temperature, the ice thickness increases and deformation of the ice cover may occur due to the occurrence of pressure when it restricts

the cross-section of the water flow. The heterogeneity of the channel morphometry and flow hydrodynamics along the length leads to alternation zones of positive and negative deformations of the river ice. From a certain moment, an increase in the ice thickness can lead to such a decrease in the channel capacity, at which the water pressure destroys the ice cover. Water comes to the surface and the over-ice process begins. It provides more intensive energy dissipation through convective heat exchange compared to conductive heat during ice-breaking. Stream icings fill mainly lowered ice cover areas, increasing its weight, and, consequently, downward deflection. In higher areas of the ice cover, the thickness increases with less intensity. Therefore, the upward deflection continues under the influence of additional pressure, leading to a new disruption of the ice cover's solidity and the ice formation. Thus, the dissipation of a part of the water flow energy by mechanical means, the beginning of which is the destruction of the ice cover, leads to a violation of the symmetry of quantitative and qualitative transformations in a self-regulating system «ice cover-water flow-channel sediments». The emergence of a new structure in the flow again leads it into a disequilibrium state. It becomes «sensitive» to the influence of many factors. Cause-and-effect relationships of processes appear to be random. That is why any attempts to develop ice thickness calculating methods on a deterministic basis for this structure have not been successful until now, judging from the results of the calculation methods analysis [13]. The aufeis rivers winter runoff characteristics calculation complexities also take place.

The positive feedback between the river and under-channel flow leads to their hydrodynamic and thermals reformation and the transformation of river valley. At low air temperatures, ice-forming waters freeze in the immediate vicinity of the groundwater discharge centers and form ice masses of considerable thickness in the same places every year. In the warm season, these waters disturb the dynamic balance between vertical and lateral erosion of loose deposits in the area, where the latter prevails. This is also facilitated by exogenous processes, which increase in the aufeis areas. As a result, ice glades are formed. The slope of the rivers here can be an order of magnitude less than the slope in adjacent ice-free sections of the rivers [25]. River runoff below the ice areas is usually absent, watercourses dry up, and channel sediments freeze over.

Thus, the violation of the symmetry of transformations of processes in RS leads to the irreversibility of ice formation, the emergence of a stable structure in the «groundwater ice—water flow—channel sediments—ice alluvium» system. Firstly, the structure stability is reflected in the formation of the winter regime of icing, which has low correlation to weather fluctuations and is stable over many years. Secondly, the stability is expressed in the limitation of possible variations in the morphological forms of ice fields, which makes it possible to reveal the relationship between their area and volume [26].

Despite the stability of connections and interactions between RS elements, there is a prerequisite for the further development and evolution of the system on a geological time scale. Symmetric transformations of the structure as a whole proceed against the background of secular irreversible, asymmetric geomorphological and geological

processes. At a certain stage of development, these mutually opposite processes come into conflict, which is resolved in the direction of a more general irreversible process.

Due to the large width and small slopes on ice glades, the transport capacity of the river flow decreases. During the periods of high water and floods, even very small fractions of sediment accumulate on them. The surface level of the ice glade decreases much more slowly than in adjacent sections of the river. With a gradual decrease in lateral erosion, vertical erosion increases. The river valley is redistributed. Its consequence is that the cross-section of friable deposits in the ice glade is extended. This leads to a decrease of aufeis capacity formation. Part of the water is used for the seasonal underground ice formation, frost mounds, and accumulation in the river valleys' friable deposits. Due to the decrease in the ice thickness, the conditions for the life of plants are improved, and more highly organized associations replace primitive plant groups. Vegetation strengthens soils and increases hydraulic roughness, which helps to reduce soil erosion and increase sediment accumulation during floods. The system comes out of a stable state again.

Seasonal underground ice and aufeises at this stage of evolution are characterized by extremely high spatial and temporal variability. In the future, even in a stationary climatic regime, either a mixing of ice-forming sources upstream may occur or groundwater will be filtered in alluvial strata along soil-filtration taliks in an ice-free regime. With a low carrying capacity of taliks, water can accumulate in the seasonally melted layer of the valley bottoms. The emergence of sporadic permafrost aquicludes leads to the accumulation of groundwater in the alluvial sediments of the river valleys for a long period, which is one of the main reasons for high runoff coefficients (often more than one) at the beginning of the warm season.

The evolution of aufeises and underground ice of ice glades on a geological time scale has not yet been sufficiently studied. Based on the considered approach and available data, various ways of their further development can be assumed. The first is the reversibility of the process in a stationary climatic situation. Ice begins to form again on the river section, gradually spreading to an ever-larger area, contributing to lateral erosion. Mounds of cryogenic heaving, seasonal underground ice are «displaced» to the periphery of the ice area. With a cooling climate, the activity of the formation of seasonal underground ice due to an increase in the thickness of sediments on the ice glade will lead to the formation of perennial underground ice. This is because of a decrease in the warming effect of the water flow in the channel with a decrease in its wetted perimeter due to deep erosion. The second reason is a decrease in the thermal conductivity of the cover deposits with an increase in their thickness and the formation of a soil-vegetation layer. The formation of perennial underground ice will reduce the intensity of water exchange in the area and the convective heat transfer by groundwater, upset the dynamic balance between the amount of heat supplied to the talik and consumed for heating the frozen rocks surrounding the talik. The size of the talik will be reduced until the water-bearing rocks the completely freezing. Frost and seasonal underground ice will be replaced by a more stable form of organization in the changed natural conditions: Perennial underground ice—permafrost.

Thus, when the external load (negative temperature field) changes, an alternation of stable and unstable structures is observed in the evolution of flow elements.

The nature of changes in the properties of elements when changing structural relationships is common for different selected cycles, creating conditions for stability and variability of the evolutionary process. This shows the fundamental principle of symmetry, which can ultimately be the basis for scientific prediction of the system's behavior.

At the same time, the process is irreversible within each cycle. It spontaneously flows only in a certain direction. Irreversibility is the starting point for evolution: The violation of time symmetry. The time scale of the evolution of structures changes from cycle to cycle. If the first cycle reflects the process on the scale of the winter season, then the second and especially the third—in the secular one. In the evolution of the last two cycles, the change in the time scale is due to the increased role of processes associated with long-term morphological transformations of river valleys with the active participation of SG. The latter conclusion must be considered when assessing the consequences of anthropogenic impact on rivers' morphology and ice-thermal regime in the permafrost zone, including the predicted climate change.

In general, the considered evolutionary processes develop according to the principle of minimum energy dissipation. Its essence: If not a single state of the system is permissible, but there is a whole set of states that agree with the conservation laws and principles, as well as the constraints imposed on the system, then the state is realized, that corresponding to the minimum energy dissipation (or, equivalently, the minimum growth of entropy (a measure of chaos)). In our case, the interaction of "cold" and water flow creates structures (order), which together are a kind of cryogenic barrage that prevents the rapid drainage of underground and river waters (including the thermal energy of the territory) in the absence of atmospheric power supply. Cold processes retain heat in the system.

4 Methodology

The methodology for determining the cryogenic regulation of rivers underground supply is based on the idea that the intra-annual variability of the storage reserves of underground aquifers recharging large rivers is insignificant. Underground water, especially from deep aquifers, is more regulated and has less variability throughout the year than surface water. The low variability of deep aquifers is confirmed by the insignificant coefficients of variation of the minimum winter and summer-autumn river runoff, which amount to 0.15–0.25 for most medium and large rivers in the northern regions of Russia [27]. In the southern regions, these coefficients are higher due to the low participation of underground water in the recharge. For example, this is manifested in the equality of the winter and summer low-water flows of the springs involved in the aufeis supply [28].

Studies of the isotopic composition of river waters have shown that the supply of rivers, especially in northern latitudes, involves groundwater with an "age" of 4 to 6 years on average, which is possible only with an appropriate volume that determines a small intra-annual variability [9, 29].



Fig. 3 Cryogenic regulation of underground supply of Russian rivers, $l/s\ km^2$

Based on the insignificant intra-annual variability of the resources of the main aquifers feeding the rivers, it can be assumed that the underground supply of the rivers in winter should be close to or equal to the low-flow summer runoff (in the absence of precipitation). If there is a difference, then there is reason to take it for the influence of various cryogenic phenomena and processes that complicate or redistribute in time the underground feeding of rivers from winter to summer (see Fig. 1.).

The difference between the winter and summer low-water runoff of rivers was determined according to the maps of the summer and winter minimum 30-day runoff of 80% availability, given in [27]. These maps were compiled on the basis of hydrological observations up to 1980 on medium rivers with catchment areas up to 50–75 thousand km^2 . During the period for which the data on runoff were used in the construction of maps, there have not yet been changes in the formation of the hydrological regime due to the climate. The fact that the calculations' low-water runoff values of 80% of availability were taken increases the objectivity of the estimates for two reasons. First, rivers are mainly fed from deeper aquifers with very little intra-annual variability in very dry years. Secondly, the role of surface (melt and rain) waters in their runoff is small. The values of the deviations of the winter from the summer minimum 30-day water flow rates of 80% of the availability, characterizing the cryogenic regulation of the underground supply of the rivers of Russia, are shown in Fig. 3.

5 Results and Discussion

The distribution over the territory of Russia of deviations of the winter underground feeding of rivers from the summer varies from 0 to 4 $l/s\ km^2$, reaching 5 $l/s\ km^2$ in the

northeastern regions. The smallest values are typical for the south of the European territory and areas of continuous permafrost. This is due to the weak development of cryogenic phenomena in the southern regions in the first case. To the south, the winter runoff is higher than the summer runoff, since the role of evaporation in the water balance of catchments in the summer period is important. A slight decrease in the difference in the northern regions is probably due to the fact that there is little participation of groundwater in feeding due to the presence of permafrost. The greatest values of the influence of cryogenic phenomena are characteristic of mountainous regions. Also, an increase in the influence of cryogenic factors can be traced in Eastern Siberia, where most rivers freeze, tens of thousands of river aufeis and underground water are formed, seasonal underground ice in river valleys and rocky ice in the mountains. In vast areas of Western Siberia, the increase in the role of negative air temperatures in the formation of river runoff is likely to be due to the freezing of the active layer saturated with water and bog hollows. The issue of accumulation of bog waters in ice and the effect of this process on the river flow with a high degree of boggy is still poorly studied. For Russia, this issue is relevant, since the country's boggy (all peat lands regardless of the thickness of the peat horizon) is 21.6% (3.69 million km²) [30]. If, for example, we take only the area of bogs with a peat thickness > 50 cm—975 thousand km², then when a 10 cm water layer freezes on it, the volume of ice will be 97 km³. Even if half of this water does not participate in the winter runoff of northern rivers, this will amount to about 0.8 l/s km² of losses in their feeding, but it will keep the wetlands waterlogged.

In general, cryogenic regulation of groundwater supply to Russian rivers is almost 500 km²/year (Table 1), which, for comparison, is, for example, 2 times more than the average annual runoff of the Volga River.

Table 1 Volume of cryogenic regulation of groundwater supply of Russian rivers

Territory of Russia	The average duration of winter, months	Average module of cryogenic flow control, l/s km ²	The area of the territory with a stable winter, Mm km ²	Volume of cryogenic regulation of river underground recharge, km ³ /year
Central and northern European territory	4	1	2.2	23
Ural and Western Siberia	5	1.7	1.6	36
Middle and North-Eastern Siberia, Far East	6	2.5	11	433
Total amount			14.8	492

It is important to note that only part of the above annual volume flows into rivers and accumulates in different types of ice. A significant volume of ground-water remains in the aquifers and the aeration zone in winter since the drainage capacity of rivers is either completely absent when the river channels freeze, or is significantly reduced due to a decrease in the throughput capacity under the ice.

During the cold season, the underground water flow to river valleys is maintained under the influence of gravity. In the absence or a significant decrease in drainage by the hydrographic network, these waters accumulate in the riverine part of the basin. At the end of winter with warming, they participate in the formation of spring floods. So, for example, on the Shamanka River in the Baikal region, it was experimentally established that underground water makes up more than 3/4 of the runoff volume [3]. Before the beginning of melt water outflow from snowpack (snow cover yield), the spring flood runoff coefficients of some Siberian rivers are equal to or more than 1 because of “underground water flood” [26]. At that the period of minimum winter runoff often shifts to the middle of winter with an increase of the catchment area. There are also known floods of underground water in spring on the rivers of Yakutia called “black water” [31].

The main part of the natural resources of underground water (without sub-aquatic discharge into the seas and under-channel runoff) discharged into the rivers of Russia (NRUW) is approximately 790 km³/year [32]. They are determined by dividing the river runoff hydrographs into surface and underground components. The above-described redistribution of a part of the underground water flow into rivers from the cold to the warm period (including the spring flood) makes it difficult to assess the natural resources of underground water by dividing the hydrograph into genetic components. This problem was partially solved by taking into account the volume of underground inflow into rivers, accumulated in river ice and auefis, in the estimates of the NRUW [12, 33].

At the same time, it is difficult to determine the part of underground water that remains in the river basin due to a decrease in the drainage capacity of the hydrographic network during the formation of ice cover and other cryogenic processes [34–36]. It is also important to note that it is not known how much of this “underdrained” in winter by river beds underground water flows into rivers during the warm season of the current year and with what intensity. The volume of underground water that did not enter the river network due to cryogenic processes for a year or a number of years is not taken into account at all in the NRUW and refers not to resources, but to underground water reserves. With the ongoing warming of winters, the weakening of cryogenic regulation of runoff, an increase in underground recharge of rivers is observed, which has been noted in many publications.

A controversial question arises—does the increase in winter runoff characterize the growth of natural resources of underground water or not [37]? Suppose the growth of winter runoff also involves those underground waters that were classified as reserves, but in new cryogenic conditions they are drained by rivers. In that case, they cannot be unambiguously considered as indicators of the NRUW. This can lead to overestimated NRUW estimates, which may be the case in some works [38]. It is not excluded that the ongoing decrease in water cut in the central and southern regions of

Russia, where there is practically no winter, is also associated with the involvement of reservoir reserves in the underground feeding of rivers [39, 40]. This can also explain the degradation of the primary hydrographic network [41], the drying up of forests in the watershed zones. But in the same period there are examples of flooding of territories [42]. Flooded areas are located mainly on the coastal areas of medium and large rivers. Here, an increase in the discharge of water coming from the upper links of the hydrographic network led to an increase in the minimum water levels in the rivers (up to 1–1.5 m), which affected a decrease in their draining role [43]. Probably, there is a gradual spatial redistribution of a part of water resources from near-watershed areas down to the river valleys of large rivers, with the "drying up" of the upper reaches. The incoming part of the water balance of underground aquifers (an increase in precipitation and infiltration with a decrease in soil freezing) increased, but the depletion of reserves increased more due to reserves. Stabilization between the input and output parts of the water balance can occur with a general decrease in the water content of the territories, when the groundwater levels of the zone of intensive water exchange decrease and, accordingly, the drainage capacity of rivers decreases. This will correspond to the state of adaptation of the water system of river basins to climate change and, possibly, to the transition to a new "quasi-stationary" state in the hydrological regime. Before the stabilization of the water balance of river basins located in the areas where the cryogenic regulation of runoff formation has stopped, the regional assessment of the NRUW based on the traditional hydrograph dissection may be incorrect. This is because of the involvement of groundwater storage capacities in the underground recharge of rivers.

It should be noted that the assessment of the cryogenic regulation of underground river recharge based on hydrological observations up to 1980 does not take into account a powerful factor—the increase in the layer of seasonal thawing of permafrost soils that has occurred in recent decades [44, 45]. It also leads to improved drainage of areas, including by improving the hydraulic connection between surface and groundwater bodies. This factor is probably no less significant. In some areas where permafrost is spread, it can be decisive in forming the water regime of territories in modern climatic conditions. For this reason, it can be argued that the performed assessment of cryogenic regulation of river flow is rather underestimated for modern climatic conditions than overestimated for the northern and eastern regions of Russia.

6 Conclusions and Foresight for Decision Making

In the formation of the winter water regime of Russian rivers, a significant role is played by the processes of phase transitions water–ice–water in catchments, in basins and in channels. Their cumulative impact is estimated at about 500 million km³/year and is expressed in two processes: Firstly, in the redistribution of a part of the underground supply of rivers from the cold to the warm one and, secondly, in the long-term regulation of the underground water storage capacity. The obtained estimate can be considered approximate since it was made on the basis of indirect

manifestations of the processes under consideration in the river runoff regime and does not take into account the effect on the formation of the water regime of the ongoing increase in the layer of seasonal thawing of permafrost. A more substantiated estimate can be obtained only using hydrogeological regime information, which is currently extremely scarce, especially in the northern and eastern regions of the country.

The ratio of the incoming and outgoing parts of the water balance of underground aquifers in modern non-stationary climatic conditions is violated due to a decrease in the regulatory role of cryogenic processes. With the unchanged supply of groundwater by atmospheric precipitation in the future, but with the weakening of cryogenic regulation, groundwater reserves (and water content of river basins) will decrease. This must be taken into account when assessing the natural and predicted groundwater resources and low-water flow of rivers.

Due to the great importance of cryogenic processes for the hydrological regime of Russian rivers, it is advisable to strengthen experimental studies of the interaction of surface and ground waters in order to identify the patterns of adaptation of the water regime of territories to climate change. Without the results of such studies, it is impossible to reasonably develop adaptation measures of the country's water management complex to the ongoing irreversible natural changes in heat and moisture turnover in river basins, to increase the reliability and validity of long-term forecasts.

7 Recommendations

The existing water management complex in Russia and many Asian countries functions according to the operating rules developed for the conditionally stationary regime of river runoff characteristic of the period preceding the climate warming. The physical and statistical analysis of the information received during this period indicated that the formation processes of the hydrological regime are described by dynamic systems, where the past uniquely determines the future. This statement was especially widely used in engineering practice, where the frequency curves were the basis. It seemed that there was complete predictability of the future state of the characteristics of water bodies if there were long observation series, adequate mathematical models and powerful computers. The ongoing climate warming has led to the occurrence of violations of the hydrological series stationarity and non-equilibrium of natural processes of the river runoff formation. One of the reasons for the non-stationarity in the water regime of rivers is the imbalance between the underground and surface components of the river runoff. This violation is associated with a decrease in cryogenic regulation of feeding and discharge of groundwater during warming winters.

The complexity of taking into account the nonstationarity of the runoff process affects many theoretical and applied sections of hydrology and water management and significantly complicates the problem of surface water resources management. Since the climate warming continues and is predicted for the future, it should be

expected that a long period of non-stationarity in the ratio of the surface and underground components of the river runoff and the water regime will persist. Therefore, in modern conditions, it is advisable to more often make adjustments to the rules for the use of water resources and the operation of engineering structures and facilities. This will reduce the risks in the operation of the water management complex due to the increasing uncertainty in predicting the state of the hydrological regime in the future.

Acknowledgements The authors express their sincere gratitude to all Russian (Soviet) and foreign researchers who have been engaged in studying the very complex problem of the influence of cryogenic processes on the hydrological regime and water resources of the northern regions of Asia. These processes and phenomena are still not well understood in modern hydrology. The authors have presented their views on this issue and will welcome any comments, criticism and discussions regarding the ideas and research presented in this chapter.

References

1. Sokolov BL (1975) *Ices and river runoff*. Gidrometeoizdat, Leningrad, p 190
2. Alekseev VR, Furman MSh (1976) *Ice and runoff*. Novosibirsk, Nauka, 118 pp
3. Kravchenko VV (1986) The role of ice in the formation of winter river runoff and ice cover of rivers in the western part of the BAM zone. *Proc State Hydrol Inst* 312:34–84
4. Obyazov VA, Smakhtin VK (2013) Climate change effects on winter river runoff in Transbaikalia. *Russ Meteorol Hydrol* 38(7):503–508. <https://doi.org/10.3103/S1068373913070091>
5. Obyazov VA, Smakhtin VK (2014) Ice regime of Transbaikalian rivers under changing climate. *Water Resour* 41(3):225–231. <https://doi.org/10.1134/S0097807814030130>
6. Markov ML, Gurevich EV (2013) On the influence of ice cover on the underground component of river flow. *Hydrosphere. Hazard processes and phenomena* 1(4):477–489 (In Russian; abstract in English). <https://doi.org/10.34753/HS.2019.1.4.477>
7. Crites H, Kokeji S, Lacelle D (2020) Icings and groundwater conditions in permafrost catchments of northwestern Canada. *Sci Rep* 10(1):3283. <https://doi.org/10.1038/s41598-020-60322-w>
8. Ensom TP, Makarieva OM, Morse PD, Kane DL, Alekseev VR, Marsh P (2020) The distribution and dynamics of aufeis in permafrost regions. *Permafr Periglac Process* 31(3):383–395. <https://doi.org/10.1002/ppp.2051>
9. Sokolov BL (1996) New results of experimental studies of the lithogenic component of river runoff. *Water Resour* 23(3):278–287
10. Markov ML (1994) The role of cryogenic barrage in the formation of river runoff in permafrost regions. *Meteorol Hydrol* 2:98–104
11. Methodical recommendations for the assessment of underground inflow into rivers (1994) Leningrad, Gidrometeoizdat pp 94
12. Calculation of underground feeding of rivers in the permafrost zone. Methodical manual (1989) Leningrad, Gidrometeoizdat pp 106
13. Chizhov AN (1990) Formation of ice cover and spatial distribution of its thickness. *Hydrometeoizdat, Leningrad*, p 127
14. Markov ML (2002) Spatial-temporal dynamics of the relationship between surface and groundwater. *Collect Work Hydrol* 25:90–104
15. Barisas A Yu (1989) Cryogenic runoff minimum. In: *Proceedings of the V All-Union Hydrological Congress. Volume 6. Theory and methods of hydrological calculations*. Leningrad, Gidrometeoizdat pp 475–478

16. Gurevich EV (2009) Influence of air temperature on winter river runoff (on the example of the Aldan river basin). *Meteorol Hydrol* 9:92–99
17. Estimation of melt water losses and forecasts of flood runoff volume (1985) Leningrad, *Gidrometeoizdat* pp 190
18. Zavileisky SV, Markov ML (2008) Experimental studies of the formation of underground river recharge at the facilities of the Valdai branch of the SHI. In: *Hydrological research in Valdai. Collection of articles for the 75th anniversary of the founding of the Valdai branch of the State Hydrological Institute (SHI)* pp 38–55
19. Georgievsky MV (2016) Water resources of the Russian rivers and their changes. *Proc. IAHS* 374:75–77. <https://doi.org/10.5194/piahs-374-75-2016>
20. Georgievsky MV, Goroshkova NI, Khomiakova VA, Georgievsky DV, Plenkina AK (2021) Impact of climate change in autumn-winter period on hydrological regime of the rivers in the Small Northern Dvina river basin. *Gidrometeorologiya i Ekologiya. J Hydrometeorol Ecol.* 64:466–479. [In Russian]. <https://doi.org/10.33933/2713-3001-2021-64-466-479>
21. Shiklomanov IA (ed.) (2008) *Water resources of Russia and their use.* – St. Petersburg, SHI pp 598
22. Shiklomanov IA, Georgievsky VYu (2002) Impact of anthropogenic climate changes on the hydrological regime and water resources. In: *Climate change and their consequences*, St. Petersburg, Nauka pp 152–164
23. Kondratev NE, Popov IV, Snishchenko BF (1982) *Fundamentals of the hydromorphological theory of the riverbed process.* Hydrometeoizdat, Leningrad, p 272
24. Donchenko RV (1987) *Ice regime of rivers of the USSR.* Hydrometeoizdat, Leningrad, p 242
25. Markov ML, Berensen AK (1988) On the formation of ice clearings and their influence on the hydrological regime of rivers. *Issues of hydrology: Reports of conference of young scientists and specialists.* Hydrometeoizdat, Leningrad, pp 46–52
26. *Practical recommendations for calculating hydrological characteristics in the zone of economic development of BAM* (1986) Leningrad, Hydrometeoizdat, pp 110
27. *Construction Norms and Specifications 2.01.14–83* (1983) *Determination of calculated hydrological characteristics*
28. Markov ML, Vasilenko NG, Gurevich EV (2017) *Ice of the BAM zone.* Saint Petersburg, Nestor-istoriya publishing house, Expedition research, p 320
29. Romanov VV, Ferronsky VI, Vakulovsky SM, Katrich IYu, Rosly EI (1983) Tritium content in natural waters of the USSR in 1979–1980. *Water resources* 3:109–115
30. Vompersky SE, Sirin AA, Tsyganova OP, Valyaeva NA, Maikov DA (2005) Swamps and wetlands of Russia: attempt to analyze spatial distribution and diversity. *Izvestiya RAS. Geografiya series* 5:21–33
31. Shepelev VV, Pavlova NA (2014) Main components of underground feeding of rivers of Yakutia. *Sci Educ* 2:117–120
32. Shvartsev SL (1996) *General hydrogeology.* Nedra, Moscow, p 423
33. *Atlas of the world's snow and ice resources* (1997) (ed. by VM Kotlyakov) Volume II, book 1, 2. IG RAS pp 270
34. Zhuravin SA, Markov ML (2010) Development of studies in small research basins in Russia and the most recent tasks. In: *Status and Perspectives of Hydrology in Small Basins* (ed. by A. Herrmann & S. Schumann), IAHS Publ. 336:219–224
35. Lavrov SA, Markov ML (2018) Assessment of the influence of atmospheric pressure on the level and flow of groundwater. *Engineering survey* 12(2) (11–12):44–51
36. Markov ML (2018) About chaos and order in cryogenic phenomena and processes that form river runoff. International scientific and practical conference “The Third Vinogradov Readings. Facets of Hydrology” in memory of the outstanding Russian scientist Yu.B. Vinogradov (March 28–31, 2018, Saint Petersburg State University, Saint Petersburg, Russia). Collection of reports. Science-Intensive Technologies Publishing House Intel Group Corporation LLC pp 92–97
37. Borevsky BV, Markov ML (2014) Is low-water flow rate of rivers a measure of groundwater recharge or total groundwater flow? *Explor Prot Miner Resour* 5:10–16

38. Dzhamalov RG, Frolova NL, Kireeva MB, Rets EP, Safronova TI, Bugrov AA, Telegina AA, Telegina EA (2015) Today's Groundwater and Surface Water Resources of European Russia (ed. by RG Dzhamalov & NL Frolova). GEOS Moscow pp 315
39. Zotov LV, Frolova NL (2016) Shum SK (2016) Gravity anomalies in 673 basins of large rivers in Russia. *Nature* 5:3–8
40. Zotov L, Shum C, Frolova N (2015) Gravity changes over Russian rivers basins 652 from GRACE, in: Jin S., Haghighipour N., Ip W. (Eds.), *Planetary Exploration and Science: 653 Recent Results and Advances*. Springer Geophysics. Springer-Verlag Berlin Heidelberg, 654:45–59. <https://doi.org/10.1007/978-3-662-45052-9>
41. Ivanova NN, Larionov GA (1996) Dynamics of the length of small rivers: factors and quantitative estimates. Causes and mechanisms of drying up of small rivers (ed. by AP Dedkova and GP Butakov). Kazan, Publishing house of Kazan University, pp 37–42
42. Razumov VV, Razumova NV, Molchanov EN (2015) Flooding of lands in the Siberian region of Russia. *Georisk* 4:22–36
43. Markov ML, Gurevich EV (2019) On the influence of ice cover on the underground component of river runoff. *Gidrosfera Danger Process Phenom* 1(4):477–489
44. Biskaborn BK, Smith SL, Noetzli J, Matthes H, Vieira G, Streletskiy DA, Schoeneich P, Romanovsky VE, Lewkowicz AG, Abramov A, Allard M, Boike J, Cable WL, Christiansen HH, Delaloye R, Diekmann B, Drozdov D, Etzelmüller B, Grosse G, Guglielmin M, Ingeman-Nielsen T, Isaksen K, Ishikawa M, Johannsson M, Johannsson H, Joo A, Kaverin D, Kholodov A, Konstantinov P, Kröger T, Lambiel C, Lanckman J-P, Luo D, Malkova G, Meiklejohn I, Moskalenko N, Oliva M, Phillips M, Ramos M, Sannel ABK, Sergeev D, Seybold C, Skryabin P, Vasiliev A, Wu Q, Yoshikawa K, Zheleznyak M, Lantuit H (2019) Permafrost is warming at a global scale. *Nat Commun* 10:264
45. Groisman PYa, Gutman (eds.) (2013) *Regional environmental changes in siberia and their global consequences*. Springer Environ Sci Eng, Springer Science+Business Media Dordrecht. https://doi.org/10.1007/978-94-007-4569-8_4

Forest Successional Change and Its Effect on Plant Species Diversity: A Case Study for Euxine Forests, NE Turkey



Alper Uzun  and Salih Terzioğlu 

Abstract In this chapter, the effect of forest succession on plant species diversity was investigated. The distribution of a total of 422 plant taxa (22 trees, 68 shrubs and 323 herbaceous plants) to forest succession stages has been revealed. Plant species diversity and relative abundance values of tree, shrub and herbaceous layers among the succession stages were calculated with the help of the Shannon–Wiener index. The Sorensen index determined similarity percentages of the succession phases. The succession, which is called sequential change of plants, was examined in three layers. The highest values of alpha diversity (H') have been reached at the ecesis-establishment stage for the herbaceous layer (3.31), at the competition stage for the shrub layer (1.95) and at the climax stage for the tree layer (1.03). When all layers were evaluated together, it was revealed that the highest value was reached at the ecesis-establishment stage (3.52). In addition, it was determined that the floristic similarity decreased from the early stage of the succession to the late stages, and each stage had the highest similarity with the previous stage. Endemism rates are also different among the succession stages and the early stages contain more endemic taxa than late stages. In particular, the discovery of a new species (*Astragalus ansinii* Uzun, Terzioğlu & Pal.-Uzun) from the establishment stage in the study area has made succession studies more important in terms of conservation biology.

Keywords Forest succession · Plant species diversity · Shannon–Wiener · Sorensen · Euxine forest · Turkey

A. Uzun (✉)

Department of Forest Botany, Faculty of Forestry, Kahramanmaraş Sütçü İmam University, Kahramanmaraş, Turkey
e-mail: auzun@ksu.edu.tr

S. Terzioğlu

Department of Forest Botany, Faculty of Forestry, Karadeniz Technical University, Trabzon, Turkey
e-mail: sterzi@ktu.edu.tr

1 Introduction

Biodiversity measurement and indicators are considered as a useful tool in forest management plans [1–3]. Although the measurements used alone are not sufficient to reach a definitive judgment in managing diversity, they constitute an important method in defining, monitoring, and comparing areas [1, 4, 5]. In addition to being a guide for the areas that require a management plan, they are important in terms of managing the ecological structure more accurately, reflecting the general course of vegetation and determining the warning signals that may arise from technical forestry or silvicultural practices [6–8].

In the last century of human history, forests have been degraded and fragmented faster than ever before due to anthropogenic factors, habitat losses, and global climate changes [9], and then subsequent forestry. Forestry activities have transformed natural forest ecosystems into different vegetation units [10, 11]. Incomplete or unavailable attribute data on degraded or fragmented forest ecosystems has always been the biggest obstacle affecting the rehabilitation of these ecosystems and decision-making mechanisms in the rehabilitation and restoration of these ecosystems [12]. The successional change model that defines and examines the course of nature is one of the most useful methods to overcome this problem [13]. However, there are quite a few studies compared to the size of the subject that trying to reveal the relationship between diversity and succession [3, 14–21]. The measurements are generally used in comparative analysis. Some questions defining certain attributes of the subject may come to mind in this regard; For instance; “Are different habitats or forest parts more diverse than each other?”, “Will plant diversity change due to processes such as succession?” or “Does disturbance affect the endemic species in a good/bad way?”. Of course, it is possible to improve these questions.

Environmental degradation includes physical effects to the land surfaces (eg desertification and soil erosion) [22], aesthetic effects to the scenic features of the landscape [23], and ecological effects to the disruption of biodiversity, habitat fragmentation and loss (eg deforestation) [24, 25]. Those all occur mostly because of human-caused reasons. Forestry activities are the biggest factor after fires that play a role in the change of forest vegetation. In this ecosystem, most plants are moderately or highly dependent on certain vegetation types [26]. On the other hand, Cosmopolitan plants can survive in many different vegetation types. Therefore, habitat degradation mostly affects species diversity and populations of most dependent or semi-dependent endemic species [27].

Species diversity is the second element of biodiversity and frequently used in calculations. It can be described as a change in the number or phylogenetic diversity of species as well as a species composition in general [28, 29]. When species diversity is considered on a global scale, it represents life in the world [30]. However, it is not enough to explain the species diversity only by the number of species. Apart from the number of species in a particular region or unit, the relative abundances of existing species are also included in the evaluations [31, 32].

The criterion of species diversity is the number of species and the taxonomic group diversity that includes these species in the ecological system and the degree of genetic information they contain [33]. Two important determinants shape the diversity of species in plant communities. The first one is the species pool. This term includes all species that are natural to a region and other species that can come from the environment and settle in that region. The second factor is the local ecological connections, which leads to the selection of the species in the species pool that can coexist in a community [34, 35]. Lévêque and Mounolou [36] state that a large number of species detected in a particular area are a good indicator of wider genetic, phylogenetic, morphological, biological and ecological diversity. On the other hand, Marques et al. [2] states that a single indicator value to be obtained by combining indicator values may be more useful in the management of areas. This value can also be used to increase the harmony between ecological structures and public judiciary. However, it is a challenging process to present biodiversity with all its components and reflect it on plans. In this case, it makes more sense to research biodiversity in sections and then establish connections.

In the last two decades, the number and variety of studies on numerical relationships of forest succession have increased considerably [3, 11, 17, 18, 37–42]. The data to be obtained by adding current concepts and methods of mapping of forest succession, monitoring forest biodiversity in various vegetation types and phytosociological studies can offer a broader perspective [5, 11, 43–49]. These also include plant species diversity in seral stages of succession, relative abundance among the stages, vegetational succession and indicators [50]. As it is known, the vegetation of a region; closely related to species diversity and abundance. On the other hand, succession allows us to predict the future formation of this diversity.

The succession is the sequential change of plant composition and vegetation structure in an ecosystem in a certain time period under the influence of various biological and physical environmental conditions [51]. Due to this change, the animal and plant species that established in the environment also change and diversify. This dynamic and progressive process usually takes place gradually over a long period of time. On the other hand, forest succession is the changes in stand age and structure, species composition and ecosystem functions over time [37, 41].

The first studies on the subsequent development of vegetation began with Cowles [52], Clements [53, 54] and Cooper [55]. Afterward, Clements formed the first theory of climax and succession and, formations and associations have been adapted as climax communities to the climates of geographical regions. Later, Clements prepared a classification based on relationships and dominant forms of development, and in the system he created, he accepted the associations as a broadly defined regional community type within the formation by gathering the basic units in the formation [54, 56, 57]. The application of the views of sequential change of plant communities is very wide in the scientific world even today [3, 11, 17, 18, 37, 39–41, 58, 59].

Clements [54, 56] characterized the succession with a 6-stage series that started with the formation of the soil and ended with the final equilibrium (climax). These

are listed as Nudation, Migration, Ecesis (Establishment), Competition, Reaction and Climax respectively.

This succession model mainly models the progression of the primary succession from the beginning to the final equilibrium. The primary succession begins with the formation of the soil and progresses until a certain vegetation. This type of succession usually takes place in new land pieces exposed by water withdrawal or empty-naked areas formed by volcanism activities and without plant reproductive organs of any vegetation [60]. Succession in existing vegetations around the world is mostly of secondary origin [35, 61]. Secondary succession is a system that occurs in an area more or less covered with vegetation. It can make sudden or gradual returns to the early stages of the vegetation cover due to the natural disasters (global warming, forest fires, insect outbreaks, lightning and storms) or human originate destructions (deforestation, habitat fragmentation and loss, intensive forestry activities, overgrazing and illegal cuttings) [51, 57]. This process is not only an indication for the determination of the course of the forests, but it can also provide the necessary data for future projections.

Nudation Stage is expressed by forming a soil layer that will allow the development of a certain vegetation on the terrain, mostly after large eruption masses, sedimentary rock fragmentation, newly formed lake shores, and dune movements in the deserts [32, 51].

Migration Stage is defined as the arrival of plant seeds and diaspores on bare soil. According to Clements, migration can often be observed in areas with no vegetation (eg dunes) or after any vegetation's sudden degradation (eg major fires). Migration may continue, albeit at a very low rate, even as other succession stages continue [15, 51].

Ecesis "Establishment" Stage is characterized by minimal competition during succession. Many pioneer plant species start to establish themselves in the new migration zones or degraded areas [15]. The physical and chemical properties of the soil change after this phase. Plant roots begin to go deep, loosen the soil, and increase aeration [32].

Competition Stage: The dominant individuals or species increase their cover and form the canopy. Then, the competition starts for more space and light above the ground, for water and nutrients below the ground. As a result, many tree individuals, shrubs or herbaceous species showing a narrow ecological tolerance leave the area since the conditions of their growing habitats are limited. This stage progresses until deaths and canopy gaps are formed. As such, the forest has entered the "Reaction" stage [15, 36].

Reaction Stage: In this stage, some species gain regional dominance and competition between plant species decreases significantly [51]. Furthermore, a marked reduction in species numbers occurs between the competition and reaction stages. According to a study, a 20% decrease in the number of plant species was recorded between these two stages in the forest ecosystem [62].

Climax Stage (Final equilibrium): In this stage, vegetation is more or less in balance with the regional climate. Floristic composition shows a certain continuity in terms of structure, physiognomy and life form. This stable vegetation phase is

called “climax vegetation or final equilibrium” and previously mentioned stages occur in certain areas and at smaller scales [15]. According to Whittaker [63], climax vegetation is a population model adapted to environmental factors. Climax vegetation can also change with the change of these factors (humidity, precipitation, temperature, etc.) [32]. Although climax stands are more or less stable stands, a certain collapse occurs in old growth forests. The vacated areas at this stage can be covered with pioneer tree species or shrubs and herbaceous taxa with high reproductive ability. Because habitat conditions have differentiated and new habitat features have become suitable for new species arrivals.

The main objectives to be achieved in the study are as follows: (1) to determine the variation of plant species diversity in the stages of forest succession; (2) to evaluate how the succession stages in tree, shrub and herbaceous layers affect the plant species replacement; and (3) to determine the distribution of abundance according to the seral stages of succession, (4) to explore the distribution of endemic and rare taxa to the succession stages.

Therefore, we investigate the relationship between forest succession and plant diversity. The results could help in transferring of plant diversity to management plans and models in terms of conservation of biodiversity. Also, it will offer a useful pathway to the forest managers, planners and technical practitioners in the forestry sector to prevent global biodiversity loss in the way of regeneration of the degraded forest areas.

2 Materials and Methods

Stratified random sampling method was used due to the suitability of the study for its purpose. This method is generally used to sample heterogeneous layers that contain internally homogeneous areas (layer/stratum/strata) in a given habitat. Habitats are rarely uniform in the areas they cover. They are mostly composed of areas smaller than the main habitat due to more or less degradation. For this reason, these strata are sampled separately from the main habitat fragment as stressed by Hill et al. [64]. Stratified random sampling is more advantageous than simple random sampling. With this sampling, variability and diversity in habitat can be recorded more accurately and differences between layers can be reflected efficiently. In addition, the presence of rare habitats in sampling is an absolute necessity for biodiversity studies.

The study area is first divided into relatively homogeneous units based on vegetation maps (Fig. 1). Then, the sample plots are randomly distributed inside the current units throughout the entire survey area. This type of sampling ensures adequate sampling of uncommon units while avoiding oversampling of the most common units [64].

Several methods are used to investigate succession. Of them; comparing the seral stages of succession in different parts of the same region (the chronosequence approach) is one of the research methods frequently used due to its ease of application [32]. By combining the information about forest understory obtained

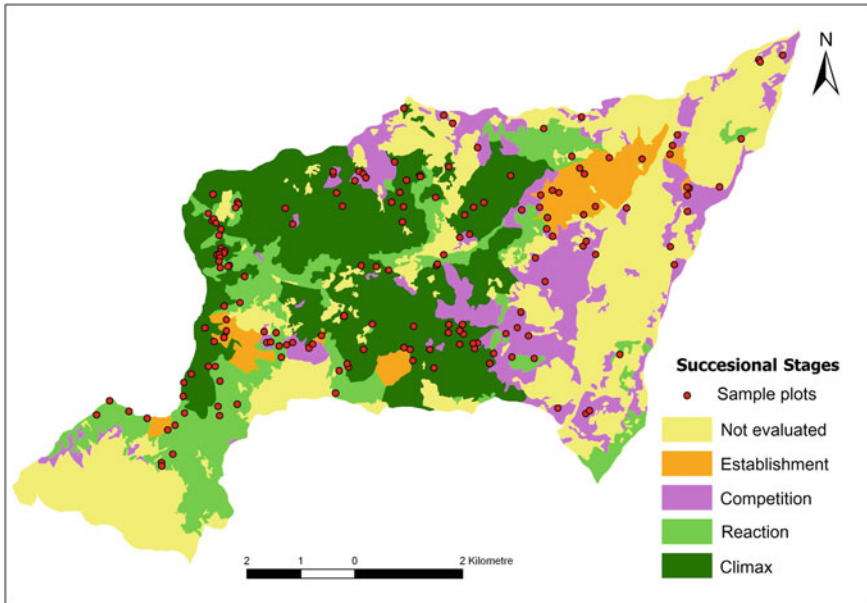


Fig. 1 Distribution of sample plots to the successional stages

in this way, the progress of succession and the change in plant compositions between seral stages can be easily monitored. For this purpose, the seral stages of Clements [54, 56] were applied to the study area [65]. For this, we used the forest stand type map of the study area obtained from the forest management plan. The preliminary field surveys determined the secondary succession stages of forest stands in the study area. Then, using averages, weighted succession stages of all forest stand types were determined and each was coded with the assigned succession stage numbers (Table 1).

The symbols in the table consist of the codes given for the dominant tree species, development stages using average diameter at breast height (dbh) and crown closure types (% cover) of forest stands shown as an example in Fig. 2. Across the entire study area, the climax stage has the largest area (1690,5 ha), while the smallest area is at the establishment stage (325,54 ha). Although the competition stage (916,4 ha) is close to the reaction stage (945,6 ha) as areal, it has a more fragmented structure (Table 2).

In diversity calculations, it is stated that it is important to consider the relative abundance along with species richness [66]. As a result of analytical discussions, mathematical models, and simulations on this subject, there is a positive, simple, and strong relationship between species richness, relative abundance of species, and proportional diversity [67]. In this context, in order to calculate the plant species diversity in the study area, the cover-abundances of the existing taxa were interpreted in each sample plot of 1,000 m² and the representative values were recorded on the

Table 1 The succession stages of forest stands

Forest stands*	Succession stages	Forest stands	Succession stages	Forest stands	Succession stages	Forest stands	Succession stages
BDy	4	KnDyLcd2	5	LDybc2	4	Lbc2	4
BDy-T	3	KnLDybc3	4	LDybc3	4	Lbc3	4
BLDy-T	3	KnLDydc3	6	LDydc2	5	Lc3	5
BL	4	KnLcd3	6	LGKncd3	6	Lcd2	5
BL-T	3	KnLd/a	4	LKnDydc3	6	Lcd3	5
BLDy	4	KnLd1	5	LKncd3	6	Ld1/a	4
Dybc3	4	LDya	3	La	3	Çsa	3

*The present symbols were described in forest management guidelines of General Directorate of Forestry in Turkey

Dominant trees; *Kn* *Fagus orientalis*, *L* *Picea orientalis*, *G* *Abies nordmanniana* subsp. *nordmanniana*, *Çs* *Pinus sylvestris*, *Dy* Mixed deciduous trees, *T* Rocky and stony places, **Development stages:** *a* regenerated stage (0–7,9 dbh) *b* young stage (8–19,9 dbh) *c* mature stage (20–35,9 dbh) *d* overmature stage (>36 dbh); **Forest crown closure types;** *B* degraded forest (<0.10), 1: low coverage (0.11–0.40), 2: medium coverage (0.41–0.70), 3: full coverage (0.71–1.0)



Fig. 2 Some examples of the succession stages of forest stands in the study area

Table 2 Areal distribution of successional stages

	Succession stage code	Number of pieces of forest stands	Area (ha)
Establishment	3	24	325.54
Competition	4	193	916.38
Reaction	5	133	945.61
Climax	6	181	1,690.53
Not evaluated	–	201	2,111.98
Total	–	732	5,990.04

Table 3 Domin scale [64]

Domin scale	% cover
10	91–100
9	75–90
8	51–74
7	34–50
6	26–33
5	11–25
4	4–10
3	<4 and many individuals
2	<4 and several individuals
1	<4 and few individuals

scorecards according to the Domin scale [64] (Table 3). Although large sample plots require more effort to determine cover-abundance values, it is a desired situation in diversity calculations. In this way, variations in diversity or relative abundance values are lower [68].

McIntosh [69] emphasizes that numerical distributions among individuals belonging to species are of great importance in the organization of communities. Plant communities around the world are diverse in terms of vertical stratification consisting of different species. Temperate forest ecosystems in the climax stage that have reached maturity are characterized by three layers that can be clearly distinguished from each other. The first of these is the tree layer found at the top and forming the canopy, the second one; shrub layer; the last one is the herbaceous layer covering the soil. Each of these layers has its own groups of species that they interact with. Similarly, communities with horizontal expansion may contain different species in different regions of the total distribution area [31]. For this reason, these 3 layers are taken into consideration while giving the cover-abundance values.

2.1 Diversity Indices Used

A diversity index is a mathematical measure of species diversity in a community, and there are many indices used today in calculating diversity. It is possible to gather these indices under three headings. These are alpha diversity indices, relative abundance indices, and beta diversity indices.

2.1.1 Alpha Diversity Index

(H') is the abbreviation used for species diversity. It treats as a dependent variable because it takes into account each factor. Since the indices developed on this subject exhibit different approaches, their interpretations also require different perspectives. In calculating alpha diversity, Shannon–Wiener [70], Simpson [71], Margalef [72] and Berger-Parker [73] are the most commonly used diversity indices [29]. Shannon–Wiener index was used in the diversity calculations in this study. This index gives more accurate interpretable results since it is more sensitive to rare taxa in the habitat than Simpson. Simpson’s index gives more accurate results when a single dominant stand type or a species is examined [44].

The Shannon–Wiener index is the most widely used diversity index that thoroughly examines community characteristics. The index is based on a logical basis of information or diversity containing code or messages that can be measured in a similar way in a natural system. This index assumes that individuals are randomly sampled from extremely large communities and samples from which all species are represented, and also gives the average degree of uncertainty of whether two randomly selected individuals from a particular community are of the same category or of the same species [28]. Uncertainty increases both as the number of species increases and when individuals belonging to the existing species show a much more even distribution. If measured correctly (H') always gives a value between “0” (low community complexity) and “4” (high community complexity). Diversity reaches maximum value when all species are distributed equally [74].

$$H' = - \sum p_i \log(p_i) \quad (1)$$

H' Species diversity

p_i The relative abundance of each species (It is calculated by proportioning the number of individuals of each species “ n_i ” to the total number of individuals “ N ” in the community)

n_i Number of individuals belonging to species “ i ” or abundance of species “ i ”.

N Total number of individuals or abundance.

$$p_i = \frac{n_i}{N} \quad (2)$$

2.1.2 Evenness Index

In this study, Pielou's evenness index was used to evaluate the relative abundance of the species. This index considers the species abundance assessment in diversity measurement. However, it is also possible to calculate a separate relative abundance measurement. Maximum diversity can be reached in the case where all species have an equal abundance. In other words, the ratio of observed variety to maximum diversity can be used as the relative abundance value (J') [75–77].

$$J' = H'/H'_{\max} = H'/\ln S \quad (3)$$

The value obtained from the formula ranges from 0 to 1. As the value approaches zero, it is understood that the individuals in the field belong to a single possible species, and when 1 is approached, each species has an equal number of individuals [78].

Ecosystems that are equal in terms of biodiversity may differ from each other in terms of relative abundance. For example, when we consider two ecosystems (A and B), both have the same taxa number (with 10 of each). Let us assume that one of the species is very common in the ecosystem A and the other nine are rare. In the ecosystem B, let's find 10 species in equal abundance. In this case, the relative abundance value in the ecosystem B will be higher than the ecosystem A.

2.1.3 Sorensen Similarity Index

The similarity index of Sorensen [79] was applied to the succession stages in which the variation change was calculated. The similarity ratios obtained in the comparisons are presented in Fig. 12.

$$\text{Sorensen index} = 2C/A + B \quad (4)$$

- A Total number of taxa in the first community
- B Total number of taxa in the second community
- C Taxa number that are common in both communities.

2.2 Programs and Statistical Methods Used in Calculation and Evaluation of Diversity

For the calculation of diversity, the plant distributions on 166 sample plots and the plant cover estimates which based on Domin scale including 10 cover values were transferred to the Species Diversity and Richness IV (SDR-IV) package program in a Excel format [74]. The program was run 4 times separately as tree, shrub, herbaceous, and all layers together. Thus, besides the general change, the variation between the

layers was tried to be revealed. Then, the obtained plant species diversity, species richness and relative abundance values were coded according to the succession stages. According to the following criteria, the diversity values obtained from the sample plots were subjected to variance analysis (ANOVA). ANOVA tested whether two groups, one of which was an independent variable, were similar in certain significance levels ($***P < 0.001$; $**P < 0.01$; $*P < 0.05$). In case of a statistically significant difference between the averages, it was investigated whether homogenous groups were formed between the averages by using Duncan test. SPSS (version 11.5) package program was used for calculations. The codes used for succession stages are given below;

- 1: Nudation (formation of soil; this stage is only available in primary succession)
- 2: Migration
- 3: Ecesis (Establishment)
- 4: Competition
- 5: Reaction
- 6: Climax.

3 Results and Discussion

A total of 422 taxa were found in 166 sample plots applied in the study area. This number corresponds to about 64% of the total taxa number (656 taxa) collected from the entire area [80]. Of the total taxa; 22 taxa (5.21%) were trees, 68 taxa (16.11%) were shrubs and 332 taxa (78.67%) were herbaceous. The number of taxa in the sample plots varies between 7 and 58.

The diversity findings were examined according to successional stages, taking into account the tree layer, shrub layer, herbaceous layer, and overall layer (3 layers together).

3.1 Succession Stages

The plant species diversity values calculated for all sample plots taken in the study area were clustered according to the succession stages and shown in Fig. 3. The diversity values gradually decrease towards the late succession stages as a general assessment. In addition, higher and much closer diversity values were reached at the early stage, ("Establishment", coded with 3). It was also observed that the range of diversity values widened towards the late succession stages (from 4 to 6).

The highest plant species diversity (Shannon–Wiener) values were determined at the establishment stage for the herbaceous layer (3.31), at the competition stage for

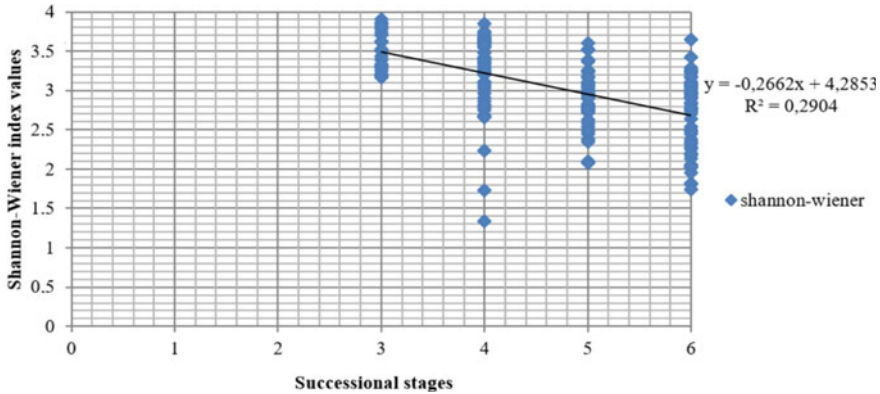


Fig. 3 Clusters of diversity values of sample plots to the successional stages

the shrub layer (1.95) and the climax stage for the tree layer (1.03) (Table 4). The highest value (3.52) was reached in the establishment stage in the calculations made for all layers together. A higher value is obtained here because many light-tolerant plant species coexist and the forest canopy is not yet fully formed. In addition, the excess of the number of species has a high multiplier effect in the calculations, as is the case here. Relative abundance values follow a different course for each layer. The highest value in the establishment stage (0.57) for the herbaceous layer shows a decreasing trend towards the climax stage (0.35). The relative abundance on the shrub level increases up to the competition stage and decreases from this stage to the final equilibrium (climax). On the tree layer, there is an increase from the establishment stage (0.22) to the competition stage (0.72) first, then followed by a decrease in the reaction stage (0.43) and again a significant increase in the climax (1.03). That is, a change in the form of a horizontal "S" curve is observed. As a result of the Duncan test, the groups which formed according to the succession stages are given in Table 4.

Taxa distributed among the successional stages were calculated together with the percentages found in the tree, shrub and herbaceous layers and are given below (Fig. 4, Table 5).

The numbers of common taxa shared in successional stages were indicated with the numbers (1–6) uppercase (A, B, C, D) and lowercase letters (a, b, c, d) as given in Table 5.

3.2 Plant Species Diversity—Succession

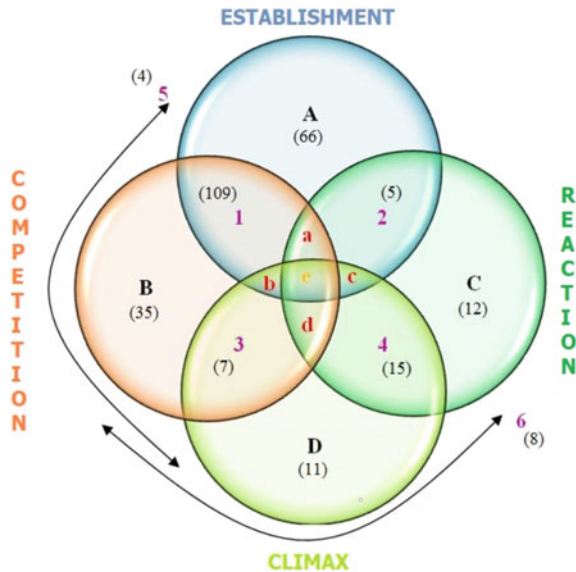
The succession stages differ from each other in terms of many structural features. While the intensity of competition varies in each stage, the percentages of the species that switch between phases in each succession process are different in terms of

Table 4 Alpha diversity (H'), richness (S) and evenness (J') mean values and their Duncan groups (arranged as horizontally) according to the layers and successional stages

Layers	Successional stages				ANOVA		
	Establishment	Competition	Reaction	Climax	Sig.	F	
Herb	H'	3.31 c	2.77 b	2.55 b	2.02 a	5.7E-12***	21.9303
	S	32.40 d	20.93 c	16.16 b	11.20 a	1.39E-17***	35.2296
	J'	0.57 c	0.48 b	0.44 b	0.35 a	5.7E-12***	21.9307
Shrub	H'	1.83 bc	1.95 c	1.63 ab	1.57 a	0.001933**	5.1739
	S	8.10 a	9.83 b	6.89 a	6.47 a	3.9E-05***	8.2394
	J'	0.43 bc	0.46 c	0.39 ab	0.37 a	0.001933**	5.1742
Tree	H'	0.22 a	0.72 b	0.43 a	1.03 c	7.86664E-11***	19.6979
	S	1.43 a	2.80 b	2.02 a	3.36 b	2.07652E-07***	12.6247
	J'	0.07 a	0.23 b	0.14 a	0.33 c	7.8668E-11***	19.6979
Overall	H'	3.52 d	3.21 c	2.92 b	2.71 a	3.66623E-12***	22.3507
	S	41.50 c	33.26 b	25.07 a	21.04 a	2.03135E-15***	29.8536
	J'	0.58 d	0.53 c	0.48 b	0.45 a	3.66713E-12***	22.3505

Sig.: Significance, *** $P < 0.001$; ** $P < 0.01$; * $P < 0.05$

Fig. 4 Venn schema representing the taxa numbers distributed to the successional stages



replacements, spreading and clinging and thus presence ratios [15]. For example, when the frequency ratios of *Picea orientalis* in the successional stages are examined, the highest ratio occurs during the reaction stage. Graphics showed that the frequency

Table 5 Numerical distribution of taxa between successional stages

Symbols	Tree layer	Shrub layer	Herb layer	Subtotal	TOTAL	RATIO
(A) Establishment	1	3	62	66	124	30.85
(B) Competition	3	3	29	35		
(C) Reaction	0	0	12	12		
(D) Climax	1	0	10	11		
(1) Estb. & Comp	3	12	94	109	148	36.82
(2) Estb. & React	0	0	5	5		
(3) Comp. & Climax	1	2	4	7		
(4) React. & Climax	0	1	14	15		
(5) Estb. & Climax	0	0	4	4		
(6) Comp. & React	0	2	6	8		
(a) Estb. & Comp. & React	2	5	20	27	69	17.16
(b) Estb. & Comp. & Climax	2	0	2	4		
(c) Estb. & React. & Climax	0	0	0	0		
(d) Comp. & React. & Climax	6	9	23	38		
(e) Intersection of all stages	3	18	40	–	61	15.17
Total	22	55	325	–	402	100

ratio of *Fagus orientalis* is low in the early stages of succession, but high in the climax stage. Also, both species overlap at approximately the same ratio value (Fig. 5).

At this point, Bell et al. [81] and Ehrenfeld and Toth [82] state that area dimensions, isolation conditions, and the connections of these areas with the environment play a decisive role in plants' presence. In addition, all plants are found in their own habitats, which are limited by various factors and have specific characteristics [83]. Ecologists acknowledge that the change in species diversity is not a direct effect of succession, but indirect effects. In other words, in the process of succession, complexity increases in the ecosystem and the system develops from inorganic structure to organic structure. As a result, species richness also changes [61]. How this change progressed in the study area is shown in Fig. 6. Accordingly, a hump-curve is obtained by distributing the taxa which determined in the sample plots to the succession stages in the area.

The number of taxa that increase in "Establishment" stage (coded with 3) reaches the highest level in the "Competition" stage (coded with 4), forming a hump and then decreasing. Figure 6 shows, while there are 301 taxa in the competition stage, this number decreases to 170 with a decline ratio of 44% in the "Reaction" stage (coded with 5). This decrease is mostly under the influence of various events that occur

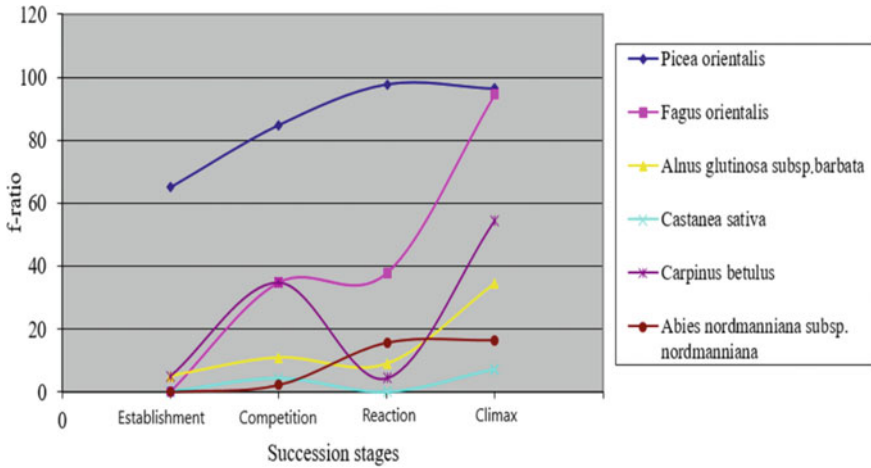


Fig. 5 Frequency ratios of major tree species

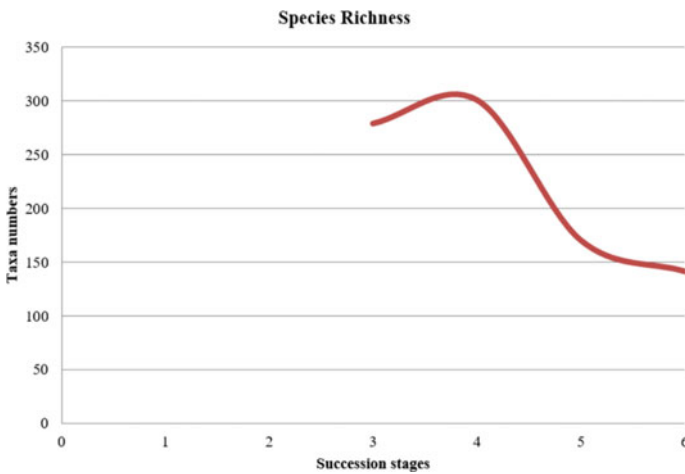


Fig. 6 Total species richness in succession stages

during succession. As the ecosystem develops during the succession, the distribution of energy among the ecosystem components also changes, the accumulation of organic matter and biomass increases, and an increasing amount of energy is spent for community functions (eg. respiration). When succession reaches the climax stage, two important events occur. On the one hand, while system metabolism is balanced, and on the other hand, more biomass (organic structure) is supported by less daily production and respiration [61].

Whether the number of taxa will peak at any intermediate stage in succession or continue to increase during the successive phases depends on a number of variables

and effects. As it is known, as succession progresses, stratification develops in vegetation and various mechanisms related to biological organization are involved in the system. As a result, potential niches emerge and the number of niches increase in the ecosystem. The proliferation of niches trigger for the increase in species diversity. Also, the population size, life span and competitiveness of the livings increase, and the species that adapt better become dominant in the environment. These contrary factors prevent both the arrival of other species and the increase in species diversity. In other words, during the succession process, some factors develop in a way to promote species diversity, while some other factors develop in a way to inhibit this [61].

Species richness is compared to the work of Palabaş-Uzun and Terzioğlu [62]. Firstly, it is noteworthy that the number of taxa in the species pools are different (Fig. 7). This difference is mostly due to the geographical locations of the areas and the variety of habitats they have. Although the number of taxa is different in these two studies, the trends of change between the stages of succession follow in the same direction. In addition, taxon richness were found to be the highest in the competition stage. The highest species diversity occurs in the intermediate stages of succession, as the pioneer species and the climax (final equilibrium) species overlap in the same environment. Also the highest recurrence rates can be achieved in the intermediate succession stages [51].

Also, as stated by Grubb [84], Ojeda et al. [16] and as Peña-Claros [37]; diversity exhibits different trends for layers (trees, shrubs, herbaceous) where different life forms are predominant. This difference can be easily observed for each layer, especially between the stages of succession (Fig. 8).

When the total taxa number is evaluated, it is seen that especially the herbaceous layer has a higher number of taxa in the early stages of succession compared to the late stages. Shrub taxa are found to be the most in the competition stage and decrease in the late stages (Fig. 8).

In this study, plant species diversity decreases from early to late stages for herbaceous and overall layer. This is an expected result. Because as vegetation matures,

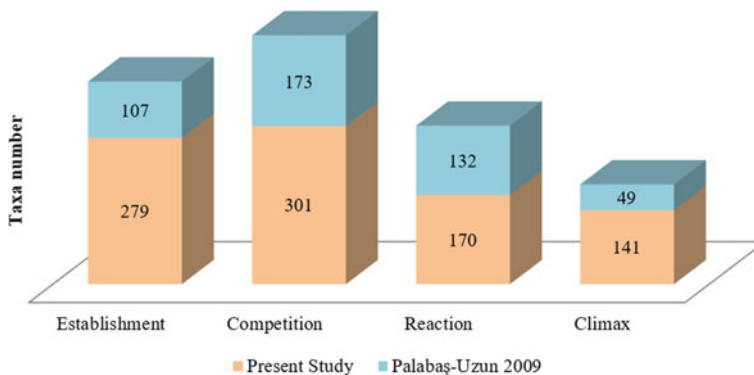


Fig. 7 Total taxon change in succession stages

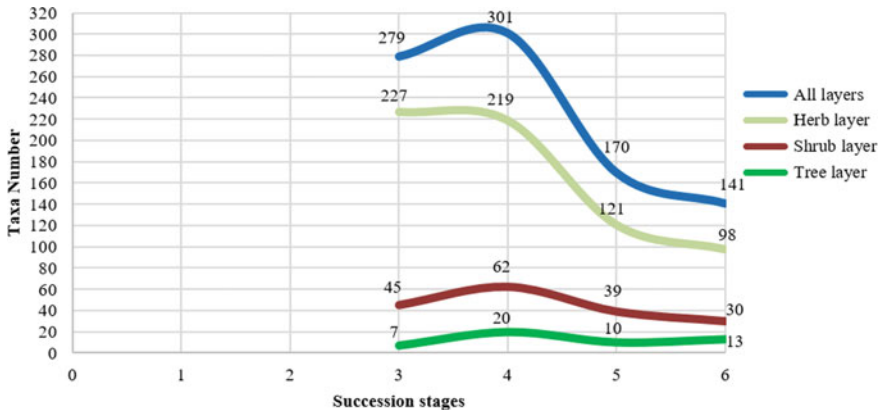


Fig. 8 Changes in the number of taxa of different layers in succession stages

competition conditions and energy circulation change [61]. Toledo and Salick [58] determined that the herbaceous layer has the highest species diversity in the early stages of succession and the tree layer has the lowest species diversity. Our current study results are generally consistent with these previous studies. However, more detailed information about the structural features and degree of change has been revealed.

When the plant species diversity is evaluated at each succession stage, a decrease from herbaceous layer to tree layer is observed. While the decreasing ratio is highest in the establishment stage, it is the lowest in the climax stage. In other words, the vegetation layers approach each other towards the final equilibrium (climax) in terms of diversity. When overall layer is evaluated, there is a gradual decrease in diversity through the succession stages (Fig. 9).

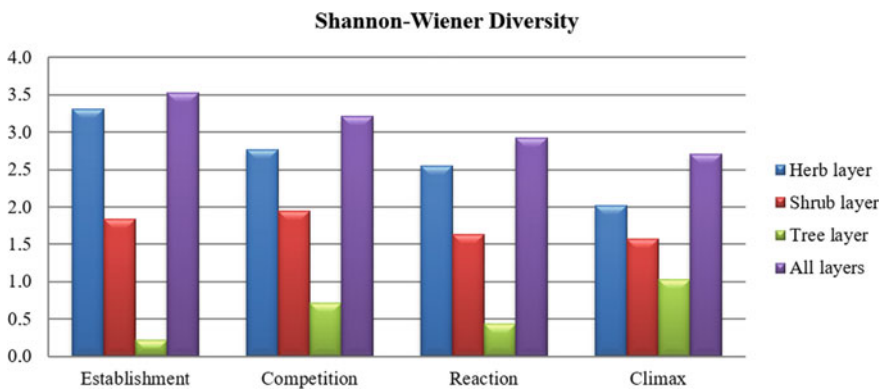


Fig. 9 Change of plant species diversity by succession stages

Nicholson and Monk [14] found that species richness increased rapidly in the phase following the establishment and placement of each layer (herbaceous, shrub, tree) at the beginning of succession, but continued to decrease throughout the remaining stages of succession. This study determined the downward trend in diversity towards the end of succession. Considering that the nudation and migration stages are not included in this study, there are no data to reveal the initial upward trend. However, it is obvious that the decrease will occur following a certain increase.

When the species richness between the phases of succession is examined, similar trends in plant species diversity are observed here (Fig. 10). While the establishment stage has the highest species richness (41.50), this number decreases towards the final equilibrium (21.04). The shrub layer reaches the highest species richness in competition stage. Because this stage provides suitable habitat conditions for shrub taxa in the study area. The canopy closure has not been formed yet and the current flow of nutrients and energy still continues in high amounts. The tree layer reaches the highest species richness in the climax stages. At this stage, climax species that adapt to the area are compatible with the tree species with living conditions identical.

When all layers are evaluated together, the relative evenness decreases from the establishment stage to the climax (Fig. 11). These values show characteristics parallel to the trend in diversity values. Suppose the relative abundance value of one community is higher than the other. In that case, the number of individuals of the species in the higher community is closer to each other than the other community. Here, the number of individuals is closest to each other in the establishment stages for overall layer.

However, the most balanced situation is observed in the climax stage (Fig. 11). The concept of self-reorganization explains this situation. According to the unbalanced thermodynamic theory of Prigogine [85]; Complex systems consisting of many parts tend to self-organize in an environment free from interference, to achieve a stable balance in the event of oscillation. A system (structure, model, or behaviour) that

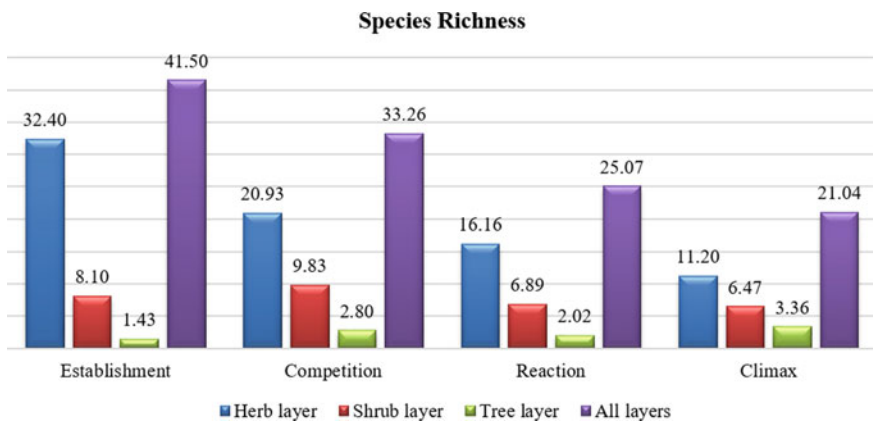


Fig. 10 Change of species richness by successional stages

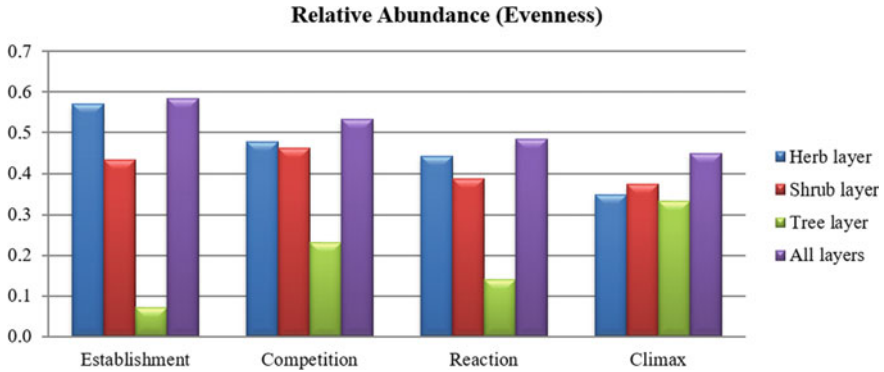


Fig. 11 Change of relative abundance by succession stages

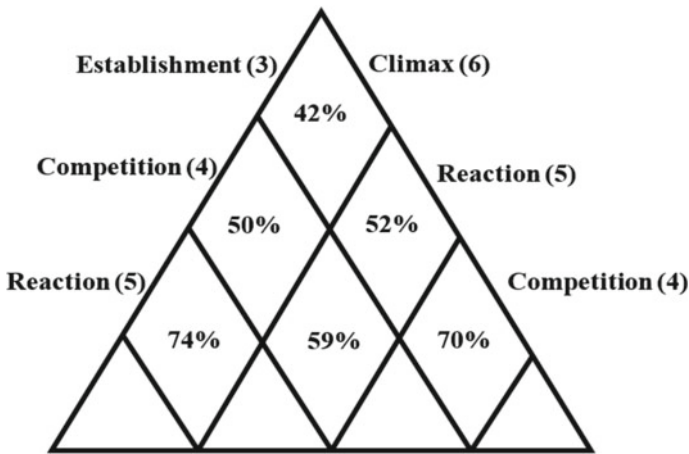


Fig. 12 Floristic similarities between successional stages

was randomly and irregularly dispersed at the beginning gets into a certain order by itself over time. In other words, in a system that is in turmoil, there is always a trend towards a regular structure and such a trend is also quite common in nature.

As a result of the field studies, taxa determined in each succession stage were subjected to Presence/Absence analysis. Based on these data, the relationship of each succession stage with other stages in terms of floristic composition was demonstrated with the help of Sorensen Similarity Index (Fig. 12).

According to the results, the highest similarity was determined between the reaction and climax stages with a ratio 74% and the lowest similarity between the establishment and climax stages with 42%. It is already expected that the similarity between reaction and climax stages will be higher than the others. Because in these two late stages, tree species that constitute the canopy have reached mature

heights. In other stages, floristic similarities have noticed significantly from the late stages since the tree layer has not yet reached sufficient maturity and the tree sizes are relatively shorter. As a result; floristic similarity rates between early succession stages and late succession stages decrease towards the final equilibrium. According to the results, each stage makes the highest similarity with the previous stage in terms of floristic composition.

The distribution of endemic and rare taxa to the succession stages is shown in Table 6. Accordingly, the most endemic and rare taxa were determined in the “Establishment” stage (with 20 taxa). The Establishment stage, including degraded areas, provides habitat conditions for more endemic species. Of course, the structure of the terrain in the area, the stony state and the proportion of rocky areas also affect this situation. Towards the later stages of the succession, a steady decrease in the number of endemic taxa (from 17 to 4) was determined. The reason for this seems to be that the majority of endemic species are highly light tolerant species. When the forest canopy is formed, it will be a negative effect for these species, but it may also positive effect the shade tolerant endemic species (eg *Hieracium gentiliforme* and *Hieracium subsilvularum*). It is a visible fact that sequential habitat use takes place here.

Some endemic taxa (eg. *Lonicera caucasica* subsp. *orientalis* and *Cyclamen parviflorum* var. *subalpinum*) are found at each stages of succession even having different presence rates, although some endemic taxa (eg. *Festuca amethystina* subsp. *orientalis* var. *turcica*, *Veronica multifida*, *Epipactis turcica*, *Onobrychis armena*, *Onosma bornmuelleri*, *Astragalus ovatus*, *Centaurea urvillei* subsp. *stepposa* and *Astrantia maxima* subsp. *haradjianii*) are specific to certain stages of succession (eg. Establishment stage). *Hieracium karagoellense* was found only in the “Competition” stage. However, the number of taxa determined at the “Reaction” and “Climax” stages were equal. As the detail; *Hieracium subsilvularum* was found only in the “Climax” stage. This results reveal that the rates of endemism are also different among the succession stages and the early stages contain more endemic taxa than the late stages. The rich habitat diversity is usually found in the early stages. The relationship between the stages of succession is very important for the vitality of many species, especially for endemic species. In this context, regulations that will include secondary succession in new forest management planning should be put into effect.

4 Conclusions

This chapter investigates the effect of forest succession on plant species diversity. The distribution of a total of 422 plant taxa (22 trees, 68 shrubs and 323 herbaceous plants) to forest succession stages has been revealed. Also, 33 endemic and 11 rare taxa were classified among the succession stages. In particular, the discovery of a new species [86] from the establishment stage in the study area has made succession studies more important in terms of conservation biology.

Table 6 Distribution of endemic and rare taxa in succession stages

Succession stages	Establishment (code: 3)	Competition (code: 4)	Reaction (code: 5)	Climax (code: 6)
Endemic Taxa	17	11	4	4
<i>Lonicera caucasica</i> subsp. <i>orientalis</i>	+	+	+	+
<i>Cyclamen parviflorum</i> var. <i>subalpinum</i>	+	+	+	+
<i>Hieracium gentiliforme</i>	–	+	+	+
<i>Melampyrum arvense</i> var. <i>elatus</i>	+	+	+	–
<i>Cirsium trachylepis</i>	+	+	–	–
<i>Galium fissurense</i>	+	+	–	–
<i>Astragalus viridissimus</i>	+	+	–	–
<i>Geranium ibericum</i> subsp. <i>jubatum</i>	+	+	–	–
<i>Geranium asphodeloides</i> subsp. <i>sintensisii</i>	+	+	–	–
<i>Dianthus carmelitarum</i>	+	+	–	–
<i>Festuca amethystina</i> subsp. <i>orientalis</i> var. <i>turcica</i>	+	–	–	–
<i>Veronica multifida</i>	+	–	–	–
<i>Epipactis turcica</i>	+	–	–	–
<i>Onobrychis armena</i>	+	–	–	–
<i>Onosma bornmuelleri</i>	+	–	–	–
<i>Centaurea urvillei</i> subsp. <i>stepposa</i>	+	–	–	–
<i>Astrantia maxima</i> subsp. <i>haradjianii</i>	+	–	–	–
<i>Astragalus ovatus</i>	+	–	–	–
<i>Hieracium karagoellense</i>	–	+	–	–
<i>Hieracium subsilvularum</i>	–	–	–	+
Rare Taxa	3	6	2	2
<i>Ruscus colchicus</i>	–	+	+	+
<i>Alchemilla speciosa</i>	+	+	–	–
<i>Anemone caucasica</i>	+	+	–	–
<i>Seseli petraeum</i>	+	+	–	–
<i>Lilium monadelphum</i> var. <i>armenum</i>	–	+	+	–
<i>Osmanthus decorus</i>	–	+	–	+
General total	20	17	6	6

The determination of plant richness and diversity in an area can primarily be used to transfer the assets of natural plant taxa to future generations. It serves the conservation and survival of target endemic plant taxa that require conservation measures. It also supports ecosystem-based planning, silvicultural practices, landscape recreation and green belt afforestation studies. It provides a basis for forestry planning involving biodiversity studies and provides data to help balance for forest use and survival.

Technical forestry activities in the region should be directed towards ensuring the continuity of current habitat conditions. Since open-stony areas show rich plant distribution, it should be a priority to avoid afforestation in habitats with endemic species and potential areas where their populations may expand. The continuity of forest partition borders and numbers in forest management plans, which are renewed at regular intervals, is also an important issue for the success of conservation activities. Continuously changing descriptive information has an effect that both prevents general focus and makes monitoring difficult.

Creating forest succession and diversity maps with the help of GIS could provide great advantages to the practitioners for monitoring. Biodiversity inventories made in this study should be repeated and mapped periodically according to their successional features. As it is known, the spread of plant populations can shrink or expand depending on changing environmental conditions. In this way, the shape and severity of the applications to be made based on the population changes can be adjusted to ensure the continuity of the population and the protection of biodiversity.

In this chapter, the change of plant biodiversity according to the succession stages of forest vegetation was investigated in detail. Accordingly, the highest alpha diversity in the study area was found to be at the "Ecesis-Establishment" stage (3.31) for herbaceous layer, at the "Competition stage" for shrub layer (1.95) and at the "Climax stage" (1.03) for tree layer. When all layers were evaluated together, it was revealed that the highest value was reached at the ecesis-establishment stage (3.52). In addition, it was determined that the floristic similarity decreased from the early stage of succession to the late stages, and also, each succession stage has the highest similarity with the previous stage. These results have revealed the necessity to consider all of the vegetation layers as a whole in future studies. Especially the values of herbaceous layer play an active role in determining the general trend of species diversity.

The insufficiency of ecological information about the original forest stand pieces has a disabling effect on transferring biodiversity to forest management plans and makes progress on this subject difficult. The biggest obstacle in this regard is that these studies are difficult, time consuming and costly. Insufficient data on the distribution areas, population sizes and dynamics of endemic and rare endangered plants and the stand types on which they depend can make this process impossible in practice. On the one hand, stands that are affected by many factors should be rehabilitated naturally, and on the other hand, biological diversity should be sustained by considering the balance of protection and use in relatively undisturbed natural stands.

5 Recommendations

Critical habitats should be defined for the continuation of plant species diversity. These habitats should be selected from different successional areas in terms of their rich environmental and biological properties. Providing the continuity of the populations in layers is very important especially in establishing a substrate for the future of diversity. For this purpose, species compositions and relative abundances of the succession stages can be used as useful guiding agents. Continuity of the areas belonging to different succession stages should be ensured. Because the plant species that constitute biodiversity form different compositions at different stages of forest succession. The spatial composition of these stages should also be taken into consideration.

In order to solve large-scale problems in the ecosystem, interactions between species, community and landscape level must be examined and the relationships between successive components should be addressed. With the monitoring system to be established in specific areas which have high conservation priority, changes in succession stages should be monitored and recorded in appropriate periods such as 5, 10 or 20 years, depending on the species diversity or the sensitivity of the ecosystem.

Acknowledgements This chapter is a part of the first author's PhD dissertation. We are indebted to Karadeniz Technical University for financial support (KTU-BAP-2003-113-001-6). We would also like to thank Dr. Cengiz Acar for his kind help in statistics.

References

1. Gaines WL, Harrod RJ, Lehmkühl JF (1999) Monitoring biodiversity: quantification and interpretation. Gen. Tech. Rep. PNW-GTR-443. Portland, OR: U.S. Department of Agriculture, Forest Service, Pacific Northwest Research Station, p 27
2. Marques JC, Salas F, Patri'cio JM, Pardal MA (2005) Application of ecological indicators to assess environmental quality in coastal zones and transitional waters: two case studies. In: Jorgensen JE, Costanza R, Xu FL (eds) Ecological indicators for assessment of ecosystem health, Chapter 3. CRC Press
3. Déleg J, Gradstein SR, Aragón G, Giordani P, Benítez A (2021) Cryptogamic epiphytes as indicators of successional changes in megadiverse lowland rain forests of western Amazonia. *Ecol Ind* 129:107890. <https://doi.org/10.1016/j.ecolind.2021.107890>
4. Jetz W, Cavender-Bares J, Pavlick R, Schimel D, Davis FW et al (2016) Monitoring plant functional diversity from space. *Nat Plants* 2:16024. <https://doi.org/10.1038/nplants.2016.24>
5. Jetz W, McGeoch MA, Guralnick R, Ferrier S, Beck J et al (2019) Essential biodiversity variables for mapping and monitoring species populations. *Nat Ecol Evol* 3(4):539–551. <https://doi.org/10.1038/s41559-019-0826-1>
6. Hansen AJ, Spies TA, Swanson FJ, Ohmann JL (1991) Conserving biodiversity in managed forests. *Bioscience* 41(6):382–392. <https://doi.org/10.2307/1311745>
7. Ehrlich PR, Ehrlich AH (1992) The value of biodiversity. *Ambio* 21(3):210–226
8. Halpern CH, Spies TA (1995) Plant species diversity in natural and managed forests of the Pacific Northwest. *Ecol Appl* 5(4):913–934. <https://doi.org/10.2307/2269343>

9. Chazdon RL (2014) *Second growth: the promise of tropical forest regeneration in an age of deforestation*. University of Chicago Press, Chicago, USA
10. Haddad NM, Brudvig LA, Clobert J, Davies KF, Gonzalez A et al (2015) Habitat fragmentation and its lasting impact on Earth's ecosystems. *Sci Adv* 1(2):e1500052. <https://doi.org/10.1126/sciadv.1500052>
11. Sánchez-Reyes UJ, Niño-Maldonado S, Barrientos-Lozano L, Treviño-Carreón J, Meléndez-Jaramillo E et al (2020) Structural changes of vegetation and its association with microclimate in a successional gradient of low thorn forest in northeastern Mexico. *Plant Ecol*. <https://doi.org/10.1007/s11258-020-01088-z>
12. Chazdon RL, Guariguata MR (2016) Natural regeneration as a tool for large-scale forest restoration in the tropics: prospects and challenges. *Biotropica* 48:716–730. <https://doi.org/10.1111/btp.12381>
13. Egerton FN (2015) History of ecological sciences, part 54: succession, community, and continuum. *Bull Ecol Soc Am* 96:426–474
14. Nicholson SA, Monk CD (1974) Plant species diversity in old field succession on the Georgia Piedmont. *Ecology* 55:1075–1085. <https://doi.org/10.2307/1940357>
15. Peet RK, Christensen NL (1988) Changes in species diversity during secondary forest succession on the North Carolina Piedmont. In: *Diversify and pattern in plant communities* pp 233–245.
16. Ojeda F, Maranon T, Arroyo J (2000) Plant diversity patterns in the Aljibe Mountains (S. Spain): a comprehensive account. *Biodivers Conserv* 9:1323–1343. <https://doi.org/10.1023/A:1008923213321>
17. Amici V, Santi E, Filibeck G, Diekmann M, Geri F et al (2013) Influence of secondary forest succession on plant diversity patterns in a Mediterranean landscape. *J Biogeogr* 40:2335–2347
18. Hilmer T, Friess N, Bässler C, Heurich M, Brandl R et al (2018) Biodiversity along temperate forest succession. *J Appl Ecol* 55:2756–2766. <https://doi.org/10.1111/1365-2664.13238>
19. Fischer DG, Antos JA, Biswas A, Zobel DB (2019) Understorey succession after burial by tephra from Mount St. Helens. *J Ecol* 107:531–544. <https://doi.org/10.1111/1365-2745.13052>
20. Koivula M, Vanha-Majamaa I (2020) Experimental evidence on biodiversity impacts of variable retention forestry, prescribed burning, and deadwood manipulation in Fennoscandia. *Ecol Process* 9:11. <https://doi.org/10.1186/s13717-019-0209-1>
21. Haeussler S, Kabzems R, McClarnon J, Bedford L (2021) Successional change, restoration success, and resilience in boreal mixedwood vegetation communities over three decades. *Can J For Res* 51:766–780. <https://doi.org/10.1139/cjfr-2020-0024>
22. Qi Y, Bhunia P, Zhang T, Luo F, Lin P, Chen Y (2020) Environmental degradation and sustainability. In: *Sustainability: fundamentals and applications* 23:483–505. <https://doi.org/10.1002/9781119434016.ch23>
23. Tribot A-S, Deter J, Mouquet N (2018) Integrating the aesthetic value of landscapes and biological diversity. *Proceed Roy Soc B: Biol Sci* 285:20180971. <https://doi.org/10.1098/rspb.2018.0971>
24. Fahrig L (2003) Effects of habitat fragmentation on biodiversity. *Annu Rev Ecol Evol Syst* 34:487–515. <https://doi.org/10.1146/annurev.ecolsys.34.011802.132419>
25. Li Y, Bearup D, Liao J (2020) Habitat loss alters effects of intransitive higher-order competition on biodiversity: a new metapopulation framework. *Proceed Roy Soc B: Biol Sci* 287:20201571. <https://doi.org/10.1098/rspb.2020.1571>
26. Işık K (2011) Rare and endemic species: why are they prone to extinction? *Turk J Bot* 35:411–417. <https://doi.org/10.3906/bot-1012-90>
27. Bazzaz FA (1991) Habitat selection in plants. *Am Nat (Suppl)* 137:S116–S130
28. Magurran AE (1988) *Ecological diversity and its measurement*. Princeton University Press, Princeton, N.J., p 179
29. Magurran AE (2004) *Measuring biological diversity*. Blackwell Publishing, Malden, MA, p 256
30. Takacs D (1996) *The idea of biodiversity: philosophies of paradise*. The Johns Hopkins University Press, p 500

31. Eldredge N (2002) Life on earth: an encyclopedia of biodiversity, ecology and evolution. ABC-CLIO, ebook
32. Kılınç M, Kutbay HG (2008) Bitki Ekolojisi. Palme Yayıncılık, Ankara, 490 s. (in Turkish)
33. Işık K, Yalırık F, Akesen A (1997) Ormanlar, biyolojik çeşitlilik ve doğal mirasın korunması. XI Dünya Ormanlık Kongresi, Bildiriler Kitabı, Antalya 2:3–27 (in Turkish)
34. Whittaker RH (1972) Evolution and measurement of species diversity. *Taxon* 21:213–251
35. Van Der Maarel E (2006) Vegetation ecology. Blackwell Publishing, UK, p 395
36. Lévêque C, Mounolou J-C (2003) Biodiversity. John Wiley & Sons Inc., Great Britain, p 284
37. Peña-Claros M (2003) Changes in forest structure and species composition during secondary forest succession in the Bolivian Amazon. *Biotropica* 35(4):450–461. <https://doi.org/10.1111/j.1744-7429.2003.tb00602.x>
38. Terzioğlu S, Başkent EZ, Kadıoğulları Aİ (2009) Monitoring forest structure at landscape level: a case study of Scots pine forest in NE Turkey. *Environ Monit Assess* 152:71–81. <https://doi.org/10.1007/s10661-008-0297-3>
39. Wöllfling M, Uhl B, Fiedler K (2019) Multi-decadal surveys in a Mediterranean forest reserve—do succession and isolation drive moth species richness? *Nat Conserv* 35:25–40. <https://doi.org/10.3897/natureconservation.35.32934>
40. Radecka A, Michalska-Hejduk D, Osińska-Skotak K, Kania A, Górski K, Ostrowski W (2019) Mapping secondary succession species in agricultural landscape with the use of hyperspectral and airborne laser scanning data. *J Appl Remote Sens* 13(3):034502. <https://doi.org/10.1117/1.JRS.13.034502>
41. Binelli EK, Gholz KL, Duryea ML (2000) Plant succession and disturbances in the urban forest ecosystem. In: Duryea ML, Binelli EK, Korhnaak LV (eds) Restoring the urban forest ecosystem. CD-ROM, Chapter 4, pp 2–23
42. Berveglieri A, Imai NN, Christovam LE, Galo LBT, M, MG Tommaselli A, Honkavaara E, (2021) Analysis of trends and changes in the successional trajectories of tropical forest using the Landsat NDVI time series. *Remote Sens Appl Soc Environ* 24:100622. <https://doi.org/10.1016/j.rsase.2021.100622>
43. Stohlgren TJ, Falkner MB, Schell LD (1995) A Modified-Whittaker nested vegetation sampling method. *Vegetatio* 117:113–121. <https://doi.org/10.1007/BF00045503>
44. Doğan HM, Doğan A (2006) A New approach to diversity indices-modelling and mapping plant biodiversity of Nallıhan (A3-Ankara/Turkey) forest ecosystem in frame of geographic information systems. *Biodivers Conserv* 15:855–878. <https://doi.org/10.1007/s10531-004-2937-4>
45. Beever EA, Swihart RK, Bestelmeyer BT (2006) Linking the concept of scale to studies of biological diversity: evolving approaches and tools. *Divers Distrib* 12:229–235. <https://doi.org/10.1111/j.1366-9516.2006.00260.x>
46. Green JL, Plotkin JB (2007) A statistical theory for sampling species abundances. *Ecol Lett* 10:1037–1045. <https://doi.org/10.1111/j.1461-0248.2007.01101.x>
47. Zobel DB, Antos JA (2016) Flowering patterns of understory herbs 30 years after disturbance of subalpine old-growth forests by Tephra from Mount St. Helen. *Int J Plant Sci* 177(2):145–156. <https://doi.org/10.1086/684181>
48. Bae S, Levick SR, Heidrich L et al (2019) Radar vision in the mapping of forest biodiversity from space. *Nat Commun* 10:4757. <https://doi.org/10.1038/s41467-019-12737-x>
49. de Almeida DRA, Almeyda Zambrano M, Broadbent EN et al (2020) Detecting successional changes in tropical forest structure using GatorEye drone-borne lidar. *Biotropica* 52(3):1155–1167. <https://doi.org/10.1111/btp.12814>
50. Asbeck T, Großmann J, Paillet Y, Winiger N, Bauhus J (2021) The Use of tree-related microhabitats as forest biodiversity indicators and to guide integrated forest management. *Curr For Rep* 7:59–68. <https://doi.org/10.1007/s40725-020-00132-5>
51. Pickett STA (1976) Succession: an evolutionary interpretation. *Am Nat* 110:107–119
52. Cowles HC (1899) The ecological relations of the vegetation of the sand dunes of Lake Michigan. *Bot Gazette* 27:95–117, 167–202, 281–308, 361–391

53. Clements FE (1905) *Research methods in ecology*. University Publishing Company, Lincoln, NE
54. Clements FE (1916) *Plant succession: an analysis of the development of vegetation*. Carnegie Inst. Pub. 242. Washington DC, p 512
55. Cooper WS (1913) The Climax forest of Isle Royale, Lake Superior, and its development. *Bot Gaz* 55:1–44
56. Clements FE (1936) Nature and structure of climax. *J Ecol* 24:252–284. <https://doi.org/10.2307/2256278>
57. Kılınç M (2005) *Bitki Sosyolojisi*, Palme Yayıncılık, Ankara
58. Toledo M, Salick J (2006) Secondary succession and indigenous management in semideciduous forest fallows of the Amazon Basin. *Biotropica* 38(2):161–170. <https://doi.org/10.1111/j.1744-7429.2006.00120.x>
59. Pickett STA, Cadenasso ML, Meiners SJ (2008) Ever since clements: from succession to vegetation dynamics and understanding to intervention. *Appl Veg Sci* 12:9–21. <https://doi.org/10.1111/j.1654-109X.2009.01019.x>
60. Glenn-Lewin DC, Peet RK, Veblen TT (1992) *Pant succession theory and prediction*. Chapman & Hall, Great Britain at the University Press, Cambridge, p 351
61. Odum EP, Barrett GW (translated by Işık K) (2008) *Ekolojinin temel ilkeleri*. Palme Yayıncılık, Ankara (in Turkish)
62. Palabaş-Uzun S, Terzioğlu S (2019) Sıldağı (Şalpazarı/Trabzon) ve yöresinin florası. *Düzce Üniversitesi Bilim ve Teknoloji Dergisi* 7:1523–1573
63. Whittaker RH (1953) A consideration of climax theory: The climax as a population and pattern. *Ecol Monogr* 23(1):41–78. <https://doi.org/10.2307/1943519>
64. Hill D, Fasham M, Tucker G, Shewry M, Shaw P (2005) *Handbook of biodiversity methods, survey, evaluation and monitoring*. Cambridge University Press, Cambridge, UK, p 573
65. Uzun A (2009) *KTU Orman Fakültesi Araştırma Ormanında Bitkisel Tür Çeşitliliğinin Saptanması ve Vejetasyonunun Haritalanması*. KTU, PhD thesis, Trabzon (in Turkish)
66. Hulbert SH (1971) The nonconcept of species diversity: a critique and alternative parameters. *Ecology* 52:577–586. <https://doi.org/10.2307/1934145>
67. Stirling G, Wilsey B (2001) Empirical relationships between species richness, evenness, and proportional diversity. *Am Nat* 158:3. <https://doi.org/10.1086/321317>
68. Kwiatkowska AJ, Symonides E (1986) Spatial distribution of species diversity indices and their correlation with plot size. *Vegetatio* 68:99–102. <https://doi.org/10.1007/BF00045060>
69. McIntosh RP (1981) *Succession and Ecological Theory*. In: West DC et al (eds) *Forest succession: concepts and application*. Springer, Berlin, pp 10–23
70. Shannon CE (1948) A mathematical theory of communication. *Bell Syst Techn J* 27:379–423 and 623–656
71. Simpson EH (1949) Measurement of diversity. *Nature* 163:688
72. Margalef R (1951) *Diversidad de especies en las comunidades naturales*. Publicaciones del Instituto de Biología Aplicada, Barcelona 6:59–72
73. Berger WH, Parker FL (1970) Diversity of planktonic foraminifera in deep-sea sediments. *Science* 168:1345–1347
74. Seaby RMH, Henderson PA (2006) *Measuring and understanding biodiversity (SDR-IV Help)*. Pisces Conservation Ltd., Hampshire, p 122
75. Pielou EC (1966) Species diversity and pattern diversity in the study of ecological succession. *J Theor Biol* 10:370–383
76. Pielou EC (1969) *An Introduction to mathematical ecology*. John Wiley, New York, p 326
77. Pielou EC (1975) *Ecological diversity*. Wiley-Interscience, New York
78. Mooers AO, Heard SB (1997) Inferring evolutionary process from phylogenetic tree shape. *Quart Rev Biol* 72:31–54. Jstor:3036810
79. Sorensen TA (1948) A method of establishing groups of equal amplitude in plant sociology based on similarity of species content, and its application to analyses of the vegetation on Danish commons. *Biologiske Skrifter* 5(4):1–34

80. Uzun A, Terzioğlu S (2021) Vascular flora and endemism of Ormanüstü planning unit (Maçka-Trabzon), Turkey. *Kastamonu Univ J For Fac* 21(2):104–121. <https://doi.org/10.17475/kastorman.1000360>
81. Bell SS, Fonseca MS, Motten LB (1997) Linking restoration and landscape ecology. *Restor Ecol* 5:318–323. <https://doi.org/10.1046/j.1526-100X.1997.00545.x>
82. Ehrenfeld JG, Toth LA (1997) Restoration ecology and the ecosystem perspective. *Restor Ecol* 5:307–317. <https://doi.org/10.1046/j.1526-100X.1997.00544.x>
83. Pickett STA (1980) Non-equilibrium coexistence of plants. *Bull Torrey Bot Club* 107:238–248
84. Grubb JP (1987) Global trends in species-richness in terrestrial vegetation: a view from the northern hemisphere. In: Gee JHR, Giller PS (eds) *Organization of communities, past and present*. Blackwell, Oxford, pp 94–118
85. Prigogine I (1962) *Introduction to non-equilibrium thermodynamics*. Wiley-Interscience, New York
86. Uzun A, Terzioğlu S, Palabaş-Uzun S, Coşkunçelebi K (2009) *Astragalus ansinii* sp. nov. (Fabaceae) from Turkey, and a contribution to the sectional taxonomy. *Nord J Bot* 27(5):397–401. <https://doi.org/10.1111/j.1756-1051.2009.00440.x>

Desertification in China: Role of Natural Succession in the Sustainable Revegetation of Drylands



Lorenz Huebner and Ayad M. Fadhil Al-Quraishi 

Abstract The “Three North Shelterbelt Development Program” and a variety of greening programs in China have been undertaken since the late 1970s, resulting in the world’s largest forestation and renaturation area over 4,800 km of sub-humid to hyper-arid climate zones across Northern China. The large-scale afforestation activities were done mainly to reduce consequences from desertification in the north, i.e. large dust storm events called “Yellow Dragon” that affected the entire country. Some planting campaigns have used non-adapted or not native tree species, leading to hydrological and/or ecological stress and subsequent tree mortality. The recent trend of worsening in some climate parameters in Northern China has further reduced billions of planted trees’ viability. We present results from example regions and review the overall efficacy of this unique long-term desertification control program. How can we restore degraded regions to achieve acceptable survival rates and adaptability of the new vegetation to climate change? Some factors that have been identified as key in the success of restoration of degraded land in Northern China will be presented, focusing on the recent concept of “natural renaturation” that was started here basically in 2006. It uses the process of natural succession, a method that relies on the self-restoration capacity of undisturbed nature to develop new vegetation over time, often many years. This method so far has only started being applied to drylands. Fifteen years after its implementation, we find encouraging results as to increases in biomass. The long-term assessment of vegetation developed in natural succession is expected to indicate superiority in ecological parameters and viability. Will this method become a successful and important component in the fight against desertification?

L. Huebner (✉)
24943 Flensburg, Germany
e-mail: L-Huebner@gmx.de

A. M. F. Al-Quraishi
Petroleum and Mining Engineering Department, Faculty of Engineering, Tishk International University, Erbil 44001, Iraq
e-mail: ayad.alquraishi@gmail.com; ayad.alquraishi@tiu.edu.iq

Keywords China · Natural succession · Active planting · Climate change · Desertification control · Drylands · Ecological renaturation

1 Introduction

Like the Mediterranean region, China has a long history of human-made causes of desertification, starting with deforestation, e.g. in the practice of fire hunting in historical times to significant deforestation, increase in population density and overuse of groundwater until recently [1]. In the semi-arid to arid desert border regions of Northern China, nomadic activity with overgrazing [2, 3] has been an important factor, paralleled in the sub-humid eastern part of Northern China by improper agricultural land use [1, 4, 5]. The average wind speed, days with strong wind and related aeolian desertification seem to increase with climate change [6, 7], leading to dust storms that are famous in China, called “Yellow Dragon”. These dust storms propagate encroachment of sand deserts., Sand dunes and sheets can build up and cover cultivated areas [8, 9].

Natural semi-arid and arid ecosystems are easily disturbed by damage to the vegetation canopy caused by livestock or active deforestation. Erosion and land degradation will then take up momentum: Ecosystems can deteriorate further in the direction of desertification, supported by extended periods of drought [10–14]. Hence, there is a high ecological and often also an agricultural need for revegetation of degraded drylands. Over the last seven decades, China has been experimenting with a wide range of different restoration concepts. In its fifth decade, the “Three North Shelterbelt Development Program” (TNSP) and different greening programs were started in China in 1978. It has become the world’s largest forestation and renaturation area over 4,800 km. It covers a wide climatic range from sub-humid to hyper-arid climate zones and different geomorphological situations across the North of China [14]. These large-scale afforestation and revegetation activities were done mainly to reduce the large dust storm events as a result of desertification that affected the capital of Beijing and the entire country.

However, trends in climate change have sometimes been unfavorable during the last 30 years in Northern China for any newly planted tree here [13], which probably has contributed to the poor survival rates reported for a number of planting efforts [10, 11, 15]. About 66 billion trees have been planted in Northern China until today. It is planned to reach 100 billion trees by the year 2050. However, tree mortality in the millions often happened only after 10 or 20 years of growth. Sometimes, the campaigns used to apply too dense planting, planting monocultures or not native trees, leading to hydro-ecological stress, often paralleled by significant suppression of native vegetation and severe ecological consequences [10, 11, 15, 16].

Today, China has learned from these campaigns and has started introducing vegetation more adapted to the local climate from a hydrological and ecological perspective. We realize that only those restoration concepts considering the consequences of a changing climate will lead to results of sustainable revegetation [17]. Under the

hostile climate of desert bordering regions, any revegetation needs to reflect perfect ecological fit.

By also reviewing a few restoration examples from regions outside of China we will highlight certain ecological criteria that can make the new vegetation better adjustable to future climate changes and further challenges. Six key success factors in revegetation were identified in a survey of the numerous restoration projects across China [16].

One of these success factors is use of natural succession, which, like any restoration measure in drylands, is cumbersome, prone to disturbance, and it needs to develop over a long time until positive results are found in terms of a measurable increase in biomass. We review China's recent "natural renaturation" concept, a campaign that was started on larger scale around 2006. It is counting on nature's own capacity for revegetation when being left undisturbed from any human or live-stock impact that would limit recovery. Finally, in 2020 first evidence was presented demonstrating that this method leads to a gain in biomass [18].

Obviously, it is too early to evaluate whether this increase in biomass after years of natural succession will effectively stop further degradation, and if done over large regions, whether it will stop sand encroachment and positively affect agriculture, regional climate, and dust storms. What is the likelihood for the "natural renaturation" method to play an important role in the future desertification control measures? And why, from ecological and sustainability perspectives, could this method be supposed to be superior to any active planting campaign? How can naturally regrown vegetation be more resistant to a future rise in temperatures, increase in drought events and aridity that has been forecasted particularly for drylands until the year 2100 [13]?

This chapter reviews relevant studies that identify the factors leading to successful and long-term sustainable revegetation of degraded semi-arid and arid drylands: Which lessons have been learned from the large-scale afforestation efforts during the recent decades in Northern China, and what is the rationale for ecological approaches to restoration? We compare ecological methods of revegetation, focusing on the process of natural succession and its implementation in China's drylands during the recent 15 years. Finally, we discuss the actual value of large-scale restoration with sustainable vegetation for the agronomy and reversal of desertification trends, and as a potential tool to directly mitigate climate warming and aridity: on local, regional, and maybe even country level.

2 World's Largest Restoration Program in China

There are 13 deserts, drylands, and sandy lands in China. Large regions of Northern China and Mongolia are at serious risk of desertification, which some believe to be caused by human activity [19]. During the last century, deforestation, industrial use of ground and water, and grasslands' transformation into arable land had markedly reduced forests and grassland areas in China [20, 21]. These land-use changes resulted in severe land desertification [22, 23] and damage to ecosystems and biodiversity

[24]. The degree of degradation was furthered by climate change parameters [25], such as the frequency of sand and dust storms and an increase in spells of drought [26, 27].

2.1 Desertification Control Programs in China

Already in the 1950s China has started to actively combat desertification [28, 29]. Since 1978 five ecological restoration programs were launched, the main one being the “Three North Shelterbelt Development Program (TNSP). Afforestation of semi-arid and arid areas is planned until 2050, it is, therefore, the longest-lasting and the largest restoration program in history [14]. It was supported by four later programs that were started around the year 2000: The Program for Conversion of Cropland to Forest, a Natural Forest Protection Program, the Program to Control Sand Source, and a Grazing Ban Program for Grassland Restoration [30]. Deforestation, overuse of water for cultivation, and overgrazing were the main causes of desertification in Northern China to be addressed by these five programs [31]. The time period and the respective achievements of the programs are summarized in Table 1.

The reversal of degradation reported so far was assessed by means of an increase in organic soil components, biodiversity, and conservation of soil and water due to the additional grasslands. A wider range of tree species with high tolerance of drought and salinity of soil was planted, such as *Populus alba*, *Pinus sylvestris* var. *mongolica*, *Ulmus pumila*, and *Salix matsudana* to protect the land from sand storms and dune migration [14]. Recent activities include the ecological enhancement of windbreaks and natural restoration projects for sand fixation [18, 31] reviewed in Sect. 4.3.

2.2 Example Region Kubuqi Desert

Kubuqi is China’s 7th largest desert, located in the Autonomous Republic of Inner Mongolia. As an outstanding example, the investment company Elion Research Ltd has planted vegetation on 6,000 km², i.e., about a third of the sand desert, supported by the local government and based on a high groundwater table. Cultures of vegetables and herbs are protected by a 5–10 km wide green belt over 242 km along the Yellow River. According to an UNEP report the annual precipitation here has increased from around 270 mm (1960 until 2000s decade) to recent 310 mm and the restoration measures had been important in the control of desertification [32]. Many local farmers use the protected land for agriculture, and the beautiful regreened area benefits from ecotourism [33].

Sandstorm days have been 10–50 per year (until 1985) and decreased since to an annual maximum of 8 days, so that the greening of the Kubuqi desert “could have caused a decrease in dust storms” [32].

Table 1 Implementation of desertification control programs in China (after [14, 30, 31, 34, 35])

Time period	Program	Outcome, achievements
Since 1978 until 2050	Three North Shelterbelt Development Program (TNSP)	<ul style="list-style-type: none"> • Afforestation of 26.5 million ha area • Forested area has increased from 5.1 to 12.4% of project area • 1.6 million ha forests for windbreak and sand fixation • Beginning reversal of degradation in the three regions: Northeast, central North, and Northwest • Reversal in regions Mu Us and Horqin sandy lands
1999–2009	Conversion of Cropland to Forest Program	<ul style="list-style-type: none"> • Farmers substituted for planting trees instead of crops • 9.3 million ha of forests newly created from cropland
2001–2010	Natural Forest Protection Program	<ul style="list-style-type: none"> • Forested area increased by 14 million ha • Timber production decreased by 220 million m³
2001–2010	Sand Source Control Program	<ul style="list-style-type: none"> • Restoration of vegetation in North eastern China to prevent sand and dust storms • 6 million ha of cropland were reforested
2003–2010	Grazing Ban Program for the Restoration of Grassland	<ul style="list-style-type: none"> • 518.7 million ha of grassland secured with fences • 12.4 million ha of grassland reseeded • Vegetation coverage increased from 59 to 71%

The report recommends to assess the available water resources and planting of species that are adapted to the local hydrological situation and at appropriate densities. It is done because the risk of overuse of water and lowering of water table have been identified, although the presence of native desert plants in addition to trees and vegetables would help to mitigate that risk [32].

2.3 *Tree Survival in Afforestation Campaigns*

The total area of afforestation in China had reached 3 million km² in 2013. However, according to the Chinese State Forestry Administrator [34, 35], less than 25% (0.69 million km²) of this area remained as forested land until 2013. Cao [10] has calculated a rather low 15% rate of tree survival for all plantations done since 1949 in Northern China [10]. Various reasons for hydro-ecological stress, leading to mortality of trees

Table 2 Reported examples of mortality of trees planted in the TNSP and other reforestation programs in China

Source	Tree mortality example	Reason given
Wang et al. [36]	Poplar (<i>Populus simonii</i>) on hill slopes, in loess and sandy lands	Poor growth due to high density planting, lack of soil moisture and nutrients, lack of management
Zheng et al. [37]	Shelterbelt with <i>Pinus sylvestris</i> in Horqin sandy land (eastern TNSP): mortality in the 1990s	Low soil moisture content after four decades of growth
Lyu et al. [31]	>333 km ² of planted poplar trees died in Zhangbei, Hebei province since 2007	Natural aging (30 years), groundwater level drawing down

and respective economic loss were identified. In many cases, this occurred only after years or decades of growth. Table 2 lists three reports with examples from Northern China and the reasons for hydro-ecological stress resulting in high tree mortality.

It seems that in order to fight erosion and sand storms, China's early afforestation efforts were aimed to increase the vegetation cover in an expedited way and by planting trees at high density. After some time of growth this often led to low soil moisture content and/or lowering of the water table. According to Wang et al. [14], most of the TNSP regions have an annual precipitation of less than 400 mm—a condition, under which plantations of trees at high density could disturb ecosystems and the water balance. They conclude that in semi-arid and arid areas with an annual mean precipitation below 400 mm, the large-scale afforestation at high density is not recommended [14]. This was confirmed in recent remote sensing studies, finding that forest loss (assessed from 2007 to 2017) was higher (35%) in the semi-arid and arid TNSP areas with less than 400 mm precipitation [38].

2.4 Hydro-Ecological Stress in Semi-Arid and Arid Afforestation

After all, the Chinese restoration efforts are realised to have successfully reduced dust storms and increased vegetation and agriculture in certain regions [14, 18]. The following attributes were shown to be essential for the planning and construction of large-scale renaturation projects on drylands [10, 11, 15, 16]:

- (1) Adaptation to the local ecological situation and climate, low percentage of shrubs and trees to allow for a natural succession of native grassland, herbs, and shrubs, yet high enough to guarantee some protection from wind, sand, and extreme temperatures.
- (2) Water consumption should be low. The available water resources offered by the semi-arid climate and water table are to be considered. Species that grow fast

- with larger amount of water but also tolerate low amounts (poikilohydric), such as *Poplar* and *Eucalyptus*, are used cautiously and planted rather widely spaced.
- (3) Preferred use of native species with proven resistance to drought and radiation.
 - (4) These projects require decades to develop and decades of certain measures for protection and maintenance.
 - (5) As observed in a very positive example region of the Chinese TNSP (Northern Jiangsu), creating a connected vegetation cover of around 20% and above can result in a climatically protected area with mitigation of hot dry sand storms and extreme temperatures, and an increase in relative humidity [39].
 - (6) Since 2006, the restoration program in China, besides active planting of trees, shrubs and grasses, also includes natural reforestation as a measure to revegetate larger areas. The closing of land is done to enable vegetation to recover in natural succession. Recently, the increase of biomass in these areas of vegetational succession was demonstrated. The authors emphasize the importance of the method because in the long-term ecosystems would benefit more, in comparison to the active planting method [18]. Natural succession may lead to biodiversity and climatic adaptability of the new vegetation.

3 Precipitation and Biomass in Northern China During Last Decades

Restoration of viable vegetation over large regions may as well restore a more humid climate in the long-term of several decades, caused by a vegetation-induced increase in precipitation and relative humidity. This is found in studies simulating the revegetation of semi-arid and arid regions [40–42]—and such strengthening of the hydrological cycle clearly would consolidate the new vegetation canopy. On the other hand, trees have a long-lasting growth cycle of several decades. The new vegetation is to be given time to develop. This fact increases the likelihood for the tree plantation to be hit by a change in climate parameters, which is likely to reduce water availability for vegetational growth, a general trend observed by Jiao et al. [43]. As shown in Fig. 1, it is precisely what happened in Northern China during recent decades of planting activities from 1980 to 2010. There is a trend of increased drought or extended sequences of years with precipitation deficit [13].

Such conditions are not as severe for a vegetation that is hydro-ecologically adapted (see Sect. 2.4) and has relatively low water requirements. Examples are grasslands, herbs, shrubs (all of which have a significantly shorter generation cycle), and in general, savanna ecosystems with low canopy of woody plants. Whereas trees, even more so newly and densely planted non-native species [10, 11, 15, 44] will struggle to survive the new climate trend.

It remains to be seen whether and if so, to what extent this intensification of vegetation on several millions of km² of desert border region may impact the regional climate in Northern China. In any case, it will be difficult to define a basis for such

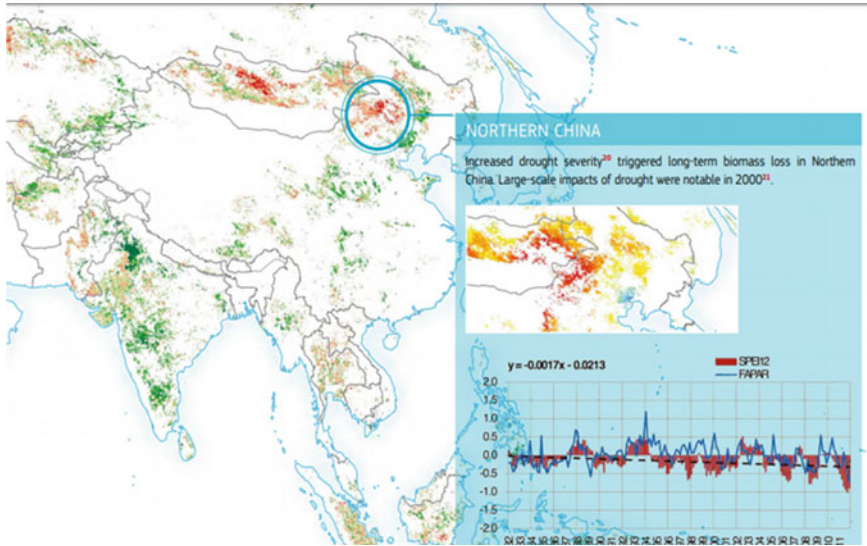


Fig. 1 Climate trend and biomass in Northern China, 1980–2010

Large map—areas of increase (green) and decrease of biomass (red) in China from 1980 to 2010
 Small map—increase in drought in Northern China from 1980 to 2010 (yellow—moderate, red—severe)

Time scale (bottom right): Red bars represent the deviation of precipitation from long-term median per year, 1982–2011. The blue line represents deviation—increase or decrease—of vegetation per year, showing some correlation with precipitation data *Source* World Atlas of Desertification (WAD) [13], European Commission, Joint Research Center Update 21.11.2018 [13]

comparison in climates and to exclude any impact of global parameters of climate change.

4 Strategies for Sustainable Revegetation

4.1 *Quality of Forests, Ecological Concepts with Native Plants*

Over recent decades, China has tackled the aim to restore desert bordering drylands over a range of almost 5,000 km in the North to prevent erosion and dust storms that drive sand and particles across the country. Active planting of forests was done by landowners, communities and was sometimes supported by the military [45]. Regions with wetter climates generally benefitted very well from these activities [46–48]. However, in drylands, the initial planting campaigns often used very limited numbers of tree species, thus were not necessarily adjusted to local climate, resulting in plant diseases and excessive damage from insects [49, 50]. Ecological mismatch

of tree species with local conditions sometimes led to the development of forests and shrubland of poor quality [10, 11, 15, 51], and the respective need for replacement by trees and shrubs of better ecological fit.

A regeneration concept, “natural restoration,” is used in China to plant and further the growth of native plant species. The process is taking time, but it certainly has its ecological advantages [52]. As an example of this concept Wang et al. [14] use the open elm woodlands that form the natural vegetation in some semi-arid areas of Northern China [14]. Species of this vegetation type were used as a reasonable choice to restore degraded land by creating sparse forests with open canopy in areas with 300–400 mm MAP.

Dry semi-arid savanna in China typically is formed by herbs and halophytic subshrubs with high water efficiency [1, 11]. It is therefore not showing the high evapotranspiration rates of fast-growing, sometimes not native species. Earlier or later the latter may have outgrown the soil water capacity resulting in hydro-ecological stress and high mortality rates during droughts. According to China state forestry statistics of the year 2017 [35] less than 25% of the total afforestation area of 3 million km² (2013) had remained as forested land [14]. In analysing the results of the various greening programs (summarized in Table 1) Wang et al. [14] find differences across the climate zones of Northern China in how the programs have achieved their purpose of an increased vegetation cover that should control desertification and reduce sand storm events. Typically, in arid and semi-arid climate water is the critical factor in the development of new vegetation, but despite having the highest increase in MAP the western region showed the lowest increase in vegetational cover. The potential reason given by Wang et al. [14] is that in the eastern and central parts, additional ecological engineering programs were run in parallel, whereas in the western region, only the TNSP had been implemented. They conclude that ecological measures of restoration and protection are factors that have contributed to the observed vegetational increase [14].

4.2 Ecological Solutions for Drylands in Other Countries

The recent planting of diverse and native species has introduced an increase in tree survival rates [18]. China is not the only country where monocultures have been planted on a large scale for an initial campaign. As we have reported earlier [17], the first “Green Dam” plantations of the 1970s over 1,500 km in Algeria with MAP of 200–300 mm were monocultures of Aleppo pine [53] planted over hundreds of km. Already in the 1980s these monocultures resulted in some denaturation of the soil, the native vegetation had been suppressed. Due to the poor ecological outcome, more diverse species were planted, including cropland and fruit gardens [54, 55], a diversity that led to improved ecosystem services.

Detailed lessons learned in Turkey were presented where planting schemes have been developed that take MAP and soil quality into account [12, 17]. Planting distances are adjusted to soil structure, ecological parameters, requirements of the

individual tree species, and local aridity. Maintenance work (thinning, weed removal) is considered important in later development stages of restoration. Optimal canopy cover was studied in Turkey to prevent erosion on steep slopes (25%) [56]. Crop, fruit trees, and spice plants were shown to be effective in erosion control, resulting in native, ecologically adapted vegetation, that even had some economic benefit.

4.3 Natural Succession as Effective Restoration Component

Since around the year 2006, China has started to implement the process of natural succession in drylands on a broader basis. For this method, called “natural reforestation” fields and grasslands are closed, allowing natural savannah vegetation to develop over years of undisturbed succession [18, 57]. China subsidizes farmers when they leave their fields and pastures for natural reforestation. As in more humid climates and degraded semi-arid drylands, the original ecosystems can recover by themselves when an external impact is removed [58]. However, measuring the outcome and success of natural reforestation activities is a challenge since there are thousands of individual areas with rather sparse vegetation to be assessed.

For a comparison of the effects of natural reforestation with those of active reforestation (planting), Gerlein-Safdi et al. [18] used Imaging Spectroradiometry at moderate resolution (MODIS) and an Enhanced Vegetation Index as remote sensing tool [18]. In addition, they applied new methods also to assess water content and photosynthetic activity in the restored vegetation areas. They were able to show for the first time that an increase in vegetation cover and biomass had taken place on areas where the natural reforestation method had been applied to China’s drylands. Shrubs and trees of the savanna that develop in natural succession are growing slowly and the process may take many years until a closed vegetation cover is gained [18]. In contrast, active planting will increase the vegetation signal immediately or only few years after plantation. Both, active and natural reforestation methods have led to increased productivity and biomass, which the authors find surprising for the active afforestation method since it often resulted in high tree mortality.

4.4 Nature of Climatically Adaptable Vegetation in Drylands

This is an encouraging result since a naturally developed vegetation cover has high biodiversity, enabling vegetation to adapt to potential climate changes. It will result in higher ecosystem services than planted forestations [59, 60]. A well thought ecological planting approach may use at least 5–10 different native species of trees and shrubs, planted in wide enough distances, similar to local examples of ecosystems found in the closer environment. This very likely would mimic certain grasslands, savanna-like ecosystems, or open woodlands for the climate zones in question.

Table 3 Advantages and disadvantages of active planting and natural succession

	Active planting (ecologically oriented)	Natural succession (natural reforestation)
Advantages	Native, ecologically adapted vegetation Predictable success within a short and foreseeable time Relatively easy to monitor progress and development	Native, ecologically adapted vegetation Due to the diversity of ecosystems vegetation is able to adapt to changes in climate in the most suitable way Sustainability and additional long-term benefits of ecosystems [59, 60] Low costs since no planting efforts and only limited maintenance is required
Disadvantages	High costs of: plant nursery, planting activity and long-term maintenance Remaining risk of vegetation that still is not 100% adjusted to (future) local water availability, i.e. risk of local hydrological stress	Takes a long time of natural development, i.e. years and decades of growth [18] Requires strong protection over one or more decades to allow for undisturbed growth

The advantages and disadvantages of such an ecological active planting approach are compared against those of natural succession methods in Table 3.

Obviously, even the most thoughtful ecological restoration by active planting will not reach the diversity of trees, shrubs, herbs, grasses, and microorganisms within a much shorter time than development in natural succession would take in the same location. So far, we do not know exactly for which degree of desertification the process of natural succession can be useful in drylands. It may have its limits [14], however, the use of the method in this climate seems too new to draw any conclusions.

We have suggested a hybrid method that combines active planting of twin green belts (native shrubs and trees) with the development of savannah vegetation in natural succession in the area between the two belts that, to some extent is protected from hot dry wind [16, 61]. These rather narrow twin belt modules are suggested to hydrologically connect existing areas of regional vegetation to form a hydrological network, and the method may extend the use of natural succession into more densely populated regions. We do not yet know whether concepts of creating an environment for natural succession that is somewhat protected from harsh semi-arid climate, particularly from constant dry wind, would have advantages on more severely degraded land. Also, the development of vegetation cover may occur in an accelerated way compared to unprotected areas. In general, the cost-effectiveness of natural succession and high adaptability of the resulting vegetation to climate changes seem to indicate superiority over other restoration methods.

As China (and other countries) have learned during the last century, only the ecologically adapted vegetation will have long-term survival chances in water-restricted environments. Adaptation and diversity are two sides of the same coin: Diverse ecosystems will contain individuals of a species (plant, animal, microorganism) that can adjust and, if a change in climatic condition, e.g. extended drought,

is not too severe—could thrive and develop better, thereby changing the ecosystem so that it fits to the new conditions.

5 Conclusions

Large-scale reforestation campaigns were started in China four to five decades ago. These are still being improved and vegetation areas are planned to be extended until 2030. World's largest restoration program is the sum of a variety of regional campaigns, it is a future-oriented initiative for which over not too long time its importance and successful reduction of erosion and mitigation of continental sand storms will become more and more evident. There are positive regional examples where we already find that revegetation efforts have improved local or regional climate parameters, such as Kubuqi desert [32] and Northern Jiangsu [39], the latter of which experienced a change to moderately sub-humid climate. These positive examples have in common that water is abundantly available despite the semi-arid climate due to high water table.

Reforestation in Jiangsu started 70 years ago, so it seems that in a semi-arid environment, the new vegetation needs to be given enough time to develop into a stable state. Conversely, this could mean that the true value of the large campaigns that started “only” 44 years ago should be reassessed 20 years from now. Many mistakes were reported to have been done in planting, leading to poor survival rates. Still, the lowest estimated percentage given with 15% [10] would have resulted in 10 billion viable adult trees! The idea was to answer large-scale desertification with a variety of large-scale revegetation efforts—this appears to be the right decision. However, with such huge program, it is “easy” to make mistakes, but China has learned from them and is already looking back on almost two decades of ecological learning and implementation of corrective action.

Trees have a long generation time of several decades. In contrast, climate parameters are changing rapidly with a trend to higher temperatures and rise in frequency and duration of drought events [62, 63], which per se already presents a high risk for any newly planted tree. The global rise in temperatures has been shown to cause tree mortality globally [64], with larger trees at higher risk [65]. This trend clearly needs to be taken into account when analyzing the outcome of planting efforts in China. Brodribb et al. [66] summarize the environmental situation of trees globally: The increase in aridity would require tree populations to adapt to higher intensities of water stress. The long generation times of most species were unlikely to allow adaptation and persistence given the rapid climate change. Genetic diversity is given as one of the factors of adaptative potential enabling trees to keep pace with the environmental changes [66].

The risks related to accelerated climate changes exist for all restoration methods, whether they use natural succession (natural reforestation) or active planting in an ecologically mindful way. The latter, however, still has a remaining intrinsic risk of failure because the selection of species or density of planting may not be precisely

adjusted to the climate of the near future. Numerous restoration programs and a multitude of methods have been applied in China, including the restriction of livestock browsing and the limitation of nomadic migration. Newer trends are the restoration of former monocultures more ecologically with higher numbers of native species, resulting in higher, more acceptable survival rates, and the closing of remote regions to let the new vegetation develop in undisturbed succession [18]. This method was systematically implemented on larger areas only 15 years ago—and it is surprising that we are already able to measure an increase in biomass in a rather early stage of ecosystem development [18].

Arguably it can be seen as an advantage that the discussion around carbon sequestration was not as present when China started the large-scale efforts 40–70 years ago. Given the foreseeable water constraints resulting from a changing climate [43], the success of these efforts in the first instance should be measured by their vegetational and climatic impact rather than by giga tons of carbon fixated. We should expect an important positive direct climatic impact that the new vegetation cover will have on regional, maybe even country level. The consolidation of vegetation in desert border regions has the potential to stabilize precipitation events and the hydrological cycle here. Zeng et al. [67] have found a net increase of permanent surface water from 2000 to 2015 in two of the TNSP afforestation regions that to some extent could have been caused by the vegetational increase here. Over long time China has seen the big picture in planning. Three generations, several hundred thousand Chinese people have made the large-scale implementation possible. It seems that now we need to be able to give the Chinese program two additional decades to develop and consolidate, to then measure its full impact, not only on dust storms and desertification—but also on wind speed, precipitation, groundwater table, humidity and regional temperatures.

6 Recommendations

We have learned that in the harsh arid climate of desert border regions, only ecologically well-adapted vegetation will survive, which in restoration often became evident within a relatively short time of one or a few decades [17]. Only vegetation with high “ecological value” will have high enough potential to adapt to the changes and challenges. The potential use of native vegetables, fruit trees, spice plants and other useful crops reported e.g., for Kubuqi desert (China) and Turkey [32, 56] should be further evaluated in erosion control, as part of an ecologically adapted restoration.

Restoration in drylands based on natural succession will take a long time, but the method should be considered superior to afforestation in terms of sustainability because the resulting vegetation will be highly adaptable. A restoration model combining the planting of native shrubs and trees with areas of natural succession was suggested to achieve protection by the planted woody greenbelts and the vegetation-ecological advantages of succession to occur between them [61]. It remains to be investigated whether such protection and assistance (e.g., soil treatment) would expedite the successional development of native vegetation.

Acknowledgements The authors are grateful to Professor Dr. Klaus Becker, Hohenheim University, Germany, for all advice and constructive discussion.

References

1. Wang X, Chen F, Hasi E, Li J (2008) Desertification in China: an assessment. *Earth Sci Rev* 88:188–206. <https://doi.org/10.1016/j.earscirev.2008.02.001>
2. Otterman J (1974) Baring high-albedo soils by overgrazing: a hypothesized desertification mechanism. *Science* 186:531–533
3. Ibanez J, Martinez J, Schnabel S (2007) Desertification due to overgrazing in a dynamic commercial livestock–grass–soil system. *Ecol Model* 205:277–288
4. D’Odorico P, Bhattachan A, Davis KF, Ravi S, Runyan CW (2013) Global desertification: drivers and feedbacks. *Adv Water Resour* 51:326–344
5. Bestelmeyer BT, Okin GS, Duniway MC, Archer SR, Sayre NF, Williamson JC, Herrick JE (2015) Desertification, land use, and the transformation of global drylands. *Front Ecol Environ* 13:28–36
6. Xue Z, Qin Z, Cheng F, Ding G, Li H (2017) Quantitative assessment of aeolian desertification dynamics—a case study in north Shanxi of China (1975–2015). *Sci Rep* 7:10460
7. Zhang CL, Li Q, Shen YP, Zhou N, Wang XS, Li J, Jia WR (2018) Monitoring of aeolian desertification on the Qinghai-Tibet Plateau from the 1970s to 2015 using Landsat images. *Sci Total Environ* 619–620:1648–1659
8. Wang X, Yang Y, Dong Z, Zhang C (2009) Responses of dune activity and desertification in China to global warming in the twenty-first century. *Glob Planet Change* 67:167–185
9. Wang F, Zhao X, Gerlein-Safdi C, Mu Y, Wang D, Lu Q (2017) Global sources, emissions, transport and deposition of dust and sand and their effects on the climate and environment: a review. *Front Environ Sci Eng* 11:12270–12279
10. Cao S (2008) Why large-scale afforestation efforts in China have failed to solve the desertification problem. *Environ Sci Technol* 42:1826–1831
11. Cao S, Chen L, Shankman D, Wang C, Wang X, Zhang H (2011) Excessive reliance on afforestation in China’s arid and semi-arid regions: lessons in ecological restoration. *Earth Sci Rev* 104:240–245
12. Boydak M, Caliskan S (2015) Afforestation in arid and semi-arid region; Chapter 5.1.3. “Spacings in the arid and semi-arid afforestation sites”. Republic of Turkey, Ministry of Forestry and Water Affairs. General Directorate of Combating Desertification and Erosion ISBN: 978-605-4610-84-6
13. WAD—World Atlas of Desertification (2018) European Commission, joint research center update 21.11.2018. <https://wad.jrc.ec.europa.eu/>
14. Wang F, Pan X, Gerlein-Safdi C, Cao X, Wang S, Gu L, Wang D, Lu Q (2019) Vegetation restoration in Northern China: a contrasted picture. *Land Degrad Dev* 2019:1–8
15. Jin TT, Fu BJ, Liu GH, Wang Z (2011) Hydrologic feasibility of artificial forestation in the semi-arid Loess Plateau of China. *Hydrol Earth Syst Sci*, 15, 2519–2530. www.hydrol-earth-syst-sci.net/15/2519/2011/. <https://doi.org/10.5194/hess-15-2519-2011>
16. Huebner L (2020) Large Scale Afforestation in Arid and Semi-Arid Climate: Hydrologic-ecological lessons learned and concept of modular hydrologic connectivity of vegetation. *J Agr Food Dev* 6:1–12
17. Huebner L, Al-Quraishi AMF (2022) Desertification in Algeria and Turkey: climate change leading to “natural selection” of restoration concepts. In: Al-Quraishi AMF and Mustafa YT (eds) *Natural resources deterioration in MENA region: Land deterioration, soil erosion, and desertification. Springer - in preparation.*

18. Gerlein-Safdi C, Keppel-Aleks G, Wang F, Frohling S, Mauzerall DL (2020) Satellite monitoring of natural reforestation efforts in China's Drylands. *One Earth* 2:98–108
19. Zhuge W, Yue Y, Shang Y (2019) Spatial-temporal pattern of human-induced land degradation in Northern China in the Past 3 decades—RESTREND approach. *Int J Environ Res Pub Health* 16:2258. <https://doi.org/10.3390/ijerph1613225>
20. Zhang P, Shao G, Zhao G, Le Master DC, Parker GR, Dunning JB, Li Q (2000) Ecology-China's forest policy for the 21st century. *Science* 288:2135–2136
21. He FN, Ge QS, Dai JH (2008) Rao YJ (2008) Forest change of China in recent 300 years. *J Geogr Sci* 18:59–72
22. Wang T, Zhu Z (2003) Study on Sandy desertification in China. *J Des Res* 23:209–214
23. Wang X, Lu C, Fang J, Shen Y (2007) Implications for development of grain-for-green policy based on cropland suitability evaluation in desertification-affected north China. *Land Use Policy* 24:417–424
24. Jiang Z, Jiang J, Wang Y, Zhang E, Zhang Y, Li L, Cai B, Luo Z, Li C, Ping X et al (2016) China's ecosystems: overlooked species. *Science* 2016(353):657
25. Huang J, Yu H, Guan X, Wang G, Guo R (2015) Accelerated dryland expansion under climate change. *Nat Clim Chang* 6:166–171. <https://doi.org/10.1038/nclimate2837>
26. Liu JG, Diamond J (2005) China's environment in a globalizing world. *Nature* 435:1179–1186
27. Sun DF, Li H, Dawson R, Tang CJ, Li XW (2006) Characteristics of steep cultivated land and the impact of the Grain-for-Green Policy in China. *Pedosphere* 16:215–223
28. Wang F, Pan X, Wang D, Shen C, Lu Q (2013) Combating desertification in China: past, present and future. *Land Use Policy* 31:311–313. <https://doi.org/10.1016/j.landusepol.2012.07.010>
29. Bryan BA, Gao L, Ye Y, Sun X, Connor JD, Crossman ND, Hou X (2018) China's response to a national land-system sustainability emergency. *Nature* 559:193–204. <https://doi.org/10.1038/s41586-018-0280-2>
30. Lyu Y, Yang Y, Guo L, Liu L, Shi P, Zhang G, Qu Z, Hu X, Wang J, Xiong Y et al (2016) Desertification and blown sand disaster in China. *J Agric Sci Technol A* 6:363–371
31. Lyu Y, Shi P, Han G, Liu L, Guo L, Hu X, Zhang G (2020) Desertification control practices in China. *Sustainability* 12:3258. <https://doi.org/10.3390/su12083258>
32. UNEP (2015) Review of the Kubuqi ecological restoration project: a desert green economy pilot initiative. United Nations Environment Programme, Nairobi
33. Yang L (2018) Kubuqi a successful example of desert greening. *China Daily*, Updated: 2018-08-06
34. State Forestry Administration (2014) Opinions of the state forestry administration on deepening the construction and reform of the Three North Shelterbelt Development Program. <http://www.forestry.gov.cn/sbj/5055/1549/4.html>
35. State Forestry Administrator (2017) China forestry statistical yearbook 2016. China Forestry Press, Beijing, China
36. Wang Y, Shao M, Zhang X (2008) Soil moisture ecological environment of artificial vegetation on steep slope of loess region in north Shaanxi province, China. *Acta Ecol Sin* 28:3769–3778
37. Zheng X, Zhu JJ, Yan QL, Song LN (2012) Effects of land use changes on the groundwater table and the decline of *Pinus sylvestris* var. *mongolica* plantations in Southern Horqin Sandy Land, Northeast China. *Agric Water Manage* 109:94–106
38. Li H, Xu F, Li Z, You N, Zhou H, Zhou Y, Chen B, Qin Y, Xiao X, Dong J (2021) Forest changes by precipitation zones in Northern China after the Three-North Shelterbelt forest program in China. *Remote Sens* 13:543. <https://doi.org/10.3390/rs13040543>
39. Zhuang J-Y, Zhang J-C, Yang Y, Zhang B, Li J (2017) Effect of forest shelter-belt as a regional climate improver along the old course of the Yellow River, China. *Agroforest Syst* 91:393–401
40. Becker K, Wulfmeyer V, Berger T, Gebel J, Muench W (2013) Carbon farming in hot, dry coastal areas: an option for climate change mitigation. *Earth Syst Dyn* 4:237–251
41. Yosef G, Walko R, Avisar R, Tatarinov F, Rotenberg E, Yakir D (2018) Large-scale semi-arid afforestation can enhance precipitation and carbon sequestration potential. *Nat Sci Rep* 8:996
42. Branch O, Wulfmeyer V (2019) Deliberate enhancement of rainfall using desert plantations. *Proc Natl Acad Sci USA* 116(38):18841–18847

43. Jiao W, Wang L, Smith WK, Chang Q, Wang H, D'Odorico P (2021) Observed increasing water constraint on vegetation growth over the last three decades. *Nat Comm* 12:3777. <https://doi.org/10.1038/s41467-021-24016-9>
44. Cao S, Sun G, Zhang Z, Chen L, Feng Q, Fu B, McNulty S, Shankman D, Tang J, Wang Y, Wei X (2011) Greening China naturally. *Ambio* 40:828–831. <https://doi.org/10.1007/s13280-011-0150-8>
45. Osborne S (2018) China reassigns 60,000 soldiers to plant trees in bid to fight pollution. *The Independent* <https://www.independent.co.uk/news/world/asia/china-tree-plant-soldiers-reassign-climate-change-globalwarming-deforestation-a8208836.html>
46. Chen Y, Wang K, Lin Y, Shi W, Song Y, He X (2015) Balancing green and grain trade. *Nat Geosci* 8:739–741
47. Tong X, Brandt M, Yue Y, Horion S, Wang K, De Keersmaecker W, Tian F, Schurgers G, Xiao X, Luo Y et al (2018) Increased vegetation growth and carbon stock in China karst via ecological engineering. *Nat Sustain* 1:44–50
48. Chen C, Park T, Wang X, Piao S, Xu B, Chaturvedi RK, Fuchs R, Brovkin V, Ciais P, Fensholt R et al (2019) China and India lead in greening of the world through land-use management. *Nat Sustain* 2:122–129
49. Liu J, Li S, Ouyang Z, Tam C, Chen X (2008) Ecological and socioeconomic effects of China's policies for ecosystem services. *Proc Natl Acad Sci USA* 105(28):9477–9482. <https://doi.org/10.1073/pnas.0706436105>
50. Stone R (2009) Nursing China's ailing forests back to health. *Science* 325:556–558. https://doi.org/10.1126/science.325_556
51. Zhu JJ, Zheng X, Wang GG, Wu BF, Liu SR, Yan CZ, Li Y, Sun YR, Yan QL, Zeng Y, Lu SL, Li XF, Song LN, Hu ZB, Yang K, Yan NN, Li XS, Gao T, Zhang JX, Ellison AM (2017) Assessment of the world largest afforestation program: success, failure, and future directions. Preprint bioRxiv Preprint Server Biol 2017. <https://doi.org/10.1101/105619>
52. Liu X, Zhang W, Cao J, Yang B, Cai Y (2018) Carbon sequestration of plantation in Beijing-Tianjin sand source areas. *J Mt Sci* 15:2148–2158
53. CEN-SAD (2008) The great green wall initiative for the Sahara and the Sahel. Introductory Note Number 3. OSS: Tunis. ISBN: 978-9973-856-27-2, S.44 ff. <http://www.fao.org/3/a-ax355e.pdf>
54. Saifi M, Boulghobra N, Fattoum L (2015) The Green Dam in Algeria as a tool to combat desertification. In: *Planet@Risk* 3(1):68–71. Global Risk Forum GRF Davos, Davos
55. Azzouzi SA, Pantaleoni AV, Bentounes HA (2018) Monitoring desertification in Biskra, Algeria using Landsat 8 and Sentinel-1A images. 2018 IEEE Access. *IEEE Access* PP(99):1–1. <https://doi.org/10.1109/ACCESS.2837081>
56. Acar A, Gül A, Bilgin F (2006) Erozyon kontrolünde bazı bitki türlerinin toprağı kapatma oranları ile üst toprak kaybını önleme yetenekleri arasındaki ilişkiler. *Türkiye'de Kurak Bölgelerde yapılan Ağaçlandırma ve Erozyon Kontrolü Uygulamalarının Değerlendirilmesi Çalıştayı* (7–10 Kasım, Ürgüp-Nevşehir), Cilt I, pp 172–182, On Ofset, Ankara
57. Li J, Yang X, Jin Y, Yang Z, Huang W, Zhao L, Gao T, Yu H, Ma H, Qin Z et al (2013) Monitoring and analysis of grassland desertification dynamics using Landsat images in Ningxia, China. *Remote Sens Environ* 138:19–26
58. Martinez-Valderrama J, Ibanez J, Del Barrio G, Sanjuan ME, Alcalá FJ, Martinez-Vicente S, Ruiz A, Puigdefabregas J (2016) Present and future of desertification in Spain: implementation of a surveillance system to prevent land degradation. *Sci Total Environ* 563–564:169–178
59. Li FR, Zhang H, Zhao LY, Shirato Y, Wang XZ (2003) Pedoecological effects of a sand-fixing poplar (*Populus simonii* Carr.) forest in a desertified sandy land of Inner Mongolia. *China. Plant Soil* 256:431–442
60. Chazdon RL (2008) Beyond deforestation: restoring forests and ecosystem services on degraded lands. *Science* 320:1458–1460
61. Huebner L, Al-Quraishi AMF, Branch O, Gaznayee HAA (2022) Sustainable renaturation in desertification control: expediting natural succession of large-scale vegetation in drylands. In: Walker T, Wendt S, Goubran S, Schwartz T (eds) *Beyond the 2 °C: business and policy trajectories to climate change adaptation*. Palgrave-Macmillan.

62. Elliott KJ, Miniati CF, Pederson N (2015) Laseter SH (2015) Forest tree growth response to hydroclimate variability in the southern Appalachians. *Glob Change Biol* 21:4627–4641
63. Piao S, Yin G, Tan J, Cheng L, Huang M, Li Y, Liu R, Mao J, Myneni RB, Peng S et al (2015) Detection and attribution of vegetation greening trend in China over the last 30 years. *Glob Change Biol* 21:1601–1609
64. Allen CD, Macalady AK, Chenchouni H, Bachelet D, McDowell NG et al (2010) A global overview of drought and heat-induced tree mortality reveals emerging climate change risks for forests. *For Ecol Manage* 259:660–684
65. Bennett AC, McDowell NG, Allen CD, Anderson-Teixeira KJ (2015) Larger trees suffer most during drought in forests worldwide. *Nat Plants* 1:15139
66. Brodribb TJ, Powers J, Cochard H, Choat B (2020) Hanging by a thread? forests and drought. *Science* 368:261–266
67. Zeng Y, Yang X, Fang N, Shi Z (2020) Large-scale afforestation significantly increases permanent surface water in China's vegetation restoration regions. *Agr For Met* 290. <https://doi.org/10.1016/j.agrformet.2020.108001>

Estimation of Satellite-Based Regional-Scale Evapotranspiration for Agriculture Water Management Using Penman–Monteith Method



Satiprasad Sahoo, Tanushree Basu Roy, Anirban Dhar,
and Anupam Debsarkar

Abstract Evapotranspiration (ET) is one of the important parameters in the hydrological cycle affecting water resource availability. Estimating surface evapotranspiration is essential for water resources evaluation, drought monitoring, crops production simulation, and providing guidance for crop water needs in irrigated lands. Reference evapotranspiration (ET₀), is a representation of efficient water management for environmental demand. Environmental degradation is crucial for humankind over the past few decades. Thus, hydro-environmental management is required for future sustainable planning purposes. The present study estimates the monthly reference evapotranspiration (ET₀) based on the FAO Penman–Monteith method using the Landsat 7 ETM + and Landsat 8 OLI seasonal data of 2014, 2015, and 2016 over the Dwarakeswar—Gandheswari river basin. Required model input parameters are emissivity, land surface temperature (LST), net radiation, soil heat flux (G), air temperature, actual & saturation vapor pressure, and wind speed. Correlation analyses have been performed of ET and field-based soil moisture data in the proposed command area. Finally, results are validated by using MODIS LST for estimated LST and MODIS ET for estimated ET. Moreover, assessment of regional-scale based evapotranspiration is a challenge to the agricultural and hydrological frame. This analysis demonstrates the potential applicability of this methodology.

S. Sahoo (✉)

Geoinformatics Division, International Institute of Geospatial Science and Technology, Kolkata, India

e-mail: satisps@gmail.com

T. B. Roy

Department of Remote Sensing & GIS, Vidyasagar University, Midnapore, India

e-mail: tanushreebasuroy@gmail.com

A. Dhar

Department of Civil Engineering, Indian Institute of Technology Kharagpur, Kharagpur, India

e-mail: anirban@civil.iitkgp.ernet.in

A. Debsarkar

Department of Civil Engineering, Jadavpur University, Kolkata, India

e-mail: anupamju1972@gmail.com

© The Author(s), under exclusive license to Springer Nature Switzerland AG 2022

A. M. F. Al-Quraishi et al. (eds.), *Environmental Degradation in Asia*,

Earth and Environmental Sciences Library,

https://doi.org/10.1007/978-3-031-12112-8_29

Keywords Evapotranspiration · Land Surface Temperature · Net radiation · PAO-56 Penman Monteith · LANDSAT · MODIS · Remote Sensing

1 Introduction

Estimation of ET is essential to know how much water is required during the growing season, to improve crop water management and hydrological applications. ET is the process that accounts for a large portion of the hydrological water budget. On the land surface, an average of about 60% of the precipitation received is returned to the atmosphere through ET.

Moderate numbers of studies are available for the estimation of ET using remote sensing techniques. Calculation of reference crop ET based on Penman evaporation equation using available weather data [1]. Tsouni et al. [2] estimated daily ET for all the 21 days of the study period using the FAO Penman–Monteith, Carlson–Buffum, and Granger method in the Thessaly plain, Greece. Spatiotemporal distribution of ET estimation based on SEBAL model in South–Central Nebraska [3]. Simulation of ET estimation using empirical methods from groundwater under different soil conditions is available in [4]. Evaluation of ET of an oasis–desert transition zone using the Penman–Monteith model in the middle stream of Heihe River, China [5]. Quantification of predicting ET using remote sensing techniques in the mixed vegetation surface areas [6]. Ficklin et al. [7] estimate Palmer Drought Severity Index (PDSI) using Penman–Monteith PET method for current and future drought projections.

Li et al. [8] studied the assessment of ecosystem ET dynamics using the Priestley–Taylor parameter in eastern Inner Mongolia, China. Wang et al. [9] estimated ET under multi-scale conditions using “thermal infrared remote sensing and three-temperature model” in the Zhangye oasis and adjacent Gobi and desert, northwest China. Estimation of ET based on the Simplified Surface Energy Balance (SSEBoP) model for the spatial distribution of water mapping in the Colorado River Basin [10]. Yao et al. [11] reported that the evaporative drought index (EDI) had been used to monitor China’s surface dryness conditions based on the ET model and Hargreaves equation from JAXA-MODIS Insolation products, GEWEX, NCEP-2, and MODIS NDVI data. Groundwater ET estimation is based on empirical equations from irrigated cropland areas [9]. ET’s future scenarios use the Hadley Centre Coupled Model version 3 data for crop production and water balance framework [12]. The Impact of ET formulations for various elevations for various climatic conditions of meteorological drought assessment [13]. Raoufi and Beighley [14] studied daily global ET estimation based on the Penman–Monteith method using land surface temperature (LST) for the period 2000–2013.

The relationship between the surface resistance and remotely sensed stress index based on modified Penman–Monteith in the semi-arid region of Tensift Al Haouz (Morocco) for optimizing irrigation management is available in [15]. Assessments of global and regional scale surface fluxes based on the Penman–Monteith model, Priestley–Taylor Jet Propulsion Laboratory model (PTJPL), and the Global Land

Evaporation Amsterdam Model (GLEAM) is available in [16]. Rozenstein et al. [17] studied cotton ET estimation based on eddy covariance, surface renewal, and heat pulse using Sentinel-2 satellite imagery in the cotton field near Gedera, in the Shfela region in Israel.

Jahanfar et al. [18] performed refined water budget analysis using a modified FAO ET model for Green Roof systems. Fernandes et al. [19] studied the estimation of water use efficiency (WUE) from Moderate Resolution Imaging Spectroradiometer (MODIS) data in the Cerrado of Minas Gerais State (western part of Minas Gerais). Wu et al. [20] identified crop drought index through the Two-Source Energy Balance (TSEB) model for monitoring and assessing winter wheat drought disasters. In a more recent paper, evapotranspiration estimation based on surface energy balance models using satellite data for sustainable agriculture water management [21–26].

However, the middle to upper portions of the river basin is high water stress areas. A Command area is proposed for agricultural water management in the middle portion of the river basin. Moderate-resolution satellite data are used for accurate ET estimations for these different years at a regional scale. Moreover, the estimated seasonal ET is very needful for regional-scale hydro-environmental (e.g., drought) planning and management framework. The proposed methodology is applied to Dwarakeswar—Gandheswari river basin, West Bengal, India.

2 Study Area

Dwarakeswar River is a major river in the western part of West Bengal in India (Fig. 1). The detailed information on the Dwarakeswar- Gandheswari river basin is available in [27]. Penman–Monteith is the best method for ET calculation compared to other methods [28]. Using satellite data, seasonal ET estimation has been performed in the small river basin.

3 Materials and Methods

Figure 2 presents the methodology adopted in the chapter in more detail in the following subsections.

3.1 Data Sources

Landsat 8 OLI (2014–2016 and Path:139–140, Row: 044) and MODIS (MODIS/Terra and MOD16) data were collected from the Earth Explorer, United

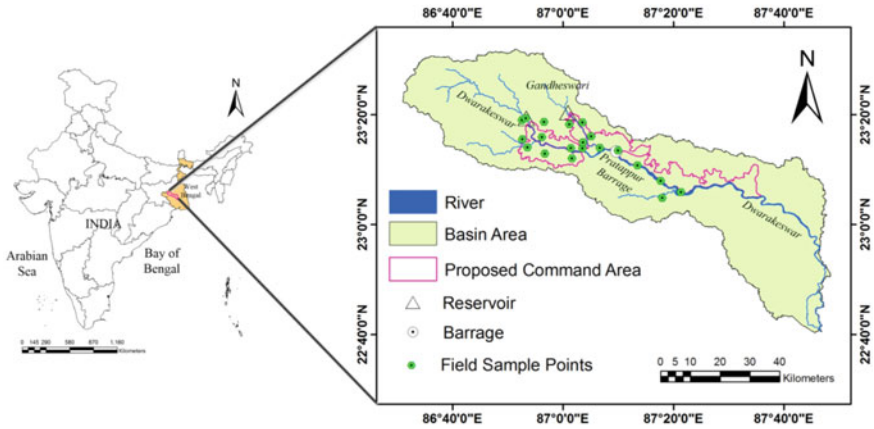


Fig. 1 Location map of the study area

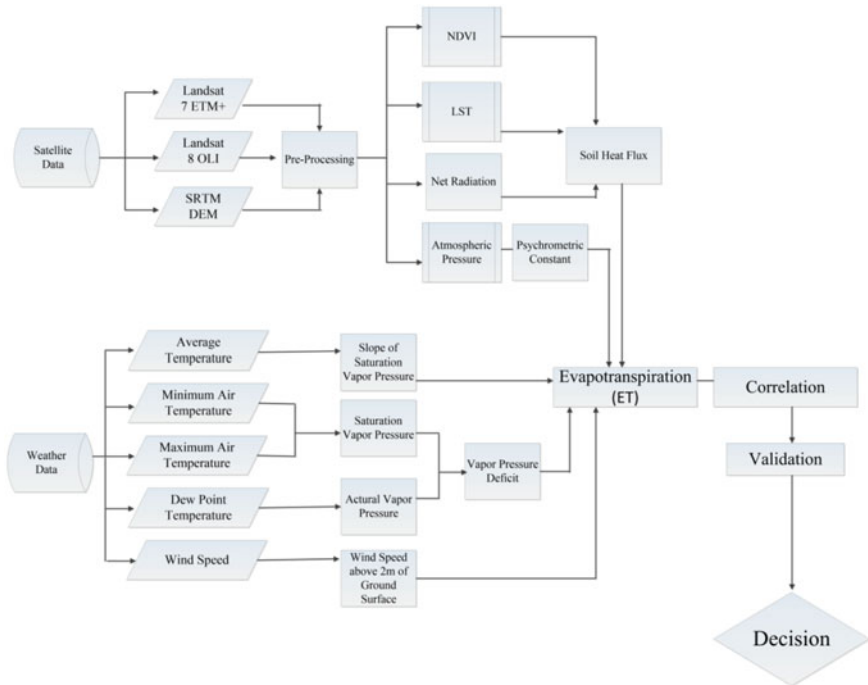


Fig. 2 Overall Methodology

States Geological Survey (USGS) (<http://glovis.usgs.gov/>). Weather data are collected from the NASA Prediction of Worldwide Energy Resources power.larc.nasa.gov site.

3.2 Methodology

3.2.1 Image Pre-processing

The images were collected in different time periods under different solar illumination, so the Sun angle correction was necessary. After Sun angle correction, the DN values of the images were converted to radiance.

Estimation of Evapotranspiration (ET)

An updated equation is recommended by FAO [28] with the FAO-56 Penman–Monteith Equation. Simplify the equation by using assumed constant parameters for a clipped grass reference crop. It was assumed that the definition for the reference crop is a hypothetical reference crop with a crop height of 0.12 m, a fixed surface resistance of, $70sm^{-1}$ and an albedo value of 0.23 [29].

The new equation is:

$$ET_0 = \frac{0.408\Delta(R_n - G) + \gamma \frac{900}{T+273} u_2 (e_s - e_a)}{\Delta + \gamma(1 + 0.34u_2)}$$

where ET_0 is the reference evapotranspiration ($mm\ day^{-1}$); R_n is the net radiation ($MJ\ m^{-2}d^{-1}$); G is the soil heat flux ($MJ\ m^{-2}d^{-1}$); T is the mean daily air temperature at 2 m height ($^{\circ}C$); u_2 is the wind speed at 2 m height ($m\ s^{-1}$); e_s is the saturation vapor pressure (kPa); e_a is the actual vapor pressure (kPa); $e_s - e_a$ is the saturation vapor pressure deficit (kPa); Δ is the slope of the vapor pressure curve ($kPa\ ^{\circ}C$); γ is the psychrometric constant ($kPa\ ^{\circ}C$).

4 Results and Discussion

4.1 Spatiotemporal Variations of Evapotranspiration

Based on the distribution of ET values in January 2014, 2015, and 2016, ET was very high in the higher elevated area of the basin, over Susanna hill, Tilaboni hill, Futiaryi dam, Saheb Bandh lake and in the Jangalmahal, Beliature forest area (Fig. 3). The ET values are also high in the West Midnapore, Hooghly, Purulia, and Bankura district over the study area. ET values are very low in the sandy region and the Burdwan

district over the area. This value has gradually increased from 2014 to 2016. The minimum value of ET was found in the Purulia district and in the sandy region. In March, Higher ET value (>120 mm) was found in the Hooghly, West Midnapore, Burdwan and western part of the Bankura district over the study area, and as usual in the higher elevated area of the basin. The maximum portion of the study area is occupied by a medium ET value. In May 2014, the highest ET value was found in the Jangalmahal area, a little bit portion of the Hooghly, West Midnapore and Bankura district. However, in 2016, some portion of the Purulia is also showing a higher ET value.

In June 2014, the lower part of the river basin showed higher ET values, and in the Jangalmahal area, some portions of the Purulia district's ET values are high. In August 2014, the higher ET value was found in the upper part of the river basin, which includes the Purulia district over the study area and the Beliatare forest, Jangalmahal, Joypur jungle area. In September 2015, ET was very high (>152 mm) in the monsoonal flood zone, which includes the western part of Bankura, West Midnapore, Burdwan, and Hooghly district over the study area and also in the Susunia hill. In October 2014, 2015, 2016, higher ET value was found almost every portion of the study area. Susunia hill is showing the highest value as well as the lake, dam,

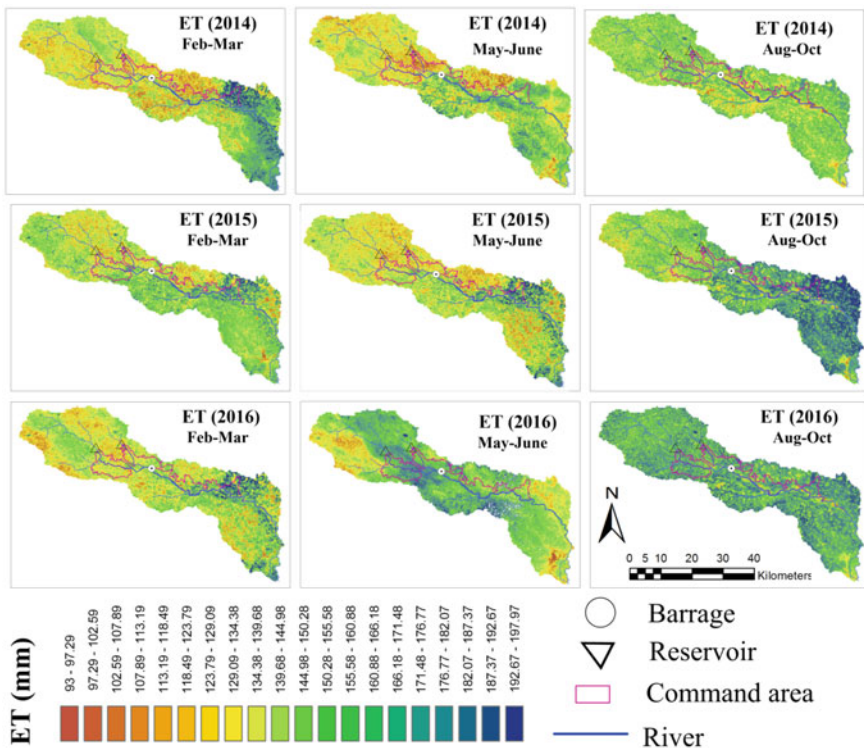


Fig. 3 Satellite-based ET mapping for Dwarakeswar-Gandheswari river basin

and forest areas. ET value was low in the sandy region. The result of ET values for October month in these three years does not vary very much.

Moreover, it could be said that the ET variation in this study area is closely related to crop growth (Fig. 4). The Hilly area and the water body like the dam and lake always show a high ET value. ET values are always lower in the sandy region and the settlement area.

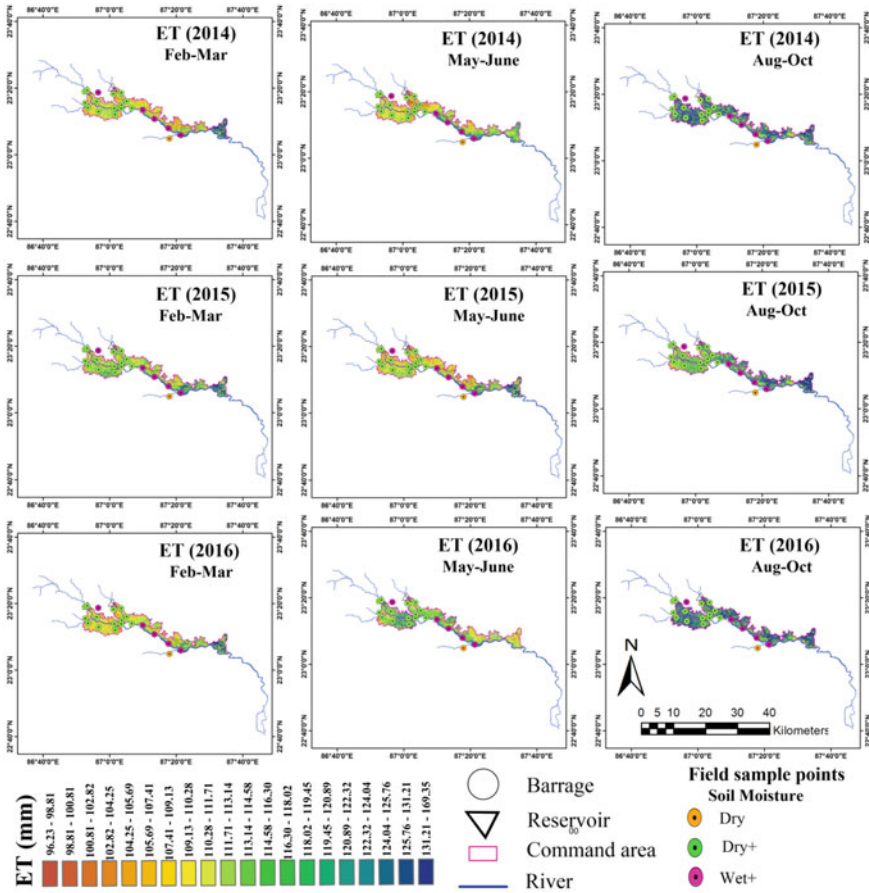


Fig. 4 Estimation of ET for proposed command area with field-based validation points

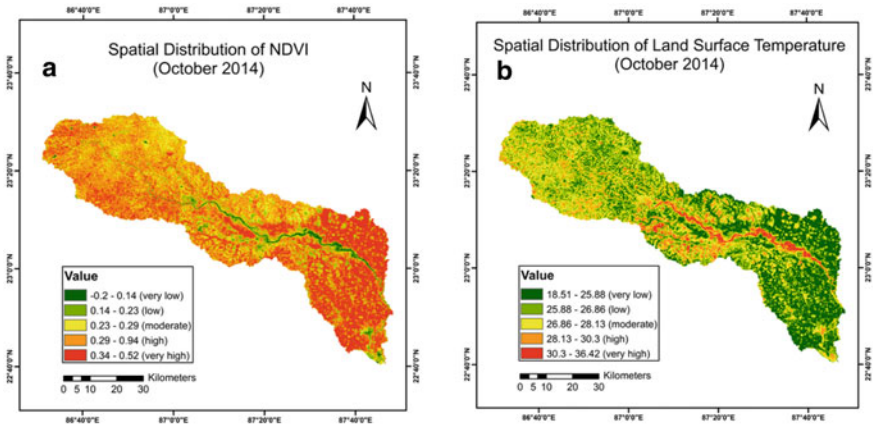


Fig. 5 a Spatial distribution of NDVI & b LST in October 2014

4.2 Correlation Analysis

4.2.1 NDVI and LST

The NDVI has been widely used for determining temporal LST changes. These images show that where NDVI values are high, LST values are low due to vegetation cover. Thus NDVI and LST represent a strong negative correlation. The water body is a special case, where both NDVI and LST values tended to be the lowest value (Fig. 5).

4.2.2 LST and Soil Heat Flux

The soil heat flux (G) is the energy that is heating the soil. Soil heat flux is positive when the soil is warming and negative when the soil is cooling. Thus Soil heat flux depends on Surface temperature and represents a positive correlation (Fig. 6).

4.2.3 NDVI and ET

Evapotranspiration is strongly related to vegetation. It is an essential component for assessing vegetation dynamics. Thus NDVI is an important variable for evapotranspiration, representing a significant positive relationship with ET (Fig. 7).

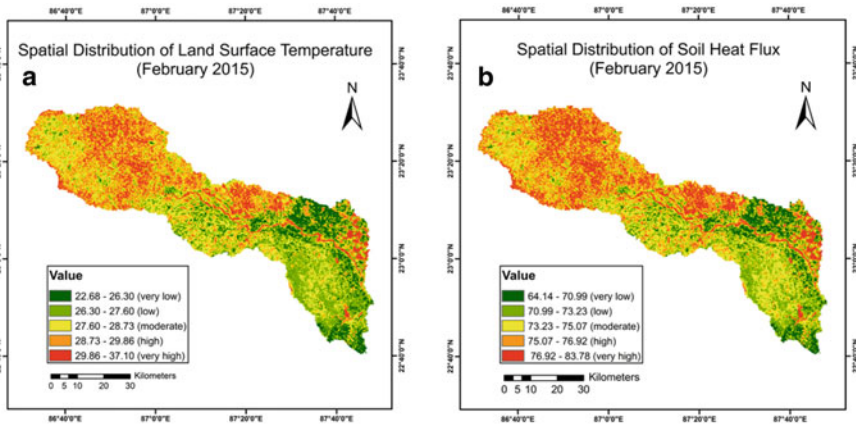


Fig. 6 a Spatial distribution of LST and b Soil heat flux in february 2015

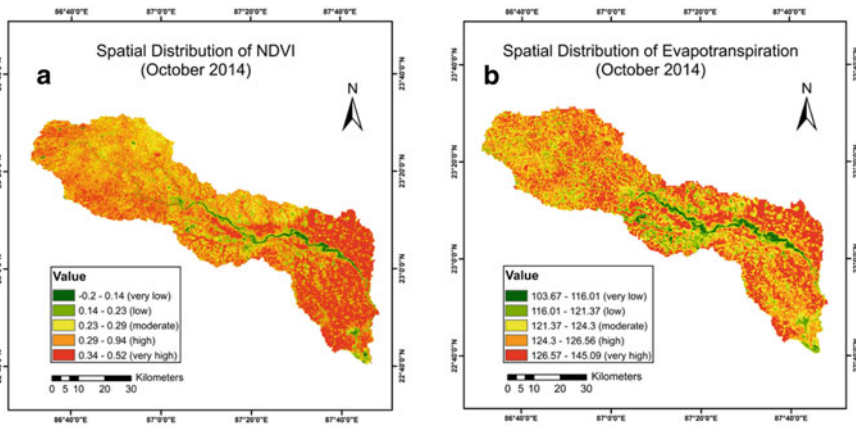


Fig. 7 a Spatial distribution of NDVI and b ET in October 2014

4.2.4 LST and ET

Evapotranspiration and LST maintain a negative relationship. Land surfaces with larger ET have lower LST. At the same time, air temperature, air humidity, wind speed, and solar radiation remain homogeneous over the land surfaces of interest (Fig. 8).

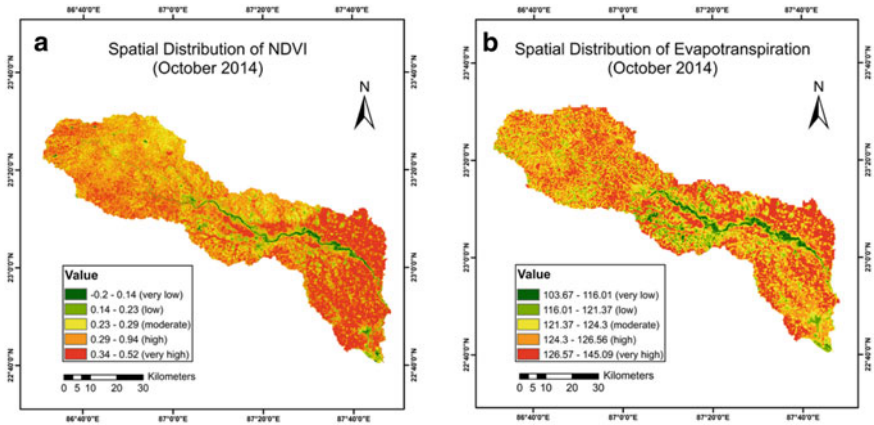


Fig. 8 a Spatial distribution of LST and b ET in October 2014

4.2.5 Net Radiation (R_n) and ET

Net radiation is the total energy that is available to influence the climate. The net radiation of the surface consists of the direct and diffused radiation and the atmospheric emission absorbed and retained by the surface. Therefore, evapotranspiration is strongly dependent on net radiation and represents a positive correlation (Fig. 9).

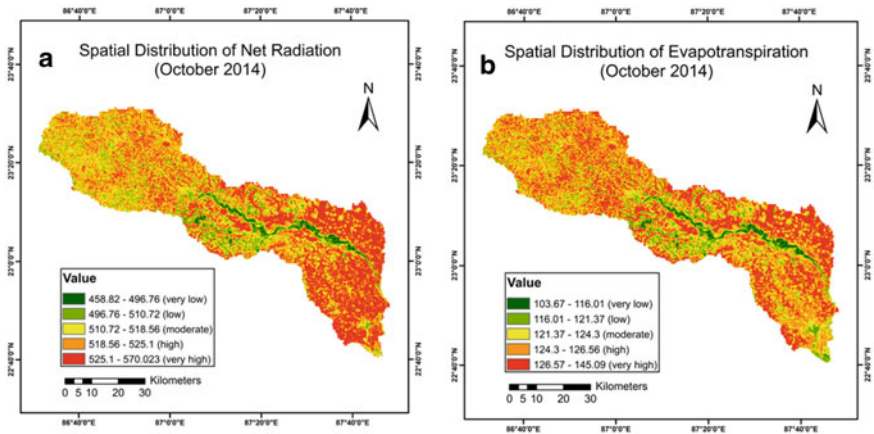


Fig. 9 (A) Spatial distribution of Net Radiation and (B) ET in October 2014

Table 1 Comparison between the estimated and the observed results of LST in 2015

Months	Minimum LST (°C)				Maximum LST (°C)			
	Estimated value	Observed value	Absolute error	Relative error (%)	Estimated value	Observed value	Absolute error	Relative error (%)
Feb-Mar	24.03	26.75	2.72	11.31918	36.57	37.07	0.5	1.367240
May-Jun	24.16	27.87	3.71	15.35596	31.21	37.45	6.24	19.99359
Aug-Oct	25.51	29.29	3.78	14.81771	36.23	36.59	0.36	0.993651

Table 2 The estimated and the observed results of ET in 2015

Month	Minimum ET (°C)				Maximum ET (°C)			
	Estimated value	Observed value	Absolute error	Relative error (%)	Estimated value	Observed value	Absolute error	Relative error (%)
Feb-Mar	100.399	94.2	6.199	6.1743	114.12	106.3	7.82	6.8524

4.3 Validation

4.3.1 Validation of Land Surface Temperature with MODIS LST

To validate the result of LST Table 1 was made to estimate the absolute and relative error between observed LST values collected from the C6 MODIS LST product (MOD11_L2) and estimated LST values using the above equations.

For minimum LST values, the maximum and absolute minimum errors are respectively 5.05 °C (relative error 26.5%) and 2 °C (relative error 10.9%). The maximum and absolute minimum error for maximum LST values are respectively 4.18 °C (relative error 14.8%) and 0 °C (relative error 0%). These results indicate that this LST estimation method has a small error that may be due to cloud cover, haze, or noise.

4.3.2 Validation of Evapotranspiration with MODIS ET

The estimated ET image of February 2015 was compared to the MODIS ET product in the same month and year (Table 2). For minimum ET values, the absolute error is 6.12 (relative error of 6.17%) and for maximum ET values, the absolute error is 7.82 (relative error of 6.85%).

5 Discussion

The ET estimation is very important for regional scale (e.g. River basin) using satellite-derived data. Penman–Monteith method is used for seasonal/monthly ET

estimation purposes using a GIS environment. All utilized parameters are derived through meteorological and satellite data. Four satellite data (SRTM, Landsat ETM + , Landsat OLI, and MODIS) are used for ET calculation. Seven MODIS/Terra LST/Emissivity 8-Day L3 Global 1 km SIN Grid products (MOD11_A1) are utilized for LST [30]. The MODerate Resolution Imaging Spectrometer (MOD16) global ET (MOD16A2) dataset is used for validation purposes [31]. The results show inconsistent comparisons with MOD16 ET. Seasonal time periods (Feb-Mar, May-June, and Aug-Oct) are considered for 2014, 2015, and 2016. The limitation of the research is that rainy season images could not be used due to high clouds, haze, and noise. The collected data used in the model directly affects the accuracy of the ET. The model involves many parameters, and errors in each parameter can affect the calculated results. Further, it is required high spatial resolution satellite data and a denser network of meteorological stations to improve the model. Sensitivity analyses are needed to level of agreement between input and output errors in the study area.

6 Conclusions

This study aims to estimate ET based on Landsat satellite dataset, and the SRTM DEM for Dwarakeswar -Gandheswari river basin based on the FAO-56 Penman-Monteith method. A comparison of the estimated results of ET with the NDVI indicates a good relationship over the study area. ET and NDVI distribution in the study area are strongly correlated. Susunia hill, Tilaboni hill, and the lower part of the river basin, including Burdwan, Hooghly, West Midnapore, and western parts of Bankura district over the study area have higher NDVI, typically have greater ET. Some portions of the Purulia district with sparse vegetation coverage normally have very low ET. ET values for the forests and vegetated areas, where the distribution of vegetation is highly variable, are relatively heterogeneous. ET change in the river basin is closely related to crop growth. The maximum monthly ET values in the entire study area were observed in irrigated cropland and the mountain areas. During the harvesting periods, ET is notably lower than in other months.

In the summer season, some portions of this area are clearly dependent on the irrigation applied. Spatial differences in yield were caused by differences in irrigation scheduling, especially during the dry season when the irrigation schedules were not able to meet the full crop requirements, the yield was reduced. Overall, the ET estimates depend on several factors, including climatic conditions and irrigation from a groundwater well, vegetation rate, and cropping pattern in these areas. High ET rates from water bodies were an indication of very high evaporative water. Moreover, ET results indicate the crop water stress scenarios and the need to differentiate between irrigated and non-irrigated areas. The present analysis is helpful for planning a water resources project with hydraulic structure(s).

7 Recommendations

A few recommendations have been proposed for a sustainable agriculture water management framework under changing climatic conditions using remote sensing & GIS techniques.

- i. High-resolution satellite data can be used for ET estimation purposes.
- ii. Different hydrological models can be used for long-term evapotranspiration estimations purposes.
- iii. Climate data can be correlated with evapotranspiration for drought assessment purposes.
- iv. The generated output can be used for future planning of agriculture water management purposes.

Acknowledgements The authors thank the Irrigation and Waterways Directorate, Government of West Bengal, India, for supporting this research work.

References

1. Valiantzas JD (2006) Simplified versions for the Penman evaporation equation using routine weather data. *J Hydrol* 331(3):690–702
2. Tsouni A, Kontoes C, Koutsoyiannis D, Elias P, Mamassis N (2008) Estimation of actual evapotranspiration by remote sensing: Application in Thessaly Plain. *Greece Sensors* 8(6):3586–3600
3. Singh RK, Irmak A, Irmak S, Martin DL (2008) Application of SEBAL model for mapping evapotranspiration and estimating surface energy fluxes in south-central Nebraska. *J Irrig Drain Eng* 134(3):273–285
4. Liu T, Luo Y (2012) An empirical approach simulating evapotranspiration from groundwater under different soil water conditions. *Environ Earth Sci* 67(5):1345–1355
5. Zhao L, Zhao W (2014) Evapotranspiration of an oasis-desert transition zone in the middle stream of Heihe River. *Northwest China J Arid Land* 6(5):529–539
6. Nouri H, Beecham S, Kazemi F, Hassanli AM, Anderson S (2013) Remote sensing techniques for predicting evapotranspiration from mixed vegetated surfaces. *Hydrol Earth Syst Sci Discuss* 10(3):3897–3925
7. Ficklin DL, Letsinger SL, Gholizadeh H, Maxwell JT (2015) Incorporation of the Penman-Monteith potential evapotranspiration method into a Palmer Drought Severity Index tool. *Comput Geosci* 85:136–141
8. Li H, Wang A, Yuan F, Guan D, Jin C, Wu J, Zhao T (2016) Evapotranspiration dynamics over a temperate meadow ecosystem in eastern Inner Mongolia. *China Environ Earth Sci* 75(11):1–11
9. Wang YQ, Xiong YJ, Qiu GY, Zhang QT (2016) Is scale really a challenge in evapotranspiration estimation? A multi-scale study in the Heihe oasis using thermal remote sensing and the three-temperature model. *Agric Meteorol* 230:128–141
10. Senay GB, Friedrichs M, Singh RK, Velpuri NM (2016) Evaluating Landsat 8 evapotranspiration for water use mapping in the Colorado River Basin. *Remote Sens Environ* 185:171–185
11. Yao Y, Qin Q, Fadhil AM, Li Y, Zhao S, Liu S, Sui X, Dong H (2011) Evaluation of EDI derived from the exponential evapotranspiration model for monitoring China's surface drought. *Environ Earth Sci* 63(2):425–436

12. Kundu S, Khare D, Mondal A (2017) Future changes in rainfall, temperature and reference evapotranspiration in the central India by least square support vector machine. *Geosci Front* 8(3):583–596
13. Mohammed R, Scholz, M (2016) Impact of evapotranspiration formulations at various elevations on the reconnaissance drought index. *Water Resour Manag* 1–18
14. Raoufi R, Beighley E (2017) Estimating daily global evapotranspiration using Penman-Monteith equation and remotely sensed land surface temperature. *Remote Sens* 9(11):1138
15. Amazirh A, Er-Raki S, Chehbouni A, Rivalland V, Diarra A, Khabba S, Merlin O (2017) Modified Penman-Monteith equation for monitoring evapotranspiration of wheat crop: Relationship between the surface resistance and remotely sensed stress index. *Biosys Eng* 164:68–84
16. Talsma CJ, Good SP, Jimenez C, Mattens B, Fisher JB, Miralles DG, McCabe MF, Purdy AJ (2018) Partitioning of evapotranspiration in remote sensing-based models. *Agric Meteorol* 260:131–143
17. Rozenstein O, Haymann N, Kaplan G, Tanny J (2018) Estimating cotton water consumption using a time series of Sentinel-2 imagery. *Agric Water Manag* 207:44–52
18. Jahanfar A, Drake J, Sleep B, Gharabaghi B (2018) A modified FAO evapotranspiration model for refined water budget analysis for Green Roof systems. *Ecol Eng* 119:45–53
19. Fernandes FHS, Sano EE, Ferreira LG, de Mello Baptista GM, de Castro VD, Fassoni-Andrade AC (2018) Degradation trends based on MODIS-derived estimates of productivity and water use efficiency: A case study for the cultivated pastures in the Brazilian Cerrado. *Remote Sens Appl: Soc Environ* 11:30–40
20. Wu X, Wang P, Huo Z, Wu D, Yang J (2018) Crop Drought Identification Index for winter wheat based on evapotranspiration in the Huang-Huai-Hai Plain, China. *Agr Ecosyst Environ* 263:18–30
21. Rahimzadegan M, Janani A (2019) Estimating evapotranspiration of pistachio crop based on SEBAL algorithm using Landsat 8 satellite imagery. *Agric Water Manag* 217:383–390
22. Guzinski R, Nieto H (2019) Evaluating the feasibility of using Sentinel-2 and Sentinel-3 satellites for high-resolution evapotranspiration estimations. *Remote Sens Environ* 221:157–172
23. Cunha J, Pereira TE, Pereira E, Rufino I, Galvão C, Valente F, Brasileiro F (2020) A high-throughput shared service to estimate evapotranspiration using Landsat imagery. *Comput Geosci* 134:104341
24. Sun SK, Li C, Wang YB, Zhao XN, Wu PT (2020) Evaluation of the mechanisms and performances of major satellite-based evapotranspiration models in Northwest China. *Agric Meteorol* 291:108056
25. Shukla G, Tiwari P, Dugesar V, Srivastava PK (2021) Estimation of evapotranspiration using surface energy balance system and satellite datasets. In: *Agricultural Water Management* (pp. 157–183). Academic Press
26. Aryalekshmi BN, Biradar RC, Chandrasekar K, Ahamed JM (2021) Analysis of various surface energy balance models for evapotranspiration estimation using satellite data. *Egypt J Remote Sens Space Sci* 24(3):1119–1126
27. Sahoo S, Sil I, Dhar A, Debsarkar A, Das P, Kar A (2018) Future scenarios of land-use suitability modeling for agricultural sustainability in a river basin. *J Clean Prod* 205:313–328
28. Allen RG, Pereira LS, Raes D, Smith M (1998) Crop evapotranspiration: guidelines for computing crop requirements. FAO Irrigation and Drainage Paper No. 56 Rome Italy pp. 282
29. Smith M, Allen R, Monteith JL, Perrier A, Santos Pereira L, Segeren A (1992) Expert Consultation on Revision of FAO Methodologies for Crop Water Requirements. Food and Agriculture Organisation of the United Nations (Land and Water Development Division) Rome 60
30. Williamson SN, Hik DS, Gamon JA, Kavanaugh JL, Flowers GE (2014) Estimating temperature fields from MODIS land surface temperature and air temperature observations in a sub-arctic alpine environment. *Remote Sens* 6(2):946–963
31. Ramoelo A, Majozi N, Mathieu R, Jovanovic N, Nickless A, Dziki S (2014) Validation of global evapotranspiration product (MOD16) using flux tower data in the African savanna. *South Africa Remote Sensing* 6(8):7406–7423